Influence of Electrostatic Interactions and Hydrogen Bonding on the Thermal and Mechanical Properties of Step-Growth Polymers

Sharlene R. Williams

Dissertation submitted to the faculty of the
Virginia Polytechnic Institute and State University
in partial fulfillment of the requirements for the degree of

Doctor of Philosophy
In
Chemistry

Timothy E. Long, Chair
Thomas C. Ward, Member
S. Richard Turner, Member
Maren Roman, Member
Susan E. Duncan, Member

October 21, 2008
Blacksburg, Virginia

Keywords: Hydrogen bonding, Electrostatic Interactions, Michael Addition, Polyurethane, Ionene, Thermomechanical Behavior

Influence of Electrostatic Interactions and Hydrogen Bonding on the Thermal and Mechanical Properties of Step-Growth Polymers

Sharlene R. Williams

ABSTRACT

Current research efforts have focused on the synthesis of novel, segmented, cross-linked networks and thermoplastics for emerging technologies. Tailoring macromolecular structures for improved mechanical performance can be accomplished through a variety of synthetic strategies using step-growth polymerization. The synthesis and characterization of novel Michael addition networks, ionene families, and ion-containing polyurethanes are described, with the underlying theme of fundamentally investigating the structure-property relationships of novel, segmented macromolecular architectures. In addition, it was discovered that both covalent and electrostatic crosslinking play an important role in the mechanical properties of all types of polymers described herein.

Novel cross-linked networks were synthesized using quantitative base-catalyzed Michael chemistry with acetoacetate and acrylate functionalities. These novel synthetic strategies offer unique thermo-mechanical performance due to the formation of a multiphase morphology. In order to fundamentally elucidate the factors that influence the kinetics of the Michael addition reaction a detailed analyses of model compounds were conducted in the presence of an in-situ IR spectrometer to optimize reaction conditions using statistical design of experiments. Networks were then prepared based on these optimized conditions. The mechanical performance was

evaluated as a function of molecular weight between crosslink points. Furthermore, the incorporation of hydrogen bonding within the monomer structure enhanced mechanical performance. The changes in morphological, thermal, and mechanical properties evaluated using dynamic mechanical analysis (DMA) and tensile behavior are described. In addition, the use of preformed urethane segments provides a safer method for incorporating hydrogen bonding functional groups into macromolecules.

In order to compare the thermomechanical and morphological properties of ion-containing polyurethanes to non-charged polyurethanes, poly(tetramethylene oxide)-based polyurethanes containing either a novel phosphonium diol or 1,4-butanediol chain extenders were prepared using a prepolymer method. The novel phosphonium polyurethane was more crystalline, and it was presumed that hydrogen bonding in the non-charged polyurethane restricted polymer mobility, and reduced PTMO crystallinity, and hydrogen bonding interactions were significantly reduced due to the presence of phosphonium cations. These results correlated well with mechanical property analysis. The phase separation and ionic aggregation were demonstrated via wide-angle X-ray scattering, small-angle X-ray scattering, scanning transmission electron microscopy, and energy-dispersive X-ray spectroscopy during STEM imaging, as described herein. In addition, a novel polyurethane containing imidazolium cations in the hard segment was synthesized and behaved very similarly to the phosphonium cation-containing polyurethane.

Ammonium ionenes, which contain quaternary nitrogen in the macromolecular repeating unit, have many potential uses in biomedical applications. They offer interesting coulombic properties, and the charge density is easily controlled through synthetic design. This property makes ionenes ideal polyelectrolyte models to investigate the influence of ionic aggregation on

many physical properties. Ammonium ionenes were prepared via the Menshutkin reaction from 1,12-dibromododecane and 1,12-bis(N,N-dimethylamino)dodecane. The absolute molecular weights were determined for the first time using an on-line multi-angle laser light scattering (MALLS) in aqueous size exclusion chromatography (SEC). Tensile testing and DMA were used to establish structure-property relationships between molecular weight and mechanical properties for a series of 12,12-ammonium ionenes. Furthermore, degradation studies in the presence of base support the possibility for water-soluble coatings with excellent mechanical durability that are amenable to triggered depolymerization. A novel synthetic strategy was utilized to prepare chain extended 12,12-ammonium ionenes containing cinnamate functional groups. In the presence of UV light, the polymers chain extended, and the resulting ionenes possessed enhanced thermomechanical properties and increased molecular weight. In addition, the novel synthesis of imidazolium ionenes was demonstrated, and the charge density was tuned for appropriate applications using either low molecular weight segments or oligomeric precursors. The change in charge density had a profound role in imidazolium ionene thermal and mechanical behavior.

ACKNOWLEDGEMENTS

I would like to thank my advisor, Tim Long, for his guidance throughout my graduate career. I thank all of my committee members for their interest and helpful suggestions concerning my research: Prof. Tom Ward, Prof. Richard Turner, Prof. Susan Duncan, and Prof. Maren Roman. My committee was also helpful with giving advice, especially Prof. Tom Ward. Various staff members made my stay at Virginia Tech a little easier, including Vicki Long, Millie Ryan, Laurie Good, Tammy Jo Hiner, Mary Jane Smith, Mary Dean Coleman, JaeHee Hong, and Jan McGinty, and I thank you for your assistance over the years. Filling the pages of this thesis would not have been possible without my collaborators, including Dr. Kevin Miller of Rohm and Haas, Prof. Craig Thatcher and Ben Lepene of Virginia-Maryland Regional College of Veterinary Medicine, Dr. Clay Bunyard of Kimberly-Clark, Prof. Karen Winey, Sunny Wang, and David Salas-de la Cruz of University of Pennsylvania. Working with a variety of people from different backgrounds made the research projects more interesting and gave the results greater depth than I could have ever accomplished alone. In addition, I acknowledge the funding sources for my research, including MILES IGERT, MAP MURI, ILEAD MURI, Rohm and Haas, and Kimberly-Clark.

I would especially like to thank fellow group members, present and past, for their camaraderie and research assistance over the years, including Tomonori, Kalpana, Emily, Shijing, Serkan, Gozde, Qin, John, Ann, Matt M., Erika, Takeo, Funda, Bill, Andy, Matthew, Matt H., Mana, Akshay, Sean, Renlong, Eva, Steve, Matt G., and Tianyu. I appreciate everything that Afia and Casey helped me with during the beginning of graduate school, especially with making it through the first year and my first reactions. I thank Brian for help with research and friendship over the years. Rebecca made graduate school a little less painful and a lot more fun with her friendship. The assistance of my undergraduate students, especially Sophie Barta and Brian Mohns, is appreciated.

My chemistry teacher at Northeastern High School, Beth Funderburg, provided inspiration to become a scientist, and I thank her for it. I also thank my professors at Wright State University, especially Prof. Eric Fossum and Prof. Kenneth Turnbull for the great experiences I had as an undergraduate researcher. I give my deepest thanks to my parents, Doug and Sharon Hopkins, for always believing in me and reminding me to do my very best. I thank

my brother Doug Jr., and his family, for providing support over the years. I also thank my entire family and friends, especially Jessica Maxson, for their support and love.

Finally, I can't imagine going though all of this without my husband, Larry. Thank you for all of your love, encouragement, and inspiration to do my best.

Attributions

- Timothy E. Long
  - VT Professor, graduate research advisor
- Erika M. Borgerding
  - VT M.S., conducted aqueous SEC experiments and analyzed data
- John M. Layman
  - VT Ph.D., conducted aqueous SEC experiments and analyzed data
- Karen I. Winey
  - UPenn Professor, advisor to Wenqin Wang and David Salas, collaborator
- Wenqin Wang
  - UPenn Ph.D. graduate student, conducted X-ray scattering experiments, analyzed data, and assisted with manuscript preparation and editing
- Zsofia Barta
  - Visiting undergraduate student, assisted with synthesis and characterization of polymers
- Sean M. Ramirez
  - VT associate research professor, synthesized a polymer and edited manuscript
- David Salas
  - UPenn Ph.D. graduate student, conducted X-ray scattering experiments, analyzed data, and assisted with manuscript preparation and editing
- Kevin M. Miller
  - Ph.D., Rohm and Haas, conducted experiments and assisted with manuscript preparation and editing
- Brian D. Mather
  - VT Ph.D., assisted with data analysis and editing of manuscript
- Benjamin S. Lepene
  - VMRCVM Ph.D. graduate student, assisted with experiments and manuscript editing
- Craig D. Thatcher
  - Former VMRCVM professor, advisor to Benjamin Lepene, collaborator

Table of Contents

Chapter 1 : Introduction 1
1.1 Dissertation Overview 1
Chapter 2 : Recent Advances in the Synthesis and Structure-Property Relationships of Ammonium Ionenes 3
2.1 Abstract 3
2.2 Scientific rationale and perspective 3
2.3 Synthesis of ionenes via the Menshutkin reaction 6
2.3.1 Historical perspective 6
2.3.2 Kinetics 7
2.4 Characterization of ionenes 8
2.4.1 Molecular weight determination 8
2.4.2 Thermal degradation of ammonium ionenes 10
2.4.3 In-situ monitoring of ionene polymerization 12
2.5 Non-segmented ionenes 14
2.5.1 Introduction 14
2.5.2 Early investigations of aliphatic ionenes with high charge density 15
2.5.3 Nanocomposites based on non-segmented ionenes 24
2.5.4 Interactions of ionenes with surfactants and zwitterionomers 25
2.6 Segmented ionenes 30
2.6.1 Introduction 30
2.6.2 Poly(tetramethylene oxide)-based ionenes 31
2.6.3 Poly(ethylene glycol)-based ionenes 43
2.6.4 Poly(propylene glycol)-based ionenes 45
2.6.5 Ionenes based on polydienes 46
2.7 Branched and cross-linked ionenes 48
2.8 Conclusions and future directions 51
2.9 Acknowledgements 54
2.10 References 55
Chapter 3 : Synthesis and Characterization of Well-Defined 12,12-Ammonium Ionenes: Evaluating Mechanical Properties as a Function of Molecular Weight 59
3.1 Abstract 59
3.2 Introduction 60
3.3 Experimental 63
3.3.1 Materials 63
3.3.2 Synthesis of 1,12-bis(N,N-dimethylamino)dodecane 64
3.3.3 Synthesis of 12,12-ammonium ionenes 64
3.3.4 Characterization 65
3.4 Results and discussion 66
3.5 Conclusions 79
3.6 Acknowledgements 80
3.7 References 80
Chapter 4 : Influence of Molecular Weight on the Cytotoxicity of 12,12-Ammonium Ionenes 83
4.1 Abstract 83

4.2 Introduction 83
4.3 Experimental 85
4.3.1 Materials 85
4.3.2 Characterization of polyionenes 85
4.3.3 Cell culture 86
4.3.4 Cell Viability Assay 86
4.4 Results and discussion 87
4.5 Conclusions 95
4.6 Acknowledgements 95
4.7 References 96
Chapter 5 : Synthesis of 12,12-Ammonium Ionenes with Functionality for Chain Extension and Cross-linking via UV Irradiation 98
5.1 Abstract 98
5.2 Introduction 98
5.3 Experimental 101
5.3.1 Materials 101
5.3.2 Synthesis of cinnamate-functionalized 12,12-ammonium ionene 102
5.3.3 Synthesis of *tert*-butyl bis(3-(dimethylamino)propyl)carbamate (bocDMPC) 103
5.3.4 Synthesis of *N,N*-bis(3-(dimethylamino)propyl)cinnamamide (cinDMPC) 103
5.3.5 Synthesis of poly(cinDMPC-*co*-bocDMPC) 104
5.3.6 Film preparation for cross-linked networks containing cinnamate-functionalized 12,12-ammonium ionenes and DMPC copolymers 104
5.3.7 Synthesis of styrenic-functionalized 12,12-ammonium ionene 105
5.3.8 Characterization of ionenes 105
5.4 Results and Discussion 107
5.4.1 Synthesis of tertiary amine end-capped 12,12-ammonium ionenes 107
5.4.2 Chain extension of 12,12-ammonium ionenes possessing cinnamate end groups 108
5.4.3 Cross-linking of cinnamate-functionalized 12,12-ammonium ionenes and cinnamate ionene copolymer (poly(cinDMPC-*co*-bocDMPC)) 114
5.4.4 Cross-linking of 12,12-ammonium ionenes possessing styrenic end groups 118
5.5 Conclusions 122
5.6 Acknowledgements 122
5.7 References 123
Chapter 6 : Ionene Segmented Block Copolymers Containing Imidazolium Cations: Structure-Property Relationships as a Function of Hard Segment Content 125
6.1 Abstract 125
6.2 Introduction 126
6.3 Experimental 128
6.3.1 Materials 128
6.3.2 Synthesis of 1,1'-(1,4-butanediyl)bis(imidazole) 129
6.3.3 Synthesis of poly(tetramethylene oxide) dibromide 129
6.3.4 Synthesis of imidazolium ionene containing 100 wt % hard segment 130
6.3.5 Synthesis of imidazolium ionene segmented block copolymers containing PTMO dibromide soft segments 130
6.3.6 Characterization 131

6.4 Results and Discussion 132
6.5 Conclusions 140
6.6 Acknowledgments 141
6.7 References 141
Chapter 7 : Influence of Imidazolium Salt Chain Extenders on the Thermomechanical Properties and Morphology of Segmented Poly(tetramethylene oxide)-Based Polyurethanes 144
7.1 Abstract 144
7.2 Introduction 145
7.3 Experimental 147
7.3.1 Materials 147
7.3.2 Synthesis of 1,1'-(1,4-butanediyl)bis(imidazole) 148
7.3.3 Synthesis of 1,1'-(butane-1,4-diyl)bis(3-(2-hydroxyethyl)-1H-imidazol-3-ium) bromide 148
7.3.4 Synthesis of polyurethanes 148
7.3.5 Characterization 149
7.4 Results and Discussion 150
7.5 Conclusions 162
7.6 Acknowledgements 162
7.7 References 163
Chapter 8 : Synthesis and Morphology of Segmented Poly(tetramethylene oxide)-Based Polyurethanes Containing Phosphonium Salts 165
8.1 Abstract 165
8.2 Introduction 166
8.3 Experimental 171
8.3.1 Materials 171
8.3.2 Synthesis of butane-1,4-bis[(2-hydroxyethyl)diphenylphosphonium] bromide chain extender 171
8.3.3 Synthesis of polyurethanes 172
8.3.4 Characterization 172
8.4 Results and Discussion 174
8.5 Conclusions 189
8.6 Acknowledgements 190
8.7 References 190
Chapter 9 : Michael Addition Reaction Kinetics of Acetoacetates and Acrylates for the Formation of Polymeric Networks 194
9.1 Abstract 194
9.2 Introduction 195
9.3 Experimental 198
9.3.1 Materials and Procedures 198
9.3.2 In-situ FTIR reactions for model studies 199
9.3.3 ^{1}H NMR spectroscopic kinetic studies 200
9.3.4 Statistical design of experiments 200
9.3.5 Network formation 201
9.3.6 Characterization 202
9.4 Results and discussion 202

9.4.1 Model Reactions with EtAcAc and EHA 202
9.4.2 Effect of base concentration 205
9.4.3 Effect of solvent on Carbon-Michael reactions 207
9.4.3.1 Effect of solvent using in-situ FTIR 207
9.4.3.2 Effect of solvent using ^{1}H NMR 209
9.4.4 Effect of acrylate concentration on Carbon-Michael kinetics 210
9.4.5 Design of Experiment (DOE) analysis 211
9.4.6 Network formation 221
9.5 Conclusions 230
9.6 Acknowledgements 231
9.7 References 231
Chapter 10 : Novel Michael Addition Networks Containing Urethane Hydrogen Bonding 233
10.1 Abstract 233
10.2 Introduction 233
10.3 Experimental 237
10.3.1 Materials and procedures 237
10.3.2 Preparation of EA-HMDI-EA 237
10.3.3 Network Formation 238
10.3.4 Characterization 238
10.4 Results and discussion 239
10.5 Conclusions 257
10.6 Acknowledgements 258
10.7 References 258
Chapter 11 : Synthesis and Characterization of Poly(ethylene glycol)-Glutathione Conjugate Self-Assembled Nanoparticles for Antioxidant Delivery 261
11.1 Abstract 261
11.2 Introduction 261
11.3 Experimental 264
11.3.1 Materials 264
11.3.2 Synthesis of GS-PEG-SG 265
11.3.3 Synthesis of FITC-labeled GS-PEG-SG 265
11.3.4 Synthesis of GS-SPEGS-SG 266
11.3.5 Characterization 266
11.3.6 Cell culture of SH-SY5Y cell line 267
11.3.7 Measure of cell viability after challenge with H_2O_2 267
11.3.8 Measure of cell viability of SH-SY5Y cells challenged with H_2O_2 and various concentrations of GS-PEG-SG and GS-SPEGS-SG 268
11.3.9 Cell viability assay 268
11.4 Results and Discussion 268
11.5 Conclusions 280
11.6 Acknowledgements 281
11.7 References 281
Chapter 12 : Oxidative Degradation of Biological Macromolecules 284
12.1 Abstract 284
12.2 Scientific rational and perspective 284

12.3 Free radical interactions 285
12.3.1 Oxygen balance in biological systems 285
12.3.1.1 Reactive oxygen species and their interactions with biological macromolecules 285
12.3.2 Radical reactions involving reactive oxygen species 287
12.3.3 Defense and repair mechanisms for biological and synthetic macromolecules 290
12.4 Protein oxidative degradation via reactive oxygen species 291
12.4.1 Oxidative degradation of amino acids 291
12.4.1.1 Aliphatic amino acids 291
12.4.1.2 Aromatic and heterocyclic amino acids 292
12.4.1.3 Amino acids containing sulfur atoms 293
12.4.2 Reactive oxygen species promoting peptide bond cleavage 295
12.4.3 Formation of carbonyl functionalities in amino acids 295
12.4.4 Protein cross-linking as a result of oxidative degradation 297
12.5 Carbohydrate oxidative degradation via reactive oxygen species 298
12.5.1 Oxidative degradation of reducing sugars and related compounds 299
12.5.1.1 The pro-oxidant and antioxidant abilities of saccharides 301
12.5.2 Nitroxide-mediated oxidation of polysaccharides 302
12.5.3 Oxidative stability of polymers with saccharide pendant groups 304
12.6 Effective means for measuring oxidative stress in biological macromolecular systems 305
12.6.1 Techniques for measuring oxidative stress or oxidative degradation 306
12.6.1.1 Electron paramagnetic resonance spectroscopy 306
12.6.1.2 Chemiluminescence and differential scanning calorimetry 307
12.6.1.3 Oxygen uptake 308
12.6.1.4 Infrared spectroscopy 308
12.7 Conclusions 310
12.8 References 310
Chapter 13 : Introduction of Saccharide Functionality into Polymers: Synthesis and Applications 314
13.1 Abstract 314
13.2 Research objectives and scientific importance 314
13.3 Advantages of utilizing bio-derived materials 316
13.3.1 Potential applications of glycopolymers 317
13.4 Incorporation of saccharide functionalities into vinyl polymers 319
13.4.1 Protection and deprotection chemistry 320
13.4.2 Synthesis 322
13.4.2.1 Conventional free radical polymerization 322
13.4.2.2 Ionic polymerization 323
13.4.2.3 Controlled free radical polymerization 324
13.4.2.4 Ring opening metathesis polymerization 328
13.4.2.5 Ring opening polymerization 329
13.5 Oxidative stress of polymers 330
13.5.1 Techniques to measure oxidative stability 332
13.5.2 Oxidative stability of polymers with saccharide pendant groups 333
13.6 Conclusions 335

13.7 References 335
Chapter 14 : Overall Conclusions 339
Chapter 15 : Suggested Future Work 345
15.1 Synthesis and structure-property relationships of novel ionenes 345
15.2 Synthesis and applications of ion-containing polyurethanes and polyureas 350
15.3 Synthesis of Michael addition networks containing ammonium, imidazolium, and phosphonium salt monomers 351
15.4 Glutathione nanoparticles for antioxidant delivery 352
15.5 References 352

List of Figures

Figure 2.1. Cartoon representing ionene structures as a function of charge density and structure type. (a) regular charge placement, (b) blocky charge placement using oligomeric precursors, (c) branched structures with regular charge placement, and (d) regular charge placement with tailored hydrophilic and hydrophobic segments. 5
Figure 2.2. Nikolai Alexandrovich Menshutkin (1842-1907), who discovered the Menshutkin reaction.[5] 6
Figure 2.3. Structure of dimethylamino-*n*-alkyl halides, originally used for ionene synthesis. 7
Figure 2.4. SEC chromatograms (MALLS traces) of 6,12-ammonium ionene polymerization over a 24 h period. Inset table includes time and M_w from MALLS.[12] 10
Figure 2.5. Kinetic plots of ionene polymerizations with monomers containing various methylene spacers at low conversion as a function of time.[23] 13
Figure 2.6. *In-situ* FT-IR spectroscopy as a function of time for 6,12-ammonium ionene polymerization. Arrow points to C-N^+ peak (903 cm^{-1}) growth and plateau after 20 h in refluxing methanol (30 wt% solids). 14
Figure 2.7. Representative examples of the aliphatic ammonium ionenes originally synthesized. 15
Figure 2.8. Transition state leading to the formation of the cyclic product that Rembaum et al. characterized.[42] 16
Figure 2.9. Reduced viscosity versus salt concentration of 6,6-ammonium ionene. (1) Water, (2) 0.5 M KBr, (3) 0.40 M KBr.[10] 18
Figure 2.10. Repeating unit structure of Tanaka's *x,y*-oxyethylene ionenes.[52] 19
Figure 2.11. Activated dichlorides used in ionene polymerizations. 22
Figure 2.12. Sukhyy's ionenes used in nanocomposite preparation.[62] 24
Figure 2.13. Ordering of surfactant and ionene as a function of charge density. (a) 3,3-ammonium ionene; (b) 6,4- and 6,6-ammonium ionene; (c) 6,12- and 12,12-ammonium ionene.[63] 27
Figure 2.14. General structure of a sulfobetaine. 28
Figure 2.15. Model for ionene complexation with PDMAPS. [67] 30
Figure 2.16. Structure of the first segmented ionene based on PTMO. 31
Figure 2.17. Dihalide structures Leir and Stark investigated for PTMO-based ionenes. 32
Figure 2.18. Proposed microphase separation model of Wilkes' PTMO ionenes.[72] 34
Figure 2.19. Dynamic mechanical behavior of the bromide (IP-Br) versus the chloride (IP-Cl) PTMO ionene.[75] 37
Figure 2.20. Schematic of PTMO ionenes as a function of counteranion (PI-Cl= chloride PTMO ionene, PI-Br= bromide PTMO ionene).[75] 39
Figure 2.21. PTMO-based ionenes and zwitterionomers. 42
Figure 2.22. Dynamic mechanical behavior of 2000 and 7000 g/mol highly branched (HBI) and linear (LI) ammonium ionenes. 43
Figure 2.23. Dielectric spectroscopy of polyisoprene ionenes.[77] 46
Figure 2.24. Structures of polybutadiene ionene (PBI) and polybutadiene urethane (PBU). 47
Figure 2.25. Cell viability as a function of 6,10-ammonium ionene concentration on normal and cancerous cells.[102] 52
Figure 2.26. Synthesis of imidazolium ionenes from 1,1'-(1,4-butanediyl)bis(imidazole) and 1,12-dibromobutane. 53

Figure 2.27. Synthesis of phosphonium ionenes from 1,4-bis(diphenylphosphino)butane and PTMO dibromide. 54
Figure 3.1. SEC MALLS traces of the bromine-terminated 12,12-ammonium ionenes. 69
Figure 3.2. ^{1}H NMR spectrum of an amino-terminated 12,12-ammonium ionene. 70
Figure 3.3. TGA curves for bromine-terminated 12,12-ammonium ionenes. Molar ratios in graph legend correspond to the diamine:dihalide molar ratios. 71
Figure 3.4. SEC dRI traces of the 12,12-ammonium ionene before and after degradation in the presence of base. 72
Figure 3.5. X-ray scattering profiles of the 1:1 12,12-ionene. a) Scattering intensity vs. q for stretched (200 %) and unstretched 12,12-ammonium ionenes films; b) Wide-angle X-ray scattering pattern of stretched (200 %) ionene film; c) Wide-angle X-ray scattering pattern of unstretched ionene film. 76
Figure 3.6. 12,12-ammonium ionene demonstrating shape memory properties..... 78
Figure 3.7. 12,12-ammonium ionenes demonstrating self-healing properties under an optical microscope equipped with a heating stage..... 79
Figure 4.1. Typical structure of an *x,y*-ionene, where x represents the number of methylenes in the diamine monomer, and y represents the number of methylenes in the dihalide monomer..... 84
Figure 4.2. MTT assay of SY5Y cells in the presence of various concentrations of 12,12-ammonium ionenes. SY5Y neuroblastoma cells ($2x10^4$ cells/well) were incubated for 24 h at 37 ºC prior to conducting the MTT assay. Data are means ± SD, n=8. 90
Figure 4.3. Luminescent cytotoxicity assay of SY5Y cells in the presence of various concentrations of 12,12-ammonium ionenes. SY5Y neuroblastoma cells ($2x10^4$ cells/well) were incubated for 24 h at 37 ºC prior to conducting the luminescent assay. Data are means ± SD, n=8. 91
Figure 4.4. MTT assay of COS-7 cells in the presence of various concentrations of 12,12-ammonium ionenes. COS-7 cells ($2x10^4$ cells/well) were incubated for 24 h at 37 ºC prior to conducting the MTT assay. Data are means ± SD, n=8..... 93
Figure 4.5. Luminescent cytotoxicity assay of COS-7 cells in the presence of various concentrations of 12,12-ammonium ionenes. COS-7 cells ($2x10^4$ cells/well) were incubated for 24 h at 37 ºC prior to conducting the luminescent assay. Data are means ± SD, n=8. 94
Figure 5.1. DMA of the 12,12-ammonium ionene. 108
Figure 5.2. Dimerization of cinnamate functional groups. 109
Figure 5.3. UV spectra demonstrating the cinnamate-functionalized ionene chain-extension process..... 111
Figure 5.4. Average (3 samples) tensile stress versus strain behavior of UV-irradiated cinnamate-functionalized 12,12-ammonium ionene. 113
Figure 5.5. SEC traces for cinnamate-functionalized 12,12-ammonium ionenes. Red traces = after UV irradiation, blue traces = after UV irradiation, solid lines = MALLS traces, dashed lines = RI traces. 114
Figure 5.6. Structure of poly(cinDMPC-*co*-bocDMPC)..... 115
Figure 5.7. UV spectra demonstrating decreasing cinnamate concentration after exposure to UV light for 88/12 wt % mixture of cinnamate-end-capped 12,12-ammonium ionene/poly(cinDMPC-*co*-bocDMPC). 117
Figure 5.8. UV spectra demonstrating decreasing cinnamate concentration after exposure to UV light for 43/57 mol % mixture of cinnamate-end-capped 12,12-ammonium ionene/ poly(cinDMPC -*co*-bocDMPC). 118

Figure 5.9. FIB-SEM image of spun cast ammonium ionene film. Layers from top to bottom: Pt, Au (~20 nm), film (~110 nm), and HF decorated quartz (from gas-assisted XeF_2 etching). Conditions: 86 pA, 5.00 kV, 4.2 mm WD, 52° tilt, 512 nm HFW, TLD detector. Scale bar = 200 nm. 120
Figure 5.10. UV spectra demonstrating the decreased absorbance of DMPA, indicating that cross-linking occurred. 121
Figure 6.1. ^{1}H NMR spectroscopy of imidazolium ionene segmented block copolymers as a function of hard segment content. 135
Figure 6.2. Dynamic mechanical behavior of PTMO-based imidazolium ionenes. Dashed line = 38 wt % HS, solid line = 20 wt % HS. 137
Figure 6.3. Multi-angle X-ray scattering intensity vs. scattering vector q plotted in log-log scale for unstretched PTMO-based imidazolium ionene films containing different concentrations of hard segment. The interdomain spacing was calculated from $d = 2\pi/q$. 140
Figure 7.1. Structure of the 2,2'-biimidazole-based chain extender used in the polyurethane synthesis of Collier et al.[24] 147
Figure 7.2. DSC traces of PTMO-HMDI-BD (solid line) and PTMO-HMDI-N+ (dashed line). Conditions: 10 °C/min, 2nd heat. 154
Figure 7.3. DMA curves demonstrating the transitions of PTMO-HMDI-BD and PTMO-HMDI-N+. Conditions: TA Instruments Q800 DMA, 3 °C/min, 1 Hz, film tension mode. 155
Figure 7.4. Multi-angle X-ray scattering intensity vs. scattering vector q plotted in log-log scale for unstretched PTMO-based polyurethane films containing different chain extenders. The inter-domain spacing was calculated from $d = 2\pi/q$. 156
Figure 7.5. High-angle angular dark field (HAADF) STEM image of PTMO-HMDI-N+ showed bright features dispersed in the dark matrix. Two types of bright features distinct in size were observed: a) microphase separation and b). macrophase separation. 157
Figure 7.6. EDS mapping of Br element for STEM image of PTMO-HMDI-N+. 158
Figure 7.7. FT-IR spectroscopy of NH (left) and C=O (right) region of PTMO-HMDI-BD and PTMO-HMDI-N+. 159
Figure 7.8. Comparison of the stress-strain behavior of linear, segmented, ion-containing polyurethane elastomers: (A) PTMO-HMDI-BD, (B) PTMO-HMDI-N+. 160
Figure 7.9 a) Scattering intensity vs. q averaged over the azimuthal angular range of 80-100° for the stretched polyurethane films. 2-D X-ray scattering patterns of stretched polyurethanes b) PTMO-HMDI-BD and c) PTMO-HMDI-N+. Arrows indicate stretching direction. 161
Figure 8.1. DSC traces for PTMO-HMDI-P+ (light gray), and PTMO-HMDI-BD (black). Conditions: 5 °C/min, 2nd heat. 178
Figure 8.2. DMA curves demonstrating the transitions of the phosphonium-containing (gray line) and non-charged polyurethanes (black line). Conditions: 3 °C/min, 1 Hz, film tension mode. 179
Figure 8.3. X-ray scattering intensity vs. scattering vector (q) plotted in log-log scale for unstretched PTMO oligomer and unstretched PTMO-based polyurethane films containing different chain extenders. 181
Figure 8.4. a. HAADF STEM image of phosphonium polyurethane showed bright, spherical ion-rich regions dispersed in the dark, hydrocarbon-rich matrix. b. Fitting the intensity profile across an isolated ionic domain with a Gaussian function provided the diameter of a STEM feature. 183

Figure 8.5. Spot EDS intensities taken from phosphonium polyurethane ultra-thin films during STEM imaging with a stationary 0.7 nm probe placed on bright and dark regions in the specimen. The quantity of Br and P is greater in the bright ion-rich domains. 184
Figure 8.6. 2-D X-ray scattering patterns of the stretched PTMO-HMDI-BD films at 600% strain (a) Wide-angle pattern shows two equatorial scattering peaks at angular positions of 14 nm^{-1} and 17 nm^{-1} that correspond to PTMO crystallization. (b) Same wide-angle pattern as (a), but in a different color scale to show the weak meridional reflections at 6 nm^{-1} that correspond to intramolecular scattering from hard segment. (c) Small-angle pattern shows meridional reflections at ~0.35 nm^{-1} that correspond to interparticle scattering from microphase-separated hard domains. The blue arrow indicates the stretching direction. (d) Chemical structure of the urethane segment in PTMO-HMDI-BD. 186
Figure 8.7. FT-IR spectroscopy of NH (left) and C=O (right) region of PTMO-HMDI-BD and PTMO-HMDI-P+..... 187
Figure 8.8. Comparison of the stress-strain behavior of linear, segmented, ion-containing polyurethane elastomer compared to the non-charged polyurethane: (A) PTMO-HMDI-BD (B) PTMO-HMDI-P+..... 189
Figure 9.1. *In-situ* FTIR spectra of EtAcAc and EHA Michael reaction waterfall plot: 1.4:1.0 acrylate to AcAc, 3 mol% K_2CO_3, in THF. 203
Figure 9.2. *In-situ* FTIR spectra of EtAcAc and EHA Michael reaction 2D plot: 1.4:1.0 acrylate to AcAc, 3 mol% K_2CO_3, in THF..... 204
Figure 9.3. Stacked ^1H NMR spectra of EHA and EtAcAc Michael reaction versus time. 205
Figure 9.4. The effect of base concentration on rate constant for the EtAcAc and EHA Michael reaction in the presence of DBU. Reaction conditions: 2.0:1.0 mol ratio acrylate to AcAc, 35 °C, neat, DBU. 206
Figure 9.5. The effect of base concentration on rate constant for EtAcAc and EHA Michael reaction in the presence of K_2CO_3. Reaction conditions: 0.8:1.0 mol ratio acrylate to AcAc, 35 °C, neat, K_2CO_3. 207
Figure 9.6. The effect of solvent on rate constant for the EtAcAc and EHA Michael reaction in the presence of DBU. Reaction conditions: 1.4:1.0 mol ratio acrylate to AcAc, 5 mol% catalyst, 35 °C, DBU..... 208
Figure 9.7. The effect of solvent on the rate constant for EtAcAc and EHA Michael reaction in the presence of K_2CO_3. Reaction conditions: 0.8:1.0 mol ratio acrylate to AcAc, 5 mol% catalyst, 35 °C, K_2CO_3. 209
Figure 9.8. The significant relationship between predicted and actual observed rate constants for reactions conducted in the presence of DBU. 212
Figure 9.9. The relationship between acrylate molar ratios and actual observed rate constants for reactions conducted in the presence of DBU. 213
Figure 9.10. The significant relationship between base concentration and actual observed rate constants for reactions conducted in the presence of DBU. 213
Figure 9.11. The significant relationship between the presence of solvent and actual observed rate constants for reactions conducted in the presence of DBU. 214
Figure 9.12. Contour plots of the effect of base concentration and acrylate molar ratios on the actual observed rate constants for reactions conducted in the presence of DBU. The plot on the left (a) represents reactions in THF, and the plot on the right (b) represents reactions in neat conditions. 215

Figure 9.13. Overlay plots of the effect of base concentration and acrylate molar ratios on the predicted observed rate constants for reactions conducted in the presence of DBU. The plot on the left (a) represents reactions in THF, and the plot on the right (b) represents reactions in neat conditions. 216
Figure 9.14. The significant relationship between predicted and actual observed rate constants for reactions conducted in the presence of K_2CO_3. 217
Figure 9.15. The relationship between acrylate molar ratios and actual observed rate constants for reactions conducted in the presence of K_2CO_3. 218
Figure 9.16. The significant relationship between base concentration and actual observed rate constants for reactions conducted in the presence of K_2CO_3. 218
Figure 9.17. The significant relationship between the presence of solvent and actual observed rate constants for reactions conducted in the presence of K_2CO_3. 219
Figure 9.18. Contour plots of the effect of base concentration and acrylate molar ratios on the actual observed rate constants for reactions conducted in the presence of K_2CO_3. The plot on the left (a) represents reactions in THF, and the plot on the right (b) represents reactions in neat conditions. 220
Figure 9.19. Overlay plots of the effect of base concentration and acrylate molar ratios on the predicted observed rate constants for reactions conducted in the presence of K_2CO_3. The plot on the left (a) represents reactions in THF, and the plot on the right (b) represents reactions in neat conditions. 221
Figure 9.20. *In-situ* FTIR profiles demonstrating decrease in absorption over time for PPG BisAcAc – PPGDA networks prepared with DBU as the base. 223
Figure 9.21. *In-situ* FTIR profiles demonstrating decrease in absorption over time for PPG BisAcAc – PPGDA networks prepared with K_2CO_3 as the base. 223
Figure 9.22. Kinetic plot of PPG BisAcAc – PPGDA network formation. 224
Figure 9.23. Storage modulus versus temperature for 1000 g/mol PPG BisAcAc – PPGDA networks. 227
Figure 9.24. Storage modulus versus temperature for 2000 g/mol PPG BisAcAc – PPGDA networks. 228
Figure 9.25. Storage modulus versus temperature for 4000 g/mol PPG BisAcAc – PPGDA networks. 229
Figure 9.26. Storage modulus versus temperature for 8000 g/mol PPG BisAcAc – PPGDA networks. 230
Figure 10.1. Tan δ versus temperature for PPG BisAcAc or TrisAcAc - NPGDA films. 244
Figure 10.2. Storage modulus versus temperature for PPG BisAcAc or TrisAcAc - NPGDA films. 245
Figure 10.3. Glass transition temperature of PPG BisAcAc – NPGDA networks as a function of inverse PPG BisAcAc molecular weight. 246
Figure 10.4. Isothermal TGA curves of 2000 g/mol PPG BisAcAc - NPGDA networks in air. 248
Figure 10.5. Tan δ versus temperature for PPG BisAcAc - EA-HMDI-EA films. 251
Figure 10.6. Storage modulus versus temperature for PPG BisAcAc - EA-HMDI-EA films. 252
Figure 10.7. DMA data comparison for 2000 g/mol PPG BisAcAc - EA-HMDI-EA network versus 2000 g/mol PPG BisAcAc - NPGDA network. 253
Figure 10.8. Tensile data comparison for 2000 g/mol PPG BisAcAc - EA-HMDI-EA network versus 2000 g/mol PPG BisAcAc - NPGDA network. 255

Figure 10.9. Isothermal TGA curves of PPG BisAcAc - EA-HMDI-EA networks in air at 125 °C. 256
Figure 10.10. Isothermal TGA data comparison for 2000 g/mol PPG BisAcAc - EA-HMDI-EA network versus 2000 g/mol PPG BisAcAc – NPGDA network in air at 125 °C. 257
Figure 11.1. Structure of glutathione (left) and its oxidized form, glutathione disulfide (right). 264
Figure 11.2. Dynamic light scattering of GS-PEG575-SG nanoparticles. Conditions: 10 mg/mL, 25 °C. 270
Figure 11.3. TEM micrograph of GS-PEG575-SG nanoparticles. Scale bar = 500nm. 271
Figure 11.4. UV-vis spectrum of FITC-labeled GS-PEG-SG nanoparticles. 273
Figure 11.5. Confocal microscopy of FITC-labeled GS-PEG575-SG nanoparticles. Scale bar = 1 μm. 274
Figure 11.6. FT-IR spectroscopy of HO-PEG-OH (black, OH indicated with arrow) and HS-PEG-SH (red, SH and C=O indicated with arrows). 276
Figure 11.7. FT-IR spectrum of GS-SPEGS-SG, where disappearance of thiol S-H is noticable. 277
Figure 11.8. SH-SY5Y cell viability in the presence of various concentrations of H_2O_2. Viability determined with conventional MTT assay methodologies. 278
Figure 11.9. MTT assay results for GS-PEG 575-GS in the presence of 100 μm H_2O_2. 279
Figure 11.10. MTT assay results for GS-SPEGS-GS in the presence of 100 μM H_2O_2..... 280
Figure 12.1. Oxidation products with carbonyl functionalities of proteins containing lysine, cysteine, and histidine.[48] 296
Figure 12.2. 2-deoxyribose, the monosaccharide in DNA..... 299
Figure 12.3. Structure of TEMPO, a persistent nitroxide. 302
Figure 12.4. Examples of glycopolymers, both linear and dendritic, where sugar portions are shown in red. 304
Figure 12.5. Infrared spectra of carbonyl and hydroxyl functionalities of oxidized poly(propylene) films over time.[86] 309
Figure 12.6. A kinetic plot to determine the rate of oxidation in carbonyl and hydroxyl functionalities of oxidized poly(propylene) films.[86] 309
Figure 13.1. Examples of protected saccharides.[31] 321
Figure 13.2. Typical nitroxides utilized in controlled free radical polymerization.[39] 326
Figure 13.3. Novel nitroxide initiator developed for lipo-glycopolymerization.[55] 327
Figure 13.4. Novel ruthenium initiators developed for ROMP.[62] 329
Figure 13.5. The auto-oxidation process in the degradation of polymers.[70] 334
Figure 15.1. Solution rheology of 15700 g/mol 12,12-ammonium ionene. Conditions: AR-G2, 25 °C, concentric cylinder geometry. 347
Figure 15.2. Schematic of ionene brushes as environmental factors are varied. 348

List of Tables

Table 2.1. Tensile properties of 12,12- and 6,12-ammonium ionenes as a function of molecular weight and charge density. The 6,6-ammonium ionenes were not mechanically strong enough for tensile test measurements. 24
Table 2.2. Reaction conditions and resulting intrinsic viscosity data for the synthesis of star-shaped ionenes. 48
Table 3.1. Ionene ditertiary amine monomer: dihalide monomer molar ratios and corresponding molecular weights. Calculated molecular weights for offset stoichiometry determined from Carother's equation. †Molecular weights are absolute and determined from the MALLS detector. *PEO/PEG equivalent molecular weights determined using dRI retention volumes/times. 68
Table 3.2. Ionene molecular weight and corresponding thermal transitions. The T_g was determined from maximum in tan δ versus temperature graphs. Second transition corresponds to the ionic aggregate disassociation. 74
Table 3.3. Tensile data for 12,12-ammonium ionene films as a function of molecular weight. . 75
Table 4.1. Molecular weight analysis via aqueous SEC, and ionene monomer molar ratios dictates final molecular weights. †Absolute weight-average molecular weights were determined from an on-line MALLS detector. *PEO/PEG equivalent molecular weights determined using dRI detection. 89
Table 5.1. Degradation onset temperatures (TGA), glass transition temperatures (DSC), and molecular weight data of the cinnamate-functionalized ionene before and after UV irradiation. 112
Table 6.1. Copolymer compositions based on molar equivalents of monomer and HS/SS content. 134
Table 6.2. TGA and DSC results of imidazolium ionene copolymers. 136
Table 9.1. DOE design. 201
Table 9.2. Effect of solvent on k_{obs} – ^{1}H NMR method. 210
Table 9.3. Effect of acrylate : acetoacetate molar ratio on k_{obs}. 211
Table 9.4. Observed rate constants from *in-situ* FTIR experiments for PPG BisAcAc – PPGDA network formation. 224
Table 9.5. Gel time analysis for PPG BisAcAc – PPGDA networks as determined from rheology experiments. The gel time was recorded when G' = G". 225
Table 9.6. Gel fraction analysis for PPG BisAcAc – PPGDA networks as determined from Soxhlet extractions. 226
Table 10.1. Molecular weight and functionality analysis of PPG AcAc network precursors. .. 240
Table 10.2. Gel fraction analysis for PPG BisAcAc (or TrisAcAc) – NPGDA films. 242
Table 10.3. Tensile data for PPG BisAcAc (or TrisAcAc) – NPGDA films. 247
Table 10.4. Isothermal TGA data summary for PPG BisAcAc (or TrisAcAc) networks in air for 5 h. 249
Table 10.5. Gel fraction analysis for PPG BisAcAc – EA-HMDI-EA films. 250
Table 10.6. Tensile data for PPG BisAcAc – EA-HMDI-EA films. 254
Table 11.1. Reactive oxygen species.[31] 263
Table 11.2. Particle diameter measured via DLS as a function of PEG molecular weight. 272
Table 11.3. Thermal properties of GS-PEG-SG nanoparticles. 274
Table 12.1. Reactive oxygen and nitrogen species.[23] 287
Table 12.2. Rate constants of reactions of amino acids with radicals. [30,37] 294

Table 12.3. Antioxidant capabilities of some saccharides.[67] 301
Table 13.1. Reactive oxygen species.[68] 331

List of Schemes

Scheme 2.1. General mechanism for S_N2 reactions. 7
Scheme 2.2. Reactions involving quaternary ammonium salts at 200 °C. 11
Scheme 2.3. Synthesis of DABCO-based ionenes using various dibromides, where R = propyl, butyl, pentyl, hexyl, octyl, decyl, dodecyl, or *o*-, *m*-, *p*-xylyl. 21
Scheme 2.4. Synthesis of pyridinium ionenes from "living" PTMO and either 4,4'-bipyridine or 1,2-bis(4-pyridinium)ethylene. 35
Scheme 2.5. Synthesis of PTMO ionenes that contain only one quaternary ammonium cation per repeating unit.[74,75] 36
Scheme 2.6. Mechanism of the base-promoted Hofmann elimination reaction for 12,12-ionenes. 38
Scheme 2.7. Synthesis of PEG-based ionenes from anionic polymerization of ethylene oxide. 44
Scheme 2.8. Synthesis of elastomeric ionenes for conductive LiTCNQ complexes. 45
Scheme 2.9. Synthesis of acrylate and allyl cross-linkers. 50
Scheme 3.1. Synthesis of 1,12-bis(N,N-dimethylamino)dodecane. 67
Scheme 3.2. Synthesis of bromine-terminated 12,12-ammonium ionenes. 67
Scheme 3.3. Mechanism of the base-promoted Hofmann elimination reaction for 12,12-ionenes. 72
Scheme 4.1. Synthesis of 12,12-ammonium ionenes via the Menschutkin reaction. 88
Scheme 5.1. Ionene polymerization via the Menshutkin reaction. 99
Scheme 5.2. a. Head-to-head and b. head-to-tail [2π + 2π] cycloaddition of cinnamate functional groups. 101
Scheme 5.3. Synthesis of 12,12-ammonium ionene. 107
Scheme 5.4. Synthesis of 11-bromundecyl-cinnamate. 109
Scheme 5.5. Synthesis of cinnamate-functionalized 12,12- ammonium ionenes. 109
Scheme 5.6. Synthesis of styrenic-functionalized ionene. 119
Scheme 6.1. Synthesis of 1,1'-(1,4-butanediyl)bis(imidazole). 132
Scheme 6.2. Synthesis of bromine-terminated PTMO. 133
Scheme 6.3. Synthesis of imidazolium ionene segmented block copolymers containing 1,12-dibromododecane and bromine-terminated PTMO. 134
Scheme 7.1. Synthetic strategy for 1,1'-(1,4-butanediyl)bis(imidazole). 151
Scheme 7.2. Synthesis of 1,1'-(butane-1,4-diyl)bis(3-(2-hydroxyethyl)-1H-imidazol-3-ium) bromide (bisimidazolium diol). 151
Scheme 7.3. Synthesis of the imidazolium-containing polyurethane (PTMO-HMDI-N+). 152
Scheme 8.1. Synthesis of butane-1,4-bis[(2-hydroxyethyl)diphenylphosphonium] bromide chain extender. 175
Scheme 8.2. Synthesis of phosphonium-containing polyurethanes (PTMO-HMDI-P+). 176
Scheme 9.1. General Carbon-Michael reaction. 196
Scheme 9.2. Second Michael addition 197
Scheme 9.3. Model reactions of EtAcAc and EHA. 203
Scheme 9.4. Network formation via the Michael reaction of PPG BisAcAc and PPGDA. 222
Scheme 10.1. Mechanism of the carbon Michael addition reaction. 235
Scheme 10.2. Preparation of PPG BisAcAc, the Michael donor. 240
Scheme 10.3. Preparation of networks based on PPG BisAcAc and NPGDA. 241
Scheme 10.4. Preparation of networks based on PPG BisAcAc and EA-HMDI-EA 241

Scheme 11.1. Synthesis of GS-PEG-SG nanoparticles. 269
Scheme 11.2. Synthesis of FITC-labeled GS-PEG-SG nanoparticles. 272
Scheme 11.3. Synthetic strategy for thiol-terminated PEG. 275
Scheme 11.4. Synthesis of GS-SPEGS-SG. 277
Scheme 12.1. The autoxidation reaction scheme.[27] 288
Scheme 12.2. Hydrogen atom abstraction of serine. 292
Scheme 12.3. Hydrogen atom abstraction of lysine. 292
Scheme 12.4. Formation of 3, 4-dihydrophenylalanine (DOPA).[30] 293
Scheme 12.5. Formation of carbonyl compounds upon oxidation of glutamyl residues. [47] 295
Scheme 12.6. Lysine oxidation though glycation – glycoxidation reaction. P represents the protein backbone.[48] 296
Scheme 12.7. Protein – protein cross-linking reactions.[48] 298
Scheme 12.8. Oxidation of an aldose yielding its lower aldonic acid and formic acid. 300
Scheme 12.9. Nitroxide mediated oxidation of alcohols.[71] 303
Scheme 15.1. Synthesis of phosphonium cation-containing ionenes with PTMO soft segments. 350

Chapter 1 : Introduction

1.1 Dissertation Overview

The effect of cross-linking, whether electrostatic or covalent, on structure-property relationships was investigated in this dissertation. Following this chapter, the structure-property relationships of a family of polyelectrolytes, specifically named ammonium ionenes, were reviewed. The third chapter describes the synthesis of 12,12-ammonium ionenes with varying molecular weights. Absolute molecular weights were determined via aqueous size exclusion chromatography using a multi-angle laser light scattering detector. Relationships between molecular weight and thermomechanical performance were investigated. The fourth chapter illustrates a fundamental investigation of the cytotoxicity of 12,12-ammonium ionenes as a function of molecular weight. Ionenes have potential applications in the biomedical arena, so it is important to understand the cytotoxicity. The fifth chapter focuses on the synthesis and thermomechanical properties of 12,12-ammonium ionenes possessing functionality appropriate for UV irradiation. Cross-linked and chain extended polymers were prepared that contained cinnamate and vinyl endgroups. The sixth chapter focuses on the synthesis and structure-property relationships of novel imidazolium ionene copolymers. A poly(tetramethylene oxide) soft segment was used, and thermomechanical properties were evaluated as a function of the hard segment content.

The seventh chapter describes the synthesis of novel imidazolium polyurethanes containing poly(tetramethylene oxide) soft segments. The thermomechanical and morphological properties were compared to non-charged polyurethanes. The eighth chapter focuses on comparing the thermomechanical and morphological properties of phosphonium chain extended

polyurethanes to non-charged analogs. Profound differences in the morphological features of the two different types of polyurethanes were observed.

The ninth chapter focuses on the kinetics of the Michael addition reaction of small molecule and cross-linked networks. A statistical design of reactions were conducted in the presence of an *in-situ* ATR FTIR spectrometer to determine the effect of solvent, base, base concentration, and reactant stoichiometry on the observed rate constant. The tenth chapter describes the synthesis and characterization of Michael cross-linked networks prepared from acetoacetate oligomers and acrylate monomers. The incorporation of urethane functionality enhanced the tensile properties compared to non-hydrogen bonded analogues.

In recent years, research at the chemistry-biology interface has received renewed interest, particularly the polymer-biology interface. The eleventh chapter focuses on synthesis of self-assembling nanoparticles containing poly(ethylene oxide) conjugated to antioxidant peptides. Glutathione, the antioxidant, was attached to poly(ethylene oxide) oligomers using a Michael addition reaction. The nanoparticles have potential in biomedical technologies. The twelfth and thirteenth chapters are original literature reviews from the Department of Chemistry and MILES oxidation course, respectively. They were included to emphasize the increasing importance of incorporating biologically based macromolecules in conventional polymer science applications and the effects they have on oxidation. The fourteenth chapter summarizes the dissertation accomplishments, and the fifteenth chapter describes potential future work.

Chapter 2 : Recent Advances in the Synthesis and Structure-Property Relationships of Ammonium Ionenes

From: Williams, S.R.; Long, T.E. *Progress in Polymer Science,* submitted, 2008.

2.1 Abstract

Ionenes are ion-containing polymers that have quaternary nitrogen atoms in the macromolecular main chain as opposed to a pendant site. They are synthesized through a Menshutkin reaction of ditertiary amines and alkyl dihalides. This review focuses on the synthesis and structure-property relationships of ammonium ionenes, which were first synthesized in 1933. Since then, many researchers have investigated the effect of charge density of novel ionene families on polymer properties, such as viscosity and dynamic mechanical behavior. In particular, emphasis is placed on the properties of non-segmented and segmented ionene polymers. Although this investigation focuses largely on linear ionenes, branched and cross-linked ionenes will also be discussed.

2.2 Scientific rationale and perspective

Polymers containing quaternary nitrogen atoms in the polymer main chain, as opposed to in a pendant site, are called ammonium polyionenes, or ionenes.[1] Although the first ionenes were prepared from dimethylamino-*n*-alkyl halides,[2] ionenes are generally prepared from a reaction of ditertiary amines and dihalides. Ionenes have received increasing attention as ideal candidates for precisely controlling the charge density in polyelectrolytes. Typically, ionomers and polyelectrolytes present a non-uniform distribution of ionic groups within a polymer chain.[3] Thus, because the properties of ionomers are highly dependent on polymer composition, their

behaviors are not easily modeled.[4] This random type of polymer structure often complicates the analysis of ionic aggregation effects. Conversely, ionenes are unique since the ionic sites are precisely situated along the macromolecular repeating unit in a very well-defined manner. Careful monomer selection provides control of the charge density, and a number of dihalides and ditertiary amines are commercially available for polymerization or are easily synthesized. This permits the synthesis of a vast array of well-defined polymers that are ideal for studying ionic aggregation.

Several cartoons representing the various types of ionene polymer structures are shown in Figure 2.1. An ionene can have a very high, regularly placed charge density (Figure 2.1a) using low molecular weight monomers or a blocky charge placement (Figure 2.1b) using an oligomeric precursor and a low molecular weight monomer. In addition, branch points are incorporated using monomers with functionalities greater than 3 (Figure 2.1c). For many emerging applications, a balance between the hydrophilic and hydrophobic blocks is typically required. This feature can also be achieved via ionene polymerization, while maintaining controlled charge placement (Figure 2.1d).

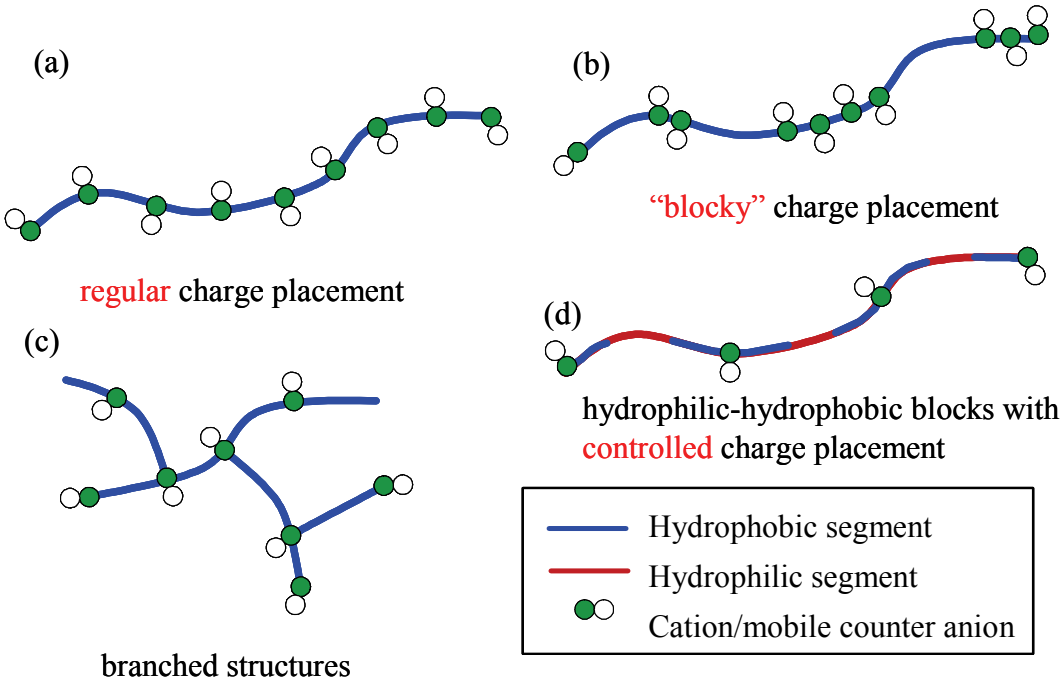

Figure 2.1. Cartoon representing ionene structures as a function of charge density and structure type. (a) regular charge placement, (b) blocky charge placement using oligomeric precursors, (c) branched structures with regular charge placement, and (d) regular charge placement with tailored hydrophilic and hydrophobic segments.

Only a few polymerizations strategies provide high mechanical strength elastomeric films with well-defined placement of cross-link points. Ionic aggregation, however, allows for the formation of physical cross-links, which imparts mechanical strength comparable to segmented, hydrogen-bond containing polyurethanes. In this review, therefore, various synthetic strategies for preparing ionenes will be discussed. Moreover, the structure-property relationships of novel ionene families will be described as a function of polymer composition.

2.3 Synthesis of ionenes via the Menshutkin reaction

2.3.1 Historical perspective

The reaction used to prepare ionenes is named after Nikolai Menshutkin (Figure 2.2). This polymerization reaction typically involves an S_N2 mechanism between a linear dihalide and a nucleophilic ditertiary amine. Typically, dibromides are used because of the suitability of the bromide anion as a leaving group in nucleophilic substitution. Other leaving groups have been investigated, but dichlorides are typically slow to react, and diiodides, if commercially available, are more expensive than dibromides.

Figure 2.2. Nikolai Alexandrovich Menshutkin (1842-1907), who discovered the Menshutkin reaction.[5]

In 1968, Rembaum et al. adopted the name "ionene" for polymers that contain ionic groups derived from amino-containing monomers.[1] The first ionenes were synthesized in 1933 from dimethylamino-*n*-alkyl halides, which are now termed AB monomers (Figure 2.3).[2] The polymerization process typically resulted in a variety of cyclic species, in addition to the polymer product.

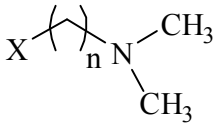

X = F, Cl, Br, I

Figure 2.3. Structure of dimethylamino-*n*-alkyl halides, originally used for ionene synthesis.

Since a number of ditertiary amines and alkyl dihalides are commercially available or easily synthesized, polymerization of ionenes is also accomplished via polymerization of a dihalide and a ditertiary amine, also referred to as the Menshutkin reaction.[6] The nomenclature of aliphatic, non-segmented, ionenes is typically associated with the number of methylene units from the monomers, namely the ditertiary amine and alkyl dihalide, respectively, i.e., *x,y*-ionene, where x = number of CH_2 units in the diamine and y = number of CH_2 units in the dihalide.[7]

2.3.2 Kinetics

As mentioned previously, ionene polymerizations typically proceed via an S_N2 mechanism. In very rare cases, such as those involving concentrated solutions, researchers have reported first order kinetics.[1] The S_N2 mechanism involves an inversion in stereochemistry at the carbon alpha to the halide. A general mechanism for an S_N2 reaction between a tertiary amine and an alkyl halide is given in Scheme 2.1.

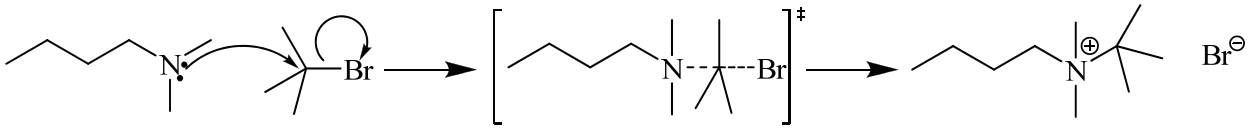

Scheme 2.1. General mechanism for S_N2 reactions.

When the reaction is second order, the rate law[8] is written as:

$$\text{Rate} = k[\text{RX}][\text{Nu:}]$$

The rate of reaction of an ionene polymerization is similar to other S_N2 reactions. The reaction will proceed most rapidly when the substrate, the dihalide, is unhindered. In the case of an ionene polymerization, the dihalide typically primary, and thus provide the most reactive centers for an S_N2 reaction, with the exception of methyl halide. Ditertiary amines serve as the nucleophile in the polymerization process, and dimethyl substitution avoids deleterious steric effects and ensures efficient nucleophilic behavior. The leaving group for an ionene polymerization is important not only from a structure-property perspective, as shown later, but also with respect to monomer reactivity. Dichlorides and dibromides are commercially available and relatively affordable, in contrast to diiodides, which are typically expensive or not commercially available. As discussed below, the most widely used halogen in ionene synthesis is bromine because the bromide anion, which is a relatively weak base, serves as an excellent leaving group.[8]

2.4 Characterization of ionenes

2.4.1 Molecular weight determination

Although ionene chemistry has been reported since the early 1930s, absolute molecular weight analysis has not received attention until recently. Typically, apparent molecular weight was only reported using intrinsic viscosity measurements. It is critical to perform molecular weight analysis for non-associating polymer chains—rather than obtaining aggregate measurements—for accurate molecular weight determination. However, since it is often difficult to eliminate all polymer interactions, the use of solvent/salt solutions is effective at screening electrostatic interactions in order to obtain accurate molecular weights.

In the 1930s, researchers would typically obtain an average molecular weight based on the ratio of non-ionic bromine to total bromide in an ionene solution.[9] Later, in the 1960s and 1970s Rembaum et al. conducted viscosity and light scattering experiments on 3,4- and 6,6-ammonium ionenes to elucidate the Mark-Houwink and Debye relationships, respectively.[10] Although these methods did result in absolute molecular weight determination, the calculations involved tedious and meticulous sample preparation.

Another important method for determining absolute molecular weight involves the use of size exclusion chromatography (SEC). In the case of polyelectrolytes, however, SEC is often challenging. First, the radius of gyration of the polymer chain in solution is used to determine absolute molecular weight. But since polyelectrolytes often aggregate in solution, determining absolute molecular weight becomes problematic. Other factors that influence the determination of polyelectrolyte molecular weight include non-size exclusion events such as ion interactions, ion exclusion, and hydrophobic interactions in the stationary phase of the chromatographic column.[11] With these factors in mind, absolute molecular weights are best achieved when SEC is coupled with multi-angle laser light scattering (MALLS). Using the MALLS method, our research group recently reported appropriate chromatographic conditions to determine the molecular weight of 12,12- and 6,12-ammonium ionenes using an aqueous-based mobile phase.[12] While several mobile phase compositions were attempted (including those previously reported in literature), the only mobile phase composition found appropriate for separating both types of ionenes consisted of a 54/23/23 mixture of water/methanol/acetic acid that contained 0.54 M NaOAc at a pH of 4.0. Dynamic light scattering (DLS) confirmed the absence of ionic aggregates, thus ensuring the feasibility of chromatographic separation in this unusual solvent composition. A plot of SEC chromatograms (MALLS traces) are shown for a 6,12-ammonium

ionene polymerization during a 24 h period in Figure 2.4.

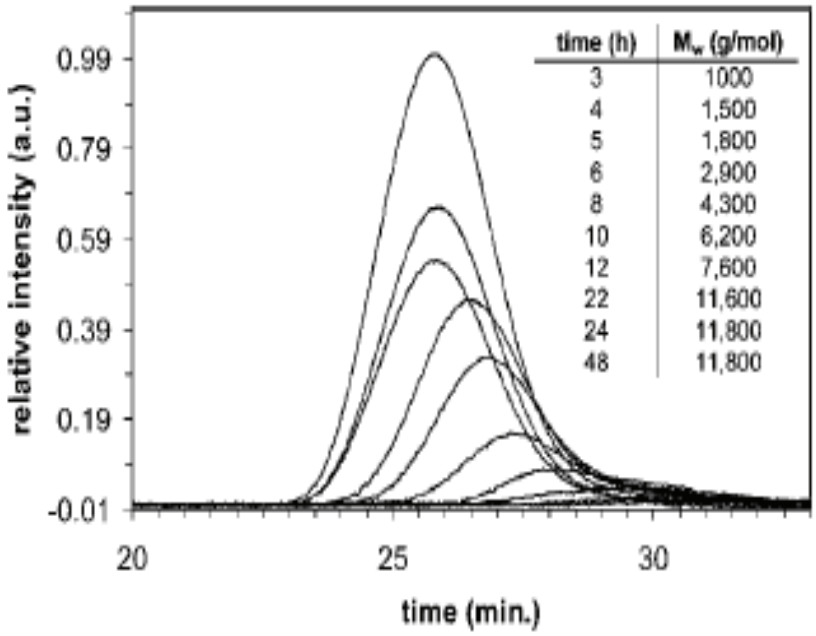

Figure 2.4. SEC chromatograms (MALLS traces) of 6,12-ammonium ionene polymerization over a 24 h period. Inset table includes time and M_w from MALLS.[12]

2.4.2 Thermal degradation of ammonium ionenes

Although specific examples of ionene degradation are detailed throughout this review, this section will describe general thermal degradation of quaternary ammonium compounds, including ionenes. The thermal decomposition of quaternary ammonium polymers is not well-documented throughout the literature; however, many researchers have investigated the thermal stability of low molecular weight ammonium salts. Quaternization is known to enhance the thermal stability of tertiary amines. For example, the quaternization of *N,N*-dimethyldodecylamine with iodomethane resulted in an ammonium salt that was thermally stable until 250 °C, whereas the tertiary amine precursor was completely degraded and/or volatilized at ~170 °C.[13]

One degradation reaction that ionenes undergo is the reverse Menshutkin reaction at higher temperatures,[14], where the products of the degradation process have functional end groups that are halides and ditertiary amines. Another viable degradation pathway is the Hofmann elimination reaction. Charlier and co-workers used a combination of TGA, high-performance liquid chromatography (HPLC), and mass spectroscopy to study the thermal stability of telechelic polystyrene containing quaternary ammonium ionic sites.[13] Based on model compounds, they proposed that three possible reactions occurred, as shown in Scheme 2.2. As they demonstrated, reaction A was confirmed via HPLC; while reactions B and C were verified using mass spectroscopy. However, it is important to note that the dequaternization reaction is highly dependent on ammonium salt composition. Specifically, a less basic amine will enhance the dequaternization process.[15]

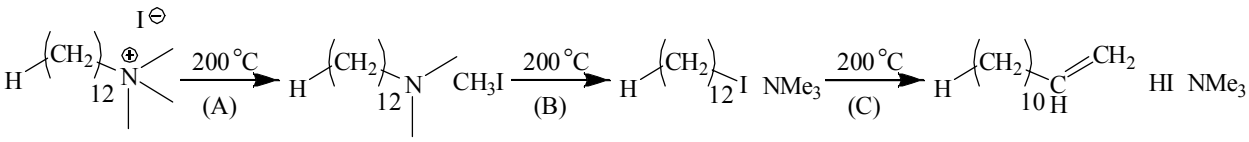

Scheme 2.2. Reactions involving quaternary ammonium salts at 200 °C.

Typically, high charge density ionenes are thermally stable to ~225-250 °C.[16] After that point, the polymer begins to degrade through a complex process that involves both of the reactions described above. The de-alkylation reaction and subsequent elimination reaction for most polymers, including ionenes, is consistent with the literature on low molecular weight ammonium salts.[17] In addition, several researchers have investigated small molecule ammonium salt decomposition and observed a tailing phenomenon in TGA curves.[18,19] This occurrence was particularly evident in high temperature regions, i.e., before complete decomposition, and increased with increasing alkyl chain length. Overall, the decomposition of small molecule and polymeric ammonium salts is a complicated process due to many competing reaction

mechanisms.[20]

2.4.3 In-situ monitoring of ionene polymerization

Due to the complexity and sensitivity of many reactions, *in-situ* analysis is a valuable characterization tool. The need for tedious sample removal is eliminated, and second, the possibility that impurities, air, and/or moisture will interfere with the reaction process and products is significantly reduced. Therefore, it is particularly amenable to polymerizations that require the absence of air and moisture, such as anionic and polyurethane polymerizations. Finally, *in-situ* instrumentation is ideal for polymerizations using limited quantities of monomers because all of the product is isolated at one time, and none is wasted on product analysis over time.[21]

Typically, monomer and polymer chain ends exhibit equal reactivity in step growth polymerizations, which leads to straightforward kinetic considerations.[22] However, Meyer et al. demonstrated via *in-situ* ^{13}C NMR spectroscopic studies that *x,y*-ionene polymerizations were quite complex for x and y = 3, 4, and 6.[23] Specifically, they detected four different reactions using NMR spectroscopy: (1) dihalide monomer reacting with ditertiary amine monomer, (2) dihalide monomer reacting with ditertiary amine end-capped polymer, (3) ditertiary amine monomer reacting with dihalide end-capped polymer, and (4) dihalide end-capped polymer reacting with ditertiary amine end-capped polymer. In addition, the Hofmann elimination reaction and intramolecular cyclization were also detected. Thus, the kinetics of their reactions were not always second order, as shown in Figure 2.5. From their NMR spectroscopic analyses, they proposed that ionenes would display broad molecular weight distributions based on the specific reaction conditions.

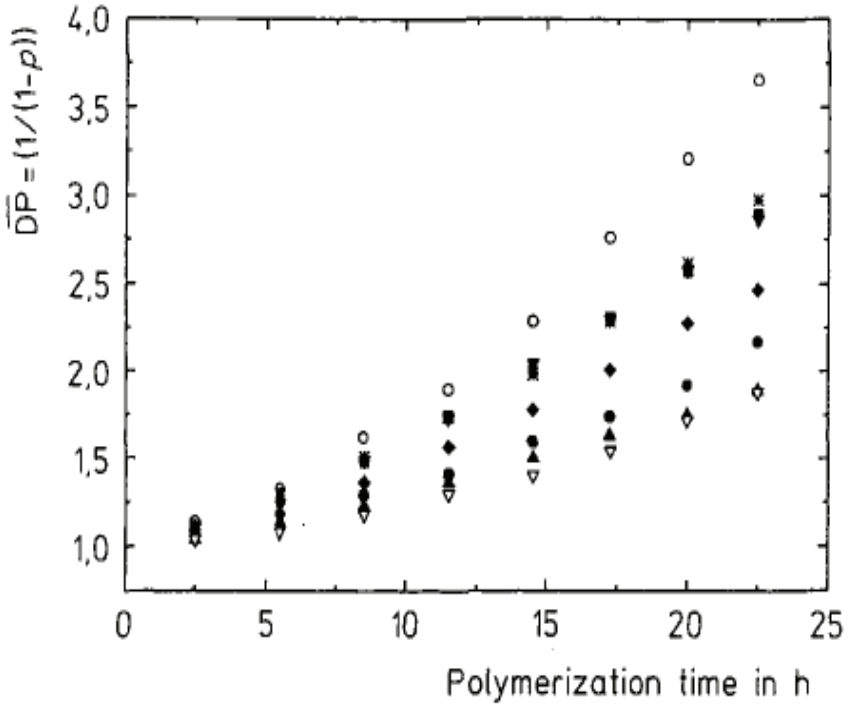

Figure 2.5. Kinetic plots of ionene polymerizations with monomers containing various methylene spacers at low conversion as a function of time.[23]

In-situ FT-IR spectroscopy is a useful tool for monitoring the IR spectrum of a reaction over time, particularly because it eliminates the need for removing samples from the reaction flask.[24-38] 6,12-Ammonium ionenes were polymerized in the presence of an *in-situ* FT-IR spectroscopic probe,[39] and the resulting spectrum is shown in Figure 2.6 for the 940-800 cm^{-1} region, where C-N^+ stretches are observed. The arrow indicates the growth and plateau of the C-N^+ stretch at 903 cm^{-1}.[40] From the plot, second order kinetics were obtained, which is consistent with the literature on non-segmented ionenes, described below. Similar observations were observed for 12,12-ammonium ionenes as well.[39,41]

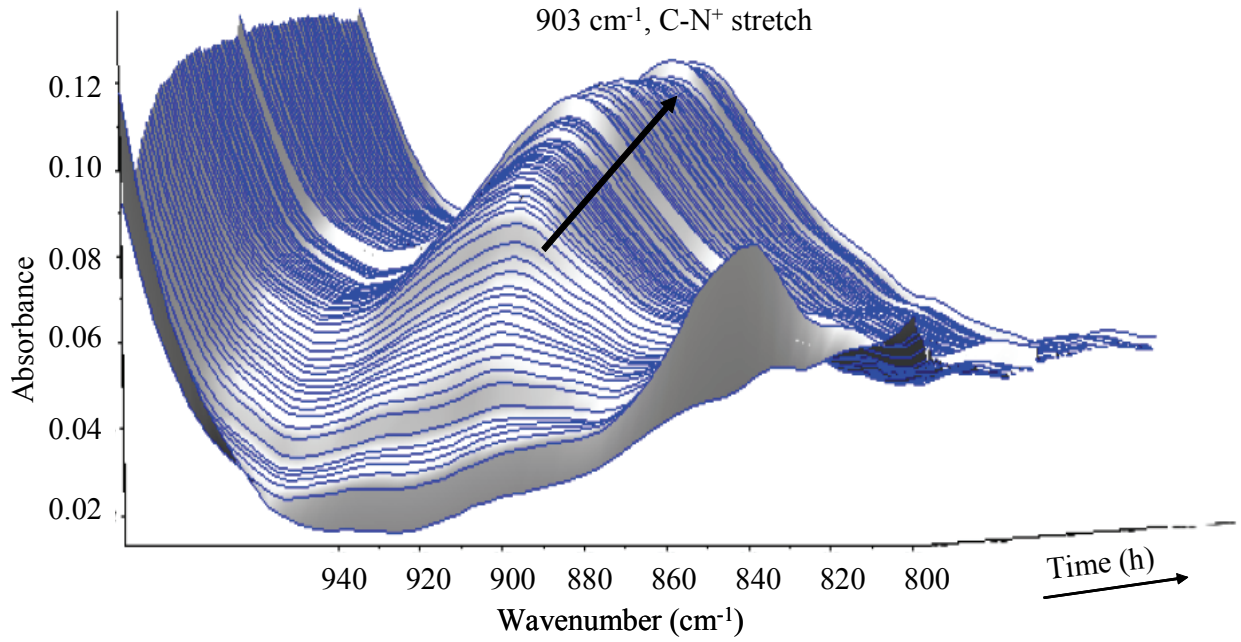

Figure 2.6. *In-situ* FT-IR spectroscopy as a function of time for 6,12-ammonium ionene polymerization. Arrow points to $C\text{-}N^+$ peak (903 cm^{-1}) growth and plateau after 20 h in refluxing methanol (30 wt% solids).

2.5 Non-segmented ionenes

2.5.1 Introduction

The literature is rich with examples involving the synthesis of *x,y*-ammonium ionenes, starting with the work of Rembaum et al., as illustrated in the next section. Since their pioneering work in the late 1960s and early 1970s, many researchers have also investigated ionic interactions with other charged species. As will be described, ionenes form complex mixtures with zwitterionomers and surfactants, resulting in unique properties. Research demonstrating the formation of novel composites based on clay and ionene mixtures will also be discussed.

2.5.2 Early investigations of aliphatic ionenes with high charge density

Rembaum et al. were the first to study high charge density ionenes, which result from the reaction of ditertiary amines with dihalides.[1] They reported the synthesis of a variety of aliphatic ionenes (Figure 2.7) in a number of solvents, including DMSO, DMF, methanol, and benzene, with reaction times ranging from several days to several weeks at 25 °C.

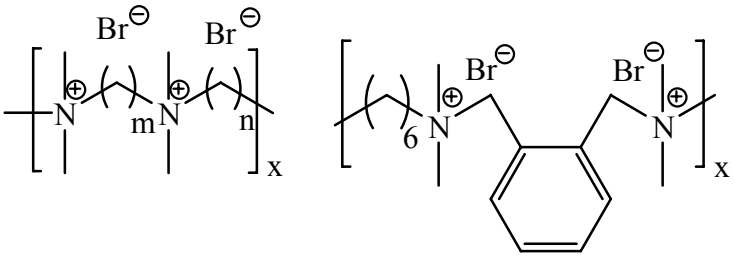

Figure 2.7. Representative examples of the aliphatic ammonium ionenes originally synthesized.

Kinetic investigations revealed that the polymerizations were second order at lower concentrations, and the reaction rate was solvent dependent. Furthermore, the rate of reaction did not change as the number of methylene spacers changed. Finally, they reported that the dichlorides reacted more slowly than the dibromides, which was consistent with typical S_N2 reactions.[8] From the kinetic data, they determined that the reaction mechanism was bimolecular, and that cyclics did not form in any appreciable amount at typical polymerization conditions. The cyclization reaction, which had the potential to occur under highly dilute conditions, was a first order kinetic process.[1]

In subsequent studies, Rembaum et al. also determined the number of methylene spacers that was required to obtain macromolecules, rather than cyclic and low molecular weight products.[42] A mixture of DMF and methanol (in a 1:1 volume ratio) was used as the reaction solvent, and a series of ionenes were synthesized with methylene spacers ranging from 1 to 6 for the ditertiary amines and dialkylbromides. When the number of methylene spacers was low (i.e.,

1-2) for one of the monomers, the result was either cyclic or linear oligomers. Interestingly, when tetramethyldiaminomethane was used as the ditertiary amine monomer, a cyclic product formed regardless of the number of methylene spacers in the dihalide, as demonstrated in Figure 2.8.

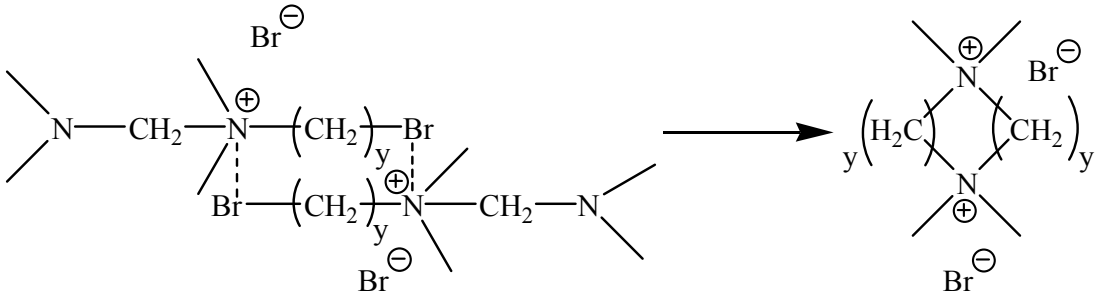

Figure 2.8. Transition state leading to the formation of the cyclic product that Rembaum et al. characterized.[42]

Many factors influence the polymerization of segmented ionenes, including choice of solvent, reaction temperature, time, and monomer concentration. Rembaum et al. demonstrated how intrinsic viscosity changed as these factors were varied for 3,3-ammonium ionenes prepared from dimethylamino-*n*-propyl chloride,[43] which is an AB monomer similar to the monomers that Marvel et al. used.[2,9] For this particular polymer, the greatest intrinsic viscosity was obtained in a 4:1 DMF:H_2O mixture, after the authors made several attempts in DMF:MeOH, DMF:H_2O, DMSO:H_2O, $CHCl_3$, and CH_3CN. DMF, DMSO, and CH_3CN are effective solvents for S_N2 reactions because they are known to raise the nucleophile's ground state energy and thus enhance the rate of reaction.[8] The temperature was varied to achieve the highest possible intrinsic viscosity levels using the 4:1 DMF:H_2O solvent system; however, the highest viscosity achieved was only 0.112 dL/g at a reaction temperature of 68 °C. With that in mind, the authors attempted the polymerization in water using a variety of conditions. They discovered that reactions

conducted at 100 °C under nitrogen resulted in ionenes with enhanced viscosity (0.223 dL/g), which likely corresponded to an increase in molecular weight.

Since an ionene has specific charge placement throughout the macromolecule, interaction with added salt will likely affect polyelectrolyte behavior. In the absence of added salt, polyelectrolyte chains associate, which causes an increase in solution viscosity. However, addition of salt effectively screens the electrostatic interactions of the polymer chains, resulting in decreased viscosity.[44] This "polyelectrolyte effect" is well-documented within the literature, including the works of Dobrynin, Rubinstein, Eisenberg, and Holliday.[45-48] Rembaum et al. studied the solution properties of two high-charge density ionenes: the 3,4- and the 6,6-ionene.[10] They reported that both ionenes exhibited rod-like behavior in solutions without added salt, which was characteristic of the polyelectrolyte effect, and the behavior followed the Fuoss equation.[49] Upon addition of 0.4 M KBr, the polyelectrolyte effect was suppressed and the ionenes behaved as uncharged polymers (Figure 2.9). As shown in Figure 2.9, all electrostatic interactions were suppressed with 0.4 M KBr, since the viscosity was constant over the added salt concentration range.

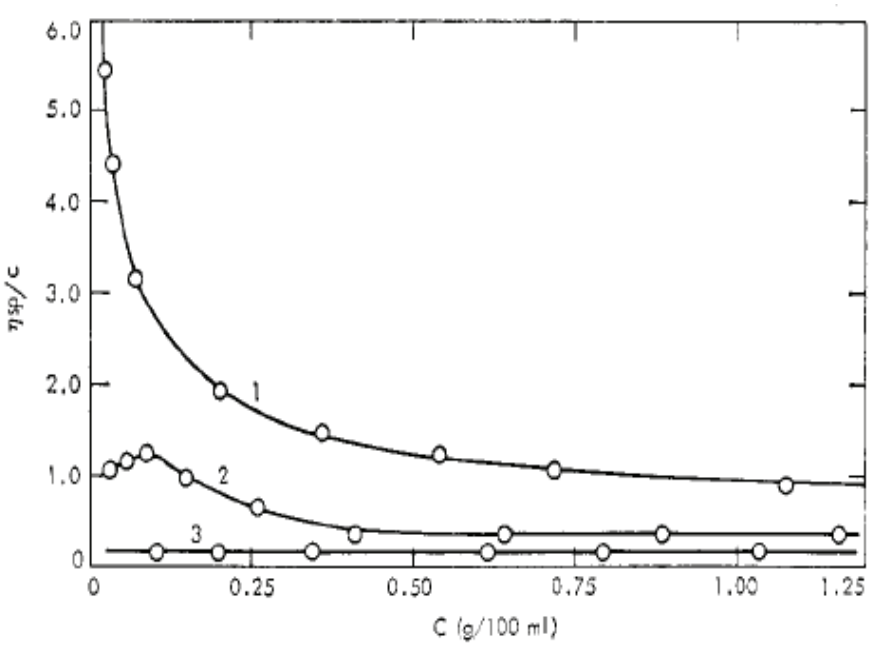

Figure 2.9. Reduced viscosity versus salt concentration of 6,6-ammonium ionene. (1) Water, (2) 0.5 M KBr, (3) 0.40 M KBr.[10]

Ander et al. studied the polyelectrolyte to polysoap transition behavior of *N,N*-disubstituted ionenes.[50,51] Most ionenes reported in the literature possess methyl substituents, as illustrated throughout this review. These researchers observed that as the length of the substituent on the nitrogen atoms increased from methyl to *n*-octyl, the ionene behaved as a polysoap rather than a polyelectrolyte. This transition behavior was attributed to differences in viscosity. For example, in high dielectric constant solvents, an ionene possessing a methyl substituent on the nitrogen atom would display polyelectrolyte behavior with increased viscosity; however, an ionene possessing an *n*-octyl substituent would exhibit polysoap behavior and show reduced viscosity in the same high dielectric constant solvent. This was attributed to the changing polarity of the polymer as the substituent length was varied, since longer alkyl substituents were shown to decrease the polarity of the ionene. The researchers also reported that the sudden transition behavior from polyelectrolyte to polysoap was due to the dominance of

the hydrophobic alkyl substituents. For the ionenes studied, the transition occurred for the 3,3- and 4,4- ammonium ionenes when the alkyl substituent was *n*-hexyl, and for the 6,6-ammonium ionene when the alkyl substituent was *n*-octyl.

All of the aliphatic ionenes discussed thus far have contained only alkyl chains between the charge sites. However, in 1975, Tanaka et al. reported the synthesis, torsional braid analysis (TBA), and wide angle X-ray scattering (WAXS) of eight different *x,y*-oxyethylene ionenes, where x and y were varied from 2 to 5 (Figure 2.10).[52]

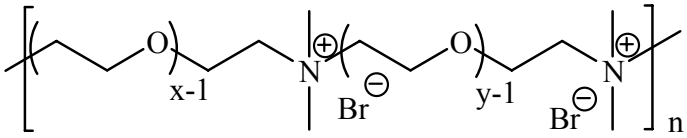

Figure 2.10. Repeating unit structure of Tanaka's *x,y*-oxyethylene ionenes.[52]

Intrinsic viscosity measurements confirmed that the molecular weights of these ionenes were in excess of 5000 g/mol. WAXS indicated the presence of crystallinity in the high charge density ionenes (2,2-, 2,3-, 2,4-, and 3,3-oxyethylene ionenes). TBA analysis revealed that the *x,y*-oxyethylene ionenes possessed two mechanical relaxations, named α-dispersions (T_α, at higher temperatures) and β-dispersions (T_β, at lower temperatures). T_α was related to both the micro-Brownian motions in the amorphous region and the glass transition temperature (T_g) of the polymer, and T_β corresponded to the local modes of the PEO-like backbone. T_α decreased in temperature as the polymer absorbed water. This was due to the low T_g of water, which was reported previously as -130 to -138 °C.[53,54] In addition, charge density increased as T_α increased. This was attributed to the ionic groups along the polymer backbone which electrostatically repelled each other, thus restricting the movement of the polymer chains. It was important to note that even though T_β was only minimally influenced with increasing charge density, this factor influenced T_β the greatest due to the increased presence of electrostatic repulsion near the

local modes of the methylene units.

Later, Tanaka et al. investigated the TBA properties of *x,y*-ionenes.[16] These polymers differ from those previously discussed because their TBA curves displayed three mechanical relaxations, T_α, T_β, and T_γ, which were attributed to the T_g (T_α), ionic portions of the polymer (T_β), and local motions of the methylene groups (T_γ). Again, Tanaka et al. demonstrated using WAXS that greater charge density increased crystallinity, and that ionic content influenced T_g. They also confirmed that ionene crystallinity and water uptake influenced the T_β.

Tanaka et al., recognizing that water influenced both T_α and T_β, also studied the influence of counterion and water uptake on the TBA properties of several 10,6-ammonium ionenes.[55] The counterions investigated in the experiments included Br^-, I^-, ClO_4^-, BF_4^-, SCN^-, and $B(C_6H_5)_4^-$. They found that both T_α and T_β decreased with increasing counterion size. Similar to the aforementioned ionenes, T_γ was only minimally influenced as the counterion size varied.

In a similar manner to Tanaka et al., Meyer and co-workers investigated the T_g and dielectric properties of non-segmented ionenes. They determined that the T_g was highly dependent on the chemical structure between charge sites, as well as the size of the counterion.[56] Clearly, incorporating flexible repeating units increased the segmental motion of the polymer, thereby lowering the T_g. In addition, small counterions allowed for increased packing of the polymer chains compared to bulky anions, such as tetraphenylborate or ethylorangesulfonate, which also lowered the T_g –particularly when small ions, such as BF_4^-, were used. Meyer et al. also used variable temperature one- and two-dimensional ^2H NMR spectroscopy to investigate polymer chain motion. They observed significant motion below the T_g which led them to conclude that the T_g was the point at which a dissociation of ionic lattice structures around the polymer chain began to occur. Furthermore, ionene dielectric behavior demonstrated that there

were two regions: one at lower temperatures that was frequency dependent, and another at higher temperatures that was essentially frequency independent.

Salamone et al. first demonstrated the synthesis of ionenes based on rigid, cyclic ditertiary amines.[57] Their rationale to utilize bulky tertiary amines resulted from prior problems with cyclic products isolated from the non-segmented ionene polymerizations that included methylene spaces between charge sites. In addition, Salamone predicted that the bulky, rigid structure would allow the nitrogen lone pair to remain exposed, thus enhancing nucleophilicity. As described in their manuscript, Salamone and Snider prepared ionenes from 1,4-diaza[2.2.2]bicyclooctane (DABCO) and various low molecular weight dihalides according to Scheme 2.3.

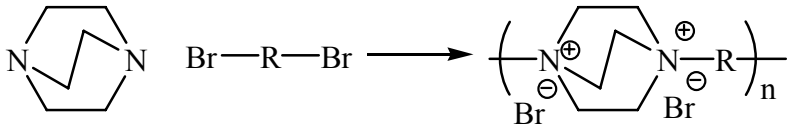

Scheme 2.3. Synthesis of DABCO-based ionenes using various dibromides, where R = propyl, butyl, pentyl, hexyl, octyl, decyl, dodecyl, or *o*-, *m*-, *p*-xylyl.

Their analysis of reaction rates revealed that the polymerization proceeded more rapidly with increases in both the dielectric constant of the solvent and the reaction temperature. In addition, they revealed that the reaction yields of ionenes prepared with aliphatic dihalides in DMF-MeOH mixtures were lower than those performed in DMSO. However, the opposite was true when ionenes were based on xylene dibromides. When intrinsic viscosities were measured for each polymer, they were similar regardless of solvent; moreover, the viscosities increased from 0.09 dL/g to 0.25 dL/g as the dialkylbromide chain length increased.

As described earlier, Rembaum et al. reported that dichlorides reacted more slowly than dibromides during ionene formation.[1] However, dichlorides are potentially more affordable

compared to dibromides, while aliphatic dichlorides are generally unreactive under conventional ionene polymerization conditions. Therefore, Bortel et al. investigated the synthesis of ionenes from dichlorides that contained functional groups which facilitated inductive effects that lowered the C-Cl bond energy.[58] Two effective dichlorides used for successful polymerizations included 1,3-dichloro-propan-2-one and bis(2-chloroethyl)ether (Figure 2.11). The reactions conducted with dichlorides were first order, in comparison to the second order kinetics observed when using dibromides, as described previously. The authors explained this discrepancy with the fact that the rate determining step was the ionization process, thus making the reaction first order.

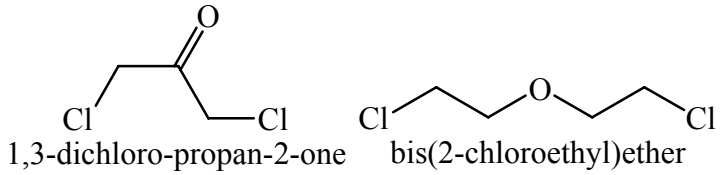

1,3-dichloro-propan-2-one bis(2-chloroethyl)ether

Figure 2.11. Activated dichlorides used in ionene polymerizations.

In 2000, Engel and co-workers reported the synthesis of cyclic ionene structures.[59] In comparison to previously described syntheses, they deliberately optimized the reaction conditions in such a manner to produce cyclized ionene precipitates. They used acetonitrile as the reaction solvent, which allowed for modest solubility of the ammonium salts, thus allowing the cyclic species to form rather than polymers. The cyclic compounds precipitated from the reaction, which enabled the resulting product to be easily isolated. All of the products were characterized via ^{1}H and ^{13}C NMR spectroscopy. Although this is not an example of polymer synthesis, it was intriguing to investigate the variety of ring structures that are possibly formed during ionene polymerizations. For example, Marvel et al. reported when the number of methylene spacers was 4 to 6, cyclic products were obtained.[60]

The first report describing the mechanical performance of 12,12-ammonium ionenes as a

function of absolute molecular weight was recently published from our laboratories.[61] Dynamic mechanical analysis (DMA) confirmed that the water-soluble ionenes possessed T_g values that increased with increasing molecular weight. In addition, the presence of ionic aggregates was observed to dissociate at approximately 88 °C, regardless of molecular weight. The higher molecular weight ionenes (M_n > 10 000 g/mol) displayed excellent tensile properties, with 22 MPa stress at yield values and elongations ranging from 230 to 440 %. While X-ray scattering determined that the methylene segments were too short to facilitate crystallization, ionic domains were observed. In addition, the triggered depolymerization of 12,12-ammonium ionenes in the presence of an aqueous sodium hydroxide solution was achieved, thus facilitating the production of degradable films with good mechanical durability.

Our group also determined the various relationships between charge density, structural symmetry, and thermal and mechanical properties of 6,6-, 6,12- and 12,12-ammonium ionenes.[39] To ensure that results were based on charge density and symmetry—rather than on molecular weight—we used polymers with similar molecular weights. As charge density was increased, the mechanical performance of the polymer diminished, as shown with tensile test measurements (Table 2.1). However, the 6,6-ammonium ionenes were able to crystallize and possessed enhanced degradation temperatures.

Polymer	Stress at Break (MPa)	Strain at Break (%)	Stress at Yield (MPa)	Modulus (MPa)
6,12-20k	--	9	9	278
12,12-20k	10 ± 4	206 ± 121	6 ± 0.4	231 ± 113
6,12-40k	16 ± 5	313 ± 41	13 ± 3	132 ± 63
12,12-40k	24 ± 2	235 ± 6	35 ± 4	489 ± 55

Table 2.1. Tensile properties of 12,12- and 6,12-ammonium ionenes as a function of molecular weight and charge density. The 6,6-ammonium ionenes were not mechanically strong enough for tensile test measurements.

2.5.3 Nanocomposites based on non-segmented ionenes

Sukhyy et al. demonstrated for the first time the use of the ammonium-based ionenes as surface modifiers in clay-based nanocomposites (Figure 2.12).[62] Typically, a surface modifier will decrease the surface energy of the clay, thus improving its wettability. Therefore, the researchers used ionenes rather than low molecular weight quaternary ammonium salts due to their potential to enhance thermal stability by ~50 °C. In addition, the authors maintained that ionenes have much lower potential to oxidatively degrade compared to low molecular weight quaternary ammonium salts. Both of these factors are critical for nanocomposite processing, which usually involves thermal treatment.

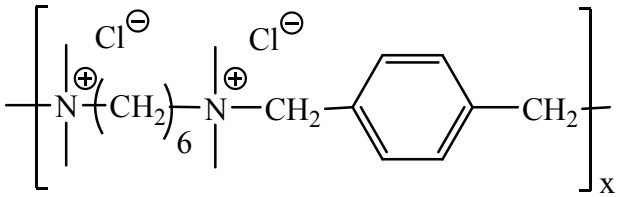

Figure 2.12. Sukhyy's ionenes used in nanocomposite preparation.[62]

The ammonium ionene shown in Figure 2.12 was mixed with bentonite clay, after which

X-ray scattering and TGA were used for comparison to pure bentonite clay. X-ray scattering results revealed that the ammonium ionene-modified bentonite clay displayed a more perfect lattice. This demonstrated that using ionenes was beneficial for exfoliating the clay. Moreover, TGA results provided conclusive evidence that there was a decrease in the thermal stability of the ionene-modified bentonite clay at 280 °C that corresponded to ionene degradation.

In order to prepare nanocomposites, the ionene-modified bentonite clay was mixed with a polyamide, polystyrene, or polypropylene. The resulting wide angle X-ray diffraction (WAXD) patterns were quite different as a function of the polymer matrix structure. Moreover, while all of the polymers exfoliated the ionene-modified bentonite clay, and each of the nanocomposites possessed enhanced mechanical properties compared to the bulk polymers, slight differences were observed. The authors showed that incorporating up to 2 wt% ionene-modified bentonite clay enhanced the mechanical properties of both the polyamide- and polystyrene-containing reinforced nanocomposites. The polypropylene nanocomposite, however, demonstrated superior mechanical strength, which the authors contributed to the thermodynamic compatibility of the hydrophobic organo-bentonite clay and polypropylene. It is important to note that if more than 2 wt% ionene-modified bentonite clay was incorporated, the resulting clay aggregates decreased nanocomposite mechanical performance. The TGA properties of the polystyrene- and polyamide-toughened nanocomposites were similar, since the ionene-modified bentonite clay acted as a barrier and prevented thermal degradation at higher temperatures. Interestingly, the authors reported no change in the thermal stability of the polypropylene nanocomposite compared to the bulk polymer; however, they offered no explanation for this trend.

2.5.4 Interactions of ionenes with surfactants and zwitterionomers

Ionic groups in polyelectrolytes interact with low molar mass surfactants and/or

zwitterionomers. The hydrophobic/hydrophilic balance, charge density, and stoichiometry are of high importance for the analysis of these interactions and subsequent aggregation effects.

Osada et al., for example, explored the interactions of *x,y*-ammonium ionenes, where x = 3, 6, 12 and y = 3, 4, 6, 12, with sodium methyl sulfate, sodium hexyl sulfate, sodium dodecyl sulfate, sodium octanesulfonate, and sodium decanesulfonate in water.[63] They reported a two-step binding process in which all steps were in equilibrium, and where the ionene and surfactant formed insoluble complexes under 1:1 stoichiometry conditions, but became soluble under non-stoichiometric conditions. The alkyl chain length and charge density dictated the interactions of the ionene with the surfactant. Specifically, higher order structures were obtained when the complex formation was modified appropriately. The 3,3-, 6,4-, and 6,6-ammonium ionenes were crystalline, while the 6,12- and 12,12-ammonium ionenes were amorphous, as characterized via X-ray scattering. The surfactants demonstrated both short- and long-range order, and depending on the charge density of the ionene, the authors proposed several mechanistic explanations for the ordering of the ionene with surfactant, as demonstrated in Figure 2.13. These results correlated well with the WAXS and SAXS analysis of these complexes.

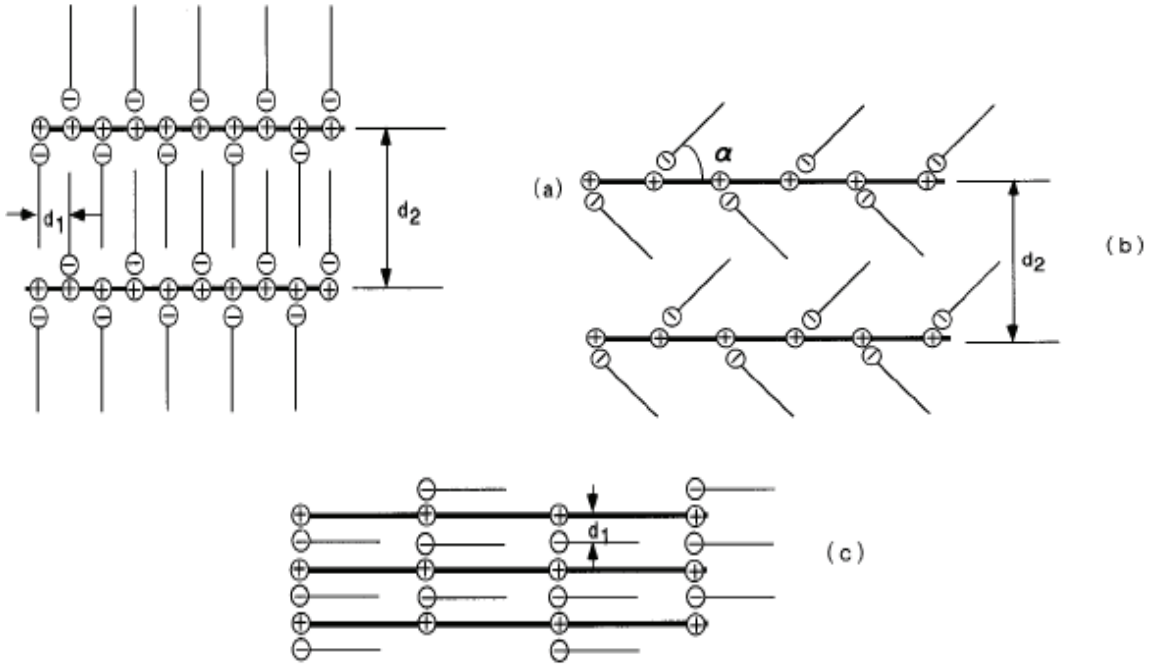

Figure 2.13. Ordering of surfactant and ionene as a function of charge density. (a) 3,3-ammonium ionene; (b) 6,4- and 6,6-ammonium ionene; (c) 6,12- and 12,12-ammonium ionene.[63]

Cao et al. investigated the effects of mixing *x,y*-ammonium ionenes, where x = 2, 4, 6 and y = 4, 6, 12, with sodium dodecyl sulfate (SDS).[64] They found that depending on the ionene charge density, the solution viscosity rose and fell at a certain molar ratio of SDS and *x,y*-ammonium ionene, which ranged from 1.00:1.00 to 1.35:1.00. The solution viscosity dropped due to the micellization of the SDS, which limited the interaction of the surfactant with the *x,y*-ammonium ionene. They noted more dramatic changes in solution viscosity with lower charge density ionenes, due to the more hydrophobic nature of the methylene spacers. The interactions with SDS, however, were more favorable due to the longer methylene spacers. In addition, the longer methylene spacer facilitated microphase separation, which was consistent with other ionene microphase separation properties described herein. Furthermore, the authors correlated their solution viscosity results with laser light scattering analyses of the hydrodynamic radii of

the aggregates in solution. The results synergistically agreed with the solution rheology results, namely the aggregate hydrodynamic radius was greatest when the solution viscosity was the highest. They also confirmed that at a high solution concentration, the ionene/SDS mixtures would gel at a critical SDS/*x,y*-ammonium ionene ratio, but would reverse upon addition of either mixture component.

Zwitterionomers belong to a special class of polyelectrolytes that contain both positive and negative charges in the pendant group of a repeating unit. Sulfobetaines are a subset class of zwitterionomers, whose structure is shown in Figure 2.14.

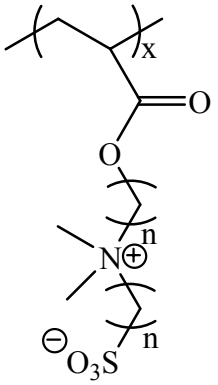

Figure 2.14. General structure of a sulfobetaine.

In 1986, Schulz et al. examined the behavior of (3-dimethyl (methacryloyloxyethyl) ammonium propane sulfonate (PDMAPS) in a variety of salt solutions. They discovered that the solubility of PDMAPS in salt solution depended on the salt composition and concentration, continuous microphase separation occurred between upper and lower critical solution temperatures, and viscosity increased with increasing salt concentration, which became known as the anti-polyelectrolyte effect.[65] Building on that previous research, Osada et al. investigated the interactions of various cationic and anionic polyelectrolytes, including *x,y*-ammonium ionenes (x = 3, 6; y = 3, 4) with PDMAPS.[66] Because of the sensitive nature of PDMAPS as reported earlier by Schultz et al., Osada's thorough analysis of the behavior of polyelectrolytes and

zwitterionomers revealed that microphase behavior changed as a function of polyelectrolyte structure. Moreover, they anticipated that the presence of macromolecules containing ionic groups (rather than small molecule salts) would have a profound influence on the upper and lower critical solution temperatures due to the cooperative segmental motion of the polymer chains. To test this hypothesis, they measured the upper and lower critical solution temperatures via transmittance experiments at temperatures ranging from 2 to 70 °C; viscosity measurements were performed using Ubbelohde viscometers at identical temperature ranges. The investigators determined that interactions of PDMAPS with the various polyelectrolytes affected the upper and lower critical solution temperatures due to intra- and inter-chain pairing. They attributed this to the quaternary ammonium functional groups on the ionene, which interacted with the pendant sulfonate groups on PDMAPS.

In a later paper, Osada et al. investigated the effect of charge density on complex formation and the upper critical solution temperature with PDMAPS.[67] Interestingly, a large amount of precipitate formed when only 1 mol% of 3,3-ammonium ionene was introduced to a solution of PDMAPS, making the complex formation non-stoichiometric. Based on the large amount of resulting precipitate, Osada et al. developed a cascade model, depicting how a small amount of ionene can initiate the complexation process. This is depicted in Figure 2.15.

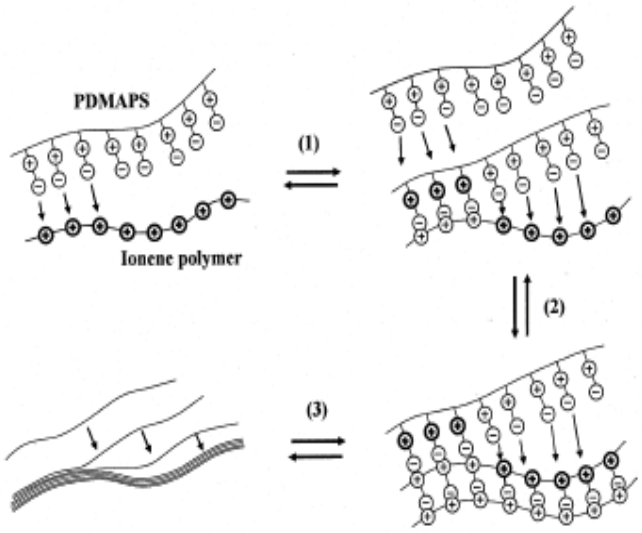

Figure 2.15. Model for ionene complexation with PDMAPS. [67]

2.6 Segmented ionenes

2.6.1 Introduction

Segmented ionenes possessing oligomeric spacers between charge sites were first synthesized in order to obtain ionene polymers with excellent mechanical properties. As shown in this section, many of these segmented ionenes behave mechanically similarly to polyurethanes. However, polyurethanes are prepared using hazardous isocyanates that produce amines upon hydrolysis. Conversely, ionene synthesis is proposed as more environmentally friendly and inherently less toxic. Furthermore, well-defined polyurethanes are typically prepared in a two-step process; however, ionenes are synthesized in a single step, suggesting a manufacturing advantage over polyurethanes.

Most literature descriptions of ionenes containing oligomeric sequences are based on poly(tetramethylene oxide) (PTMO), as described below. Only recently have researchers begun to incorporate other oligomers, such as poly(propylene glycol) (PPG), poly(ethylene glycol) (PEG), or polydienes, including polybutadiene and polyisoprene. Typically, low molecular

weight, high charge density ionenes are brittle materials and display poor mechanical performance. However, reducing the charge density can enhance important film mechanical properties, especially in the case of PTMO ionenes, where PTMO has the potential to crystallize thereby increasing mechanical performance. In the following section, the synthesis and structure-property relationships of various ionenes containing oligomeric spacers between the charge sites will be discussed.

2.6.2 Poly(tetramethylene oxide)-based ionenes

Kohjiya et al. reported the first segmented ionene based on PTMO in 1981 (Figure 2.16).[68] Their overall objective was to prepare elastomeric ionenes; earlier non-segmented ionenes were non-elastomeric, brittle powders. As mentioned previously, the non-elastomeric properties were likely due to the use of high charge density ionenes, but could also have resulted from the use of low molecular weight polymers. Nevertheless, Kohjiya and co-workers synthesized an ionene based on the structure shown below that exhibited promising elastomeric behavior, namely, 1.37 MPa tensile stress at break and 510% elongation at break. It is important to note that the authors possibly could have obtained improved mechanical performance if the reaction was allowed to achieve higher conversion, since the reaction time and temperature was only 1 h at 50 °C. Moreover, a rate enhancement might have been attained if dibromides were used, as discussed previously. Thus, these initial segmented systems were most likely limited in molecular weight and SEC data was not reported.

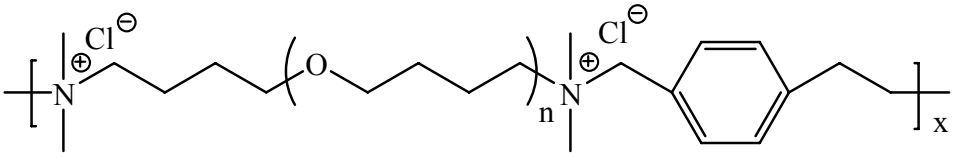

Figure 2.16. Structure of the first segmented ionene based on PTMO.

One issue associated with using high molecular weight polymer precursors is the limited availability of reactive chain ends. Since the concentration of chain ends is reduced in a segmented ionene relative to a non-segmented system, the reaction rates and degree of polymerization tend to decrease. To investigate this phenomenon further, Leir and Stark prepared PTMO-based ionenes with a variety of dihalides and investigated the rate of reaction based on the dihalide structure (Figure 2.17).[69]

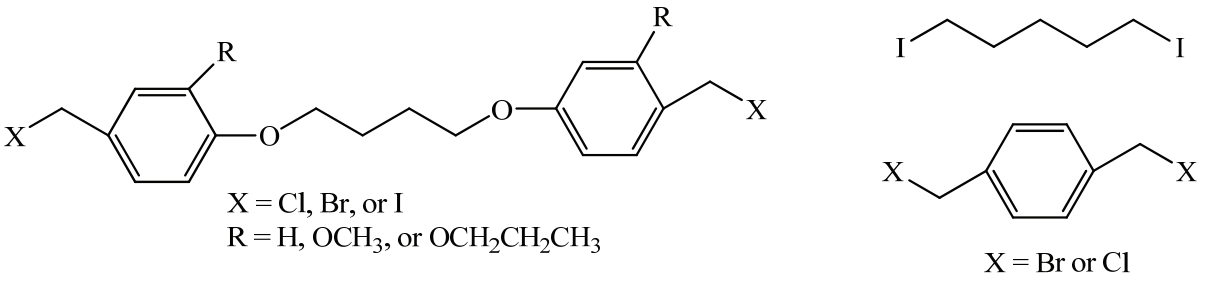

Figure 2.17. Dihalide structures Leir and Stark investigated for PTMO-based ionenes.

Previously, Yamashita had demonstrated that the incorporation of aromatic groups in the dihalide enhanced the reaction rate of PTMO-dibenzyl chloride ionenes.[68] Leir and Stark, however, included dihalide structures containing an oxygen atom *para* to the benzyl group. The added electron donating group stabilized the structure and provided improved leaving group ability. They also determined that the rate increased from Cl<Br<I, while the rest of the dihalide structure remained unchanged.[69] Later, in collaboration with Wilkes and co-workers, Leir and Stark investigated the structure-property relationships of the same PTMO ionenes.[70] The thermal and mechanical properties of these ionenes were studied in order to determine the effect of the following four characteristics: 1) the molecular weight of the PTMO soft segment, 2) the counterions of the ionenes (Br^- vs. Cl^-), 3) the structural differences of the ionene hard segments, and 4) the influence of charge on microphase separation. Interestingly, the polymers

behaved similarly to polyurethane ionomers, even though the PTMO ionenes did not possess the hydrogen bonding abilities that the polyurethane ionomers have within their hard segments. This is intriguing because polyurethanes typically display excellent thermomechanical behavior due to the incompatibility of the hard (featuring hydrogen bonding) and soft segments, in contrast to the ionene polymers which microphase separate due to the electrostatic interactions of the ionic groups. The microphase separation was investigated via small-angle X-ray scattering (SAXS), as well as other testing methods, including DMA. Due to the presence of PTMO segments, the ionenes displayed desirable stress-strain behavior, with elongations at break and stress at break approaching 1000% and 40 MPa, respectively. A sharp upturn in the stress-strain curve was observed, which was attributed to the strain-induced crystallization of PTMO. This phenomenon was consistent with results obtained for other PTMO-based elastomers.[71] Wilkes et al. also observed a significant difference in the PTMO ionene series due to the effect of the counterion. Ionenes containing chlorine anions (rather than bromine anions) always displayed greater tensile stress at break values, which the researchers attributed to the more efficient packing of the electronegative chlorine anions.[70]

Wilkes et al. also analyzed the structure-property relationships of ionenes prepared from a dimethylamino-terminated PTMO oligomer that was reacted with 1,4-dibromo-*p*-xylene.[72] The ionenes possessed elastomeric behavior due to the microphase separation of ionic aggregates with adjacent low T_g soft segments. Multiple peaks were observed in the SAXS profiles, which indicated that ionic aggregation was present in the ionene films. Rod-like structures were observed via transmission electron microscopy (TEM), which further demonstrated the microphase separation of the ionic domains from the PTMO soft segment. Based on these consistent TEM and SAXS results, Wilkes et al. proposed a schematic of the microphase

separation of the ionic domains from the PTMO segments (Figure 2.18).

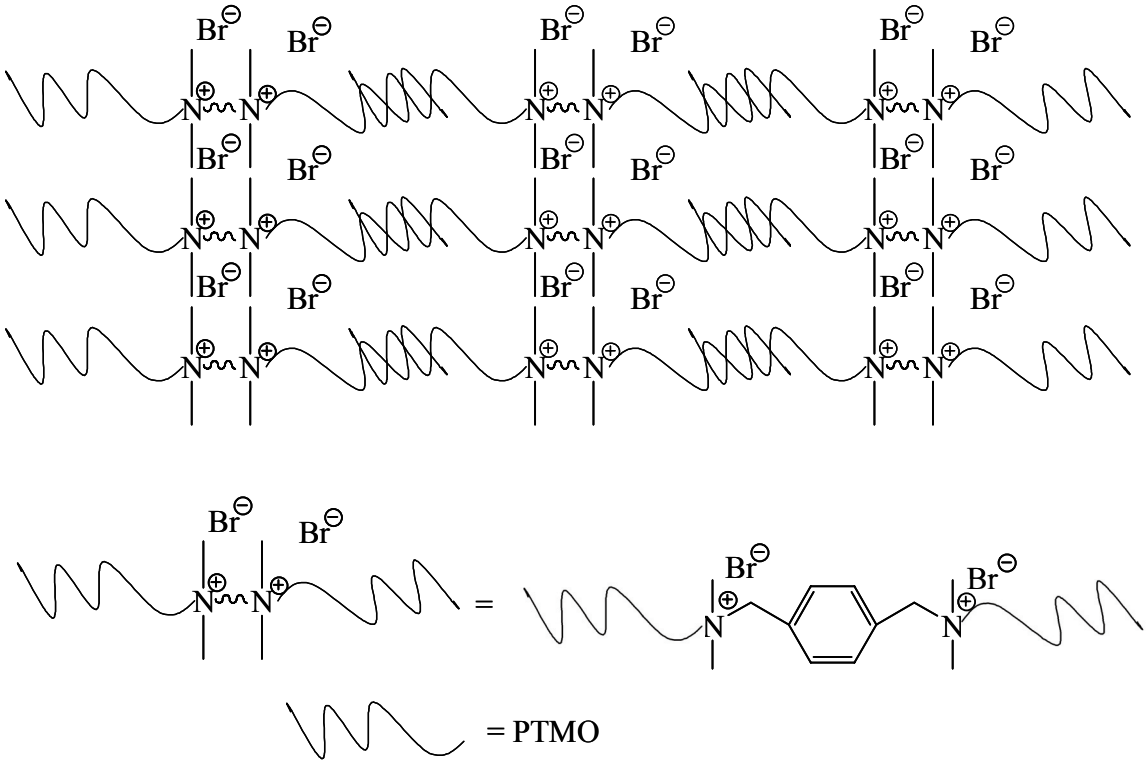

Figure 2.18. Proposed microphase separation model of Wilkes' PTMO ionenes.[72]

Later, Wilkes et al. prepared ionenes from a reaction of telechelic PTMO dioxonium ions and either 4,4'-bipyridine or 1,2-bis(4-pyridinium)ethylene (Scheme 2.4).[73] The pyridinium ionenes possessed superior thermal stability compared to the benzyl ionenes. Specifically, the pyridinium ionenes softened around 210 °C, while the benzyl ionenes softened at approximately 175 °C. This enhanced thermal stability afforded a greater processing temperature and service window. Similar to the previously mentioned PTMO ionenes, the pyridinium ionenes formed ionic aggregates, as evidenced via SAXS. However, the absence of higher-order scattering peaks indicated that a long-range ordered structure had not formed. Nevertheless, the ionenes still possessed excellent mechanical properties, including tensile strengths greater than 30 MPa and elongations greater than 800%. These results were similar to those previously obtained for the

benzyl ionenes.

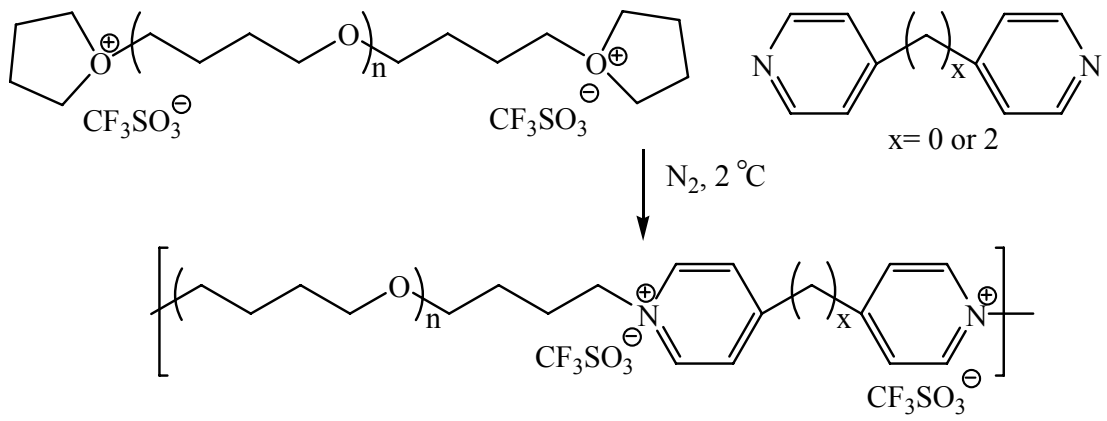

Scheme 2.4. Synthesis of pyridinium ionenes from "living" PTMO and either 4,4'-bipyridine or 1,2-bis(4-pyridinium)ethylene.

Typically, ionenes possess two ionic sites for every repeating unit because the reaction proceeds via the step-growth polymerization of a ditertiary amine and an alkyl dihalide. Ikeda and co-workers demonstrated the novel synthesis of PTMO-based ionenes that contained only one ionic group in each repeating unit through a one-pot living PTMO chain extension reaction (Scheme 2.5).[74,75] They proposed that the one ammonium cation per repeating unit influenced the thermomechanical properties of the ionenes. Specifically, Ikeda et al. suggested that the incorporation of one ammonium group per repeating unit lowered the overall tensile stress and increased the elongation. They attributed this to the fact that the ionic aggregates were not as large as conventional ionenes that contain two ionic sites per repeating unit. This was further analyzed via SAXS, where the Bragg spacing between ionic sites was 53 Å.

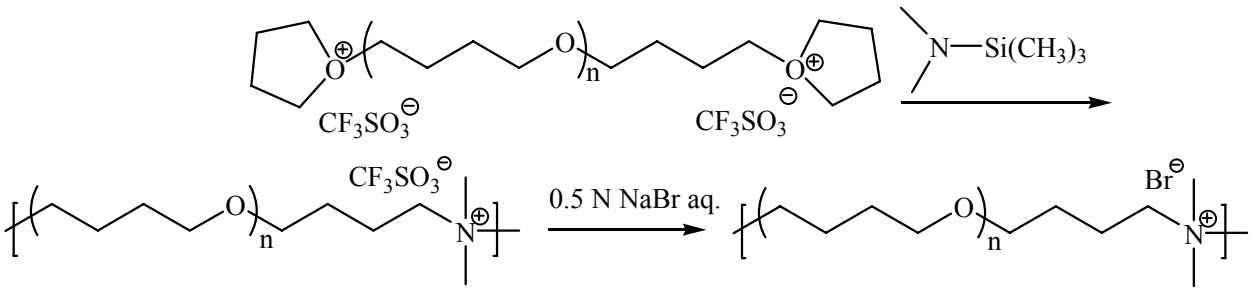

Scheme 2.5. Synthesis of PTMO ionenes that contain only one quaternary ammonium cation per repeating unit.[74,75]

In a subsequent study, Ikeda et al. investigated the effects of counterion on the structure-property relationships of the same PTMO-based ionene shown in Scheme 2.5.[75] Specifically, the effect of incorporating chloride versus bromide anions was determined for matching molecular weight ionenes using SAXS, WAXD, DMA, differential scanning calorimetry (DSC), and tensile measurements. It was presumed based on previous work that counteranions influenced the ionic domain size. Ikeda et al. observed that ionenes with bromide anions have smaller and shorter ionic domains, while those with chloride anions have larger and longer ionic domains. Therefore, they proposed that ionenes containing different anions would exhibit distinctive mechanical and thermal properties. Indeed, the tensile properties of the chloride and bromide ionenes were drastically different at high elongation levels (>900%). Moreover, the ionene containing the bromide anion demonstrated a greater tensile strength at break than the chloride ionene (30 MPa vs. 10 MPa), which indicated that the stress-induced crystallization of PTMO was more evident in the bromide ionene. These results differ from the earlier work of Wilkes et al., who demonstrated that ionenes having chlorine anions consistently displayed higher tensile strength values compared to the bromide ionenes.[70] It was presumed that the difference in chemical structure produced these tensile property variations, since the Ikeda ionenes had only one ionic site per repeating unit, while the Wilkes ionenes had two.

The dynamic mechanical behavior of both counteranion ionenes was very similar prior to the melting temperature (T_m) (Figure 2.19). The T_g of the amorphous PTMO phase was approximately -80 ºC, while the T_m of the PTMO crystalline phase was approximately 20 ºC. Although the dissociation of the ionic aggregates occurred at the same temperature (200 ºC), the storage modulus, G', of the bromide ionene was greater than the chloride ionene.

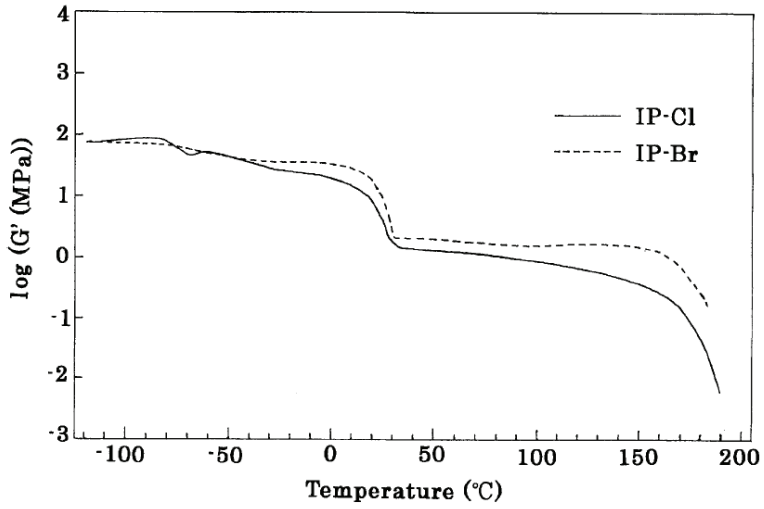

Figure 2.19. Dynamic mechanical behavior of the bromide (IP-Br) versus the chloride (IP-Cl) PTMO ionene.[75]

The thermal properties of PTMO ionenes changed as a function of anion incorporation as well.[75] The authors reported that the ionic aggregate dissociation temperatures of the chloride ionene was lower (200 ºC) in comparison to the bromide ionene (227 ºC). However, our research group (as well as others) has shown that at those high temperatures, ionenes begin to depolymerize and degrade via the Hofmann elimination (Scheme 2.6).[13,14,16,61,76,77] As shown in this scheme, even though hydroxyl anions mount an initial attack, at high temperatures the halide counterion is sufficiently strong enough to abstract the proton from the methylene group near the ammonium cation site. Technically, the ionic domains are dissociating, but this is primarily due

to the degradation of the macromolecule.

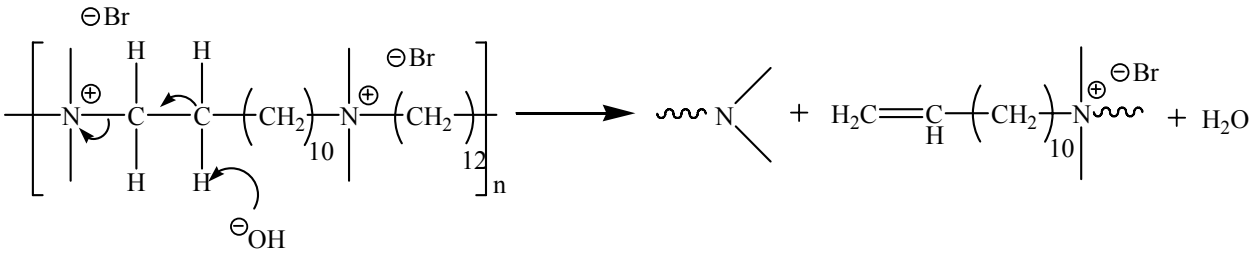

Scheme 2.6. Mechanism of the base-promoted Hofmann elimination reaction for 12,12-ionenes.

Furthermore, DSC results confirmed that the ionic domains in bromide ionenes prevented crystallization of PTMO segments at room temperature, indicating that the bromide ionene is primarily amorphous under ambient conditions. In contrast, the chloride ionene displayed a T_m of 29 ºC, which was associated with the melting of the PTMO segments. Overall, these DSC results indicated that the morphological structures of the ionenes differed as a function of anion selection. Moreover, SAXS results indicated that ionic domains were present with one peak, but well-ordered morphology was not observed. WAXD confirmed the DSC results, in which the crystalline nature of the chloride anion ionene was revealed by the appearance of a diffraction ring and an amorphous halo observed at room temperature. In contrast, only an amorphous halo was observed for the bromide ionene—a phenomenon which further confirmed the amorphous characteristic of the bromide ionene as measured by DSC.

Overall, Ikeda et al. proposed a schematic of the morphology of the ionenes as a function of anion selection based on the thermal and morphological data described above (Figure 2.20). The chloride ionene displayed three distinct phases: amorphous PTMO segments, PTMO crystallites, and ionic aggregates. Conversely, the bromide ionene schematic displayed only two phases: amorphous PTMO segments and ionic aggregates. Based on this research and the associated schematic, one can presume that ionenes contain ionic aggregates which act as

physical cross-links, thereby imparting these elastomeric properties. In addition, the presence of counteranions greatly influenced the mechanical properties and resulting morphology.

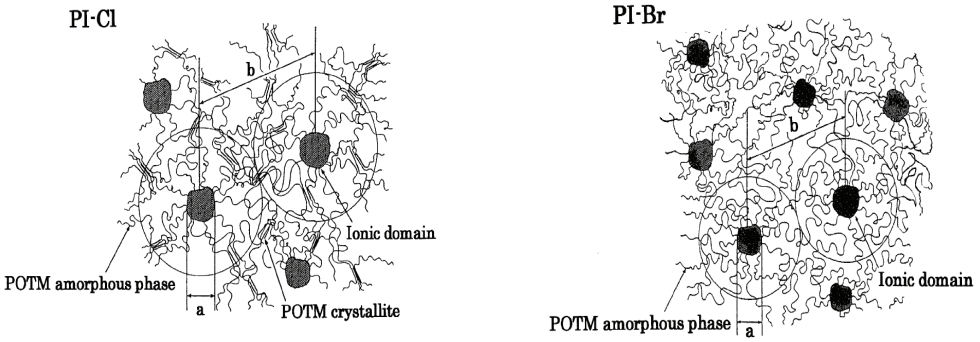

Figure 2.20. Schematic of PTMO ionenes as a function of counteranion (PI-Cl= chloride PTMO ionene, PI-Br= bromide PTMO ionene).[75]

Klun et al. extensively studied the structure-property relationships of PTMO-based ionenes.[78] Molecular weight studies were conducted in 0.1 % LiBr in DMF, with resulting molecular weights ranging from ~5000 to 110,000 g/mol. The variation in molecular weight was attributed to monomer selection. In other words, high degrees of polymerization were achieved when non-sterically crowded tertiary amines were used. Dihalide selection was also critical. When activated dihalides, such as dibromides were utilized, the polymerization proceeded at a faster rate. This is consistent with the rate analysis described above for non-segmented ionenes.

Thermal analysis was conducted using DSC and TGA. The T_g of PTMO was observed at -66 °C to -80 °C, indicating that the polymers were essentially microphase separated, with the PTMO and ionic clusters in separate phases.[78] Ionenes that contained a longer PTMO segment (~100 repeating units) possessed T_ms, while ionenes with shorter segments were amorphous. However, when crystallization was induced with heating, the polymers displayed well-ordered structures. The thermal stability of these materials as measured via TGA ranged from 120 °C to

200 °C. The tensile behavior of the PTMO ionenes was consistent with typical microphase separated elastomers. Ionenes with amorphous PTMO segments demonstrated elastomeric properties due to the formation of ionic domains that served as physical cross-links. Conversely, semi-crystalline ionenes displayed a higher modulus and yield point with increased toughness relative to the amorphous ionenes. At 300 % elongation, all the polymers exhibited some extent of stress induced crystallization. Interestingly, the polymers possessed what is known as shape-memory properties.[79] In other words, after stretching the ionene polymer film using a tensile test apparatus, the polymer possessed some form of permanent set. However, the film returned to its original state upon application of heat. With respect to mechanical performance, while it is known that stress-strain behavior is predominantly influenced by the soft segment structure, this study also confirmed that the choice of anion can influence mechanical performance. The investigators noted that when the anion was bromide, tensile strengths were higher in comparison to ionenes with chloride anions.[78] This was consistent with the work of Ikeda et al., described above,[75] but conflicts with the results that Wilkes et al reported.[70] It is also important to note that ionene polymers are very hygroscopic in nature due to their ionic domains. This is critical for mechanical testing because the presence of water weakens ionic domain interactions. In other words, if ionic clusters are disrupted, lower tensile strengths will result. DMA results demonstrated that the PTMO ionenes did not behave like polyurethane elastomers, since the rubbery plateau was very flat. This is similar to the DMA results obtained by Ikeda et al, which was depicted earlier in Figure 2.19.[75] To determine their functional potential, Klun et al. tested the PTMO ionenes for anti-static and permeability properties. Quaternary ammonium polymers are typically used as anti-static coatings because they attract water to the surface and disrupt any static buildup. Even though the PTMO ionenes possessed good anti-static coating properties at

higher humidity levels, when the air was drier their anti-static properties were diminished relative to conventional anti-static coatings. Furthermore, testing their permeability properties revealed the moisture-sensitive nature of the PTMO ionenes, indicating that they would not suitable as membranes for packaging. Although Klun et al. reported good moisture-vapor transmission values, their oxygen permeability was poor.

Polyelectrolytes are sometimes compared to zwitterionomers in the literature. However, zwitterionomers differ from polyelectrolytes in that they contain both a bound positive and negative charge within each repeat unit. This characteristic imparts interesting properties to these materials due to the presence of these opposite charges on the polymer chain. Galin et al. synthesized 2000 – 7000 g/mol PTMO-based ionenes and compared their properties to corresponding PTMO-based zwitterionomers (Figure 2.21).[76] The zwitterionomers were prepared through the demethylation of the quaternary ammonium nitrogen, and subsequent reaction of the tertiary nitrogen site to enable the formation of typical zwitterionic functional groups. TGA analyses revealed that both the zwitterionomers and ionenes displayed high thermal stabilities, with T_d at 5% weight loss ranging from 312 – 432 °C. Moreover, both the zwitterionomers and ionenes showed good microphase separation, as indicated via DSC measurements with a PTMO T_g and a hard segment T_g.[80] These results were consistent with Eisenberg's multiplet-cluster theory.[46] However, Galin et al. demonstrated with both DSC and solid state ^{1}H NMR spectroscopy that the zwitterionomers they studied were more efficient at forming ionic clusters than the ionenes. In a later manuscript, Galin et al. confirmed via SAXS and small-angle neutron scattering (SANS) that the zwitterionomers displayed long-range order—in contrast to the ionenes which did not.[81]

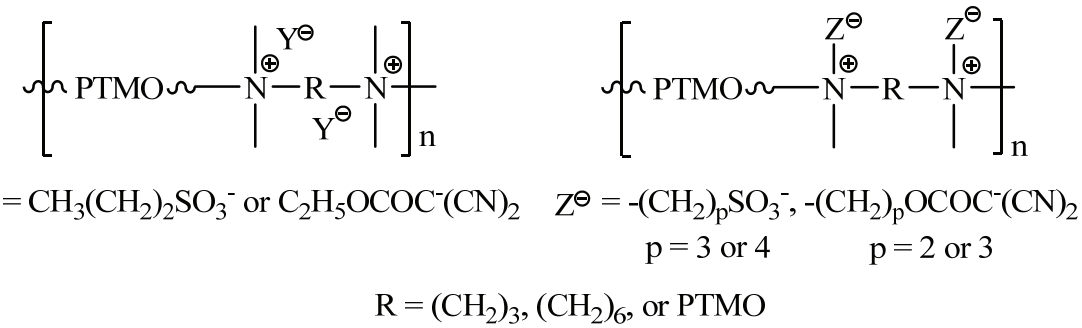

Figure 2.21. PTMO-based ionenes and zwitterionomers.

A recent study of PTMO-based ionenes focused on the effect of polymer architecture and molecular weight using linear and highly branched PTMO ionenes.[82] Our research group determined that branching negatively influenced ionic aggregation, regardless of PTMO segment molecular weight. In addition, polymer architecture did not influence T_g. DMA results verified that the ionic aggregates did not persist once the PTMO soft segment had melted in highly branched PTMO ionenes. However, the linear PTMO ionenes demonstrated excellent DMA behavior, with a linear rubbery plateau region that persisted until ~175 °C (Figure 2.22). Under ambient conditions, the linear PTMO ionenes possessed excellent mechanical properties similar to thermoplastic polyurethanes (35 MPa tensile strength and elongations >1000%), while the highly branched ionenes possessed lower tensile strengths and elongations. This data suggested that the presence of branching disrupted ionic aggregate formation, which was consistent with the work of Loveday et al. who asserted that ionic groups placed regularly along the backbone in a linear fashion were important for favorable mechanical performance.[83]

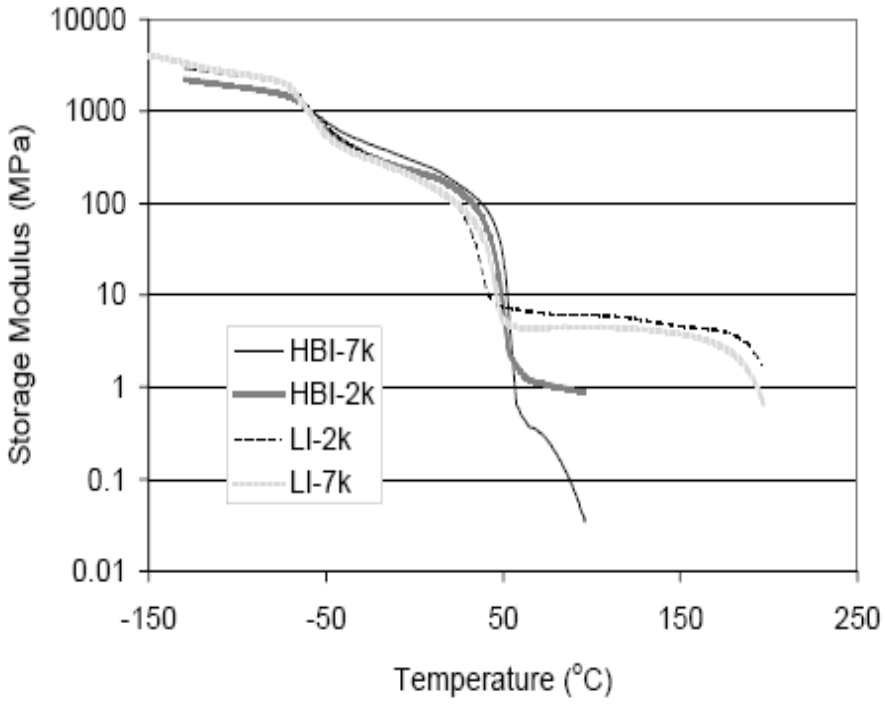

Figure 2.22. Dynamic mechanical behavior of 2000 and 7000 g/mol highly branched (HBI) and linear (LI) ammonium ionenes.

2.6.3 Poly(ethylene glycol)-based ionenes

PEG-containing polymers are ideal for biomedical applications due to their biocompatibility and low toxicity.[84] Dimitrov et al. synthesized PEG-based ionenes using an anionic polymerization of ethylene oxide in the presence of a *N*-methyldiethanolamine initiator.[85] They subsequently used dichloromethane in the presence of CsOH or KOH to increase the molecular weight of the PEG segment using a Williamson-type reaction. The polymer was then quaternized to yield a PEG-based ionene (Scheme 2.7). The various functionalized polymers displayed different solution behaviors. For example, when R = CH_3, the ionene demonstrated typical polyelectrolyte behavior; however, when R was zwitterionic or perfluorinated, the hydrodynamic radius decreased due to dipole-dipole and hydrophobic interactions.

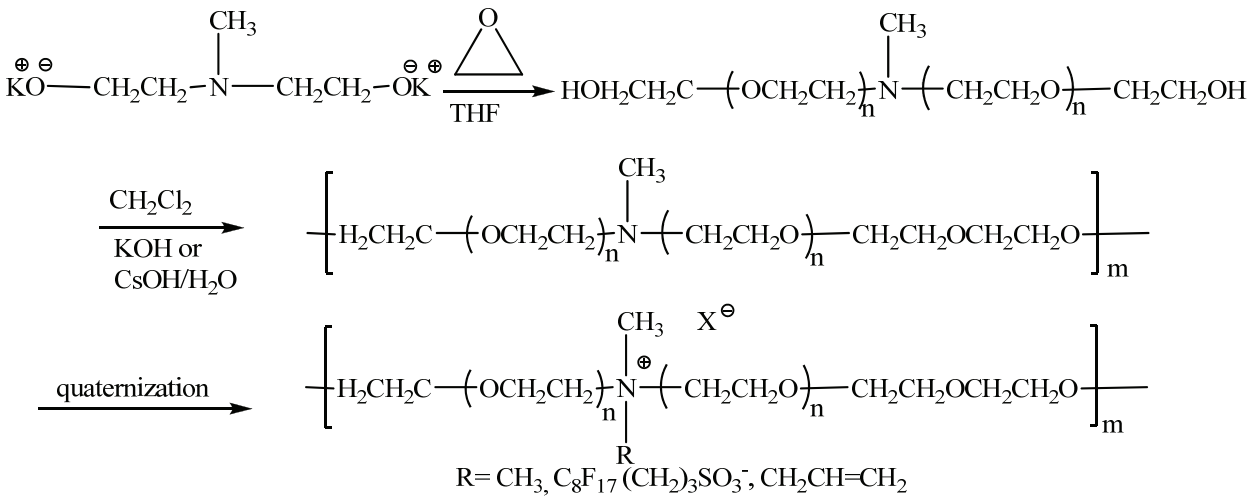

Scheme 2.7. Synthesis of PEG-based ionenes from anionic polymerization of ethylene oxide.

Sukhyy et al. recently reported the synthesis, thermal property characterization, and ionic conductivity of novel PEG-based ionenes.[86] As they described, changing the PEG oligomer molecular weight controlled the charge density. As expected for polyelectrolytes, the T_g increased with increasing charge content. For the PEG ionenes that Sukhyy et al. examined, the T_g ranged from -52 to -10 °C as the PEG repeat unit decreased from 21 to 2. WAXS analysis revealed that the longest PEG spacer facilitated polymer crystallization, while decreasing the length of the PEG spacer produced amorphous characteristics. These results were similar to those reported by Wagener et al., who synthesized well-defined polyelectrolytes consisting of poly(ethylene-co-acrylic acid) (EAA) copolymers with 9, 15 or 21 methylene groups between the pendant carboxylic acid groups.[87] In their work, the EAA copolymer with the longest polyethylene spacer (21 methylene units) exhibited crystallinity and multiple reflections in X-ray scattering results, indicating that packing was more regular; conversely, the shorter methylene spacer ionomers were amorphous. Sukhyy et al. also observed the effect of charge density via SAXS results. The longest PEG spacer ionene allowed for enhanced microphase separation with larger soft domains. DC conductivities were measured for the PEG ionenes, and it was found

that as the PEG chain increased, there was a corresponding decrease in conductivity. In addition, the higher charge density ionenes possessed Arrhenius behavior, while the lower charge density ionenes displayed Vogel-Tammann-Fulcher (VTF) behavior. It is interesting to note that even though the importance of a well-defined morphology for polymers is typically emphasized; in the case of polymer conductivity, crystalline structures are not desired.

2.6.4 Poly(propylene glycol)-based ionenes

In 1970, Rembaum et al. studied the electronic conductivity of elastomeric ammonium ionenes containing PPG segments. The ionenes had weight average molecular weights ranging from 10000 to 40000 g/mol, and were complexed with lithium tetracyano-quinodimethane (LiTCNQ).[88] Their desirable elastomeric properties resulted from a polyurethane prepolymer that was chain extended with dimethylamino ethanol and a dihalide (Scheme 2.8). Reported resistivities ranged from 10^4 to 10^7 ohm-cm, which was proportional to the distance between charge sites.

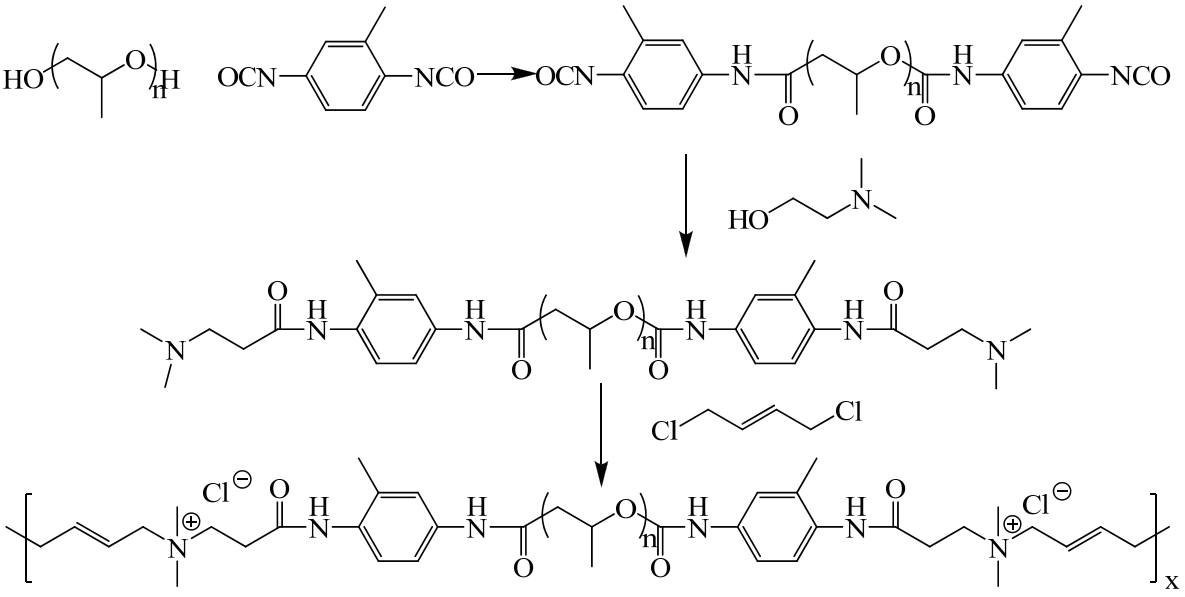

Scheme 2.8. Synthesis of elastomeric ionenes for conductive LiTCNQ complexes.

2.6.5 Ionenes based on polydienes

Very few studies have investigated ionenes based on polyolefins. Jérôme et al. were the first to report the novel synthesis of polyisoprene-based ionenes from 5000 g/mol *α,ω*-bis(dimethylamino)polyisoprene and dibromo-*p*-xylene.[77] Dielectric spectroscopy was utilized to determine thermal transitions (Figure 2.23).

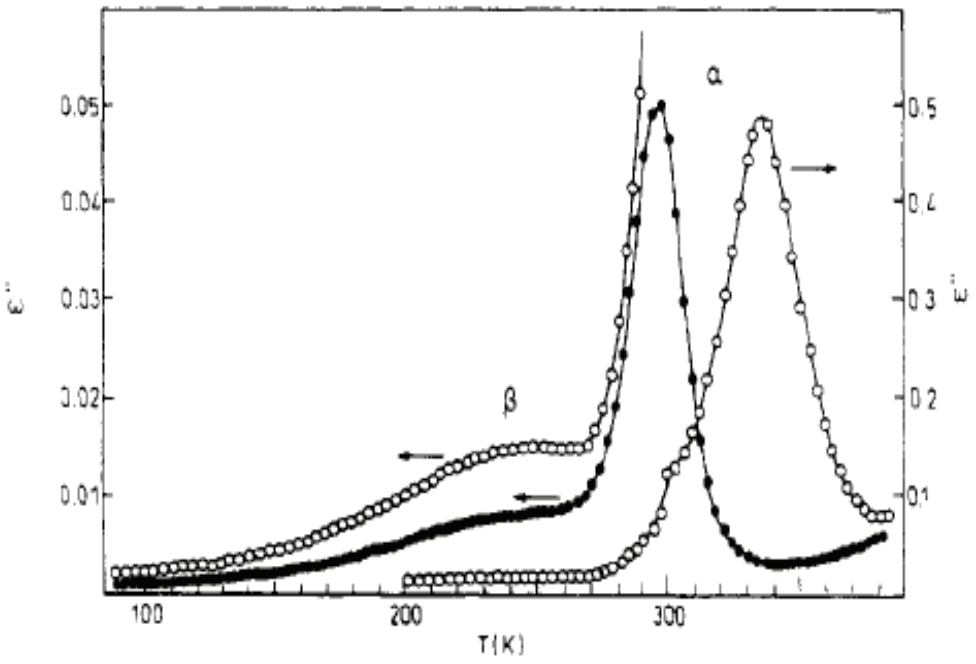

Figure 2.23. Dielectric spectroscopy of polyisoprene ionenes.[77]

Because the investigators understood that the microstructure of polyisoprene would influence the results, they consistently used polyisoprene that possessed 65 % of 3,4 and 35% of 1,2 content. Similar to *x,y*-oxyethylene ionenes that Tanaka et al. reported,[52] the polyisoprene ionenes possessed a T_α and a T_β, where T_α was attributed to the glass transition temperature and T_β was attributed to the local scale motions of the polymer backbone below the T_g. The dielectric increment, Δε, for T_β remained unchanged upon nitrogen quaternization. This further supported the hypothesis that T_β occurred as a result of local polymer chain motion. Conversely, the Δε for

T_α was 5-10 times larger for the ionene in comparison to the polyisoprene oligomeric precursor. The authors hypothesized that the shoulder observed in Figure 2.23 was possibly due to the formation of multiplets of ionic aggregates, which could have restricted the mobility of the polymer chain close to the ionic groups. To further clarify, the authors compared the polyisoprene ionene multiplet formation to Eisenberg's sodium salts of styrene-(methacrylic acid) copolymers.[89,90]

Yamashita et al. conducted an investigation to elucidate the role of ionic aggregation on the swelling and mechanical properties of novel polybutadiene ionenes (PBIs) (Figure 2.24).[91] The ionenes were synthesized in a two-step process beginning with a commercially available isocyanate-terminated polybutadiene, which they then reacted with 2-dimethylaminoethanol. The isolated product was subsequently reacted with 1,4-dibromobutane. In order to establish a benchmark, polybutadiene urethanes (PBUs) (Figure 2.24) were also synthesized from hydroxyl-terminated polybutadiene and 2,4-toluene diisocyanate. The microstructures of both the hydroxyl-terminated and isocyanate-terminated polybutadiene oligomers were identical, and consisted of 20 % *cis*, 60 % *trans*, and 20 % vinyl.

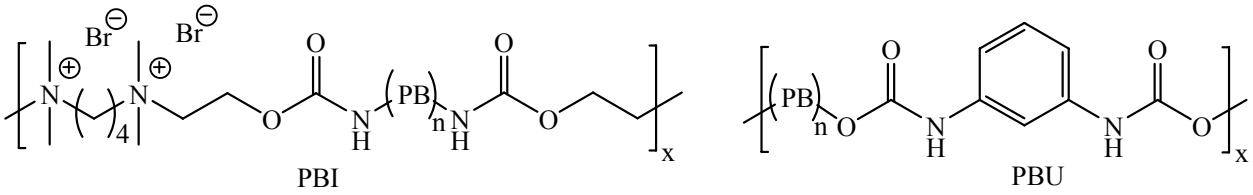

Figure 2.24. Structures of polybutadiene ionene (PBI) and polybutadiene urethane (PBU).

Swelling experiments were conducted to determine the effect of ionic groups on the solubility parameter of PBI. The results demonstrated that regardless of the choice of solvent, the polybutadiene solubility parameter values did not vary from prior literature reports. This indicated that the presence of quaternary ammonium ionic sites did not alter the solvent

interactions with the polymer. The authors attributed this phenomenon to low ionic content relative to polybutadiene content. To evaluate mechanical performance, tensile measurements were conducted on both the PBU and PBI. From 10-140 °C, PBI consistently displayed superior tensile strength and elongation relative to PBU. This increase in mechanical strength was attributed to the presence of ionic aggregates that imparted non-covalent cross-linking, which was consistent with previous results showing that ionenes can form ionic aggregates that enhance mechanical properties.

2.7 Branched and cross-linked ionenes

Rembaum et al. reported the first example of star-shaped and branched ionenes in 1973.[43] 3-Dimethylamino-*n*-propyl chloride was reacted with 2,4,6-tri(chloromethyl)mesitylene and 1,2,4,5-tetra(chloromethyl)benzene to achieve star-shaped ionenes. Reaction conditions and intrinsic viscosity data are provided in Table 2.2.

Compound	Solvent	Temperature (°C)	Time (h)	Mol AB monomer/mol compound	$[\eta]^a$ dL/g
2,4,6-tri(chloromethyl)mesitylene	4:1 DMF:H_2O	54	168	10	0.180
1,2,4,5-tetra(chloromethyl)benzene	4:1 DMF:H_2O	54	168	10	0.150
1,2,4,5-tetra(chloromethyl)benzene	H_2O	95	60	10	0.245

Table 2.2. Reaction conditions and resulting intrinsic viscosity data for the synthesis of star-shaped ionenes.

In the same paper, Rembaum and co-workers described branched polymers synthesized with the same monomers in a reaction with poly(4-vinylpyridine), poly(ethyleneimine), and poly(vinylbenzyl chloride). Elemental analysis indicated that branched structures had formed, and that intrinsic viscosity increased. However, other characterization methods were not reported.

Until Rembaum et al. first synthesized ionene cross-linking reagents and explored the properties of networks prepared from these materials,[92] the effects of cationic sites on cross-linking agents and the properties of the resulting polymers were unexplored. In their 1969 report, they proposed three types of cross-linking agents: acrylate/methacrylate, divinylpyridinium, and diallylammonium compounds. The pyridinium cross-linking agents were never successfully isolated due to spontaneous polymerization and cross-linking. They did, however, successfully prepare acrylate and allyl cross-linking reagents, and those structures are shown below (Scheme 2.9). The R structure between the dihalide and ditertiary amine varied from aliphatic to aromatic. In total, four diacrylate, four dimethacrylate, and two diallylammonium bromides were prepared. They confirmed the bromide content via titration with silver nitrate and a chromate indicator. Three polymerization methods were used to synthesize the cross-linked polymers: (1) redox initiation with sodium persulfate and sodium metabisulfite, (2) cobalt γ irradiation with a 10^6 rads dose, and (3) photopolymerization with visible and UV light. The diallylammonium bromide cross-linker was not successfully polymerized because of the stability of the radical, which was stabilized through resonance. In addition, they demonstrated the successful synthesis of copolymers using methacrylate and acrylate cross-linkers.

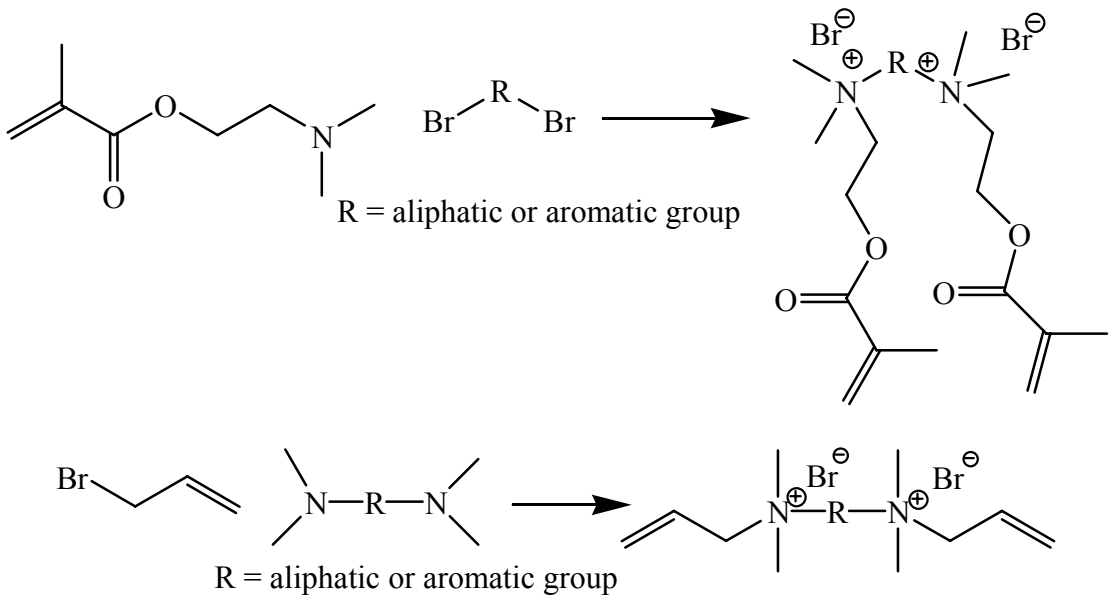

Scheme 2.9. Synthesis of acrylate and allyl cross-linkers.

Thermally reversible cross-linked networks are desirable due to facile processing at elevated temperature, and upon cooling, elastomeric properties are potentially obtained via cross-linking. In 2000, Ruckenstein et al. prepared cross-linked ionenes and demonstrated their thermal reversible cross-linking properties.[14] Polymers possessing chloride or ditertiary amine functionality were cross-linked with each other or with low molecular weight ditertiary amines or dichlorides, respectively. Chloromethylstyrene and styrene-*r*-chloromethylstyrene copolymers, as well as 2-(dimethylamino)ethyl acrylate and 2-(dimethylamino)ethyl acrylate-*r*-butyl acrylate copolymers, were used in their investigation. Several methods including IR spectroscopy, NMR spectroscopy, solubility testing, and DSC were utilized to investigate the cross-linking and thermal de-cross-linking processes. Ruckenstein et al. elucidated that cross-linking efficiency depended on the structure of the low molecular weight ditertiary amine and dichloride. Specifically, when the cross-linker possessed an increased number of methylene sites, the cross-linking reaction occurred more rapidly. However, when a rigid structure was utilized, the cross-linking reaction took longer to complete. De-cross-linking took place at higher

temperatures, usually above 200 °C. At this temperature, however, a variety of competing reactions can occur. For example, the Hofmann degradation is the primary side reaction, which would render the cross-linking/de-cross-linking process irreversible. The formation of C=C bond was easily detectable via NMR and IR spectroscopy.

2.8 Conclusions and future directions

This review focused on the synthesis and structure-property relationships of ammonium ionene polymers. Ionenes are useful model polyelectrolytes that allow for systematic studies of polyelectrolyte behavior due to their controlled charge placement. The charge density is well-defined through monomer selection, which differs from polyelectrolytes where charge placement is random. This property makes ionenes potentially useful as ion channel forming polymers. In addition, ionenes with oligomeric spacers, such as PTMO, have elastomeric properties comparable in performance to polyurethanes. However, ionene synthesis is more environmentally friendly and inherently less toxic, since the starting materials are not as toxic and reactive as the isocyanate monomers used in polyurethane synthesis.

Well-defined ionenes have a variety of potential applications, as shown in the literature and patent records. The primary emphasis with respect to ionene applications has focused on biomedical technologies, such as gene transfection agents,[93-96] antimicrobials,[97-101] and cancer therapeutics.[102] For example, certain non-segmented ionenes, such as 6,10-ammonium ionene, prevented cancer growth, while not harming normal cells (Figure 2.25).[102]

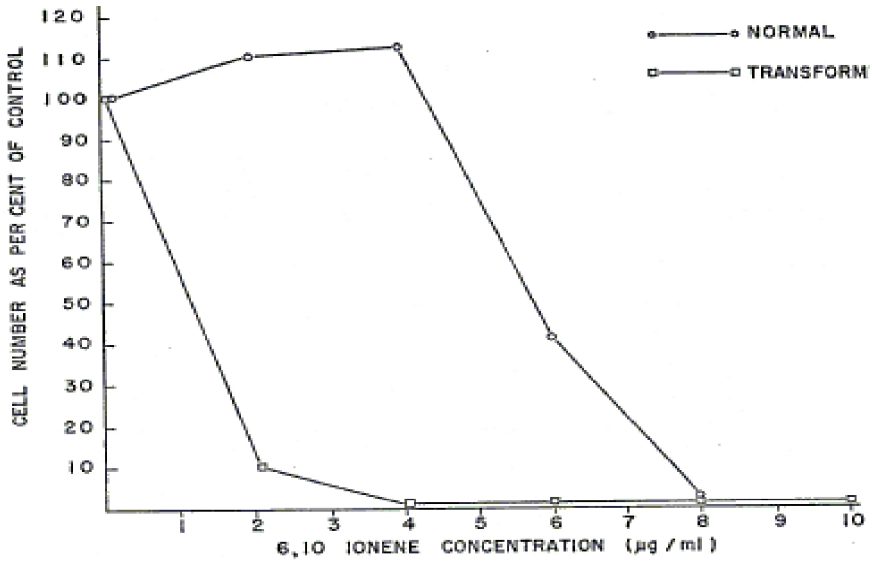

Figure 2.25. Cell viability as a function of 6,10-ammonium ionene concentration on normal and cancerous cells.[102]

Antimicrobial coatings are typically comprised of quaternary ammonium salts.[103] Rembaum et al. and Narita et al. have demonstrated that ionenes possess excellent antimicrobial properties.[99,100] In fact, the antimicrobial properties of quaternary ammonium polymers have facilitated the development of new antimicrobial coatings.[104,105] To their detriment, ionenes are not suitable as gene delivery agents in their unmodified state. This is due to the permanent positive charge of their quaternary nitrogens. Generally, polymers used in gene therapy applications must feature a way to control pH through protonatable sites, since this is believed to aid in endosomal release and encourage active gene delivery. However, ionenes are useful models for gene therapy because their charge density and molecular weights are easily controlled through careful monomer selection.

To address these issues, new research conducted in the Long group has focused on synthesizing novel ionenes and thoroughly investigating their structure-property

relationships.[12,39,41,61,82,106] In addition, functionalized ammonium ionenes show promise as successful gene therapy agents.[107] The most recent investigation has involved the novel synthesis of imidazolium and phosphonium ionenes. We have demonstrated the successful synthesis of imidazolium-based ionenes using a bisimidazolium monomer (1,1'-(1,4-butanediyl)bis(imidazole))[108] prepared from imidazole and dibromobutane.[41] Since a number of dihalides are either commercially available or are easily synthesized, we have pursued several avenues for synthesizing novel ionenes, including the use of low molecular weight dihalides (Figure 2.26) and oligomeric sequences, such as PEG, PPG, and PTMO. These novel ionenes have potential in a variety of applications, including in electro-active devices and antimicrobial coatings.

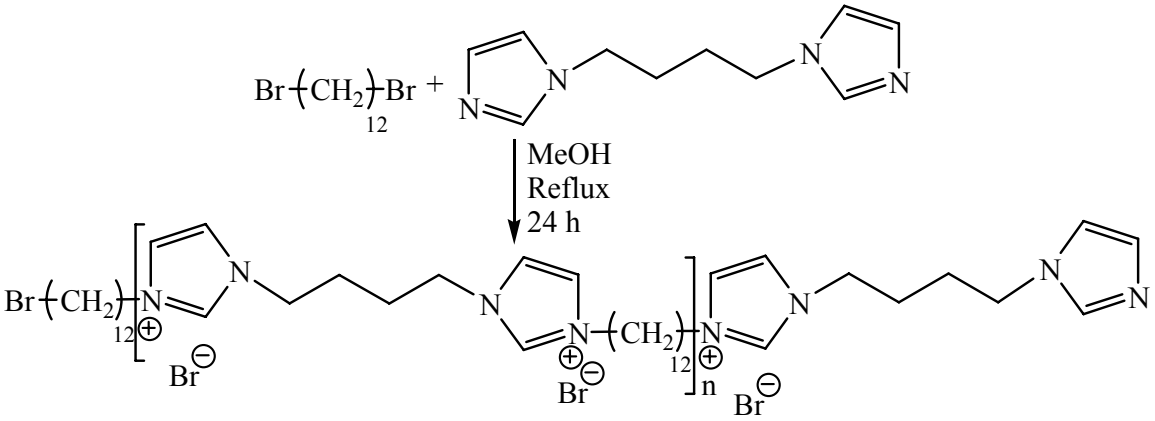

Figure 2.26. Synthesis of imidazolium ionenes from 1,1'-(1,4-butanediyl)bis(imidazole) and 1,12-dibromobutane.

It is well known that phosphonium salts typically possess greater thermal stability compared to ammonium salts.[109,110] Therefore, the synthesis of phosphonium ionenes was conducted with a commercially available monomer, 1,4-bis(diphenylphosphino)butane. We have also shown that it is possible to synthesize novel phosphonium ionenes using similar dihalides as described above, such as the PTMO-based phosphonium ionenes shown in Figure 2.27 below.

Our research group has shown that these ionenes are more thermally stable (>50 °C higher thermal decomposition temperature) when a phosphonium cation is used instead of ammonium or imidazolium cations. In addition, the phosphonium salt is not water soluble, thus diminishing the hygroscopic nature that is typical of ionenes.

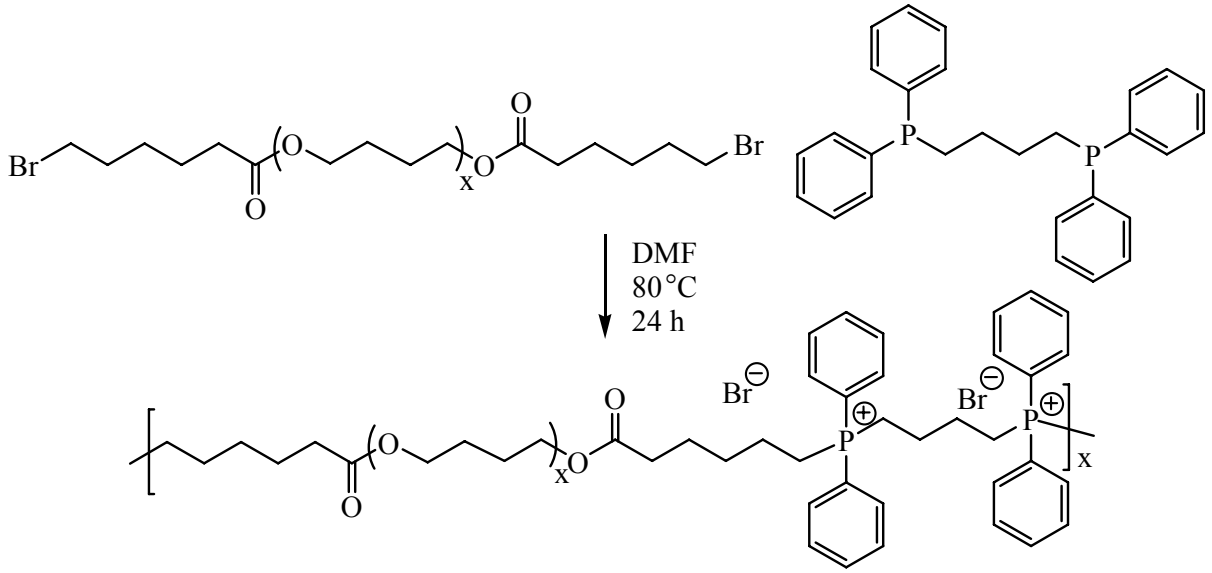

Figure 2.27. Synthesis of phosphonium ionenes from 1,4-bis(diphenylphosphino)butane and PTMO dibromide.

Careful molecular weight analysis of ionenes and all polyelectrolytes is crucial for developing accurate structure-property relationships. In particular, the use of light scattering detectors in combination with dynamic light scattering is needed to ensure that molecular weight measurements are conducted on single polymer chains rather than on aggregates.

2.9 Acknowledgements

This material is based upon work supported in part by the Macromolecular Interfaces with Life Sciences (MILES) Integrative Graduate Education and Research Traineeship (IGERT) of the National Science Foundation under agreement no. DGE-0333378. This material is based upon work supported in part by the U.S. Army Research Office under grant number W911NF-

07-1-0452 Ionic Liquids in Electro-Active Devices (ILEAD) MURI. The Kimberly Clark Corporation is also gratefully acknowledged for support of this research, and discussions with Clay Bunyard were helpful. Finally, we thank Ms. Laurie Good for manuscript review.

2.10 References

(1) Rembaum, A.; Baumgartner, W.; Eisenberg, A. *J. Polym. Sci. Polym. Lett. Ed.* **1968,** 6, (3), 159-171.
(2) Gibbs, C. F.; Littman, E. R.; Marvel, C. S. *J. Am. Chem. Soc.* **1933,** 55, 753.
(3) Tant, M. R.; Mauritz, K. A.; Wilkes, G. L., *Ionomers: Synthesis, structure, properties, and applications*. Blackie Academic and Professional: London, 1997.
(4) Schlick, S., *Ionomers: characterization, theory, and applications*. CRC Press: Boca Raton, 1996.
(5) http://www.alhimikov.net/biograf/menshutkin.html
(6) Abboud, J. L. M.; Notario, R.; Bertran, J.; Sola, M. *Prog. Phys. Org. Chem.* **1993,** 19, 1-182.
(7) Rembaum, A.; Noguchi, N. *Macromolecules* **1972,** 5, (3), 261-269.
(8) McMurray, J., *Organic chemistry*. 5th ed.; Brooks-Cole: Pacific Grove, 2000.
(9) Lehman, M. R.; Thompson, C. D.; Marvel, C. S. *J. Am. Chem. Soc.* **1935,** 57, 1137-1139.
(10) Casson, D.; Rembaum, A. *Macromolecules* **1972,** 5, (1), 75-81.
(11) Wu, C., *Handbook of size exclusion chromatography*. Dekker: New York, 1995; Vol. 69.
(12) Layman, J. M.; Borgerding, E. M.; Williams, S. R.; Heath, W. H.; Long, T. E. *Macromolecules* **2008,** 41, (13), 4635-4641.
(13) Charlier, P.; Jerome, R.; Teyssie, P.; Prud'homme, R. E. *J. Polym. Sci. A* **1993,** 31, 128-134.
(14) Ruckenstein, E.; Chen, X. N. *Macromolecules* **2000,** 33, (24), 8992-9001.
(15) Patai, S., *The chemistry of the amino group*. Wiley: New York, 1968.
(16) Tsutsui, T.; Tanaka, R.; Tanaka, T. *J. Polym. Sci. Polym. Phys. Ed.* **1976,** 14, (12), 2259-2271.
(17) Cotter, R. J., Pyrolysis and desorption mass spectroscopy. In *Analytical pyrolysis. Techniques and applications*, Voorhees, K. J., Ed. Butterworths: London, 1984.
(18) Avram, E. *Rev. Roum. Chim* **2001,** 46, (1), 49-53.
(19) Lubkowski, J.; Blazejowski, J. *Thermochimica Acta* **1990,** 157, (2), 259-277.
(20) Haskins, N. J.; Mitchell, R. *Analyst* **1991,** 116, (9), 901-903.
(21) Pasquale, A. J.; Long, T. E. *Journal of Applied Polymer Science* **2004,** 92, (5), 3240-3246.
(22) Flory, P. J., *Principles of Polymer Chemistry*. Cornell University Press: 1953.
(23) Wang, J.; Meyer, W. H.; Wegner, G. *Macromol. Chem. Phys.* **1994,** 195, 1777-1795.
(24) Karikari, A. S.; Edwards, W. F.; Mecham, J. B.; Long, T. E. *Biomacromolecules* **2005,** 6, (5), 2866-2874.
(25) Lepene, B. S.; Long, T. E.; Meyer, A.; Kranbuehl, D. E. *J. Adhes.* **2002,** 78, (4), 297-312.
(26) Lizotte, J. R.; Erwin, B. M.; Colby, R. H.; Long, T. E. *J. Polym. Sci., Part A: Polym. Chem.* **2002,** 40, (4), 583-590.
(27) Lizotte, J. R.; Long, T. E. *Macromol. Chem. Phys.* **2003,** 204, (4), 570-576.
(28) Lizotte, J. R.; Long, T. E. *Macromol. Chem. Phys.* **2004,** 205, (5), 692-698.
(29) McGrath, J. E.; Rasmussen, L.; Shultz, A. R.; Shobha, H. K.; Sankarapandian, M.; Glass, T.; Long, T. E.; Pasquale, A. J. *Polymer* **2006,** 47, (11), 4042-4057.

(30) Pasquale, A. J.; Allen, R. D.; Long, T. E. *Macromolecules* **2001,** 34, (23), 8064-8071.
(31) Pasquale, A. J.; Fornof, A. R.; Long, T. E. *Macromol. Chem. Phys.* **2004,** 205, (5), 621-627.
(32) Pasquale, A. J.; Karro, R.; Allen, R. D.; Long, T. E. *Abstracts of Papers, 220th ACS National Meeting, Washington, DC, United States, August 20-24, 2000* **2000**, POLY-444.
(33) Pasquale, A. J.; Long, T. E. *J. Appl. Polym. Sci.* **2004,** 92, (5), 3240-3246.
(34) Wiles, K. B.; Bhanu, V. A.; Pasquale, A. J.; Long, T. E.; McGrath, J. E. *Abstracts of Papers, 222nd ACS National Meeting, Chicago, IL, United States, August 26-30, 2001* **2001**, POLY-532.
(35) Wiles, K. B.; Bhanu, V. A.; Pasquale, A. J.; Long, T. E.; McGrath, J. E. *J. Polym. Sci., Part A: Polym. Chem.* **2004,** 42, (12), 2994-3001.
(36) Williams, S. R.; Miller, K. M.; Long, T. E. *Prog. React. Kinet. Mech.* **2007,** 32, (4), 165-194.
(37) Williamson, D. T.; Buchanan, T. D.; Elkins, C. L.; Long, T. E. *Macromolecules* **2004,** 37, (12), 4505-4511.
(38) Yilgor, I.; Mather, B. D.; Unal, S.; Yilgor, E.; Long, T. E. *Polymer* **2004,** 45, (17), 5829-5836.
(39) Borgerding, E. M. Synthesis, molecular weight characterization, and structure-property relationships of ammonium ionenes. Virginia Tech, Blacksburg, VA, 2007.
(40) Colthup, N. B.; Daly, L. H.; Wiberley, S. E., *Introduction to infrared and raman spectroscopy*. 3rd ed.; Academic Press: New York, 1975.
(41) Williams, S. R.; Long, T. E. *unpublished results*.
(42) Noguchi, N.; Rembaum, A. *J. Polym. Sci. Polym. Lett. Ed.* **1969,** 7, 383-394.
(43) Yen, S. P. S.; Casson, D.; Rembaum, A. *Polymer Science and Technology* **1973**, 291-312.
(44) Fuoss, R. M. *J. Polym. Sci.* **1948,** 3, 603.
(45) Dobrynin, A. V.; Rubinstein, M. *Prog. Polym. Sci.* **2005,** 30, 1049-1118.
(46) Eisenberg, A.; Hird, B.; Moore, R. B. *Macromolecules* **1990,** 23, 4098.
(47) Eisenberg, A.; King, M., *Ion containing polymers*. Academic Press: New York, 1977.
(48) Holliday, L., Ed., *Ionic polymers*. Halstead Press: New York, 1975.
(49) Leyte, J. C.; Mandel, M. *J. Polym. Sci. A* **1964,** 2, (4), 1879-91.
(50) Sonnessa, A. J.; Cullen, W.; Ander, P. *Macromolecules* **1980,** 13, 195-196.
(51) Knapick, E. G.; Hirsch, J. A.; Ander, P. *Macromolecules* **1985,** 18, 1015-1021.
(52) Tsutsui, T.; Tanaka, R.; Tanaka, T. *J. Polym. Sci. Polym. Phys. Ed.* **1975,** 13, (11), 2091-2102.
(53) Sugisaki, M.; Suga, H.; Seki, S. *Bull. Chem. Soc. Japan* **1968,** 41, 2591.
(54) Yue, Y. Z.; Angell, C. A. *Nature* **2004,** 427, (6976), 717-720.
(55) Tsutsui, T.; Tanaka, R.; Tanaka, T. *J. Polym. Sci. Polym. Phys. Ed.* **1976,** 14, (12), 2273-2284.
(56) Meyer, W. H.; Rietz, R. R.; Schaeffer, D.; Kremer, F. *Electrochim. Acta* **1992,** 37, (9), 1491-1494.
(57) Salamone, J. C.; Snider, B. *J. Polym. Sci. A-Polym. Chem.* **1970,** 8, (12), 3495-3501.
(58) Bortel, E.; Kochanowski, A. *Makromol. Chem.* **1987,** 188, 2019-2026.
(59) Cohen, J. I.; Shteto, V.; Engel, R. *Synthesis* **2000,** 9, 1263-1268.
(60) Littman, E. R.; Marvel, C. S. *J. Am. Chem. Soc.* **1930,** 52, 287.
(61) Williams, S. R.; Borgerding, E. M.; Layman, J. M.; Wang, W.; Winey, K. I.; Long, T. E. *Macromolecules* **2008,** 41, (14), 5216–5222.
(62) Burmistr, M. V.; Sukhyy, K. M.; Shilov, V. V.; Pissis, P.; Spanoudaki, A.; Sukha, I. V.; Tomilo, V. I.; Gomza, Y. P. *Polymer* **2005,** 46, 12226-12232.
(63) Chen, L.; Yu, S.; Kagami, Y.; Gong, J.; Osada, Y. *Macromolecules* **1998,** 31, 787-794.
(64) Zheng, X.; Cao, W. *Eur. Polym. J.* **2001,** 37, 2259-2262.
(65) Schultz, D. N.; Peiffer, D. G.; Agarwal, P. K.; Laladas, J.; Soni, L.; Handwerker, B.; Garner,

R. T. *Polymer* **1986,** 27, 1734.
(66) Chen, L.; Honma, Y.; Mizutani, T.; Liaw, D.-J.; Gong, J. P.; Osada, Y. *Polymer* **2000,** 41, 141-147.
(67) Okawa, K.; Gong, P. P.; Osada, Y. *Macromolecular Rapid Communications* **2002,** 23, (7), 423-425.
(68) Kohjiya, S.; Ohtsuki, T.; Yamashita, S. *Makromolekulare Chemie-Rapid Communications* **1981,** 2, (6-7), 417-420.
(69) Leir, C. M.; Stark, J. E. *Journal of Applied Polymer Science* **1989,** 38, (8), 1535-1547.
(70) Feng, D.; Venkateshwaran, L. N.; Wilkes, G. L.; Leir, C. M.; Stark, J. E. *Journal of Applied Polymer Science* **1989,** 38, (8), 1549-1565.
(71) Das, S.; Yilgor, I.; Yilgor, E.; Inci, B.; Tezgel, O.; Beyer, F. L.; Wilkes, G. L. *Polymer* **2007,** 48, 290-301.
(72) Feng, D.; Wilkes, G. L.; Leir, C. M.; Stark, J. E. *J. Macromol. Sci.-Chem.* **1989,** A26, (8), 1151-1181.
(73) Feng, D.; Wilkes, G. L.; Lee, B.; McGrath, J. E. *Polymer* **1992,** 33, (3), 526-535.
(74) Ikeda, Y.; Murakami, T.; Urakawa, H.; Kohjiya, S.; Grottenmuller, R.; Schmidt, M. *Polymer* **2002,** 43, 3483-3488.
(75) Ikeda, Y.; Yamato, J.; Murakami, T.; Kajiwara, K. *Polymer* **2004,** 45, 8367-8375.
(76) Grassl, B.; Galin, J. C. *Macromolecules* **1995,** 28, (21), 7035-7045.
(77) Yano, S.; Tadano, K.; Jerome, R. *Macromolecules* **1991,** 24, (24), 6439-6442.
(78) Klun, T. C.; Wendling, L. A.; Van Bogart, J. W. C.; Robbins, A. F. *J. Polym. Sci. A* **1987,** 25, (1), 87-109.
(79) Williams, K. A.; Dreyer, D. R.; Bielawski, C. W. *MRS Bull.* **2008,** 33, 759-765.
(80) Grassl, B.; Meurer, B.; Scheer, M.; Galin, J. C. *Macromolecules* **1997,** 30, 236-245.
(81) Grassl, B.; Mathis, A.; Rawiso, M.; Galin, J. C. *Macromolecules* **1997,** 30, 2075-2084.
(82) Fornof, A. R. Synthesis and characterization of multiphase, highly branched polymers. Virginia Tech, Blacksburg, VA, 2006.
(83) Loveday, D.; Wilkes, G. L.; Bheda, M. C.; Shen, Y. X.; Gibson, H. W. *J. Macro. Sci., Part A* **1995,** 32, (1), 1-27.
(84) Petersen, H.; Fechner, P. M.; Martin, A. L.; Kunath, K.; Stolnik, S.; Roberts, C. J.; Fischer, D.; Davies, M. C.; Kissel, T. *Bioconjugate Chem* **2002,** 13, (4), 845-854.
(85) Dimitrov, I. V.; Berlinova, R. V. *Macromol. Rap. Comm.* **2003,** 24, (9), 551-555.
(86) Burmistr, M. V.; Sukhyy, K. M.; Shilov, V. V.; Pissis, P.; Polizos, G.; Spanoudaki, A.; Gomza, Y. P. *Solid State Ionics* **2005,** 176, 1787-1792.
(87) Baughman, T. W.; Chan, C. D.; Winey, K. I.; Wagener, K. B. *Macromolecules* **2007,** 40, 6564-6571.
(88) Somoano, R.; Yen, S. P. S.; Rembaum, A. *J. Polym. Sci. Polym. Lett. Ed.* **1970,** 8, 467-479.
(89) Arai, K.; Eisenberg, A. *J. Macromol. Sci. Phys.* **1980,** B17, 803.
(90) Hodge, I. M.; Eisenberg, A. *Macromolecules* **1978,** 11, 283.
(91) Yamashita, S.; Itoi, M.; Kohjiya, S.; Kidera, A. *J. Appl. Polym. Sci.* **1988,** 35, 1927-1935.
(92) Rembaum, A.; Singer, S.; Keyzer, H. *J. Polym. Sci. Polym. Lett. Ed.* **1969,** 7, 395-402.
(93) Zelikin, A. N.; Akritskaya, N. I.; Izumrudov, V. A. *Macromol. Chem. Phys.* **2001,** 202, (15), 3018-3026.
(94) Zelikin, A. N.; Litmanovich, A. A.; Paraschuk, V. V.; Sybatchin, A. V.; Izumrudov, V. A. *Macromolecules* **2003,** 36, (6), 2066-2071.
(95) Zelikin, A. N.; Putnam, D.; Shastri, P.; Langer, R.; Izumrudov, V. A. *Bioconjugate Chem.*

2002, 13, (3), 548-553.
(96) Wahlund, P.-O.; Izumrudov, V. A.; Gustavsson, P.-E.; Larsson, P.-O.; Galaev, I. Y. *Macromol. Biosci.* **2003,** 3, (8), 404-411.
(97) Fitzpatrick, R.; Klinger, J. D.; Shackett, K. K. Ionene polymers and their use as antimicrobial agents. WO 2002080939, 2002.
(98) Jen, J. S.; Jones, R. E.; Homesley, P. M.; Petisce, J. Methods for providing biomedical devices with hydrophilic antimicrobial coatings. US 2005-68008 20050228, 2006.
(99) Narita, T.; Nishino, M.; Gong, J. P.; Osada, Y. *Colloid and Polymer Science* **2000,** 278, 884-887.
(100) Rembaum, A., Biological activity of ionene polymers. In *Polymeric Materials for Unusual Service Conditions*, Golub, M. A.; Parker., J. A., Eds. Wiley: New York, 1973; pp 299-317.
(101) Tashiro, T. *Macromolecular Materials and Engineering* **2001,** 286, 63-87.
(102) Rembaum, A. Ionene polymers for selectively inhibiting the vitro growth of malignant cells. 4,013,507, 1977.
(103) Cakmak, I.; Ulukanli, Z.; Tuzcu, M.; Karabuga, S.; Genctav, K. *European Polymer Journal* **2004,** 40, (10), 2373-2379.
(104) Lan, J.; Vanderlaan, D.; Willcox, M.; Aliwarga, Y. Biomedical devices with antimicrobial cationic peptide and protein coatings. WO 2002064183, 2002.
(105) Lydon, M.; Gravett, D. M.; Whitbourne, R. J. Antimicrobial needle coating for extended infusion. WO2006053007 2006.
(106) Tamami, M.; Long, T. E. *unpublished results*.
(107) Ramirez, S.; Long, T. E., *unpublished results*.
(108) So, Y. H. *Macromolecules* **1992,** 25, (2), 516-520.
(109) Nakajima, H.; Ohno, H. *Polymer* **2005,** 46, (25), 11499-11504.
(110) Tsunashima, K.; Sugiya, M. *Electrochemistry Communications* **2007,** 9, (9), 2353-2358.

Chapter 3 : Synthesis and Characterization of Well-Defined 12,12-Ammonium Ionenes: Evaluating Mechanical Properties as a Function of Molecular Weight

Reproduced in part with permission from: Williams, S.R.; Borgerding, E.M.; Layman, J.M.; Wang, W.; Winey, K.I; Long, T.E. *Macromolecules,* 41 (14), 5216–5222, 2008. Copyright 2008. American Chemical Society.

3.1 Abstract

Water-soluble 12,12-ammonium ionenes were prepared via the Menschutkin reaction from 1,12-dibromododecane and 1,12-bis(N,N-dimethylamino)dodecane. A stoichiometric imbalance of monomers controlled the final molecular weights of the polymers. The absolute molecular weights were determined for the first time using an on-line multi-angle laser light scattering (MALLS) detector in aqueous size exclusion chromatography (SEC). Weight-average molecular weights ranged from 4,300 to 20,900 g/mol. Relationships between weight-average molecular weight and mechanical properties were established for a series of 12,12-ammonium ionenes using both tensile testing and dynamic mechanical analysis (DMA). Tensile analysis of the higher molecular weight ionenes revealed an average tensile strength of 20 MPa and elongations ranging from 230-440%. Dissociation of ionic aggregates was observed at 85-88 °C in DMA experiments, and the glass transition temperatures increased with increasing molecular weight (61-88 °C). X-ray scattering revealed an amorphous polyethylene peak at approximately 14 nm^{-1} and a sharp ionic group correlation peak at 4.38 nm^{-1}. These correlations agreed well

with the proposed macromolecular structure. In addition, the 12,12-ammonium ionenes possessed shape memory and self-healing properties.

3.2 Introduction

Ammonium polyionenes, or ionenes, are ion-containing polymers that contain quaternary nitrogen atoms in the macromolecular main chain as opposed to a pendant site. In 1933, Gibbs and co-workers were the first to report the synthesis of ionenes from dimethylamino-*n*-alkyl halides via a step-growth polymerization process.[1] Ionene synthesis also occurs via polymerization of an alkyl dihalide and a ditertiary amine according to the Menschutkin reaction.[2] Rembaum et al. used the Menschutkin reaction to synthesize ionenes with a variety of methylene spacers and extensively explored their solution properties.[3-5] The polymer is commonly named from the number of methylene units, which correspond to the diamine and dihalide monomers, respectively (i.e., x,y-ionene).[5] Rembaum et al. studied the solution properties of high-charge density ionenes with structures of 3,4- and 6,6-ionenes.[3] They reported that both ionenes exhibited rod-like behavior in solutions without additional salt, which is known as the polyelectrolyte effect.[6] Upon addition of 0.4 M KBr, the polyelectrolyte effect was suppressed and the ionenes behaved as uncharged polymers. Ander et al. also studied the transition of polyelectrolyte to polysoap behavior of N,N-disubstituted ionenes.[7,8] They observed that as the length of the substituent on the nitrogen atoms increased from methyl to *n*-octyl, the ionene behaved as a polysoap rather than a polyelectrolyte. Salamone et al. demonstrated the successful synthesis of ionenes via the Menschutkin reaction using bulky ditertiary amines such as 1,4-diaza[2.2.2]bicyclooctane.[9] This manuscript established that there are a wide range of possibilities for ionene synthesis because of the number of ditertiary amines and dibromoalkanes available in sufficient purity for polymerization.

Wilkes et al. analyzed the structure-property relationships of ionenes prepared from a dimethylamino-terminated poly(tetramethylene oxide) (PTMO) oligomer that was reacted with 1,4-dibromo-*p*-xylene.[10] The ionenes possessed elastomeric behavior due to the microphase separation of ionic aggregates with adjacent low glass transition temperature soft segments. Multiple peaks were observed in small-angle X-ray scattering (SAXS) profiles, which indicated that ionic aggregation was present in the ionene films. Rod-like structures were observed with transmission electron microscopy (TEM), which further demonstrated microphase separation of the ionic domains from the PTMO soft segment. Later, Wilkes et al. prepared ionenes from a reaction of telechelic PTMO dioxonium ions and either 4,4'-bipyridine or 1,2-bis(4-pyridinium)ethylene.[11] These ionenes showed a single scattering peak in SAXS profiles, which indicated the presence of ionic aggregates. The absence of higher-order scattering peaks indicated that a long-range ordered structure was not formed. However, the ionenes still possessed excellent mechanical properties, including tensile strengths greater than 30 MPa and elongations greater than 800%.

Ionenes offer many potential uses in emerging biomedical applications. Earlier research in non-viral gene delivery vectors has typically involved cationic polymers such as poly(ethylene imine) (PEI),[12] poly(L-lysine),[13] and poly(2-dimethylaminoethyl methacrylate) (PDMAEMA).[14,15] Since DNA does not efficiently cross cell membranes in the absence of a vector due to charge repulsion, cationic ionenes also complex DNA, which allows DNA to be transported across the cell membrane.[16] Izumrudov et al. formed polyelectrolyte complexes (PEC) of symmetric and asymmetric aliphatic ionenes with calf thymus DNA to explore the influence of added salt on PEC stability.[17] Later, in collaboration with Langer et al., Izumrudov explored the effect of polymer chain length and charge density on effective gene delivery.[18]

Ionenes are also used in antimicrobial applications due to their ability to disrupt bacterial cellular membranes.[19] The concentration, charge density, hydrophobicity, and molecular weight dictate whether an ionene is suitable for DNA delivery or antimicrobial applications.[20,21]

One potential limitation of conventional ionenes compared to pendant tertiary amines, such as PDMAEMA, is the presence of permanent positive charge on all quaternary nitrogens. The endosome must release the polyplex to deliver the therapeutic DNA.[22,23] Polymers containing tertiary amines allow for pH-sensitivity, since the presence of a charge is pH dependent. It is hypothesized that the polymers buffer the endosome and release the polyplex that contains the therapeutic DNA through a pH-controlled mechanism.[22,23] However, ionenes, which bear a permanent positive charge, perhaps are not suitable for efficient gene therapy due to the lack of pH control and corresponding mode of endosomal release. Nevertheless, ionenes are useful in gene therapy as model polyelectrolytes, as the charge density and molecular weight are easily adjusted.[18] In addition, the delivery of DNA from PECs based on ionene vectors does suggest a more complex endosomal release mechanism.

Ion-containing polymers typically exhibit moduli and glass transition temperatures (T_g) that are significantly higher than their non-ionic counterparts. This is primarily attributed to ionic aggregates that form physical crosslinks.[24,25] For example, Eisenberg et al. studied the aggregation phenomenon in vinylpyridinium cationic ionomers.[26] The ionic aggregates decreased the mobility of the main chain, and increasing ionic content subsequently raised the T_g. An ion-containing polymer has a higher apparent molecular weight and possesses similar mechanical properties and thermal transitions as non-ionic polymers of higher molecular weight. Reversible crosslinks, formed from ionic aggregates, allow for easier melt processability, higher melt stability, and lower melt viscosity than non-ionic polymers. Added salt has a profound

effect on the chain conformation of the polyelectrolyte, and this is well-documented within the literature, including the works of Dobrynin, Rubinstein, Eisenberg, and Holliday.[24,25,27,28] Briefly, the expanded polymer chains collapse in the presence of added salt, allowing the salt to effectively screen electrostatic interactions. Previous work in our laboratory has focused on the synthesis of telechelic poly(ethylene terephthalate) sodium sulfonate ionomers.[29] Melt rheology confirmed that the ionic end groups increased the melt viscosity compared to uncharged analogs at equivalent molecular weights. In addition, we have recently reported the novel synthesis of polymers containing complementary hydrogen bonding and cationic phosphonium salts.[30] The addition of the cationic guest drastically changed the dynamic mechanical behavior and morphology compared to the polymer in the absence of the cationic phosphonium salt. In this work, we describe the synthesis and mechanical properties of 12,12-ammonium ionenes as a function of weight-average molecular weight, and X-ray scattering revealed for the first time the morphology of 12,12-ionenes.

3.3 Experimental

3.3.1 Materials

1,12-dibromododecane (98%) was purchased from Aldrich and recrystallized from ethanol. Dimethylamine solution (60% in water) was purchased from Aldrich and used as received. Methanol (MeOH, Fisher, HPLC grade) was distilled from calcium hydride. Tetrahydrofuran (THF, EMD Science, HPLC grade), diethyl ether (Fisher, 99.9%, anhydrous), and sodium hydroxide (Mallinckrodt Chemicals, 99%) were used as received.

3.3.2 Synthesis of 1,12-bis(N,N-dimethylamino)dodecane

A modified literature procedure was used to synthesize 1,12-bis(N,N-dimethylamino)dodecane.[31] THF (125 mL) and 1,12-dibromododecane (10.10 g, 0.0308 mol) were introduced into a one-neck, round-bottomed flask, equipped with a stir bar. The flask was cooled to -78 °C for 30 min. The solution of dimethylamine (478 mL total solution) was slowly added to the flask. The flask was warmed to room temperature and the reaction was allowed to proceed for 24 h. Upon completion, the solvent was removed via rotary evaporation. The product was redissolved in ether and subsequently stirred with 2 M NaOH (aq). The layers were separated, and the ether layer was dried over magnesium sulfate and evaporated to yield a pale yellow oil. The oil was further purified via vacuum distillation (100 °C and 150 mTorr) to yield a colorless liquid. The final product was obtained in 47% yield. ^{1}H NMR (400 MHz, CD_3OD) δ = 2.81 (t, 4H), 2.16 (s, 12H), 1.39 (dd, 4H), 1.22 (m, 16H). ^{13}C NMR (100 MHz, CD_3OD): δ=123.8, 59.7, 44.3, 29.6, 29.5, 27.5, 27.2. FAB MS: m/z = 257.29 (found), m/z = 256.48 (calculated).

3.3.3 Synthesis of 12,12-ammonium ionenes

1,12-dibromododecane (1.28 g, 0.0039 mol) and 1,12-bis(N,N-dimethylamino)dodecane (1.00 g, 0.0039 mol) were added to a two-neck, round-bottomed flask equipped with a stir bar, condenser, and nitrogen inlet. Freshly distilled MeOH was added to the flask via syringe. The reaction was allowed to proceed for 24 h at 80 °C. Upon completion, the polymer was cast into a film for further characterization. The drying procedure for film preparation was critical, and slow removal of methanol was required to avoid formation of film defects. First, the polymer was dissolved in MeOH (approximately 50 wt%) and poured in a Teflon™ mold. Methanol was allowed to evaporate in ambient conditions for 3 days. Subsequently, the films were heated in

the Teflon™ molds at approximately 60-70 °C for at least 2-3 days. Finally, the polymer films were subsequently dried *in vacuo* (0.1 mm Hg) at room temperature for 24 h to ensure complete removal of MeOH. ^{1}H NMR (400 MHz, CD_3OD) δ = 3.31 (m, 8H per repeating unit, $CH_2N^+(CH_3)_2CH_2$), 3.05 (s, 12H per repeating unit, $CH_2N^+(CH_3)_2CH_2$), 1.75 (m, 8H per repeating unit, $CH_2CH_2N^+(CH_3)_2CH_2CH_2$), 1.3-1,4 (m, 32H per repeating unit, $(CH_2)_8CH_2CH_2N^+(CH_3)_2$).

3.3.4 Characterization

^{1}H NMR was utilized to determine monomer and polymer composition in $CDCl_3$ or CD_3OD at 23 °C with a 400 MHz Varian UNITY spectrometer. FAB-MS was obtained on a JOEL HX110 dual focusing mass spectrometer. Thermogravimetric analysis (TGA) was conducted on a TA Instruments Hi-Res TGA 2950 with a temperature ramp of 10 °C/min in a nitrogen atmosphere. Dynamic mechanical analysis (DMA) was conducted on a TA Instruments Q800 dynamic mechanical analyzer in tension mode at a frequency of 1 Hz and temperature ramp of 3 °C/min. The glass transition temperature (T_g) was determined at the peak of the tan δ curve. Stress-strain experiments were conducted with dogbone-shaped film specimens, which were cut with a die according to ASTM D3368 specifications. Tensile tests were performed on a 5500R Instron universal testing instrument with a cross-head speed of 13 mm/min using manual grips at ambient temperature.

Size exclusion chromatography (SEC) was performed using a Waters size exclusion chromatograph. The instrument was equipped with Waters 1515 isocratic HPLC pump, Waters 717plus autosampler, Wyatt miniDAWN multiangle laser light scattering (MALLS) detector operating a He-Ne laser at 690 nm, Viscotek 270 viscosity detector, and a Waters 2414 differential refractive index detector operating at 880 nm and 35 °C. A flow rate of 0.8 mL/min

in 54:23:23 H_2O:MeOH:acetic acid (v/v/v), 0.54 M NaAc, 200 ppm NaN_3, pH = 4 was used. Reported weight-average molecular weights are based on absolute measurements using the MALLS detector. The specific refractive index increment (*dn/dc*) was calculated using a Wyatt OptiRex differential/absolute refractive index detector operating at 690 nm and 30 °C. After allowing the polymers to dissolve in the SEC solvent for 18 h, samples were injected via a syringe pump that was equipped with a 0.45 μm PTFE syringe filter into the RI detector at a rate of 0.8 mL/min. The *dn/dc* values were determined using the Wyatt Astra V software package.

The solvent-cast and dried ionene films were used directly for X-ray scattering characterization. The multi-angle X-ray scattering system (MAXS) generated Cu X-ray from a Nonius FR 591 rotating-anode generator operated at 40 kV and 85 mA. The beam was focused by doubly-focusing mirror-monochromator optics in an integral vacuum system. The scattering data were collected over an interval of 1 h using a Bruker Hi-Star multiwire detector with a sample to detector distance of 11 and 54 cm. The 2-D data reduction and analysis were performed using *Datasqueeze* software.[32]

3.4 Results and discussion

The synthetic strategy (Scheme 3.1) for the preparation of 1,12-bis(N,N-dimethylamino)dodecane was adapted from Spencer et. al.[31] ^{1}H NMR spectroscopy confirmed the structures of the diamine and dihalide. 1,12-dibromododecane was recrystallized from ethanol and subsequently dried *in vacuo* (0.1 mm Hg) at room temperature for 24 h prior to polymerization. A series of 12,12-ammonium ionenes were successfully synthesized via the Menschutkin reaction in a single step from the dihalide and diamine (Scheme 3.2). The reactions were allowed to proceed for 24 h in refluxing methanol. ^{1}H NMR spectroscopy confirmed the final polymer structure.

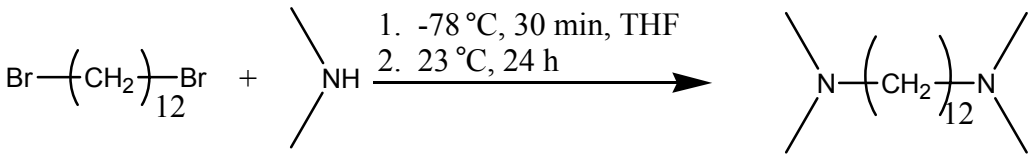

Scheme 3.1. Synthesis of 1,12-bis(N,N-dimethylamino)dodecane.

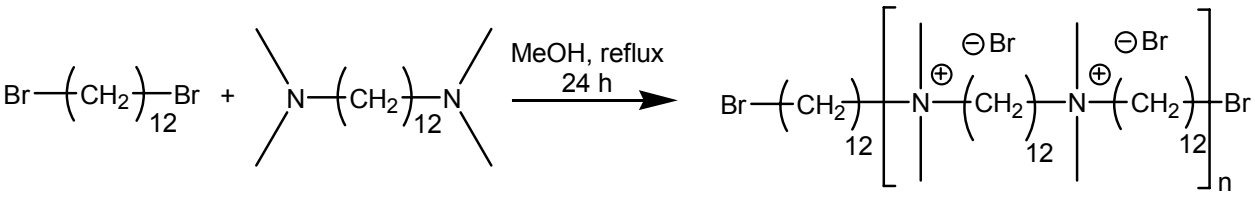

Scheme 3.2. Synthesis of bromine-terminated 12,12-ammonium ionenes.

It is well known that a 1:1 stoichiometry is required to obtain high molecular weight polymers via step growth polymerizations;[33] however, in some cases, it is advantageous to limit molecular weight. One can achieve molecular weight control in step-growth polymerization through the addition of monofunctional reagents, limited difunctional monomer conversion, or through a stoichiometric imbalance of difunctional monomers.[34] The latter method is preferred because the resulting polymers possess chain ends with the same functionality as the excess monomer. In this case, both monomers are completely consumed, and this results in a stable polymer that cannot increase in molecular weight during a post-polymerization process.[34,35] In our work, excess dihalide resulted in polymers possessing alkyl bromide end groups. The Carother's equation was utilized to predict molecular weights as a function of the monomer stoichiometry.[35] As shown in Table 3.1, the obtained experimental M_w values were consistent with the calculated molecular weight values, as expected for a controlled step-growth polymerization process. Controlled weight-average molecular weights ranging from 4,300 to 20,900 g/mol (Table 3.1 and Figure 3.1) were obtained using a stoichiometric imbalance. The chromatograms based on the light scattering detector are shown in Figure 3.1. It is important to note that the chromatograms are monomodal, and significant interaction of the polymer with the

stationary phase of the column was not observed. Performing successful aqueous SEC on polyelectrolytes is often difficult due to problems associated with polymer-column interactions and sample aggregation in the mobile phase.[36] A manuscript, which describes the establishment of these suitable chromatographic conditions in more detail, was recently submitted.[37]

Monomer Molar Ratio	**Calculated Molecular Weight (g/mol)**	M_w **(g/mol)**†	M_n **(g/mol)***	M_w **(g/mol)***	M_w/M_n*
1.00:1.00	-	20900	10700	26900	2.52
1.00:1.03	19800	17800	9700	23000	2.36
1.00:1.05	12000	14600	6900	17000	2.45
1.00:1.07	8600	12300	6800	17000	2.50
1.00:1.10	3200	4300	1900	4900	2.63

Table 3.1. Ionene ditertiary amine monomer: dihalide monomer molar ratios and corresponding molecular weights. Calculated molecular weights for offset stoichiometry determined from Carother's equation. †Molecular weights are absolute and determined from the MALLS detector. *PEO/PEG equivalent molecular weights determined using dRI retention volumes/times.

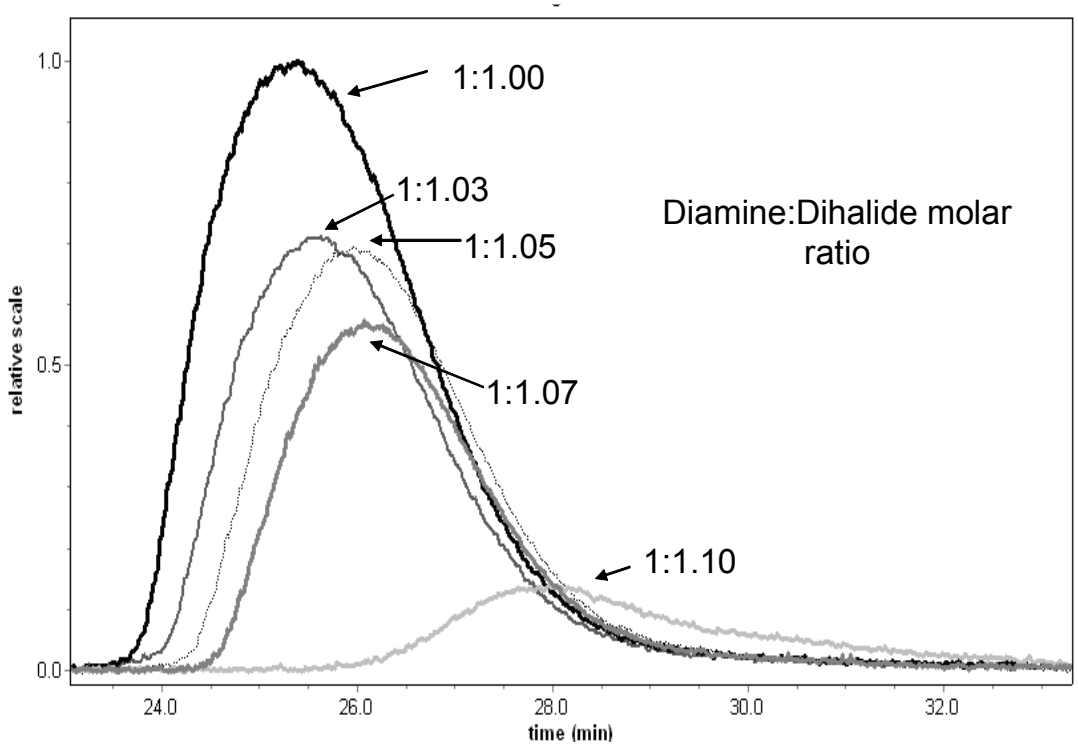

Figure 3.1. SEC MALLS traces of the bromine-terminated 12,12-ammonium ionenes.

An amino-terminated polymer was also synthesized using a 1.05:1.00 molar ratio of 1,12-bis(N,N-dimethylamino)dodecane and 1,12-dibromododecane. The reaction was allowed to proceed for 24 h in refluxing methanol. The amino-terminated polymer was prepared to compare ^{1}H NMR spectroscopy number-average molecular weights and SEC molecular weights, and thus determine if the SEC measurements were reliable. The methyl groups attached to the amino nitrogen end group were easily detected with ^{1}H NMR spectroscopy. End group analysis indicated a number average molecular weight of 7600 g/mol (Figure 3.2). Aqueous SEC was utilized to determine the molecular weight of the identical polymer, and the resulting M_n was 8400 g/mol. Saito and co-workers examined the reliability of SEC-MALLS and ^{1}H NMR to confirm the molecular weight of low molecular weight polystyrene standards that ranged from 500 to 2400 g/mol.[38] Their study concluded that MALLS detection was reliable, even at low molecular weights. Thus, the results obtained with ^{1}H NMR and SEC-MALLS were comparable

for the amino-terminated 12,12-ammonium ionene and supported the reliability of the SEC-MALLS reported herein.

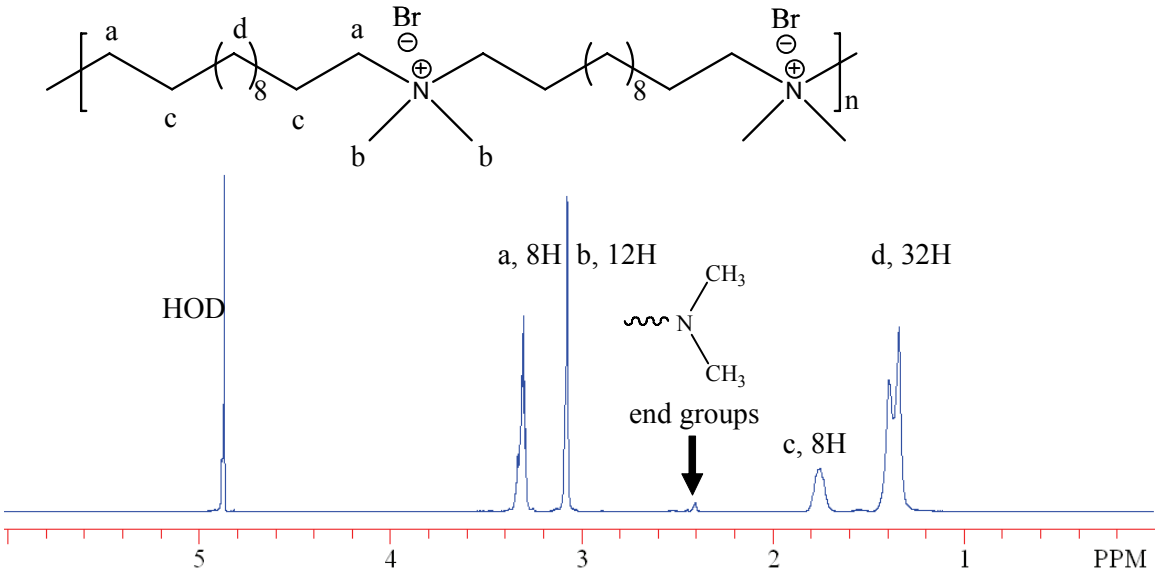

Figure 3.2. ^{1}H NMR spectrum of an amino-terminated 12,12-ammonium ionene.

Thermal stability was measured via thermogravimetric analysis (TGA), and all polymers typically exhibited 5% weight loss at approximately 225 °C (Figure 3.3). The thermal degradation occurred in a single step, which Ruckenstein et al.[39] and Jerome et al.[40] attributed to the dequaternization of the nitrogen, although the actual mechanism of thermal decomposition is complex.[41] Charlier and co-workers extensively studied the thermal stability of telechelic polystyrene containing quaternary ammonium ionic groups.[42] They concluded that the Hofmann elimination occurred at the end groups of the telechelic polymers via the analysis of both pristine and degraded polymers using a combination of TGA, high-performance liquid chromatography (HPLC), and mass spectroscopy. The onset degradation values reported herein are similar to those reported by Tanaka et al. for various ionenes including 12,n-ionenes (250 °C).[43]

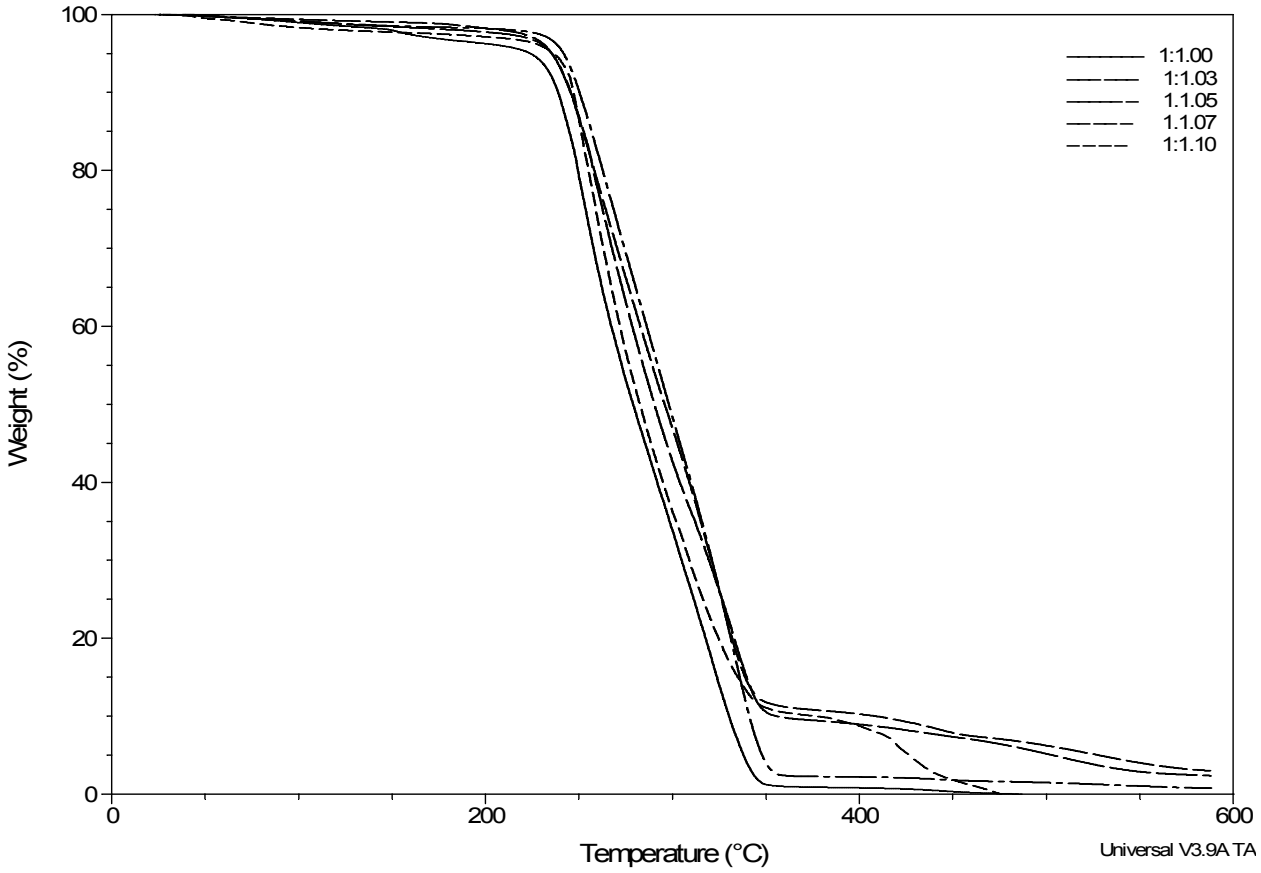

Figure 3.3. TGA curves for bromine-terminated 12,12-ammonium ionenes. Molar ratios in graph legend correspond to the diamine:dihalide molar ratios.

It is well-documented in the literature that the Hofmann elimination also occurs in the presence of base, converting a tetraalkylammonium salts to an alkenes and dimethylamines (Scheme 3.3).[44,45] Chemical degradation of the 20,900 g/mol 12,12-ionene was also observed in the presence base. An experiment was conducted in 1 M NaOH solution at 23 °C for 24 h. After the reaction was complete, the SEC results indicated that the polymer was partially degraded, as the M_n decreased from 20,900 to 2,500 g/mol. Differential RI traces before and after the reaction are shown in Figure 3.4. The monomodal, symmetrical peak for the 20,900 g/mol 12,12-ammonium ionene became multi-modal and unsymmetrical after the reaction. Furthermore, the presence of dimethyl amino groups was observed in the ^{1}H NMR spectrum, which indicated that

the nitrogen of the tetraalkylammonium salt was the site of degradation. The degradation study was performed at a concentration of 0.01 g/mL. Although concentration was not addressed in this study, it is presumed that concentration may influence the formation of various side products including cyclic species at more dilute concentrations. This will be the focus of a future study. Ionene degradation in the presence of base shows promise as a means to convert mechanically strong films and coatings to low mass monomers in the presence of base upon disposal. In fact, our current efforts involve monomer selection to ensure more environmentally friendly byproducts upon degradation.

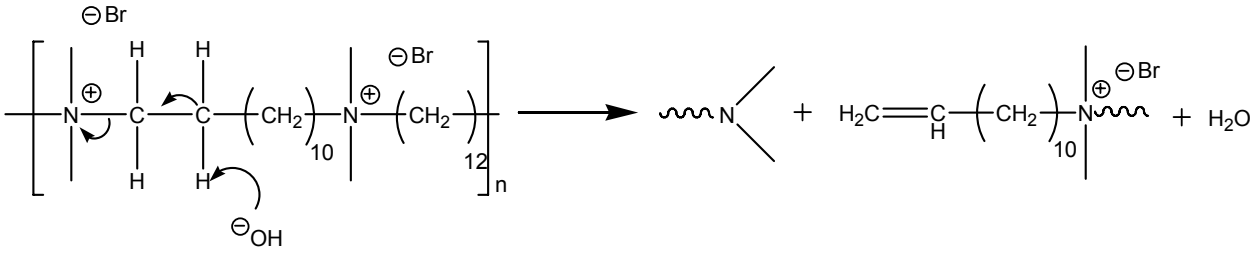

Scheme 3.3. Mechanism of the base-promoted Hofmann elimination reaction for 12,12-ionenes.

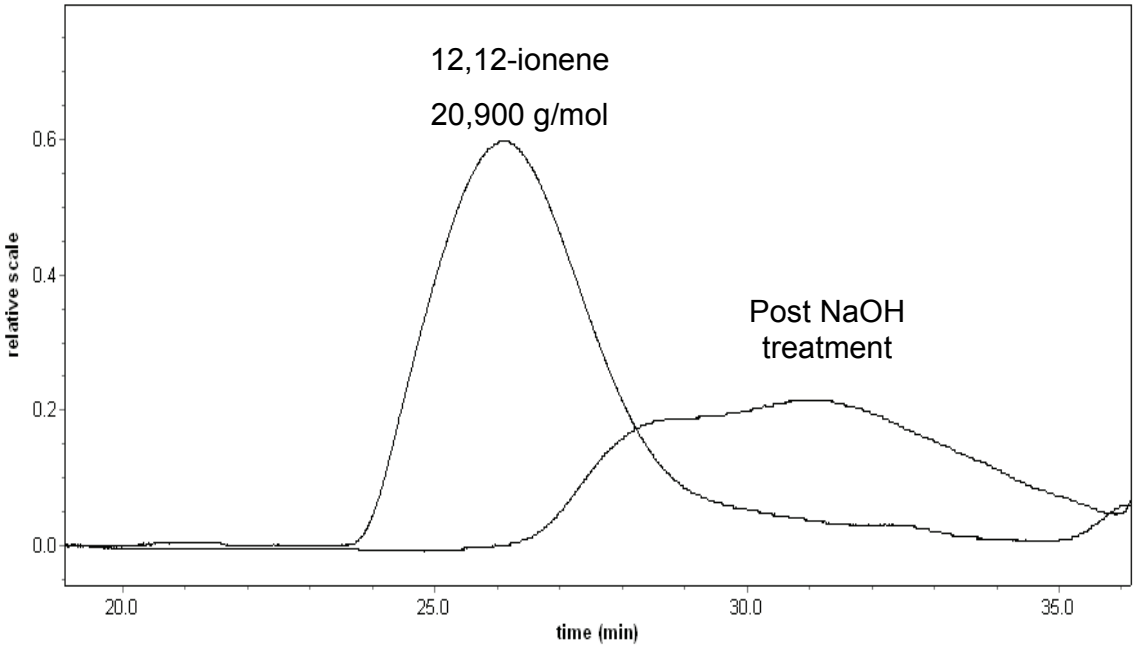

Figure 3.4. SEC dRI traces of the 12,12-ammonium ionene before and after degradation in the

presence of base.

DSC analysis revealed the expected dependence of T_g on molecular weight. The highest molecular weight ionene had the greatest T_g, and the values ranged from 24-69 °C. A melting transition was not observed to 200 °C. Thus, the presence of a crystalline melting point would have to occur above 200 °C, which is near the degradation temperature (~225 °C). DMA of the ammonium ionenes revealed two transitions, as expected for ion-containing polymers that form ionic aggregates.[28,46,47] The lower temperature transition was assigned to the T_g and the second, higher temperature transition was attributed to ionic aggregate dissociation (Table 3.2). The dissociation of ionic aggregates in aliphatic ionenes has not been previously reported. Eisenberg and co-workers have extensively studied the dynamic mechanical properties of ionomers with various ionic contents.[48] At lower ionic content, a second transition occurred at temperatures above the matrix T_g, and this transition was termed the cluster T_g. As the ionic content increased, both the matrix and cluster T_g increased. Kim and co-workers studied the dynamic mechanical behavior of sulfonated poly(butylene succinate) ionomers and found that ion-pair associations caused the polymer chains to collapse and cause a decrease in the viscosity and radius of gyration.[49,50] Eisenberg and co-workers determined with sodium salts of styrene-methacrylic acid copolymers that macromolecular ionic dissociation only occurred if the ion content was sufficient for aggregates to form.[28,46,47] In the case of ionenes, the T_g (tan δ maximum) increased with increasing molecular weight, and ranged from 61-88 °C, and the ionic aggregate dissociation occurred at higher temperatures, typically 85-88 °C. It is interesting to note that the ionic aggregate dissociation was independent of molecular weight. The T_g was not reported from the onset of storage modulus loss, since the transition was broad. In fact, the temperature that corresponded to the onset of storage modulus loss was approximately the same temperature as T_g

midpoint as determined via DSC. Interestingly, there was overlap of the T_g and the ionic aggregate dissociation temperature for the 20,900 g/mol ionene due to increasing molecular weight. It was presumed that the ionic aggregate dissociation temperature remained nearly constant, since the ion content remained unchanged as molecular weight increased. In addition, the presence of end groups is presumed to have an insignificant effect on the ionic aggregate dissociation temperature, since over the range of molecular weights, the aggregate dissociation temperature did not change. Furthermore, all of the ionenes have equal equivalent molecular weight and ion content.

M_w (g/mol)	T_g (°C)	Ionic Dissociation (°C)
20900	88	88
17800	69	85
14600	69	88
12300	61	87

Table 3.2. Ionene molecular weight and corresponding thermal transitions. The T_g was determined from maximum in tan δ versus temperature graphs. Second transition corresponds to the ionic aggregate disassociation.

Tensile properties revealed high ultimate mechanical strength, as shown in Table 3.3. This is the first report of tensile analysis of 12,12-ionenes to the best of our knowledge. As the M_n of the ionene decreased, the stress at break decreased from 26.4 MPa to 16.2 MPa. Furthermore, the strain at break decreased from 440% to 230%. Yield stress was approximately identical for all three polymers (22 MPa). The relaxation of the polymer chains during tensile testing and subsequent collapse of the ionic aggregates may cause similar yield points, despite the variation in polymer molecular weights.[51] Tensile analysis was not performed on the lower

molecular weight samples due to their brittle nature. The tensile performance of 12,12-ionene compared well to the earlier literature for polyurethane ionene rotaxanes.[51] In Wilkes' earlier work, the stress at break ranged from 17 to 34 MPa, and the elongation ranged from 114 to 807%.

M_w (g/mol)	Stress at Break (MPa)	Strain at Break (%)	Stress at Yield (MPa)	Toughness (MPa)
20900	26.4 ± 1.0	440 ± 45	21.5 ± 2.8	84.3 ± 7.1
17800	33.0 ± 3.0	360 ± 42	22.9 ± 3.9	85.8 ± 13.1
14600	16.2 ± 2.4	230 ± 31	22.9 ± 9.2	39.8 ± 5.9

Table 3.3. Tensile data for 12,12-ammonium ionene films as a function of molecular weight.

X-ray scattering was performed on stretched and unstretched 20,900 g/mol 12,12-ionene films. The stretched sample was elongated ~ 200% with heating at 70 °C. Both stretched and unstretched films were isotropic as evident in the two-dimensional scattering patterns (Figure 3.5). Both films were also amorphous with a broad amorphous peak at ~ 14 nm^{-1}, and crystalline peaks corresponding to polyethylene were not observed. This result was consistent with DSC and DMA data. In addition, there was a scattering peak at 4.38 nm^{-1}, which corresponded to a real-space distance of 1.43 nm. While the ammonium groups prevented crystallization, these ionic groups assembled into ionic domains. The correlation distance between these domains was well-defined because the separation between ionic groups was exactly 12 methylene groups. If this polyethylene segment was in the all-*trans* crystalline conformation, the ammonium-ammonium separation would be 1.60 nm. The somewhat smaller separation observed here was consistent with the amorphous morphology.

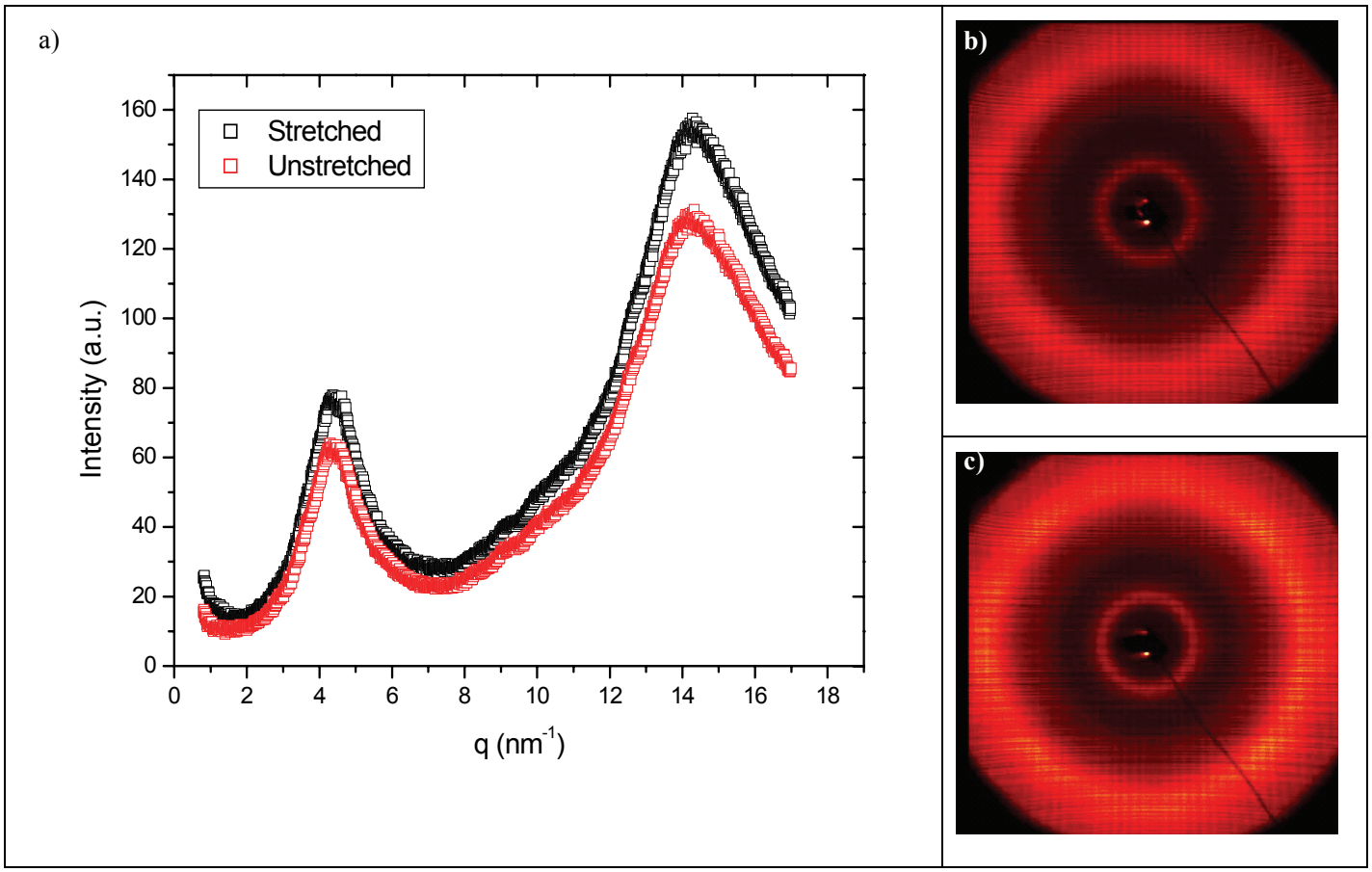

Figure 3.5. X-ray scattering profiles of the 1:1 12,12-ionene. a) Scattering intensity vs. q for stretched (200 %) and unstretched 12,12-ammonium ionenes films; b) Wide-angle X-ray scattering pattern of stretched (200 %) ionene film; c) Wide-angle X-ray scattering pattern of unstretched ionene film.

Wagener and co-workers have also synthesized a periodic ionomer, and their reported morphology was similar to this work.[52] The poly(ethylene-*co*-acrylic acid) (EAA) copolymer had 9, 15 or 21 methylene groups between pendant carboxylic acid groups. As in the 12,12-ionene, the correlation lengths between acid groups was comparable or somewhat smaller than the all-*trans* polyethylene conformation. However, in sharp contrast to the 12,12-ionene, the EAA copolymer with the longest polyethylene spacer (21 methylene units) exhibited crystallinity

and multiple reflections indicated that packing was more regular. In a similar fashion to the 12,12-ionene, the EAA copolymer with the 15 methylene units between acid groups remained anisotropic upon stretching. In both the EAA copolymers and 12,12-ionenes, the primary structure of the polymers dictated the nanoscale morphology. The comparison of ammonium ionenes to EAA copolymers may also suggest the relatively more efficient aggregation of metal carboxylates versus large, organic ammonium cations as reported earlier.[53,54]

The shape memory properties of 12,12-ammonium ionenes was evaluated using a sample that was deformed from tensile analysis. After tensile tests, the ionenes remain tough, in a curled state, as shown in Figure 3.6. At ambient temperatures and low humidity, the sample remained in this conformation for approximately 2 years. Upon heating at 90 ± 1 °C, the ionic aggregate dissociation temperature, the sample returned to the original shape and dimensions. This phenomenon took place over ~ 30 s. It is important to note that flow of the polymer chains does not occur until ~120 °C, as evidenced via DMA. Therefore, the ionic aggregates must be responsible for this behavior.

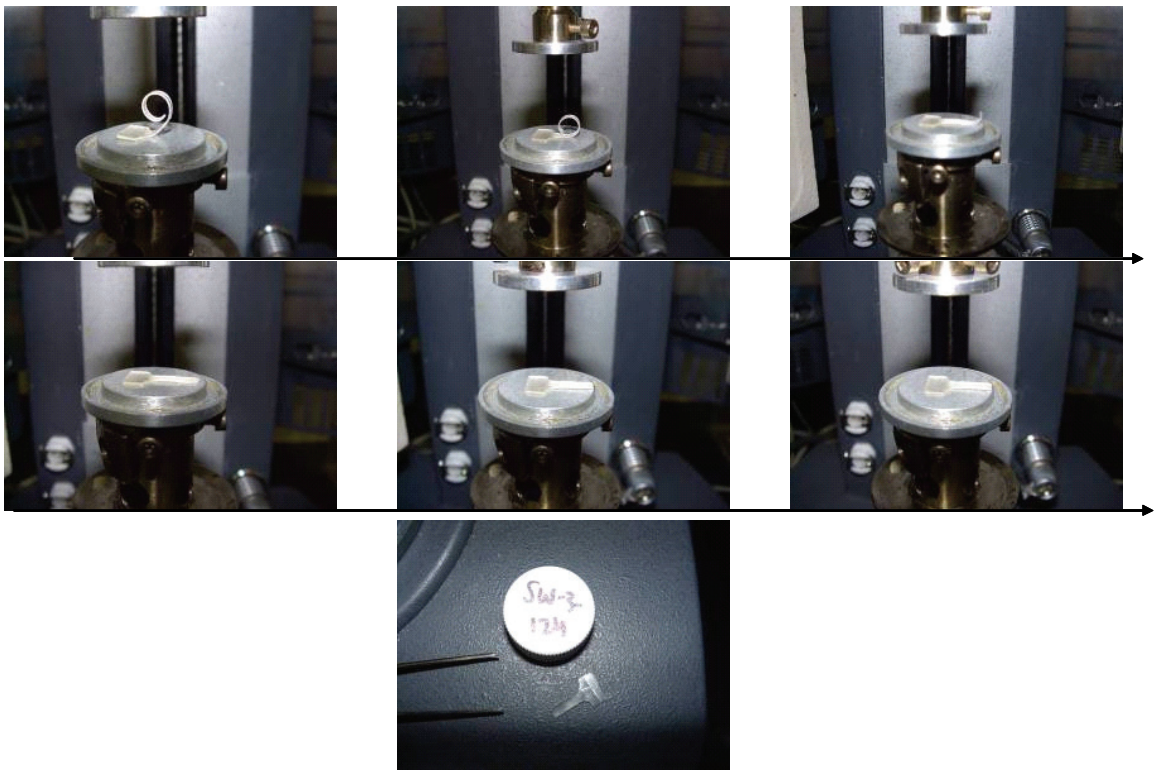

Figure 3.6. 12,12-ammonium ionene demonstrating shape memory properties.

The surface of a 12,12-ammonium ionene film (M_w = 20900 g/mol) was scribed with a razor blade in an "X" shape to evaluate the self-healing properties. The film was placed under an optical microscope equipped with a heating stage. Upon heating, the "X" fills in and becomes almost invisible, as shown in Figure 3.7, particularly where the arrow indicated the most evidence for self-healing. Again, this property was attributed to the presence of ionic aggregates, which dissociate with heating prior to the flow temperature.

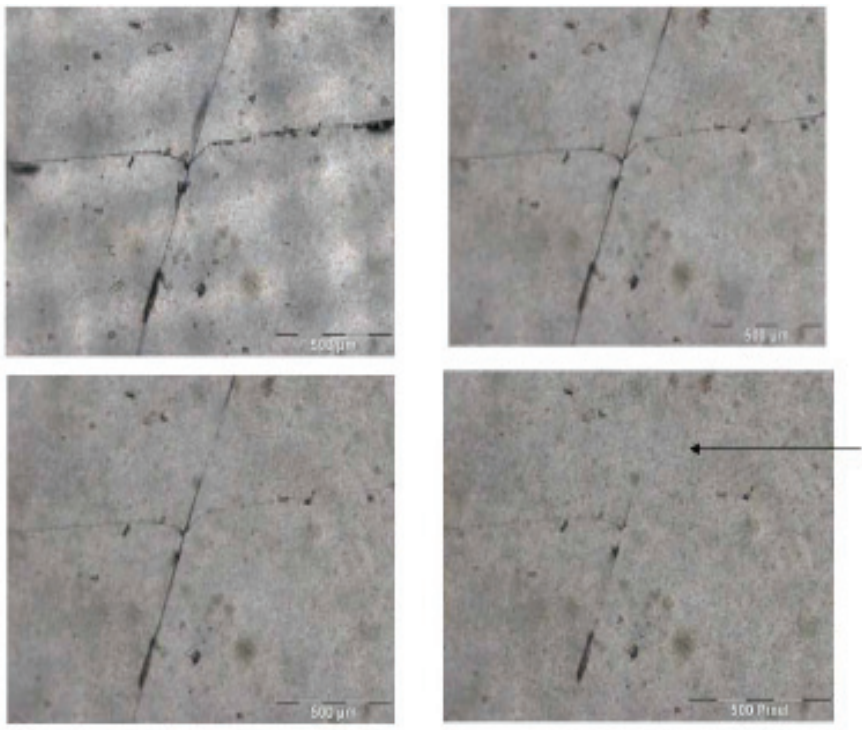

Figure 3.7. 12,12-ammonium ionenes demonstrating self-healing properties under an optical microscope equipped with a heating stage.

3.5 Conclusions

The Menschutkin reaction was used to prepare a series of water-soluble 12,12-ammonium ionenes from 1,12-dibromododecane and 1,12-bis(N,N-dimethylamino)dodecane. The macromolecular structures were confirmed with ^{1}H NMR spectroscopy, and the absolute weight-average molecular weights were determined for the first time using multi-angle laser light scattering (MALLS) with aqueous size exclusion chromatography (SEC). Relationships between molecular weight and mechanical performance were established for a series of 12,12-ammonium ionenes using tensile testing and dynamic mechanical analysis (DMA). The water-soluble polymers possessed greater than room temperature glass transition temperatures and ionic aggregate disassociation temperatures of 85 to 88 °C. Tensile analysis of the higher molecular

weight ionenes revealed an average yield stress of 22 MPa and elongations ranging from 230 to 440%. The morphology was examined with X-ray scattering, and it was discovered that the steric hindrance of ammonium groups inhibited the close packing and crystallization of the relatively short polyethylene segment between the charges. Specifically, X-ray scattering indicated the formation of ion-rich domains, with an average separation that correlated with the methylene spacer length between the charged groups. Degradation studies in the presence of base support the possibility for water-soluble coatings with excellent mechanical durability that are amenable to triggered depolymerization. Shape memory and self-healing experiments were successful and demonstrated for the first time the ability of ionenes to self-heal and possess shape memory.

3.6 Acknowledgements

This material is based upon work supported in part by the Macromolecular Interfaces with Life Sciences (MILES) Integrative Graduate Education and Research Traineeship (IGERT) of the National Science Foundation under agreement no. DGE-0333378. This material is based upon work supported in part by the U.S. Army Research Office under grant number W911NF-07-1-0452 Ionic Liquids in Electro-Active Devices (ILEAD) MURI. This material is based upon work supported in part by the Kimberly Clark Corporation, and we acknowledge helpful discussions with Dr. Clay Bunyard.

3.7 References

(1) Gibbs, C. F.; Littman, E. R.; Marvel, C. S. *J. Am. Chem. Soc.* **1933,** 55, 753.
(2) Abboud, J. L. M.; Notario, R.; Bertran, J.; Sola, M. *Prog. Phys. Org. Chem.* **1993,** 19, 1-182.
(3) Casson, D.; Rembaum, A. *Macromolecules* **1972,** 5, (1), 75-81.
(4) Noguchi, N.; Rembaum, A. *Macromolecules* **1972,** 5, (3), 253-260.
(5) Rembaum, A.; Noguchi, N. *Macromolecules* **1972,** 5, (3), 261-269.

(6) Leyte, J. C.; Mandel, M. *J. Polym. Sci. A* **1964,** 2, (4), 1879-91.
(7) Sonnessa, A. J.; Cullen, W.; Ander, P. *Macromolecules* **1980,** 13, 195-196.
(8) Knapick, E. G.; Hirsch, J. A.; Ander, P. *Macromolecules* **1985,** 18, 1015-1021.
(9) Salamone, J. C.; Snider, B. *J. Polym. Sci. A-Polym. Chem.* **1970,** 8, (12), 3495-3501.
(10) Feng, D.; Wilkes, G. L.; Leir, C. M.; Stark, J. E. *J. Macromol. Sci.-Chem.* **1989,** A26, (8), 1151-1181.
(11) Feng, D.; Wilkes, G. L.; Lee, B.; McGrath, J. E. *Polymer* **1992,** 33, (3), 526-535.
(12) Boussif, O.; Lezoualch, F.; Zanta, M. A.; Mergny, M. D.; Scherman, D.; Demeneix, B.; Behr, J.-P. *Proc. Natl. Acad. Sci. USA* **1995,** 92, 7297-7301.
(13) Zauner, W.; Ogris, M.; Wagner, E. *Advanced Drug Delivery Reviews* **1998,** 30, (1-3), 97-113.
(14) Layman, J. M.; Hirani, A. A.; McKee, M. G.; Britt, P. F.; Pickel, J. M.; Lee, Y. W.; Long, T. E. *Polymer Preprints* **2006,** 47, (1), 39-40.
(15) Layman, J. M.; Hirani, A. A.; Pickel, J. M.; Britf, P. F.; Lee, Y. W.; Long, T. E. *Polymer Preprints* **2006,** 47, (2), 70-71.
(16) Trukhanova, E. S.; Litmanovich, A. A.; Zelikin, A. N. *Biomacromolecules* **2005,** 6, 3198-3201.
(17) Zelikin, A. N.; Litmanovich, A. A.; Paraschuk, V. V.; Sybatchin, A. V.; Izumrudov, V. A. *Macromolecules* **2003,** 36, (6), 2066-2071.
(18) Zelikin, A. N.; Putnam, D.; Shastri, P.; Langer, R.; Izumrudov, V. A. *Bioconjugate Chemistry* **2002,** 13, (3), 548-553.
(19) Fitzpatrick, R. J.; Shackett, K. K. *WO 2004045629* **2004,** PCT Int. Appl.
(20) Narita, T.; Nishino, M.; Gong, J. P.; Osada, Y. *Colloid and Polymer Science* **2000,** 278, 884-887.
(21) Tashiro, T. *Macromolecular Materials and Engineering* **2001,** 286, 63-87.
(22) Putnam, D.; Gentry, C. A.; Pack, D. W.; Langer, R. *Proc. Natl. Acad. Sci. USA* **2001,** 98, (3), 1200-1205.
(23) Zhao, X.; Pan, F.; Zhang, Z.; Grant, C.; Ma, Y.; Armes, S. P.; Tang, Y.; Lewis, A. L.; Waigh, T.; Lu, J. R. *Biomacromolecules* **2007,** 8, 3493-3502.
(24) Eisenberg, A.; King, M., *Ion containing polymers*. Academic Press: New York, 1977.
(25) Holliday, L., Ed., *Ionic polymers*. Halstead Press: New York, 1975.
(26) Gauthier, S.; Duchesne, D.; Eisenberg, A. *Macromolecules* **1987,** 20, 753-759.
(27) Dobrynin, A. V.; Rubinstein, M. *Prog. Polym. Sci.* **2005,** 30, 1049-1118.
(28) Eisenberg, A.; Hird, B.; Moore, R. B. *Macromolecules* **1990,** 23, 4098.
(29) Kang, H.; Lin, Q.; Armentrout, R. S.; Long, T. E. *Macromolecules* **2002,** 35, 8738-8744.
(30) Mather, B. D.; Baker, M. B.; Beyer, F. L.; Green, M. D.; Berg, M. A. G.; Long, T. E. *Macromolecules* **2007,** 40, 4396-4398.
(31) Spencer, T. A.; Onofrey, T. J.; Cann, R. O.; Russel, J. S.; Lee, L. E.; Blanchard, D. E.; Castro, A.; Gu, P.; Jiang, G. J.; Shechter, I. *J. Org. Chem.* **1999,** 64, (3), 807-818.
(32) Heiney, P. A. *Comm Powder Diffr Newsletter* **2005,** 32, 9-11.
(33) Rogers, M. E.; Long, T. E.; Turner, S. R., Introduction to synthetic methods in step-growth polymers. In *Synthetic Methods in Step-Growth Polymers*, Rogers, M. E.; Long, T. E., Eds. Wiley-Interscience: Hoboken, N.J., 2003; pp 1-16.
(34) Odian, G., *Priciples of polymerization*. 4th ed.; Wiley-Interscience: Hoboken, 2004.
(35) Stevens, M. P., *Polymer chemistry*. 3rd ed.; Oxford University Press: Oxford, 1999.
(36) Jiang, X.; van der Horst, A.; van Steenbergen, M. J.; Akeroyd, N.; van Nostrum, C. F.;

Schoenmakers, P. J.; Hennink, W. E. *Pharm. Res.* **2006,** 23, (3), 595-603.
(37) Layman, J. M.; Borgerding, E. M.; Williams, S. R.; Heath, W. H.; Long, T. E. *Macromolecules* **2008,** 41, (13), 4635-4641.
(38) Saito, T.; Lusenkova, M. A.; Matsuyama, S.; Shimada, K.; Itakura, M.; Kishine, K.; Sato, K.; Kinugasa, S. *Polymer* **2004,** 45, 8355-8365.
(39) Ruckenstein, E.; Chen, X. N. *Macromolecules* **2000,** 33, (24), 8992-9001.
(40) Yano, S.; Tadano, K.; Jerome, R. *Macromolecules* **1991,** 24, (24), 6439-6442.
(41) Grassl, B.; Galin, J. C. *Macromolecules* **1995,** 28, (21), 7035-7045.
(42) Charlier, P.; Jerome, R.; Teyssie, P.; Prud'homme, R. E. *J. Polym. Sci. A* **1993,** 31, 128-134.
(43) Tsutsui, T.; Tanaka, R.; Tanaka, T. *J. Polym. Sci. Polym. Phys. Ed.* **1976,** 14, (12), 2259-2271.
(44) Vollhardt, K. P. C.; Schore, N. E., *Organic chemistry: Structure and function*. 3rd ed.; W.H. Freeman and Company: New York, 1999.
(45) March, J., *Advanced organic chemistry: reactions, mechanisms, and structure*. 3rd ed.; Wiley: New York, 1985.
(46) Arai, K.; Eisenberg, A. *J. Macromol. Sci. Phys.* **1980,** B17, 803.
(47) Hodge, I. M.; Eisenberg, A. *Macromolecules* **1978,** 11, 283.
(48) Kim, J.-S.; Wu, G.; Eisenberg, A. *Macromolecules* **1994,** 27, 814-824.
(49) Han, S.-I.; Ima, S. S.; Kim, D. K. *Polymer* **2003,** 44, 7165-7173.
(50) Lundberg, R. D.; Phillips, R. R. *J. Polym. Sci., Polym. Phys. Ed.* **1982,** 20, 1143.
(51) Loveday, D.; Wilkes, G. L.; Bheda, M. C.; Shen, Y. X.; Gibson, H. W. *J. Macro. Sci., Part A* **1995,** 32, (1), 1-27.
(52) Baughman, T. W.; Chan, C. D.; Winey, K. I.; Wagener, K. B. *Macromolecules* **2007,** 40, 6564-6571.
(53) Capek, I. *Advances in Colloid and Interface Science* **2004,** 112, (1-3), 1-29.
(54) Capek, I. *Advances in Colloid and Interface Science* **2005,** 118, 73-112.

Chapter 4: Influence of Molecular Weight on the Cytotoxicity of 12,12-Ammonium Ionenes

4.1 Abstract

Ionenes are ideal candidates for model polyelectrolytes in biomedical applications. A thorough analysis was conducted on SY5Y and COS-7 cell lines to determine the cytotoxicity of ionenes at various concentrations that are typical for gene transfection and antimicrobial action. Specifically, 12,12-ammonium ionenes prepared via a Menschutkin reaction of 1,12-dibromododecane and 1,12-bis(N,N-dimethylamino)dodecane were used in the present investigation. Concentrations of ionenes ranged from 1-800 μg/mL, and significant cell viability was observed at concentrations less than 25 μg/mL, regardless of cell line utilized. Overall, there was not a direct correlation between ionene weight-average molecular weight and cell viability for the molecular weight range described herein. To determine the effect of assay type, Promega CellTiter 96® non-radioactive cell proliferation and Cell Titer-Glo® luminescent cell viability assays were compared.

4.2 Introduction

Cationic polyelectrolytes offer potential in many biomedical applications, including antimicrobial coatings,[1,2] gene delivery,[3,4] tissue scaffolds,[5] drug delivery systems,[6] and coatings for medical devices.[7] Several authors have extensively reviewed the emerging applications of polyelectrolytes.[8,9] The charged site of cationic polyelectrolytes promotes binding of biological molecules, such as DNA, RNA, proteins, and specific polysaccharides. Polyelectrolytes enable many potential applications in the biomedical field, and it is imperative to develop a clear

understanding of the influence of structure and molecular weight on toxicity. The toxicity of polyelectrolytes for biomedical applications has received significant attention in the literature,[10-14] however, the literature has not revealed the toxicity of ammonium ionenes as a function of controlled molecular weight.

Ammonium polyionenes, which are commonly termed ionenes, are ion-containing polymers that contain ammonium cations in the macromolecular main chain as opposed to a pendant site. The length of each methylene spacer is denoted in ionene common nomenclature, and the common name is derived from the number of methylenes corresponding to the diamine and dihalide monomers, respectively, i.e., *x,y*-ionene (Figure 4.1).[15]

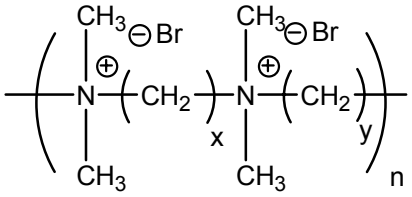

Figure 4.1. Typical structure of an *x,y*-ionene, where x represents the number of methylenes in the diamine monomer, and y represents the number of methylenes in the dihalide monomer.

The solution concentration, charge density, hydrophobicity, and molecular weight dictate suitability for DNA binding or antimicrobial applications.[16,17] For example, Izumrudov and coworkers explored the effect of degree of polymerization (DP) and charge density on effective polyelectrolyte complex (PEC) formation with (2,4- and 2,8-) ammonium ionenes and poly(methacrylic acid). They measured the PEC stability in saltwater solutions.[18] Later, Izumrudov et al. collaborated with Langer's research group to reveal structure-property relationships of ionene and DNA-based PECs.[19] It was shown that DP and charge density were critical factors for determining the stability of the complex. The authors maintained that their analysis was useful for correlating gene delivery efficiency with PEC formation. In 2003, the

Izumrudov group formed PECs of symmetric and asymmetric aliphatic ionenes with calf-thymus DNA to explore the influence of added salt on PEC stability.[20]

Ionenes are also used in antimicrobial applications due to their ability to disrupt cellular membranes.[21,22] Osada and coworkers investigated the antimicrobial properties of several aliphatic and aromatic ionenes with yeast protoplasts.[16] They determined that the concentration that caused significant cell death varied with the length of the hydrophobic segment between charged sites. Furthermore, several patents describe the use of ionenes as antimicrobial coatings.[21,23]

4.3 Experimental

4.3.1 Materials

1,12-dibromododecane (98%) was purchased from Aldrich and recrystallized from ethanol. Dimethylether solution (60% in water) was purchased from Aldrich and used as received. Methanol (MeOH, Fisher, HPLC grade) was distilled from calcium hydride. Tetrahydrofuran (THF, EMD Science, HPLC grade), diethyl ether (Fisher, 99.9%, anhydrous), and sodium hydroxide (Mallinckrodt Chemicals, 99%) were used as received.

4.3.2 Characterization of polyionenes

^{1}H NMR was utilized to determine monomer and polymer composition in $CDCl_3$ and d-MeOD at ambient temperature with a 400 MHz Varian UNITY spectrometer. Size exclusion chromatography (SEC) was performed using a Waters size exclusion chromatograph. The instrument was equipped with Waters 1515 isocratic HPLC pump, Waters 717plus autosampler, Wyatt miniDAWN multiangle laser light scattering (MALLS) detector operating a He-Ne laser at 690 nm, Viscotek 270 viscosity detector, and a Waters 2414 differential refractive index

detector operating at 880 nm and 35 °C. A flow rate of 0.8 mL/min in 54:23:23 H_2O:MeOH:acetic acid (v/v/v), 0.54 M NaAc, 200 ppm NaN_3, pH = 4 was used. Reported molecular weights are based on absolute measurements using the MALLS detector. The specific refractive index increment (*dn/dc*) was calculated using a Wyatt OptiRex differential/absolute refractive index detector operating at 690 nm and 30 °C. After allowing the polymer samples to dissolve in the SEC solvent for 18 h, they were injected via a syringe pump equipped to a 0.45 μm PTFE syringe filter into the RI detector at a rate of 0.8 mL/min. The *dn/dc* values were determined using the Wyatt Astra V software package.

4.3.3 Cell culture

Human neuroblastoma cells (SY5Y) were cultured in 1:1 mixture of Eagle's Minimum Essential Medium (EMEM) containing 1.5 g/L sodium bicarbonate, 2 mM L-glutamine, 1 mM sodium pyruvate and 0.1 mM nonessential amino acids and Ham's F12 Medium containing 1.5 g/L sodium bicarbonate and 2 mM L-glutamine, nonessential amino acids, vitamins, 100 U/ml of penicillin, and 100 μg/ml of streptomycin, and 10% fetal bovine serum. African green monkey kidney fibroblast cells (COS-7) were cultured in Dulbecco's modified Eagle's medium with 4 mM L-glutamine adjusted to contain 1.5 g/L sodium bicarbonate and 4.5 g/L glucose, and 10 % fetal bovine serum. Cultures were incubated at 37 °C in a humid atmosphere of 5% CO_2.

4.3.4 Cell Viability Assay

Cell viability was determined with Promega CellTiter-Glo luminescent and CellTiter 96® non-radioactive cell proliferation (MTT) assays. The cells were harvested during the log phase. A 90 μL cell suspension was dispensed in a 96 well plate ($2x10^4$ cells/well) and was allowed to incubate for 24 h at 37 °C, 5% CO_2. Ionene solutions were prepared at the appropriate

concentration, and 10 μL of ionene solution was added to each well. The plate was incubated for 24 h at 37 °C, 5% CO_2.

For the CellTiter 96® non-radioactive cell proliferation assay, 15 μL of dye solution containing MTT was added to each well and was allowed to incubate for 4 h at 37 °C, 5% CO_2. Solubilization/stop solution (100 μL) was added to each well and the plate was incubated for 1 h at 23 °C in a sealed box. Absorbance at 570 nm was measured for each well using a SpectraMax M5 microplate reader (Molecular Devices Corp.).

For the Cell Titer-Glo luminescent cell viability assay, the 96-well plate containing the cells was equilibrated at room temperature for approximately 30 min. CellTiter-Glo reagent (100 μL), which releases the ATP from cells was added and mixed with an orbital shaker for 2 min to induce cell lysis. After incubating the plate at room temperature for 10 min, the luminescence was recorded using a SpectraMax M5 microplate reader (Molecular Devices Corp.) with an integration time of 0.50 s per well.

4.4 Results and discussion

We report herein a thorough analysis of 12,12-ammonium ionene cytotoxicity as a function of weight-average molecular weight. Although the cytotoxicity of polyelectrolytes is well-documented in the literature, very little is known about the cytotoxicity of ionenes, especially ionenes of well-defined molecular weight. We used two assays and two cell lines to verify that our biological assay measurements were accurate and to ascertain the differences in assay type and cell line.

Two cytotoxicity assays were utilized, including a 3-(4,5-dimethylthiazol-2-yl)-2,5-diphenyltetrazolium bromide (MTT) assay and a luminescent assay that measures adenosine

triphosphate (ATP) activity of living cells. Mosmann developed the widely accepted and utilized MTT assay in 1983.[24] The cellular reaction consists of the conversion of a soluble tetrazolium salt into an insoluble formazan product. More recently, a luminescent cell viability assay that measures ATP activity of living cells was developed.[25] ATP is required and present in living cells, however, cells consume ATP when injured or in environments where nutrient or oxygen levels are too low. Thus, the ATP concentrations are correlated to the number of living cells. Specifically, Promega CellTiter 96® non-radioactive cell proliferation and Cell Titer-Glo® luminescent cell viability assays were compared. The Promega CellTiter 96® assay was employed since others optimized the procedure and reagents to overcome technical problems associated with the original MTT assay.[26,27]

A thorough analysis was conducted on human brain SY5Y neuroblastoma and COS-7 African green monkey kidney cell lines to determine the cytotoxicity of the ionenes at various concentrations. These cell lines were chosen due to their well-established correlation to DNA binding and transfection efficiencies.

Ammonium ionenes were prepared via the Menschutkin reaction from 1,12-dibromododecane and 1,12-bis(N,N-dimethylamino)dodecane (Scheme 4.1). ^{1}H NMR spectroscopy confirmed the polymer structure.

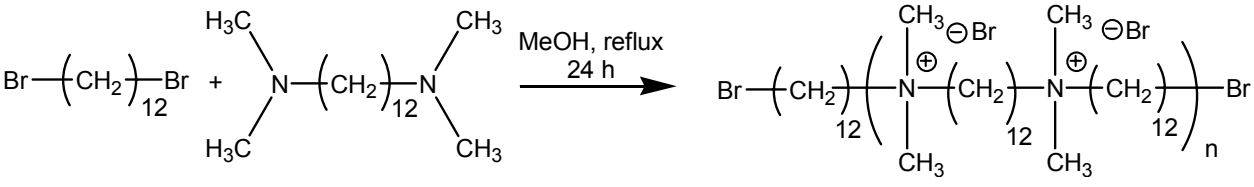

Scheme 4.1. Synthesis of 12,12-ammonium ionenes via the Menschutkin reaction.

A stoichiometric imbalance of monomers provided polymers with varying molecular weights. One can achieve molecular weight control in step-growth polymerization through the addition of monofunctional reagents, limited difunctional monomer conversion, or through a non-

stoichiometric imbalance of difunctional monomers.[28] The latter method is preferred because the resulting polymers possess chain ends with the same functionality as the excess monomer. In this case, both monomers are completely consumed, and this results in a stable polymer that cannot increase in molecular weight during a post-polymerization process.[28,29] Specifically, five weight-average molecular weights of ionenes, which ranged from 4300 to 20900 g/mol (Table 4.1), were used in the cytotoxicity analysis. These polymers were prepared to determine the effect of molecular weights on the cytotoxicity of 12,12-ammonium ionenes. Previously, our group has published the determination of absolute molecular weights and thermomechanical property characterization of 12,12-ammonium ionenes.[30,31] The polymers were not dialyzed before the cytotoxicity measurements; therefore, any residual monomer potentially had an influence on the toxicity. However, monomer was not detected according to ^{1}H NMR and *in-situ* FT-IR spectroscopy.

Diamine : Dihalide Molar Ratio	M_w **(g/mol)**†	M_n **(g/mol)***	M_w **(g/mol)***	M_w/M_n*
1.00:1.00	20900	10700	26900	2.52
1.00:1.03	17400	9700	23000	2.36
1.00:1.05	13200	6900	17000	2.45
1.00:1.07	12300	6800	17000	2.50
1.00:1.10	4300	1900	4900	2.63

Table 4.1. Molecular weight analysis via aqueous SEC, and ionene monomer molar ratios dictates final molecular weights. †Absolute weight-average molecular weights were determined from an on-line MALLS detector. *PEO/PEG equivalent molecular weights determined using dRI detection.

The ionene concentration in the presence of SY5Y and COS-7 cells ranged from 1-800 μg/mL. Eight replicates were used for each concentration at each molecular weight. In addition,

eight control wells without polymer were used in each experiment. As shown in Figure 4.2-Figure 4.5, a broad range in viability was obtained as a function of 12,12-ammonium ionene concentration. Interestingly, we did not observe a significant difference in toxicity over the ionene molecular weight range studied, which is also revealed in Figure 4.2-Figure 4.5.

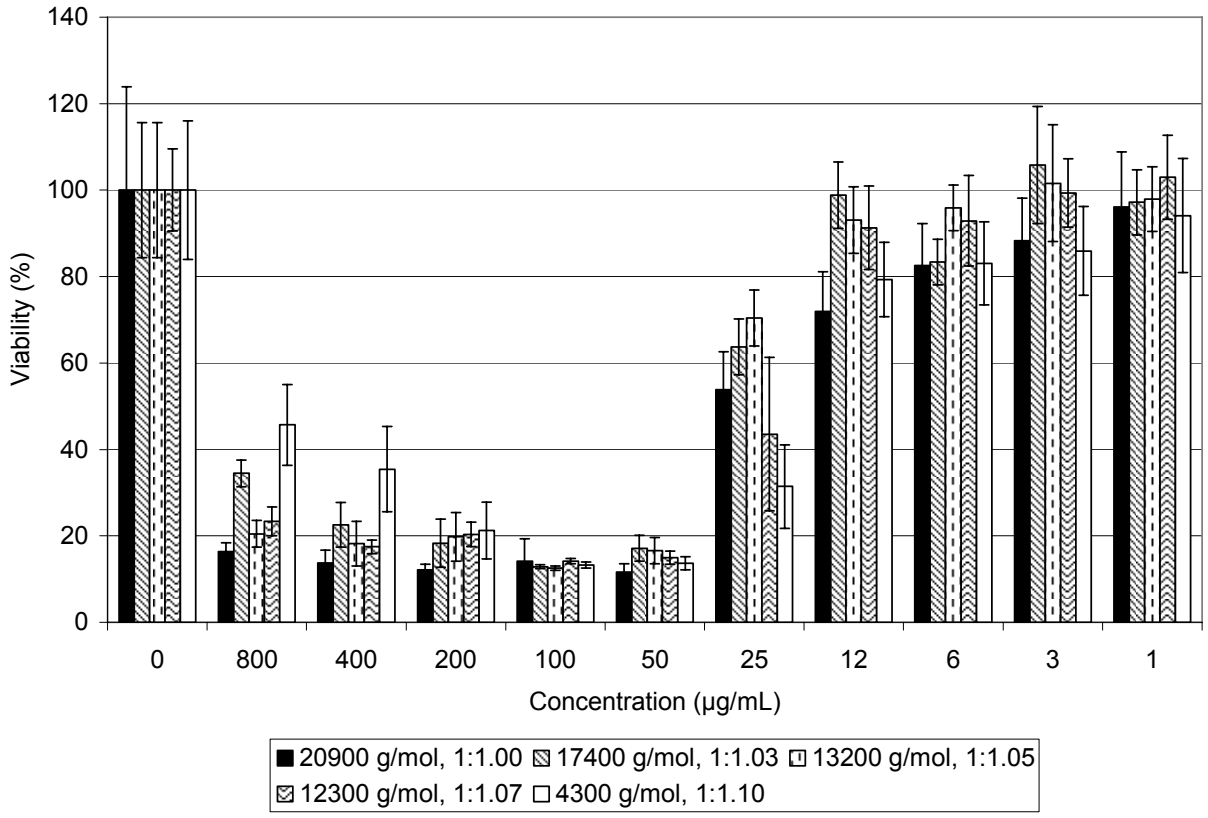

Figure 4.2. MTT assay of SY5Y cells in the presence of various concentrations of 12,12-ammonium ionenes. SY5Y neuroblastoma cells ($2x10^4$ cells/well) were incubated for 24 h at 37 ºC prior to conducting the MTT assay. Data are means ± SD, n=8.

Figure 4.2 summarizes the results for the MTT assay for the SY5Y cells. At concentrations ranging from 400-800 µg/mL of ammonium ionene, SY5Y cell viability ranged from approximately 20-40%, and SY5Y cell viability slightly decreased to less than 20% at concentrations of 50-200 µg/mL. As shown in Figure 4.2, we observed an increase in the SY5Y

cell viability, at 25 μg/mL and at concentrations less than 12 μg/mL, SY5Y cell viability ranged from 80 to greater than 100%. Overall, the MTT assay resulted in a bimodal distribution of viability from 100-800 μg/mL and 1-50 μg/mL. One hypothesis for the bimodal viability issue is that at high concentrations, ionenes bind with ions in the cell culture media and alter the pH of media, which results in a change in the tetrazolium reduction.[32,33] This change will lead to a shift in the absorbancies and thus alter the results. The bimodality was observed to have the most pronounced effect with the lowest molecular weight 12,12-ammonium ionene.

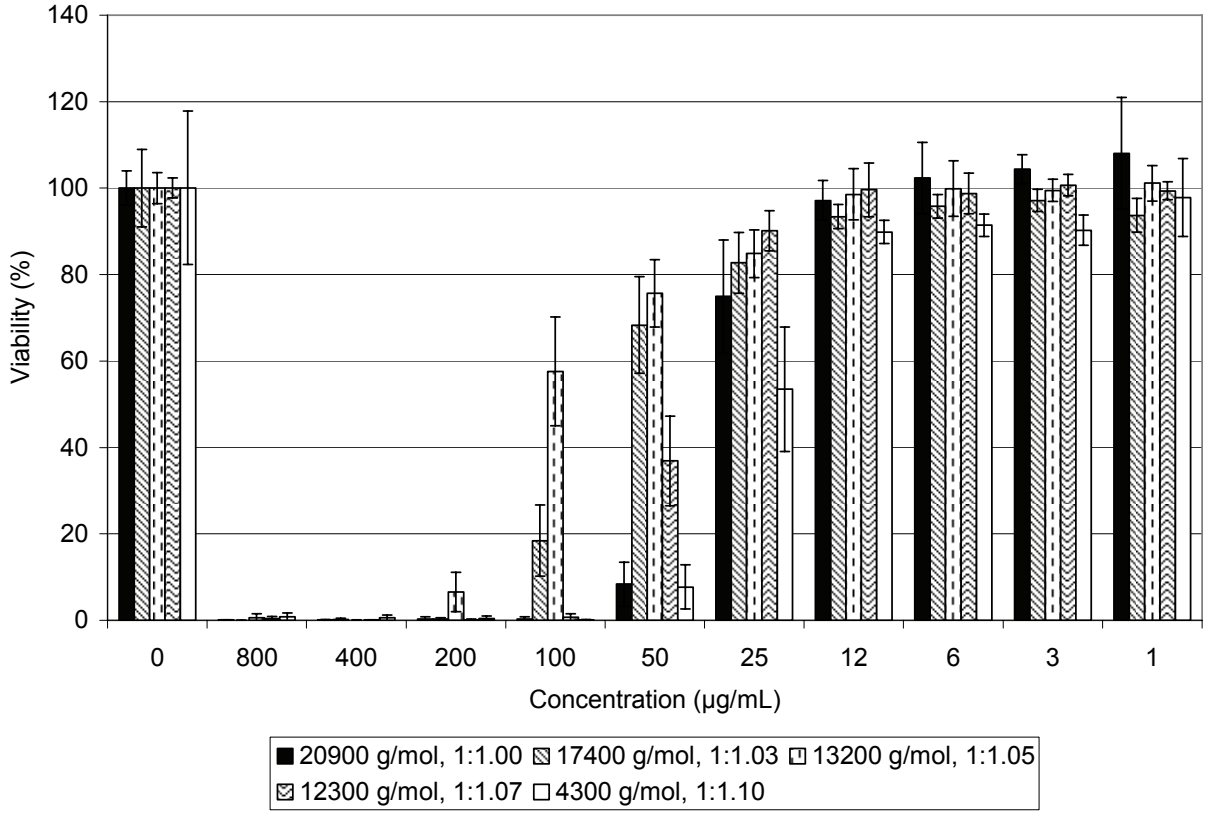

Figure 4.3. Luminescent cytotoxicity assay of SY5Y cells in the presence of various concentrations of 12,12-ammonium ionenes. SY5Y neuroblastoma cells ($2x10^4$ cells/well) were incubated for 24 h at 37 ºC prior to conducting the luminescent assay. Data are means ± SD, n=8.

The SY5Y cell viability at high concentrations was markedly different using the luminescent assay compared to the MTT assay. As shown in Figure 4.3, a extensive range in viability was obtained for SY5Y cells in the presence of 12,12-ammonium ionenes. At concentrations of 200-800 μg/mL, SY5Y cell viability was nearly 0%, which was expected at high concentrations. This is in contrast to the MTT assay results, which demonstrated viabilities of approximately 20% at the higher concentrations of 200-800 μg/mL. A sharp increase in SY5Y cell viability was observed beginning at 100 μg/mL, and at concentrations less than 12 μg/mL, minimal SY5Y cell death was observed. As shown in Figure 4.2 and Figure 4.3, the SY5Y cell viabilities at lower concentrations were nearly indistinguishable for both cell viability assays. Bimodal cytotoxicity profiles were not observed using the luminescent assay, and this supported the hypothesis previously described.

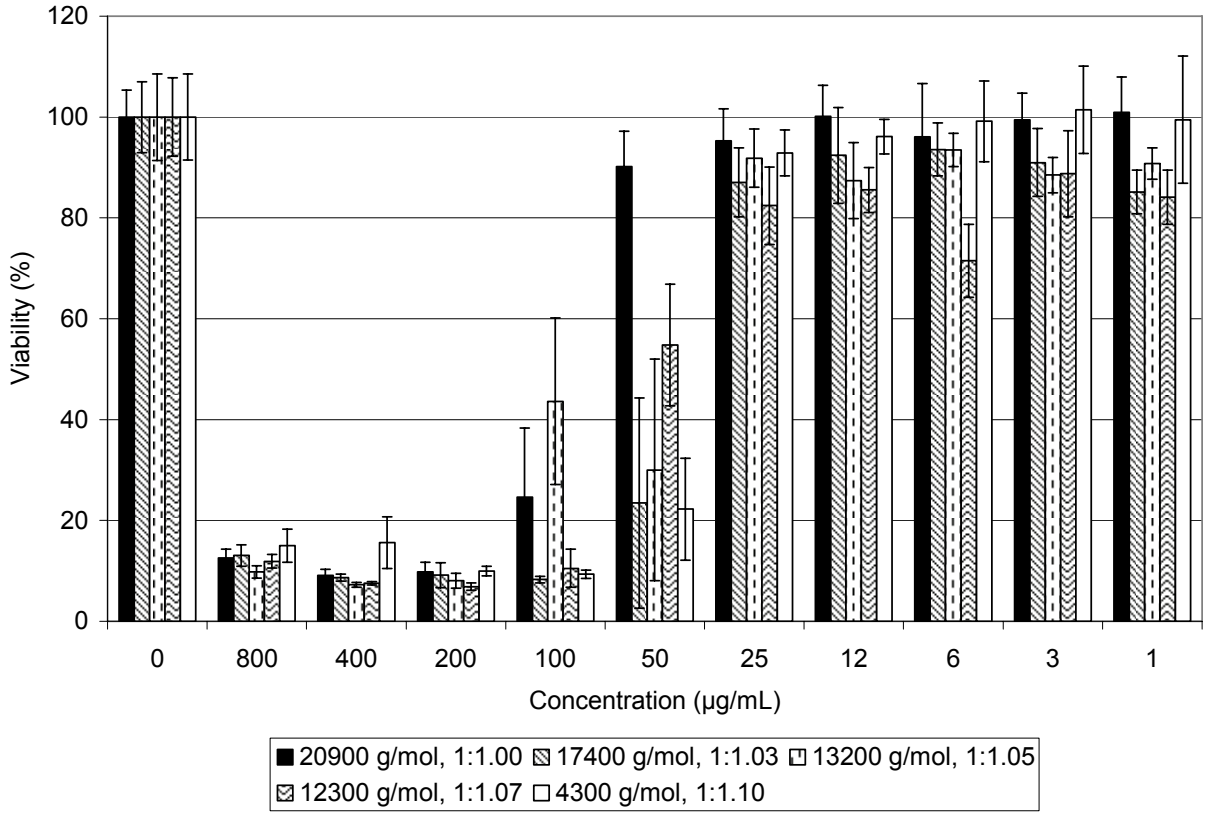

Figure 4.4. MTT assay of COS-7 cells in the presence of various concentrations of 12,12-ammonium ionenes. COS-7 cells ($2x10^4$ cells/well) were incubated for 24 h at 37 ºC prior to conducting the MTT assay. Data are means ± SD, n=8.

Figure 4.4 demonstrates the effect of 12,12-ammonium ionenes on COS-7 cell viability using the MTT assay. In comparison to the SY5Y cells, COS-7 cells were more resilient to the medium range concentrations (~50 µg/mL). In Figure 4.2, at 50 µg/mL concentration of 12,12-ammonium ionene, SY5Y cell viability was less than 20%. However, as shown in Figure 4.4, COS-7 cell viability was significantly greater. At high concentrations (~100-800 µg/mL), COS-7 cell viability was generally less than 20%. A distinct increase in COS-7 cell viability was observed at 50 µg/mL, and at lower concentrations, minimal COS-7 cell death was observed.

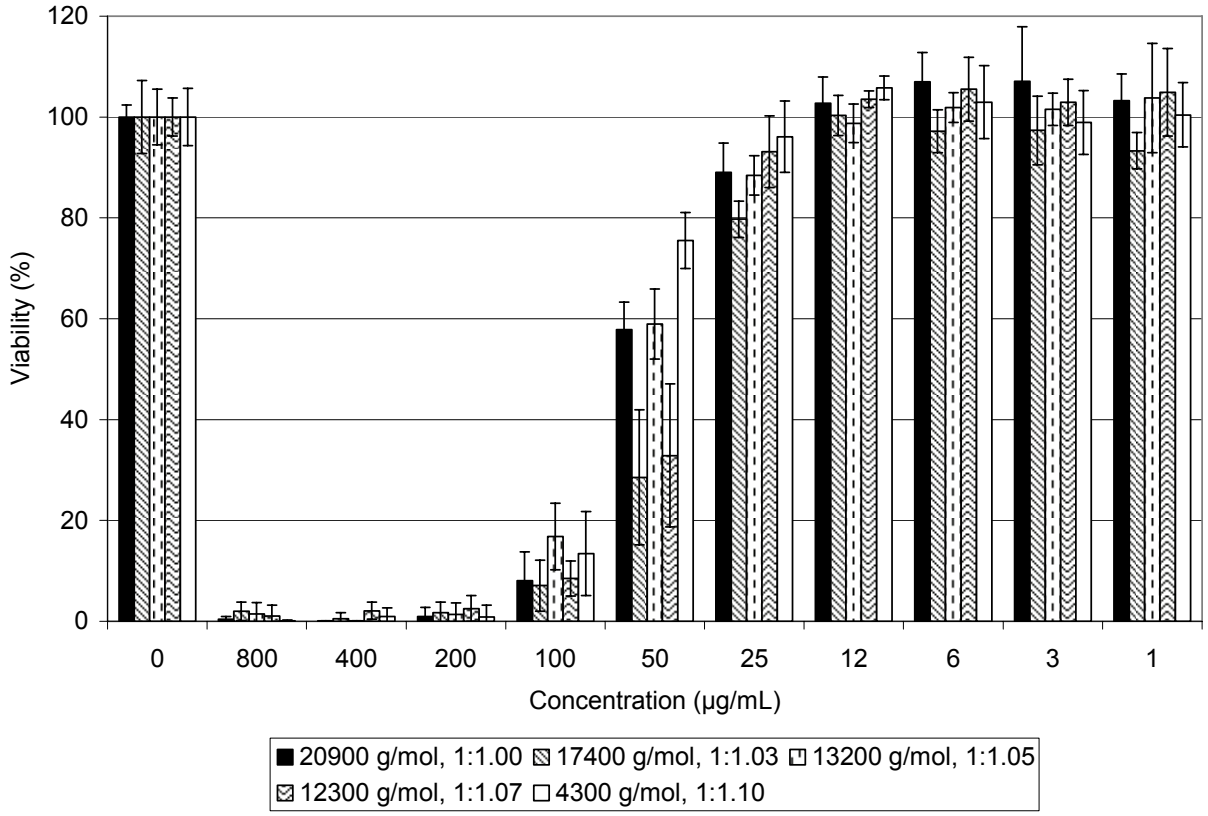

Figure 4.5. Luminescent cytotoxicity assay of COS-7 cells in the presence of various concentrations of 12,12-ammonium ionenes. COS-7 cells ($2x10^4$ cells/well) were incubated for 24 h at 37 ºC prior to conducting the luminescent assay. Data are means ± SD, n=8.

The luminescent cytotoxicity assay results for COS-7 cells in the presence of 12,12-ammonium ionenes are shown in Figure 4.5. In a similar fashion to the SY5Y cell line luminescent cytotoxicity assay results, COS-7 cell viability was negligible at high concentrations. An increase in COS-7 cell viability was not observed until 12,12-ammonium ionene concentrations of 50-100 µg/mL were used. Concentrations of 25 µg/mL resulted in minimal COS-7 cell death, as shown in Figure 4.5, and 12,12-ammonum ionene concentrations less than and equal to 12 µg/mL did not cause any apparent COS-7 cell death, regardless of ionene molecular weight.

To the best of our knowledge, this is the first report of the cytotoxicity of ammonium ionenes as a function of molecular weight with a variety of cell lines and assays. Osada et al. previously reported cytotoxicity properties of aliphatic ionenes as a function of charge density with microbial cell lines.[16] Interestingly, the 12,12-ammonium ionene cytotoxicity profile that their group obtained with yeast protoplast cells agreed very well with the results reported herein.

4.5 Conclusions

In conclusion, ammonium ionenes were prepared via the Menschutkin reaction from 1,12-dibromododecane and 1,12-bis(N,N-dimethylamino)dodecane. A thorough analysis was conducted on SY5Y and COS-7 cell lines to determine the cytotoxicity of ionenes at various concentrations that are typical for gene transfection and antimicrobial action. Specifically, Promega CellTiter 96® non-radioactive cell proliferation and Cell Titer-Glo® luminescent cell viability assays were compared. Concentrations of ionenes ranged from 1-800 μg/mL, and significant cell viability was observed at concentrations less than 25 μg/mL, regardless of cell line utilized. There also was not a direct correlation between ionene weight-average molecular weight and cell viability. In future gene delivery studies, it appears that 12,12-ammonium ionene concentration should be used at the lower concentration ranges (< 12 μg/mL).

4.6 Acknowledgements

This material is based upon work supported in part by the Macromolecular Interfaces with Life Sciences (MILES) Integrative Graduate Education and Research Traineeship (IGERT) of the National Science Foundation under Agreement No. DGE-0333378.

4.7 References

(1) Cakmak, I.; Ulukanli, Z.; Tuzcu, M.; Karabuga, S.; Genctav, K. *European Polymer Journal* **2004,** 40, (10), 2373-2379.

(2) Kenawy, E. R.; Mahmoud, Y. A. G. *Macromolecular Bioscience* **2003,** 3, (2), 107-116.

(3) Heath, W. H.; Senyurt, A. F.; Layman, J.; Long, T. E. *Macromolecular Chemistry and Physics* **2007,** 208, (12), 1243-1249.

(4) Tan, J. F.; Hatton, T. A.; Tam, K. C.; Too, H. P. *Biomacromolecules* **2007,** 8, (2), 448-454.

(5) Rajagopalan, P.; Shen, C. J.; Berthiaume, F.; Tilles, A. W.; Toner, M.; Yarmush, M. L. *Tissue Engineering* **2006,** 12, (6), 1553-1563.

(6) Zhang, Y. Q.; Li, L. L.; Tang, F. Q.; Ren, J. *Journal of Nanoscience and Nanotechnology* **2006,** 6, (9-10), 3210-3214.

(7) Samoilova, N. A.; Krayukhina, M. A.; Novikova, S. P.; Babushkina, T. A.; Volkov, I. O.; Komarova, L. I.; Moukhametova, L. I.; Aisina, R. B.; Obraztsova, E. A.; Yaminsky, I. V.; Yamskov, I. A. *Journal of Biomedical Materials Research Part A* **2007,** 82A, (3), 589-598.

(8) Kabanov, V. A., *Macromolecular complexes in chemistry and biology*. Springer-Verlag: New York, 1994.

(9) Izumrudov, V. A., *Smart polymers for bioseparation and bioprocessing*. Taylor and Francis: New York, 2002.

(10) Scranton, A. B.; Rangarajan, B.; Klier, J., Biomedical applications of polyelectrolytes. In *Advances in Polymer Science*, Peppas, N. A.; Langer, R. S., Eds. Springer-Verlag: Berlin, 1995; Vol. 122, pp 1-54.

(11) Lv, H. T.; Zhang, S. B.; Wang, B.; Cui, S. H.; Yan, J. *Journal of Controlled Release* **2006,** 114, (1), 100-109.

(12) Senior, J. H.; Trimble, K. R.; Maskiewicz, R. *Biochimica Et Biophysica Acta* **1991,** 1070, (1), 173-179.

(13) Hartig, S. M.; Greene, R. R.; Dikov, M. M.; Prokop, A.; Davidson, J. M. *Pharmaceutical Research* **2007,** 24, (12), 2353-2369.

(14) Choi, J. S.; Lee, E. J.; Jang, H. S.; Park, J. S. *Bioconjugate Chemistry* **2001,** 12, (1), 108-113.

(15) Rembaum, A.; Noguchi, N. *Macromolecules* **1972,** 5, (3), 261-269.

(16) Narita, T.; Nishino, M.; Gong, J. P.; Osada, Y. *Colloid and Polymer Science* **2000,** 278, 884-887.

(17) Tashiro, T. *Macromolecular Materials and Engineering* **2001,** 286, 63-87.

(18) Zelikin, A. N.; Akritskaya, N. I.; Izumrudov, V. A. *Macromol. Chem. Phys.* **2001,** 202, (15), 3018-3026.

(19) Zelikin, A. N.; Putnam, D.; Shastri, P.; Langer, R.; Izumrudov, V. A. *Bioconjugate Chem.* **2002,** 13, (3), 548-553.

(20) Zelikin, A. N.; Litmanovich, A. A.; Paraschuk, V. V.; Sybatchin, A. V.; Izumrudov, V. A. *Macromolecules* **2003,** 36, (6), 2066-2071.

(21) Fitzpatrick, R. J.; Shackett, K. K. *WO 2004045629* **2004,** PCT Int. Appl.

(22) Rembaum, A., Biological activity of ionene polymers. In *Polymeric Materials for Unusual Service Conditions*, Golub, M. A.; Parker., J. A., Eds. Wiley: New York, 1973; pp 299-317.

(23) Fitzpatrick, R.; Klinger, J. D.; Shackett, K. K. Ionene polymers and their use as antimicrobial agents. WO 2002080939, 2002.
(24) Mosmann, T. *J Immunol Methods* **1983,** 65, (1-2), 55-63.
(25) Crouch, S. P.; Kozlowski, R.; Slater, K. J.; Fletcher, J. *J Immunol Methods* **1993,** 160, (1), 81-8.
(26) Denizot, F.; Lang, R. *J Immunol Methods* **1986,** 89, (2), 271-7.
(27) Carmichael, J.; DeGraff, W. G.; Gazdar, A. F.; Minna, J. D.; Mitchell, J. B. *Cancer Res* **1987,** 47, (4), 936-42.
(28) Odian, G., *Priciples of polymerization*. 4th ed.; Wiley-Interscience: Hoboken, 2004.
(29) Stevens, M. P., *Polymer chemistry*. 3rd ed.; Oxford University Press: Oxford, 1999.
(30) Layman, J. M.; Borgerding, E. M.; Williams, S. R.; Heath, W. H.; Long, T. E. *Macromolecules* **2008,** 41, (13), 4635-4641.
(31) Williams, S. R.; Borgerding, E. M.; Layman, J. M.; Wang, W.; Winey, K. I.; Long, T. E. *Macromolecules* **2008,** 41, (14), 5216–5222.
(32) Vistica, D. T.; Skehan, P.; Scudiero, D.; Monks, A.; Pittman, A.; Boyd, M. R. *Cancer Res* **1991,** 51, (10), 2515-20.
(33) Plumb, J. A.; Milroy, R.; Kaye, S. B. *Cancer Res* **1989,** 49, (16), 4435-40.

Chapter 5 : Synthesis of 12,12-Ammonium Ionenes with Functionality for Chain Extension and Cross-linking via UV Irradiation

5.1 Abstract

A novel synthetic methodology for preparing chain-extended and cross-linked ionenes using UV irradiation is described. 12,12-Ammonium ionenes were functionalized with either cinnamate or styrenic functionality at the chain ends and were subsequently exposed to UV irradiation. In addition, a novel copolymer (poly(cinDMPC-*co*-bocDMPC)) was mixed with the cinnamate-functionalized 12,12-ammonium ionene to prepare photo-cross-linked networks. The UV irradiation process was monitored via UV-vis spectroscopy after each exposure. The chain-extended 12,12-ammonium ionene possessed superior tensile properties compared to the original 12,12-ammonium ionene. Successful cross-linking was confirmed with solubility testing of the thin films in methanol. The results indicated that photo-cross-linked 12,12-ammonium ionenes offer potential in membrane technology applications.

5.2 Introduction

Ammonium ionenes are polyelectrolytes that contain quaternary nitrogen atoms in the main polymeric chain, and Gibbs et al. were the first to synthesize ammonium ionenes from dimethylamino-*n*-alkyl halides.[1] It is also possible to synthesize ionenes via step-growth polymerization of alkyl dihalides and ditertiary amines in a Menshutkin reaction (Scheme 5.1).[2]

Rembaum et al. used this strategy to synthesize ammonium ionenes with a variety of methylene spacers and explored their solution properties.[3-5] The ionenes are named as *x,y*-ionene, where the x and y represent the number of methylene groups between quaternized nitrogen atoms for the ditertiary amine and alkyl dihalide, respectively.

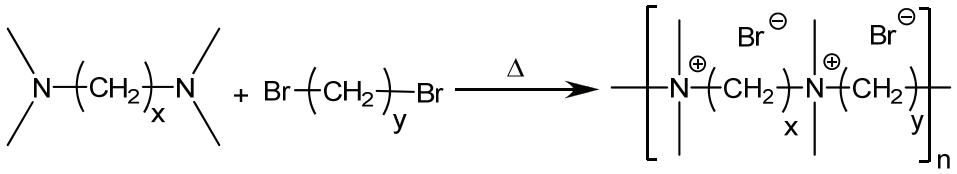

Scheme 5.1. Ionene polymerization via the Menshutkin reaction.

Our research group recently reported appropriate chromatographic conditions to determine the absolute molecular weight of 12,12- and 6,12-ammonium ionenes using an aqueous-based mobile phase and multi-angle laser light scattering (MALLS).[6] While several mobile phase compositions were attempted (including those previously reported in literature), the only mobile phase composition found appropriate for separating both types of ionenes consisted of a 54/23/23 mixture of water/methanol/acetic acid that contained 0.54 M NaOAc at a pH of 4.0. Dynamic light scattering (DLS) confirmed the absence of ionic aggregates, thus ensuring the feasibility of chromatographic separation in this unusual solvent composition. Moreover, in a separate article, relationships between absolute molecular weight and thermomechanical performance were investigated.[7] Dynamic mechanical analysis (DMA) confirmed that the water-soluble ionenes possessed T_g values that increased with increasing molecular weight. In addition, the presence of ionic aggregates was observed to dissociate at approximately 88 °C, regardless of molecular weight. Higher molecular weight 12,12-ammonium ionenes (M_n > 10000 g/mol) displayed excellent tensile properties. While X-ray scattering determined that the methylene segments were too short to facilitate crystallization, ionic domains were observed. In

addition, the base-catalyzed depolymerization of 12,12-ammonium ionenes was achieved, thus facilitating the production of degradable films with good mechanical durability.

Photoreactive ionenes are not well-documented in the literature, but a few examples demonstrate the combination of photoreactive groups with ionenes that inherently possess coulombic interactions. For example, Suzuki et al. reported the synthesis of various ammonium ionene structures that possessed pendent (9-anthryl)methyl functional groups.[8] Many factors that influenced the photodimerization reaction, including polymer structure, molecular weight, chromophore concentration, and solvent selection were investigated. They determined that hydrophobic and coulombic interactions were both important factors in the rate of dimerization in the presence of UV light. In another example, Hong et al. reported the synthesis, photoisomerization, and photoorientation of multi-layered structures containing azobenzene functionality in novel ionene polymers.[9] They determined that ionene alkyl spacer length influenced the UV-light induced orientational order.

As described above, ammonium ionenes containing UV-reactive functionality are reported in the literature; however, the incorporation of cinnamate functional groups was not reported earlier. Cinnamate dimerization is an advantageous methodology for chain extension and cross-linking, as it occurs without the need for a photoinitiator in the presence of ultraviolet (UV) light. Specifically, the cinnamate functional group dimerizes in the presence of ultraviolet B (UVB) light,[10] and either head-to-head or head-to-tail [$2\pi + 2\pi$] cycloaddition occurs to convert two C=C bonds into a single cyclobutane ring (Scheme 5.2). The cinnamate functional group offers potential in cross-linking technologies. Previously, our research group reported the novel preparation of electrospun fibers consisting of cinnamate-functionalized poly(methyl methacrylate-*co*-2-hydroxyethyl acrylate) copolymers.[11] Cross-linking of the copolymer

occurred during the electrospinning process using a modified electrospinning apparatus equipped with a UV light source.

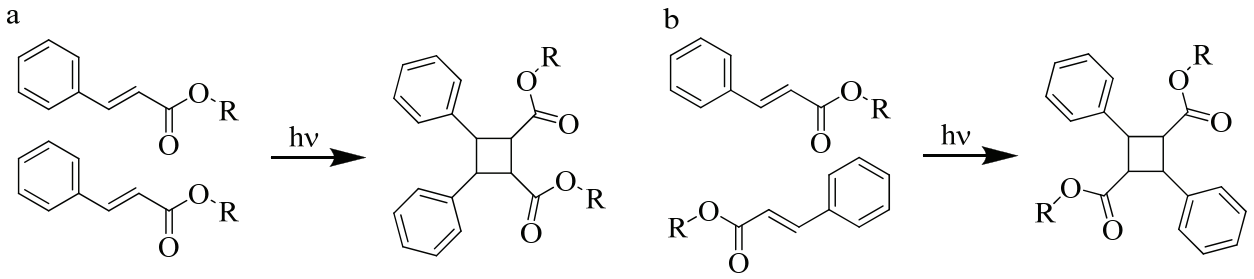

Scheme 5.2. **a.** Head-to-head and **b.** head-to-tail [2π + 2π] cycloaddition of cinnamate functional groups.

Well-defined ionenes enable a variety of potential technologies; however, most emphasis is placed on biomedical technologies, such as model gene transfection agents,[12-15] antimicrobials,[16-20] and cancer therapeutics.[21] Herein, the synthesis of 12,12-ammonium ionenes possessing UV-reactive end groups is described. Through exposure to UV irradiation, chain-extended and cross-linked polymers, which possessed enhanced mechanical properties compared to non-UV irradiated ammonium ionene polymers, were synthesized. The novel cross-linked ionenes offer potential as membranes for water purification purposes. Upon cross-linking, the membranes achieved complete insolubility in water. In addition, the charge on the macromolecular repeating unit is expected to repel filtered particles, which reduces membrane clogging and enhances membrane efficiency.

5.3 Experimental

5.3.1 Materials

1,12-dibromododecane (98%) was purchased from Aldrich and recrystallized from ethanol. Dimethylamine solution (60% in water), 2,6-bis(1,1-dimethylethyl)-4-methylphenol

(BHT), 3,3'-iminobis(*N,N*-dimethylpropylamine) (IDMPA), di-*tert*-butyl dicarbonate (di-*tert*Boc), triethylamine (TEA, anhydrous), dichloromethane (CH_2Cl_2, anhydrous), and 2,2-dimethyl-2-phenol acetophenone (DMPA) were purchased from Aldrich and used as received. Methanol (MeOH, Fisher, HPLC grade) and chloroform ($CHCl_3$, Fisher, HPLC grade) were distilled from calcium hydride. Tetrahydrofuran (THF, EMD Science, HPLC grade) was used as received. Cinnamoyl chloride was purchased from Aldrich and purified via sublimation. 11-Bromundecanol was purchased from Alfa Aesar and used as received. (Chloromethyl)styrene was purchased from Fluka and purified via aluminum oxide column. 1,12-bis(*N,N*-dimethylamino)dodecane was synthesized according to Spencer et al.[22] and used in previous 12,12-ammonium ionene synthesis.[7] Tertiary amine-terminated 12,12-ammonium ionenes were synthesized using a molar ratio of 1.05:1.00 (ditertiary amine: alkyldihalide), as reported previously.[7] Synthesis of 11-bromundecyl cinnamate was prepared according to Wegner et al.[23]

5.3.2 Synthesis of cinnamate-functionalized 12,12-ammonium ionene

Tertiary amine end-capped 12,12-ammonium ionene (1.017 g, 0.134 mmol), 11-bromundecyl cinnamate (0.153 g, 0.402 mmol), and methanol (20 wt % solids) were introduced into a two-necked, round-bottomed flask equipped with a condenser and magnetic stir bar. The mixture was purged under nitrogen and allowed to react for 24 h at 70 °C. Upon completion, the amount of solvent was reduced via rotary evaporation and the polymer was cast into Teflon™ molds to enable film formation. ^{1}H NMR (400 MHz, CD_3OD) confirmed f = 2. δ = 7.53-7.69 (cinn), 7.37 (cin), 6.48 (cin), 3.36-4.42 (cinn-ionene alkyl linker), 3.28 (8H per repeating unit, $CH_2N^+(CH_3)_2CH_2$), 3.03 (12H per repeating unit, $CH_2N^+(CH_3)_2CH_2$), 2.81 (12H, $(CH_3)_2$-N-R_2 closest to chain end), 1.71 (8H per repeating unit, $CH_2CH_2N^+(CH_3)_2CH_2CH_2$), 1.49 (cinn-ionene alkyl linker), 1.33 (32H per repeating unit, $(CH_2)_8CH_2CH_2N^+(CH_3)_2$).

5.3.3 Synthesis of *tert*-butyl bis(3-(dimethylamino)propyl)carbamate (bocDMPC)

A 500-mL, round-bottomed flask equipped with magnetic stir bar and 100-mL addition funnel was charged with IDMPA (16 g, 87 mmol), TEA (33 mL, 261 mmol), and anhydrous CH_2Cl_2 (250 mL), then cooled to 0 °C under a nitrogen atmosphere. A solution of di-*tert*Boc (37.9 g, 174 mmol) in anhydrous CH_2Cl_2 (75 mL) was added dropwise over 1 h via addition funnel, and the reaction mixture was stirred for 2 h at 0 °C and 18 h at 23 °C. The reaction mixture was extracted with brine (100 mL) and aqueous $NaHCO_3$ solution (100 mL). (*Caution*: During the extractions excess degassing was observed.) The organic layer was collected, dried over Na_2SO_4, and concentrated to yield a yellow liquid (22.2 g). The yellow liquid was distilled to yield a clear, viscous liquid (14.71g, 61%). b.p.= 84-86 °C (0.160 mTorr). ^{1}H NMR (400 MHz, CD_3OD) δ3.23 (4H, CH_2NH), 2.35 (4H, $CH_2N(CH_3)_2$), 2.25 (12H, CH_3N), 1.73 (4H, CH_2CH_2), 1.47 (9H, $(CH_3)_3C$)); ^{13}C NMR (400 MHz, $CDCl_3$) δ 155.9, 79.5, 57.6, 45.9, 28.9, 27.3, 27.0. FAB-MS $(M+H)^+$: Calculated for $C_{15}H_{34}N_3O_2$: 288.2651, Found: 288.2654.

5.3.4 Synthesis of *N,N*-bis(3-(dimethylamino)propyl)cinnamamide (cinDMPC)

A two-necked, 250-mL, round-bottomed flask equipped with magnetic stir bar and 100-mL addition funnel was charged with IDMPA (5.89 g, 31 mmol), TEA (12 mL, 93 mmol), and anhydrous CH_2Cl_2 (80 mL), then cooled to 0 °C under a nitrogen atmosphere. A solution of cinnamoyl chloride (5.23 g, 31 mmol) in anhydrous CH_2Cl_2 (35 mL) was added dropwise over 1 h via addition funnel, and the reaction mixture was stirred 24 h at 23 °C. The reaction mixture was extracted with brine (100 mL) and aqueous $NaHCO_3$ solution (100 mL). The organic layer was collected, dried over Na_2SO_4, and concentrated to yield a yellow oil (9.5 g). The yellow oil was passed through a short basic alumina column with pentanes to yield a clear oil (4.5 g, 45%). ^{1}H NMR (400 MHz, $CDCl_3$) δ7.67 (1H, J= 14Hz), 7.52 (2H), 7.37 (3H), 7.07 (1H, J= 14Hz)

3.52 (4H, CH_2NH), 2.29 (4H, $CH_2N(CH_3)_2$), 2.29 (12H, CH_3N), 1.79 (4H, CH_2CH_2); ^{13}C NMR (400 MHz, $CDCl_3$) δ 166.5, 142.4, 136.6, 129.5, 128.8, 127.9, 117.9, 57.2, 56.2, 46.0, 45.5, 45.1, 27.6, 26.1. FAB-MS $(M+H)^+$: Calculated for $C_{15}H_{34}N_3O_2$: 318.2546, Found: 318.2545.

5.3.5 Synthesis of poly(cinDMPC-*co*-bocDMPC)

A two-necked, 50-mL, round-bottomed flask equipped with mechanical stirrer and condenser was charged with bocDMPC (788 mg, 2.74 mmol), cinDMPC (96 mg, 0.30 mmol), 1,12-dibromododecane (1.00 g, 3.04 mmol), and methanol (3 mL) under nitrogen. The reaction vessel was submerged in an oil bath (~75 °C) and refluxed for 40 h under continuous mechanical stirring (45 rpm). To this flask was added methanol (50 mL), and the solution was concentrated and dried in a vacuum oven (70 °C) for 24 h to yield a clear solid polymer (1.82 g). T_g = 91 °C, $T_{d(onset)}$ = 175 °C. M_n = 13,000; M_w = 20,600; PDI = 1.6; ^1H NMR (400 MHz, D_2O) δ7.72 (cinn), 7.64 (cinn), 7.48 (cinn), 7.13 (cinn), 3.30 (12H) 3.06 (12H), 2.02 (4H), 1.70 (4H), 1.47 (9H), 1.27-1.39 (16H).

5.3.6 Film preparation for cross-linked networks containing cinnamate-functionalized 12,12-ammonium ionenes and DMPC copolymers

DMPC copolymer and cinnamate functionalized 12,12-ammonium ionene were weighed and combined in a glass vial. The polymers were dissolved in methanol (80 wt % solids) and spun cast on cleaned quartz glass at 2500 rpm for 30 sec. The films were subsequently exposed to UV irradiation at a speed of 6 ft/min, and the cross-linking process was observed with an Ocean Optics USB2000 UV-VIS fiber optic spectrometer for qualitative analysis.

5.3.7 Synthesis of styrenic-functionalized 12,12-ammonium ionene

Tertiary amine end-capped 12,12-ammonium ionene (0.506 g, 0.066 mmol), *p*-chloromethyl(styrene) (0.0213 g, 0.1398 mmol), BHT (20 mg/g, 0.42 mg), and methanol (20 wt % solids) were added into a two-necked, round-bottomed flask equipped with a magnetic stir bar and condenser and purged under nitrogen. The solution was allowed to react for 24 h at 60 °C. Upon completion, the amount of solvent was reduced via rotary evaporation, and 4 wt % DMPA photoinitiator was added. The mixture was cast into Teflon™ molds to enable film formation. The polymers were dissolved in methanol (80 wt % solids) and spun cast on cleaned quartz glass at 2500 rpm for 30 sec. In addition, the films were subsequently exposed to UV irradiation, and the cross-linking process was observed with an Ocean Optics USB2000 UV-VIS fiber optic spectrometer for qualitative analysis. ^{1}H NMR (400 MHz, CD_3OD) confirmed f = 2. δ = 7.36 (sty), 6.92 (sty), 5.78 (sty), 5.21 (sty), 4.43 (sty), 3.28 (8H per repeating unit, $CH_2N^+(CH_3)_2CH_2$), 3.03 (12H per repeating unit, $CH_2N^+(CH_3)_2CH_2$), 2.81 (12H, $(CH_3)_2$-N-R_2 closest to chain end), 1.71 (8H per repeating unit, $CH_2CH_2N^+(CH_3)_2CH_2CH_2$), 1.33 (32H per repeating unit, $(CH_2)_8CH_2CH_2N^+(CH_3)_2$).

5.3.8 Characterization of ionenes

^{1}H NMR spectroscopy was utilized to determine monomer and polymer composition in $CDCl_3$ and CD_3OD at ambient temperature with a 400 MHz Varian UNITY spectrometer. Thermogravimetric analysis (TGA) was conducted on a TA Instruments Hi-Res TGA 2950 with a temperature ramp rate of 10 °C/min in a nitrogen atmosphere. Dynamic mechanical analysis (DMA) was conducted on a TA Instruments Q800 Dynamic Mechanical Analyzer in tension mode at a frequency of 1 Hz and temperature ramp rate was 3 °C/min. Differential scanning calorimetry (DSC) was performed using a TA Instruments Q1000 differential scanning

calorimeter under a nitrogen flow of 50 mL/min. Stress-strain experiments were conducted with dogbone-shape film specimens, cut with a die according to ASTM D3368 specifications. Tensile tests were performed on a 4411 Instron universal testing instrument with a cross-head speed of 50 mm/min at ambient temperature. Size exclusion chromatography (SEC) was performed using a Waters size exclusion chromatograph. The instrument was equipped with Waters 1515 isocratic HPLC pump, Waters 717plus autosampler, Wyatt miniDAWN multiangle laser light scattering (MALLS) detector operating a He-Ne laser at 690 nm, Viscotek 270 viscosity detector, and a Waters 2414 differential refractive index detector operating at 880 nm and 35 °C. A flow rate of 0.8 mL/min in 54:23:23 H_2O:MeOH:acetic acid (v/v/v), 0.54 M NaAc, 200 ppm NaN_3, pH = 4 was used. Reported molecular weights are based on absolute measurements using the MALLS detector. The specific refractive index increment (d*n*/d*c*) was calculated using a Wyatt OptiRex differential/absolute refractive index detector operating at 690 nm and 30 °C. After allowing the polymer samples to dissolve in the SEC solvent for 18 h, they were injected via a syringe pump equipped to a 0.45 μm PTFE syringe filter into the RI detector at a rate of 0.8 mL/min. The d*n*/dc values were determined as described previously[6] using the Wyatt Astra V software package. The ionene films were passed through a LC-6B Fusion UV system at 6 ft/min belt speeds and 1.42 ± 0.05 W/cm^2 for each pass to achieve photo-cross-linking or chain extension. An EIT UV Power Puck radiometer was used to measure the irradiance and temperature. Qualitative UV-vis spectroscopy was performed on an Analytical Instrument Systems, Inc. spectrometer that was equipped with fiber-optic light guides, a DT1000CE light source, and an Ocean Optics USB2000 UV-vis detector. Film thickness measurements were conducted on a Helios 600 NanoLab focused ion beam (FIB)-scanning electron microscopy (SEM) operating with a beam current of 86 pA, 5.00 kV voltage, 4.2 mm working distance, 52°

tilt, 512 nm horizontal field width, and a TLD detector. Gas-assisted etching was accomplished with XeF_2. The spun cast film (2500 rpm) was coated with 20 nm of Au, and a protective Pt layer was applied during imaging.

5.4 Results and Discussion

5.4.1 Synthesis of tertiary amine end-capped 12,12-ammonium ionenes

12,12-Ammonium ionenes were synthesized as reported previously (Scheme 5.3).[7] To ensure the polymers were end-capped with tertiary amine functionality, an excess of 1,12-bis(N,N-dimethylamino)dodecane was used (1.05:1.00 monomer stoichiometry, ditertiary amine: dialkyl halide), and difunctionality was confirmed via ^{1}H NMR spectroscopy. SEC-MALLS and ^{1}H NMR spectroscopy were used to determine M_n, and the resulting molecular weights were 7600 g/mol and 9200 g/mol, respectively. Although SEC is often difficult for polyelectrolytes due to aggregation, polymer-solvent interactions, and polymer-column interactions, the appropriate aqueous SEC solvent for successful chromatography of 12,12-ammonium ionenes was previously reported.[6]

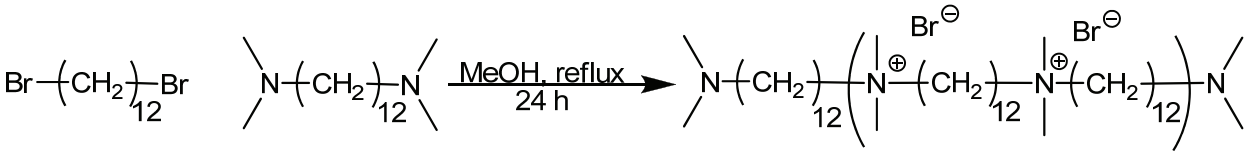

Scheme 5.3. Synthesis of 12,12-ammonium ionene.

Thermal analysis was conducted via TGA and DSC. The 7600 g/mol 12,12-ammonium ionene possessed a single T_g of 35 ºC and was thermally stable to 222 ºC. Ammonium ionenes are known to degrade at elevated temperatures in order to form many degradation products that result from various reactions, including reverse Menshutkin reactions and Hoffman eliminations.[24-31] The dimethylamino-terminated 12,12-ammonium ionene formed a brittle film,

and the dynamic mechanical behavior was evaluated. However, the film was too brittle to evaluate via tensile testing. DMA results revealed that the ionene possessed an ionic dissociation temperature of 82 ºC, and a T_g of 40 ºC (Figure 5.1). Moreover, these results were consistent with prior results concerning 12,12-ammonium ionenes published from our research group, where low molecular weight 12,12-ammonium ionenes possessed low T_gs, and the T_gs of high molecular weight (> 20000 g/mol) approach 90 ºC.[7]

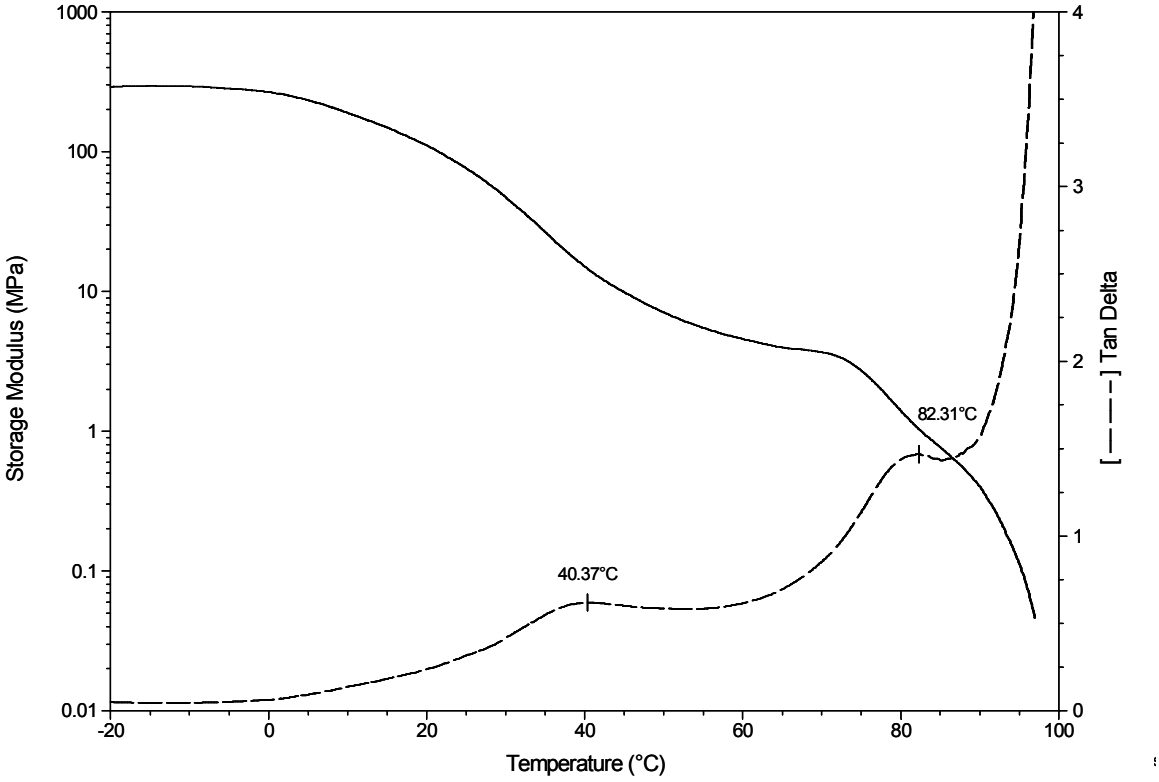

Figure 5.1. DMA of the 12,12-ammonium ionene.

5.4.2 Chain extension of 12,12-ammonium ionenes possessing cinnamate end groups

11-Bromundecyl-cinnamate was synthesized according to a literature procedure (Scheme 5.4), and the structure was confirmed via ^{1}H NMR spectroscopy.[23] The resulting end-capping reagent reacted with the chain ends of the dimethylamino-terminated 12,12-ammonium ionene according to Scheme 5.5. This resulted in a novel ammonium ionene with well-defined end

groups that undergo chain extension during UV irradiation. The UV irradiation process allows cinnamate functional groups to react in a chain extending process in a [2π + 2π] cycloaddition reaction (Figure 5.2). The cinnamate-functionalized 12,12-ammonium ionene possessed a lower T_g (15 ºC) compared to the 12,12-ammonium ionene with dimethylamino end groups (35 ºC). This clearly demonstrated that the bulky cinnamate end groups with long alkyl chains influenced the T_g, which was expected, since it was consistent with previous literature.[32,33] It is important to note that lowering of the T_g was not due to residual solvent or water, since the second heat from DSC was reported and multiple DSC experiments were conducted on different samples, and a change in T_g was not observed.

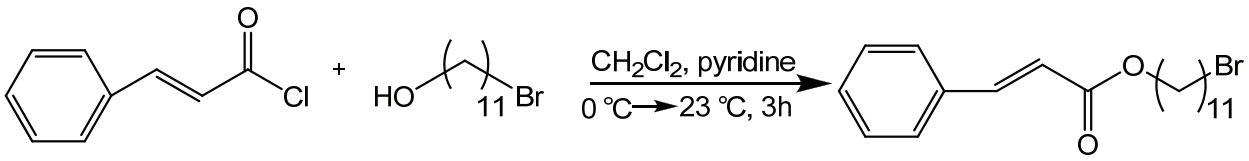

Scheme 5.4. Synthesis of 11-bromundecyl-cinnamate.

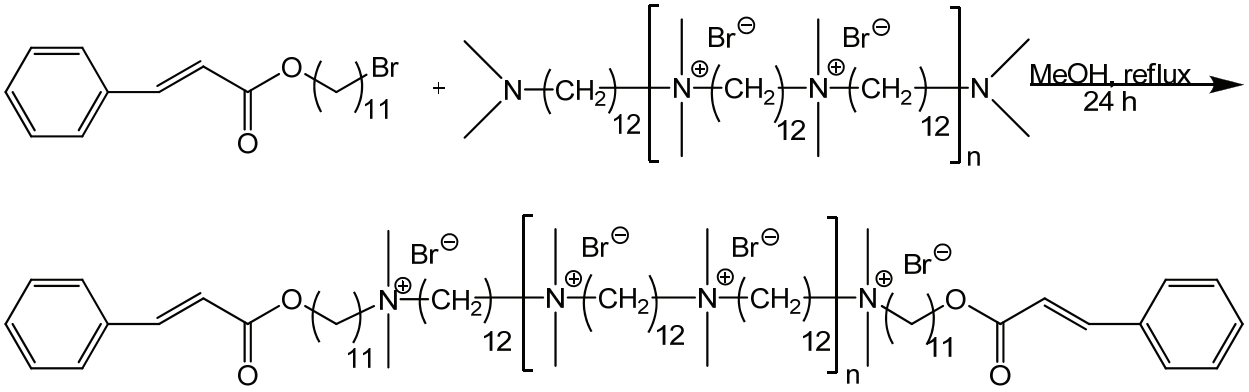

Scheme 5.5. Synthesis of cinnamate-functionalized 12,12- ammonium ionenes.

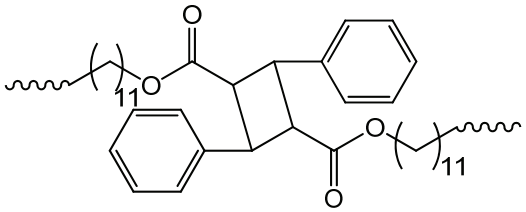

Figure 5.2. Dimerization of cinnamate functional groups.

In order to prepare chain-extended free-standing films, cinnamate-functionalized 12,12-ammonium ionenes were passed through an 1800 W UV Fusion system. It is well known that cinnamates absorb UV light at 278 nm due to the C=C vinylene functional group.[34] As shown in Figure 5.3, the absorbance before exposure to UV light was the largest. After one pass through the UV Fusion instrument, the UV spectrum was recorded again, and the absorbance decreased upon exposure to UV light. This process was continued until the UV spectra remained unchanged after UV light exposure. For the cinnamate-functionalized ionenes, the cinnamate absorbance decreased with each pass under the UV light, and the irradiation was complete after twenty passes under the UV light, according to the UV spectra shown in Figure 5.3. Multiple exposures to UV light were required, and this was attributed to the thickness of the film (~0.4 mm). It is important to note that the UV lamp generated heat over time (typically above the T_g of the polymer and maximum of 65 °C), which potentially contributed to the enhanced mobility of the chain ends, thus causing an increased number of chain end collisions to aid in successful photodimerization of cinnamate functional groups. In addition, the film was flipped after each exposure to UV light to ensure equal exposure of light to both sides and through the bulk of the polymer film.

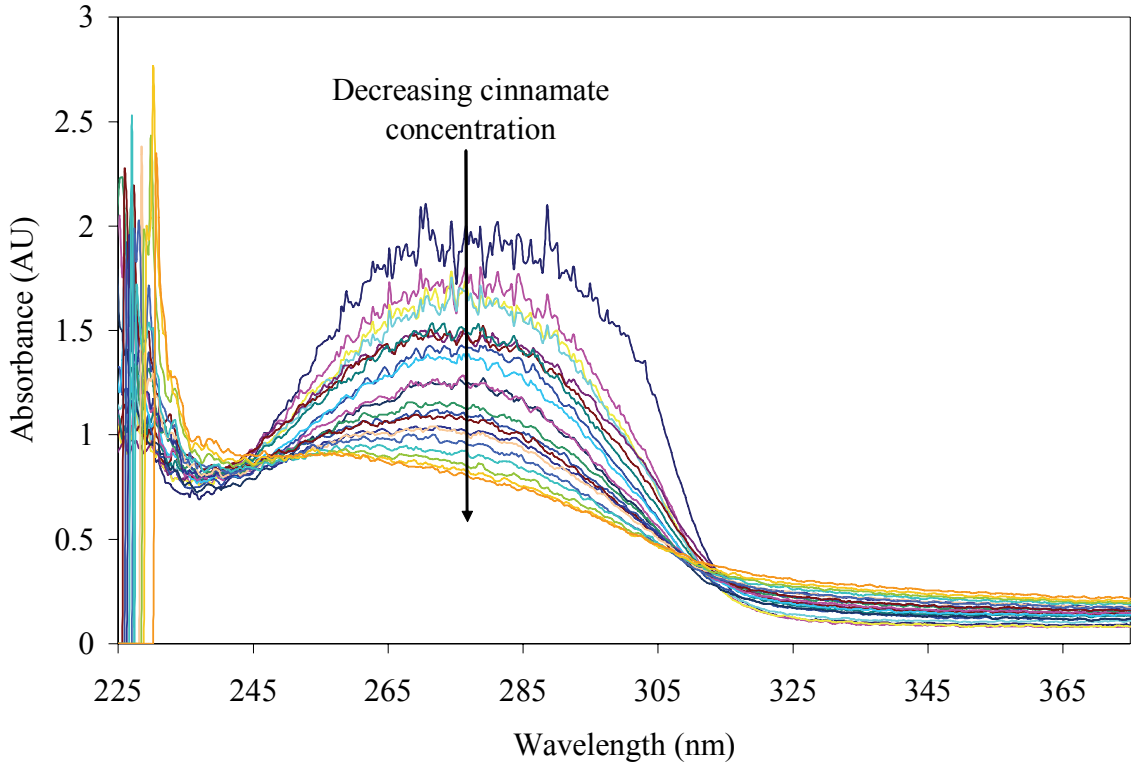

Figure 5.3. UV spectra demonstrating the cinnamate-functionalized ionene chain-extension process.

After UV irradiation, thermal properties were evaluated and compared to the original 12,12-ammonium ionene containing cinnamate end groups. As shown in Table 5.1, the T_g increased with increasing exposure to UV light. Before UV irradiation, the cinnamate-functionalized 12,12-ammonium ionene possessed a T_g of 13 °C, according to DSC, and the onset of degradation was 227 °C. After five passes through the UV Fusion instrument, a sample of the film was analyzed using TGA and DSC. The results, shown in the third column of Table 5.1, clearly demonstrated that the chain extension process occurred, due to an increase in T_g to 26 °C. Upon further UV irradiation, the T_g increased to 34 °C. Also indicated in the table was a lack of degradation upon UV exposure, which confirmed that the UV irradiation process did not degrade the 12,12-ammonium ionene to any extent.

Cinnamate-12,12-ionene	$T_{d\ onset}$ (°C)	T_g (°C)
Before UV irradiation	227	13
After UV irradiation	230	26
After multiple exposures to UV irradiation	227	34

Table 5.1. Degradation onset temperatures (TGA), glass transition temperatures (DSC), and molecular weight data of the cinnamate-functionalized ionene before and after UV irradiation.

Before UV irradiation, the 12,12-ammonium ionene film was very brittle, and after UV irradiation the film became increasingly flexible and elastomeric. The enhancement in mechanical properties was due to chain extension that occurred during UV irradiation. Tensile analysis was conducted on the cinnamate-functionalized 12,12-ammonium ionene after UV irradiation was complete. Before UV irradiation, it was not possible to test the sample due to its brittleness. After UV irradiation, the tensile stress at break was 43.1 ± 0.4 MPa, and the tensile strain at break was 640 ± 140 % (Figure 5.4). This suggested that the chain-extended 12,12-ammonium ionene possessed a higher molecular weight than before UV irradiation. Indeed, aqueous SEC analysis confirmed that increased molecular weight was achieved, as shown in the SEC traces in Figure 5.5. The enhanced molecular weight and improved mechanical performance were consistent with previously published results.[7] Specifically, 15 700 g/mol 12,12-ammonium ionenes possessed 26.4 ± 1.0 MPa stress at break and 440 ± 45 % elongation at break. To ensure that the increase in molecular weight was due to cinnamate dimerization and not unintended reactions occurring on the polymer backbone, a dimethylamino-endcapped 12,12-ammonium ionene was exposed to UV light in a similar fashion as the cinnamate-functionalized 12,12-ammonium ionene. Aqueous SEC analysis indicated that the dimethylamino-endcapped

12,12-ammonium ionene possessed the same molecular weight and molecular weight distribution before and after exposure to UV light.

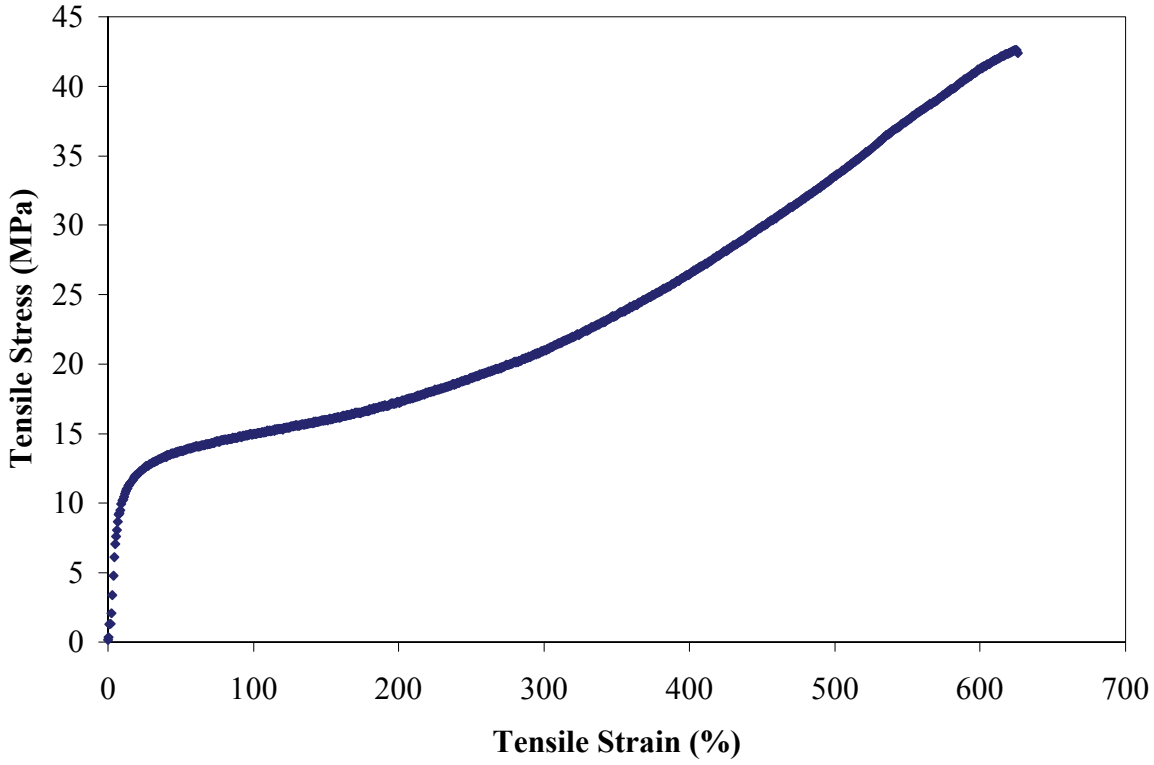

Figure 5.4. Average (3 samples) tensile stress versus strain behavior of UV-irradiated cinnamate-functionalized 12,12-ammonium ionene.

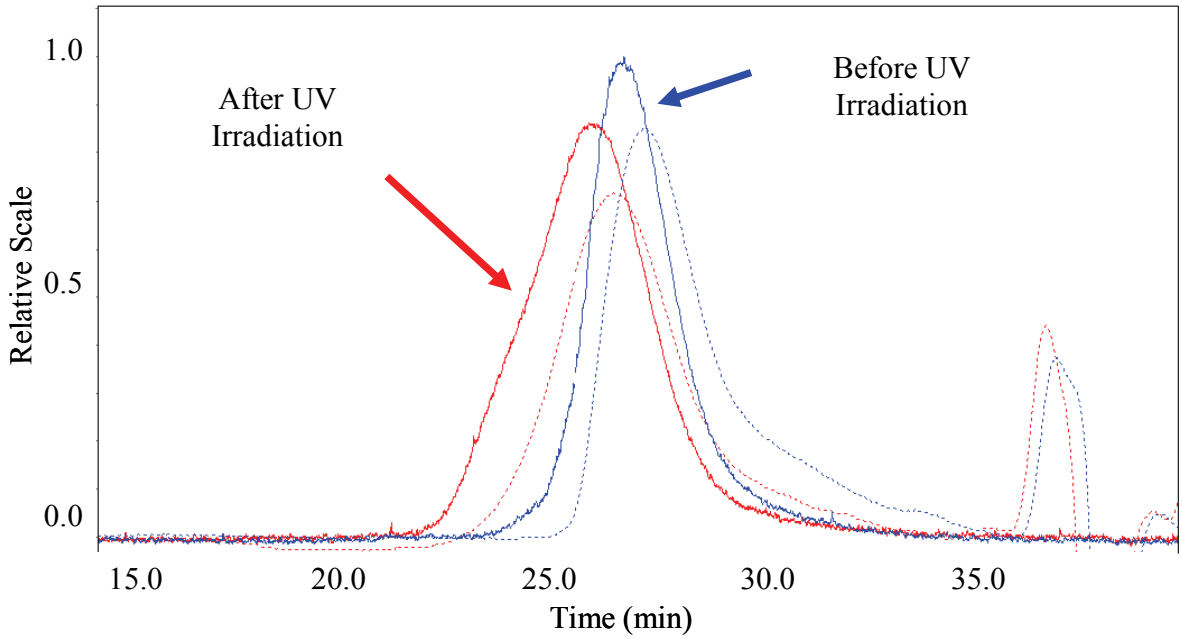

Figure 5.5. SEC traces for cinnamate-functionalized 12,12-ammonium ionenes. Red traces = after UV irradiation, blue traces = after UV irradiation, solid lines = MALLS traces, dashed lines = RI traces.

5.4.3 Cross-linking of cinnamate-functionalized 12,12-ammonium ionenes and cinnamate ionene copolymer (poly(cinDMPC-*co*-bocDMPC))

Novel monomers (cinDMPC and bocDMPC) were synthesized from 3,3'-iminobis(*N,N*-dimethylpropylamine) for the preparation of a cinnamate-containing copolymer. Modification of the monomer was achieved with a reaction of the secondary amine of the monomers with cinnamoyl chloride or di-*tert*boc, respectively. The structures were confirmed via ^{1}H and ^{13}C NMR spectroscopy and FAB-MS.

An ammonium ionene possessing cinnamate functionality pendant to the polymer main chain was synthesized from cinDMPC and bocDMPC in the presence of 1,12-dibromododecane via a conventional Menshutkin reaction in methanol (Figure 5.6). The resulting copolymer possessed a number average molecular weight (M_n) of 13 000 g/mol and a weight average

molecular weight (M_w) of 20 600 g/mol, as determined via aqueous SEC (RI detector). The composition was examined via ^{1}H NMR spectroscopy, and the results corresponded exactly to the copolymer containing 10 mol % cinDMPC. Thermal analysis was conducted via DSC and TGA, and poly(cinDMPC-*co*-bocDMPC) possessed a T_g of 91 °C, and a $T_{d(onset)}$ of 175 °C. The $T_{d(onset)}$ was consistent with the loss of the *t*-boc group.

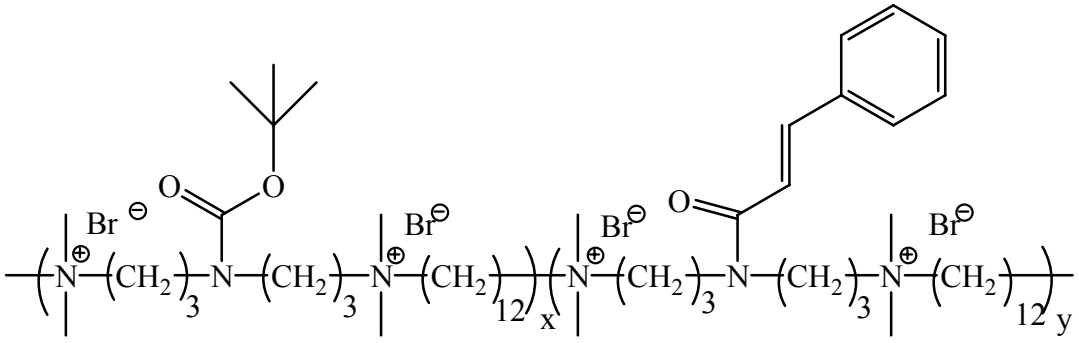

Figure 5.6. Structure of poly(cinDMPC-*co*-bocDMPC).

Poly(cinDMPC-*co*-bocDMPC) was mixed with cinnamate-functionalized 12,12-ammonium ionenes to prepare cross-linked ammonium ionenes. The polymer shown in Figure 5.6 has cinnamate functionality along the backbone, which allows for cross-linking to occur. Two mixtures of cinnamate-containing ionenes were prepared for cross-linking investigations. Initially, a 88/12 wt % mixture of cinnamate-end-capped 12,12-ammonium ionene/poly(cinDMPC-*co*-bocDMPC) were combined in a viscous methanol solution. Thick films (~0.4 mm) were cast on Teflon™ molds, and once free-standing film formation occurred, the films were removed from the mold and exposed to UV light at a rate of 6 ft/min. After 65 passes under the UV light, solubility tests indicated that cross-linking was not successful. This was attributed to the thickness of the film, which would not allow UV light to completely penetrate. A previous study from Wilkes and Long et al. indicated that cinnamate functional groups must be close to each other for successful dimerization to occur.[11] Perhaps the thick

films were chain extending in a similar manner to the cinnamate-functionalized ionenes described above, but the concentration of cinnamate functional groups was not large enough to enable cross-linking to occur in the solid state. In addition, the higher T_g (91 °C) of the copolymer possibly attributed to unsuccessful cross-linking since the UV light did not produce sufficient temperature during UV irradiation to impart mobility on the polymer chains ($T \leq 65$ °C). Therefore, thin films were prepared via spin casting onto quartz glass. The film was exposed to UV light five times, and UV-vis spectra were recorded after each exposure (Figure 5.7), until the cinnamate peak in the UV-vis spectrum remained unchanged. After UV irradiation, the solubility properties were evaluated. The film partially dissolved in methanol, and few fiber-like strands were observed in the solution. This indicated that the film was only partially cross-linked, and that the cinnamate functional groups on the ionene copolymer were perhaps unavailable for cross-linking due to the rest of the polymer chain shielding the UV reactive groups from each other. However, to confirm that forming cross-linked ammonium ionenes was possible, the amount of poly(cinDMPC-*co*-bocDMPC) was increased to 57 wt %. Thin films were spun cast on quartz glass using the same casting conditions. Upon UV irradiation, successful cross-linking occurred. As shown in Figure 5.8, the cinnamate absorbance decreased dramatically after only one exposure to UV light. This indicated that the majority of cinnamate functional groups were in close proximity to photodimerize, unlike the previous example, when more than one exposure was required to decrease the cinnamate absorbance. To ensure all cinnamate functional groups reacted, two additional exposures to UV light were performed, and the cinnamate absorbance remained unchanged. The quartz glass coated with the cross-linked ionene was placed in methanol and the film remained intact on the glass slide. Thus, successful cross-linking occurred for the cinnamate copolymer.

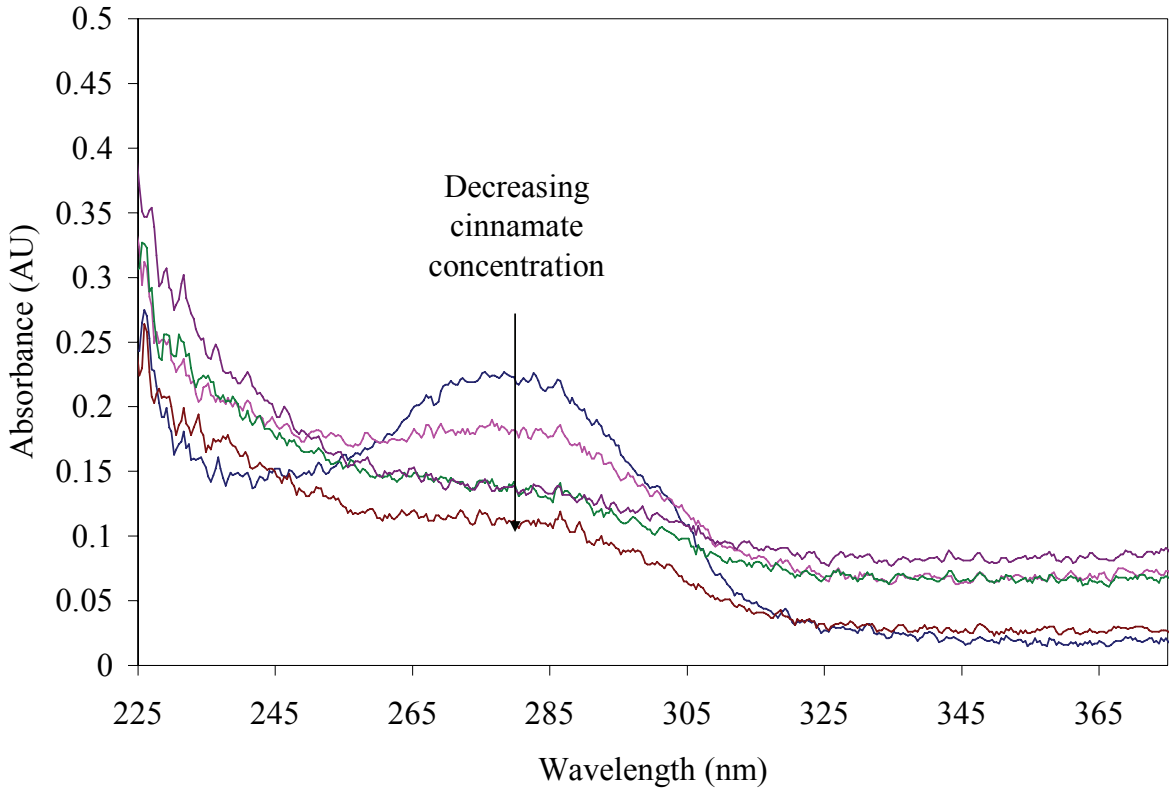

Figure 5.7. UV spectra demonstrating decreasing cinnamate concentration after exposure to UV light for 88/12 wt % mixture of cinnamate-end-capped 12,12-ammonium ionene/poly(cinDMPC-*co*-bocDMPC).

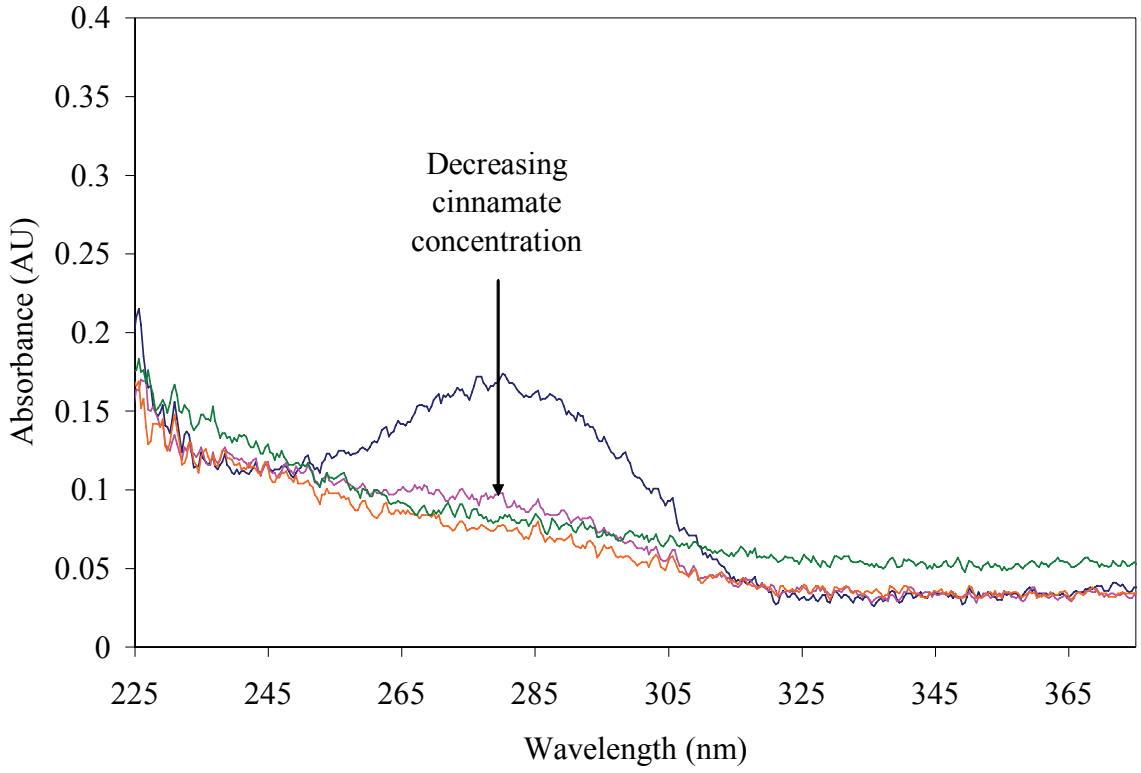

Figure 5.8. UV spectra demonstrating decreasing cinnamate concentration after exposure to UV light for 43/57 mol % mixture of cinnamate-end-capped 12,12-ammonium ionene/ poly(cinDMPC -*co*-bocDMPC).

5.4.4 Cross-linking of 12,12-ammonium ionenes possessing styrenic end groups

Chloromethyl styrene was used to synthesize a novel styrenic-functionalized ionene (Scheme 5.6). An inhibitor, BHT, was used during the end-capping synthetic procedure to prevent premature cross-linking. It is important to note that after the functionalization reaction, the end groups possessed quaternary nitrogen sites with chloride counteranions. Chloride anion containing ionenes are known to have lower degradation temperatures compared to bromide anion containing ionenes, since chloride anions are stronger bases than bromide anions.[35] Ikeda et al. demonstrated that poly(tetramethylene oxide) (PTMO)-based ionenes with chloride counteranions degraded at 200 °C, while PTMO-based ionenes with bromide counteranions

degraded at 227 °C.[35] Therefore, it was expected that the degradation temperature of the styrenic-end-capped ionene was lower than the parent 12,12-ammonium ionene polymer. In fact, the styrenic-functionalized 12,12-ammonium ionene possessed an onset decomposition temperature of 203 ± 4 °C, which was lower than the parent 12,12-ammonium ionene described above (222 ± 3 °C).

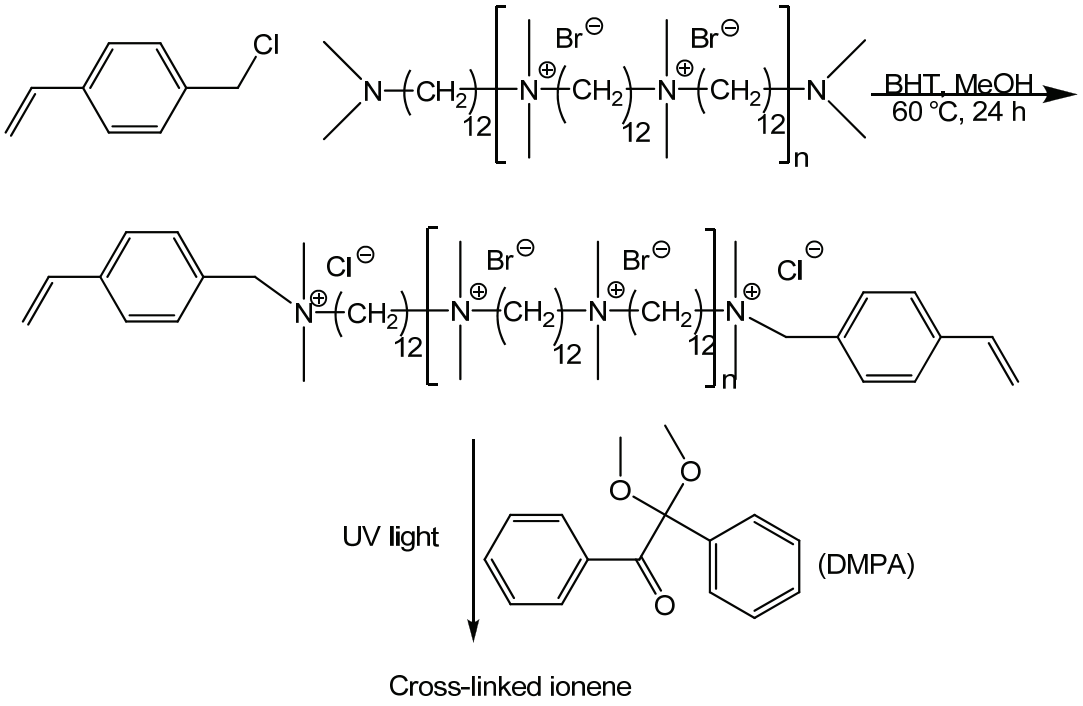

Scheme 5.6. Synthesis of styrenic-functionalized ionene.

This ionene was synthesized to form a cross-linked network in the presence of a photoinitiator and UV light due to the presence of two vinyl groups on the chain ends. DMPA (4 wt %) was used as the photoinitiator and was added to the ionene solution. Thin films were prepared via spin casting on quartz glass. Film thickness was approximately 110 nm across the uniform film, as determined via FIB-SEM (Figure 5.9). Before UV light exposure, the UV spectrum of the polymer in the presence of DMPA was recorded (Figure 5.10). A peak at ~254 nm was observed and attributed to the presence of DMPA. After one exposure to UV light the

absorbance at 254 nm was minimal. Repeated exposures to UV light and the lack of change in the UV spectra indicated that the photo-cross-linking was complete, as shown in Figure 5.10.

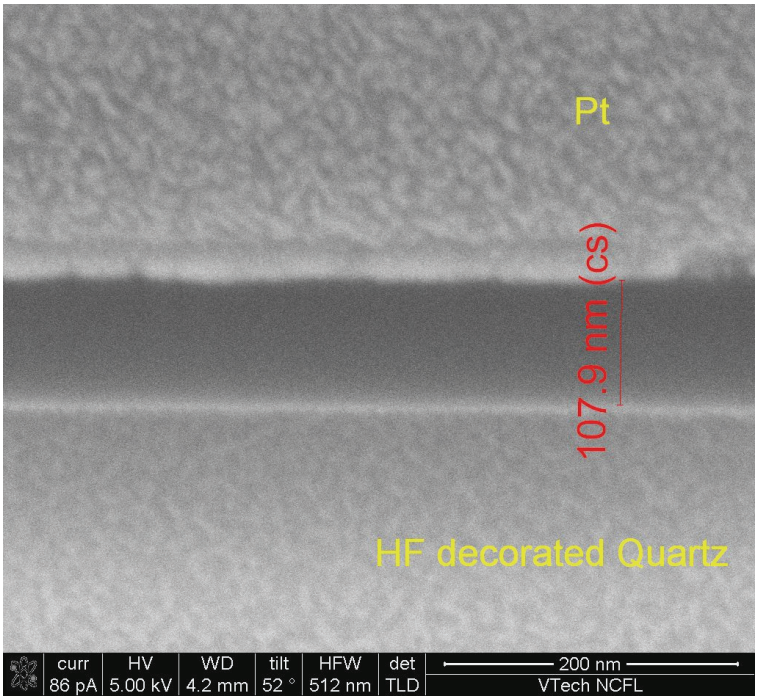

Figure 5.9. FIB-SEM image of spun cast ammonium ionene film. Layers from top to bottom: Pt, Au (~20 nm), film (~110 nm), and HF decorated quartz (from gas-assisted XeF_2 etching). Conditions: 86 pA, 5.00 kV, 4.2 mm WD, 52° tilt, 512 nm HFW, TLD detector. Scale bar = 200 nm.

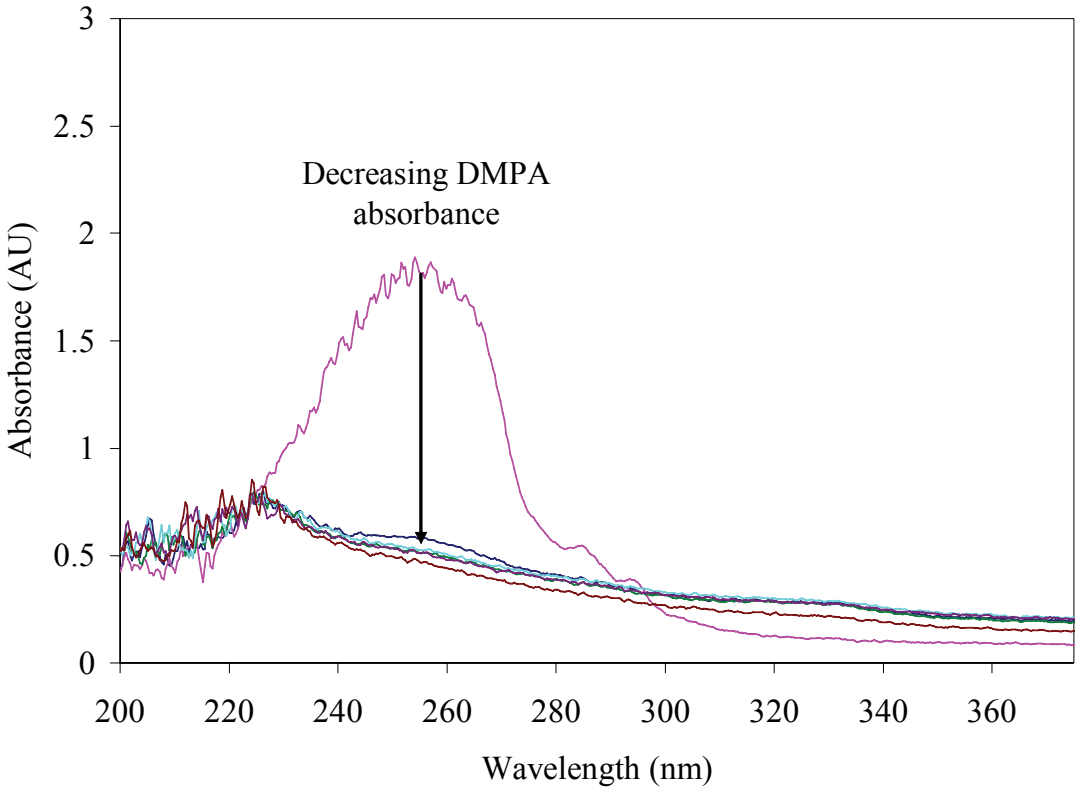

Figure 5.10. UV spectra demonstrating the decreased absorbance of DMPA, indicating that cross-linking occurred.

In the case of the styrenic-functionalized ionene, it was difficult to completely cross-link a thicker (~0.3 mm), free-standing film in the solid state. In fact, the film was swollen in isopropanol for 30 min before exposed to UV light to enhance the polymer chain end mobility. After UV irradiation, the polymer was mostly insoluble in methanol, as it was falling apart into many fine fiber-like pieces, which were insoluble in methanol after 48 h. This photo-cross-linked 12,12-ammonium ionene possessed an onset degradation temperature of 221 °C, which indicated a slight increase in thermal stability occurred upon cross-linking. Before photo-cross-linking, the styrenic-functionalized 12,12-ammonium ionene possessed a T_g of 37 °C. This indicated that the styrenic end groups did not affect the T_g in the same manner as the cinnamate-functionalized 12,12-ammonium ionene. The reason that the T_g did not lower considerably was

presumably due to the relative size of the end groups. The cinnamate end group was considerably larger than the styrenic end group, since the cinnamate end group possessed a long alkyl chain. After exposure to UV light, the cross-linked 12,12-ammonium ionene did not possess a T_g according to DSC.

5.5 Conclusions

12,12-Ammonium ionenes were prepared via the Menshutkin reaction from 1,12-dibromododecane and 1,12-bis(*N,N*-dimethylamino)dodecane. For the first time, the ionenes were functionalized with either cinnamate or styrenic groups and were then chain-extended or cross-linked via UV irradiation. The novel cinnamate-functionalized 12,12-ammonium ionene possessed enhanced mechanical properties (43.1 ± 0.4 MPa tensile stress and 640 ± 140 % elongation) compared to the 12,12-ammonium ionene prior to UV irradiation, which was too brittle for tensile measurements. Thin films of cinnamate ionene copolymers and styrenic-functionalized 12,12-ammonium ionenes were successfully cross-linked in the presence of UV light. The UV spectra were recorded after each exposure to UV light, indicating that cross-linking occurred. These results demonstrated that cross-linked ionenes show promise as mechanically durable polyelectrolytes that offer potential as membrane materials. In addition, utilization of UV light to prepare chain-extended, high molecular weight ionenes was demonstrated. This novel technique is a viable option to prepare high molecular weight polymers using step-growth polymerization techniques in concert with UV irradiation.

5.6 Acknowledgements

This material is based upon work supported in part by the Macromolecular Interfaces with Life Sciences (MILES) Integrative Graduate Education and Research Traineeship (IGERT)

of the National Science Foundation under agreement no. DGE-0333378. This material is based upon work supported in part by the U.S. Army Research Office under grant number W911NF-07-1-0452 Ionic Liquids in Electro-Active Devices (ILEAD) MURI. This material is based upon work supported in part by the Kimberly Clark Corporation.

5.7 References

(1) Gibbs, C. F.; Littman, E. R.; Marvel, C. S. *J. Am. Chem. Soc.* **1933,** 55, 753.
(2) Abboud, J. L. M.; Notario, R.; Bertran, J.; Sola, M. *Prog. Phys. Org. Chem.* **1993,** 19, 1-182.
(3) Casson, D.; Rembaum, A. *Macromolecules* **1972,** 5, (1), 75-81.
(4) Noguchi, N.; Rembaum, A. *Macromolecules* **1972,** 5, (3), 253-260.
(5) Rembaum, A.; Noguchi, N. *Macromolecules* **1972,** 5, (3), 261-269.
(6) Layman, J. M.; Borgerding, E. M.; Williams, S. R.; Heath, W. H.; Long, T. E. *Macromolecules* **2008,** 41, (13), 4635-4641.
(7) Williams, S. R.; Borgerding, E. M.; Layman, J. M.; Wang, W.; Winey, K. I.; Long, T. E. *Macromolecules* **2008,** 41, (14), 5216–5222.
(8) Suzuki, Y.; Tazuke, S. *Macromolecules* **1980,** 13, 25-30.
(9) Jung, B.-D.; Stumpe, J.; Hong, J.-D. *Thin Solid Films* **2003,** 441, 261-270.
(10) Robertson, E.; Deusen, W.; Minsk, L.; 1959, 308-311. *J. Appl. Polym. Sci.* **1959,** 2, (6), 308-311.
(11) Gupta, P.; Trenor, S. R.; Long, T. E.; Wilkes, G. L. *Macromolecules* **2004,** 37, 9211-9218.
(12) Wahlund, P.-O.; Izumrudov, V. A.; Gustavsson, P.-E.; Larsson, P.-O.; Galaev, I. Y. *Macromol. Biosci.* **2003,** 3, (8), 404-411.
(13) Zelikin, A. N.; Akritskaya, N. I.; Izumrudov, V. A. *Macromol. Chem. Phys.* **2001,** 202, (15), 3018-3026.
(14) Zelikin, A. N.; Litmanovich, A. A.; Paraschuk, V. V.; Sybatchin, A. V.; Izumrudov, V. A. *Macromolecules* **2003,** 36, (6), 2066-2071.
(15) Zelikin, A. N.; Putnam, D.; Shastri, P.; Langer, R.; Izumrudov, V. A. *Bioconjugate Chem.* **2002,** 13, (3), 548-553.
(16) Fitzpatrick, R.; Klinger, J. D.; Shackett, K. K. Ionene polymers and their use as antimicrobial agents. WO 2002080939, 2002.
(17) Jen, J. S.; Jones, R. E.; Homesley, P. M.; Petisce, J. Methods for providing biomedical devices with hydrophilic antimicrobial coatings. US 2005-68008 20050228, 2006.
(18) Narita, T.; Nishino, M.; Gong, J. P.; Osada, Y. *Colloid and Polymer Science* **2000,** 278, 884-887.
(19) Rembaum, A., Biological activity of ionene polymers. In *Polymeric Materials for Unusual Service Conditions*, Golub, M. A.; Parker., J. A., Eds. Wiley: New York, 1973; pp 299-317.
(20) Tashiro, T. *Macromolecular Materials and Engineering* **2001,** 286, 63-87.

(21) Rembaum, A. Ionene polymers for selectively inhibiting the vitro growth of malignant cells. 4,013,507, 1977.
(22) Spencer, T. A.; Onofrey, T. J.; Cann, R. O.; Russel, J. S.; Lee, L. E.; Blanchard, D. E.; Castro, A.; Gu, P.; Jiang, G. J.; Shechter, I. *J. Org. Chem.* **1999,** 64, (3), 807-818.
(23) Mathauer, K.; Schmidt, A.; Knoll, W.; Wegner, G. *Macromolecules* **1995,** 28, 1214-1220.
(24) Charlier, P.; Jerome, R.; Teyssie, P.; Prud'homme, R. E. *J. Polym. Sci. A* **1993,** 31, 128-134.
(25) Ruckenstein, E.; Chen, X. N. *Macromolecules* **2000,** 33, (24), 8992-9001.
(26) Patai, S., *The chemistry of the amino group*. Wiley: New York, 1968.
(27) Tsutsui, T.; Tanaka, R.; Tanaka, T. *J. Polym. Sci. Polym. Phys. Ed.* **1976,** 14, (12), 2259-2271.
(28) Cotter, R. J., Pyrolysis and desorption mass spectroscopy. In *Analytical pyrolysis. Techniques and applications*, Voorhees, K. J., Ed. Butterworths: London, 1984.
(29) Avram, E. *Rev. Roum. Chim* **2001,** 46, (1), 49-53.
(30) Lubkowski, J.; Blazejowski, J. *Thermochimica Acta* **1990,** 157, (2), 259-277.
(31) Haskins, N. J.; Mitchell, R. *Analyst* **1991,** 116, (9), 901-903.
(32) Muggli, M. W.; Ward, T. C.; Tchatchoua, C.; Ji, Q.; McGrath, J. E. *J. Polym. Sci. B. Polym. Phys.* **2003,** 41, 2850-2860.
(33) Wooley, K. L.; Hawker, C. J.; Pochan, J. M.; Frechet, J. M. J. *Macromolecules* **1993,** 26, (7), 1514-1519.
(34) Assaid, I.; Bosc, D.; Hardy, I. *J. Phys. Chem. B* **2004,** 108, (9), 2801-2806.
(35) Ikeda, Y.; Yamato, J.; Murakami, T.; Kajiwara, K. *Polymer* **2004,** 45, 8367-8375.

Chapter 6 : Ionene Segmented Block Copolymers Containing Imidazolium Cations: Structure-Property Relationships as a Function of Hard Segment Content

From: Williams, S.R.; Salas-de la Cruz, D.; Winey, K.I.; Long, T.E., to be submitted, 2008

6.1 Abstract

Imidazolium ionene segmented block copolymers were synthesized from 1,1'-(1,4-butanediyl)bis(imidazole) and 1,12-dibromododecane hard segments and 2000 g/mol PTMO dibromide soft segments. The polymer structures were confirmed using ^{1}H NMR spectroscopy, and resonances associated with methylene spacers from 1,12-dibromododecane became more apparent as the hard segment content increased. TGA revealed thermal stabilities ≥ 250 °C for all of the imidazolium ionene copolymers. DSC analysis demonstrated that the imidazolium ionenes containing PTMO soft segments possessed crystallinity, and a T_m of approximately 22 °C was observed. In addition, T_gs attributed to the PTMO segments were observed at approximately -80 °C for PTMO-containing imidazolium ionenes. The imidazolium ionene without PTMO soft segments possessed only a single T_g at 27 °C. The observation of thermal transitions in DMA data indicated that the PTMO imidazolium ionenes were microphase separated. IAXS and SAXS region showed evidence of microphase separation for the PTMO-containing imidazolium ionenes. The small-angle scattering peaks were believed to arise from the inter-particle scattering, with interdomain spacings ranging from approximately 10.5-18.5 nm for the imidazolium ionenes containing PTMO soft segments.

6.2 Introduction

Ionenes are ion-containing polymers that contain quaternary nitrogen atoms in the macromolecular main chain, as opposed to a pendant site, and are synthesized through a Menschutkin reaction of ditertiary amines and alkyl dihalides. Ammonium ionenes are widely reported in literature,[1-10] but the synthesis and structure-property relationships of imidazolium ionenes are not well-documented. In fact, only a few examples in the literature exist. For example, although the researchers did not refer to their systems as imidazolium ionenes, only two research groups have reported the preparation of quasi-solid state dye-sensitized solar cells containing imidazolium salts within the repeating unit of the polymer backbone.[11,12] Yanagida et al. were the first to report the synthesis of imidazolium salt-containing ionene polymers from alkyl bis(imidazoles) and alkyl diiodides for this purpose.[12] The second report originated from the group of Chen et al.[11] The researchers conducted investigations with imidazolium ionenes containing ethylene oxide chains, which are known for improving charge-transport properties.[13] The resulting dye-sensitized solar cells containing ethylene oxide repeating units possessed light-to-electricity conversion efficiencies of 1.56 %.

Typically, imidazolium cation-containing polymers are prepared from vinyl, acrylate, and methacrylate monomers using conventional free radical polymerization techniques. Ohno et al. synthesized organoboron and imidazolium salt-containing polymers via hydroboration polymerization for lithium cation transport purposes.[14] The resulting polymers possessed ionic conductivities of $3.74 \times 10^{-5} - 1.93 \times 10^{-5}$ S/cm at 50 °C when combined with equimolar concentrations of lithium bis(trifluoromethylsulfonyl)imide. In addition, Ohno et al. reported the synthesis of polymer brushes that contained imidazolium salts and poly(ethylene oxide) (PEO).[15]

The imidazolium polymer exhibited a conductivity of 1.49 x 10^{-4} S/cm at 30 °C and a T_g that was consistent with pure PEO.

Imidazolium cation-containing ionenes offer many advantages compared to conventional imidazole-containing polymers. The reactivity and charge density are easily controlled through variation in the alkylene spacer length between the bis(imidazole) monomer and the alkyl dihalide. In addition, the polymerization process does not require initiators or produce by-products. Segmented ionenes offer many interesting thermal, mechanical, and morphological properties due to the presence of oligomeric precursors. Poly(tetramethylene oxide) (PTMO) is a suitable oligomer for ionene polymers, and Kohjiya et al.[16] reported the first segmented ammonium ionene based on PTMO. The ammonium ionenes exhibited promising elastomeric behavior, namely, 1.37 MPa tensile stress at break and 510% elongation at break. Since then, many researchers have conducted ammonium ionene syntheses using PTMO segments. Leir and Stark conducted investigations on the reactivity of various dihalides with ditertiary amine end-capped PTMO.[17] However, in their synthetic strategy further alkylation can occur in the presence of dimethylamine. Therefore, the PTMO segment was not well-defined before the ionene polymerization. In a later collaboration with Wilkes et al., they determined the effect PTMO molecular weight, counteranion (Br^- vs Cl^-), and structural differences of the ionene hard segment on the thermal and mechanical properties of the ammonium ionenes. Overall, they concluded that PTMO ionenes behaved similar to polyurethane ionomers, despite the absence of hydrogen bonding that polyurethane ionomers have within their hard segments.[1] Furthermore, Wilkes et al. discovered that reacting an amino-terminated PTMO oligomer with 1,4-dibromo-*p*-xylene resulted in an ionene that microphase separated into rod-like structures.[18]

In this manuscript, the synthesis of novel imidazolium ionene copolymers containing PTMO soft segments is reported. The PTMO soft segment was prepared using a quantitative derivatization of PTMO using 6-bromohexanoyl chloride. This superior synthetic strategy avoids potential further alkylation which was a possible side reaction from a previously reported synthetic route.[17] To enhance the film formation properties, segmented block copolymers containing 1,12-dibromododecane hard segments were also synthesized. Thermal and mechanical properties were evaluated, and structure-property relationships were established as a function of hard segment content.

6.3 Experimental

6.3.1 Materials

Poly(tetramethylene oxide) (PTMO) oligomer (Terathane, Du Pont) with number-average molecular weight of 2000 g/mol was purchased from Aldrich and dried *in vacuo* (0.1 mm Hg) at 23 °C for 24 h prior to use. 1,12-Dibromododecane (Aldrich, 98%) was recrystallized from ethanol. Imidazole (Aldrich, ≥99%), dimethyl ether solution (Aldrich, 60% in water), 6-bromohexanoyl chloride (Alfa Aesar, 97%), toluene (EMD Chemicals, 99.5%), dimethylsulfoxide (DMSO, Aldrich, anhydrous grade), and diethyl ether (Fisher Scientific, 99.9%, anhydrous) were used as received. Sodium hydroxide pellets (Aldrich, ≥98%) were used to prepare a 50 wt % aqueous solution. 1,4-Dibromobutane (Aldrich, 99%) and triethylamine (TEA, Aldrich, 99%) were distilled prior to use. Dimethylformamide (DMF, Aldrich, 99.8%, anhydrous) and tetrahydrofuran (THF, EMD Science, HPLC grade) were passed through alumina and molecular sieves columns before use. Chloroform ($CHCl_3$, Fisher, Optima grade)

was distilled from sodium/benzophenone immediately prior to use. 1,12-Bis(*N,N*-dimethylamino)dodecane was synthesized according to a modified literature procedure.[10,19]

6.3.2 Synthesis of 1,1'-(1,4-butanediyl)bis(imidazole)

The procedure of So et al.[20] was used to synthesize 1,1'-(1,4-butanediyl)bis(imidazole), except 1,4-dibromobutane was used rather than 1,4-dichlorobutane. The final product was obtained in 89% yield. ^{1}H NMR (400 MHz, $(CD_3)_2SO$) δ = 7.58 (s, 2H), 7.11 (s, 2H), 6.86 (s, 2H), 3.92 (m, 4H), 1.59 (m, 4H). FAB MS: M+H = 191.12 (found), molecular weight = 190.12 (calculated).

6.3.3 Synthesis of poly(tetramethylene oxide) dibromide

PTMO (10.0 g, 0.005 mol) was dissolved in 200 mL dry $CHCl_3$ in a 500-mL round-bottomed flask containing a magnetic stirbar. TEA (1.53 mL, 0.011 mol, 2.2 eq) were added via syringe. The flask was equipped with an addition funnel and 100 mL of dry $CHCl_3$ was added to the funnel. 6-Bromohexanoyl chloride (1.68 mL, 0.011 mol, 2.2 eq) was syringed into the addition funnel. The reaction flask was cooled with an ice bath and the acid chloride was added dropwise to the reaction, and the reaction was allowed to warm to room temperature (23 °C). Stirring was continued for 18 h. When the reaction was complete, the solution was filtered through a Celite column to ensure complete removal of the triethylamine salt, and the reaction mixture was evaporated. The final product was obtained in 44% yield. ^{1}H NMR (400 MHz, $CDCl_3$) δ = 4.13 (t, 4H), 3.35 (m, 134H), 2.26 (t, 4H), 1.82 (q, 4H) 1.61 (q, 4H), 1.56 (m, 134 H), 1.42 (q, 4H). SEC-MALLS M_n = 2850 g/mol, M_w = 4000 g/mol, M_w/M_n = 1.39.

6.3.4 Synthesis of imidazolium ionene containing 100 wt % hard segment

1,12-dibromododecane (1.0 g, 3.05 mmol) and 1,1'-(1,4-butanediyl)bis(imidazole) (0.58 g, 3.05 mmol) were added to a two-neck, round-bottomed flask equipped with a stir bar, condenser, and nitrogen inlet. Dry DMF (20 wt % solids) was added to the flask via syringe. The reaction was allowed to proceed for 24 h at 80 °C. Upon completion, the polymer was cast into a film for further characterization. The drying procedure for film preparation was critical, and slow removal of DMF was required to avoid formation of film defects. DMF was allowed to evaporate in ambient conditions for 1 day. Subsequently, the films were heated in the Teflon™ molds at approximately 80 °C for at least 2-3 days. Finally, the polymer films were subsequently dried *in vacuo* (0.1 mm Hg) at 80 °C for 72 h to ensure complete removal of DMF. ^{1}H NMR (400 MHz, CD_3OD) δ = 9.17 (2H per repeating unit), 7.69 (4H per repeating unit), 4.23-4.33 (8H per repeating unit), 1.90-1.98 (8H per repeating unit), 1.30-1.35 (16H per repeating unit).

6.3.5 Synthesis of imidazolium ionene segmented block copolymers containing PTMO dibromide soft segments

The copolymer containing 38 wt % hard segment is used as an example; however, all copolymers were prepared in a similar fashion. 1,12-dibromododecane (0.194 g, 0.591 mmol), PTMO dibromide (0.562, 0.197 mmol), and 1,1'-(1,4-butanediyl)bis(imidazole) (0.15 g, 0.788 mmol) were added to a two-neck, round-bottomed flask equipped with a stir bar, condenser, and nitrogen inlet. Dry DMF (20 wt % solids) was added to the flask via syringe. The reaction was allowed to proceed for 24 h at 80 °C. Upon completion, the polymer was cast into a film for further characterization. The drying procedure for film preparation was critical, and slow removal of DMF was required to avoid formation of film defects. DMF was allowed to

evaporate in ambient conditions for 1 day. Subsequently, the films were heated in the Teflon™ molds at approximately 80 °C for at least 2-3 days. Finally, the polymer films were subsequently dried *in vacuo* (0.1 mm Hg) at 80 °C for 72 h to ensure complete removal of DMF. ^{1}H NMR (400 MHz, CD_3OD) δ = 9.17 (2H per repeating unit), 7.68 (4H per repeating unit), 4.23-4.33 (8H per repeating unit), 4.10 (t, 4H per repeating unit), 3.44 (m, 134H PTMO), 2.35 (t, 4H per repeating unit), 1.91-1.98 (8H per repeating unit), 1.89 (q, 4H per repeating unit) 1.66 (q, 4H per repeating unit), 1.62 (m, 134 H PTMO), 1.40 (q, 4H), 1.30-1.36 (16H per repeating unit).

6.3.6 Characterization

^{1}H NMR spectroscopy was utilized to determine monomer composition in $CDCl_3$ at 23 °C with a 400 MHz Varian UNITY spectrometer. FAB-MS was obtained on a JOEL HX110 dual focusing mass spectrometer. A TA Instruments Hi-Res TGA 2950 with a temperature ramp of 10 °C/min in a nitrogen atmosphere was used for thermogravimetric analysis (TGA) Dynamic mechanical analysis (DMA) was conducted on a TA Instruments Q800 dynamic mechanical analyzer in tension mode at a frequency of 1 Hz and temperature ramp of 3 °C/min. The sample was cooled from room temperature to -30 °C prior to heating. The glass transition temperature (T_g) was determined at the peak of the tan δ curve. Differential scanning calorimetry (DSC) was performed using a TA Instruments Q100 differential scanning calorimeter under a nitrogen flow of 50 mL/min. The sample was first heated from -100 °C to 125 °C at a heating rate of 10 °C/min. The cooling rate was 20 °C/min, and a subsequent heating from -100 °C to 125 °C at a heating rate of 10 °C/min was conducted.

The solvent-cast and dried imidazolium ionene films were used directly for X-ray scattering characterization. The polymer films were dried *in vacuo* (0.1 mm Hg) at 60 °C for 24 h to ensure complete removal of solvent. The multi-angle X-ray scattering system (MAXS)

generated Cu X-ray from a Nonius FR 591 rotating-anode generator operated at 40 kV and 85 mA. The bright, highly collimated beam was obtained via Osmic Max-Flux optics and pin collimation in an integral vacuum system. The scattering data were collected using a Bruker Hi-Star multiwire detector with a sample to detector distance of 7, 11, 54 and 124 cm. The 2-D data reduction and analysis were performed using *Datasqueeze* software.[21] The MAXS system provides an uncommonly wide range of scattering angles that was critical in evaluating the morphology of these segmented copolymers.

6.4 Results and Discussion

The bisimidazole monomer, (1,1'-(1,4-butanediyl)bis(imidazole)), was prepared from imidazole and 1,4-dibromobutane, according to a literature procedure (Scheme 6.1).[20] In the first step, imidazole was deprotonated, and in the subsequent step, the anionic nucleophile attacked the primary alkyl bromide, yielding the final structure shown in Scheme 6.1. The final structure, confirmed with ^{1}H NMR spectroscopy and FAB-MS, corresponded well to previous literature results.

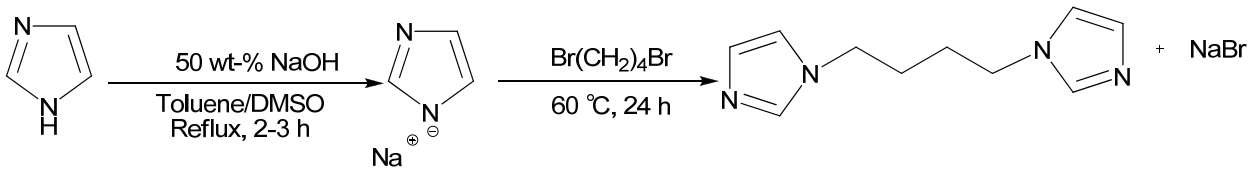

Scheme 6.1. Synthesis of 1,1'-(1,4-butanediyl)bis(imidazole).

The soft segment, bromine-terminated PTMO, was prepared via quantitative derivatization of 2000 g/mol PTMO with 6-bromohexanoyl chloride to yield an oligomeric dibromide (Scheme 6.2). This novel structure was confirmed using ^{1}H NMR spectroscopy, and the absolute molecular weights were determined from SEC-MALLS and ^{1}H NMR spectroscopy. After derivatization, SEC-MALLS revealed a typical M_n of 2850 g/mol, M_w of 4000 g/mol, and

M_w/M_n of 1.39. These values correlated well to the ^{1}H NMR M_n of 2800 g/mol. This synthetic route was facile and the soft segment molecular weight is easily varied with perfectly difunctional and commercially available PTMO diols that have low polydispersity. It is important to note that the five carbon spacer was not critical for successful oligomeric dibromide synthesis when the reaction was conducted in $CHCl_3$. Other acid chlorides are commercially available, including bromoacetyl chloride. However, Schneider et al. reported that bromoacetyl bromide cleaved ethers, including THF.[22] Therefore, all quantitative derivatizations of PTMO were conducted in $CHCl_3$ to prevent any deleterious side reactions. Synthesis of this bromine terminated soft segment is novel, since Sukhyy et al. were the only researchers to report the synthesis of oligomeric ionene precursors using chloroacetyl chloride and poly(ethylene glycol); however, the exact synthetic details were omitted from their manuscript, and different starting materials were utilized.

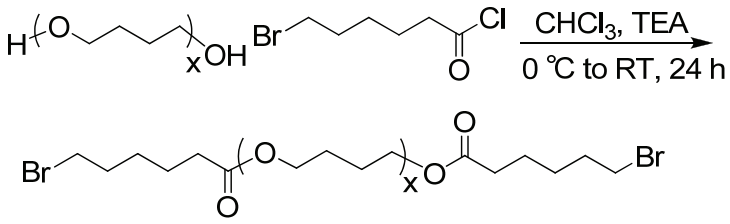

Scheme 6.2. Synthesis of bromine-terminated PTMO.

Imidazolium ionenes were prepared according to Scheme 6.3. The amount of soft segment (SS) and hard segment (HS) were varied, while maintaining a 1:1 molar ratio of bisimidazole : dibromide. In all, five novel polymer compositions were synthesized, as shown in Table 6.1. HS compositions were calculated from the amount of 1,12-dibromododecane and 1,1'-(1,4-butanediyl)bis(imidazole) added; the HS content varied from 6 – 100 wt %. The 1:1

molar ratios of monomers, shown in Table 6.1, is ideal for high molecular weight step-growth polymers.[23,24]

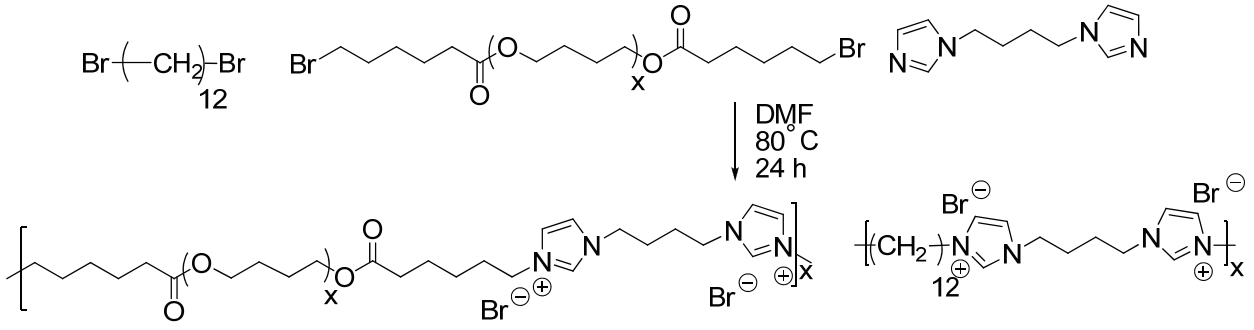

Scheme 6.3. Synthesis of imidazolium ionene segmented block copolymers containing 1,12-dibromododecane and bromine-terminated PTMO.

PTMO Dibromide (mol eq.)	1,12-Dibromide (mol eq.)	Bisimidazole (mol eq.)	HS (wt %)	SS (wt %)
1.00	0.00	1.00	6	94
0.75	0.25	1.00	9	91
0.50	0.50	1.00	20	80
0.25	0.75	1.00	38	62
0.00	1.00	1.00	100	0

Table 6.1. Copolymer compositions based on molar equivalents of monomer and HS/SS content.

Copolymer composition was evaluated using ^{1}H NMR spectroscopy. The HS/SS ratio corresponded well to the feed ratios of monomers. Figure 6.1 demonstrates the change in ^{1}H NMR spectra as the hard segment content was varied. As expected, the resonances associated with the methylene spacers (~1.2 ppm) of 1,12-dibromododecane became more apparent as the hard segment content increased.

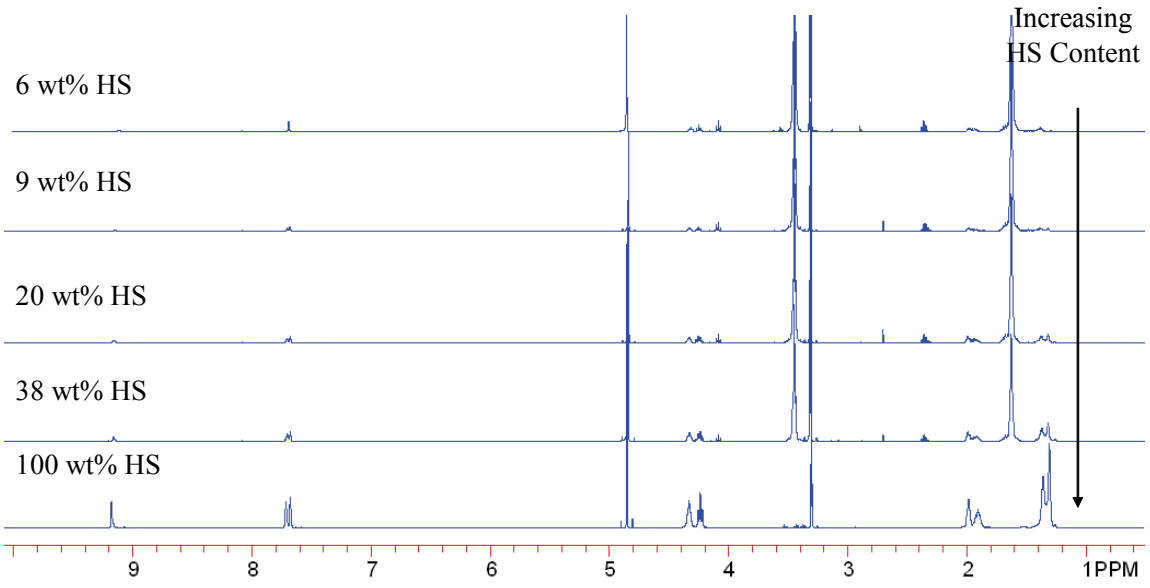

Figure 6.1. ^{1}H NMR spectroscopy of imidazolium ionene segmented block copolymers as a function of hard segment content.

Thermogravimetric analysis (TGA) of the ionenes demonstrated high thermal stability for these polymers (Table 6.2). An exact trend in thermal stability as a function of HS content was not observed, but all imidazolium copolymers were stable to ≥ 250 °C. These values were slightly greater than those previously reported for conventional ammonium ionenes.[10,25] However, the ionenes were not as thermally stable as imidazole-containing acrylate copolymers, which reportedly possessed onset degradation temperatures approaching 400 °C.[26]

The effect of hard segment content on thermal transitions was investigated using DSC, and the results for the imidazolium ionene copolymers are shown in Table 6.2. Each copolymer that contained PTMO soft segments possessed a T_g near -80 °C, which was similar to the T_g of pure PTMO. All imidazolium ionenes containing PTMO segments also possessed T_ms, which were similar to the T_m of pure PTMO, indicating that the imidazolium ionenes containing PTMO segments possessed crystallinity. Furthermore, these results indicated that if ionic aggregates were present, they were not mixed with the PTMO soft segment, since the T_gs of the copolymers

were nearly identical to values for the precursor PTMO oligomer. Therefore, the imidazolium ionene copolymers were microphase separated.

HS (wt %)	SS (wt %)	$T_{d5\%}$ (°C)	T_g (°C)	T_m (°C)
6	94	262	-82	23
9	91	263	-80	24
20	80	266	-83	22
38	62	270	-84	22
100	0	257	27	-

Table 6.2. TGA and DSC results of imidazolium ionene copolymers.

As expected, a variety of film-forming properties resulted as a function of hard segment content for the imidazolium ionene copolymers. As hard segment concentration increased, the toughness of the polymer film increased to a critical level, and then became brittle with an increasing amount of hard segment. The two copolymers containing 20 and 38 wt % hard segment formed free-standing films and were easily characterized using DMA (Figure 6.2). However, the imidazolium ionene consisting of 100 wt % hard segment was too brittle to examine using DMA. The imidazolium ionene with 20 wt % HS content possessed a higher glassy modulus (3200 MPa at -100 °C) compared to the 38 wt % HS imidazolium ionene (1700 MPa at -100 °C) since a higher amount of 2000 g/mol PTMO segments were present. This is in agreement with Wilkes et al.[27] and Long et al.,[28] where both research groups reported that the presence of PTMO crystals increased the glassy modulus. The imidazolium ionenes did not show an extended rubbery plateau, and many transitions were observed as temperature increased. Three transitions were observed in the 20 wt % HS imidazolium ionene, including a T_g at -75 °C, a broad decrease in modulus centered near -20 °C, and a large decrease in modulus attributed to

flow and melting of crystalline PTMO segments at 33 °C.[29] Four transitions were observed in the 38 wt % HS imidazolium ionene. Similar to the 20 wt % HS imidazolium ionene, the 38 wt % imidazolium ionene had a T_g at -80 °C and a broad decrease in modulus centered around -20 °C. In addition, a decrease in modulus was observed at 24 °C, approximately the same temperature at which pure PTMO melts. Finally, a large decrease in modulus attributed to flow was observed at 39 °C. The imidazolium ionenes had similar flow temperatures, indicating that the ionic aggregates persisted to approximately the same temperature as the PTMO crystallites.

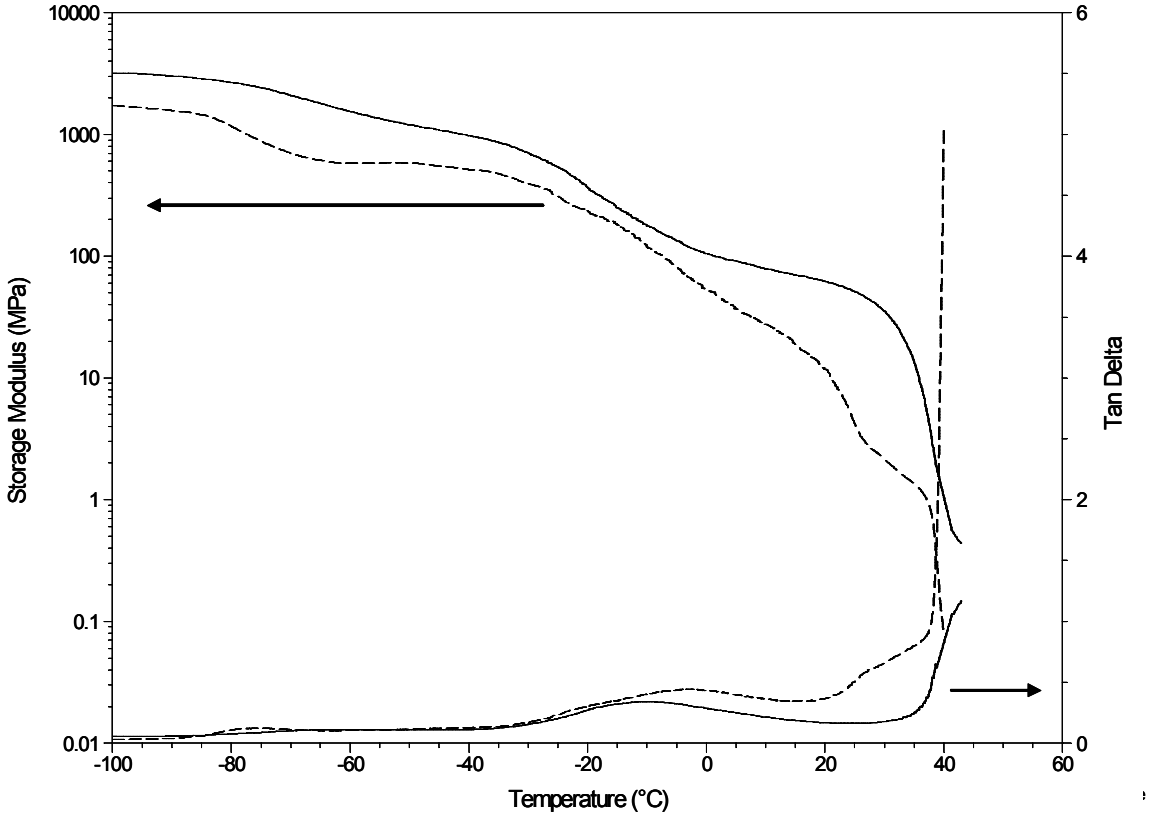

Figure 6.2. Dynamic mechanical behavior of PTMO-based imidazolium ionenes. Dashed line = 38 wt % HS, solid line = 20 wt % HS.

Scattering patterns were recorded at the small, intermediate and wide angle regions. The majority of the samples exhibited isotropic behavior with the exception of the imidazolium ionenes possessing 9 wt % HS; this sample showed anisotropic behavior at the intermediate and small angle regions. Figure 6.3 shows the combined multi-angle X-ray scattering intensity versus scattering vector q plotted in a log-log scale of the imidazolium ionenes as a function of HS content. The scattering data of the PTMO-containing imidazolium ionene containing 6 wt % HS illustrated typical peaks arising from PTMO soft segments.[30] Two sharp crystalline reflection peaks at a scattering vector q of 14.2 nm^{-1} and 17.3 nm^{-1} corresponded to the (020) and (110) peaks of PTMO crystals.[30] This imidazolium ionene also showed two scattering peaks at 0.42 nm^{-1} and 0.87 nm^{-1} that corresponded to a spacing of 15.0 nm. PTMO typically crystallizes as a monoclinic crystal structure, with molecular chains having a planar zig-zag conformation along the c-axis of the unit cell.[31] The length of a fully extended crystalline PTMO chain of 2000 g/mol is approximately 16.8 nm, comparable to the inter-lamellar spacing given via X-ray scattering.

Similarly, the imidazolium ionene possessing 9 wt % HS displayed peaks at q = 14.2 nm^{-1} and q = 17.3 nm^{-1}, corresponding to the crystalline region of PTMO. The two peaks at q ~ 0.3 nm^{-1} and q ~ 1.03 nm^{-1} broadened with the wt % increase of HS, and the inter-lamellar spacing distribution increased with increasing HS content. Furthermore, this sample exhibited anisotropic scattering at these two scattering vectors. When the HS content increased to 20 wt %, the intensity of the two crystalline peaks at the wide angle region decreased, and the peak overlapped with a broad amorphous peak associated with the imidazolium ionene. In addition, two higher order scattering peaks were observed at q ~ 0.6 nm^{-1} and q ~ 1.2 nm^{-1}. Furthermore, a

very weak peak seems to appear at q ~ 3.12 nm^{-1}. Therefore, this sample exhibited hierarchical transitional morphology.

Likewise, the imidazolium ionene containing 38 wt % HS had overlap of the two crystalline peaks and the broad amorphous imidazolium ionene peak at q = 15.6 nm^{-1}. Moreover, an ionic correlation peak at q = 3.2 nm^{-1} was observed which corresponded to a real space distance of 1.9 nm. The correlation distance between these domains was well-defined because the separation between bisimidazolium functional groups was exactly 12 methylene groups. If this polyethylene segment was in the all-*trans* crystalline conformation, the imidazolium-imidazolium separation would be 1.60 nm. In addition, three high order peaks were observed at q ~ 0.5 nm^{-1}, 1.0 nm^{-1}, and 1.5 nm^{-1}. The 2-D scattering changed from anisotropic to isotropic upon the increase of the percent of HS from 20-38 wt%.

The 100 wt % HS imidazolium ionene showed two peaks at q ~2.7 nm^{-1} and q ~15.6 nm^{-1}. The peak at q ~15.6 nm^{-1} was attributed to the amorphous regions of the polymer. The peak at q ~2.7 nm^{-1} has a real-space distance of 2.3 nm and corresponds to ionic aggregation. The peak associated with ionic aggregation was located in the intermediate angle region, and had similar peak values as the 12,12-ammonium ionenes (4.38 nm^{-1}, 1.43 nm) reported previously.[10] It was expected that the ionic aggregates were larger for the imidazolium ionenes compared to those for the ammonium ionenes, since each repeating unit of the imidazolium ionenes contained two imidazolium salt units. In summary, the IAXS and SAXS region showed evidence of microphase separation for the PTMO-containing imidazolium ionenes. The small-angle scattering peaks were believed to arise from the inter-particle scattering, with interdomain spacings ranging from approximately 10.5-18.5 nm for the imidazolium ionenes containing PTMO soft segments. Others have observed the incompatibility between soft and hard segments,

resulting in the formation of multiphase structures in various segmented polymers.[32-36] The driving force for the microphase separation in the PTMO imidazolium ionenes was due to the incompatibility of the PTMO segments and the ionic domains. The multiple reflections are an X-ray scattering phenomena due to highly oriented structures.

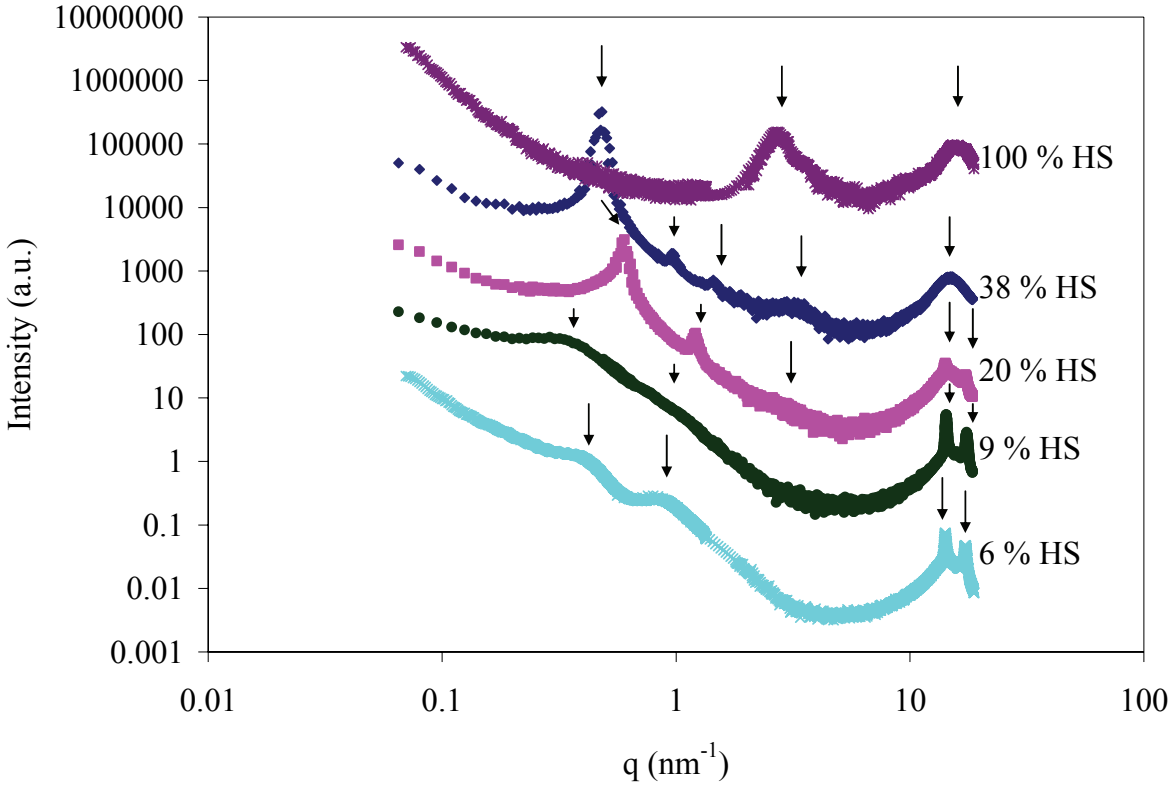

Figure 6.3. Multi-angle X-ray scattering intensity vs. scattering vector q plotted in log-log scale for unstretched PTMO-based imidazolium ionene films containing different concentrations of hard segment. The interdomain spacing was calculated from $d = 2\pi/q$.

6.5 Conclusions

This paper reports the first synthesis of imidazolium cation-containing ionene segmented block copolymers. The copolymers were prepared from novel PTMO dibromide oligomers, 1,12-dibromododecane, and 1,1'-(1,4-butanediyl)bis(imidazole), with hard segment contents

ranging from 6-100 wt %. Structure-property relationships were established as a function of hard segment content. Thermal stabilities were ≥ 250 °C. DSC indicated that the imidazolium ionenes containing PTMO segments possessed a T_g similar to pure PTMO, while the imidazolium ionene containing 100 wt % HS possessed a T_g of 27 °C. Film formation ability varied as a function of hard segment content and were enhanced when hard segment content increased to a critical level, above which the films were brittle. Dynamic mechanical behavior of the 20- and 38 wt % HS copolymers demonstrated microphase separation. IAXS and SAXS region showed evidence of microphase separation for the PTMO-containing imidazolium ionenes. The small-angle scattering peaks were believed to arise from the inter-particle scattering, with interdomain spacings ranging from approximately 10.5-18.5 nm for the imidazolium ionenes containing PTMO soft segments.

6.6 Acknowledgments

This material is based upon work supported in part by the Macromolecular Interfaces with Life Sciences (MILES) Integrative Graduate Education and Research Traineeship (IGERT) of the National Science Foundation under agreement no. DGE-0333378. This material is based upon work supported in part by the U.S. Army Research Office under grant number W911NF-07-1-0452 Ionic Liquids in Electro-Active Devices (ILEAD) MURI. This material is based upon work supported in part by the Kimberly Clark Corporation.

6.7 References

(1) Feng, D.; Venkateshwaran, L. N.; Wilkes, G. L.; Leir, C. M.; Stark, J. E. *Journal of Applied Polymer Science* **1989,** 38, (8), 1549-1565.
(2) Feng, D.; Wilkes, G. L.; Lee, B.; McGrath, J. E. *Polymer* **1992,** 33, (3), 526-535.
(3) Layman, J. M.; Borgerding, E. M.; Williams, S. R.; Heath, W. H.; Long, T. E. *Macromolecules* **2008,** 41, (13), 4635-4641.

(4) Loveday, D.; Wilkes, G. L.; Bheda, M. C.; Shen, Y. X.; Gibson, H. W. *J. Macro. Sci., Part A* **1995,** 32, (1), 1-27.
(5) Rembaum, A., Biological activity of ionene polymers. In *Polymeric Materials for Unusual Service Conditions*, Golub, M. A.; Parker., J. A., Eds. Wiley: New York, 1973; pp 299-317.
(6) Rembaum, A. Ionene polymers for selectively inhibiting the vitro growth of malignant cells. 4,013,507, 1977.
(7) Rembaum, A.; Baumgartner, W.; Eisenberg, A. *J. Polym. Sci. Polym. Lett. Ed.* **1968,** 6, (3), 159-171.
(8) Rembaum, A.; Noguchi, N. *Macromolecules* **1972,** 5, (3), 261-269.
(9) Rembaum, A.; Singer, S.; Keyzer, H. *J. Polym. Sci. Polym. Lett. Ed.* **1969,** 7, 395-402.
(10) Williams, S. R.; Borgerding, E. M.; Layman, J. M.; Wang, W.; Winey, K. I.; Long, T. E. *Macromolecules* **2008,** 41, (14), 5216–5222.
(11) Li, F.; Cheng, F.; Shi, J.; Cai, F.; Liang, M.; Chen, J. *J. Power Sources* **2007,** 165, 911-915.
(12) Suzuki, K.; Yamaguchi, M.; Hotta, S.; Tanabe, N.; Yanagida, S. *J. Photochem. Photobio. A: Chem.* **2004,** 164, 81-85.
(13) Fragiadakis, D.; Dou, S.; Colby, R. H.; Runt, J. *Macromolecules* **2008,** 41, (15), 5723-5728.
(14) Matsumi, N.; Sugai, K.; Miyake, M.; Ohno, H. *Macromolecules* **2006,** 39, 6924-6927.
(15) Yoshizawa, M.; Ohno, H. *Electrochem. Acta* **2001,** 46, 1723-1728.
(16) Kohjiya, S.; Ohtsuki, T.; Yamashita, S. *Makromolekulare Chemie-Rapid Communications* **1981,** 2, (6-7), 417-420.
(17) Leir, C. M.; Stark, J. E. *Journal of Applied Polymer Science* **1989,** 38, (8), 1535-1547.
(18) Feng, D.; Wilkes, G. L.; Leir, C. M.; Stark, J. E. *J. Macromol. Sci.-Chem.* **1989,** A26, (8), 1151-1181.
(19) Spencer, T. A.; Onofrey, T. J.; Cann, R. O.; Russel, J. S.; Lee, L. E.; Blanchard, D. E.; Castro, A.; Gu, P.; Jiang, G. J.; Shechter, I. *J. Org. Chem.* **1999,** 64, (3), 807-818.
(20) So, Y. H. *Macromolecules* **1992,** 25, (2), 516-520.
(21) Heiney, P. A. *Comm Powder Diffr Newsletter* **2005,** 32, 9-11.
(22) Schneider, D. F.; Viljoen, M. S. *Synthetic Communications* **2002,** 32, (5), 721-728.
(23) Odian, G., *Priciples of polymerization*. 4th ed.; Wiley-Interscience: Hoboken, 2004.
(24) Stevens, M. P., *Polymer chemistry*. 3rd ed.; Oxford University Press: Oxford, 1999.
(25) Tsutsui, T.; Tanaka, R.; Tanaka, T. *J. Polym. Sci. Polym. Phys. Ed.* **1976,** 14, (12), 2259-2271.
(26) Nakajima, H.; Ohno, H. *Polymer* **2005,** 46, (25), 11499-11504.
(27) Das, S.; Yilgor, I.; Yilgor, E.; Inci, B.; Tezgel, O.; Beyer, F. L.; Wilkes, G. L. *Polymer* **2007,** 48, 290-301.
(28) Williams, S. R.; Wang, W.; Winey, K. I.; Long, T. E. *Macrmolecules* **2008,** in preparation.
(29) Hu, C. B.; Ward, R. S.; Schneider, N. S. *Journal of Applied Polymer Science* **1982,** 27, (6), 2167-2177.
(30) Sun, Y.; Jeng, U.; Huang, Y.; Liang, K.; Lin, T.; Tsao, C. *Physica B* **2006,** 385, 650-652.
(31) Tadokoro, H. *J. Poly. Sci., Part C* **1966,** 15, 1-15.
(32) Aneja, A.; Wilkes, G. L. *Polymer* **2003,** 44, (23), 7221-7228.

(33) Klinedinst, D. B.; Yilgor, E.; Yilgor, I.; Beyer, F. L.; Wilkes, G. L. *Polymer* **2005,** 46, (23), 10191-10201.
(34) O'Sickey, M. J.; Lawrey, B. D.; Wilkes, G. L. *Polymer* **2002,** 43, (26), 7399-7408.
(35) Sheth, J. P.; Klinedinst, D. B.; Wilkes, G. L.; Iskender, Y.; Yilgor, E. *Polymer* **2005,** 46, (18), 7317-7322.
(36) Sheth, J. P.; Unal, S.; Yilgor, E.; Yilgor, I.; Beyer, F. L.; Long, T. E.; Wilkes, G. L. *Polymer* **2005,** 46, (23), 10180-10190.

Chapter 7 : Influence of Imidazolium Salt Chain Extenders on the Thermomechanical Properties and Morphology of Segmented Poly(tetramethylene oxide)-Based Polyurethanes

From: Williams, S.R.; Wang, W.; Winey, K.I.; Long, T.E., to be submitted, 2008.

7.1 Abstract

This chapter demonstrates the synthesis of a novel PTMO-based polyurethane containing bisimidazolium functionality in the hard segment. Comparisons with a non-ion containing polyurethane revealed that the novel imidazolium-containing polyurethane possessed unique thermomechanical, tensile, and morphological behaviors. Thermogravimetric analysis revealed that both types of polyurethanes possessed similar thermal stabilities; however, differential scanning calorimetry revealed that the imidazolium containing polyurethane possessed crystallinity, with a T_m of 15 °C, while both polyurethanes possessed T_gs similar to pure PTMO. Dynamic mechanical behaviors were also different as a function of hard segment structure. While the T_gs were similar, the behavior after the T_g was different. Specifically, the non-charged polyurethane exhibited an extended rubbery plateau to 125 °C, while the imidazolium-containing polyurethane flowed at approximately 50 °C. The X-ray scattering data demonstrated that both polyurethane compositions were of low crystallinity or amorphous at ambient temperature. STEM images revealed that ionic domains were rich in bromine. FT-IR spectroscopy indicated that ion-containing hard segments disrupted hydrogen bonding and thus, lowered the mechanical performance. Wide-angle X-ray scattering of the stretched films indicated that PTMO crystallization was induced.

7.2 Introduction

Polyurethanes consist of alternating hard and soft segments, where the hard segment results from a reaction between a diisocyanate and chain extender. The soft segments typically consist of low T_g polyols that possess molecular weights of ~500-5000 g/mol. Polyurethanes are high performance materials used in a variety of applications due to their elastomeric behavior and excellent mechanical properties. The driving force for elastomeric behavior is microphase separation of hard and soft segments.[1] Microphase separation occurs due to the incompatibility of hard and soft segments, where the hard segment contains urethane functionality that is more polar than the oligomeric soft segment and hydrogen bonding that further enhances microphase separation.[2] Due to the excellent mechanical behavior and elasticity of polyurethanes, they are used in a variety of applications including foams, coatings, fibers, and biomaterials.[3-9]

Ion-containing polyurethanes are used in many of the same applications as conventional polyurethanes, but are particularly well-suited for biomedical[10,11] and conductive polymer[12-15] applications. However, ion-containing polyurethanes add a new complexity to typical polyurethane syntheses with the addition of ionic functionality, and the incorporation of ions can either disrupt or enhance typical microphase separation.[16] Polyurethane ionomers, first reviewed in 1970,[17] have received widespread attention due to the many types of interactions among soft segments, urethane hydrogen bonding groups, and ionic groups. Ionic group location (either in the hard or soft segment) contributes significantly to the potential electrostatic interactions, multiphase morphology, and mechanical performance of ion-containing polyurethane elastomers.

The synthesis of cation-containing polyurethanes is generally achieved using two different synthetic methodologies: (1) the cationic functionality is incorporated through a cationic diol chain extender, or (2) non-charged polyurethanes are derivatized to introduce ionic

sites.[17] Typically, post-polymerization functionalization, the latter method, is used to introduce quaternary ammonium groups into polyurethanes.[17-19] Quaternary ammonium-containing polyurethanes are prevalent in the literature,[2,11,20,21] including polyurethanes that are cross-linked at nitrogen atoms using α,ω-dialkylhalides.[11,22,23] The synthesis of imidazolium salt-containing polyurethanes is not well-documented, and typically, imidazole-containing polymers are reported rather than the corresponding cationic imidazolium-containing polymers. For example, Collier et al. reported the synthesis of 2,2'-biimidazole-containing polyurethanes to investigate their metal chelating properties (Figure 7.1).[24] Their polyurethanes did not possess cationic imidazolium groups within the main chain, but did possess nitrogen atoms that could accept a proton or metal ion, such as cobalt, nickel, copper, or zinc. In 2001, Meyer et al. synthesized polyurethanes containing imidazole functionality within the polymer main chain for ion transport applications, including fuel cells, sensors, and batteries.[25] In 2005, the successful synthesis of cross-linked polyurethane cationomers containing pyridinium functionality was achieved. The novel polymers possessed enhanced thermal stability compared to conventional polyurethanes, and thus offered a greater processing temperature range for industrial applications.[26] Zhang et al. recently integrated imidazolium/poly(propylene glycol)/toluenediisocyanate prepolymers into epoxy resins in order to toughen cured products.[27] However, the synthesis, mechanical performance, and morphological properties of polyurethanes containing bisimidazolium diols remains unexplored. Recently, Ohno et al. reported bisimidazolium diols as intermediates in the synthesis of diacrylate cross-linkers for incorporation into polymer gels.[28] As shown herein, these bisimidazolium diols are also useful chain extenders for polyurethane synthesis.

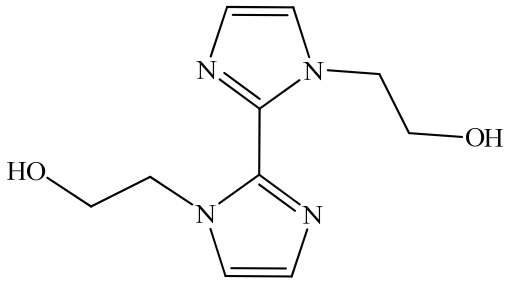

Figure 7.1. Structure of the 2,2'-biimidazole-based chain extender used in the polyurethane synthesis of Collier et al.[24]

In this work, the synthesis of a novel polyurethane containing a imidazolium bromide salt chain extender was achieved. The resulting polymer was compared to a non-charged polyurethane, containing a 1,4-butane diol chain extender, with regard to thermomechanical and morphological properties. The presence of ionic interactions in the hard segment drastically influenced the properties.

7.3 Experimental

7.3.1 Materials

PTMO oligomer (Terathane, Du Pont) with number-average molecular weight of 2000 g/mol and 1,4-butanediol were purchased from Aldrich and dried *in vacuo* (0.1 mm Hg) at 23 °C for 24 h prior to use. Bayer kindly provided bis(4-isocyanatocyclohexyl)methane (HMDI) with purity greater than 99.5%. Imidazole (Aldrich, ≥99%), toluene (EMD Chemicals, 99.5%), dimethylsulfoxide (Aldrich, anhydrous grade), and diethyl ether (Fisher Scientific, 99.9%, anhydrous) were used as received. Dibutyl tin dilaurate (DBTDL, 99%) was dissolved in THF as a 1 wt % solution. Sodium hydroxide pellets (Aldrich, ≥98%) were used to prepare a 50 wt% aqueous solution. 2-Bromoethanol (Aldrich, 95%) and 1,4-dibromobutane (Aldrich, 99%) were distilled prior to use. Dimethylformamide (Aldrich, 99.8%, anhydrous) was passed through an alumina column and a molecular sieves column before use.

7.3.2 Synthesis of 1,1'-(1,4-butanediyl)bis(imidazole)

The procedure of So et al.[29] was used to synthesize 1,1'-(1,4-butanediyl)bis(imidazole), except 1,4-dibromobutane was used rather than 1,4-dichlorobutane. The final product was obtained in 89% yield. ^{1}H NMR (400 MHz, $(CD_3)_2SO$) δ = 7.58 (s, 2H), 7.11 (s, 2H), 6.86 (s, 2H), 3.92 (m, 4H), 1.59 (m, 4H). FAB MS: M+H = 191.12 (found), molecular weight = 190.12 (calculated).

7.3.3 Synthesis of 1,1'-(butane-1,4-diyl)bis(3-(2-hydroxyethyl)-1H-imidazol-3-ium) bromide

The procedure of Ohno et al. was used to synthesize the imidazolium diol chain extender.[28] The final product was obtained in 78 % yield. ^{1}H NMR (400 MHz, D_2O) δ = 8.73 (s, 2H), 7.40 (m, 4H), 4.12-4.19 (m, 8H), 3.80 (m, 4H), 1.79 (m, 4H). FAB MS: M+Br = 358.12 (found), molecular weight = 278.22 (calculated).

7.3.4 Synthesis of polyurethanes

All reactions were conducted in three-necked, round-bottomed flasks equipped with an addition funnel, nitrogen inlet, and overhead stirrer. In the first step, HMDI end-capped PTMO prepolymers were prepared in the absence of solvent at 80 °C with 1 wt % DBTDL in THF (0.01 mL) as the catalyst, according to a literature procedure.[1] In the second step, the chain extenders (1,1'-(butane-1,4-diyl)bis(3-(2-hydroxyethyl)-1*H*-imidazol-3-ium) bromide or 1,4-butanediol) were dissolved in DMF (20 wt% solids), and the polyurethanes were prepared via the dropwise addition (over 1 h) of the chain extender solution into the HMDI end-capped PTMO prepolymer. The polymerization reactions were allowed to proceed for 24 h at 80 °C.

7.3.5 Characterization

^{1}H NMR spectroscopy was utilized to determine monomer composition in $CDCl_3$ at 23 °C with a 400 MHz Varian UNITY spectrometer. FAB-MS was obtained on a JOEL HX110 dual focusing mass spectrometer. A TA Instruments Hi-Res TGA 2950 with a temperature ramp of 10 °C/min in a nitrogen atmosphere was used for thermogravimetric analysis (TGA) Dynamic mechanical analysis (DMA) was conducted on a TA Instruments Q800 dynamic mechanical analyzer in tension mode at a frequency of 1 Hz and temperature ramp of 3 °C/min. The sample was cooled from room temperature to -150 °C prior to heating. The glass transition temperature (T_g) was determined at the first decrease in the storage modulus. Differential scanning calorimetry (DSC) was performed using a TA Instruments Q2000 differential scanning calorimeter under a nitrogen flow of 50 mL/min. The sample was first heated from -20 °C to 200 °C at a heating rate of 10 °C/min and held for 5 min to erase the thermal history. The cooling rate was 10 °C/min, and a subsequent heating from -130 °C to 200 °C at a heating rate of 5 °C/min was conducted. Dogbone-shaped film specimens, cut with a die according to ASTM D3368 specifications, were used for tensile tests performed on a 5500R Instron universal testing instrument with a cross-head speed of 50 mm/min using manual grips at 23 °C. The extent of hydrogen bonding of solvent-cast films was evaluated using a MIDAC M2004 ATR-FTIR at ambient conditions. The spectra, including the background scan, were collected at a resolution of 4 cm^{-1} and averaged over 128 scans.

Morphological analysis was conducted using a variety of complementary techniques. The solvent-cast and dried polyurethane films were used directly for X-ray scattering characterization. The polymer films were dried *in vacuo* (0.1 mm Hg) at 60 °C for 24 h to ensure complete removal of $CHCl_3$. The multi-angle X-ray scattering system (MAXS) generated Cu X-ray from a Nonius FR 591 rotating-anode generator operated at 40 kV and 85 mA. The

beam was focused via doubly-focusing mirror-monochromator optics in an integral vacuum system. The scattering data were collected over an interval of 1 h using a Bruker Hi-Star multiwire detector with a sample to detector distance of 7, 11, 54 and 124 cm. The 2-D data reduction and analysis were performed using *Datasqueeze* software.[30] Scanning transmission electron microscopy (STEM) specimens were sectioned from a solvent-cast and dried film using a Reichert-Jung ultramicrotome equipped with a diamond knife and a cryo unit operated at -145 °C. The nominal thickness of the thin section was about 50 nm. STEM experiments were performed using a JEOL 2010F field emission transmission electron microscope equipped with a Gatan Image Filter (GIF). High-angle annular dark field (HAADF) images were recorded with a 0.7 nm STEM probe at an accelerating voltage of 200 keV. X-ray energy dispersive spectroscopy (EDS) experiments were performed in a JEOL 2010F equipped with a Princeton Gamma Tech (PGT) X-ray energy dispersive spectrometer and a Bruker digital processing unit. Spectra were acquired through the placement of a stationary 0.7 nm probe at the point of interest and collecting a spectrum for 60 s. Data analysis was performed with the ESPRIT EDS Software.

7.4 Results and Discussion

(1,1'-(1,4-Butanediyl)bis(imidazole)) was prepared from imidazole and 1,4-dibromobutane, according to a literature procedure (Scheme 7.1).[29] The structure was confirmed with ^{1}H NMR spectroscopy and FAB-MS. The bisimidazole monomer was converted to 1,1'-(butane-1,4-diyl)bis(3-(2-hydroxyethyl)-1*H*-imidazol-3-ium) bromide (bisimidazolium diol) with 2-bromoethanol using a literature procedure (Scheme 7.2),[28] and structural analysis of the bisimidazolium diol was conducted using ^{1}H NMR spectroscopy and FAB-MS. It is also possible to synthesize other diols with varying alkyl chain lengths between the hydroxyl and the

imidazolium rings, providing an interesting investigation of the role of spacer length and charge density on the mechanical performance of the cation-containing polyurethanes.

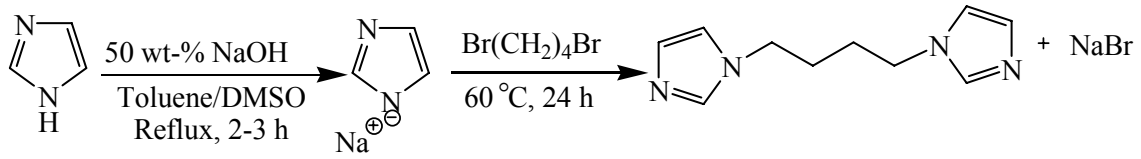

Scheme 7.1. Synthetic strategy for 1,1'-(1,4-butanediyl)bis(imidazole).

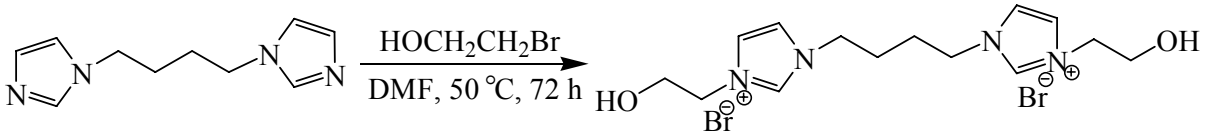

Scheme 7.2. Synthesis of 1,1'-(butane-1,4-diyl)bis(3-(2-hydroxyethyl)-1H-imidazol-3-ium) bromide (bisimidazolium diol).

A novel polyurethane was synthesized using the bisimidazolium diol (Scheme 7.3) as the chain extender in a conventional two-step prepolymer process.[1] In the first step, an oligomeric bis(4-isocyanatocyclohexyl)methane (HMDI) end-capped poly(tetramethylene oxide) (PTMO) was prepared based on 2000 g/mol PTMO. In the second step, the chain extender, dissolved in *N,N*-dimethylformamide (DMF, 20 wt% solids), was added dropwise via addition funnel to the reaction flask over 1 h. The polymerization was allowed to proceed for 24 h at 80 °C. After the reaction was cooled to room temperature, films were cast directly from the reaction flask. The imidazolium-based polyurethane containing PTMO soft segments and HMDI were referred to as PTMO-HMDI-N+. For comparison purposes, a non-charged polyurethane containing a 1,4-butanediol (BD) chain extender was synthesized (PTMO-HMDI-BD).

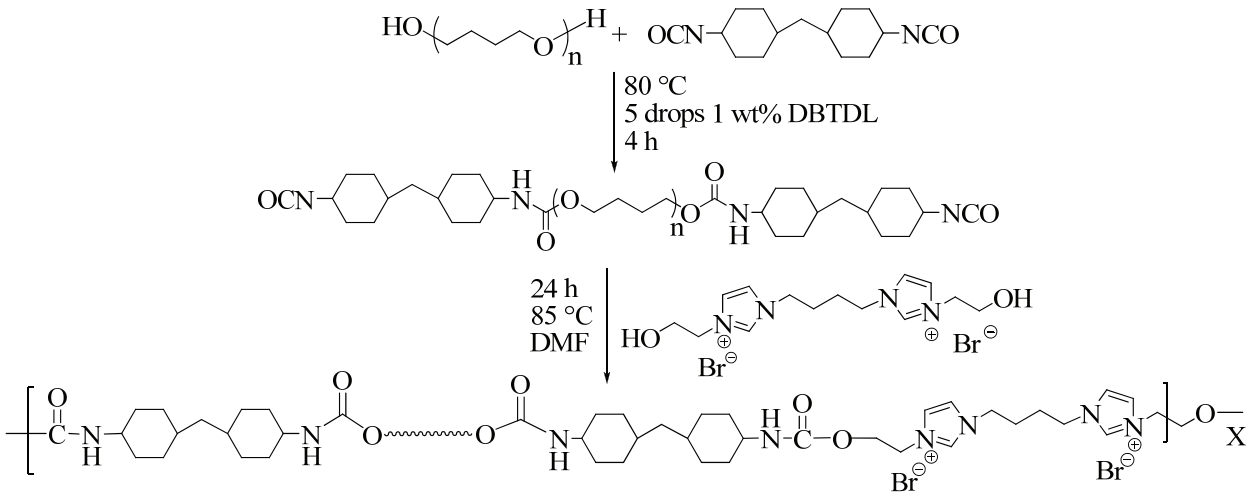

Scheme 7.3. Synthesis of the imidazolium-containing polyurethane (PTMO-HMDI-N+).

All polymers had an equal concentration of hard segment on a mol % basis, and a similar content on a wt % basis, based on the Equation 1:

Hard segment wt % = 100*[(HMDI+Chain Extender)/(HMDI+Chain Extender+PTMO)] (1)

These values were calculated based on the charged amounts of reactants. PTMO-HMDI-N+ contained 75 mol % or 32 wt % hard segment, and PTMO-HMDI-BD possessed 75 mol % or 24 wt % hard segment. Both polyurethane compositions contained 24 mol % chain extender. It is known that using 1,4-butanediol as a chain extender results in polyurethanes that possess excellent tensile properties and elasticity.[4] For this reason, 1,4-butanediol was utilized as the chain extender in the non-charged polyurethane.

Thermal stability was measured via thermogravimetric analysis (TGA). Both polyurethane compositions degraded in a single step. PTMO-HMDI-N+ exhibited a $T_{d5\%}$ of 276 °C, while PTMO-HMDI-BD exhibited a $T_{d5\%}$ of 263 °C, indicating that both polyurethane compositions possessed similar thermal stabilities. It is known that imidazolium salts typically impart thermal stability to polymers.[28,31] However, in this case, an enhanced thermal stability was not observed to any appreciable extent. Since the polyurethanes described herein contain 2000 g/mol PTMO segments within the main chain, it was proposed that the soft segment

contributed greatly towards the thermal stability of the polyurethane, and that the imidazolium bromide salt was not present at high enough concentrations to greatly influence the thermal stability. Ohno et al. have shown that homopolymerization of imidazolium acrylate monomers results in thermally stable polymers ($T_{d5\%}$ = > 350 °C).[28] In that work, the concentration of imidazolium cations was high, thus the presence of the salt greatly enhanced the thermal stability.

Differential scanning calorimetry (DSC) provided interesting information regarding the presence of crystalline domains, if any, in PTMO-HMDI-BD and PTMO-HMDI-N+. The second heat was reported to minimize any effects of thermal history. As shown in Figure 7.2, PTMO-HMDI-BD was completely amorphous, and possessed a T_g of -78 °C. Conversely, PTMO-HMDI-N+ possessed crystallinity, with a T_m at 15 °C, in addition to a T_g of -77 °C. Both T_gs were similar regardless of the chain extender used and were consistent with the T_g of pure PTMO (-79 °C). From the DSC results, it was proposed that the mobility of the polymer chain was restricted and the crystallinity of the PTMO segment was lower due to the presence of hydrogen bonding for PTMO-HMDI-BD polyurethanes. Others have shown that hydrogen bonding in non-ion containing polyurethanes and polyureas can impede crystallization when the polymers contained ether soft segments.[32]

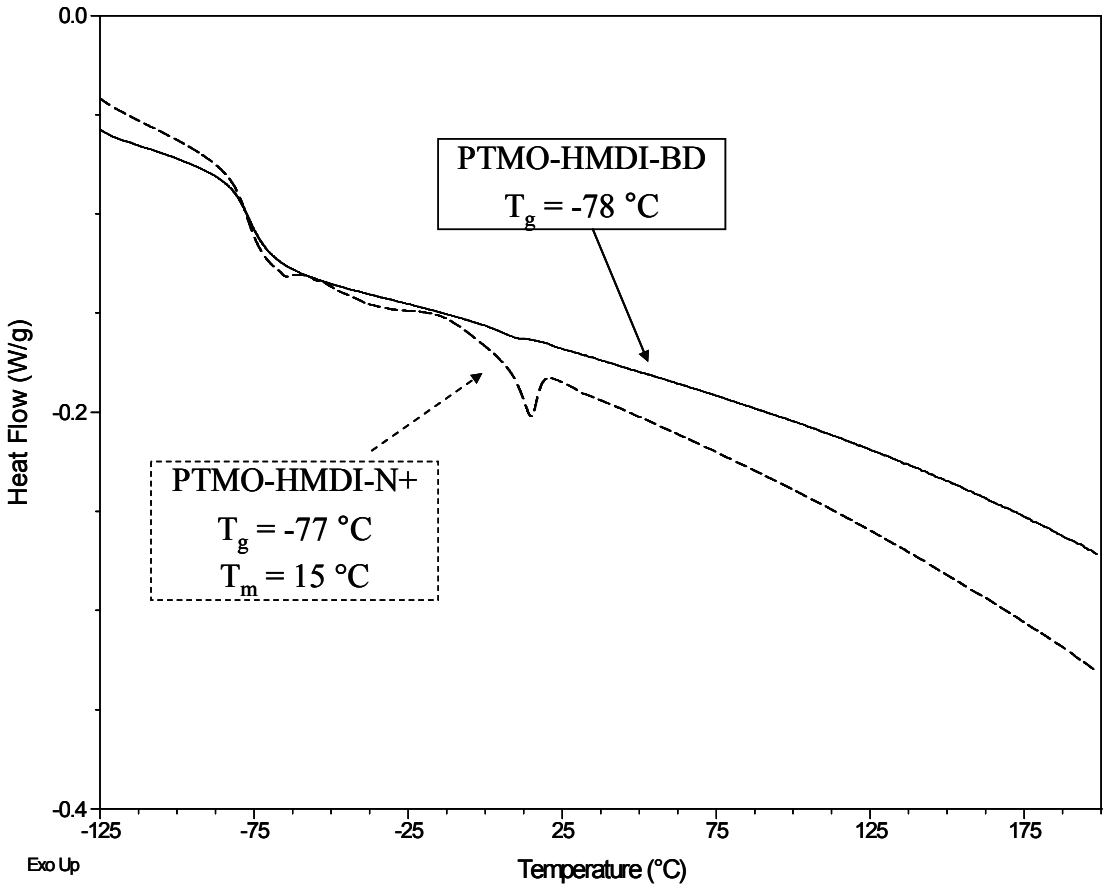

Figure 7.2. DSC traces of PTMO-HMDI-BD (solid line) and PTMO-HMDI-N+ (dashed line). Conditions: 10 °C/min, 2nd heat.

Figure 7.3 summarizes the dynamic mechanical behavior of the ion-containing and non-charged polyurethanes, PTMO-HMDI-N+ and PTMO-HMDI-BD. Both polymers demonstrated a similar PTMO soft segment T_g, with the values ranging from -64 to -67 °C. This transition is higher than that of pure PTMO (-79 °C), which could indicate that some phase mixing occurred. After the T_g, quite different dynamic mechanical behaviors were observed as a function of chain extender composition. A second transition, causing a significant decrease in the storage modulus, occurred in PTMO-HMDI-N+ at 31 °C. Thus, the ion-containing polyurethane did not possess a long rubbery plateau modulus, while PTMO-HMDI-BD maintained a rubbery plateau modulus until approximately 125 °C. Furthermore, there was a slight temperature dependence on the rubbery plateau of PTMO-HMDI-BD, since the plateau modulus was not completely

constant from -25 – 125 °C. The hydrogen bonds of PTMO-HMDI-BD began to dissociate at 125 °C and were completely dissociated at the flow temperature of 157 °C. It was interesting that the ionic associations of the imidazolium functional groups did not persist beyond 50 °C. Wilkes et al. also observed flow temperature of ~50 °C for polyurethanes containing single hard segment molecules based on asymmetric diisocyanates and 1000 g/mol PTMO soft segments;[33] however, their polyurethanes consisted of very different compositions compared to the ion-containing polyurethane described herein.

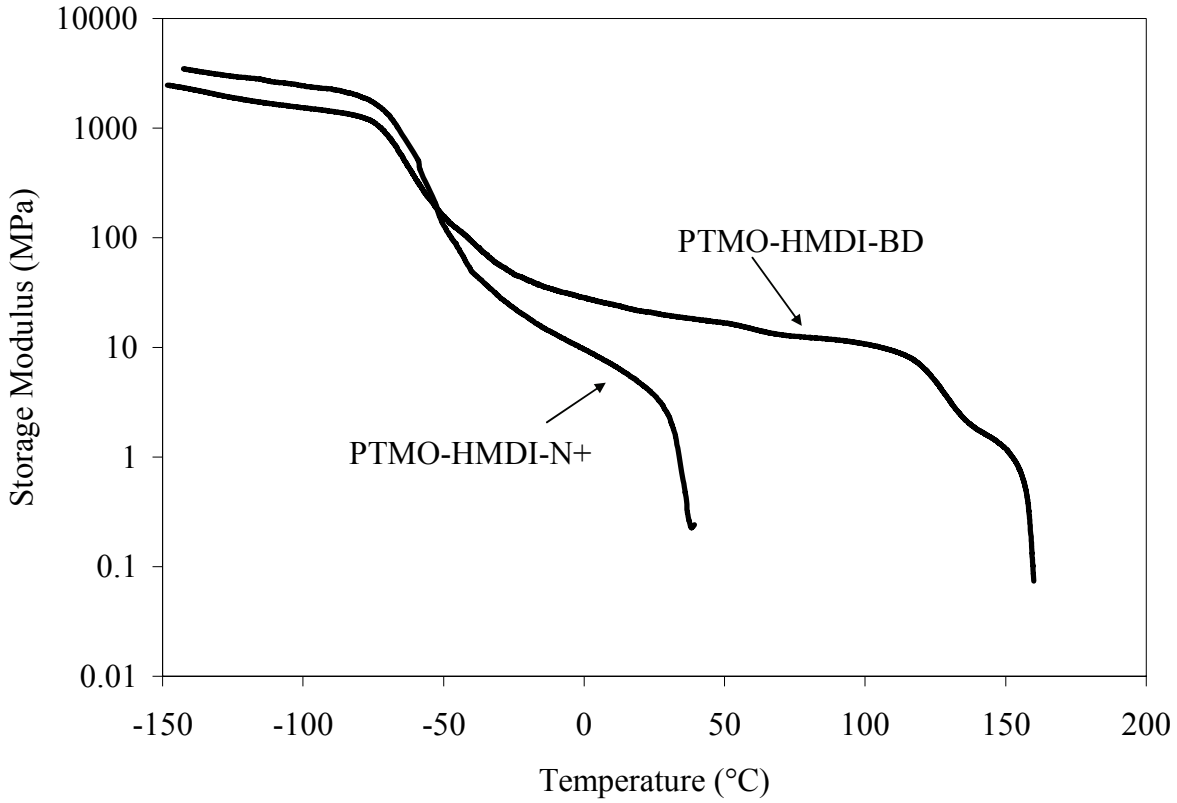

Figure 7.3. DMA curves demonstrating the transitions of PTMO-HMDI-BD and PTMO-HMDI-N+. Conditions: TA Instruments Q800 DMA, 3 °C/min, 1 Hz, film tension mode.

Figure 7.4 shows combined X-ray scattering data from three different experimental X-ray scattering angle ranges. The X-ray scattering data demonstrated that both polyurethane compositions were of low crystallinity or amorphous at ambient temperature, which is characterized via an amorphous PTMO peak at ~14 nm^{-1}. The weak broad peak near 6 nm^{-1} was

attributed to the HMDI hard segment of polyurethanes. In addition, a single broad peak was observed at 0.59 nm^{-1} for PTMO-HMDI-N+, indicating the existence of microphase separation, with Bragg spacing of 10.6 nm. It was found that PTMO-HMDI-BD also displayed hard segment microphase separation, represented with a scattering peak at an angular position of 0.49 nm^{-1}, which corresponded to an inter-domain spacing of 12.8 nm. Other researchers have observed the multiphase structures in several segmented PU elastomers due to the incompatibility between soft and hard segment.[34-38]

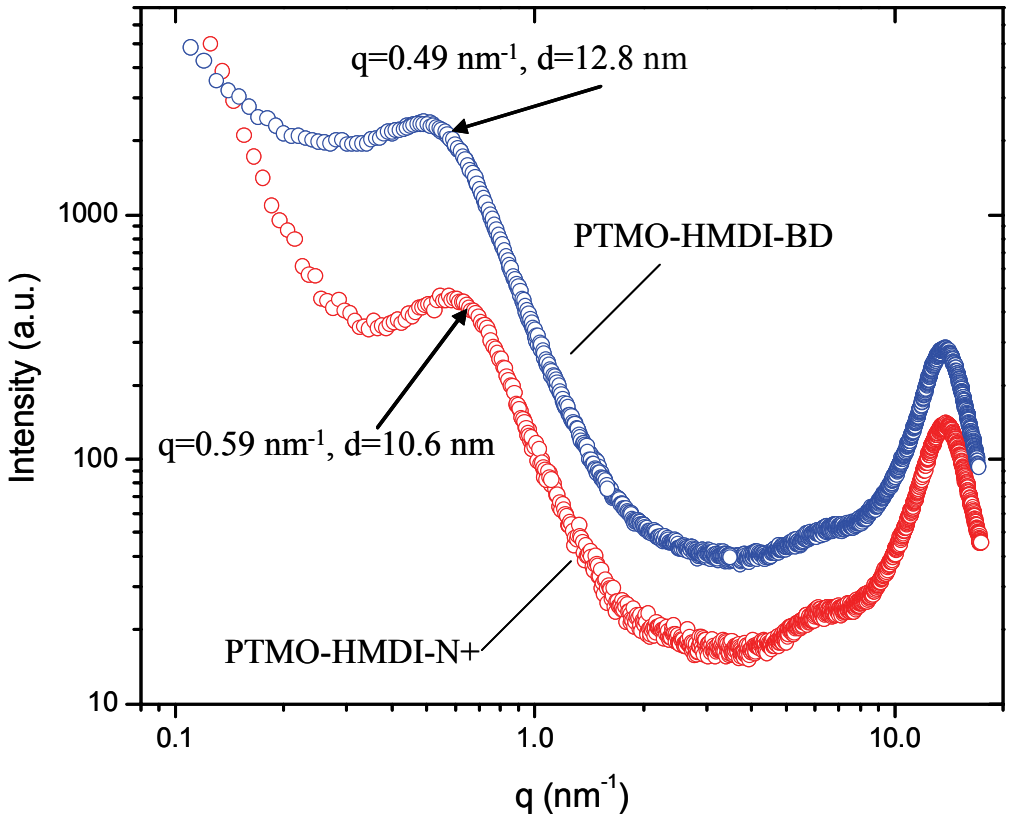

Figure 7.4. Multi-angle X-ray scattering intensity vs. scattering vector q plotted in log-log scale for unstretched PTMO-based polyurethane films containing different chain extenders. The inter-domain spacing was calculated from $d = 2\pi/q$.

To investigate ionic aggregation, scanning transmission electron microscopy (STEM) imaging was utilized. The STEM images of PTMO-HMDI-N+ showed two types of bright features, distinct in size (Figure 7.5). These bright features corresponded to regions of atoms

with higher atomic number, such as the bromide anion from the imidazolium salt chain extender. The formation of the bigger ionic domains (~100-600 nm) indicated macrophase separation.

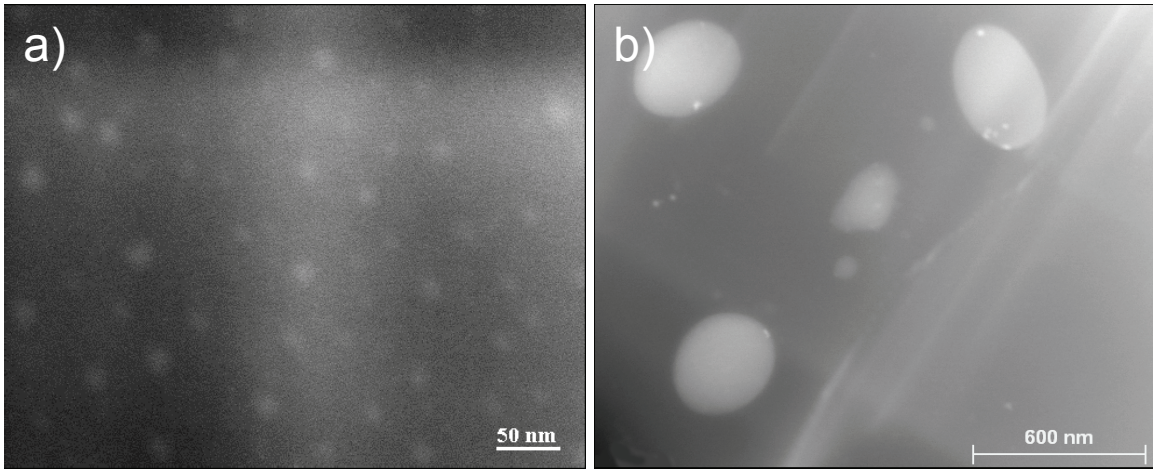

Figure 7.5. High-angle angular dark field (HAADF) STEM image of PTMO-HMDI-N+ showed bright features dispersed in the dark matrix. Two types of bright features distinct in size were observed: a) microphase separation and b). macrophase separation.

The elemental composition of ion-containing hard segment was studied via energy-dispersive X-ray spectroscopy (EDS) during STEM imaging. Because EDS is not sensitive to atoms with low atomic numbers, such as nitrogen or oxygen, only the bromine mapping result is shown in Figure 7.6. The bromine rich regions in the 2-D map corresponded well to the bright features in the STEM image shown in Figure 7.5b.

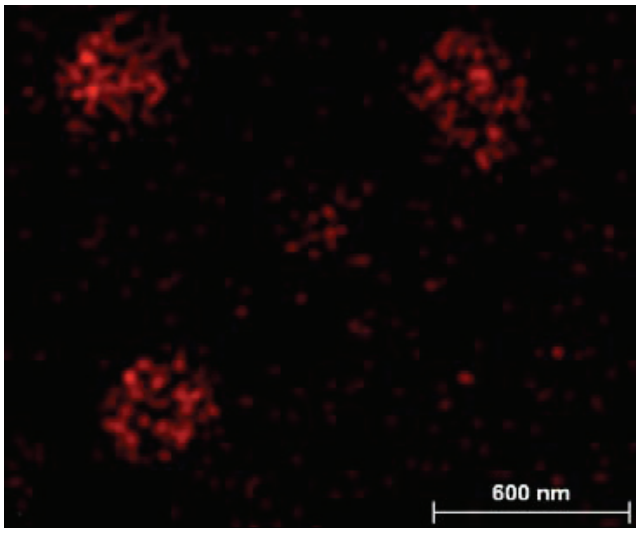

Figure 7.6. EDS mapping of Br element for STEM image of PTMO-HMDI-N+.

FT-IR spectroscopic analysis was used to determine the approximate levels of hydrogen bonding in both polyurethanes. Specifically, the carbonyl absorbing region (1610-1760 cm^{-1}) and N-H absorbing region (3000-3500 cm-1) are useful regions to determine the extent of hydrogen bonding.[39,40] Individual peaks characteristic of hydrogen bond interactions with carbonyls and amides are visible in both regions of a FT-IR spectrum. In particular, peaks at higher wavenumbers are a result of carbonyl functional groups not participating in hydrogen bonding interactions, and N-H peaks are more narrow and well-defined when hydrogen bonding interactions are present in the polymer. Both regions were helpful for qualitatively evaluating the differences in hydrogen bonding for PTMO-HMDI-BD and PTMO-HMDI-N+. As shown in Figure 7.7, the N-H region of the FT-IR spectrum was more well-defined and slightly narrower for PTMO-HMDI-BD than it was for PTMO-HMD-N+. In the carbonyl region, PTMO-HMDI-BD possessed two well-defined peaks in the FT-IR spectrum at 1716 cm^{-1} and 1686 cm^{-1}, while the PTMO-HMDI-N+ FT-IR spectrum did not have a peak at 1686 cm^{-1}. These results indicated that PTMO-HMDI-BD possessed more hydrogen bonding interactions than PTMO-HMDI-N+ and that the presence of ionic functional groups reduced the number of hydrogen bond

interactions. Accordingly, it was hypothesized that the driving force for microphase separation is the presence of ionic groups in PTMO-HMDI-N+. In addition, the results of the FT-IR investigation supported the thermomechanical data described herein.

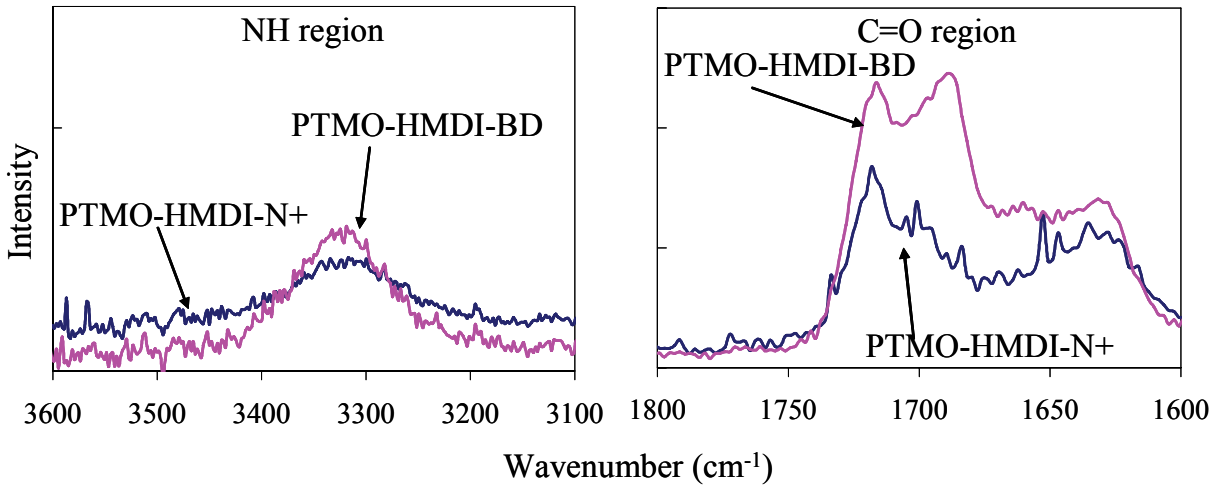

Figure 7.7. FT-IR spectroscopy of NH (left) and C=O (right) region of PTMO-HMDI-BD and PTMO-HMDI-N+.

Stress-strain curves for both PTMO-HMDI-BD and PTMO-HMDI-N+ are shown in Figure 7.8. The polyurethanes possessed very different tensile properties as a function of chemical composition. PTMO-HMDI-BD had greater elongation (1330 ± 63 %) and tensile stress at break (23.97 ± 1.23 MPa), while the PTMO-HMDI-N+ polyurethane demonstrated decreased tensile stress at break (9.26 ± 0.21 MPa) and slightly lower elongation (1160 ± 170 %). After the tensile test, both types of polyurethanes possessed excellent recovery to their original shape. As described in the above discussion, the presence of ionic groups greatly influenced the thermomechanical performance. Thus, it was likely that the presence of ionic groups would also affect the tensile performance. Indeed, this effect on tensile performance was demonstrated with lower tensile stress at break values for PTMO-HMDI-BD relative to those of PTMO-HMDI-N+. In addition, both polyurethane compositions contained PTMO segments,

explaining the exhibited strain hardening behavior typical of strain induced crystallization of polyurethanes containing PTMO soft segments.[33,41,42]

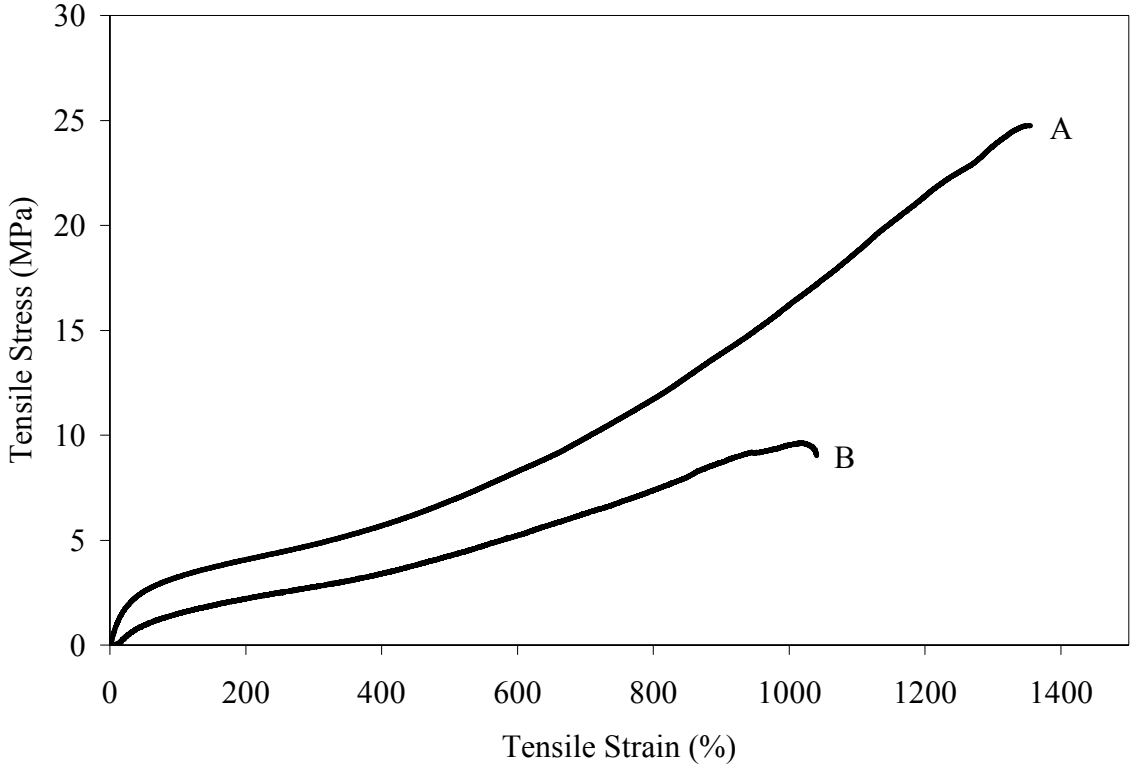

Figure 7.8. Comparison of the stress-strain behavior of linear, segmented, ion-containing polyurethane elastomers: (A) PTMO-HMDI-BD, (B) PTMO-HMDI-N+.

Wide-angle scattering data of PTMO-HMDI-N+ and PTMO-HMDI-BD exhibited quite different morphologies (Figure 7.9). Stretching the films at room temperature to about 200% of their original length for 8 h before running the experiment introduced anisotropy in both WAXS and SAXS patterns for PTMO-HMDI-N+. This stretching aligned the polymer backbone along the stretching direction, introduced crystallization of the PTMO segment, and oriented the ion-rich domain perpendicular to the stretching direction. For PTMO-HMDI-N+, the formation of the distorted crystalline phase of PTMO is characterized through the appearance of diffuse equatorial scattering at an angular position of 14.1 nm^{-1} and 16.9 nm^{-1}, corresponding to two

intense (020) and (110) reflection peaks of PTMO crystals. Conversely, PTMO-HMDI-BD was amorphous after 8 h of uniaxial stretching at 200%, and therefore did not exhibit analogous crystalline reflection peaks (Figure 7.9b). Although the PTMO segment, with number average molecular weight of 2000 g/mol, is amorphous at room temperature due to its low melting temperature, stretching the film promoted the formation of crystallites with higher melting temperature, making it possible to detect crystalline reflection peaks at room temperature. The percent crystallinity depended on the extent of stretching and aging time of polymer under stretched state. Similarly, the amount of extension in the films affected the degree of alignment of ion-rich region. It should be noted that stretching the film may also result in the shift of SAXS scattering peak to a smaller angular range, since the average spacing of ion-rich region will be increased after stretching.

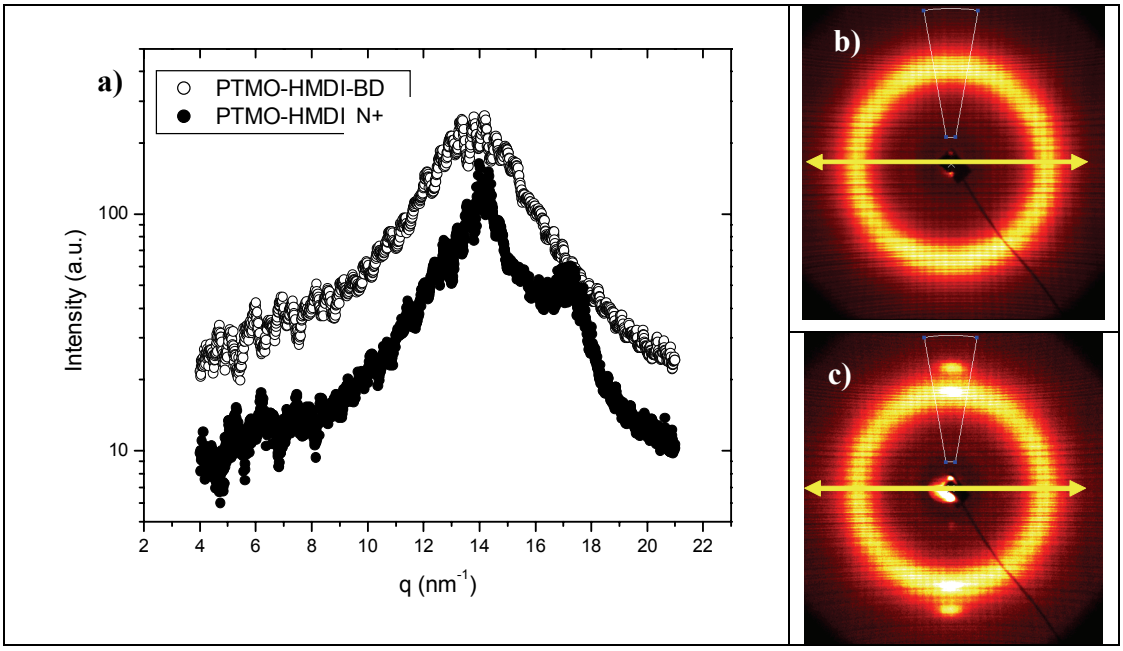

Figure 7.9 a) Scattering intensity vs. q averaged over the azimuthal angular range of 80-100° for the stretched polyurethane films. 2-D X-ray scattering patterns of stretched polyurethanes b) PTMO-HMDI-BD and c) PTMO-HMDI-N+. Arrows indicate stretching direction.

7.5 Conclusions

In conclusion, this paper demonstrated the synthesis of novel, ion-containing polyurethanes containing bisimidazolium functionality in the hard segment. The thermomechanical properties and morphology were drastically different as a function of hard segment structure. Specifically, DSC revealed that the imidazolium containing polyurethane was crystalline, with a T_m of 15 °C, while both polyurethanes possessed T_gs similar to pure PTMO. Dynamic mechanical behaviors were also different as a function of hard segment structure, since the non-charged polyurethane exhibited an extended rubbery plateau to 125 °C, while the imidazolium-containing polyurethane flowed at approximately 50 °C. The X-ray scattering data demonstrated that both polyurethane compositions were of low crystallinity or amorphous at ambient temperature. However, upon stretching, PTMO crystallization was induced, according to wide-angle X-ray scattering. The presence of ionic domains was investigated via STEM imaging, which revealed that they were rich in bromine. FT-IR spectroscopy indicated that ionic domains disrupted hydrogen bonding and thus, lowered the mechanical performance. Overall, all characterization methods indicated that the presence of ion-containing hard segments disrupted hydrogen bonding and lowered mechanical performance.

7.6 Acknowledgements

This material is based upon work supported by the U.S. Army Research Laboratory and the U.S Army Research Office under grant number W911NF-07-1-0452 Ionic Liquids in Electroactive Devices (ILEAD) MURI.

7.7 References

(1) Unal, S.; Yilgor, I.; Yilgor, E.; Sheth, J. P.; Wilkes, G. L.; Long, T. E. *Macromolecules* **2004,** 37, (19), 7081-7084.
(2) Goddard, R. J.; Cooper, S. L. *J. Polym. Sci. B. Polym. Phys.* **1994,** 32, (8), 1557-1571.
(3) Woods, G., *The ICI polyurethanes book*. John Wiley: New York, 1990.
(4) Szycher, M., *Szycher's handbook of polyurethanes*. CRC Press: Boca Raton, 1999.
(5) Chattopadhyay, D. K.; Raju, K. V. S. N. *Progress in Polymer Science* **2007,** 32, (3), 352-418.
(6) Petrovic, Z. S.; Ferguson, J. *Prog. Polym. Sci.* **1991,** 16, (5), 695-836.
(7) Hepburn, C., *Polyurethane elastomers*. 2nd ed.; Elsevier Applied Science: London, 1992.
(8) Thomson, T., *Polyurethanes as specialty chemicals : principles and applications*. CRC Press: Boca Raton, 2005.
(9) *The polyurethanes book*. J. Wiley: New York, 2002.
(10) Dickinson, R. B.; Nagel, J. A.; Proctor, R. A.; Cooper, S. L. *Journal of Biomedical Materials Research* **1997,** 36, (2), 152-162.
(11) Jeong, E. H.; Yang, H.; Youk, J. H. *Materials Letters* **2007,** 61, (18), 3991-3994.
(12) Krol, P.; Krol, B.; Subocz, L.; Andruszkiewicz, P. *Colloid and Polymer Science* **2006,** 285, (2), 177-183.
(13) Polizos, G.; Georgoussis, G.; Kyritsis, A.; Shilov, V. V.; Shevchenko, V. V.; Gomza, Y. P.; Nesin, S. D.; Klimenko, N. S.; Wartewig, S.; Pissis, P. *Polymer International* **2000,** 49, (9), 987-992.
(14) Shilov, V. V.; Shevchenko, V. V.; Pissis, P.; Kyritsis, A.; Georgoussis, G.; Gomza, Y. P.; Nesin, S. D.; Klimenko, N. S. *Molecular Crystals and Liquid Crystals* **2001,** 361, 269-274.
(15) Vatalis, A. S.; Kanapitsas, A.; Delides, C. G.; Viras, K.; Pissis, P. *Journal of Applied Polymer Science* **2001,** 80, (7), 1071-1084.
(16) Reiff, H.; Dieterich, D., Urethane-based dispersions. In *Ionomers: Synthesis, Structure, Properties, and Applications*, Tant, M. R.; Mauritz, K. A.; Wilkes, G. L., Eds. Blackie Academic and Professional: London, 1997; pp 444-501.
(17) Dieterich, D.; Keberle, W.; Witt, H. *Angew. Chem., Int. Ed.* **1970,** 9, (1), 40-50.
(18) Chen, S. A.; Hsu, J. S. *Polymer* **1993,** 34, (13), 2769-2775.
(19) Chen, S. A.; Hsu, J. S. *Polymer* **1993,** 34, (13), 2776-2782.
(20) Buruiana, E. C.; Buruiana, T.; Strat, G.; Strat, M. *Journal of Polymer Science Part A-Polymer Chemistry* **2002,** 40, (11), 1918-1928.
(21) Chen, S.-A.; Chan, W.-C. *J. Polym. Sci. B. Polym. Phys.* **1990,** 28, 1499-1514.
(22) Sriram, V.; Aruna, P.; Naresh, M. D.; Radhakrishnan, G. *J. Macro. Sci., Part A* **2001,** 38, (9), 945-959.
(23) Sundar, S.; Aruna, P.; Venkateshwarlu, U.; Radhakrishnan, G. *Colloid Polym. Sci.* **2004,** 283, 209-218.
(24) Liu, F. J.; Kokorudz, J. S.; Collier, H. L. *J. Polym. Sci. A. Polym. Chem.* **1988,** 26, 3015-3029.
(25) Yoon, C. B.; Meyer, W. H.; Wegner, G. *Syn. Met.* **2001,** 119, 465-466.
(26) Sriram, V.; Radhakrishnan, G. *Polym. Bull.* **2005,** 55, 165-172.
(27) He, S.; Shi, K.; Bai, J.; Zhang, Z.; Li, L.; Du, Z.; Zhang, B. *Polymer* **2001,** 42, 9641-9647.
(28) Nakajima, H.; Ohno, H. *Polymer* **2005,** 46, (25), 11499-11504.

(29) So, Y. H. *Macromolecules* **1992,** 25, (2), 516-520.
(30) Heiney, P. A. *Comm Powder Diffr Newsletter* **2005,** 32, 9-11.
(31) Tsunashima, K.; Sugiya, M. *Electrochemistry Communications* **2007,** 9, (9), 2353-2358.
(32) Hu, C. B.; Ward, R. S.; Schneider, N. S. *Journal of Applied Polymer Science* **1982,** 27, (6), 2167-2177.
(33) Das, S.; Cox, D. F.; Wilkes, G. L.; Klinedinst, D. B.; Yilgor, I.; Yilgor, E.; Beyer, F. L. *J. Macro. Sci., Part B* **2007,** 46, (5), 853-875.
(34) Sheth, J. P.; Unal, S.; Yilgor, E.; Yilgor, I.; Beyer, F. L.; Long, T. E.; Wilkes, G. L. *Polymer* **2005,** 46, (23), 10180-10190.
(35) Aneja, A.; Wilkes, G. L. *Polymer* **2003,** 44, (23), 7221-7228.
(36) Klinedinst, D. B.; Yilgor, E.; Yilgor, I.; Beyer, F. L.; Wilkes, G. L. *Polymer* **2005,** 46, (23), 10191-10201.
(37) O'Sickey, M. J.; Lawrey, B. D.; Wilkes, G. L. *Polymer* **2002,** 43, (26), 7399-7408.
(38) Sheth, J. P.; Klinedinst, D. B.; Wilkes, G. L.; Iskender, Y.; Yilgor, E. *Polymer* **2005,** 46, (18), 7317-7322.
(39) Wu, Y.; Xu, Y.; Wang, D.; Zhao, Y.; Weng, S.; Xu, D.; Wu, J. *J. Appl. Polym. Sci.* **2004,** 91, 2869-2875.
(40) Yilgor, I.; Yilgor, E.; Guler, I. G.; Ward, T. C.; Wilkes, G. L. *Polymer* **2006,** 47, 4105-4114.
(41) Das, S.; Yilgor, I.; Yilgor, E.; Inci, B.; Tezgel, O.; Beyer, F. L.; Wilkes, G. L. *Polymer* **2007,** 48, 290-301.
(42) Feng, D.; Wilkes, G. L.; Leir, C. M.; Stark, J. E. *J. Macromol. Sci.-Chem.* **1989,** A26, (8), 1151-1181.

Chapter 8 : Synthesis and Morphology of Segmented Poly(tetramethylene oxide)-Based Polyurethanes Containing Phosphonium Salts

8.1 Abstract

A fundamental investigation of the influence of novel phosphonium bromide salts within the polymer main chain (23.75 mol%) of polyurethanes was conducted to elucidate the effect of ionic associations on hard segment hydrogen bonding. Novel poly(tetramethylene oxide) (PTMO)-based polyurethanes containing a phosphonium diol chain extender were prepared using a conventional prepolymer method. In addition, polyurethanes containing 1,4-butanediol chain extenders were synthesized for comparison with the thermomechanical and morphological properties of the phosphonium ion-containing analogs. Moreover, the unprecedented comparison of morphological development in the presence of cationic ionic sites is described herein. Differential scanning calorimetry (DSC) revealed that phosphonium polyurethanes were relatively more crystalline compared to non-charged analogs, and it was presumed that enhanced hydrogen bonding in the non-charged polyurethanes restricted polymer mobility and reduced PTMO crystallinity. Moreover, FT-IR spectroscopy demonstrated that hydrogen bonding interactions were significantly reduced in the presence of phosphonium cations. These results correlated well with tensile properties, i.e., the non-charged polyurethanes offered superior tensile strength compared to phosphonium polyurethanes. X-ray scattering indicated that both

polyurethanes were amorphous at room temperature and exhibited hard segment microphase separation. Upon stretching, the interparticle scattering between the microphase-separated domains aligned preferentially along the stretching direction. Scanning transmission electron microscopy (STEM) and energy dispersive X-ray spectroscopy (EDS) in the STEM indicated that charged polyurethanes exhibited ionic domains that were rich in P and Br.

8.2 Introduction

Polyurethanes, which are often segmented block copolymers, consist of alternating hard and soft segments. The hard segments arise from a reaction of an isocyanate with a low molecular weight diol chain extender, and the soft segments are typically derived from a low T_g polyol. Polyurethanes are useful thermoplastic elastomers due to their superior mechanical strength and elastomeric behavior that is derived from microphase separation and hydrogen bonding.[1] Polyurethanes are used in many applications such as abrasion-resistant components, biomaterials, durable coatings, and foams.[2-8] Polyurethane ionomers have also received attention as high-strength elastomers for biomedical[9,10] and conductive polymer[11-14] applications. The incorporation of ions into macromolecular structure causes the formation of more complex morphological features, and ions potentially disrupt typical microphase separation in common polyurethanes.[15] Early reports of cation-containing polyurethanes typically involved post-polymerization functionalization to introduce quaternary ammonium groups.[16-18] Anionic polyurethanes, which commonly consist of either sulfonate or carboxylate groups in the hard segment, are typically more prevalent in the literature, and many researchers have modeled the presence of ionic aggregates within the microphase-separated polyurethane morphology.[19-23]

Dieterich et al. initially reviewed polyurethane ionomers in 1970.[16] Polyurethane ionomers continue to receive intense attention because of the potential synergistic interactions of

hydrophobic soft segments, hydrogen bonding groups, and ionic groups. At low ion concentrations, the incorporation of ionic groups into polyurethanes leads to water-dispersible products. However, many factors influence water dispersibility, including ion type, counterion, ion concentration, and soft segment composition.[24] With increasing attention to more environmentally friendly chemical syntheses and processing in the absence of volatile organic compounds (VOCs), ion-containing polyurethanes are attractive materials because water is the only solvent required for dispersion.[15,25] One potential limitation of water-dispersible polyurethanes is the hydrolytic instability of ester and urethane functional groups. However, Mequanint et al. determined that ionic domains "protected" the hydrophobic soft segments from hydrolytic degradation, depending on the polymer structure.[25] Specifically, their group revealed that polyurethanes containing ionic groups in the soft segment were more hydrolytically stable in aqueous solutions than analogs with ionic groups in the hard segment. Typically, water-dispersible polyurethanes contain either carboxylic acid or tertiary amine groups that are neutralized to their corresponding salts.[24]

Polyurethane ionomers offer unique mechanical properties due to the presence of ionic groups. The location of the ionic group and the ion content drastically influence the morphological and mechanical behavior of polyurethane ionomers. In some cases, ionic groups increase the degree of microphase separation and increase the tensile performance, but the results are highly dependent on polymer composition. For example, mechanical properties are especially dependent on whether the ionic groups are located in the hard or soft segment. Due to the expected hydroscopic nature of the ionic domains, water acts as a plasticizer and significantly influences the mechanical performance. Polyurethane ionomer research has expanded greatly in the past 30 years, and polymer structures are becoming more sophisticated. For example, Buruiana and co-workers synthesized poly(tetramethylene oxide) (PTMO)-based

polyurethanes that contained a hard segment consisting of a novel, cationic stilbene diol based on 4-chloromethylphenylcarbamoyloxymethyl-*p*-stilbene.[26,27] Quaternary ammonium groups were also introduced for enhancing water dispersibility while the stilbene group imparted interesting optical properties. Kim et al. synthesized polyurethane ionomers containing carboxylate ionic domains in polypropylene glycol soft segments.[28] The resulting polyurethanes possessed increased phase mixing and decreased solution viscosity and particle size.

The literature on phosphonium halide salt containing polymers is abundant; however, as far as the authors know, researchers have not reported the synthesis of polyurethanes containing phosphonium groups in the hard segment. McGrath et al. reported the synthesis of poly(arylene ether) phosphonium ionomers for high-performance polymers in a variety of applications including ion-exchange membranes and conductive polymers.[29] However, in sharp contrast to our work, the phosphonium ionomers were prepared via reduction of polymeric phosphine oxides to phosphines in the presence of phenylsilane and subsequently quaternizing the phosphines with alkyl halides. Other researchers have reported the synthesis and characterization of phosphonium elastomers. Parent et al. synthesized poly(isobutylene-*co*-isoprene) phosphonium and ammonium elastomers that possessed dynamic mechanical behavior properties similar to ZnO-cured brominated poly(isobutylene-*co*-isoprene).[30] The rubbery plateau modulus was approximately 1×10^6 Pa, and the T_g of all elastomers were similar, regardless of preparation. However, the solution behavior of the ionomers differed greatly compared to the non-charged elastomer that was covalently crosslinked with ZnO. The non-charged elastomer had solution viscosity behavior that was independent of solvent selection; however, the influence of solvent polarity was discernible for the ionomers due to ionic aggregate formation and disruption. Soutar et al. reported another example of polyolefin-based elastomers that contained ionic groups. Living anionic polymerization techniques were used to

prepare telechelic, phosphonium salt poly(butadiene)s with high 1,4-content. A temperature dependence of the ionic aggregate interactions was observed with dynamic mechanical thermal analysis, and the ionic aggregates dissociated at temperatures ranging from 70-120 °C.[31]

Previous work in our laboratories has focused recently on the structure-property relationships of linear and highly branched polyurethanes using a variety of soft segments including poly(propylene glycol) (PPG) and poly(tetramethylene oxide) (PTMO).[1,32-38] Oligomeric A_2 + B_3 methodology was used to prepare branched polyurethanes resulted in microphase-separated, low T_g segmented block polymers with excellent strain-hardening properties.[1,39] Recently, we demonstrated the synthesis of completely amorphous, highly branched poly(caprolactone)-based polyurethanes and poly(urethane urea)s that possessed dynamic mechanical behavior similar to a linear analog, without difficulties attributed to the semi-crystalline nature of poly(caprolactone).[39,40] In addition to highly branched and linear polyurethanes, we have also prepared crosslinked Michael networks containing urethane functionality and investigated the effect of urethane sites on the thermomechanical performance. In particular, we ascertained the influence of polymer networks containing urethane linkages on the mechanical performance of poly(propylene glycol) (PPG)-based networks prepared via the carbon Michael addition reaction using acrylate and acetoacetate functionalities.[41] Urethane linkages improved the mechanical performance compared to non-hydrogen bond-containing crosslinked networks, and synergistic effects were observed when the crosslink density was decreased while incorporating urethane segments. Previously, we also reported the influence of hydrogen bonding in photo-crosslinked star-shaped poly(D,L-lactide) (PDLLA) polymers that contained either methacrylate or urethane methacrylate functional groups on the periphery.[42,43] Both networks were highly crosslinked (>99%), but the tensile properties of the urethane

methacrylate PDLLA networks were superior compared to the methacrylate PDLLA networks. The resulting PDLLA networks were promising high performance bioadhesives.

Our group has also reported the potential advantages of phosphonium-salt containing polymers. We previously reported the synthesis of phosphonium-based methacrylic ionomers using conventional free radical polymerization techniques. The resulting polymers formed free-standing ductile films, and the ionic interactions influenced the mechanical performance of the ionomer.[39] Furthermore, we recently reported the synergy of ionic interactions and hydrogen bonding where phosphonium salts containing a uracil hydrogen bond were blended with adenine-containing ABA triblock copolymers.[44] Novel adenine-containing triblock polymers were prepared via nitroxide mediated polymerization, and these served as excellent templates for the nanoscale dispersion of uracil-containing phosphonium salts. The addition of the ionic guest altered the dynamic mechanical behavior and morphology compared to the polymer in the absence of the cationic phosphonium salt. It was concluded that the phosphonium salt was located in the adenine-containing blocks. X-ray scattering indicated a change in morphology from cylindrical to lamellar structure as the uracil-containing phosphonium salt was incorporated. ^{1}H NMR spectroscopy revealed complementary hydrogen bonding in the presence of the phosphonium salt.

In this work, urethane hydrogen bonding and phosphonium salt functionality were incorporated into the same polyurethane to elucidate the fundamental structure-property relationships of phosphonium-containing polyurethanes. This differs from the previous work described above, where the ionic group was the guest molecule and the hydrogen bonding was based on more sophisticated complementary structures. Specifically, the effect of ionic interactions in a polyurethane hard segment on morphology and mechanical properties was elucidated using a variety of complementary analytical techniques. Appropriate non-charged

polyurethanes containing only urethane hydrogen bonding interactions were prepared for comparison.

8.3 Experimental

8.3.1 Materials

PTMO oligomer (Terathane, Du Pont) with number-average molecular weight of 2000 g/mol and 1,4-butanediol were purchased from Aldrich and dried *in vacuo* (0.1 mm Hg) at 23 °C for 24 h prior to use. Bayer kindly provided bis(4-isocyanatocyclohexyl)methane (HMDI) with purity greater than 99.5%. Chloroform ($CHCl_3$, Fisher Scientific, Optima grade) was distilled from calcium hydride. Tetrahydrofuran (THF, EMD Science, HPLC grade), hexanes (Fisher Scientific, HPLC grade), dichloromethane (Fisher Scientific, HPLC grade), and diethyl ether (Fisher Scientific, 99.9%, anhydrous) were used as received. Dibutyl tin dilaurate (DBTDL, 99%) was dissolved in THF as a 1 wt % solution. A mixed solvent recrystallization was used to purify 1,4-bis(diphenylphosphino)butane (Aldrich, 98%) using hexanes and dichloromethane. The recrystallization was performed under nitrogen to minimize phosphine oxide formation. ^{31}P NMR spectroscopy revealed one peak after recrystallization. 2-Bromoethanol (Aldrich, 95%) was distilled prior to use.

8.3.2 Synthesis of butane-1,4-bis[(2-hydroxyethyl)diphenylphosphonium] bromide chain extender

In a two-necked, round-bottomed flask, equipped with a stir bar and condenser, 1,4-bis(diphenylphosphino)butane (5.694 g, 0.0134 mol) was introduced and purged under nitrogen. Chloroform (dry, 15 mL) and 2-bromoethanol (2.83 mL, 0.0401 mol) were subsequently syringed into the flask. The reaction was allowed to proceed at 60 °C for 24 h. The reaction

product was precipitated into diethyl ether twice. The final product was obtained in 90 % yield. ^{1}H NMR (400 MHz, CD_3Cl_3) δ = 7.56-7.80 (m, 20H), 5.36 (s, 2H), 3.88-3.97 (m, 4H), 3.46 (m, 4H), 3.19 (m, 4H), 1.99 (m, 4H). FAB MS: M+Br = 595.15 (found), molecular weight = 515.25 (calculated). Melting point = 123.8-124.1 °C.

8.3.3 Synthesis of polyurethanes

All reactions were conducted in three-necked, round-bottomed flasks that were equipped with an addition funnel, nitrogen inlet, and overhead stirrer. In the first step, HMDI end-capped PTMO prepolymers were prepared in the absence of solvent at 80 °C with 1 wt % DBTDL in THF (0.01 mL) as the catalyst.[1] In the second step, the chain extenders (butane-1,4-bis[(2-hydroxyethyl)diphenylphosphonium] bromide or 1,4-butanediol) were dissolved in $CHCl_3$ (20 wt% solids), and the polyurethanes were prepared via the dropwise addition (over 60 min) of the chain extender solution into the HMDI end-capped PTMO prepolymer. The polymerizations were allowed to proceed for 24 h at 80 °C, and the solutions remained homogeneous throughout the polymerization. The polymer films containing butane diol chain extenders were optically clear; however, films containing butane-1,4-bis[(2-hydroxyethyl)diphenylphosphonium] bromide were opaque.

8.3.4 Characterization

^{1}H NMR spectroscopy was utilized to determine monomer composition in $CDCl_3$ at 23 °C with a 400 MHz Varian UNITY spectrometer. FAB-MS was obtained on a JOEL HX110 dual focusing mass spectrometer. A TA Instruments Hi-Res TGA 2950 with a temperature ramp of 10 °C/min in a nitrogen atmosphere was used for thermogravimetric analysis (TGA) Dynamic mechanical analysis (DMA) was conducted on a TA Instruments Q800 dynamic

mechanical analyzer in tension mode at a frequency of 1 Hz and temperature ramp of 3 °C/min. The sample was cooled from room temperature to -30 °C prior to heating. The glass transition temperature (T_g) was determined at the peak of the tan δ curve. Differential scanning calorimetry (DSC) was performed using a TA Instruments Q2000 differential scanning calorimeter under a nitrogen flow of 50 mL/min. The sample was first heated from -20 °C to 200 °C at a heating rate of 10 °C/min and held for 5 min to erase the thermal history. The cooling rate was 10 °C/min, and a subsequent heating from -130 °C to 200 °C at a heating rate of 5 °C/min was conducted. Dogbone-shaped film specimens, which were cut with a die according to ASTM D3368 specifications, were used for tensile tests performed on a 5500R Instron universal testing instrument with a cross-head speed of 50 mm/min using manual grips at 23 °C. The extent of hydrogen bonding of solvent-case films was evaluated using a MIDAC M2004 ATR-FTIR at ambient conditions. The spectra, including the background scan, were collected at a resolution of 4 cm^{-1} and 128 scans were averaged. In all characterization methods, great care was used in drying polymer samples before testing.

Morphological analysis was conducted using a variety of complementary techniques. X-ray scattering was performed on solvent-cast polyurethane films that were dried *in vacuo* (0.1 mm Hg) at 60 °C for 24 h to ensure complete removal of $CHCl_3$. The multi-angle X-ray scattering system (MAXS) used Cu X-ray from a Nonius FR 591 rotating-anode generator operated at 40 kV and 85 mA. The bright, highly collimated beam was obtained via Osmic Max-Flux optics and pin collimation in an integral vacuum system. The scattering data were collected using a Bruker Hi-Star multiwire detector with a sample to detector distance of 7, 11, 54 and 150 cm. The MAXS system provides an uncommonly wide range of scattering angle that was critical in evaluating the morphology of these segmented copolymers. The 2-D data reduction and analysis were performed using *Datasqueeze* software.[45] Scanning transmission electron

microscopy (STEM) specimen were sectioned from solvent-cast and dried films using a Reichert-Jung ultramicrotome equipped with a cryo unit operated at -145 °C. Thin sections with nominal thickness of 50 nm were obtained with a dry diamond knife and transferred onto copper grids. The grids were stored in a vacuum desiccator at room temperature prior to imaging. STEM experiments were performed using a JEOL 2010F field emission scanning transmission electron microscope equipped with a Gatan Image Filter (GIF). High-angle annular dark field (HAADF) images were recorded with a 0.7 nm STEM probe at an accelerating voltage of 200 keV. As with most ion-containing polymers, it is important to note that the PTMO-HMDI-P+ polyurethanes have potential to be hygroscopic. Thus, the ultra-thin films used for STEM imaging might have absorbed water after cryo-microtomy during grid transfer at ambient conditions. Moisture is difficult to remove under room temperature vacuum in the microscope. X-ray energy dispersive spectroscopy (EDS) experiments were performed in the JEOL 2010F, which is equipped with a Princeton Gamma Tech (PGT) X-ray energy dispersive spectrometer and a Bruker digital processing unit. Spectra were acquired through the placement of a stationary 0.7 nm probe at the point of interest and collecting a spectrum for 60 s. Data analysis was performed with the ESPRIT EDS Software.

8.4 Results and Discussion

A novel phosphonium diol chain extender was prepared from 1,4-bis(diphenylphosphino)butane and bromoethanol, as shown in Scheme 8.1. The resulting butane-1,4-bis[(2-hydroxyethyl)diphenylphosphonium] bromide salt, which was purified after several precipitations into diethylether, was confirmed with ^{1}H NMR spectroscopy and FAB-MS. The salt was soluble in a variety of solvents including chloroform, methanol, and isopropanol, but

was insoluble in water. The salt was not classified as an ionic liquid, since the melting point was above 100 °C (123.8-124.1 °C).

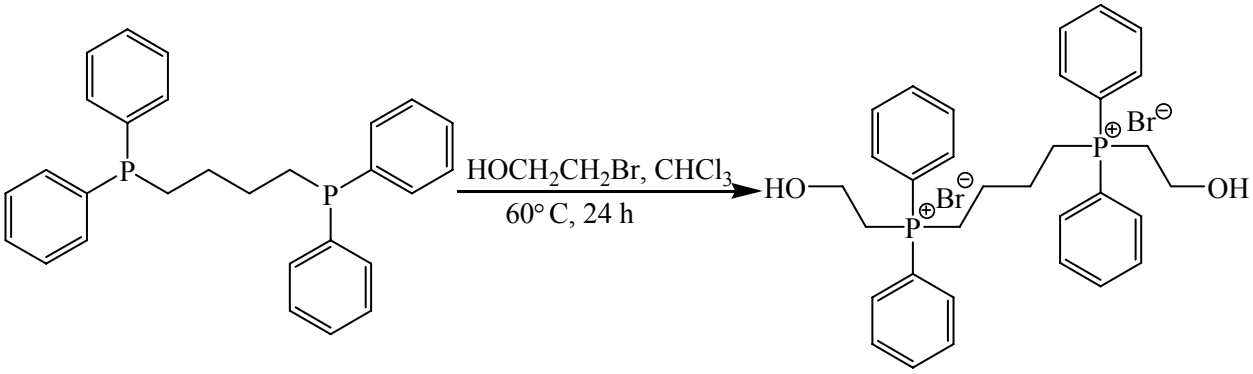

Scheme 8.1. Synthesis of butane-1,4-bis[(2-hydroxyethyl)diphenylphosphonium] bromide chain extender.

Novel ion-containing polyurethanes were synthesized in a two-step process using 2000 g/mol PTMO as the soft segment, butane-1,4-bis[(2-hydroxyethyl)diphenylphosphonium] bromide as the chain extender, and HMDI as the diisocyanate (Scheme 8.2). The phosphonium-based polyurethanes containing PTMO soft segments and HMDI was referred to as PTMO-HMDI-P+. The prepolymer method was utilized to synthesize novel polyurethanes, and the first step involved the conventional preparation of an oligomeric HMDI end-capped PTMO.[1] After the reaction was cooled to room temperature, films were cast directly from the reaction mixture. For comparative purposes, non-charged polyurethanes containing a 1,4-butanediol chain extender were synthesized (PTMO-HMDI-BD). The chemical compositions of both the ion-containing and non-charged polyurethanes were similar. Each polymer had an equal concentration of hard segment on a mol % basis, and a similar content on a wt % basis, based on Equation 1:

Hard segment content = 100*[(HMDI+Chain Extender)/(HMDI+Chain Extender+PTMO)] (1)

These values were calculated based on the charged amounts of reactants. PMTO-HMDI-P+ contained 75 mol % and 37 wt % hard segment, and PTMO-HMDI-BD possessed 75 mol % and 24 wt % hard segment. Additionally, the ion-containing polyurethane contained 20 wt % chain extender. Researchers have shown that using 1,4-butanediol as a chain extender resulted in polyurethanes that possessed excellent tensile properties and elasticity.[3] For this reason, 1,4-butanediol was utilized as the chain extender in the non-charged polyurethanes.

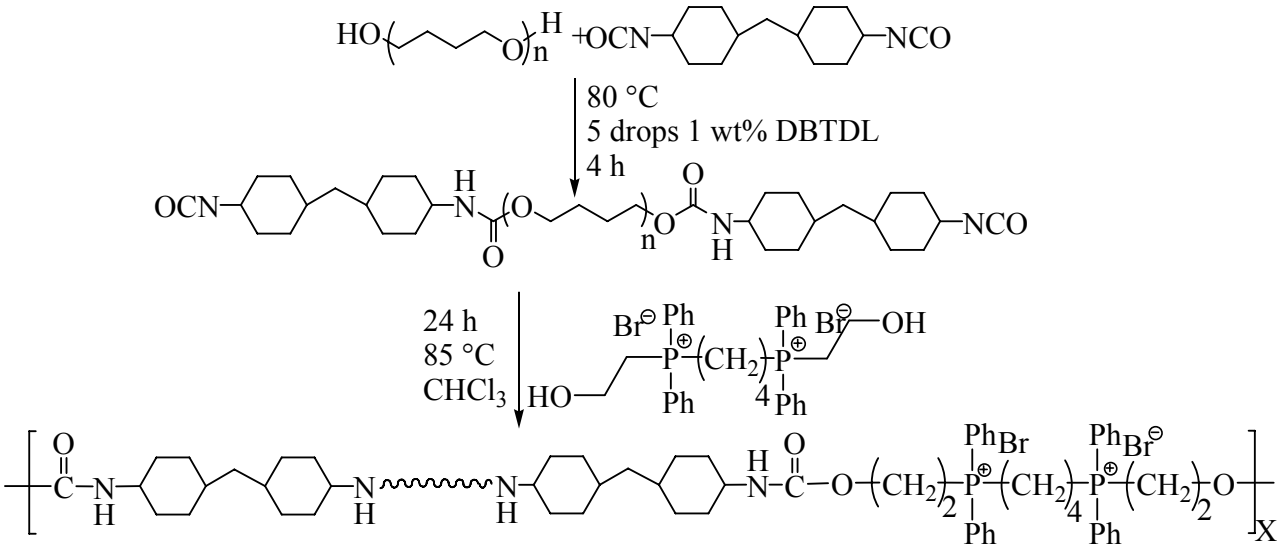

Scheme 8.2. Synthesis of phosphonium-containing polyurethanes (PTMO-HMDI-P+).

The water dispersibility of the ion-containing polyurethane was examined, and it was found that it was not dispersible in stirring water, even with heating to 60 °C. There are several possibilities, including the relatively hydrophobic nature of PTMO soft segments. Furthermore, the ionic chain extender contained a substantial amount of hydrocarbon character, including phenyl rings, so the structure was perhaps too hydrophobic to promote water dispersibility of the polyurethane. In addition, since the molecular weight of butane-1,4-bis[(2-hydroxyethyl)diphenylphosphonium] bromide salt is relatively high for an ionic chain extender (515.25 g/mol), the ionic content of the polyurethane is greater than most ion-containing water dispersible polyurethanes. For example, Yamada et al. reported incorporating 3 wt% of an ionic

chain extender into water-dispersible polyurethanes.[46] The ionic content (23.75 mol%, 14 wt%) of the phosphonium polyurethanes possibly was too high, and ionic aggregation in solution prevented dispersion in water.

The PTMO-HMDI-P+ polyurethane had a T_d of 280 °C, and the PTMO-HMDI-BD non-charged polyurethane had a slightly lower T_d of 263 °C, according to TGA analysis. The difference in thermal stabilities was considered insignificant, since the error in TGA is approximately 2 %, and the thermal stability difference between the two types of polyurethanes was only 17 °C.

DSC provided interesting information about crystallinity differences between the phosphonium bromide containing and non-charged polyurethanes and confirmed many of the DMA results described below. Both DSC traces (Figure 8.1) are from the second heat in order to minimize effects of thermal history. The phosphonium polyurethane possessed crystallinity, and a T_g, T_c, and T_m were observed at -79 °C, -35 °C, and 14 °C, respectively. Conversely, only a T_g at -78 °C was observed for the non-charged polyurethane. Based on this observation, it appeared that hydrogen bonding restricted the mobility of the polymer chain and reduced the crystallinity of PTMO segment for the non-charged polyurethanes. This was in agreement with Schneider et al., who reported that hydrogen bonding occurred between ether oxygens within the soft segment and urethane and urea units, and, thus hindered crystallization of the soft segment.[47] Moreover, the organic nature and bulkiness of the ionic groups suggested less dense packing of ionic groups in the hard segment, thus the geometric constraint on the PTMO segments surrounding the ionic domains was much less than those traditional ionomers with metal cations.

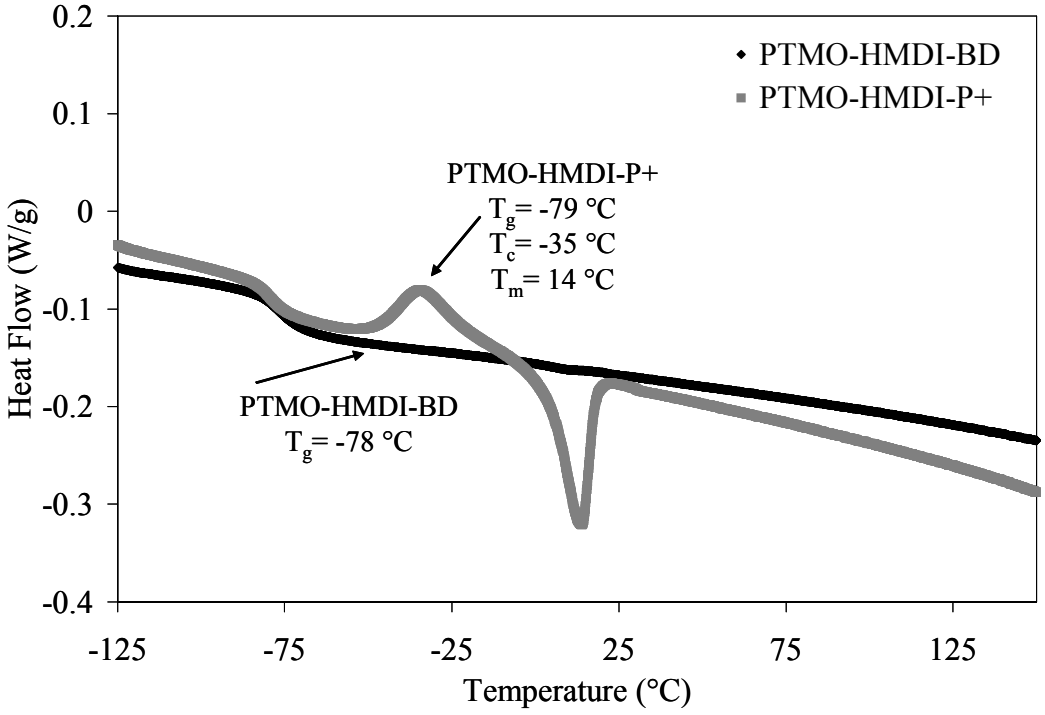

Figure 8.1. DSC traces for PTMO-HMDI-P+ (light gray), and PTMO-HMDI-BD (black). Conditions: 5 °C/min, 2nd heat.

Figure 8.2 summarizes the comparative dynamic mechanical behavior of the phosphonium-containing and non-charged polyurethanes, PTMO-HMDI-P+ and PTMO-HMDI-BD. Both polymers showed similar PTMO soft segment T_gs, with the values ranging from -60 to -64 °C. This transition was higher than pure PTMO (-79 °C), which suggested some phase mixing. The greater glassy modulus of the phosphonium polyurethane indicated that the polymer had higher crystallinity, which was consistent with DSC as described above. This is in agreement with Wilkes et al., where they reported that the presence of PTMO crystals increased the glassy modulus.[48] A second transition that caused a decrease in the storage modulus occurred in the phosphonium-containing polyurethane at 47 °C, and this was attributed to the melting of the crystalline PTMO segments.[47] The same transition occurred in the PTMO-HMDI-BD polyurethanes, but to a much lesser extent, since the decrease in modulus is very slight. The higher modulus in the rubbery plateau region (30 MPa) for the non-charged polyurethane

suggested a greater extent of hydrogen bonding[49] in comparison to the phosphonium polyurethane, which had a lower rubbery plateau modulus (1 MPa). The lower plateau modulus could also suggest that the phosphonium polyurethane had a lower entanglement density,[50-52] which was possibly due to the presence of bulky aryl groups around the phosphonium cations. Both polymers possessed similar flow temperatures at ~135 °C, and retained a relatively flat rubbery plateau modulus prior to the onset of flow. It is interesting that both polyurethanes have similar flow temperatures, which indicated that the ion-containing hard segments persist to approximately the same temperature as the urethane hydrogen bonds.

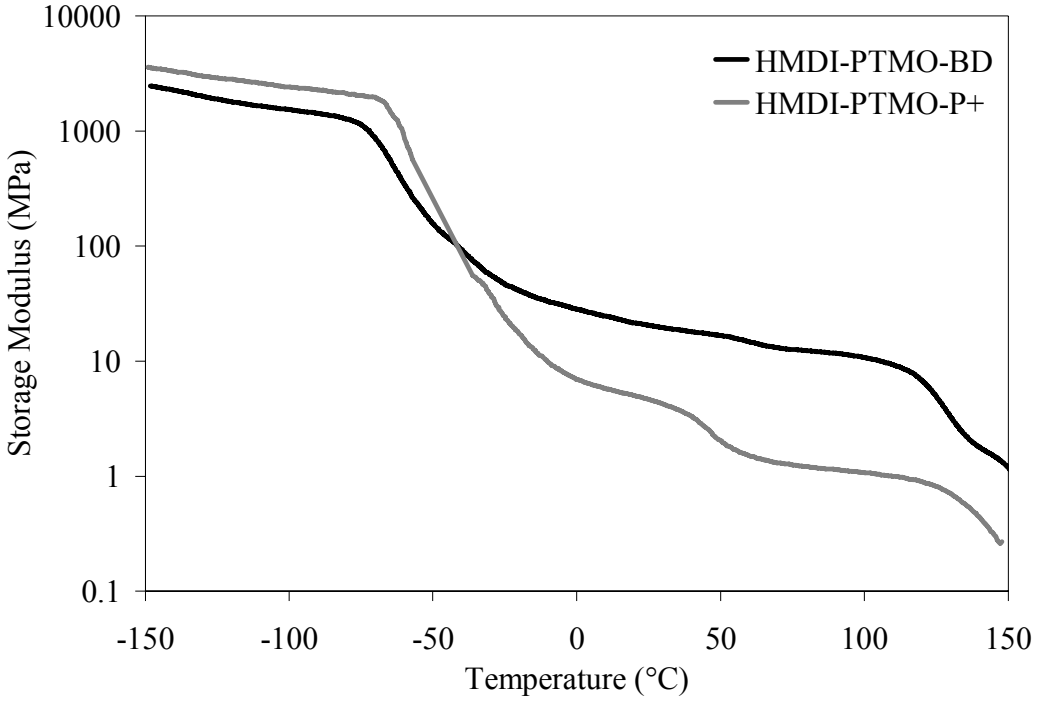

Figure 8.2. DMA curves demonstrating the transitions of the phosphonium-containing (gray line) and non-charged polyurethanes (black line). Conditions: 3 °C/min, 1 Hz, film tension mode.

Figure 8.3 shows the combined multi-angle X-ray scattering data plotted in log-log scale. PTMO oligomers (M_n = 2000 g/mol) used in the synthesis of the polyurethanes were highly crystalline, showing two sharp crystalline reflection peaks at angular positions of 14 nm^{-1} and 17

nm^{-1}, which corresponded to (020) and (110) peaks of PTMO crystals.[53] The PTMO oligomers also showed three crystalline lamellae-lamellae peaks at 0.36 nm^{-1}, 0.78 nm^{-1}, and 1.23 nm^{-1} that corresponded to a spacing of 16.3 nm. PTMO typically crystallizes into a monoclinic crystal structure with molecular chains having a planar zigzag confirmation along the c axis of the unit cell.[54] The length of a fully extended, crystalline PTMO chain of 2000 g/mol is ~16.8 nm, which is comparable to the inter-lamellar spacing given via X-ray scattering.

The scattering data of both PTMO-HMDI-P+ and PTMO-HMDI-BD displayed an amorphous peak at ~14 nm^{-1}, arising from PTMO soft segment.[53] In addition, both charged and non-charged polyurethanes also showed a weak broad peak at ~6 nm^{-1} that was absent in the pure PTMO oligomer X-ray profile. This broad peak was attributed to the intramolecular scattering from the diisocyanate hard segments. The amorphous nature of both the soft and hard segments detected via X-ray scattering at room temperature was consistent with DSC results, which showed a T_m of PTMO at 14 °C for PTMO-HMDI-P+ and non-crystalline behavior of PTMO-HMDI-BD. The crystallinity of hard segments is highly dependent on the structure and symmetry of diisocyanate groups.[55] Wilkes et al. previously showed that hard segments containing a kinked diisocyanate structure or a mixture of isomers, i.e. HMDI in this case, are less able to form ordered crystalline structures,[56] as observed herein.

In addition to the two higher-angle peaks, PTMO-HMDI-BD also demonstrated a well-defined scattering peak at an angular position of ~0.49 nm^{-1}, indicating microphase separation. This scattering peak was believed to arise from the interparticle scattering of hard domain, with an average interdomain spacing of ~12.8 nm in PTMO-HMDI-BD. Others have observed the incompatibility between soft and hard segments resulting in the formation of microphase-separated structures in various segmented polyurethane elastomers.[34,55-58] Small-angle X-ray scattering data also revealed a broad peak for PTMO-HMDI-P+ at a lower angle relative to the

non-charged polyurethane, and this peak appeared less distinct due to the overlap with the small-angle upturn. The degree of microphase separation is highly dependent on the chemical composition. The PTMO-HMDI-BD polyurethanes did not possess bulky ionic groups in the middle of urethane hard segments, and thus had better packing of the hard segments to form well-defined microphase-separated domains. For polyurethanes containing ionic groups, there were two driving forces for microphase separation, namely hydrogen-bonding interactions and ionic interactions. Additional experiments described below, were conducted to clarify the morphology of the materials.

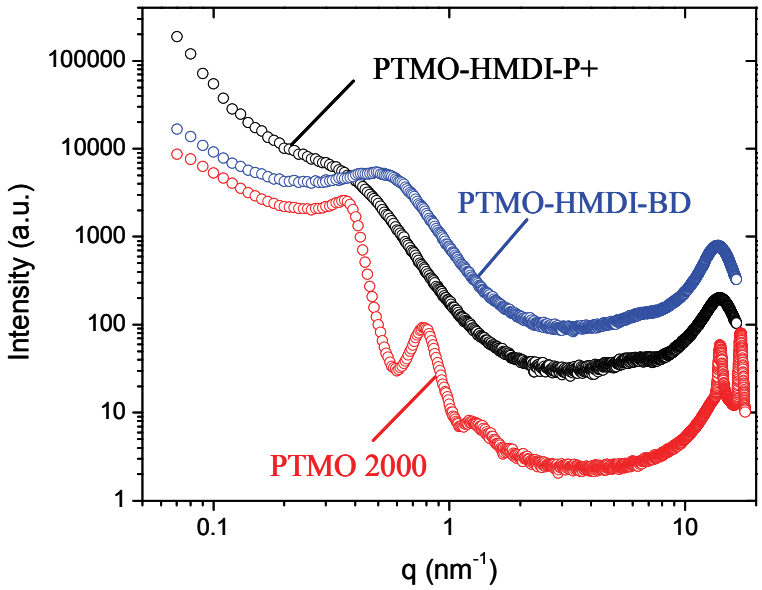

Figure 8.3. X-ray scattering intensity vs. scattering vector (q) plotted in log-log scale for unstretched PTMO oligomer and unstretched PTMO-based polyurethane films containing different chain extenders.

Scanning transmission electron microscopy (STEM) was applied to directly image the nanoscale morphology of PTMO-HMDI-P+. The high-angle annular dark-field (HAADF) STEM image of PTMO-HMDI-P+ (Figure 8.4a) showed bright, circular ion-rich regions dispersed in dark, hydrocarbon-rich matrix. The mean diameter of STEM features was 43 nm ± 15 nm (Figure 8.4b), which was determined using Gaussian fits to line scans of intensity on >50

ion-containing hard segments. The size of ionic hard domains observed in STEM images was unexpected given the angular position of the broad X-ray scattering peak (Figure 8.3), which was ~ 0.2-0.4 nm^{-1}. It is important to note that polyurethanes are potentially hydrophilic due to the presence of hydrogen bonds. Thus, the ultra-thin films used for STEM imaging might have absorbed water after cryo-microtomy during grid transfer at ambient conditions. Any moisture would be difficult to remove under room temperature vacuum in the microscope. However, TGA analysis confirmed that our drying conditions adequately removed water from the samples within the error of TGA as discussed above. It is not expected that an organic cation, especially one with four phenyl rings and an alkylene spacer would exhibit significantly more water retention. The extensive projection overlap in the STEM images and the diffuse boundary of the bright features also increased the error during the measurement of the feature sizes. These ion-containing hard domains in the phosphonium polyurethane were much bigger than those observed in ion-containing vinyl polymers, such as poly(styrene-*ran*-sulfonated styrene) and poly(styrene-*ran*-methacrylic acid) copolymers neutralized with metal cations.[59,60] Previous STEM images of those solvent-cast ionomers have shown monodisperse, spherical ionic aggregates of 1-2 nm in diameters.[59,60] The large size of ionic domains observed here might have partially resulted from the bulkiness of the phosphonium ions, which each possess two phenyl groups. In addition, the rigid diisocyanate hard segments adjacent to the ionic groups may also participate in the observed ion-rich domains.

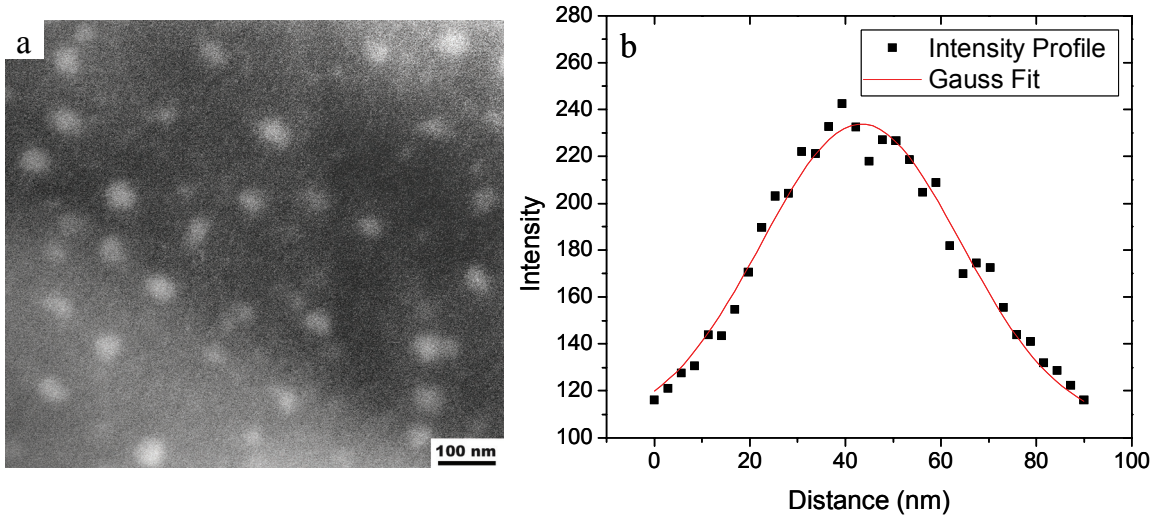

Figure 8.4. a. HAADF STEM image of phosphonium polyurethane showed bright, spherical ion-rich regions dispersed in the dark, hydrocarbon-rich matrix. **b.** Fitting the intensity profile across an isolated ionic domain with a Gaussian function provided the diameter of a STEM feature.

Energy-dispersive X-ray spectroscopy (EDS) was used to determine the elemental composition of ionic domains during STEM imaging (Figure 8.5). The spectra were collected by placing a focused electron beam of 0.7 nm diameter on bright and dark regions in the same field of view at high magnification to ensure similar thickness of the two spots. EDS results indicated that the bright, ion-rich region contained more Br and P elements in comparison to the matrix. A small amount of Br, P and O elements were also detected in the dark matrix region. However, a definite conclusion was not made about whether there were any ionic groups dispersed in the matrix exclusively based on the EDS results due to the limited lateral resolution of EDS.

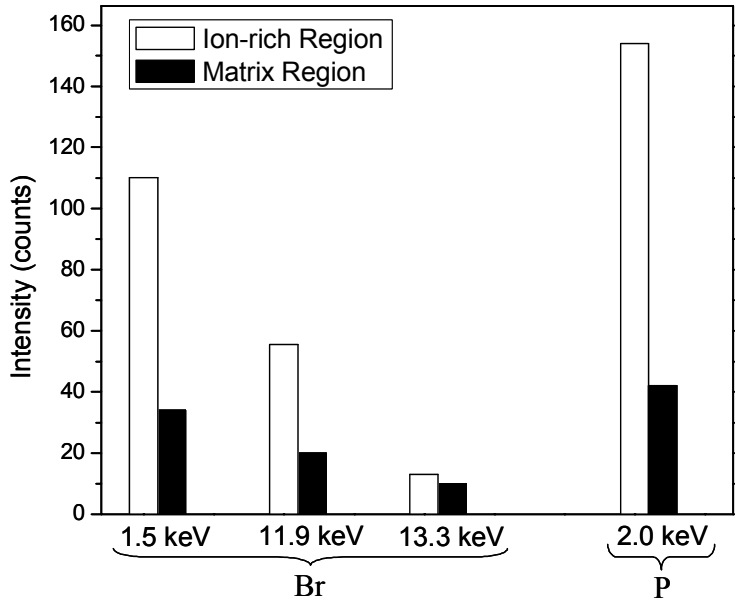

Figure 8.5. Spot EDS intensities taken from phosphonium polyurethane ultra-thin films during STEM imaging with a stationary 0.7 nm probe placed on bright and dark regions in the specimen. The quantity of Br and P is greater in the bright ion-rich domains.

To further refine the morphological description of the polyurethanes, the PTMO-HMDI-BD film was stretched to ~600% strain at room temperature using a tensile testing instrument and studied via X-ray scattering in the stretched state. The 2-D wide-angle scattering pattern showed two equatorial scattering peaks at angular positions of 14 nm^{-1} and 17 nm^{-1} (Figure 8.6a), which was the same as the crystalline reflection peaks of PTMO oligomers. Strain-introduced crystallization has been observed in various polymers.[61-63] Uniaxial stretching aligned the soft segment of the polymer backbone along the drawing direction, which effectively reduced the entropy of the polymer chain and promoted crystallization of the PTMO segment at room temperature. Furthermore, at high strain of 600%, the intramolecular hydrogen bonding that restricted the mobility of PTMO segments was broken, thereby rendering more freedom for PTMO chain to reorganize into crystalline structures. Moreover, the 2-D wide-angle scattering pattern revealed weak meridional reflections at 6 nm^{-1} (Figure 8.6b), indicating alignment of the hard segment along the stretching direction. As shown previously in Figure 8.3, this peak at 6

nm^{-1} was absent in the PTMO oligomers. It was attributed to the urethane-urethane spacing along the backbone (Figure 8.6d). The peak position of 6 nm^{-1} corresponded to a real-space distance of 1.05 nm. The intramolecular distance between the two urethane groups was estimated to be 1.15 nm.[64] Stretching also introduced meridional scattering in the 2-D small-angle scattering pattern (Figure 8.6c), indicating that the orientation of the interparticle scattering between the microphase-separated hard domains was parallel to the stretching direction. Compared to the unstretched PTMO-HMDI-BD, the peak position in the stretched film shifted from 0.49 nm^{-1} to 0.35 nm^{-1}, signifying a larger spacing between the microphase-separated domains due to the elongation of PTMO soft segments. Thus, uniaxial stretching altered the morphology in ways that were consistent with the proposed peak assignments. The intermolecular crystalline scattering signified PTMO chain crystallized along the stretching direction. The intramolecular scattering from the hard segment also showed the alignment of hard segment along the stretching direction, and the interparticle scattering from the domains indicated that the alignment of the microphase-separated domains was parallel to the stretching direction.

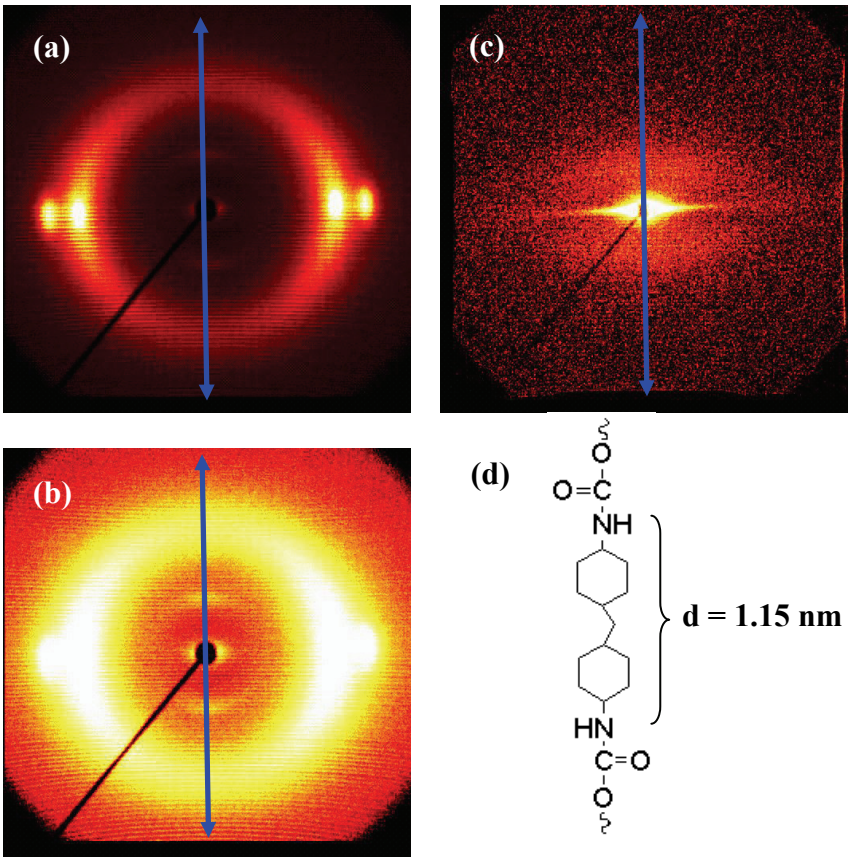

Figure 8.6. 2-D X-ray scattering patterns of the stretched PTMO-HMDI-BD films at 600% strain (a) Wide-angle pattern shows two equatorial scattering peaks at angular positions of 14 nm^{-1} and 17 nm^{-1} that correspond to PTMO crystallization. (b) Same wide-angle pattern as (a), but in a different color scale to show the weak meridional reflections at 6 nm^{-1} that correspond to intramolecular scattering from hard segment. (c) Small-angle pattern shows meridional reflections at ~0.35 nm^{-1} that correspond to interparticle scattering from microphase-separated hard domains. The blue arrow indicates the stretching direction. (d) Chemical structure of the urethane segment in PTMO-HMDI-BD.

FT-IR spectroscopy was utilized to observe the extent of hydrogen bonding in both polyurethanes (Figure 8.7). Wilkes et al. demonstrated FT-IR spectroscopy was a simple and efficient means to determine the extent of hydrogen bonding in the carbonyl absorbing region of 1610-1760 cm^{-1} for non-charged polyurethanes.[65] Specifically, they confirmed that there are distinct peaks in the carbonyl region that are attributed to hydrogen bond interactions for carbonyl groups. Non-hydrogen-bonded carbonyls have a peak at higher wavenumbers than hydrogen-bonded carbonyls. Furthermore, Wu et al. investigated the extent of hydrogen bonding

in Nylon-6,6 in the presence of lithium salts.[668] They determined that the NH peak in the FT-IR spectrum narrows as the extent of hydrogen bonding increased. In the case of PTMO-HMDI-BD and PTMO-HMDI-P+, FT-IR spectroscopy was a very powerful tool to examine the extent of hydrogen bonding. As shown in Figure 8.7, the NH region is distinctly sharper for PTMO-HMDI-BD than PTMO-HMDI-P+. In addition, the carbonyl region of PTMO-HMDI-BD had two peaks, at 1716 cm^{-1} and 1686 cm^{-1}. The peak at 1716 cm^{-1} was attributed to free carbonyl groups, and the peak at 1686 cm^{-1} was attributed to carbonyls that participated in hydrogen bonding. Clearly, a lack of hydrogen bonding was demonstrated for PTMO-HMDI-P+, as evidenced with the absence of a peak in the hydrogen bond carbonyl region at 1686 cm^{-1}. This demonstrated that the hydrogen bonding interactions were significantly reduced due to the presence of ionic groups. As a result, ionic interactions were the primary driving force for microphase separation in the phosphonium polyurethanes. Furthermore, this finding supported the tensile property results that are described below.

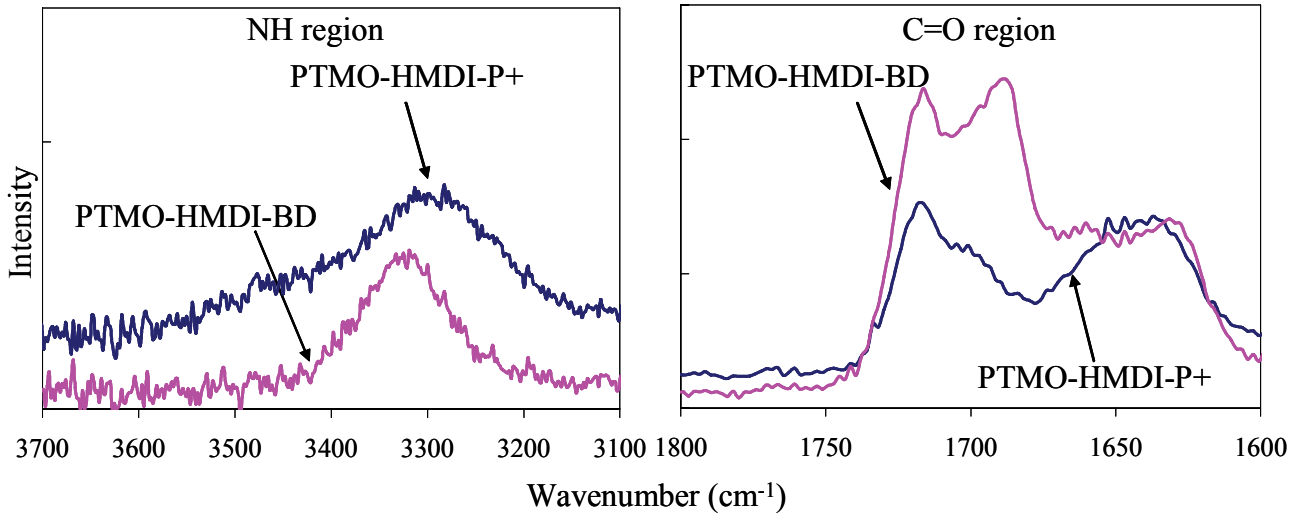

Figure 8.7. FT-IR spectroscopy of NH (left) and C=O (right) region of PTMO-HMDI-BD and PTMO-HMDI-P+.

Representative stress-strain curves for both the phosphonium-containing and non-charged polyurethanes are shown in Figure 8.8. The charged and non-charged polyurethanes had

comparable maximum elongation, which were 1330 ± 63 % and 1170 ± 180 %, respectively. The tensile stress at break was slightly higher for non-charged polyurethanes (24.0 ± 1.2 MPa) comparing to PTMO-HMDI-P+ polyurethanes (19.2 ± 1.1 MPa). It is important to note that all polyurethanes displayed excellent recovery after elongation. However, the presence of ionic groups disrupted hydrogen bonding and resulted in the slightly lower tensile performance of the phosphonium polyurethanes in comparison to the non-charged polymers. Interestingly, the tensile behavior after ~200 % elongation was quite different as the PTMO-HMDI-BD polyurethane displayed pronounced strain hardening behavior. The strain-induced crystallization was confirmed previously with X-ray scattering (Figure 8.6a), and was due to the recognized strain induced crystallization of PTMO.[48,67,68] In addition, during uniaxial stretching, it was speculated that the intramolecular hydrogen bonding between the ether oxygen in PTMO segments and urethane group was broken and replaced with intermolecular hydrogen bonds,[70] which also increased the number of physical cross-links and resulted in the straining-hardening behavior. In contrast, the presence of disruptive ionic groups prevented an upturn in modulus for the phosphonium polyurethane. Repeated experiments of PTMO-HMDI-P+ polyurethanes resulted in the reproducible behavior as shown in Figure 8.8.

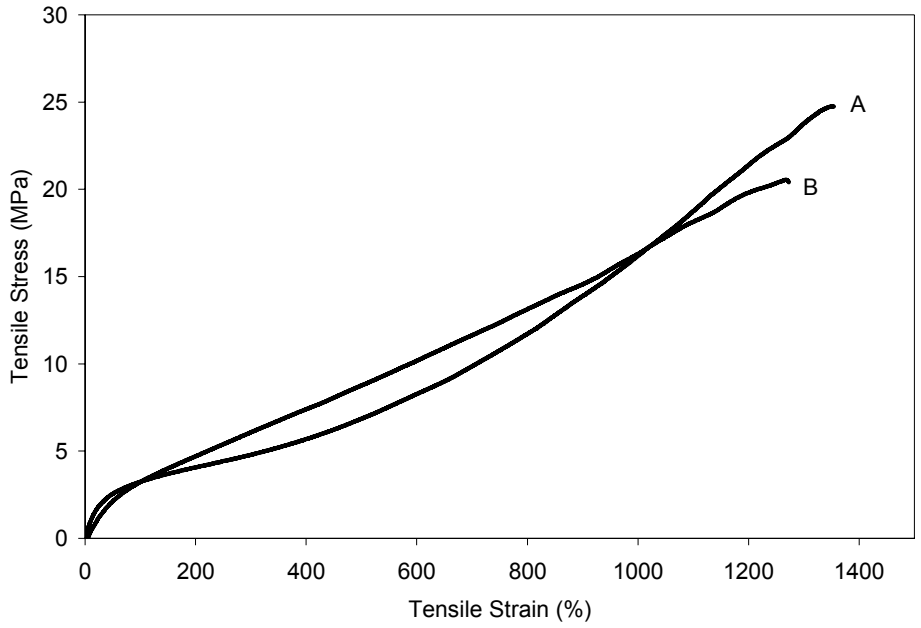

Figure 8.8. Comparison of the stress-strain behavior of linear, segmented, ion-containing polyurethane elastomer compared to the non-charged polyurethane: (A) PTMO-HMDI-BD (B) PTMO-HMDI-P+.

8.5 Conclusions

Novel phosphonium-containing polyurethanes were synthesized using a prepolymer method and characterized using a variety of methods. For comparative purposes, polyurethanes containing 1,4-butanediol as the chain extender were also synthesized. The non-charged PTMO-based polyurethane had hydrogen bonding as evident by FT-IR spectroscopy, while secondary bonding in the charged PTMO-based polyurethanes was dominated by the ionic interactions. Hydrogen-bonding interactions in PTMO-HDMI-BD reduced chain mobility and crystallinity of the PTMO segment. DSC detected crystallization in PTMO-HMDI-P+ with a T_c (-30 °C) and a T_m (14 °C). At room temperature, X-ray scattering of both polyurethanes indicated that they were amorphous, with scattering features corresponding to interparticle scattering between microphase-separated hard domains (~ 0.2-0.5 nm^{-1}), intramolecular scattering from hard segments (~ 6 nm^{-1}), and intermolecular amorphous scattering at ~ 14 nm^{-1}. For ion-containing

polyurethanes, STEM imaging confirmed the presence of ionic domains that were enriched with Br and P, although the observed size of domains was surprisingly large, perhaps due to their hygroscopic nature. X-ray scattering on stretched films verified the assignments of scattering peaks and detected strain-induced crystallization. Strain-induced crystallization was also observed in tensile testing, wherein PTMO-HMDI-BD had an upturn in modulus at the high strain region. Both charged and non-charged polyurethanes exhibited excellent elasticity, high strain to break (>1100 %), and high tensile strengths (>19 MPa). A future study will investigate the antimicrobial properties of these novel phosphonium polyurethanes. Furthermore, this type of phosphonium diol chain extender opens a wide field of potential research in polyurethane ionomers.

8.6 Acknowledgements

This material is based upon work supported by the U.S. Army Research Laboratory and the U.S Army Research Office under grant number W911NF-07-1-0452 Ionic Liquids in Electroactive Devices (ILEAD) MURI. The authors also thank Prof. Garth Wilkes and Dr. Sudipto Das for helpful discussions and assistance with FT-IR spectroscopic interpretations.

8.7 References

(1) Unal, S.; Yilgor, I.; Yilgor, E.; Sheth, J. P.; Wilkes, G. L.; Long, T. E. *Macromolecules* **2004,** 37, (19), 7081-7084.
(2) Woods, G., *The ICI polyurethanes book*. John Wiley: New York, 1990.
(3) Szycher, M., *Szycher's handbook of polyurethanes*. CRC Press: Boca Raton, 1999.
(4) Chattopadhyay, D. K.; Raju, K. V. S. N. *Progress in Polymer Science* **2007,** 32, (3), 352-418.
(5) Petrovic, Z. S.; Ferguson, J. *Prog. Polym. Sci.* **1991,** 16, (5), 695-836.
(6) Hepburn, C., *Polyurethane elastomers*. 2nd ed.; Elsevier Applied Science: London, 1992.
(7) Thomson, T., *Polyurethanes as specialty chemicals : principles and applications*. CRC Press: Boca Raton, 2005.

(8) *The polyurethanes book*. J. Wiley: New York, 2002.
(9) Dickinson, R. B.; Nagel, J. A.; Proctor, R. A.; Cooper, S. L. *Journal of Biomedical Materials Research* **1997,** 36, (2), 152-162.
(10) Jeong, E. H.; Yang, H.; Youk, J. H. *Materials Letters* **2007,** 61, (18), 3991-3994.
(11) Krol, P.; Krol, B.; Subocz, L.; Andruszkiewicz, P. *Colloid and Polymer Science* **2006,** 285, (2), 177-183.
(12) Polizos, G.; Georgoussis, G.; Kyritsis, A.; Shilov, V. V.; Shevchenko, V. V.; Gomza, Y. P.; Nesin, S. D.; Klimenko, N. S.; Wartewig, S.; Pissis, P. *Polymer International* **2000,** 49, (9), 987-992.
(13) Shilov, V. V.; Shevchenko, V. V.; Pissis, P.; Kyritsis, A.; Georgoussis, G.; Gomza, Y. P.; Nesin, S. D.; Klimenko, N. S. *Molecular Crystals and Liquid Crystals* **2001,** 361, 269-274.
(14) Vatalis, A. S.; Kanapitsas, A.; Delides, C. G.; Viras, K.; Pissis, P. *Journal of Applied Polymer Science* **2001,** 80, (7), 1071-1084.
(15) Reiff, H.; Dieterich, D., Urethane-based dispersions. In *Ionomers: Synthesis, Structure, Properties, and Applications*, Tant, M. R.; Mauritz, K. A.; Wilkes, G. L., Eds. Blackie Academic and Professional: London, 1997; pp 444-501.
(16) Dieterich, D.; Keberle, W.; Witt, H. *Angew. Chem., Int. Ed.* **1970,** 9, (1), 40-50.
(17) Chen, S. A.; Hsu, J. S. *Polymer* **1993,** 34, (13), 2769-2775.
(18) Chen, S. A.; Hsu, J. S. *Polymer* **1993,** 34, (13), 2776-2782.
(19) Ding, Y. S.; Register, R. A.; Yang, C. Z.; Cooper, S. L. *Polymer* **1989,** 30, (7), 1204-1212.
(20) Register, R. A.; Cooper, S. L. *Abstracts of Papers of the American Chemical Society* **1989,** 197, 203-POLY.
(21) Register, R. A.; Pruckmayr, G.; Cooper, S. L. *Macromolecules* **1990,** 23, (11), 3023-3026.
(22) Register, R. A.; Yu, X. H.; Cooper, S. L. *Polymer Bulletin* **1989,** 22, (5-6), 565-571.
(23) Yang, C. Z.; Grasel, T. G.; Bell, J. L.; Register, R. A.; Cooper, S. L. *Journal of Polymer Science Part B-Polymer Physics* **1991,** 29, (5), 581-588.
(24) Hourston, D. J.; Williams, G. D.; Satguru, R.; Padget, J. C.; Pears, D. *Journal of Applied Polymer Science* **1999,** 74, (3), 556-566.
(25) Mequanint, K.; Sanderson, R. *Eur. Polym. J.* **2006,** 42, 1145-1153.
(26) Buruiana, E. C.; Buruiana, T.; Strat, G.; Strat, M. *Journal of Polymer Science Part A-Polymer Chemistry* **2002,** 40, (11), 1918-1928.
(27) Buruiana, T.; Buruiana, E. C. *J. Polym. Mat.* **2001,** 18, (1), 97-102.
(28) Kim, B. K.; Yang, J. S.; Yoo, S. M.; Lee, J. S. *Colloid Polym. Sci.* **2003,** 281, 461-468.
(29) Ghassemi, H.; Riley, D. J.; Curtis, M.; Bonaplata, E.; McGrath, J. E. *Appl. Organometal. Chem.* **1998,** 12, 781-785.
(30) Parent, J. S.; Penciu, A.; Guillen-Castellanos, S. A.; Liskova, A.; Whitney, R. A. *Macromolecules* **2004,** 37, (20), 7477-7483.
(31) Lindsell, W. E.; Radha, K.; Soutar, I.; Stewart, M. J. *Polymer* **1990,** 31, (7), 1374-1378.
(32) Fornof, A. R.; Glass, T. E.; Long, T. E. *Macromolecular Chemistry and Physics* **2006,** 207, (14), 1197-1206.
(33) McKee, M. G.; Park, T.; Unal, S.; Yilgor, I.; Long, T. E. *Polymer* **2005,** 46, (7), 2011-2015.
(34) Sheth, J. P.; Unal, S.; Yilgor, E.; Yilgor, I.; Beyer, F. L.; Long, T. E.; Wilkes, G. L. *Polymer* **2005,** 46, (23), 10180-10190.

(35) Sheth, J. P.; Wilkes, G. L.; Fornof, A. R.; Long, T. E.; Yilgor, I. *Macromolecules* **2005,** 38, (13), 5681-5685.
(36) Supriya, L.; Unal, S.; Long, T. E.; Claus, R. O. *Chemistry of Materials* **2006,** 18, (10), 2506-2512.
(37) Yilgor, I.; Mather, B. D.; Unal, S.; Yilgor, E.; Long, T. E. *Polymer* **2004,** 45, (17), 5829-5836.
(38) Lepene, B. S.; Long, T. E.; Meyer, A.; Kranbuehl, D. E. *J. Adhes.* **2002,** 78, (4), 297-312.
(39) Unal, S. Synthesis and characterization of branched macromolecules for high performance elastomers, fibers, and films. PhD Thesis. Virginia Tech, Blacksburg, VA, 2005.
(40) Unal, S.; Ozturk, G.; Sisson, K.; Long, T. E. *J. Polym. Sci. A* **2008,** submitted.
(41) Williams, S. R.; Mather, B. D.; Miller, K. M.; Long, T. E. *J. Polym. Sci. A-Polym. Chem.* **2007,** 45, (17), 4118-4128.
(42) Karikari, A. S.; Edwards, W. F.; Mecham, J. B.; Long, T. E. *Biomacromolecules* **2005,** 6, (5), 2866-2874.
(43) Karikari, A. S.; Williams, S. R.; Heisey, C. L.; Rawlett, A. M.; Long, T. E. *Langmuir* **2006,** 22, (23), 9687-9693.
(44) Mather, B. D.; Baker, M. B.; Beyer, F. L.; Green, M. D.; Berg, M. A. G.; Long, T. E. *Macromolecules* **2007,** 40, 4396-4398.
(45) Heiney, P. A. *Comm Powder Diffr Newsletter* **2005,** 32, 9-11.
(46) Chinwanitcharoen, C.; Kanoh, S.; Yamada, T.; Hayashi, S.; Sugano, S. *J. Appl. Polym. Sci.* **2004,** 91, 3455-3461.
(47) Hu, C. B.; Ward, R. S.; Schneider, N. S. *Journal of Applied Polymer Science* **1982,** 27, (6), 2167-2177.
(48) Das, S.; Yilgor, I.; Yilgor, E.; Inci, B.; Tezgel, O.; Beyer, F. L.; Wilkes, G. L. *Polymer* **2007,** 48, 290-301.
(49) Christenson, C. P.; Harthcock, M. A.; Meadows, M. D.; Spell, H. L.; Howard, W. L.; Creswick, M. W.; Guerra, R. E.; Turner, R. B. *Journal of Polymer Science Part B-Polymer Physics* **1986,** 24, (7), 1401-1439.
(50) Fetters, L. J.; Lohse, D. J.; Graessley, W. W. *Journal of Polymer Science Part B-Polymer Physics* **1999,** 37, (10), 1023-1033.
(51) Llorens, J.; Rude, E.; Marcos, R. M. *Journal of Polymer Science Part B-Polymer Physics* **2000,** 38, (11), 1539-1546.
(52) Wang, D. H.; Shen, Z. H.; Guo, M. M.; Cheng, S. Z. D.; Harris, F. W. *Macromolecules* **2007,** 40, (4), 889-900.
(53) Sun, Y.; Jeng, U.; Huang, Y.; Liang, K.; Lin, T.; Tsao, C. *Physica B* **2006,** 385, 650-652.
(54) Tadokoro, H. *J. Poly. Sci., Part C* **1966,** 15, 1-15.
(55) Aneja, A.; Wilkes, G. L. *Polymer* **2003,** 44, (23), 7221-7228.
(56) Klinedinst, D. B.; Yilgor, E.; Yilgor, I.; Beyer, F. L.; Wilkes, G. L. *Polymer* **2005,** 46, (23), 10191-10201.
(57) O'Sickey, M. J.; Lawrey, B. D.; Wilkes, G. L. *Polymer* **2002,** 43, (26), 7399-7408.
(58) Sheth, J. P.; Klinedinst, D. B.; Wilkes, G. L.; Iskender, Y.; Yilgor, E. *Polymer* **2005,** 46, (18), 7317-7322.
(59) Benetatos, N. M.; Chan, C. D.; Winey, K. I. *Macromolecules* **2007,** 40, (4), 1081-1088.
(60) Zhou, N.; Chan, C. D.; Winey, K. I. *Macromolecules* **2008,** 41, ASAP.
(61) Martins, C. I.; Cakmak, M. *Polymer* **2007,** 48, (7), 2109-2123.
(62) Bartczak, Z.; Kozanecki, A. *Polymer* **2005,** 46, (19), 8210-8221.

(63) Klimov, E.; Hoffmann, G. G.; Gumenny, A.; Siesler, H. W. *Macromolecular Rapid Communications* **2005,** 26, (13), 1093-1098.
(64) The distance is calculated based on the size of cyclohexane (0.45 nm) and the carbon-carbon bond length of 0.145 nm with bond angle of 120^{o}.
(65) Yilgor, I.; Yilgor, E.; Guler, I. G.; Ward, T. C.; Wilkes, G. L. *Polymer* **2006,** 47, 4105-4114.
(66) Wu, Y.; Xu, Y.; Wang, D.; Zhao, Y.; Weng, S.; Xu, D.; Wu, J. *J. Appl. Polym. Sci.* **2004,** 91, 2869-2875.
(67) Das, S.; Cox, D. F.; Wilkes, G. L.; Klinedinst, D. B.; Yilgor, I.; Yilgor, E.; Beyer, F. L. *J. Macro. Sci., Part B* **2007,** 46, (5), 853-875.
(68) Feng, D.; Wilkes, G. L.; Leir, C. M.; Stark, J. E. *J. Macromol. Sci.-Chem.* **1989,** A26, (8), 1151-1181.

Chapter 9 : Michael Addition Reaction Kinetics of Acetoacetates and Acrylates for the Formation of Polymeric Networks

Reproduced with permission from: Williams, S.R.; Miller, K.M.; Long, T.E. *Progress in Reaction Kinetics and Mechanism*, 32, 165-194, 2007. Copyright 2007. Science Reviews

9.1 Abstract

2-Ethylhexyl acrylate and ethyl acetoacetate were reacted in a Carbon-Michael addition reaction as a model for subsequent studies of polymer networks. A statistical design of reactions were conducted in the presence of an *in-situ* ATR FTIR spectrometer to determine the effect of solvent, base, base concentration, and reactant stoichiometry on the observed rate constant. In particular, a central composite statistical design of experiments analysis was performed for model reactions that were catalyzed using either 1,8-diazbicyclo[5.4.0]undec-7-ene (DBU) or K_2CO_3 at various concentrations. Poly(propylene glycol) bisacetoacetate (PPG BisAcAc) and poly(propylene glycol) diacrylate (PPGDA) networks were then prepared in the absence of solvent at 23 °C based on optimized conditions in the presence of DBU and K_2CO_3. In a similar fashion to model studies, *in-situ* FTIR spectroscopy was utilized, and observed rate constants were determined. The influence of PPG BisAcAc molecular weight on dynamic mechanical properties was determined and gel fraction analysis was conducted. It appears that the selection of base significantly altered the rate of the reaction, but had an insignificant effect on mechanical properties.

9.2 Introduction

The Michael reaction, which was discovered by Arthur Michael in the late 1800's, is an efficient and versatile reaction. The carbon-Michael addition reaction has received significant attention in recent literature for the preparation of novel polymers and composites.[1-11] The Michael reaction typically refers to the base-catalyzed addition of an enolate anion (Michael donor) to an activated α,β-unsaturated carbonyl-containing compound (Michael acceptor).[5-8] One of the most well-known Carbon-Michael transformations is the base-catalyzed addition of ethyl acetoacetate to methyl acrylate.[12] The mechanism of the reaction is relatively straightforward, and every step is in equilibrium and thermodynamically dependant on the relative strength of the base and the type of acetoacetate. The acetoacetate is first deprotonated with a base, which provides an enolate anion in equilibrium. The enolate anion then reacts in a 1,4-conjugate addition to the olefin of the methyl acrylate. The carbonyl of the acrylate stabilizes the resulting anion until proton transfer occurs, which regenerates the base. The overall driving force for the conjugate addition is the replacement of a π bond with a σ bond. Thus, there is the preference for 1,4-addition rather than 1,2-addition. However, in some cases, kinetically controlled reaction conditions afford attack at the carbonyl carbon rather than at the β-carbon of the olefin.[13]

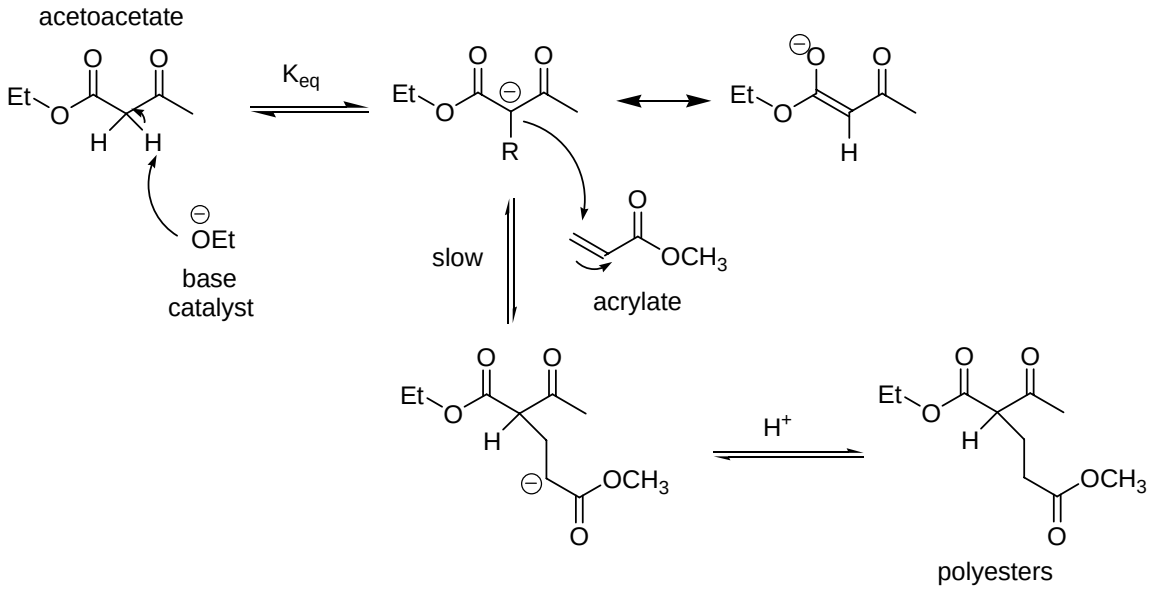

Scheme 9.1. General Carbon-Michael reaction.

From Scheme 9.1, one can observe that the rate determining step is the attack of the enolate anion on the activated olefin. The reaction rate is therefore second order overall with respect to the enolate anion and the olefin acceptor. The concentration of the enolate is a function of the base strength and the K_{eq} of the deprotonation of the active methylene hydrogen. It follows that the equilibrium constant is dependant on the relative strength of the base and the structure of the acetoacetate.

It is worthy to note that the product of the first Michael addition has one remaining active methylene hydrogen which can be deprotonated and thus undergo a second addition to another acrylate (Scheme 9.2). Clemens et. al. has documented that the second pK_a is expected to have a value of 13 (versus the pK_a of the initial active hydrogen of 12).[14] The second deprotonation therefore has a different equilibrium constant (K_{eq}) and it is assumed that the concentration of the first Michael adduct will be low. As a result, the concentration of the enolate at any rate (especially in the early stages of the reaction) is not effected by this secondary reaction.

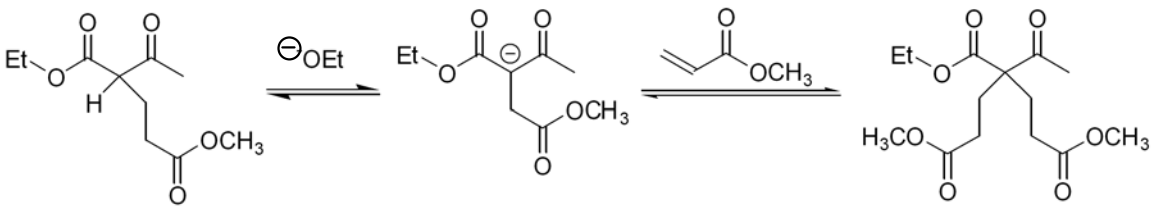

Scheme 9.2. Second Michael addition

It follows that a rate law can be determined for the above reaction sequence. Writing the reactions in terms of the Michael addition, the following reaction sequences are obtained:

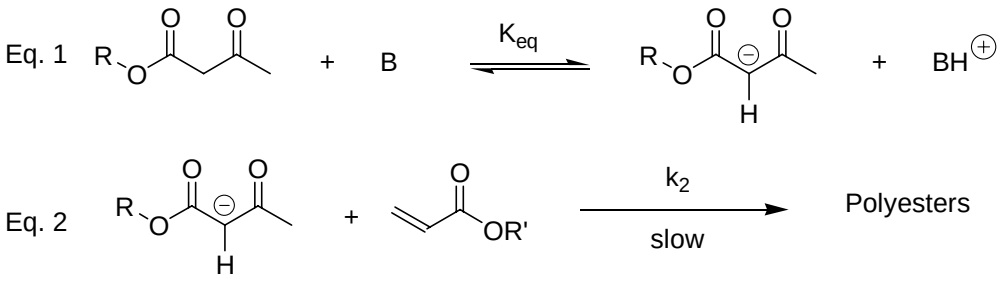

The subsequent rate equations based on the reaction sequence are the following:

Eq. 3 $K_{eq} = [AcAc^-][BH^+] / [AcAc][B]$

Eq. 4 $Rate = k_2[AcAc^-][Acrylate] = k_2K_{eq}([B] / [BH^+])[AcAc][Acrylate]$

The choice of catalyst has a tremendous effect on the reaction kinetics. As previously noted, the concentration of the enolate and therefore the value of K_{eq} is highly dependant on the relative base strength. In the case of strong bases, K_{eq} will lie to the right and the concentration of the enolate anion is approximately equal to the concentration of the base (achieving a steady state concentration). The resulting rate law follows pseudo first-order kinetics (Eq. 5). In this rate expression, there is a pseudo first-order dependence on acrylate concentration, where k_{obs} is a function of base concentration.

Eq. 5 $Rate = k_{obs}[Acrylate]$

In the case of weaker base catalysts, K_{eq} has a moderate value, but is not large. This

introduces the equilibrium constant into the rate law and results in the reaction following second order kinetics (Eq. 4). Clemens et. al. has completed an extensive study on how base strength effects reaction kinetics and molecular weight when the Michael addition is used to prepare crosslinked acetoacetate resins for thermoset coatings.[14] In his model study, Clemens analyzed the ability of weaker bases such as tetramethylguanidine (TMG), triethylamine (TEA), 1,8-diazabicyclo[5.4.0]undec-7-ene (DBU) and 1,5-diazabicyclo[4.3.0]non-5-ene (DBN) and found that, as indicated by Eq. 4, the rate of the reaction is dependant on catalyst concentration. In the cases of stronger bases such as hydroxide, a steady-state concentration of enolate anion is achieved and pseudo-first order kinetics are observed (Eq. 5).

Our current research seeks to fundamentally understand the kinetics of the Michael reaction with both homogeneous and heterogeneous catalysts. Model reactions as described herein allowed us to understand the kinetics of the Michael reaction as a function of acrylate to acetoacetate molar ratio, base concentration, and solvent. We subsequently applied our understanding of the model reactions to the formation of polymeric networks containing poly(propylene glycol) (PPG). The kinetics of the network formation as well as dynamic mechanical analysis of the networks are described.

9.3 Experimental

9.3.1 Materials and Procedures

tert-Butyl acetoacetate (tBuAcAc, 98%), 800 g/mol poly(propylene glycol) diacrylate (PPGDA), ethyl acetoacetate (EtAcAc, 99%) and 1,8-diazbicyclo[5.4.0]undec-7-ene (DBU, 98%) were purchased from Aldrich and used as received. 2-Ethylhexyl acrylate (EHA, 98%) was purchased from Aldrich, and the inhibitors were removed by passing the as received EHA

through a column of alumina. Tetrahydrofuran (THF, EMD Science, HPLC grade), ethanol (Aldrich, anhydrous, ≥ 99.5%), *m*-xylene (Aldrich, anhydrous, 99+%), and dimethylsulfoxide (DMSO, Aldrich, anhydrous, ≥ 99.5%) were used as received. Finely ground potassium carbonate (K_2CO_3) and poly(propylene glycol) bisacetoacetate (PPG BisAcAc) oligomers of 2000, 4000, and 8000 g/mol were kindly supplied by Rohm and Haas, the synthesis of which has been previously described.[3,15] All ARCOL™ and ACCLAIM™ polyols were kindly supplied by Bayer Co. PPG BisAcAc of 1000 g/mol was prepared from ARCOL™ poly(propylene glycol) diol. PPG BisAcAc oligomers of 2000, 4000, and 8000 g/mol were prepared from ACCLAIM™ poly(propylene glycol) diols, using a method described previously and described below.[3,15]

In a typical procedure, Arcol™ PPG (10.0 g, 10 mmol) and tBuAcAc (6.3 g, 40 mmol, 4 equiv.) were charged to a two-necked 100-mL flask, equipped with a short-path distillation head, receiving flask, and magnetic stirrer. The mixture was maintained at 150 °C for 3 h and vacuum (0.1 mmHg) was applied to remove the *tert*-butanol byproduct and excess tBuAcAc. An additional 6.3 g tBuAcAc was added and heating continued for 3 h at 150 °C in order to ensure quantitative functionalization. Vacuum (0.1 mmHg) at 150 °C was applied to remove volatile starting reagents and reaction byproducts. ^{1}H NMR spectroscopy of the PPG BisAcAc oligomers confirmed the desired composition. ^{1}H NMR (400 MHz, $CDCl_3$) of the 1000 g/mol PPG BisAcAc: δ=1.12 ppm (br, PPG C*H*$_3$),1.24 ppm (dd, 6H, CHC*H*$_3$OAcAc), 2.26 ppm (s, 6H,COCH$_2$COC*H*$_3$), 3.4 ppm (br, PPG C*H*), 3.6 ppm (br, PPG C*H*$_2$), 5.08 ppm (m, 4H, C*H*$_2$CHCH$_3$OAcAc), 5.29 ppm (s, enol C=C*H*–C=O).

9.3.2 In-situ FTIR reactions for model studies

A typical reaction consisted of a 1.4:1 mol ratio of acrylate to acetoacetate and 3 mol% 1,8-diazabicyclo-[5.4.0]-undec-7-ene (DBU) as the base in the presence of the *in-situ* FTIR

spectrometer. The *in-situ* FTIR ATR probe was cleaned with THF prior to running a background scan in air. A 3-necked, round-bottomed flask that was equipped with a stir bar was charged with 6.000 g (0.04610 mol) ethyl acetoacetate, and 11.895 g (0.06455 mol) 2-ethylhexyl acrylate was weighed in a separate vial. The round-bottomed flask and vial were placed in a 35 °C oil bath. DBU (3 mol%, 511 μL) was added to the round-bottomed flask, and the contents were allowed to equilibrate for 60 min. After the 60 min pre-equilibration, the reaction was monitored with the *in-situ* FTIR spectrometer. Once the first scan was complete, the acrylate was quickly added to the round-bottomed flask. For the reactions with solvent, the reaction flask was diluted 50% with THF by weight.

9.3.3 ^{1}H NMR spectroscopic kinetic studies

For the reactions completed in solvent, ^{1}H NMR spectroscopy was also used to determine relative rates of reaction. In a typical procedure, ethyl acetoacetate (5.00 g, 0.038 mol) was diluted 50% w/w with 5.00 g solvent (THF, DMSO, EtOH, *m*-xylene) was warmed to 35 °C using an oil bath. Once at 35 °C, 1 mol% potassium carbonate was added and allowed to stir for 30 minutes. Butyl acrylate (4.93 g, 0.038 mol), pre-warmed to 35 °C, was added, and loss of acrylate signal was monitored by ^{1}H NMR over time. Plots of ln[acrylate] versus time resulted in a linear fit ($r^2 > 0.998$) of which the slope was the observed pseudo-first order rat constant. Analysis of the post reaction products resulted in >99:1 ratio of the mono to bis Carbon-Michael substitution products.

9.3.4 Statistical design of experiments

A central composite statistical design of experiments (DOE) was developed for the investigation of the kinetics of the Michael reaction. The constants for the DOE included stir

rate, reaction temperature (35 °C), air atmosphere, and an acetoacetate with base pre-equilibration time (1 h). The factors for the DOE included the EHA : EtAcAc molar ratio, choice of basic catalyst, catalyst concentration, and the presence or absence of solvent. Specifically, EHA : EtAcAc molar ratio ranged from 0.8 to 2.0, choice of basic catalyst was DBU or K_2CO_3, catalyst concentration ranged from 1-5 mol%, and the solvent was THF or bulk. The observed rate constant was the response modeled for the DOE. Stat-Ease software Design-Expert version 6.0.1 was used, and the DOE experimental design is given in Table 9.1.

Std	Run	Factor 1: Acrylate Molar Ratio (relative to AcAc)	Factor 2: Base Concentration (mol%)	Factor 3: Solvent
2	1	1.4 : 1.0	3.0	Bulk
11	2	0.8 : 1.0	1.0	Bulk
17	3	2.0 : 1.0	1.0	THF
9	4	2.0 : 1.0	5.0	THF
1	5	1.4 : 1.0	3.0	THF
14	6	2.0 : 1.0	1.0	Bulk
6	7	0.8 : 1.0	1.0	THF
8	8	2.0 : 1.0	3.0	Bulk
15	9	1.4 : 1.0	1.0	Bulk
7	10	1.4 : 1.0	5.0	THF
16	11	0.8 : 1.0	3.0	Bulk
12	12	0.8 : 1.0	5.0	THF
18	13	2.0 : 1.0	3.0	THF
5	14	1.4 : 1.0	5.0	Bulk
10	15	2.0 : 1.0	5.0	Bulk
3	16	0.8 : 1.0	3.0	THF
13	17	0.8 : 1.0	5.0	Bulk
4	18	1.4 : 1.0	1.0	THF

Table 9.1. DOE design.

9.3.5 Network formation

2000 g/mol PPG BisAcAc (0.75 g, 3.75 x 10^{-4} mol) and PPGDA (0.42 g, 5.25 x 10^{-4} mol, 1.4 equiv) were mixed thoroughly to form a clear, homogeneous liquid. DBU catalyst was

quickly added and mixed thoroughly. The mixture was then transferred to a Teflon™ mold and was allowed to cross-link for 24 h at room temperature. The resulting films were dried at reduced pressure (0.1 mm Hg) for 18 h at room temperature. Similar preparations were used to form all Carbon-Michael networks described in this manuscript, with the exception that K_2CO_3 was substituted for DBU.

9.3.6 Characterization

^{1}H NMR spectroscopy was utilized to determine PPG BisAcAc oligomer composition, number average molecular weight, percent functionalization, and confirm Michael reactions. A 400 MHz Varian UNITY spectrometer was used to characterize the oligomers and polymerizations in $CDCl_3$ at 23 °C. Dynamic mechanical analysis (DMA) was conducted on a TA Instruments Q800 dynamic mechanical analyzer in tension mode at a frequency of 1 Hz, an oscillatory amplitude of 15 μm, and a static force of 0.01 N. The temperature ramp was 3 °C/min. The glass transition temperature (T_g) was determined from the storage modulus curves. The resulting networks were characterized for gel fraction via Soxhlet extractions in THF for 3 h and subsequently dried in an oven at reduced pressure (0.1 mmHg) at 60 °C for 18 h, or until constant weight was observed. The gel fraction was determined by dividing the initial mass (m_i) with the final mass (m_f). Rheological experiments were conducted on a TA Instruments AR2000 Rheometer at a frequency of 1 Hz and a temperature of 25 °C. The gel time was recorded when the storage modulus (G') and loss modulus (G") were equal.

9.4 Results and discussion

9.4.1 Model Reactions with EtAcAc and EHA

The kinetics of the Michael reaction were analyzed using an *in-situ* FTIR spectrometer

and DOE software. During the *in-situ* FTIR reactions, the disappearance of the vinyl CH_2 out-of-plane wag was monitored at 810 cm^{-1}. Scheme 9.3 depicts the reaction strategy.

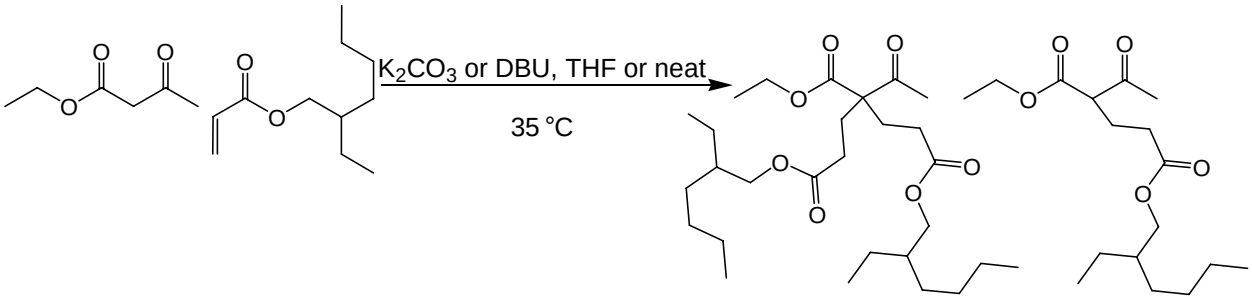

Scheme 9.3. Model reactions of EtAcAc and EHA.

A waterfall plot, which shows the *in-situ* FTIR absorbance as a function of time, is shown in Figure 9.1 for a reaction of EtAcAc and EHA with a 1.4:1.0 acrylate to AcAc molar ratio, 3 mol% K_2CO_3, in THF. As demonstrated in the FTIR data, this reaction was complete within 1 h. A 2-dimensional plot also reveals the disappearance of the vinyl CH_2 out-of-plane wag, with the peak decreasing in intensity as the reaction proceeded (Figure 9.2).

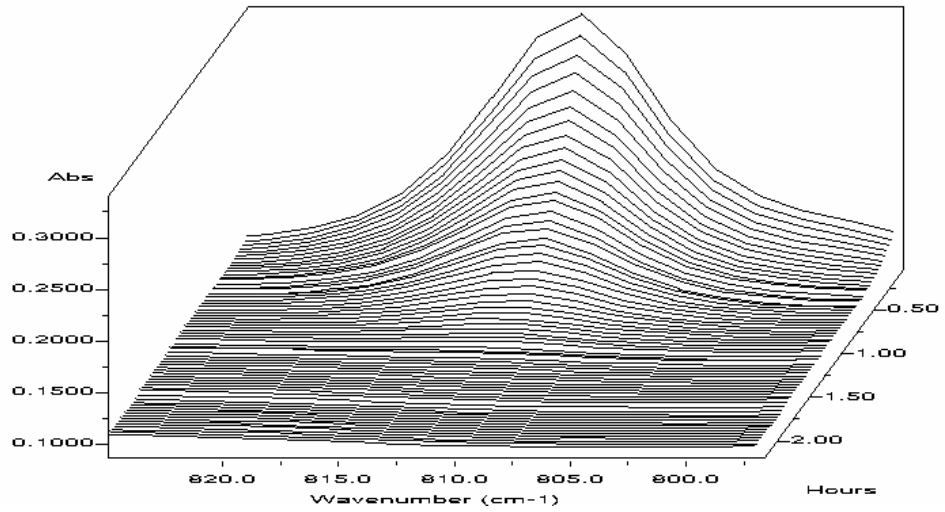

Figure 9.1. *In-situ* FTIR spectra of EtAcAc and EHA Michael reaction waterfall plot: 1.4:1.0 acrylate to AcAc, 3 mol% K_2CO_3, in THF.

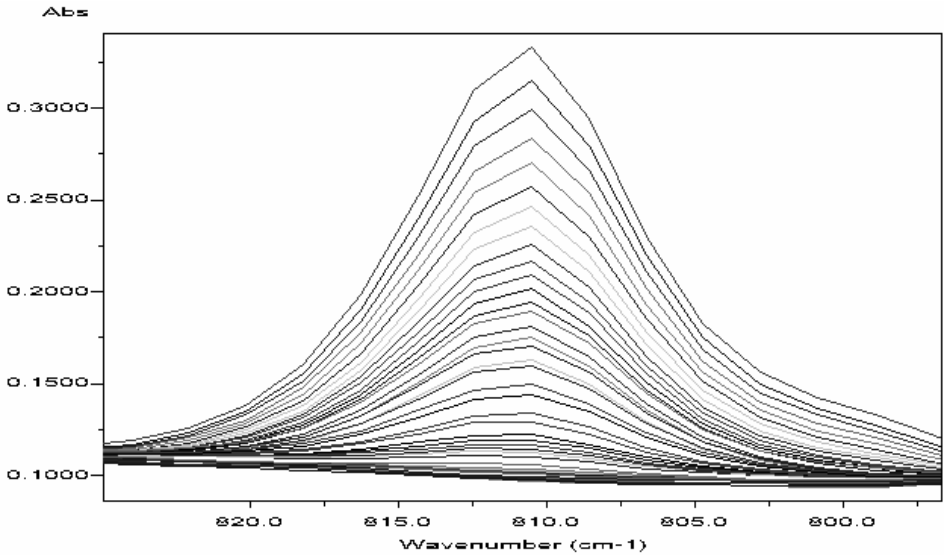

Figure 9.2. *In-situ* FTIR spectra of EtAcAc and EHA Michael reaction 2D plot: 1.4:1.0 acrylate to AcAc, 3 mol% K_2CO_3, in THF.

To further confirm that the vinyl groups of EHA were consumed during the reaction, samples were removed from a Michael reaction of EHA and EtAcAc and quenched with 0.65 M trifluoroacetic acid in $CDCl_3$. As demonstrated in Figure 9.3, the acrylate protons are consumed over time, and after 1 h, the acrylate is quantitatively consumed.

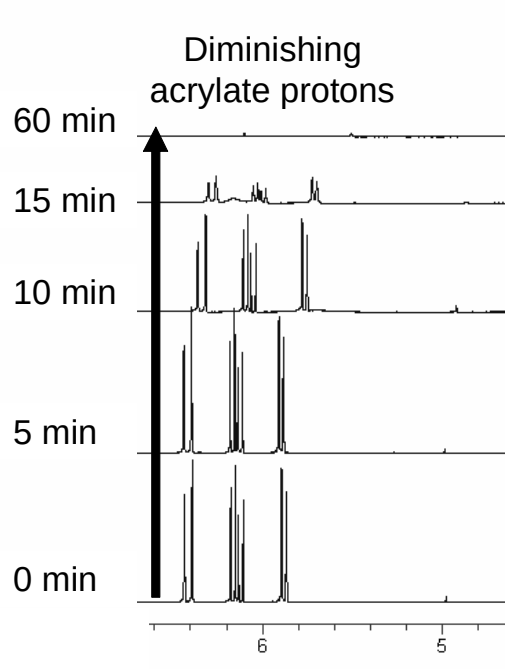

Figure 9.3. Stacked ^{1}H NMR spectra of EHA and EtAcAc Michael reaction versus time.

In the following section, three areas of interest are investigated with respect to the kinetics of the Carbon-Michael reaction, i.e., base concentration, solvent effects, and acrylate concentration. The goal is to provide a fundamental understanding of the reaction kinetics which may provide some help in understanding the kinetics of formation and mechanical properties of the corresponding polymer networks.

9.4.2 Effect of base concentration

As shown in Table 9.1, a series of reactions were performed, with various base concentrations and acrylate to acetoacetate molar ratios. Furthermore, the base was varied either as ground K_2CO_3 or DBU, and the reaction was performed in either THF solvent or in the absence of solvent. The vinyl CH_2 out-of-plane wag was monitored over time and compared to a baseline for every experiment. From this, the pseudo-first order plots were constructed and the observed rate constants were calculated from the slopes of the linear fits. The effect of DBU

concentration is depicted in Figure 9.4. As the base concentration was increased from 1 to 5 mol%, there was a systematic increase in the observed rate constant. Observed rate constants of 4.20×10^{-4}, 8.30×10^{-4}, and 2.00×10^{-3} s^{-1} for 1, 3, and 5 mol% DBU, respectively, were calculated.

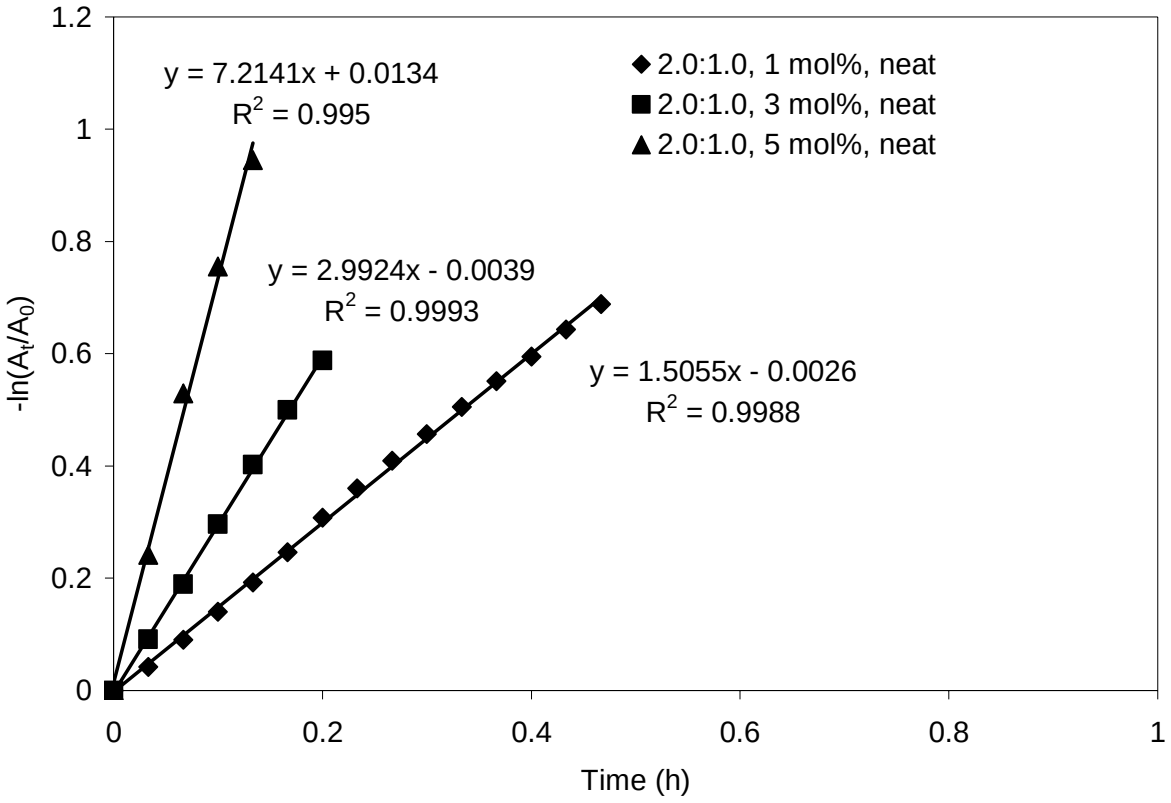

Figure 9.4. The effect of base concentration on rate constant for the EtAcAc and EHA Michael reaction in the presence of DBU. Reaction conditions: 2.0:1.0 mol ratio acrylate to AcAc, 35 °C, neat, DBU.

Similar experiments were conducted with K_2CO_3 as the basic catalyst in the model Michael reactions. The effect of K_2CO_3 concentration is depicted in Figure 9.5. As expected, when the base concentration is increased from 1 to 5 mol%, there was a systematic increase in the slopes, and thus an increase in the observed rate constant. Observed rate constants of 2.90×10^{-4}, 2.43×10^{-3}, and 4.6×10^{-3} s^{-1} for 1, 3, and 5 mol% K_2CO_3, respectively, were calculated.

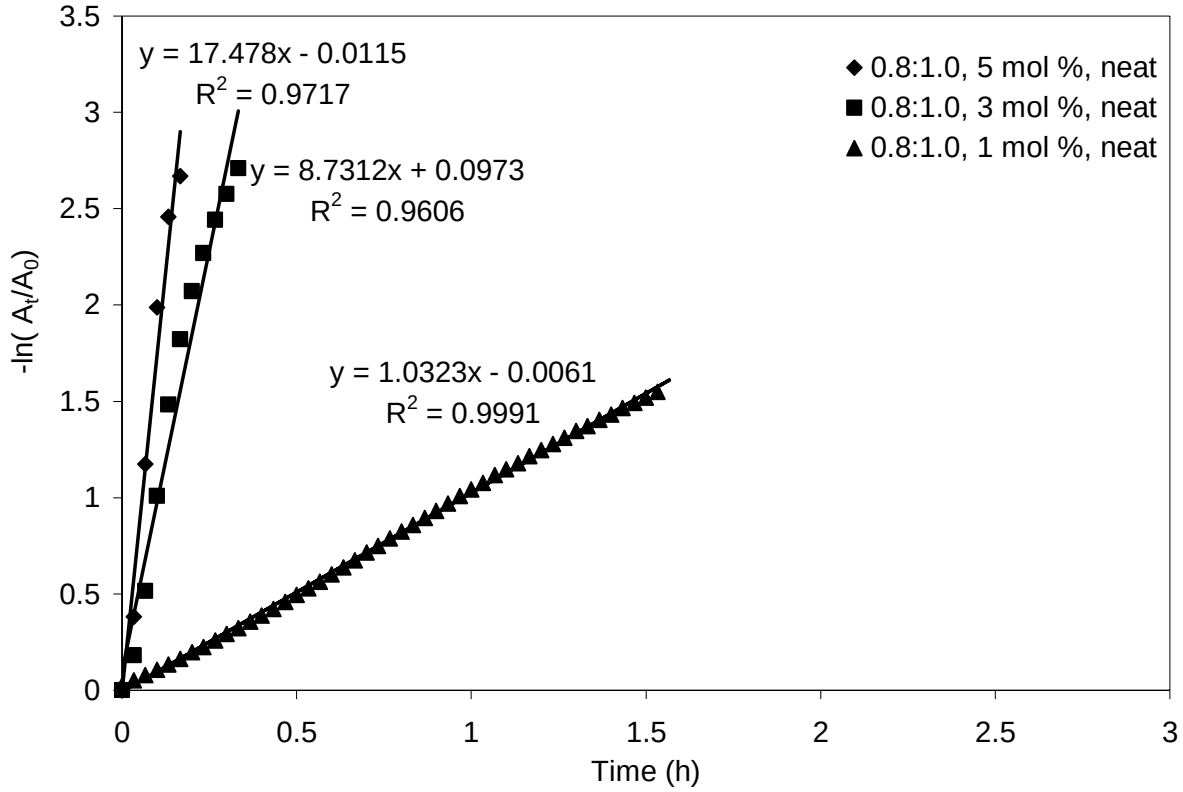

Figure 9.5. The effect of base concentration on rate constant for EtAcAc and EHA Michael reaction in the presence of K_2CO_3. Reaction conditions: 0.8:1.0 mol ratio acrylate to AcAc, 35 °C, neat, K_2CO_3.

9.4.3 Effect of solvent on Carbon-Michael reactions

9.4.3.1 Effect of solvent using in-situ FTIR

Typical Carbon-Michael reaction solvents include methanol, ethanol, diethyl ether, tetrahydrofuran, benzene, xylene, dioxane and mixtures of these solvents. Initially, protic solvents were desirable in the Carbon-Michael reaction to promote rapid proton transfer, however, Schlessinger et al. has shown that high yielding reactions could also be achieved using aprotic solvents.[16,17] The choice of solvent strongly depends on the solubility of the catalyst, donor and acceptor as well as sensitivity to side reactions. For example, if the reactants or

products are susceptible to alcoholysis (ester exchange or hydrolysis), self-condensation of the substrate, or the 'retro-Michael' reaction, a non-hydroxylic solvent should be chosen.[18] Reactions can even be run neat utilizing bases such as sodium amide.

As expected, the presence of solvent significantly influenced the observed rate constant in the reactions catalyzed by both DBU and potassium carbonate, as shown in Figure 9.6 and Figure 9.7. The calculated observed rate constants were 3.70×10^{-4} s^{-1} for the reaction conducted in THF, and 3.81×10^{-3} s^{-1} for the reaction conducted without solvent. The presence of the relatively non-polar THF solvent leads to a decrease in reaction rate due to the lower dielectric constant (DE = 7.6 for THF) compared with the solventless system.[19]

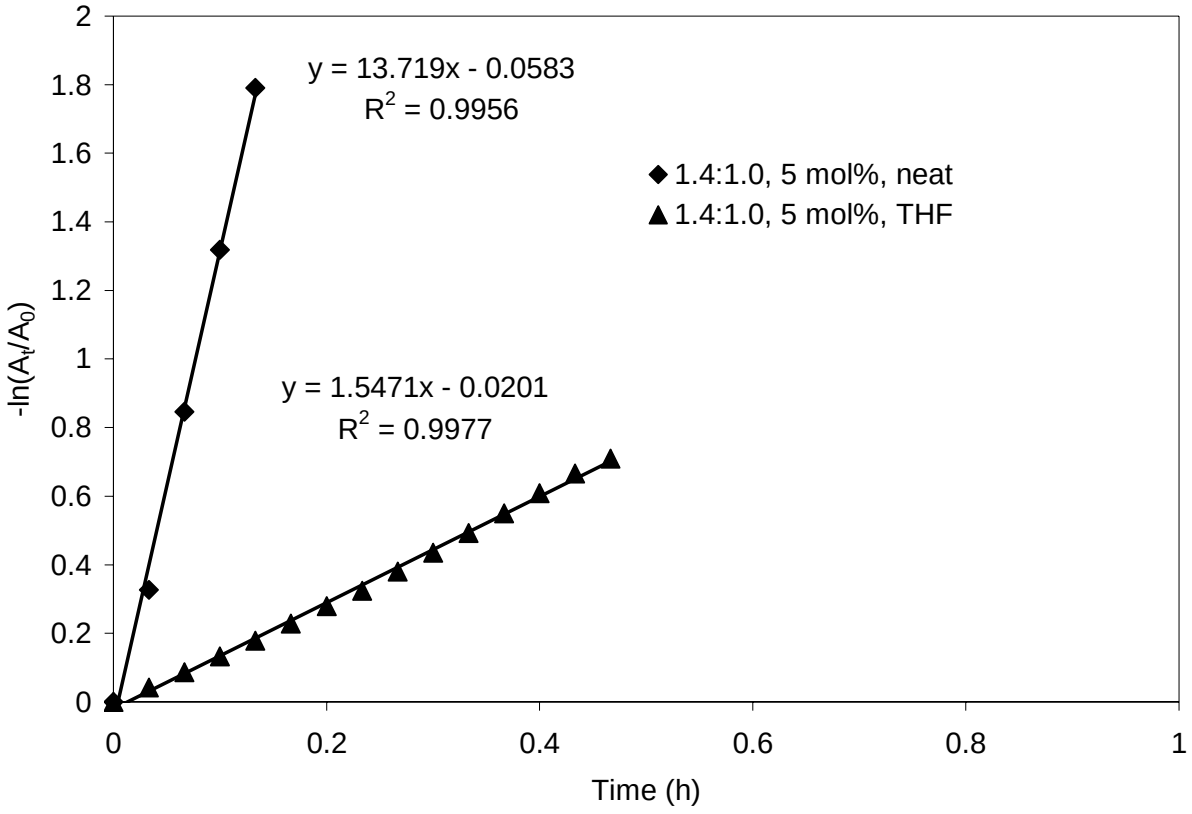

Figure 9.6. The effect of solvent on rate constant for the EtAcAc and EHA Michael reaction in the presence of DBU. Reaction conditions: 1.4:1.0 mol ratio acrylate to AcAc, 5 mol% catalyst, 35 °C, DBU.

For the reactions catalyzed with K_2CO_3 (Figure 9.7), the calculated observed rate constants are 9.60×10^{-4} s^{-1} for the reaction conducted in THF, and $4.86 \times 10^{-3} s^{-1}$ for the reaction conducted in the absence of solvent. As expected, the higher concentrations of functional groups lead to a more rapid reaction.

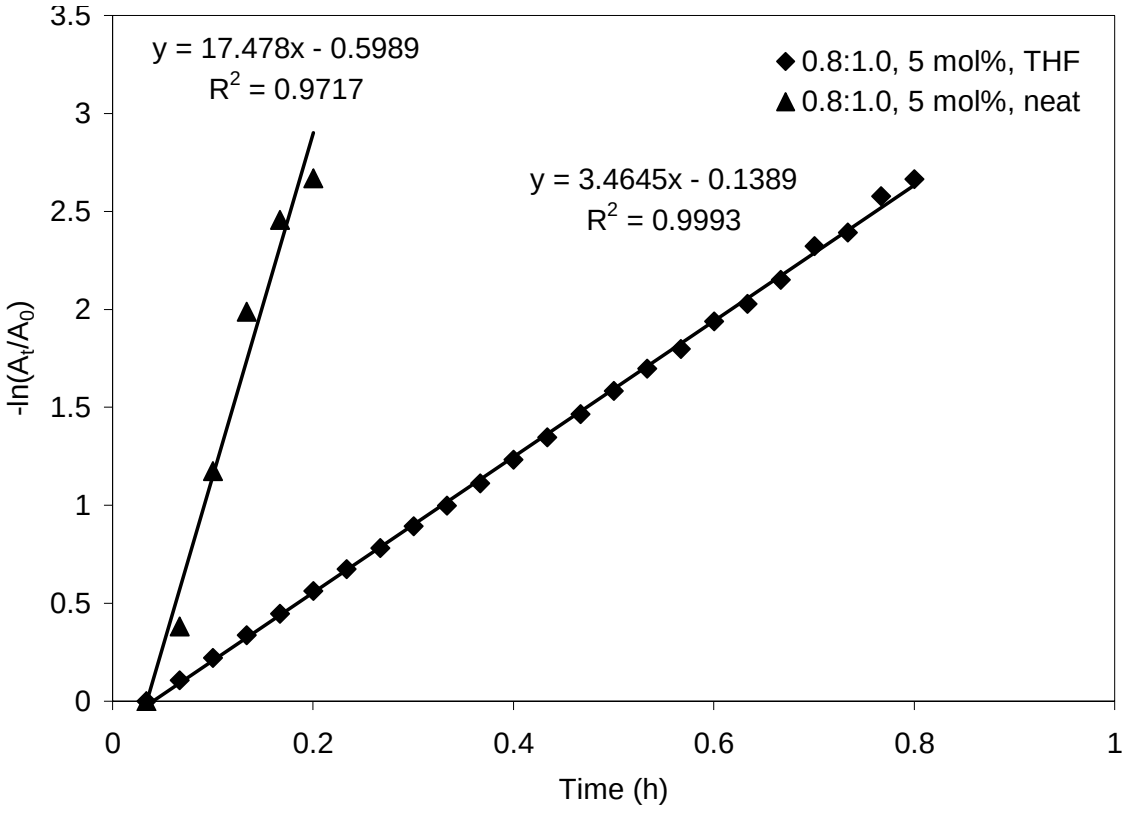

Figure 9.7. The effect of solvent on the rate constant for EtAcAc and EHA Michael reaction in the presence of K_2CO_3. Reaction conditions: 0.8:1.0 mol ratio acrylate to AcAc, 5 mol% catalyst, 35 °C, K_2CO_3.

9.4.3.2 Effect of solvent using ^{1}H NMR

To validate the effects of THF solvent in the above in-situ FTIR studies, a similar study was conducted using ^{1}H NMR to determine reaction kinetics that investigated a wider range of solvents. The same model reaction of EtAcAc and EHA was used, but at a 1:1 molar ratio. Two

solvents of lower dielectric constant (*m*-xylene and THF) and two solvents of higher dielectric constant (ethanol and DMSO) were chosen.[20] In Table 9.2, a clear correlation was observed between solvent polarity and the k_{obs}. Note that when a solvent with a lower dielectric constant was used (*m*-xylene, THF), the observed reaction rate decreased compared to the neat reaction. Both ethanol and DMSO provided a rate enhancement. The highly polar solvents stabilized the transition state(s) of the reaction, leading to lower activation energies and faster kinetics.

Solvent	DE	k_{obs} (min^{-1})	Relative Rate
THF	2.3	$9.68x10^{-4}$	0.08
m-xylene	7.6	$1.85x10^{-3}$	0.16
no solvent	--	$1.15x10^{-2}$	1.00
ethanol	24.5	$2.85x10^{-2}$	2.48
DMSO	78	$1.86x10^{-1}$	16.2

Table 9.2. Effect of solvent on k_{obs} – ^{1}H NMR method.

9.4.4 Effect of acrylate concentration on Carbon-Michael kinetics

Although a continued increase in starting acrylate concentration lead to an increase in the bis Carbon-Michael product (and thus leading to more complex kinetics), it was of interest to investigate concentration changes on k_{obs}. Table 9.3 provides a summary of the *in*-situ FTIR data for observed rates of reaction when the acrylate : acetoacetate ratio was varied from 0.8:1.0 to 1.4:1.0 to 2.0:1.0. These reactions were completed without solvent in the presence of 5 mol% catalyst. There was no clear trend when the acrylate : acetoacetate ratio was at 1.4:1.0 or 2.0:1.0 since the fluxuations in acrylate concentration lead to complex kinetics where the k_{obs} value reflects both the reaction rate of the first and second Carbon-Michael addition. However, the observed rates of reaction were always slowest for the reactions conducted with a 0.8:1.0

acrylate : acetoacetate ratio.

Base	Acrylate : AcAc	k_{obs} (s^{-1})
DBU	0.8:1.0	$4.58x10^{-3}$
DBU	1.4:1.0	$3.81x10^{-3}$
DBU	2.0:1.0	$2.00x10^{-3}$
K_2CO_3	0.8:1.0	$9.30x10^{-4}$
K_2CO_3	1.4:1.0	$1.14x10^{-3}$
K_2CO_3	2.0:1.0	$5.90x10^{-4}$

Table 9.3. Effect of acrylate : acetoacetate molar ratio on k_{obs}.

9.4.5 Design of Experiment (DOE) analysis

Once all 36 experiments were conducted and observed rate constants were determined, a statistical analysis was conducted to determine the influence of each component on the observed rate constant. The statistical design software provided a model for the observed rate constant as a function of base concentration and acrylate to acetoacetate molar ratios. The equations in terms of these factors in the presence of DBU are:

DBU THF k_{obs} = 3.63618 x 10^{-4} -1.28056 x 10^{-4} * Acrylate Mol Ratio +1.67167 x 10^{-4} * Base Concentration -6.83333 x 10^{-5} * Acrylate Mol Ratio * Base Concentration (4)

DBU Neat k_{obs} = -1.55772 x 10^{-3} +6.625 x 10^{-4} * Acrylate Mol Ratio+1.605 x 10^{-3} * Base Concentration -5.79167 x 10^{-4} * Acrylate Mol Ratio * Base Concentration (5)

From these equations and actual observed rate constants measured from *in-situ* FTIR experiments, a plot of predicted versus actual observed rate constants was constructed, as depicted in Figure 9.8. Each experimental rate constant is represented with a square. The statistical design model shows a good agreement between predicted and actual observed rate constants.

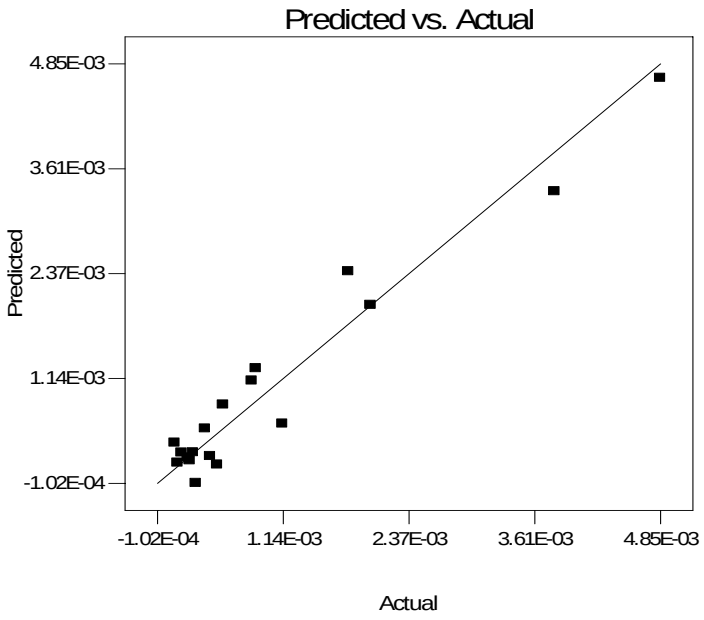

Figure 9.8. The significant relationship between predicted and actual observed rate constants for reactions conducted in the presence of DBU.

The effects of each of the factors on the observed rate constants are depicted in Figure 9.9-Figure 9.11 for reactions conducted in the presence of DBU. The observed rate constant was the smallest for the 0.8:1.0 acrylate to acetoacetate molar ratio and varied for the other molar ratios (Figure 9.9). Increasing the base concentration and conducting the reactions in neat conditions resulted in greater observed rate constants, as depicted in Figure 9.10 and Figure 9.11, respectively.

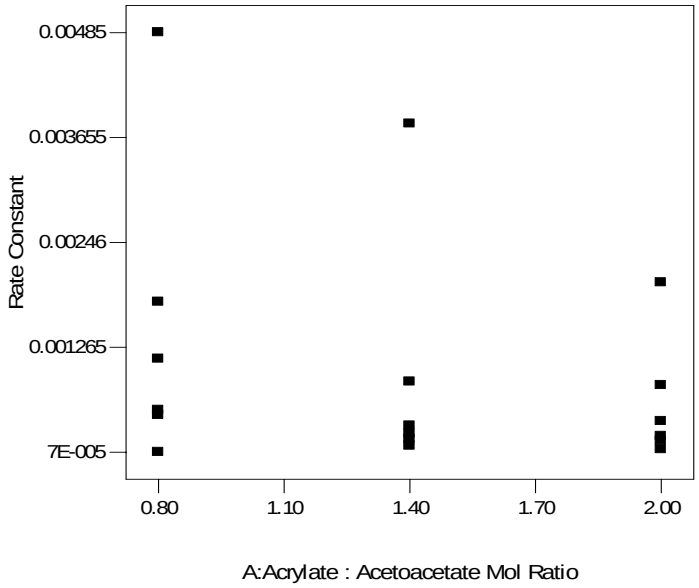

Figure 9.9. The relationship between acrylate molar ratios and actual observed rate constants for reactions conducted in the presence of DBU.

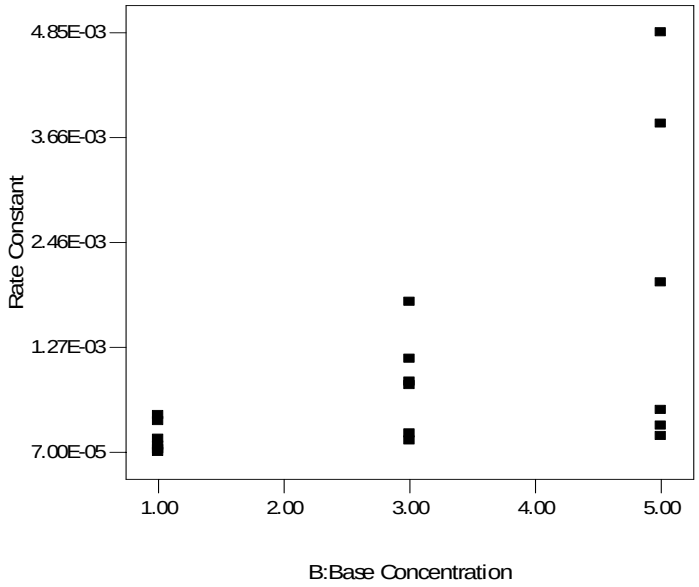

Figure 9.10. The significant relationship between base concentration and actual observed rate constants for reactions conducted in the presence of DBU.

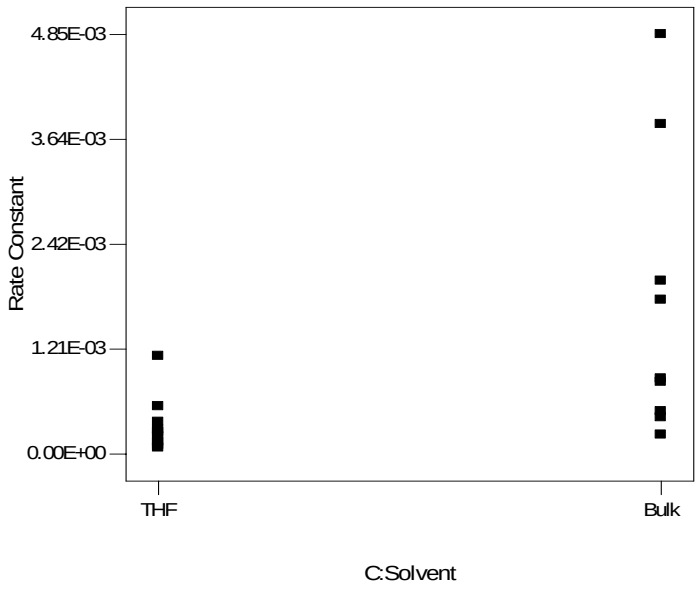

Figure 9.11. The significant relationship between the presence of solvent and actual observed rate constants for reactions conducted in the presence of DBU.

Contour plots, shown in Figure 9.12, demonstrate the effect of base concentration and acrylate : AcAc molar ratios on the actual observed rate constants for reactions conducted in the presence of DBU. Figure 9.12a represents reactions in THF, and Figure 9.12b represents reactions in neat conditions. A wider range of observed rate constants were achieved in the absence of solvent.

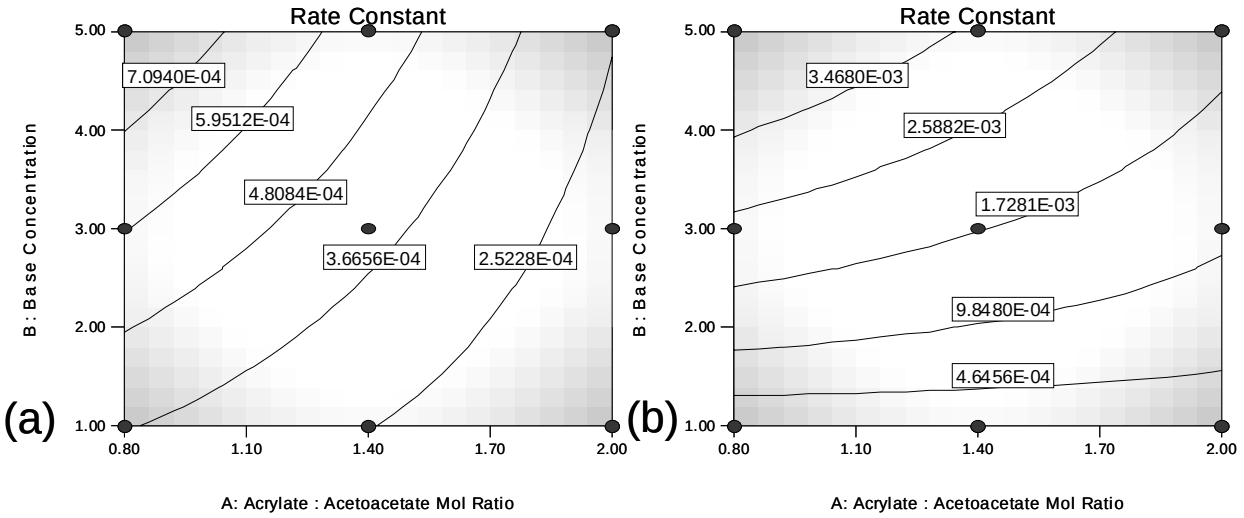

Figure 9.12. Contour plots of the effect of base concentration and acrylate molar ratios on the actual observed rate constants for reactions conducted in the presence of DBU. The plot on the left (a) represents reactions in THF, and the plot on the right (b) represents reactions in neat conditions.

To optimize observed rate constants above 5 x 10^{-4} s^{-1}, an overlay plot was constructed. As depicted in Figure 9.13, to achieve a rate constant of at least 5 x 10^{-4} s^{-1}, one must use reaction conditions in such a manner that the base concentration and acrylate : AcAc molar ratio are within the shaded area of the graph. Since the rates of reaction are faster in the absence of solvent, there is a greater shaded area for the reaction performed in neat conditions. Figure 9.13a represents reactions in THF, and Figure 9.13b represents reactions in neat conditions.

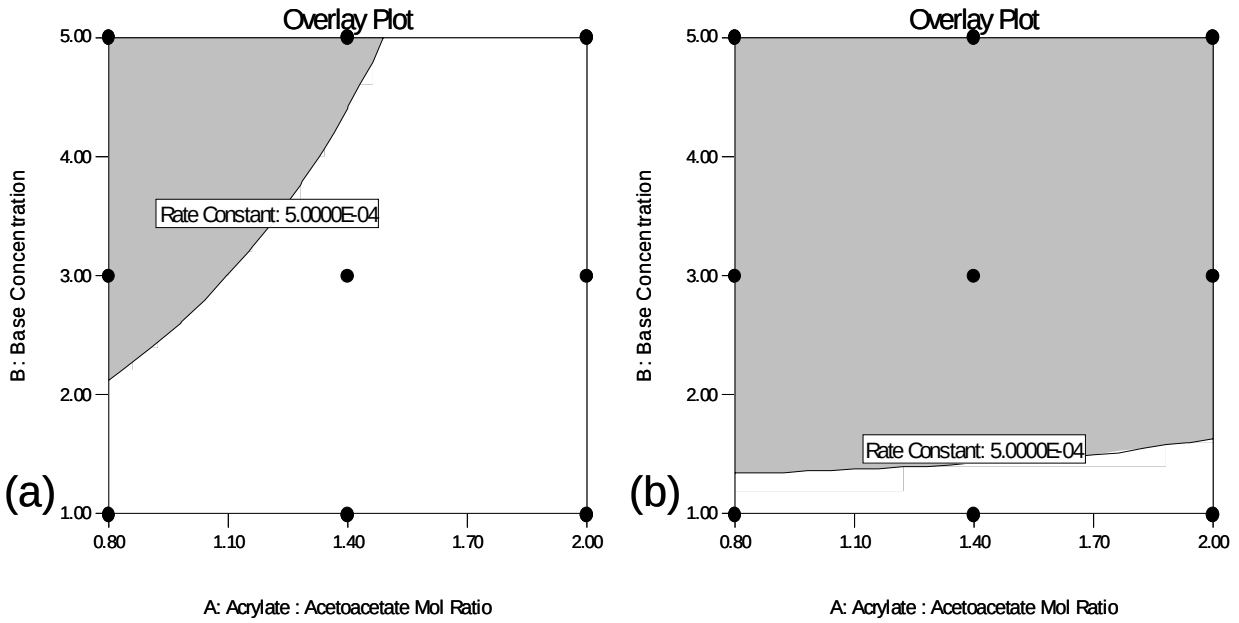

Figure 9.13. Overlay plots of the effect of base concentration and acrylate molar ratios on the predicted observed rate constants for reactions conducted in the presence of DBU. The plot on the left (a) represents reactions in THF, and the plot on the right (b) represents reactions in neat conditions.

A similar DOE was prepared and analyzed for reactions conducted in the presence of K_2CO_3. The equations in terms of the factors in the presence of K_2CO_3 are:

K_2CO_3 THF $k_{obs} = 5.79132 \times 10^{-5} + 1.06519 \times 10^{-4}$ * Acrylate Mol Ratio $+ 2.43935 \times 10^{-4}$ * Base Concentration $- 8.91017 \times 10^{-5}$ * Acrylate Mol Ratio * Base Concentration (6)

K_2CO_3 Neat $k_{obs} = -9.05646 \times 10^{-4} + 6.58163 \times 10^{-4}$ * Acrylate Mol Ratio $+ 1.22873 \times 10^{-3}$* Base Concentration $- 4.89694 \times 10^{-4}$ * Acrylate Mol Ratio * Base Concentration (7)

In a similar manner as above, from these equations and actual observed rate constants measured from *in-situ* FTIR experiments, a plot of predicted versus actual observed rate constants was constructed, as depicted in Figure 9.14. The statistical design model shows a close agreement between predicted and actual observed rate constants. The model did not predict any

outlying observed rate constants.

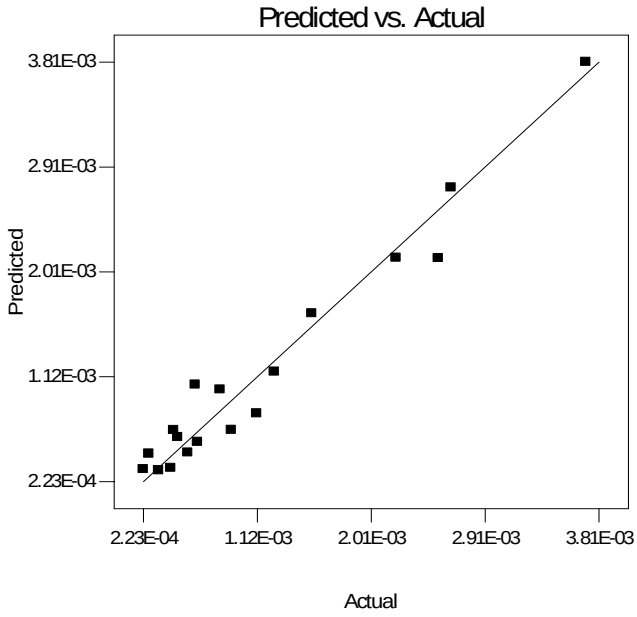

Figure 9.14. The significant relationship between predicted and actual observed rate constants for reactions conducted in the presence of K_2CO_3.

The effect of each of the factors on the observed rate constants are depicted in Figure 9.15-Figure 9.17 for reactions conducted in the presence of K_2CO_3. In a similar fashion to reactions conducted in the presence of DBU, the observed rate constant was the smallest for the 0.8:1.0 acrylate to acetoacetate molar ratio and varied for the other molar ratios (Figure 9.15). Increasing the base concentration and conducting the reactions without solvent resulted in greater observed rate constants, as depicted in Figure 9.16 and Figure 9.17, respectively.

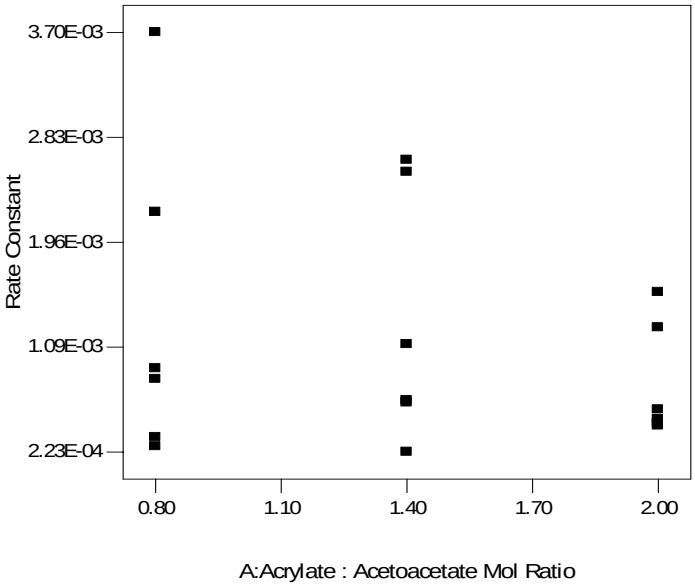

Figure 9.15. The relationship between acrylate molar ratios and actual observed rate constants for reactions conducted in the presence of K_2CO_3.

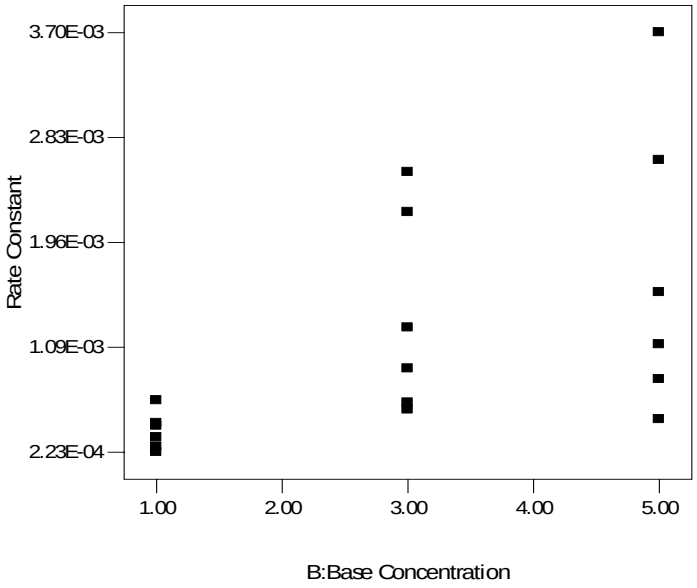

Figure 9.16. The significant relationship between base concentration and actual observed rate constants for reactions conducted in the presence of K_2CO_3.

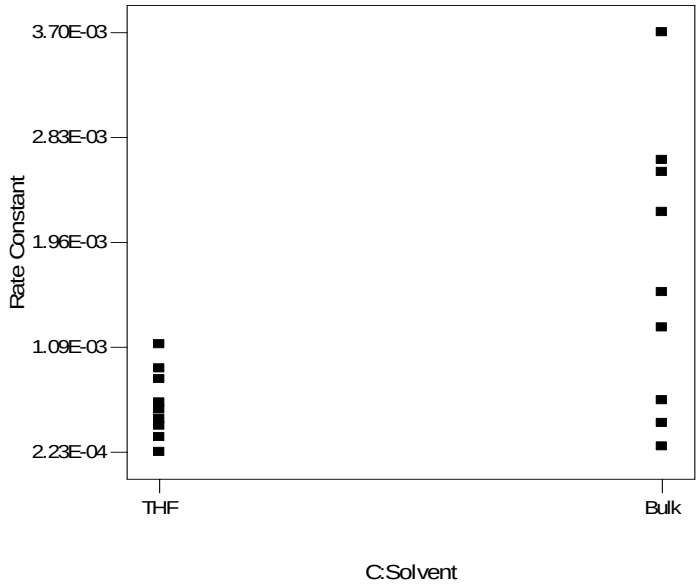

Figure 9.17. The significant relationship between the presence of solvent and actual observed rate constants for reactions conducted in the presence of K_2CO_3.

Contour plots, shown in Figure 9.18, demonstrate the effect of base concentration and acrylate molar ratios on the actual observed rate constants for reactions conducted in the presence of K_2CO_3. Figure 9.18a represents reactions in THF, and Figure 9.18b represents reactions in neat conditions. A wider range of observed rate constants are achieved in neat reaction conditions.

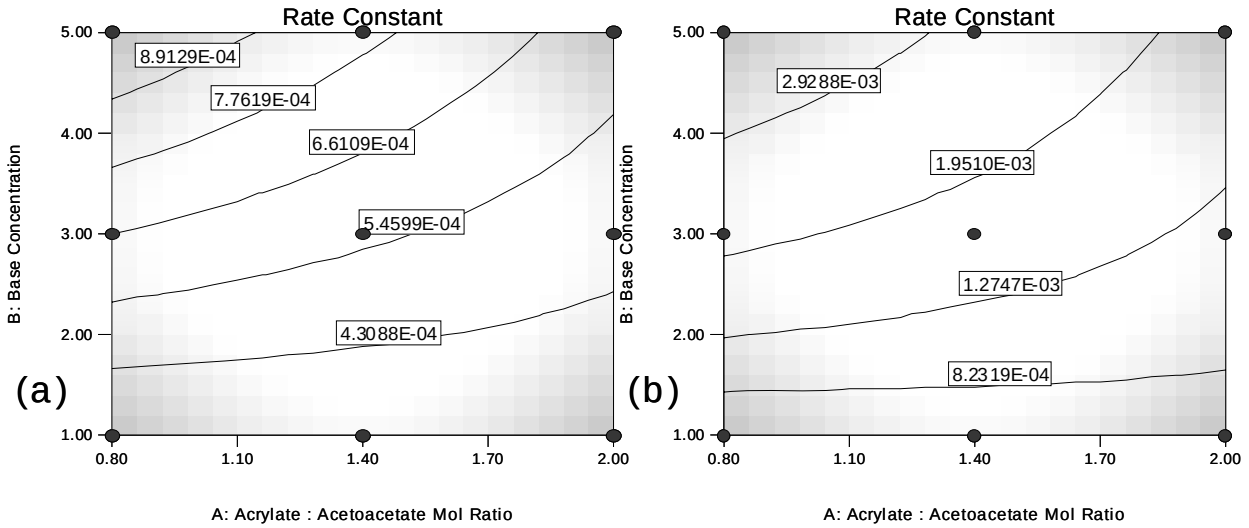

Figure 9.18. Contour plots of the effect of base concentration and acrylate molar ratios on the actual observed rate constants for reactions conducted in the presence of K_2CO_3. The plot on the left (a) represents reactions in THF, and the plot on the right (b) represents reactions in neat conditions.

To predict observed rate constants in the presence of K_2CO_3, an overlay plot was constructed. As depicted in Figure 9.19, to achieve a rate constant of at least 9 x 10^{-4} s^{-1}, one must use reaction conditions in such a manner that the base concentration and acrylate molar ratio are within the shaded area of the graph. Since the rates of reaction are faster in the absence of solvent, there is a greater shaded area for the reaction performed in neat conditions. The plot on the left (a) represents reactions in THF, and the plot on the right (b) represents reactions in neat conditions.

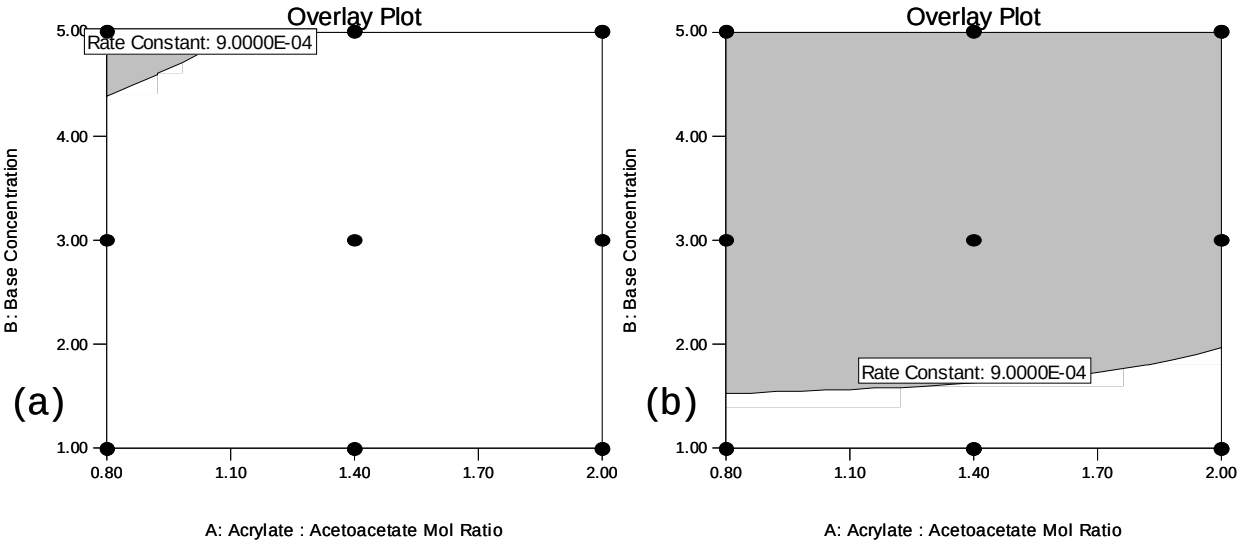

Figure 9.19. Overlay plots of the effect of base concentration and acrylate molar ratios on the predicted observed rate constants for reactions conducted in the presence of K_2CO_3. The plot on the left (a) represents reactions in THF, and the plot on the right (b) represents reactions in neat conditions.

Of several factors, the presence of solvent and base concentration contributed the greatest to the observed rate constant. Overall, greater observed rate constants were observed when DBU was used as the base.

9.4.6 Network formation

A series of networks were synthesized from PPG BisAcAc and PPGDA, using DBU or K_2CO_3 as the basic catalyst. The molecular weight of the PPGDA was 800 g/mol, and the molecular weights of the PPG BisAcAc ranged from 1000 to 8000 g/mol. A total of 8 different networks were prepared.

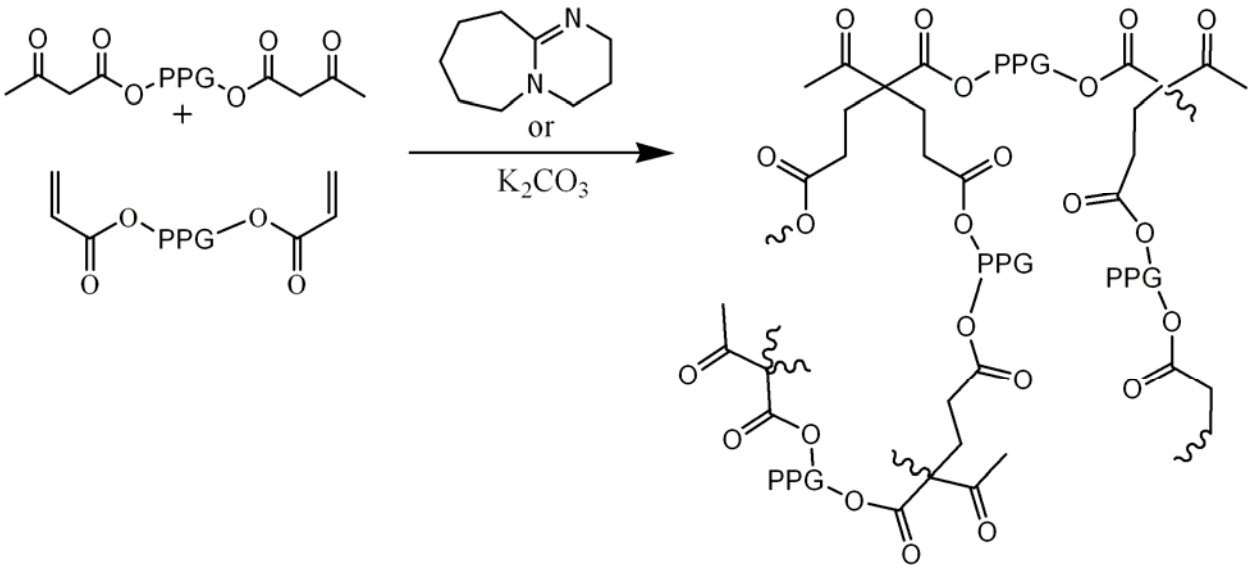

Scheme 9.4. Network formation via the Michael reaction of PPG BisAcAc and PPGDA.

In a similar fashion to the model studies *in-situ* FTIR spectroscopy was used to observe the change in the vinyl stretch over the reaction period for each network. The absorbance profiles versus time in seconds are demonstrated in Figure 9.20 and Figure 9.21 for networks prepared in the presence of DBU and K_2CO_3, respectively. As the molecular weight of the PPG BisAcAc segment increased from 1000 g/mol to 8000 g/mol, the change in the intensity of the absorbance profile was not as pronounced, indicating slower reaction rates due to decreased reactive chain end concentration. Furthermore, the decrease in absorbance was not as pronounced for networks prepared with K_2CO_3 as the base.

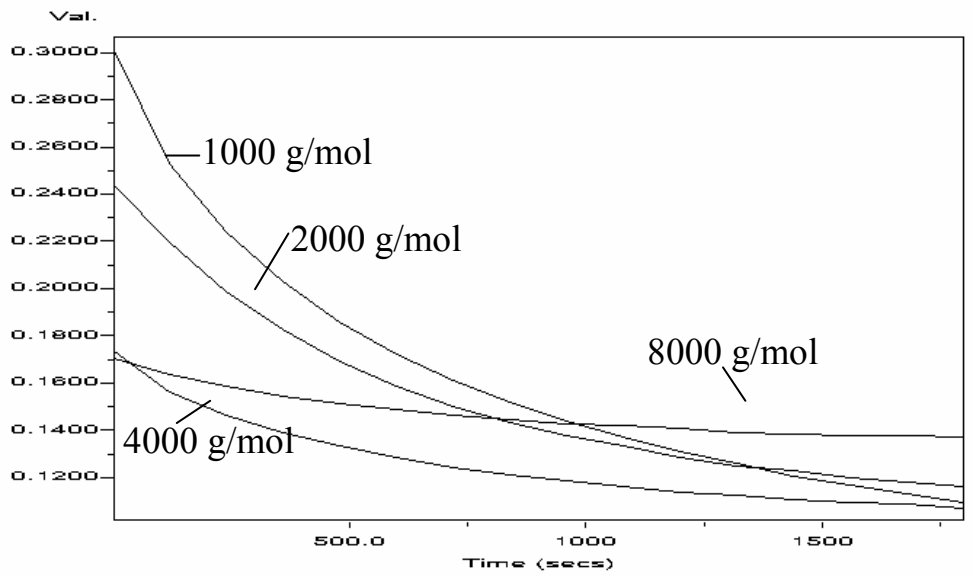

Figure 9.20. *In-situ* FTIR profiles demonstrating decrease in absorption over time for PPG BisAcAc – PPGDA networks prepared with DBU as the base.

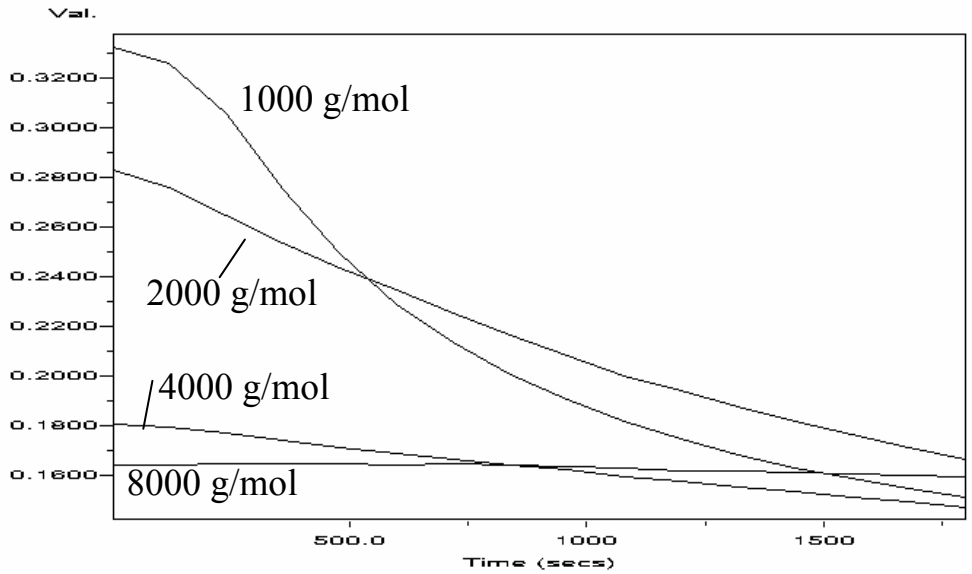

Figure 9.21. *In-situ* FTIR profiles demonstrating decrease in absorption over time for PPG BisAcAc – PPGDA networks prepared with K_2CO_3 as the base.

From the profiles shown in Figure 9.20 and Figure 9.21, kinetic plots were constructed and are shown in Figure 9.22. As the molecular weight of the PPG BisAcAc segment increased, the rate of the reaction decreased. In addition, the rate of the reaction was considerably slower

for the networks prepared with K_2CO_3 as the basic catalyst, than with the networks prepared with DBU. The observed rate constants were calculated from the plots and are summarized in Table 9.4.

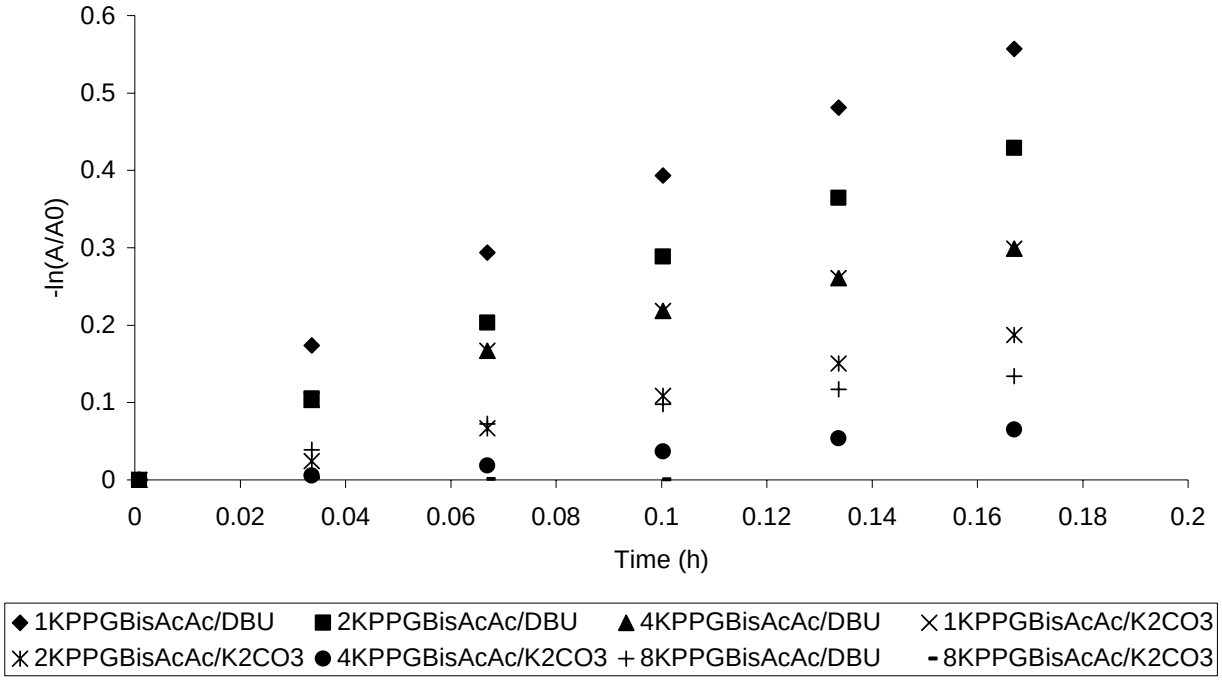

Figure 9.22. Kinetic plot of PPG BisAcAc – PPGDA network formation.

Polymer	Base	k_{obs} (s^{-1})
1000 g/mol PPG BisAcAc-PPGDA	DBU	9.08×10^{-4}
2000 g/mol PPG BisAcAc-PPGDA	DBU	7.18×10^{-4}
4000 g/mol PPG BisAcAc-PPGDA	DBU	4.81×10^{-4}
8000 g/mol PPG BisAcAc-PPGDA	DBU	2.22×10^{-4}
1000 g/mol PPG BisAcAc-PPGDA	K_2CO_3	4.81×10^{-4}
2000 g/mol PPG BisAcAc-PPGDA	K_2CO_3	3.24×10^{-4}
4000 g/mol PPG BisAcAc-PPGDA	K_2CO_3	1.17×10^{-4}
8000 g/mol PPG BisAcAc-PPGDA	K_2CO_3	2.23×10^{-5}

Table 9.4. Observed rate constants from *in-situ* FTIR experiments for PPG BisAcAc – PPGDA network formation.

To determine the precise gel point, rheological experiments were conducted. Rheology revealed a dependence of PPG BisAcAc molecular weight on the gel time, as observed from the crossover point of the storage modulus (G') and loss modulus (G"). The gel point increased as the molecular weight of the PPG BisAcAc segment increased. Considerably longer gel times were observed for the networks prepared with heterogeneous base, K_2CO_3. The result of the gel point analysis is shown in Table 9.5.

Polymer	Base	Gel Time (s)
1000 g/mol PPG BisAcAc-PPGDA	DBU	243
2000 g/mol PPG BisAcAc-PPGDA	DBU	414
4000 g/mol PPG BisAcAc-PPGDA	DBU	932
8000 g/mol PPG BisAcAc-PPGDA	DBU	1925
1000 g/mol PPG BisAcAc-PPGDA	K_2CO_3	1422
2000 g/mol PPG BisAcAc-PPGDA	K_2CO_3	1525
4000 g/mol PPG BisAcAc-PPGDA	K_2CO_3	1735
8000 g/mol PPG BisAcAc-PPGDA	K_2CO_3	6530

Table 9.5. Gel time analysis for PPG BisAcAc – PPGDA networks as determined from rheology experiments. The gel time was recorded when G' = G".

Films were prepared in Teflon™ molds for gel fraction mechanical property analysis. Soxholet extractions were performed in THF for 3 h. The results are demonstrated in Table 9.6. All networks were highly cross-linked, with the exception of the networks prepared with 8000 g/mol PPGBisAcAc. As the distance between cross-link points increased and concentration of functional endgroups decreased, the gel fraction decreased. We hypothesized that the use of

inorganic, insoluble, heterogeneous K_2CO_3 would result in lower gel fractions. However, as shown in Table 9.3, the gel fraction analyses for the two sets of networks were quite similar.

Polymer	Base	Gel Fraction (%) (±2%)
1000 g/mol PPG BisAcAc-PPGDA	DBU	93
2000 g/mol PPG BisAcAc-PPGDA	DBU	91
4000 g/mol PPG BisAcAc-PPGDA	DBU	88
8000 g/mol PPG BisAcAc-PPGDA	DBU	71
1000 g/mol PPG BisAcAc-PPGDA	K_2CO_3	97
2000 g/mol PPG BisAcAc-PPGDA	K_2CO_3	96
4000 g/mol PPG BisAcAc-PPGDA	K_2CO_3	92
8000 g/mol PPG BisAcAc-PPGDA	K_2CO_3	72

Table 9.6. Gel fraction analysis for PPG BisAcAc – PPGDA networks as determined from Soxholet extractions.

The mechanical properties were also very similar for matching molecular weight sets of networks with either DBU or K_2CO_3 as the base, as shown in Figure 9.23-Figure 9.26. DMA revealed a molecular weight dependence as well. Increasing T_g was observed as the molecular weight of the PPG BisAcAc segment decreased. Furthermore, as the crosslink density increased, the modulus of the rubbery plateau increased.

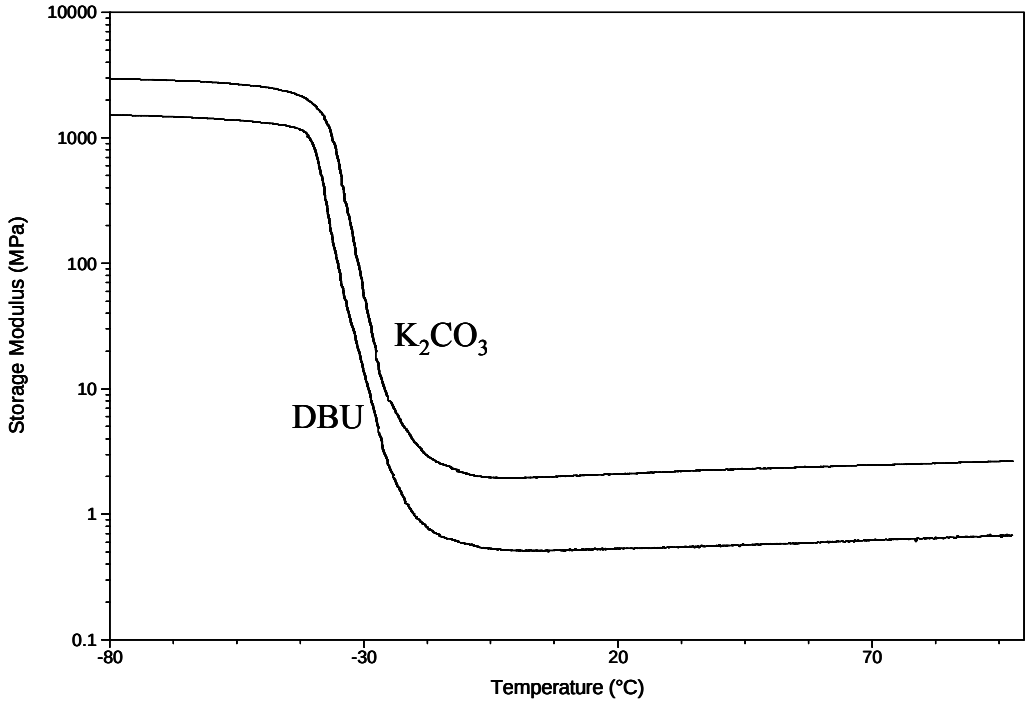

Figure 9.23. Storage modulus versus temperature for 1000 g/mol PPG BisAcAc – PPGDA networks.

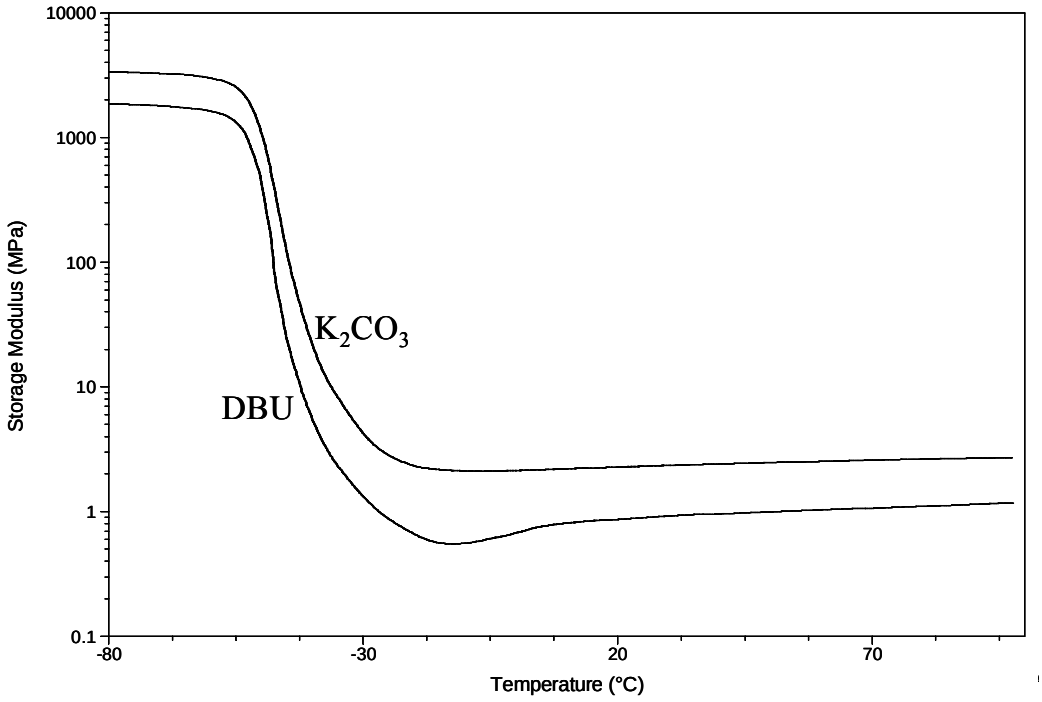

Figure 9.24. Storage modulus versus temperature for 2000 g/mol PPG BisAcAc – PPGDA networks.

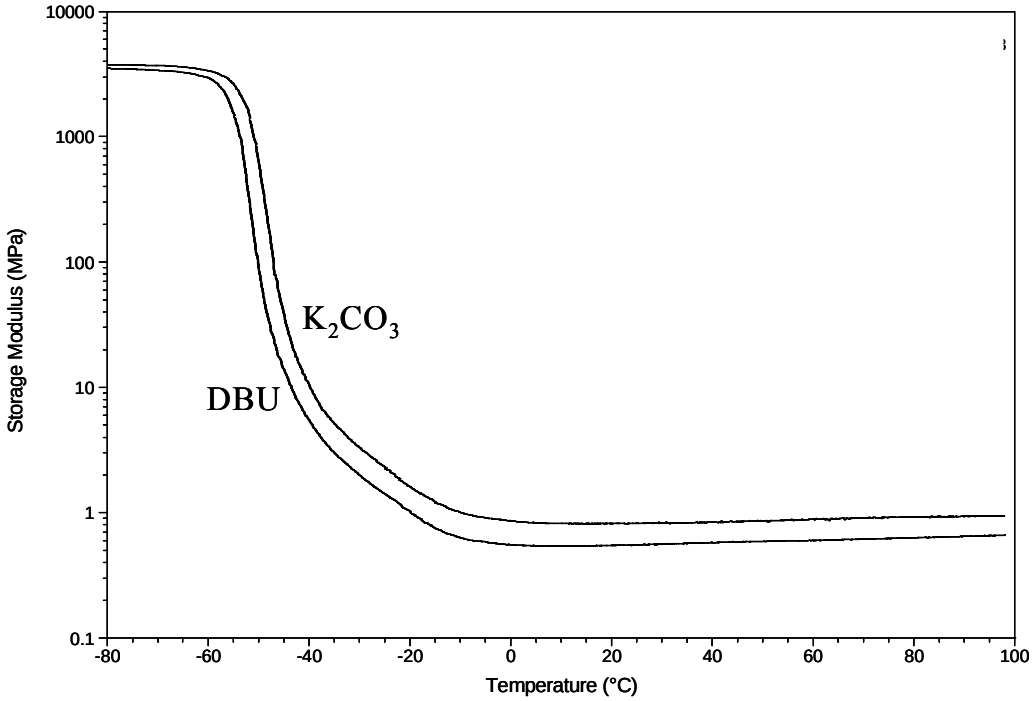

Figure 9.25. Storage modulus versus temperature for 4000 g/mol PPG BisAcAc – PPGDA networks.

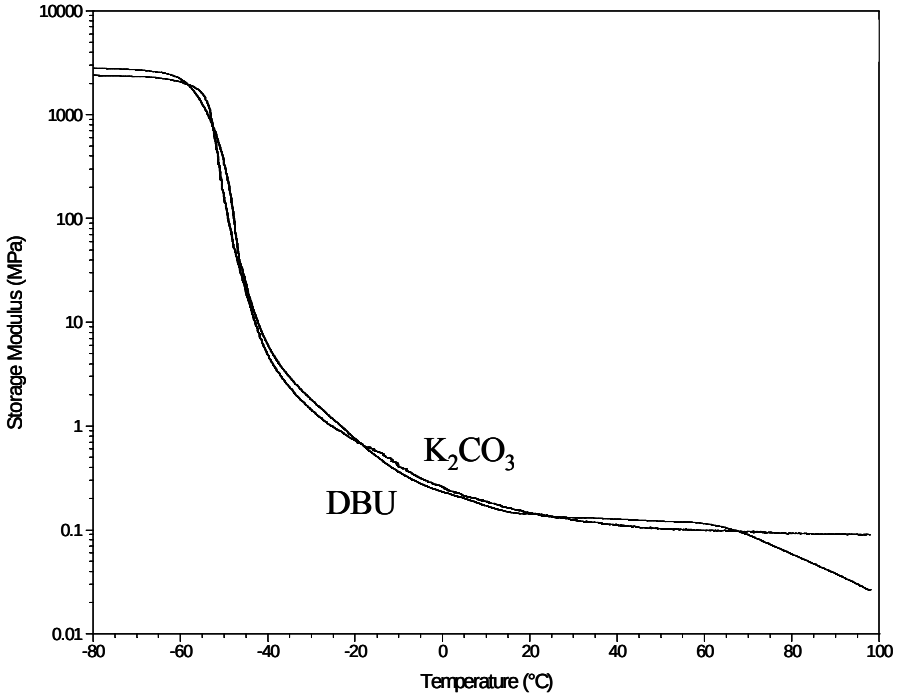

Figure 9.26. Storage modulus versus temperature for 8000 g/mol PPG BisAcAc – PPGDA networks.

9.5 Conclusions

Model Michael addition reactions were conducted with EHA and EtAcAc to determine the effect of solvent, base, base concentration, and reactant molar ratio on the observed rate constant. The observed rate constants were determined via *in-situ* FTIR. A DOE analysis was conducted for small molecule Michael reactions prepared with DBU and K_2CO_3 as the base. Cross-linked films were then prepared from PPG BisAcAc and PPGDA in the presence of DBU and K_2CO_3. These networks were prepared in the absence of solvent at 23 °C, without the formation of byproducts. Network formation was monitored via *in-situ* FTIR, and observed rate constants were calculated. As the molecular weight of the PPG BisAcAc segment increased, the observed rate constant decreased. The influence on PPG BisAcAc molecular weight on mechanical properties was determined via DMA and gel fraction analysis. A dependence on

PPG BisAcAc molecular weight on gel fraction analysis was observed, and revealed that increasing the molecular weight of PPG BisAcAc precursor resulted in lower gel fractions. However, the base did not change the mechanical properties, according to the DMA results. Therefore, it appears that base type is significant for the rate of the reaction, but not for mechanical properties.

9.6 Acknowledgements

The authors acknowledge the partial financial support of Rohm and Haas Company and the Department of Energy under agreement number DE-FG36-04GO14317, as well as support in part by the Macromolecular Interfaces with Life Sciences (MILES) Integrative Graduate Education and Research Traineeship (IGERT) of the National Science Foundation under agreement number DGE-0333378 and support in part by the U.S. Army Research Laboratory and the U.S. Army Research Office under grant number DAAD19-02-1-0275 Macromolecular Architecture for Performance (MAP) MURI.

9.7 References

(1) Moy, T. M.; Dammann, L.; Loza, R. Liquid Oligomers Containing Unsaturation. US 5,945,489, 1999.
(2) Kim, Y.-B.; Kim, H. K.; Nishida, H.; Endo, T. *Macromol Mater Eng* **2004,** 289, (10), 923-926.
(3) Mather, B. D.; Miller, K. M.; Long, T. E. *Macromol Chem Phys* **2006,** 207, (15), 1324-1333.
(4) Mather, B. D.; Viswanathan, K. V.; Miller, K. M.; Long, T. E. *Prog Polym Sci* **2006,** 31, (5), 487-531.
(5) Kauffman, T. F.; Whitman, D. W.; Zajackowski, M. J. Surface promoted Michael cure compositions US 2006078742, April 13, 2006, 2006.
(6) Kauffman, T. F.; Whitman, D. M.; Zajaczkowski, M. J.; Vietti, D. E. Biomass based Michael addition composition. EP 1640388, 2006.
(7) Wang, D.; Liu, Y.; Hong, C.-Y.; Pan, C.-Y. *Polymer* **2006,** 47, (11), 3799-3806.
(8) Rizzi, S. C.; Hubbell, J. A. *Biomacromolecules* **2005,** 6, (3), 1226-1238.
(9) Elbert, D. L.; Pratt, A. B.; Lutolf, M. P.; Halstenberg, S.; Hubbell, J. A. *J Control Release* **2001,** 76, (1-2), 11-25.

(10) Lutolf, M. P.; Hubbell, J. A. *Biomacromolecules* **2003,** 4, (3), 713-722.
(11) Rizzi, S. C.; Ehrbar, M.; Halstenberg, S.; Raeber, G. P.; Schmoekel, H. G.; Hagenmuller, H.; Muller, R.; Weber, F. E.; Hubbell, J. A. *Biomacromolecules* **2006,** 7, (11), 3019-3029.
(12) Albertson, N. F. *J. Am. Chem. Soc.* **1948,** 70, (2), 669-670.
(13) Schultz, A. G.; Yee, Y. K. *J Org Chem* **1976,** 41, (45), 4044-4045.
(14) Clemens, R. J.; Rector, F. D. *J Coat Technol* **1989,** 61, (770), 83-91.
(15) Williams, S. R.; Mather, B. D.; Miller, K. M.; Long, T. E. *J Polym Sci (A) Chem* **2007,** 45, (17), 4118-4128.
(16) Little, R. D.; Masjedizadeh, M. R.; Wallquist, O.; McLoughlin, J. I., The Intramolecular Michael Reaction. In *Organic Reactions*, Wiley: New York, 1995; Vol. 47, pp 315-552.
(17) Jung, M. E., Stabilized Nucleophiles with Electron Deficient Alkenes and Alkynes. In *Comprehensive Organic Synthesis*, Pergamon: Oxford, 1991; pp 1-67.
(18) Bergman, E. D., Ginsburg D., Pappo, R., The Michael Reaction. In *Organic Reactions*, 1959; Vol. 10, pp 179-556.
(19) Carey, F. A.; Sundberg, R. J., *Advanced Organic Chemistry : Part A. Structure and Mechanisms*. 3rd ed.; Plenum Press: New York, 1999; p 233-235.
(20) Smith, M. B.; March, J., *March's Advanced Organic Chemistry*. 5th ed.; Wiley-Interscience: 2001; p 450-454

Chapter 10 : Novel Michael Addition Networks Containing Urethane Hydrogen Bonding

10.1 Abstract

Covalently cross-linked networks based on poly(propylene glycol) bis(acetoacetate) with either neopentyl glycol diacrylate or hydroxyethyl acrylate derivatized bis(4-isocyanatocyclohexyl)methane (HMDI) were prepared utilizing the Michael addition reaction in the presence of catalytic quantities of diazabicyclo[5.4.0]undec-7-ene (DBU). These networks were prepared in the absence of solvent at 23 °C without the formation of byproducts. Mechanical and thermal analyses of the networks were performed utilizing DMA, tensile testing, and TGA. Tensile analysis revealed that the introduction of hydrogen-bonding urethane linkages in the diacrylate segment resulted in higher tensile strengths and elongation to break compared to non-hydrogen bonding analogs. All cross-linked products exhibited high gel fractions and excellent thermomechanical properties.

10.2 Introduction

The Carbon-Michael addition reaction has received significant attention in recent literature for the preparation of novel polymers and composites.[1-11] Our research group recently extensively reviewed the versatility of the Michael addition reaction in macromolecular

synthesis.[4] Pan and co-workers[12,13] recently utilized the Michael addition reaction using trifunctional amines with difunctional acrylamides and trifunctional acrylamides with difunctional amines to prepare novel hyperbranched polymers. In general, many researchers have investigated novel, cross-linked networks using diverse synthetic organic methodologies. For example, Hawker and co-workers[14,15] prepared networks via Click chemistry, which was initially developed by Sharpless and co-workers[16] for the synthesis of small molecule enzymatic inhibitors. Cross-linked networks with shape-memory properties were also recently prepared by Langer and co-workers[17] via photopolymerization of oligo-(ε-caprolactone) dimethacrylates. In the present work, we investigate a Michael addition reaction between a low molar mass diacrylate and an oligomeric bis- or tris-acetoacetate to produce a cross-linked network. The Michael addition reaction offers many advantages, including mild reaction conditions at ambient temperature, absence of undesirable byproducts, and tolerance of a variety of functional groups. In addition, many acrylates that are suitable for the Michael addition reaction are commercially available or easily prepared.

The Michael addition reaction mechanism consists of three steps, as illustrated in Scheme 10.1. First, deprotonation of the β-keto ester in the presence of catalytic base yields an enolate anion that is resonance stabilized and nucleophilic; this intermediate is known as the Michael donor. Second, the Michael donor adds to a Michael acceptor, such as an α, β- unsaturated ester, that has electrophilic character to generate a second enolate intermediate. The final product is formed upon proton transfer to the enolate from either solvent or the starting β-keto ester.[18]

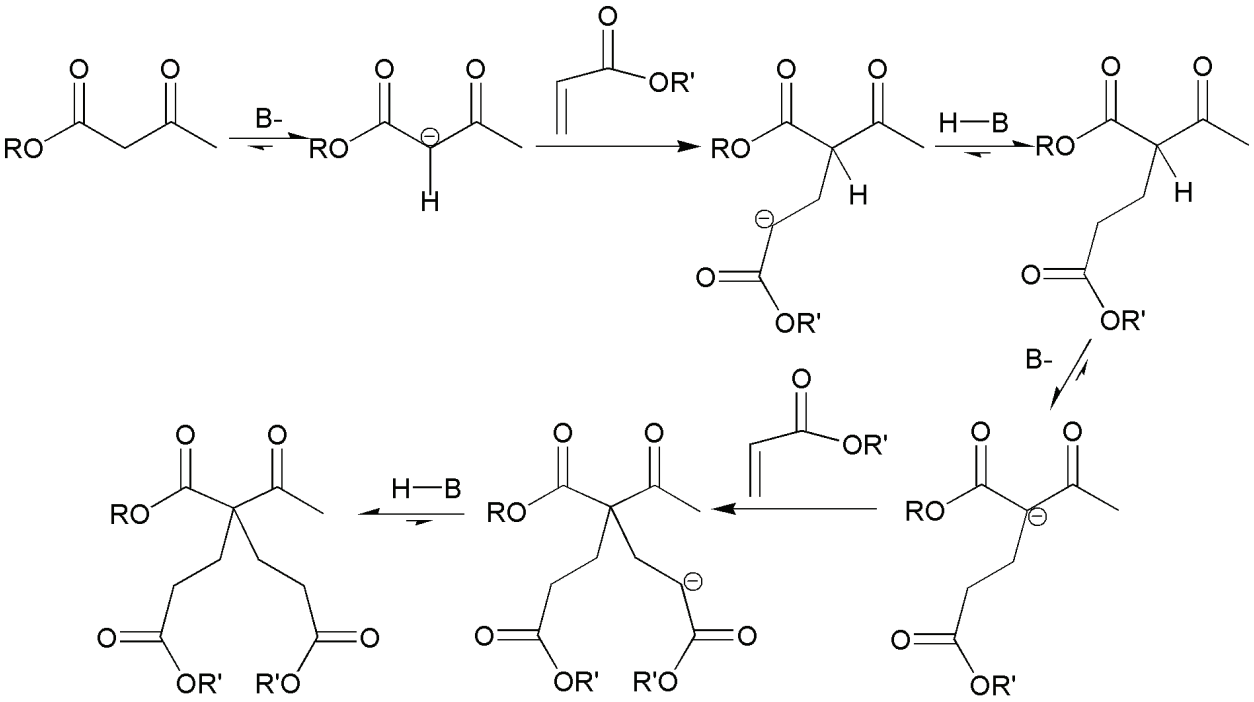

Scheme 10.1. Mechanism of the carbon Michael addition reaction.

The reaction rate is highly dependent on the strength of the basic catalyst.[19] Since the pKa's of the two acidic acetoacetate hydrogens vary significantly (pK_{a1} = 12, pK_{a2} = 13),[19] different network structures are obtained as a function of base selection and concentration. In earlier literature, Clemens and Rector contrasted amidine and guanidine bases to inorganic bases, such as potassium hydroxide, for the carbon-Michael addition reaction of isobutyl acetoacetate to ethyl acrylate at 25 °C. These workers demonstrated that amidine and guanidine bases were convenient for synthesis since these bases are readily soluble in organic solvents and react in a controlled fashion at ambient temperature.[19] Thus, we chose an amidine base, 1,8-diazabicyclo[5.4.0]undec-7-ene (DBU), for our carbon-Michael addition cross-linking reactions as reported herein.

ACCLAIM™ hydroxyl-endcapped poly(propylene glycol) (PPG) is a telechelic oligomer available from Bayer in a variety of molecular weights with nearly perfect difunctionality.[20] PPG and PPG copolymers are used in a variety of applications including drug delivery,[21,22]

protein delivery,[23] coatings,[24,25] polyurethanes,[26-28] and surfactants.[29-31] For example, poly(propylene glycol) acetoacetate (PPG AcAc) was shown as an effective component in body tissue adhesives.[32] Previous research in our laboratory has focused on the synthesis and characterization of cross-linked networks based on PPG AcAc and poly(ethylene glycol) diacrylate.[3] The hydroxyl endgroups of PPG were quantitatively functionalized in an uncatalyzed transesterification with *tert*-butyl acetoacetate (tBuAcAc) to yield PPG AcAc. Networks were subsequently formed upon Michael addition of acetoacetate-functional oligomers with poly(ethylene glycol) diacrylate under basic conditions to yield well-defined networks with uniform molecular weights between cross-link points.[3]

The present study describes a detailed analysis of the structure-property relationships of networks prepared via the Michael addition reaction as a function of the molecular weight of the PPG oligomer. In order to achieve well-defined, highly cross-linked networks with desired mechanical and thermal properties, we have synthesized networks based on PPG AcAc and neopentyl glycol diacrylate as well as networks based on PPG AcAc and 2-hydroxyethyl acrylate derivatized bis(4-isocyanatocyclohexyl)methane (EA-HMDI-EA). The mechanical and thermal properties as a function of cross-link density were investigated for cross-linked networks prepared using the carbon-Michael addition reaction, and the influence of hydrogen bonding on mechanical and thermal properties was revealed. Tensile testing and dynamic mechanical analysis (DMA) were used to analyze the mechanical properties of the free-standing cross-linked networks, and thermogravimetric analysis (TGA) was used to explore the thermooxidative stability of the networks.

10.3 Experimental

10.3.1 Materials and procedures

tert-Butyl acetoacetate (tBuAcAc, 98%), neopentyl glycol diacrylate (NPGDA), 1,8-diazbicyclo[5.4.0]undec-7-ene (DBU, 98%), and bis(4-isocyanatocyclohexyl)methane (HMDI, 90%) were purchased from Aldrich and used as received. 2-Hydroxyethyl acrylate (HEA, 96%) was purchased from Aldrich and purified as described previously.[33] Tetrahydrofuran (THF, EMD Science, HPLC grade) was distilled from sodium/benzophenone immediately prior to use. Dibutyl tin dilaurate (DBTDL, 99%) was dissolved in THF as a 1 wt % solution. Poly(propylene glycol) bis(acetoacetate) (PPG BisAcAc) of 1000 g/mol was prepared from ARCOL™ poly(propylene glycol) diol. PPG BisAcAc oligomers of 2000, 4000, and 8000 g/mol were prepared from ACCLAIM™ poly(propylene glycol) diols. Poly(propylene glycol) tris(acetoacetate) (PPG TrisAcAc) of 6000 g/mol was prepared from trifunctional ACCLAIM™ poly(propylene glycol). These acetoacetates were prepared using the method described previously.[3] ^{1}H NMR spectroscopy of the PPG BisAcAc oligomers confirmed the desired composition. ^{1}H NMR (400 MHz, $CDCl_3$) of the 1000 g/mol PPG BisAcAc: δ=1.12 ppm (br, PPG C*H*$_3$),1.24 ppm (dd, 6H, CHC*H*$_3$OAcAc), 2.26 ppm (s, 6H,COCH$_2$COC*H*$_3$), 3.4 ppm (br, PPG C*H*), 3.6 ppm (br, PPG C*H*$_2$), 5.08 ppm (m, 4H, C*H*$_2$CHCH$_3$OAcAc), 5.29 ppm (s, enol C=C*H*–C=O). All ARCOL™ and ACCLAIM™ polyols were kindly supplied by Bayer Co.

10.3.2 Preparation of EA-HMDI-EA

Freshly distilled THF (80 mL), HMDI (9.35 mL, 38 mmol), HEA (8.45 mL, 80 mmol, 2.1 equiv), and DBTDL (0.01 mL) were introduced into a one-neck, round-bottomed flask equipped with a stir bar and nitrogen inlet. The reaction was allowed to proceed for 3 h at 60 °C.

Upon completion, 25 mg of hydroquinone were added to prevent polymerization of the product, and the reaction solution was precipitated from hexanes. The resulting white powder was subsequently dried *in vacuo* (0.1 mm Hg) at room temperature for 24 h.

10.3.3 Network Formation

2000 g/mol PPG BisAcAc (1.75 g, 0.875 mmol) and NPGDA (0.260 g, 1.23 mmol, 1.4 equiv) were mixed thoroughly to form a clear, homogeneous liquid. DBU catalyst was quickly added and mixed thoroughly. The mixture was then transferred to a Teflon™ mold and was allowed to cross-link for 24 h at room temperature. The resulting films were dried at reduced pressure (0.1 mm Hg) for 18 h at room temperature. Similar preparations were used to form carbon-Michael networks containing EA-HMDI-EA, except that the solid acrylate monomer was dissolved in a minimal amount of THF (< 0.5 mL) to facilitate homogeneous mixing.

10.3.4 Characterization

Size exclusion chromatography (SEC) was performed using a Waters size exclusion chromatograph. The instrument was equipped with an autosampler, three 5 μm PLgel Mixed-C columns, a Waters 2410 refractive index (RI) detector operating at 880 nm, a Wyatt Technologies miniDAWN multi-angle laser light scattering (MALLS) detector operating at 690 nm, and a Viscotek 270 viscosity detector at 40 °C at a flow rate of 1 mL/min in THF. Reported molecular weights are based on absolute measurements using the MALLS detector. The RI increment (d*n*/d*c*) was calculated online. ^{1}H NMR spectroscopy was utilized to determine PPG AcAc oligomer composition, number average molecular weight, and percent functionalization. A 400 MHz Varian UNITY spectrometer was used to characterize the oligomers in $CDCl_3$ at 23 °C. Dynamic mechanical analysis (DMA) was conducted on a TA Instruments Q800 Dynamic

Mechanical Analyzer in tension mode at a frequency of 1 Hz, an oscillatory amplitude of 15 μm, and a static force of 0.01 N. The temperature ramp was 3 °C/min. The glass transition temperature (T_g) was determined at the peak of the tan δ curve. Stress-strain experiments were conducted with dogbone-shape film specimens, cut with a die according to ASTM D3368 specifications. The reported data represents an average of five specimens. Tensile tests were performed on an Instron 4411 universal testing instrument with a cross-head speed of 13 mm/min using manual grips at ambient temperature. Oxidative stability of the networks was measured with a TA Instruments Hi-Res Thermogravimetric Analyzer 2950, with a temperature ramp of 10 °C/min in an air atmosphere. The samples were tested in an isothermal fashion for 5 h at 37 °C, 75 °C, and/or 125 °C. The remaining weight percent was measured. The networks were characterized for gel fraction via Soxhlet extractions in THF for 6 h and subsequently dried in an oven at reduced pressure (0.1 mmHg) at 60 °C for 18 h, or until constant weight was observed. The gel fraction was determined gravimetrically, via dividing the initial mass (m_i) by the final mass (m_f).

10.4 Results and discussion

Carbon-Michael addition chemistry was utilized to prepare networks based on PPG AcAc and either NPGDA or EA-HMDI-EA. The preparation of the Michael donor is depicted in Scheme 10.2. ARCOL™ 1000, which is a 1000 g/mol PPG diol, was functionalized using tBuAcAc. The byproducts from this reaction, *tert*-butanol and excess tBuAcAc, were quantitatively removed at reduced pressure (0.1 mm Hg) at 150 °C. ^{1}H NMR spectroscopy confirmed the intended composition and the absence of either by-product.

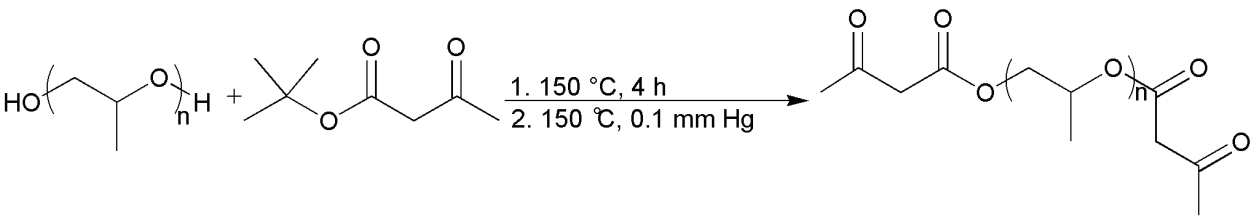

Scheme 10.2. Preparation of PPG BisAcAc, the Michael donor.

^{1}H NMR and SEC were used to analyze the number average molecular weight, molecular weight distribution, and functionality of the Michael donor. The Michael donors included 1000 g/mol PPG BisAcAc, 2000 g/mol PPG BisAcAc, 4000 g/mol PPG BisAcAc, and 6000 g/mol PPG TrisAcAc. Table 10.1 compares the molecular weight and AcAc functionality for the Michael donors. The Michael donors were reacted with NPGDA or EA-HMDI-EA, using DBU as the base.

PPG AcAc	M_n (^{1}H NMR)	M_n (SEC)	M_w/M_n	Degree of Functionalization
	g · mol^{-1}	g · mol^{-1}		%
1 000	1 300	1 200	1.10	100
2 000	2 400	2 400	1.05	100
4 000	4 300	4 700	1.01	92
6 000 (tris)	6 600	6 800	1.11	97

Table 10.1. Molecular weight and functionality analysis of PPG AcAc network precursors.

The carbon-Michael addition networks were formed using a stoichiometry of 1.40 acrylates per 1.00 acetoacetate (assumes acetoacetate f = 1-2), and the base concentration was typically 1 wt%. Reaction schemes for this process are given in Scheme 10.3 and Scheme 10.4. Cross-linking reactions were allowed 24 h at room temperature prior to subjecting the films to reduced pressure for 18 h, and the onset of gelation was observed after only 5 min. Previous results indicated that a stoichiometry of 1.4:1.0 resulted in cross-linked networks with greater tensile strengths and Young's moduli than cross-linked networks prepared at 2.0:1.0.[3] The strength of DBU allowed for deprotonation of both acetoacetate methylene protons (ideal

acetoacetate functionality of 2).

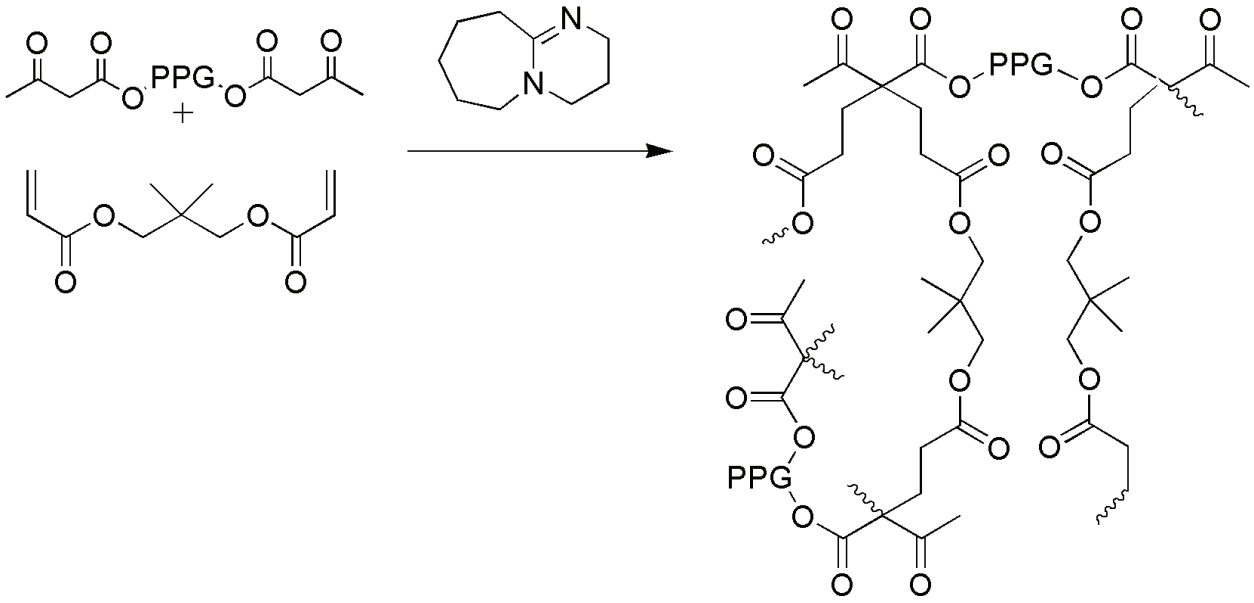

Scheme 10.3. Preparation of networks based on PPG BisAcAc and NPGDA.

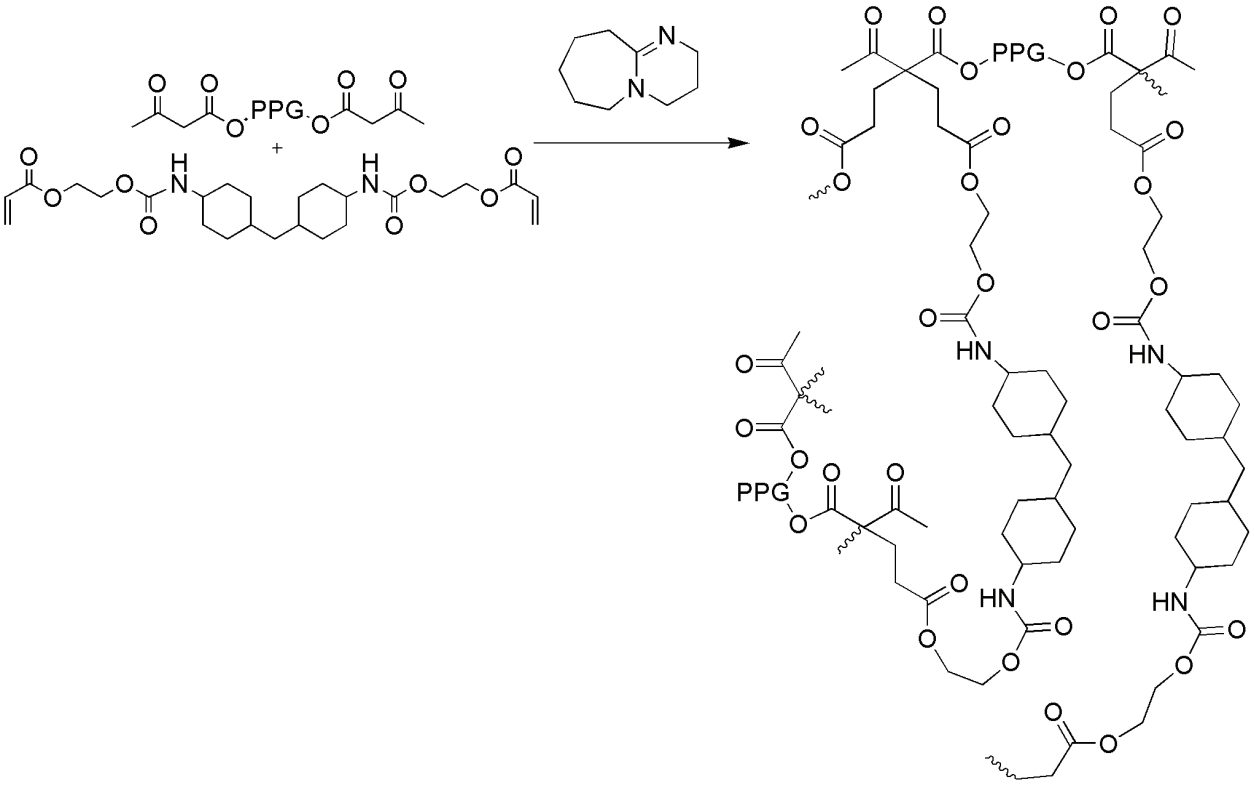

Scheme 10.4. Preparation of networks based on PPG BisAcAc and EA-HMDI-EA.

Gel fraction analyses were conducted on the Michael networks to ascertain the efficacy of

the cross-linking reaction and the influence of gel fraction on mechanical properties of the cross-linked films, and data is summarized in Table 10.2. It appeared that the carbon-Michael networks that were prepared with a lower molecular weight PPG AcAc precursor were more efficiently cross-linked than networks with a higher molecular weight PPG AcAc precursor. This was attributed to a slower cross-linking reaction at identical reaction conditions for the higher molecular weight PPG oligomers with reduced chain end concentration. Furthermore, the acetoacetate functionality was greater for the lower molecular weight PPG oligomers, which resulted in higher gel content for the cross-linked networks.

Network	Gel Fraction (%) (± 2%)
1000 g/mol PPG BisAcAc - NPGDA	95
2000 g/mol PPG BisAcAc - NPGDA	98
4000 g/mol PPG BisAcAc - NPGDA	95
6000 g/mol PPG TrisAcAc - NPGDA	94

Table 10.2. Gel fraction analysis for PPG BisAcAc (or TrisAcAc) – NPGDA films.

Dynamic mechanical analysis (DMA) was used to analyze the resulting Michael addition networks including 1000 g/mol PPG BisAcAc, 2000 g/mol PPG BisAcAc, 4000 g/mol PPG BisAcAc, and 6000 g/mol PPG TrisAcAc cross-linked with NPGDA. The tan δ versus temperature and storage modulus versus temperature plots are included in Figure 10.1 and Figure 10.2, respectively. In order to demonstrate the influence of the molecular weight of the PPG BisAcAc oligomer, a plot of T_g versus PPG BisAcAc molecular weight was constructed, as shown in Figure 10.3. In addition, it is important to note that the critical molecular weight of entanglement (M_c) for PPG is 7700 g/mol.[34] Although all of the oligomeric PPG BisAcAc network precursors were below the M_c, it is possible for linear segments to form during the

Michael addition cross-linking process if the second deprotonation reaction does not occur. This is expected to slightly affect the overall observed mechanical properties. However, in order to minimize mono-addition products and maximize bis-addition products of the acrylate to the acetoacetate, a relatively strong base (DBU) was utilized. Clemens and Rector showed that weaker inorganic bases, such as potassium carbonate, lead to greater amounts of mono-addition products (mono:bis AcAc ratio = 0.04), while organic bases, such as DBU, lead to greater amounts of bis-addition products(mono:bis AcAc ratio = 0.7).[19] The effect of acetoacetate functionality (f = 2 or 3) is observed in the intensity of the tan δ curves, and the network based on the 6000 g/mol TrisAcAc (f = 3) having the greatest tan δ intensity that occurs at a temperature between the 4000 g/mol (f = 2) and 2000 g/mol (f = 2) PPG BisAcAc networks.

As shown in Figure 10.1, the T_g's of the carbon-Michael addition networks were -14 °C for the 1000 g/mol PPG BisAcAc – NPGDA network, -37 °C for the 2000 g/mol PPG BisAcAc – NPGDA network, -44 °C for the 4000 g/mol PPG BisAcAc – NPGDA network, and -44 °C for the 6000 g/mol PPG TrisAcAc – NPGDA network, as determined using DMA. The T_g decreased with increasing molecular weight of the PPG BisAcAc segment (Figure 10.3), and this observation was attributed to less restriction on segmental motion due to increased molecular weight between cross-link points. In addition, the trifunctional Michael donor network had a T_g value that was identical to the 4000 g/mol PPG BisAcAc network.

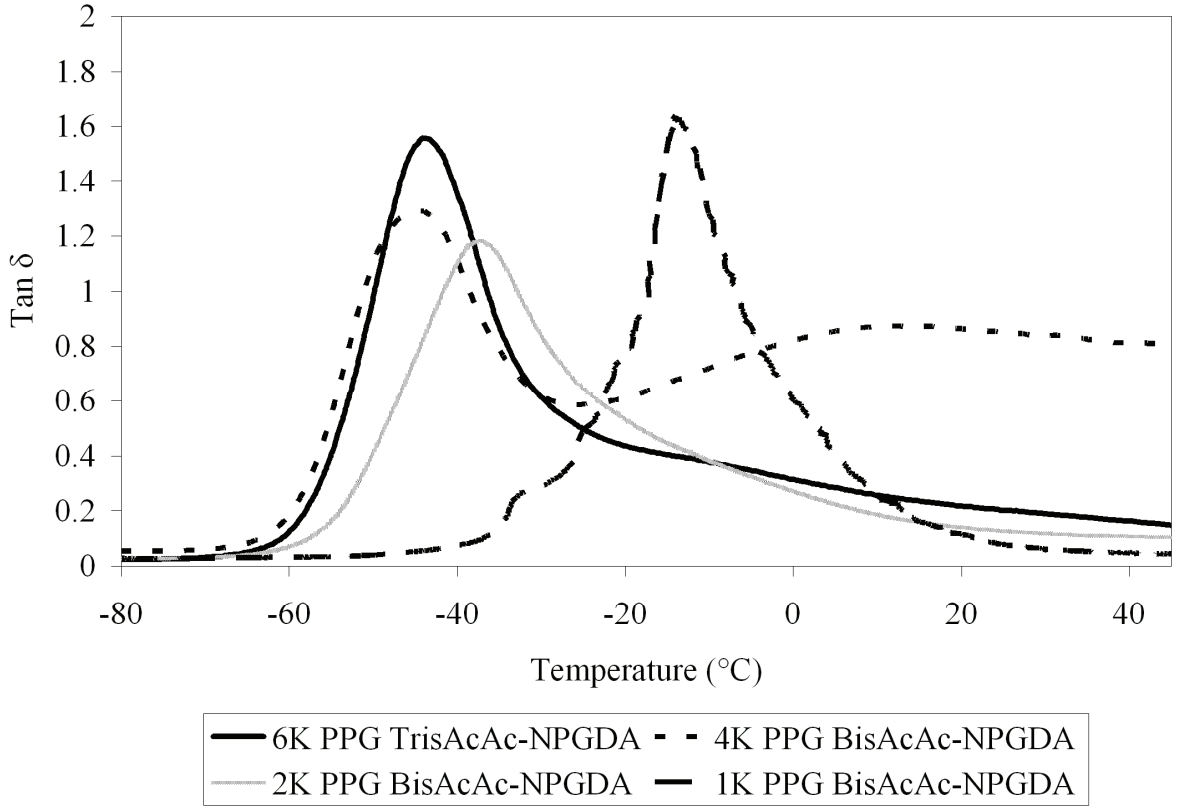

Figure 10.1. Tan δ versus temperature for PPG BisAcAc or TrisAcAc - NPGDA films.

The presence of the branch point in the trifunctional Michael donor was proposed to reduce the motion of the 6000 g/mol PPG Tris AcAc. Essentially, each arm length of the trifunctional Michael donor was presumed to have a molecular weight of 2000 g/mol. The breadth of the T_g is observed in Figure 10.2. As the molecular weight between cross-link points decreases, the segmental motion close to the cross-link junctions is more limited. This results in an overall broadening of the viscoelastic region, and the relaxation occurs at a higher temperature.[35,36]

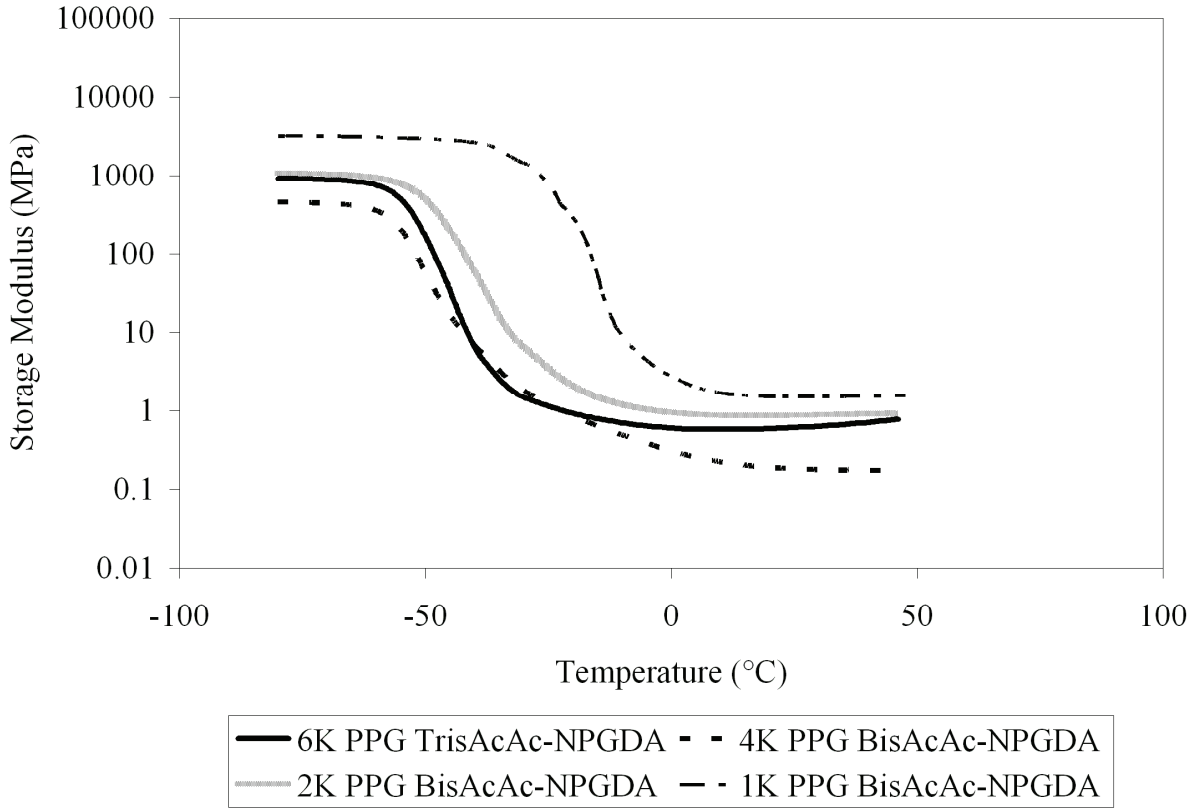

Figure 10.2. Storage modulus versus temperature for PPG BisAcAc or TrisAcAc - NPGDA films.

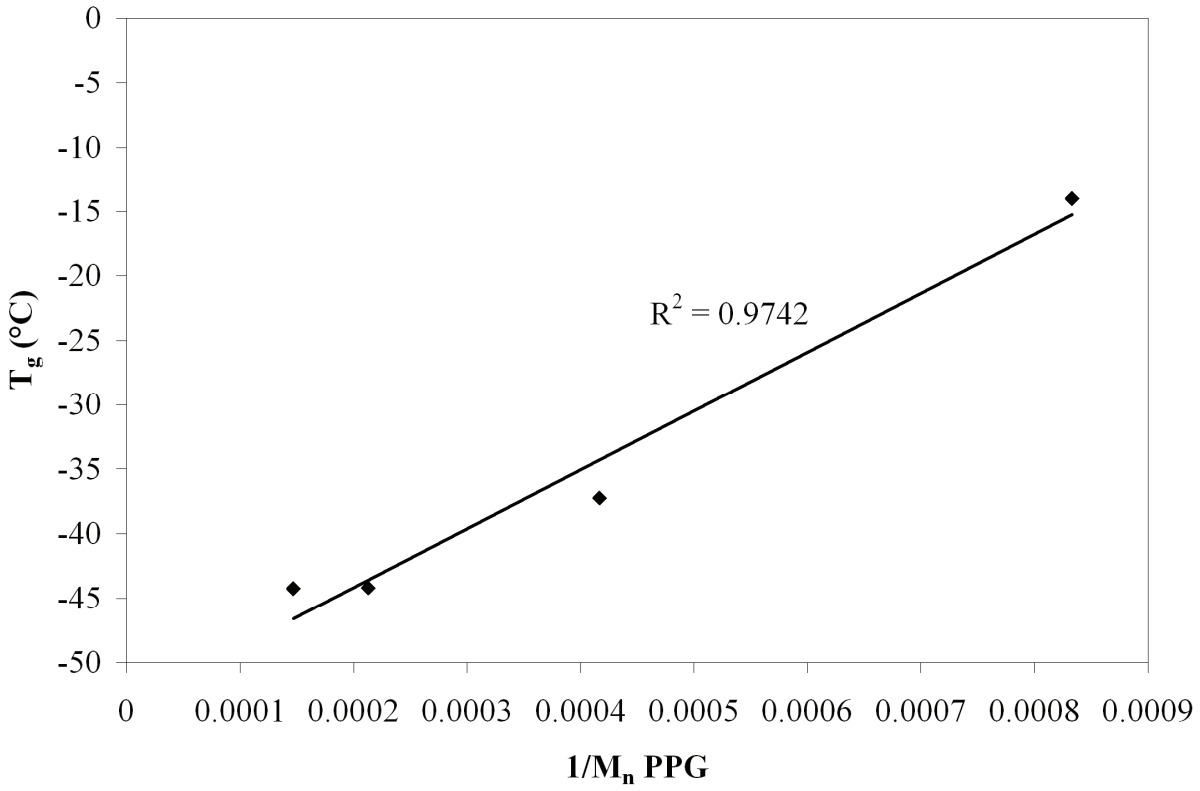

Figure 10.3. Glass transition temperature of PPG BisAcAc – NPGDA networks as a function of inverse PPG BisAcAc molecular weight.

Tensile properties of the networks were analyzed using an Instron 4411 testing machine with a minimum of 5 samples for each network. The films exhibited low Young's moduli, stress at break values, and elongations (Table 10.3). As the PPG precursor molecular weight increased, the Young's modulus and stress at break decreased for the 2000 g/mol and the 4000 g/mol PPG BisAcAc carbon-Michael networks. In addition, the elongation at break increased from 52 to 117%. These trends were attributed to the decrease in cross-link density as the PPG precursor M_n increased. In addition, these trends are attributed to the functionality of the PPG BisAcAc network precursor decreasing slightly as the PPG M_n increased. The 6000 g/mol PPG TrisAcAc carbon-Michael network exhibited properties approximately between the values for the 2000

g/mol and 4000 g/mol PPG BisAcAc networks. This intermediate performance was also confirmed using DMA analysis. The network prepared from 1000 g/mol PPG Bis AcAc had similar mechanical performance as the 2000 g/mol PPG BisAcAc network, which is probably due to fast cross-linking for the 1000 g/mol PPG BisAcAc network.

Network	Young's Modulus (MPa)	Stress at Break (MPa)	Elongation at Break (%)	Toughness (MPa)
1000 g/mol PPG BisAcAc - NPGDA	0.72 ± 0.03	0.40 ± 0.01	65 ± 1	0.04 ± 0.002
2000 g/mol PPG BisAcAc - NPGDA	0.98 ± 0.06	0.43 ± 0.01	52 ± 5	0.03 ± 0.002
4000 g/mol PPG BisAcAc - NPGDA	0.61 ± 0.02	0.35 ± 0.07	117 ± 8	0.02 ± 0.003
6000 g/mol PPG TrisAcAc - NPGDA	0.43 ± 0.05	0.27 ± 0.04	98 ± 6	0.04 ± 0.001

Table 10.3. Tensile data for PPG BisAcAc (or TrisAcAc) – NPGDA films.

Isothermal thermogravimetric analysis (TGA) was used to characterize the oxidative degradation of the networks. Polyethers are inherently unstable to oxidative conditions. Poly(ethylene glycol) (PEG) degrades at a fast rate at 70-80 °C due to hydrogen atom abstraction adjacent to ether functionalities and subsequent peroxide formation.[37] The oxidative stability of ARCOL 1000 g/mol PPG in air was determined via isothermal TGA at 125 °C for 5 h. After the 5 h, only 68% of the sample remained. The PPG BisAcAc (or TrisAcAc) – NPGDA films samples were maintained at three temperatures, 37 °C, 75 °C, and 125 °C for 6 h in air. Representative TGA curves are given in Figure 10.4 for 2000 g/mol PPG BisAcAc – NPGDA film. As shown in Figure 10.4, at 37 °C, there was minimal degradation, and more degradation occurred at 75 °C and 125 °C. However, after 5 h, only 2% of the sample was degraded at 125

°C, and over this temperature range, the networks were oxidatively stable. A summary of all TGA data is provided in Table 10.4. All networks, despite differences in PPG precursor molecular weight and functionality, had a similar extent of oxidative degradation. Thus, the oxidative stability of the networks is greatly enhanced when compared to the original oligomer. The observation of enhanced oxidative stability of the cross-linked networks enables new applications for these cross-linked networks.

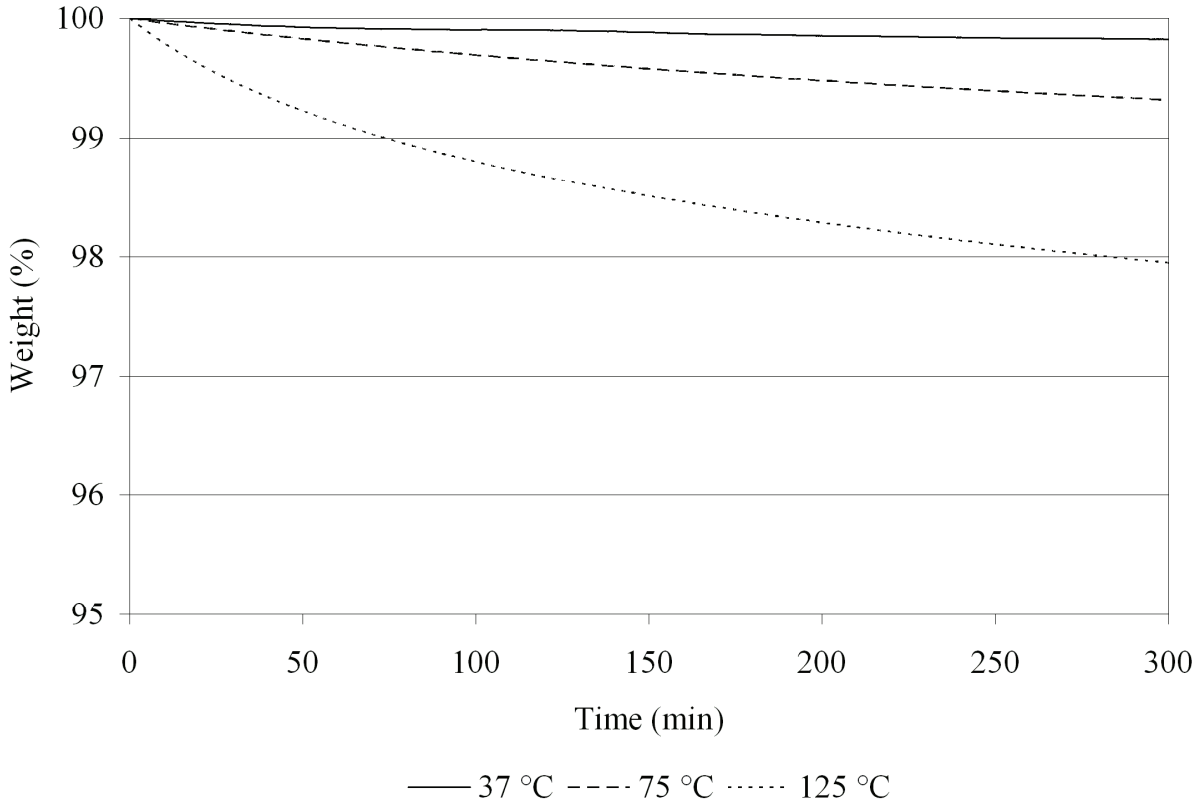

Figure 10.4. Isothermal TGA curves of 2000 g/mol PPG BisAcAc - NPGDA networks in air.

Network	% Weight Remaining		
	37 °C	75 °C	125 °C
1000 g/mol PPG BisAcAc - NPGDA	>99%	94%	94%
2000 g/mol PPG BisAcAc - NPGDA	>99%	>99%	98%
4000 g/mol PPG BisAcAc - NPGDA	>99%	99%	97%
6000 g/mol PPG TrisAcAc - NPGDA	>99%	98%	92%

Table 10.4. Isothermal TGA data summary for PPG BisAcAc (or TrisAcAc) networks in air for 5 h.

In order to probe the influence of urethane sites on the thermal and mechanical performance, three Michael addition networks were prepared using 1000 g/mol PPG BisAcAc, 2000 g/mol PPG BisAcAc, a 4000 g/mol PPG BisAcAc that were cross-linked with EA-HMDI-EA, which contained urethane functionality within the diacrylate. Gel fraction analysis was conducted on the resulting hydrogen bonded carbon-Michael networks, and is given in Table 10.5. A similar trend to the non-hydrogen bonded networks was observed, as the carbon-Michael networks prepared with lower molecular weight PPG AcAc precursor were more efficiently cross-linked than the networks with a higher molecular weight PPG AcAc precursor. It was also observed that the gel fractions for the hydrogen bonded networks (89% average) were slightly lower than the non-hydrogen bonded networks (95% average). The error in gel fraction analyses is typically 2%, however, there are several possible explanations for the slightly lower gel fractions. These include diacrylate solubility differences, catalyst deactivation, and reduced chain end mobility due to hydrogen bonding interactions. Future efforts will be directed towards a more fundamental understanding of the basis for the influence of urethane units on cross-linking kinetics.

Network	Gel Fraction (%) (± 2%)
1000 g/mol PPG BisAcAc – EA-HMDI-EA	94
2000 g/mol PPG BisAcAc – EA-HMDI-EA	88
4000 g/mol PPG BisAcAc – EA-HMDI-EA	84

Table 10.5. Gel fraction analysis for PPG BisAcAc – EA-HMDI-EA films.

DMA was used to analyze the resulting hydrogen bonded Michael addition networks. The tan δ versus temperature and storage modulus versus temperature plots are shown in Figure 10.5 and Figure 10.6, respectively. According to the tan δ data, the networks behaved differently as molecular weight varied. The maxima of the tan δ curves range from -42 °C to 12 °C. This observation is in sharp contrast to the damping behavior of the non-urethane containing networks, which had similar damping behavior. Thus, we conclude that the incorporation of urethane linkages greatly influences the thermal transitions of the cross-linked networks.

As shown in Figure 10.5, the T_g's of the carbon-Michael addition networks were -12 °C for the 1000 g/mol PPG BisAcAc – NPGDA network, -20 °C for the 2000 g/mol PPG BisAcAc – NPGDA network, and -42 °C for the 4000 g/mol PPG BisAcAc – NPGDA network as determined using DMA. The T_g significantly decreased with increasing molecular weight of the PPG BisAcAc segment. The breadth of the viscoelastic region is also observed in Figure 10.6, in a similar manner to Figure 10.2. Broadening of the viscoelastic region is observed as the molecular weight between cross-link points decreases, due to restricted segmental motion near the cross-link junctions.

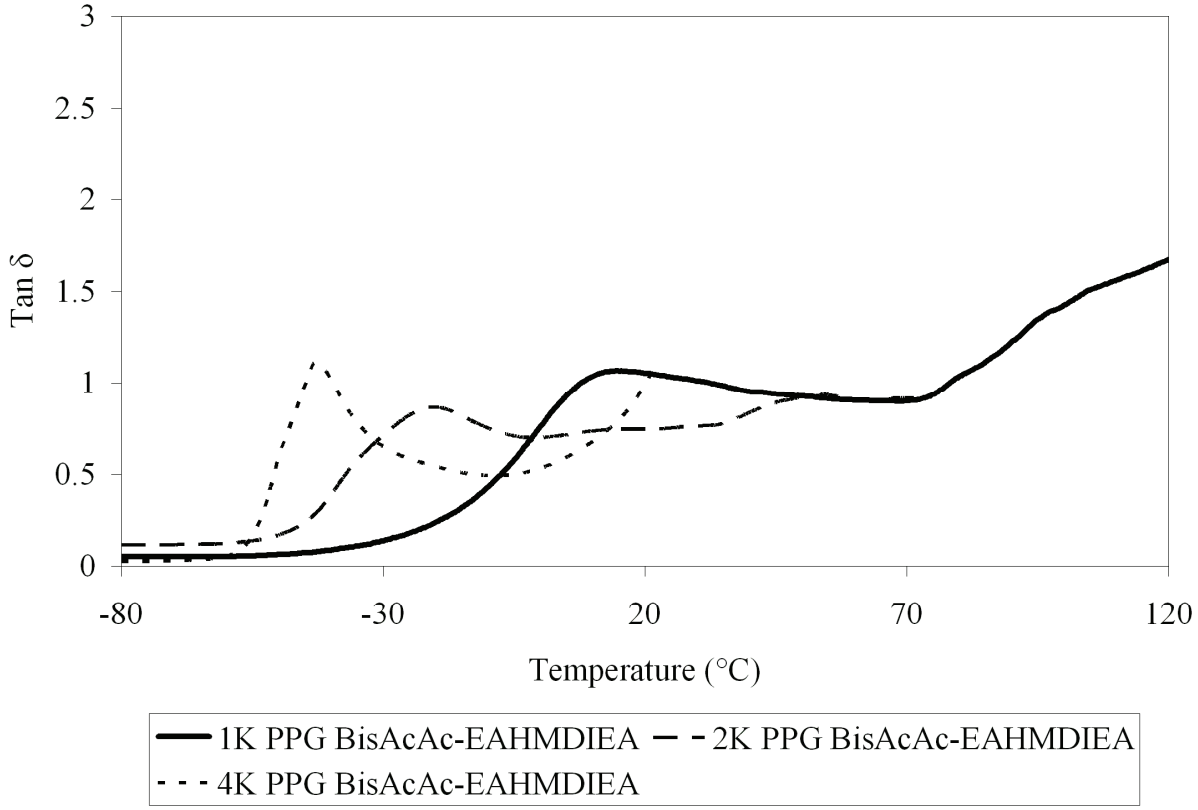

Figure 10.5. Tan δ versus temperature for PPG BisAcAc - EA-HMDI-EA films.

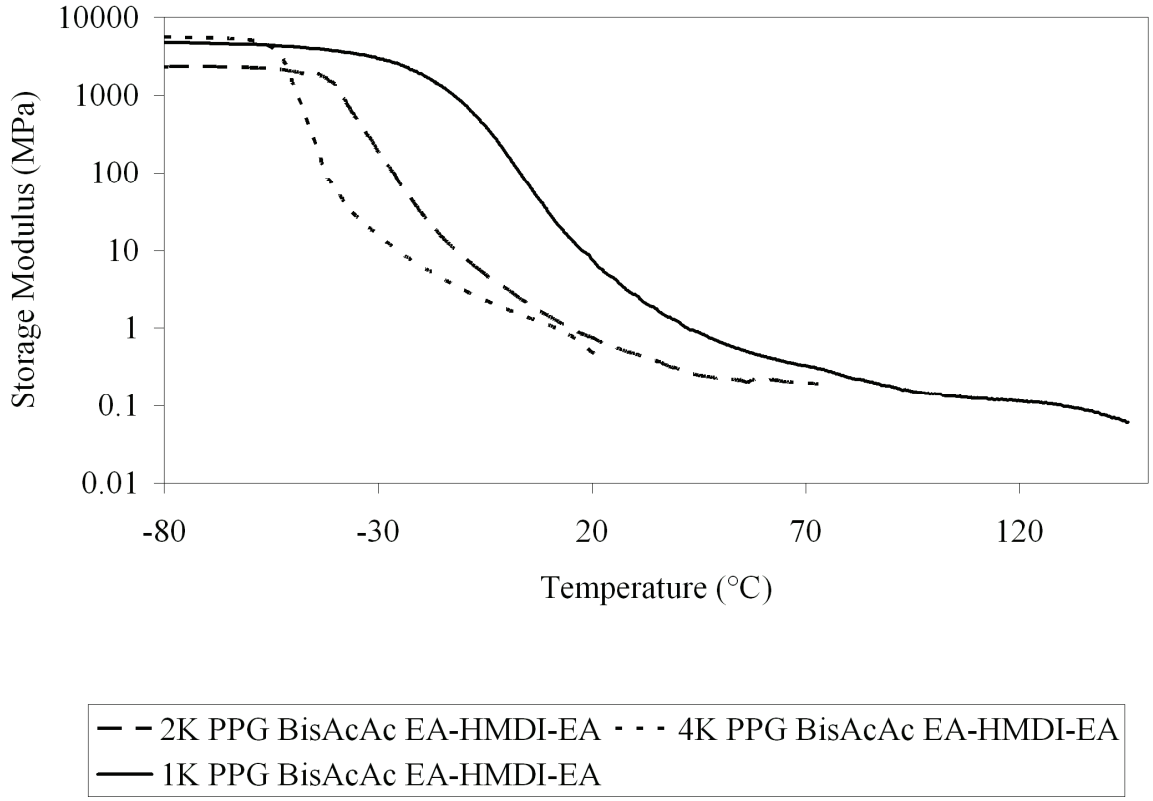

Figure 10.6. Storage modulus versus temperature for PPG BisAcAc - EA-HMDI-EA films.

A direct comparison on the DMA behavior of the non-hydrogen and hydrogen bonding Michael networks is depicted in Figure 10.7. The storage modulus that corresponded to the 2000 g/mol PPG BisAcAc – EA-HMDI-EA network was higher (1070 MPa to 2320 MPa at -80 °C) than the non-hydrogen bonded counterpart, thus showing the influence of hydrogen bonding within a cross-linked network. In addition, an increased glass transition temperature (-37 °C to -19 °C) was observed from the tan δ curve. Although the two diacrylates are different in structure, we propose the difference in mechanical properties is due to mostly the effect of hydrogen bonding. However, it cannot be eliminated that the difference in diacrylate structure is not affecting the properties. Meijer and co-workers[38-42] and Long and co-workers[43-46] have shown that hydrogen bonds have high association constants and thus can greatly improve

mechanical properties based solely on non-covalent interactions.

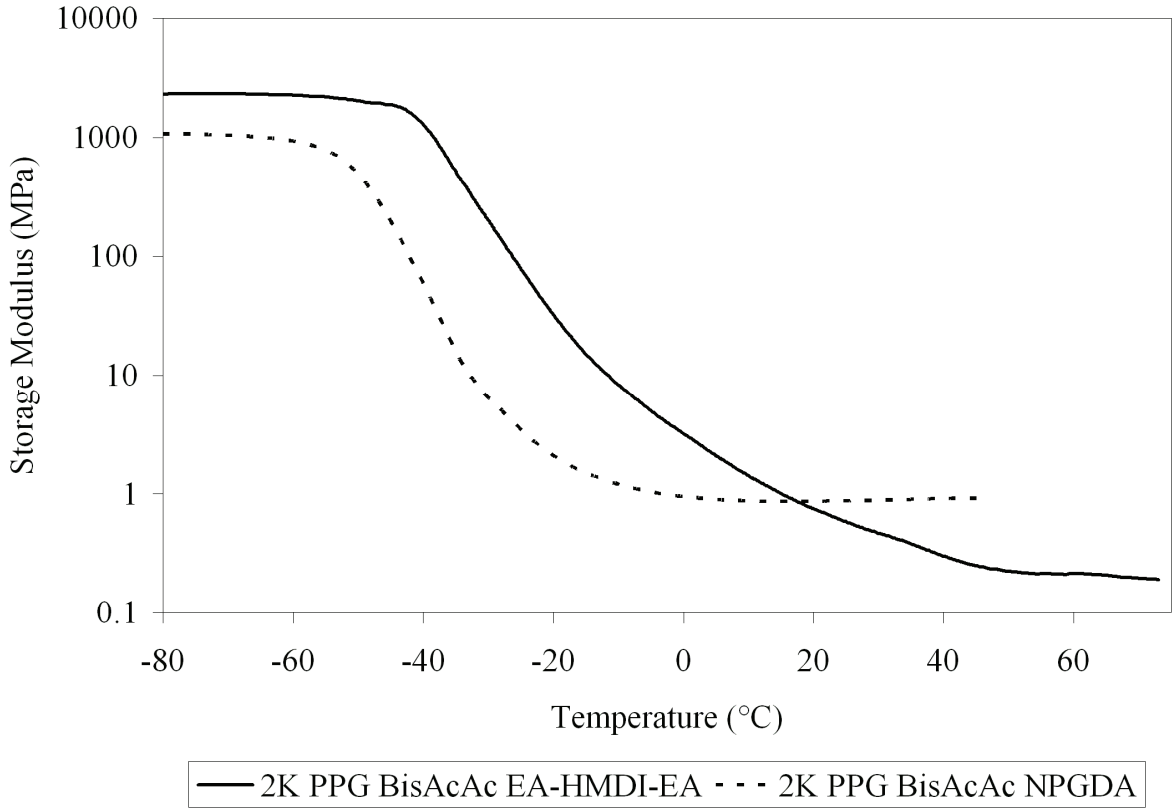

Figure 10.7. DMA data comparison for 2000 g/mol PPG BisAcAc - EA-HMDI-EA network versus 2000 g/mol PPG BisAcAc - NPGDA network.

The tensile properties were analyzed in an identical fashion to the non-urethane containing networks, and the data is summarized in Table 10.6. In a consistent fashion as the PPG BisAcAc molecular weight increased, the Young's modulus and stress at break decreased. The elongation at break increased significantly compared to non-hydrogen bonded networks, and at constant PPG BisAcAc molecular weight, the intermolecular hydrogen bonding of urethane linkages improved tensile properties.

Network	Young's Modulus (MPa)	Stress at Break (MPa)	Elongation at Break (%)	Toughness (MPa)
1000 g/mol PPG BisAcAc – EA-HMDI-EA	0.58 ± 0.05	0.54 ± 0.09	96 ± 5	0.17 ± 0.02
2000 g/mol PPG BisAcAc - EA-HMDI-EA	0.25 ± 0.05	0.27 ± 0.05	346 ± 25	0.04 ± 0.003
4000 g/mol PPG BisAcAc - EA-HMDI-EA	0.10 ± 0.01	0.10 ± 0.02	507 ± 33	0.01 ± 0.002

Table 10.6. Tensile data for PPG BisAcAc – EA-HMDI-EA films.

A direct comparison on the stress versus strain behavior of the non-hydrogen and hydrogen bonding Michael networks is depicted in Figure 10.8. The tensile behavior that corresponded to the 2000 g/mol PPG BisAcAc – EA-HMDI-EA network exhibited similar tensile strength, however, extent of elongations were significantly higher than the non-hydrogen bonded analog, thus showing the influence of hydrogen bonding within a cross-linked network. Both Michael networks produced films that were transparent with a slight yellow color due to the enolate formation during the cross-linking reaction.

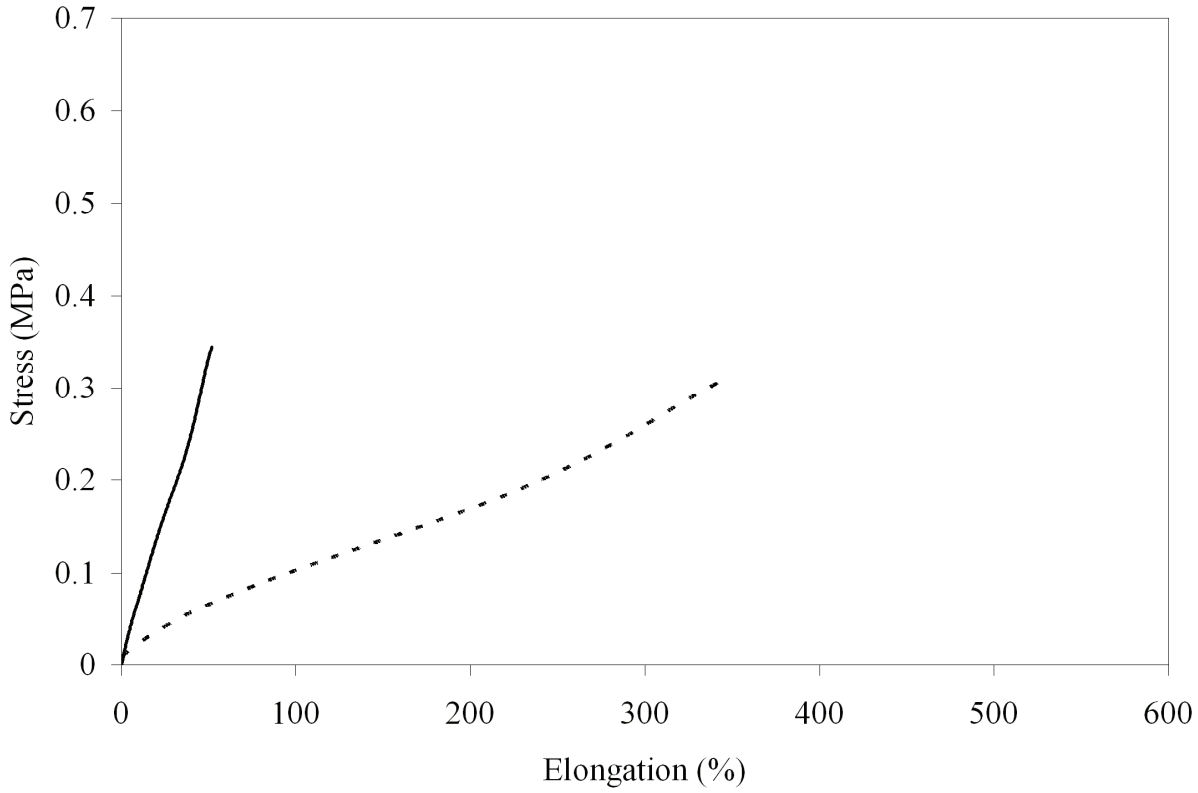

Figure 10.8. Tensile data comparison for 2000 g/mol PPG BisAcAc - EA-HMDI-EA network versus 2000 g/mol PPG BisAcAc - NPGDA network.

Oxidative degradation of the hydrogen-bonded carbon-Michael networks was characterized via isothermal thermogravimetric analysis (TGA) only at 125 °C, since the non-hydrogen bond containing networks had minimal weight loss over time at 37 °C and 75 °C. The samples were held isothermally at 125 °C for 5 h in an atmosphere of air. Isothermal TGA curves are given in Figure 10.9 for all three hydrogen bonded carbon-Michael networks. A slight decrease in oxidative stability compared to the non-hydrogen bonded networks was observed for the hydrogen-bonded carbon-Michael networks, but the decrease is within TGA error. However, the hydrogen bonded carbon-Michael networks were still considerably more stable than the ARCOL 1000 g/mol PPG diol. A direct comparison of the hydrogen bonded carbon-Michael

networks versus the non-hydrogen bonded carbon-Michael networks is depicted in Figure 10.10.

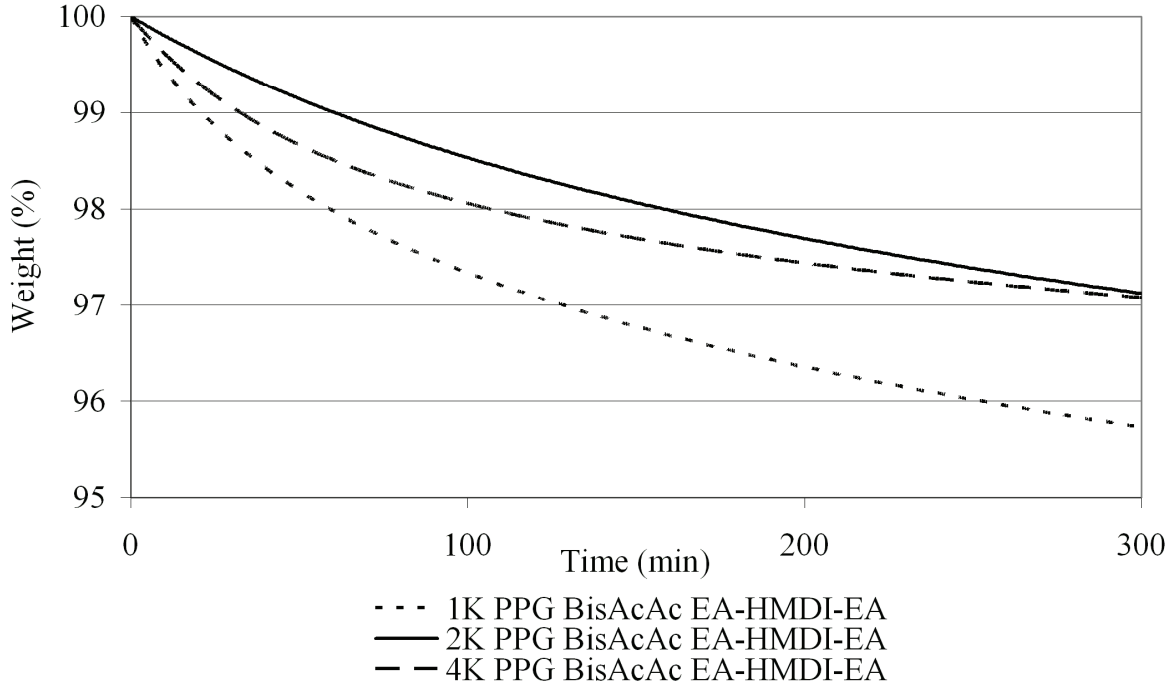

Figure 10.9. Isothermal TGA curves of PPG BisAcAc - EA-HMDI-EA networks in air at 125 °C.

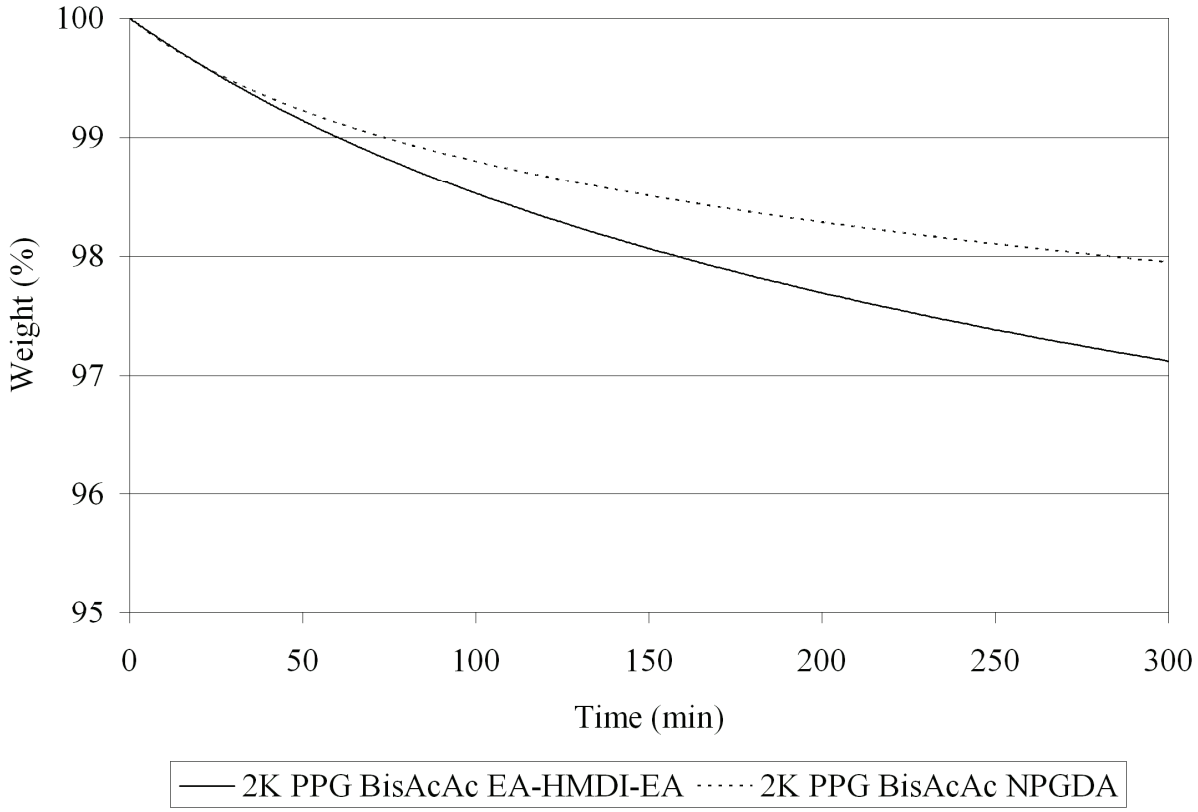

Figure 10.10. Isothermal TGA data comparison for 2000 g/mol PPG BisAcAc - EA-HMDI-EA network versus 2000 g/mol PPG BisAcAc – NPGDA network in air at 125 °C.

10.5 Conclusions

PPG was successfully functionalized to incorporate acetoacetate endgroups through a transesterification reaction. Cross-linked films were then prepared from the PPG AcAc and NPGDA or EA-HMDI-EA. The influence on PPG AcAc molecular weight on mechanical properties was determined for both NPGDA and EA-HMDI-EA carbon-Michael networks via tensile testing and DMA. The stress at break and elongations at break for PPG BisAcAc (or TrisAcAc) – NPGDA networks ranged from 0.27 to 0.43 MPa and 52-117%, respectively. Additionally, urethane functionality significantly improved network mechanical performance. The stress at break and elongations at break for PPG BisAcAc – EA-HMDI-EA networks ranged

from 0.10 to 0.54 MPa and 96-507%, respectively. Isothermal TGA revealed excellent thermal stability in air over several hours for all cross-linked networks (> 92 wt % remaining). A dependence on PPG AcAc molecular weight on gel fraction analysis was observed, and revealed that increasing the molecular weight of PPG AcAc precursor resulted in lower gel fractions. These networks could find potential applications in packaging and adhesives.

10.6 Acknowledgements

We thank Ms. Rebecca Huyck for assistance with size-exclusion chromatography and Mr. Tomonori Saito for assistance with thermogravimetric analysis. The authors acknowledge the financial support of Rohm and Haas Company and the Department of Energy under agreement number DE-FG36-04GO14317, as well as support in part by the Macromolecular Interfaces with Life Sciences (MILES) Integrative Graduate Education and Research Traineeship (IGERT) of the National Science Foundation under agreement number DGE-0333378.

10.7 References

(1) Moy, T. M.; Dammann, L.; Loza, R. Liquid Oligomers Containing Unsaturation. US 5,945,489, 1999.
(2) Kim, Y.-B.; Kim, H. K.; Nishida, H.; Endo, T. *Macromol Mater Eng* **2004,** 289, (10), 923-926.
(3) Mather, B. D.; Miller, K. M.; Long, T. E. *Macromol Chem Phys* **2006,** 207, (15), 1324-1333.
(4) Mather, B. D.; Viswanathan, K. V.; Miller, K. M.; Long, T. E. *Prog Polym Sci* **2006,** 31, (5), 487-531.
(5) Kauffman, T. F.; Whitman, D. W.; Zajackowski, M. J. Surface promoted Michael cure compositions US 2006078742, April 13, 2006, 2006.
(6) Kauffman, T. F.; Whitman, D. M.; Zajaczkowski, M. J.; Vietti, D. E. Biomass based Michael addition composition. EP 1640388, 2006.
(7) Wang, D.; Liu, Y.; Hong, C.-Y.; Pan, C.-Y. *Polymer* **2006,** 47, (11), 3799-3806.
(8) Rizzi, S. C.; Hubbell, J. A. *Biomacromolecules* **2005,** 6, (3), 1226-1238.
(9) Elbert, D. L.; Pratt, A. B.; Lutolf, M. P.; Halstenberg, S.; Hubbell, J. A. *J Control Release* **2001,** 76, (1-2), 11-25.
(10) Lutolf, M. P.; Hubbell, J. A. *Biomacromolecules* **2003,** 4, (3), 713-722.
(11) Rizzi, S. C.; Ehrbar, M.; Halstenberg, S.; Raeber, G. P.; Schmoekel, H. G.; Hagenmuller,

H.; Muller, R.; Weber, F. E.; Hubbell, J. A. *Biomacromolecules* **2006,** 7, (11), 3019-3029.
(12) Wang, D.; Liu, Y.; Hong, C.-Y.; Pan, C.-Y. *J Polym Sci (A) Chem* **2005,** 43, 5127-5137.
(13) Wang, D.; Zheng, Z.; Hong, C.; Liu, Y.; Pan, C. *J Polym Sci (A) Chem* **2006,** 44, 6226-6242.
(14) Hawker, C. J.; Wooley, K. L. *Science* **2005,** 309, 1200-1205.
(15) Malkoch, M.; Vestberg, R.; Gupta, N.; Mespouille, L.; Dubois, P.; Mason, A. F.; Hedrick, J. L.; Liao, Q.; Frank, C. W.; Kingsburye, K.; Hawker, C. J. *Chem. Commun.* **2006**, 2774-2776.
(16) Kolb, H. C.; Finn, M. G.; Sharpless, K. B. *Angew Chem Int Ed* **2001,** 40, 2004-2021.
(17) Lendlein, A.; Schmidt, A. M.; Schroeter, M.; Langer, R. *J Polym Sci (A) Chem* **2005,** 43, 1369-1381.
(18) McMurray, J., *Organic Chemistry*. 5th ed.; Brooks/Cole: Pacific Grove, 2000.
(19) Clemens, R. J.; Rector, F. D. *J Coat Technol* **1989,** 61, (770), 83-91.
(20) O'Sickey, M. J.; Lawrey, B. D.; Wilkes, G. L. *J Appl Polym Sci* **2002,** 84, (2), 229-243.
(21) Nguyen, P. M.; Hammond, P. T. *Langmuir* **2006,** 22, 7825-7832.
(22) Liaw, J.; Lin, Y.-C. *J Control Release* **2000,** 68, (2), 273-282.
(23) Oh, K. S.; Han, S. K.; Lee, H. S.; Koo, H. M.; Kim, R. S.; Lee, K. E.; Han, S. S.; Cho, S. H.; Yuk, S. H. *Biomacromolecules* **2006,** 7, 2362-2367.
(24) Sinclair, A. R.; Okell, P. R.; Akbar, S. Soluble deverting agents. August 10, 2006, 2006.
(25) Harris, L. A.; Riffle, J. S.; Johnson, M.; Wilkes, G. L. *J Adhes* **2005,** 81, (5), 473-494.
(26) Kaushiva, B. D.; Dounis, D. V.; Wilkes, G. L. *J Appl Polym Sci* **2000,** 78, 766-786.
(27) Moreland, J. C.; Wilkes, G. L.; Turner, R. B. *J Appl Polym Sci* **1991,** 43, (4), 801-815.
(28) Armistead, J. P.; Wilkes, G. L.; Turner, R. B. *J Appl Polym Sci* **1988,** 35, (3), 601-629.
(29) Ortona, O.; D'Errico, G.; Paduano, L.; Vitagliano, V. *J Colloid Interface Sci* **2006,** 301, 63-77.
(30) Dufour, M.; Guyot, A. *Colloid Polym Sci* **2003,** 281, (2), 97-104.
(31) Dufour, M. G.; Guyot, A. *Colloid Polym Sci* **2003,** 281, (2), 105-112.
(32) Arthur, S. D. Polymer-based tissue-adhesive for medical use. US 20060079599, April 13, 2006, 2006.
(33) Coca, S.; Jasieczek, C. B.; Beers, K. L.; Matyjaszewski, K. *J Polym Sci (A) Chem* **1998,** 36, 1417-1424.
(34) Wilkes, G. L., Mechanical Properties. In *Comprehensive Desk Reference of Polymer Characterization and Analysis*, Robert F. Brady, J., Ed. American Chemical Society: Washington, D.C., 2003; pp 624-668.
(35) Roland, C. M.; Ngai, K. L.; Plazek, D. J. *Comput Theor Polym Sci* **1998,** 7, (3-4), 133-137.
(36) Roland, C. M. *Macromolecules* **1994,** 27, 4242-4247.
(37) Glastrup, J. *Polym Degrad Stab* **2003,** 81, 273-278.
(38) Keizer, H. M.; Kessel, R. v.; Sijbesma, R. P.; Meijer, E. W. *Polymer* **2003,** 44, 5505-5511.
(39) Wisse, E.; Spiering, A. J. H.; Leeuwen, E. N. M. v.; Renken, R. A. E.; Dankers, P. Y. W.; Brouwer, L. A.; Luyn, M. J. A. v.; Harmsen, M. C.; Sommerdijk, N. A. J. M.; Meijer, E. W. *Biomacromolecules* **2006,** 7, 3385-3395.
(40) Dankers, P. Y. W.; Zhang, Z.; Wisse, E.; Grijpma, D. W.; Sijbesma, R. P.; Feijen, J.; Meijer, E. W. *Macromolecules* **2006,** 39, 8763-8771.
(41) Kautz, H.; Beek, D. J. M. v.; Sijbesma, R. P.; Meijer, E. W. *Macromolecules* **2006,** 39, 4265-4267.

(42) Keizer, H. M.; Sijbesma, R. P.; Jansen, J. F. G. A.; Pasternack, G.; Meijer, E. W. *Macromolecules* **2003,** 36, 5602-5606.
(43) Elkins, C. L.; Park, T.; McKee, M. G.; Long, T. E. *Journal of Polymer Science Part a-Polymer Chemistry* **2005,** 43, (19), 4618-4631.
(44) Elkins, C. L.; Viswanathan, K.; Long, T. E. *Macromolecules* **2006,** 39, (9), 3132-3139.
(45) Karikari, A. S.; Edwards, W. F.; Mecham, J. B.; Long, T. E. *Biomacromolecules* **2005,** 6, (5), 2866-2874.
(46) Viswanathan, K.; Ozhalici, H.; Elkins, C. L.; Heisey, C.; Ward, T. C.; Long, T. E. *Langmuir* **2006,** 22, (3), 1099-1105.

Chapter 11 : Synthesis and Characterization of Poly(ethylene glycol)-Glutathione Conjugate Self-Assembled Nanoparticles for Antioxidant Delivery

11.1 Abstract

Functional oligomers based on glutathione (GSH) and poly(ethylene glycol) diacrylate (PEGDA) were synthesized via Michael addition. Well-defined, spherical, nanoparticle self-assembly was confirmed via dynamic light scattering and transmission electron microscopy. In addition, a series of Michael addition oligomers containing GSH were prepared with various molecular weights of poly(ethylene glycol) (PEG). Thermal analysis indicated the oligomers were thermally stable to ~160 °C, and the T_g increased as the PEG molecular weight increased. In addition, thiol-terminated PEG was synthesized and reacted with GSH to form disulfide-linked oligomers in order to probe potential antioxidant therapies. SH-SY5Y cells were utilized in cell culture experiments, and hydrogen peroxide induced oxidative stress on the cells. Disulfide-linked GSH oligomers were 100 % effective at protecting SH-SY5Y cells from oxidative stress, while the Michael addition glutathione oligomers did not offer protection.

11.2 Introduction

Biology provides limitless inspiration for polymer scientists in terms of the potential synergy of structure and function that biological molecules richly possess. Polymer and oligomer conjugation to peptides has emerged as an important topic in polymer science.[1-8] Many

researchers have shown that polymer-peptide conjugates provide the opportunity for novel biomaterials that form self-assembled nanostructures based on the interactions of well-defined amino acid residues. For example, Hennink et al. synthesized a series of poly(alkyl methacrylate)s, including poly(2-dimethylaminoethyl methacrylate), that was conjugated to various peptide structures.[9] The nanostructure of the peptide sequences varied from a random coil to an α-helix as a function of pH. The incorporation of peptide units also enhanced the transfection efficiency compared to conventional quaternary ammonium methacrylates due to changing the nanostructure's ability to interact with cells. Furthermore, self-assembled nanomaterials are useful in many other applications, including electronic device fabrication[10,11] and various biomedical applications.[12,13] Kiick et al. recently synthesized a series of noncovalent hydrogel networks containing peptide sequences for controlled growth factor delivery.[14-19] Hubbell et al. demonstrated that recombinant protein-polymer hydrogel conjugates are useful for regenerative tissue engineering.[20,21]

One of the greatest dilemmas of biological systems is their dependence on oxygen and their concurrent degradation due to oxidation. While oxygen is required for life in eukaryotic cells, it also promotes oxidative degradation of biological molecules through the formation of radical species, which are often termed reactive oxygen species (ROS).[22-24] ROS are considered major contributors to the cause of many diseases and ailments including Alzheimer's disease, aging, ischemic injuries, and cancer.[25-28] The major producer of ROS in the body are mitochondria,[29] and ROS are products of the electron transport chain.[30] When cells are healthy, normal defense mechanisms alleviate high concentrations of ROS in the body. However, a symptom of many diseases is an increase in ROS that requires supplemental antioxidant therapy. ROS are typically radicals or reactive intermediates that convert other molecules into deleterious

species. For example, peroxides are considered ROS because under the appropriate conditions, peroxides can undergo homolytic bond cleavage to yield two radical species. Typical ROS are shown in Table 11.1.

ROS	Chemical Formula
Alkoxyl radical	RO•
Hydroperoxide	ROOH
Hydroperoxyl radical	HOO•
Hypochlorite	$^{-}$OCl
Hydrogen peroxide	H_2O_2
Hydroxyl radical	HO•
Nitric oxide radical	NO•
Peroxyl radical	ROO•
Peroxynitrite	$ONOO^{-}$
Singlet Oxygen	$^1\Delta O_2$

Table 11.1. Reactive oxygen species.[31]

Oxidative stress is an imbalance of oxidants and antioxidants. To slow the process of oxidative degradation, antioxidants are synthesized naturally in biological systems or are incorporated during chemical syntheses.[32] Antioxidants are synthetic or natural compounds that inhibit or slow the rate of oxidative damage resulting from ROS in a system. There are two key classes of antioxidants, chain-breaking and preventative. Chain-breaking antioxidants, also termed primary antioxidants, eliminate radical species, while preventative antioxidants (secondary antioxidants) obstruct radical formation.[33] Antioxidants synthesized naturally include superoxide dismutase, catalases, peroxidases, GSH, urate, and ubiquinol.[34]

GSH, or γ-glutamylcysteinylglycine, is a water-soluble, endogenous antioxidant that consists of a tripeptide of glutamic acid, cysteine, and glycine. It is the most abundant non-protein thiol in cells and protects cells from oxidative stress.[35] The molecular structure of GSH and its oxidized form, glutathione disulfide (GSSG), are depicted in Figure 11.1. The antioxidant action of GSH is due to the redox reaction that readily occurs between GSH and GSSG.[36] Through scavenging singlet oxygen, hydroxyl radicals, and superoxide radicals, GSH can protect

cells from oxidative stress. GSSG is formed during the quenching of ROS, and in the presence of glutathione reductase, GSSG is reduced to GSH.[37]

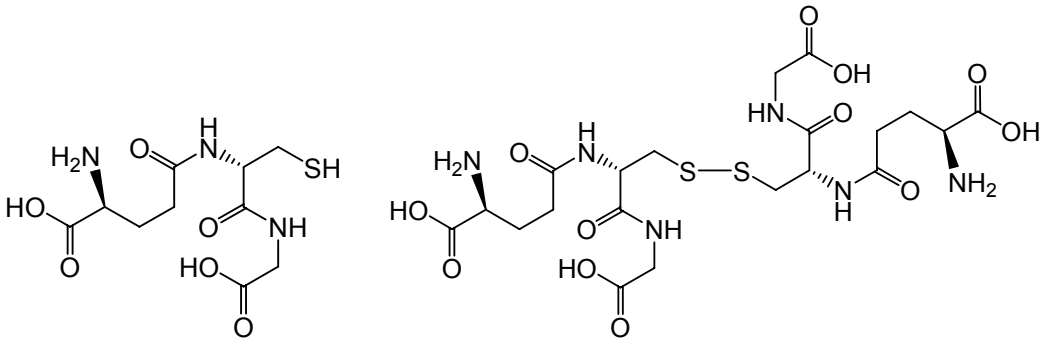

Figure 11.1. Structure of glutathione (left) and its oxidized form, glutathione disulfide (right).

As described herein, Michael addition, a facile, room temperature, base-catalyzed reaction,[38] was utilized to synthesize GSH-containing oligomers. Many others have shown that the Michael addition reaction is widely used for conjugation of acrylates to thiols,[21,39-44] and our research group has previously utilized the Michael reaction to prepare cross-linked networks.[38,45-47] We report in this manuscript that the functionalized oligomers formed unprecedented self-assembled uniform nanoparticles of sizes suitable for antioxidant delivery. In addition, disulfide-linked oligomers possessing GSH end groups were synthesized and were shown to alleviate oxidative stress in SH-SY5Y cells challenged with H_2O_2.

11.3 Experimental

11.3.1 Materials

Poly(ethylene glycol) (PEG, M_n = 600 g/mol), PEG diacrylate (PEGDA, M_n = 300 g/mol, 575 g/mol, and 700 g/mol), mercaptoacetic acid (98%), fluorescein isothiocyanate (FITC, 99%), and L-GSH (99%) were purchased from Aldrich and were used as received. Sodium hydroxide (NaOH, 99%) was obtained from Mallinckrodt. Toluene (Fisher Scientific, HPLC grade) and

tetrahydrofuran (THF, EM Science, HPLC grade) were passed through an alumina column and a molecular sieves column immediately prior to use. Sulfuric acid (95-98%) was purchased from VWR International. Anhydrous diethyl ether was purchased from Fisher Scientific and used as received. Solutions of H_2O:THF (2:1) were prepared from nanopure water and THF. Aqueous sodium hydroxide was prepared from nanopure water and sodium hydroxide. Thiol-terminated PEG (600 g/mol) was functionalized according to an earlier literature procedure.[48]

11.3.2 Synthesis of GS-PEG-SG

GSH and PEGDA (300 g/mol, 575 g/mol, and 700 g/mol) were reacted in a Michael addition fashion. PEGDA (575 g/mol, 5 g, 8.696 mmol) was dissolved in 250 mL of 2:1 H_2O:THF in a 500-mL round-bottomed flask equipped with magnetic stir bar. GSH (5.345 g, 2 eq) was introduced into a 100-mL round-bottomed flask equipped with magnetic stir bar and then dissolved in 60 mL 0.1 M NaOH. The GSH and PEGDA solutions were then combined, the solution was adjusted to pH 8, and the reaction was allowed to proceed for 18 h at 23 °C. Upon completion, THF was removed via rotary evaporation, and the water was removed via lyophilization (10.3 g, 99%). GS-PEG-SG consisting of the 300 g/mol and 700 g/mol PEGDA were prepared in a similar fashion. ^{1}H NMR of GS-PEG575-SG (400 MHz, D_2O) δ = 4.44 (2H, CH_2-C*H*(C=O)(NH)), 4.15 (4H, O=C-C*H*$_2$-NH), 3.64 (2H, CH_2-C*H*(C=O)(NH_2), 3.55 (48H, PEG C*H*$_2$), 2.95 (4H, CH-C*H*$_2$-S), 2.71 (4H, S-C*H*$_2$-CH_2), 2.60 (4H, CH_2-C*H*$_2$-C=O), 2.38 (4H, CH-C*H*$_2$-CH_2), 1.99 (4H, CH_2-C*H*$_2$-C=O). FAB MS: m/z = 1181 (found), m/z = 1182 (calculated).

11.3.3 Synthesis of FITC-labeled GS-PEG-SG

GS-PEG575-SG (0.1 g, 8.41 x 10^{-5} mol) and FITC (0.0655 g, 1.68 x 10^{-4} mol) were

added to a round-bottomed flask equipped with a magnetic stir bar. A solution of 0.1 M Na_2CO_3 (5 mL) was added to the flask, and the reaction was allowed to proceed for 2 h at 23 °C in the absence of light. Upon completion, the reaction mixture was passed through a Sephadex G-25 column, and fractions were collected for UV-vis spectroscopy. Fractions containing the FITC-labeled GS-PEG-SG were combined and lyophilized (0.14 g, 84 %). UV-vis spectroscopy confirmed the attachment of FITC due to absorbance peaks at 275 nm (GSH) and 495 nm (FITC) for all FITC-labeled GS-PEG-SG oligomers.

11.3.4 Synthesis of GS-SPEGS-SG

HS-PEG-SH (0.551 g, 7.45 x 10^{-4} mol) was stirred with GSH (0.4589 g, 1.49 x 10^{-3} mol, 2 eq) in a 100-mL round-bottomed flask equipped with a magnetic stir bar. The reaction was allowed to proceed for 18 h at 23 °C. The solution was then lyophilized to yield a white powder (1.0 g, 99 %). FT-IR spectroscopy indicated a clear disappearance of the thiol S-H peak. ^{1}H NMR (400 MHz, D_2O) δ = 4.40 (2H, CH_2-C*H*(C=O)(NH)), 4.16 (4H, O=C-C*H*$_2$-NH), 3.82 (4H, S-S-C*H*$_2$-C=O), 3.65 (2H, CH_2-C*H*(C=O)(NH_2), 3.54 (46H, PEG C*H*$_2$), 2.79 (4H, CH-C*H*$_2$-S-S), 2.39 (4H, CH-C*H*$_2$-CH_2), 2.00 (4H, CH_2-C*H*$_2$-C=O).

11.3.5 Characterization

^{1}H NMR spectroscopy was utilized to determine monomer and oligomer composition in D_2O or $CDCl_3$ at 23 °C with a 400 MHz Varian UNITY spectrometer. FAB-MS was obtained on a JOEL HX110 dual focusing mass spectrometer. Thermogravimetric analysis (TGA) was conducted on a TA Instruments Hi-Res TGA 2950 with a temperature ramp of 10 °C/min in a nitrogen atmosphere. Thermal transitions were determined on a TA Instruments Q2000 DSC at a heating rate of 10 °C/min under a nitrogen purge, and reported data were obtained from the

second heating cycle. Dynamic light scattering (DLS) was performed at 25 °C in nanopure water using a Malvern CGS-3 DLS instrument. Transmission electron microscopy (TEM) was performed on a Philips 420T TEM operating at 100 kV. UV-vis spectroscopy was performed on a Cary UV-vis spectrometer. Confocal microscopy was conducted on a ZEISS LSM 510 laser scanning microscope equipped with an argon laser operating at 488 nm. FT-IR spectroscopy was conducted on a MIDAC M2004 ATR-FTIR at ambient conditions. The spectra, including the background scan, were collected at a resolution of 4 cm^{-1} and 128 scans were averaged.

11.3.6 Cell culture of SH-SY5Y cell line

Human brain neuroblastoma cells (SH-SY5Y) were obtained from ATCC and grown and harvested according to ATCC protocol. SH-SY5Y were cultured in 1:1 mixture of Eagle's Minimum Essential Medium (containing 1.5 g/L sodium bicarbonate, 2 mM L-glutamine, 1 mM sodium pyruvate and 0.1 mM nonessential amino acids, ATCC) and Ham's F12 Medium (containing 0.5 g/L sodium bicarbonate and 2 mM L-glutamine, Mediatech), 10% fetal bovine serum (Hyclone), and 10,000 U/mL penicillin, 10,000 µg/mL streptomycin, and 25 µg/mL amphotericin B (Hyclone). Cultures were incubated at 37 °C in a humid atmosphere of 5% CO_2 for approximately 7 d, with medium renewal every 2-3 d.[49]

11.3.7 Measure of cell viability after challenge with H_2O_2

The cells were harvested according to ATCC protocol and were treated with 25, 50, 100, 200, 400, and 800 µM of H_2O_2 in 96 well plates for 24 h. Upon completion, the cell viability was determined via MTT assay as described below.

11.3.8 Measure of cell viability of SH-SY5Y cells challenged with H_2O_2 and various concentrations of GS-PEG-SG and GS-SPEGS-SG

SH-SY5Y cells were cultured and treated with various concentrations of either Michael addition or disulfide-linked glutathione oligomers for 24 h. The cells were then exposed to 100 μM of H_2O_2 for 24 h, and the cell viability was subsequently determined via MTT assay, as described below.

11.3.9 Cell viability assay

All cell viability experiments were conducted with CellTiter 96® non-radioactive cell proliferation assays. The cells were harvested during the log phase. A 90 μL cell suspension was dispensed in a 96 well plate ($2x10^4$ cells/well) and was allowed to incubate for 24 h at 37 °C, 5% CO_2. Glutathione-containing oligomer solutions were prepared at the appropriate concentration, and 10 μL of the solution was added to each well. The plate was incubated for 24 h at 37 °C, 5% CO_2. Dye solution containing MTT (15 μL) was added to each well and was allowed to incubate for 4 h at 37 °C, 5% CO_2. Solubilization/stop solution (100 μL) was added to each well and the plate was incubated for 1 h at 23 °C in a sealed box. Absorbance at 570 nm was measured for each well using a SpectraMax M5 microplate reader (Molecular Devices Corp.). Concentrations of both GS-PEG-SG and GS-SPEGS-GS oligomers were varied as such: 100, 125, 250, 500, and 1000 μM of oligomer, as well as 100 μM of H_2O_2. The assay also consisted of three controls, one neutral control containing only media, a positive control (100 μM GSH) and negative control (100 μM H_2O_2)

11.4 Results and Discussion

GS-PEG-SG oligomers were synthesized via Michael addition according to Scheme 11.1,

where Michael donors were GSH and Michael acceptors were PEGDA oligomers. PEG was used due to its well-established biocompatibility, low immunogenicity, low antigenicity, and low toxicity.[50] In the presence of base, the thiol of GSH is readily deprotonated, and the thiolate serves as a nucleophile and adds to the Michael acceptor. To demonstrate a successful Michael strategy, three molecular weights of GS-PEG-SG were synthesized using 300, 575, and 700 g/mol PEGDA. The final compositions were confirmed using ^{1}H NMR spectroscopy and FAB-MS. In the ^{1}H NMR spectrum, the most notable change was the disappearance of peaks attributed to C=C functional groups at 5.8 – 6.3 ppm.

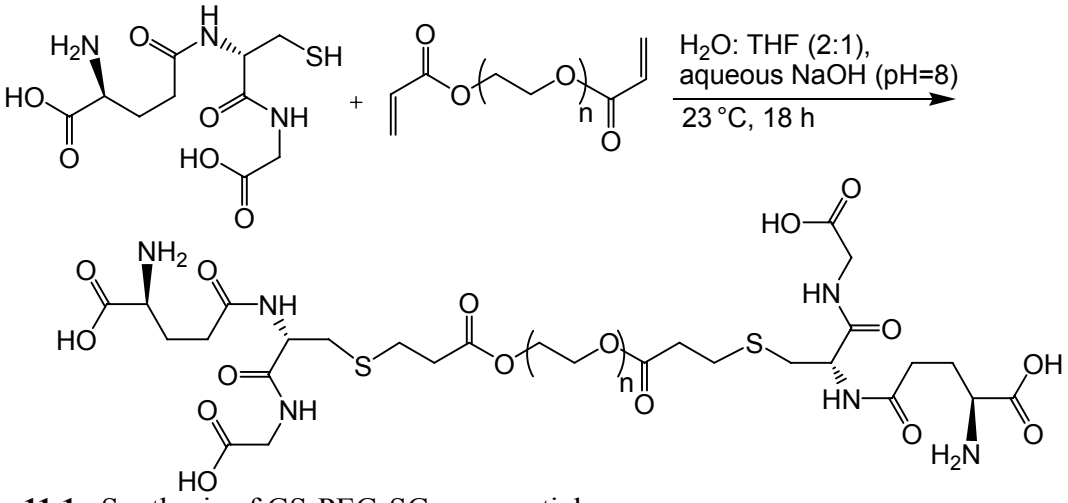

Scheme 11.1. Synthesis of GS-PEG-SG nanoparticles.

Dilute solutions in nanopure water were required for proper DLS investigations. Solutions of 10 mg/mL were prepared, and a minimum of five replicates were analyzed. Interestingly, DLS revealed that GS-PEG-SG formed monodisperse, uniform nanoparticles in aqueous solution. The average particle size determined for the GS-PEG575-SG nanoparticles was 283 ± 4 nm, as shown in Figure 11.2. It was proposed that the nanoparticles formed due to self-assembled aggregation and phase separation of internal PEG segments from glutathione external segments. Messersmith et al. and Kros et al. have reported the synthesis of PEG-peptide conjugates, and both groups proposed that a PEG shell coated the peptide core in the

aggregates.[51,52] In addition, peptides are known to form various shaped nanostructures, such as spheres, coiled coils, and fibrils, due to the propensity for inter- and intramolecular hydrogen bonding.

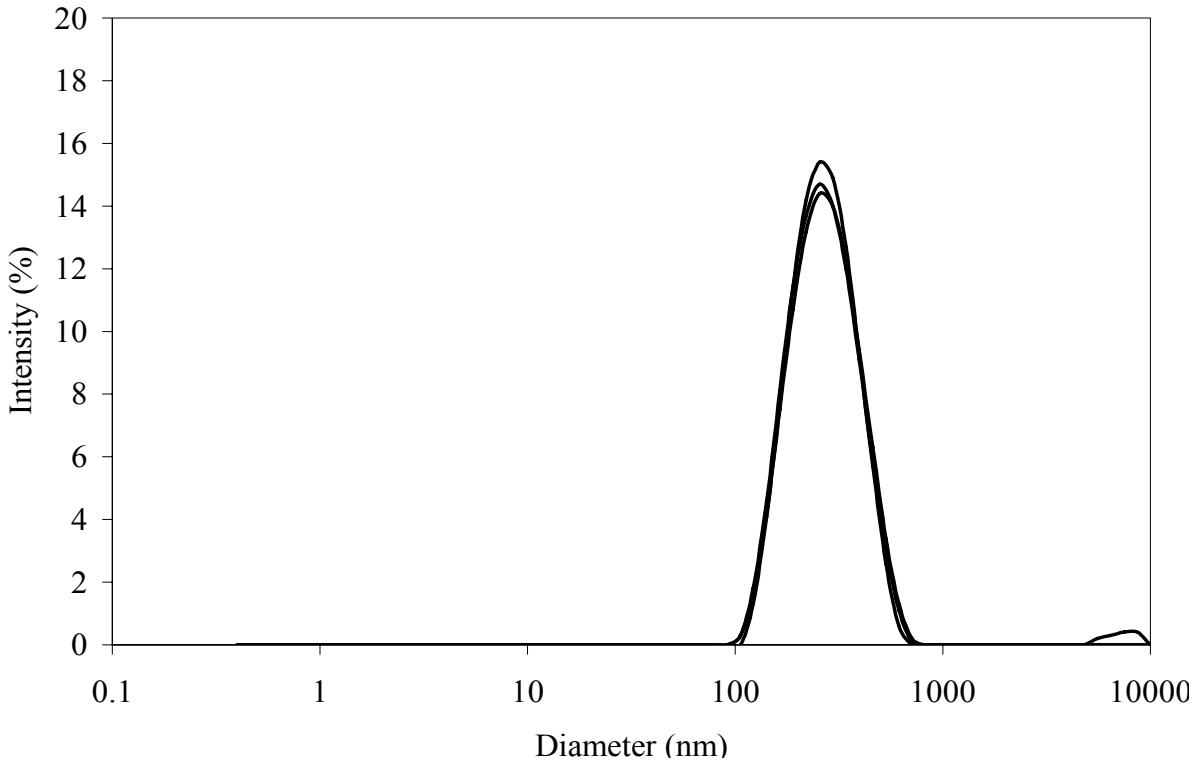

Figure 11.2. Dynamic light scattering of GS-PEG575-SG nanoparticles. Conditions: 10 mg/mL, 25 °C.

To further confirm the existence of nanoparticles, TEM was employed to investigate the nanoscale morphology. Aqueous solutions (1 mg/mL) of GS-PEG575-SG were prepared and slowly coated onto carbon-coated TEM grids, and the water was allowed to evaporate slowly over 24 h. TEM analysis revealed the existence of monodisperse GS-PEG575-SG nanoparticles that were approximately 100 nm (Figure 11.3). The discrepancy in size was attributed to the presence of water in DLS investigations and the absence of water in TEM experiments. Obviously water solvated the nanoparticles in the DLS experiments, since the size of the nanoparticles in aqueous solution increased ~180 nm.

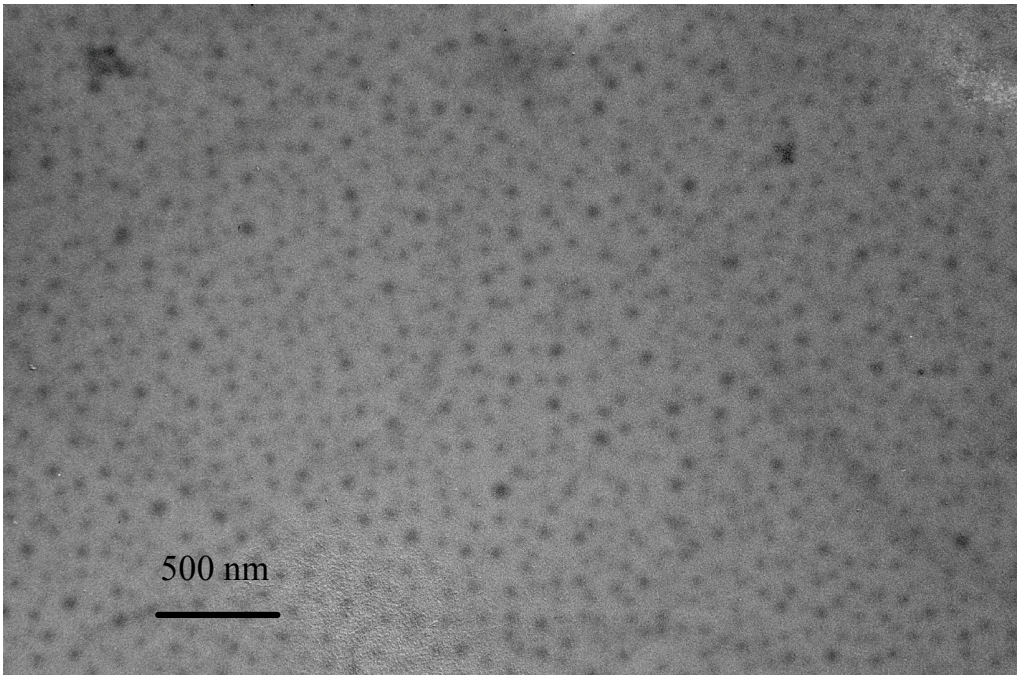

Figure 11.3. TEM micrograph of GS-PEG575-SG nanoparticles. Scale bar = 500nm.

In addition, DLS was employed to determine the change in particle size as a function of molecular weight. However, a consistent trend in particle size for this narrow range of molecular weight was not observed, although uniformly sized particles for all three samples were observed. As shown in Table 11.2, the particle sizes were 283 ± 23, 283 ± 4, and 315 ± 39 for GS-PEG300-SG, GS-PEG575-SG, and GS-PEG700-SG oligomers, respectively. Overall, the particle diameter increased when 700 g/mol PEGDA was used in the Michael reaction; however, the measured diameter was not considered significant due to the error in particle size measurement. The insignificant change in particle size was expected,[53] since the large diameter from DLS measurements indicated that self-assembled aggregates formed, instead of individual molecules.

Oligomer	Diameter (nm)
GS-PEG300-SG	283 ± 23
GS-PEG575-SG	283 ± 4
GS-PEG700-SG	315 ± 39

Table 11.2. Particle diameter measured via DLS as a function of PEG molecular weight.

Each of the three GS-PEG-SG oligomers was reacted with FITC in a stoichiometric fashion to react with the amine functional groups of the glutathione external segments (Scheme 11.2). The reaction mixture was passed through a Sephadex G-25 column to obtain pure oligomer product and ensure that free dye was not present. UV-vis spectroscopy confirmed the attachment of the dye to the GS-PEG-SG, since an absorbance was observed at 275 nm (GSH) and 495 nm (FITC) for all FITC-labeled GS-PEG-SG oligomers (Figure 11.4).

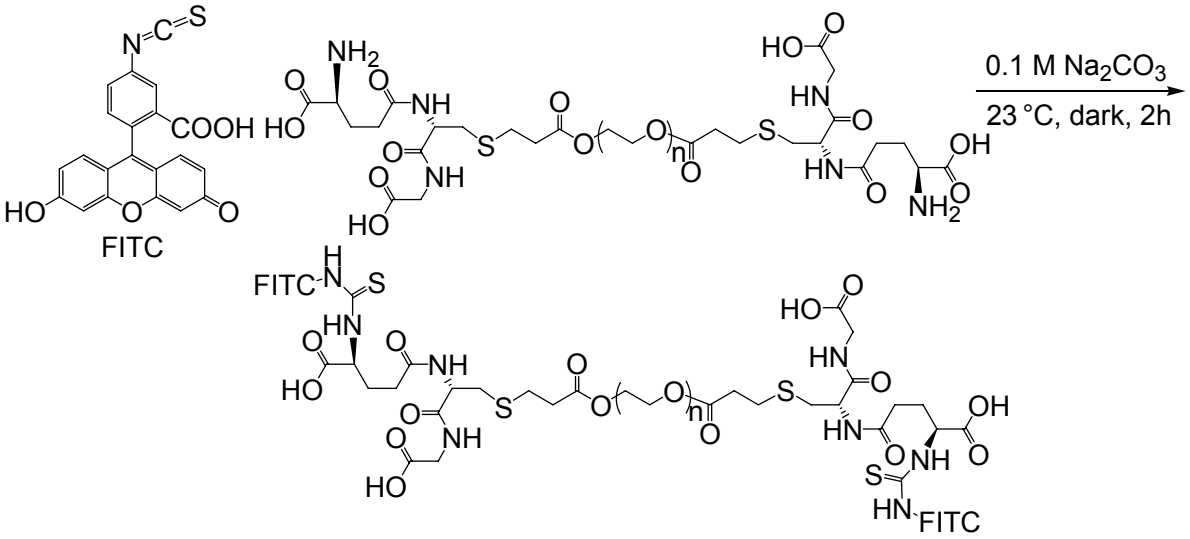

Scheme 11.2. Synthesis of FITC-labeled GS-PEG-SG nanoparticles.

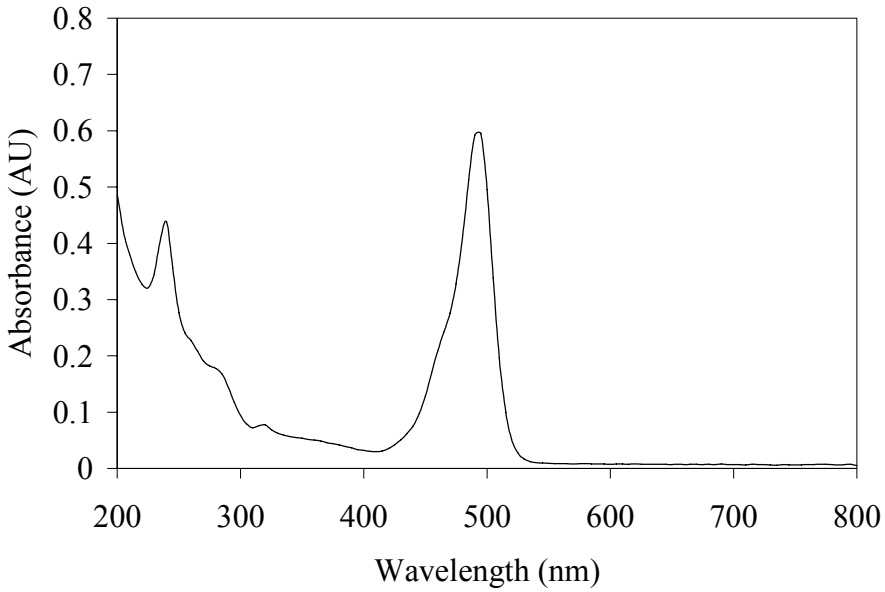

Figure 11.4. UV-vis spectrum of FITC-labeled GS-PEG-SG nanoparticles.

A fluorescent green color was observed when FITC modified GS-PEG-SG oligomers were subjected to an argon laser operating at 488 nm in the presence of a confocal microscope. Confocal microscopy revealed monodisperse particles in solution, although the resolution of the microscope was only 1 μm (Figure 11.5, GS-PEG575-SG). Essentially, confocal microscopy was utilized to observe if large scale aggregates formed. It is significant to note that the appearance of the FITC fluorescence was evenly distributed over the entire microscope viewing area, which indicated a lack of large-scale aggregates. Similar results were observed for GS-PEG300-SG and GS-PEG700-SG (data not shown).

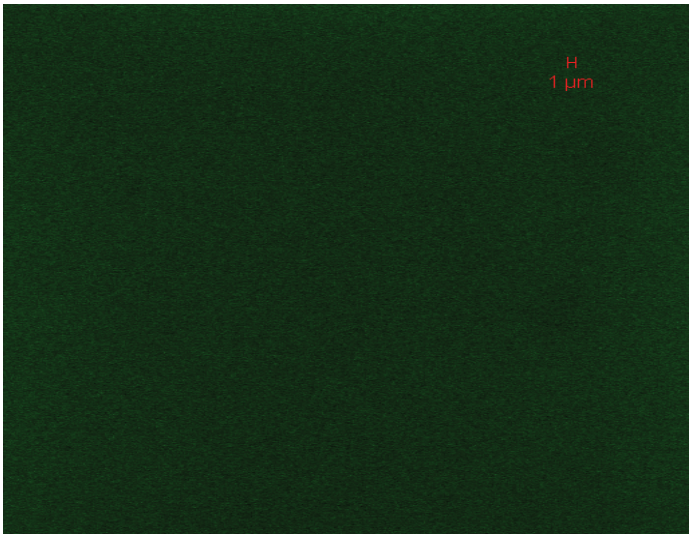

Figure 11.5. Confocal microscopy of FITC-labeled GS-PEG575-SG nanoparticles. Scale bar = 1 µm.

Thermal analysis of the GS-PEG-SG oligomers was conducted via TGA and DSC. As shown in Table 11.3, the T_g was dependent on PEG molecular weight. The T_g was the highest for GS-PEG700-SG (-35 °C), and decreased as the PEG molecular weight decreased to 575 g/mol (-57 °C). DSC did not reveal a T_g for the oligomer possessing the lowest molecular weight PEG segment. It is well-known that as molecular weight increases, T_g increases to a certain level, after which it plateaus.[54,55] The results herein were consistent with that general observation. The degradation temperatures were similar for all modified PEG oligomers, and GS-PEG300-SG, GS-PEG575-SG, GS-PEG700-SG possessed degradation onset temperatures of 168 °C, 165 °C, and 160 °C, respectively.

Oligomer	**T_g (°C)**	**$T_{d\ onset}$ (°C)**
GS-PEG300-SG	--	168
GS-PEG575-SG	-57	165
GS-PEG700-SG	-35	160

Table 11.3. Thermal properties of GS-PEG-SG nanoparticles.

Since the oligomers formed monodisperse nanoparticles, antioxidant delivery was proposed as a potential application. However, glutathione acts as an antioxidant through its thiol functionality;[36,37] therefore, the above described GS-PEG-SG nanoparticles were not viable options for antioxidant delivery systems since the thiol groups were consumed during Michael addition. A disulfide bridge was proposed for successful antioxidant delivery. A disulfide linkage would release the antioxidant when the pH was low enough to enable thiol formation. Therefore, thiol-terminated PEG, HS-PEG-SH, was synthesized according to Brash et al (Scheme 11.3).[48] A 600 g/mol PEG oligomer was used in the synthesis to ensure that the resulting conjugate would possess a comparable molecular weight to GS-PEG575-SG. The structure and difunctionality of HS-PEG-SH was confirmed using ^{1}H NMR spectroscopy. In addition, FT-IR spectroscopy was used to determine external segment structure, as shown in Figure 11.6. Prior to the addition of the thiol functionality, the presence of hydroxyl functionality was clearly observed at ~3300 cm^{-1}. After a reaction of mercaptoacetic acid with PEG, disappearance of hydroxyl functionality was observed, and the appearance of two thiol peaks (2555 cm^{-1} (S-H) and 751 cm^{-1} (C-S)) and one carbonyl peak (1739 cm^{-1}) were also observed.

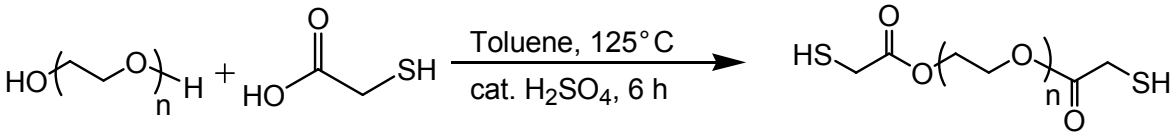

Scheme 11.3. Synthetic strategy for thiol-terminated PEG.

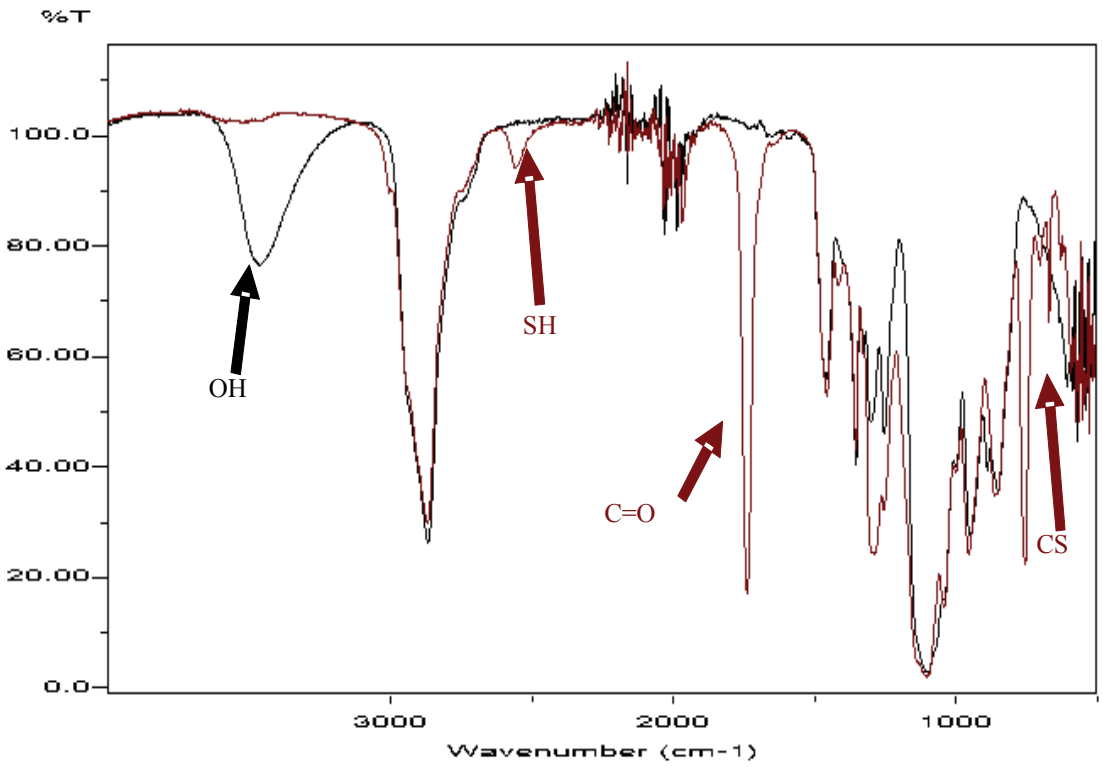

Figure 11.6. FT-IR spectroscopy of HO-PEG-OH (black, OH indicated with arrow) and HS-PEG-SH (red, SH and C=O indicated with arrows).

To prepare oligomers possessing disulfide linkages, the synthetic strategy shown in Scheme 11.4 was used. The pH was altered in a manner to ensure the reaction medium was slightly basic throughout the reaction in order to facilitate disulfide linkage formation. The structure was confirmed via ^{1}H NMR spectroscopy and FT-IR spectroscopy (Figure 11.7). The disappearance of the thiol functional group (S-H) at 2555 cm^{-1} was indicative of disulfide formation. Furthermore, TGA analysis revealed that GS-SPEGS-SG possessed an onset of degradation temperature at 174 °C, which was only slightly higher than the degradation temperature of the Michael-derived GS-PEG-SG nanoparticles. Thus, the impact of the disulfide linkage on thermal stability of the antioxidant particles was minimal. However, this data suggested that the nanoparticles were stable at physiological temperatures.

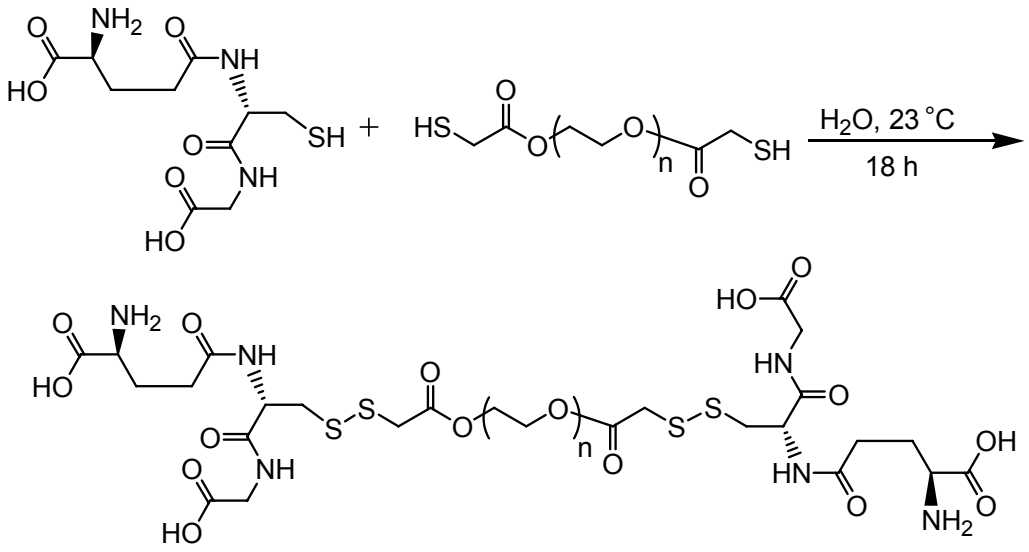

Scheme 11.4. Synthesis of GS-SPEGS-SG.

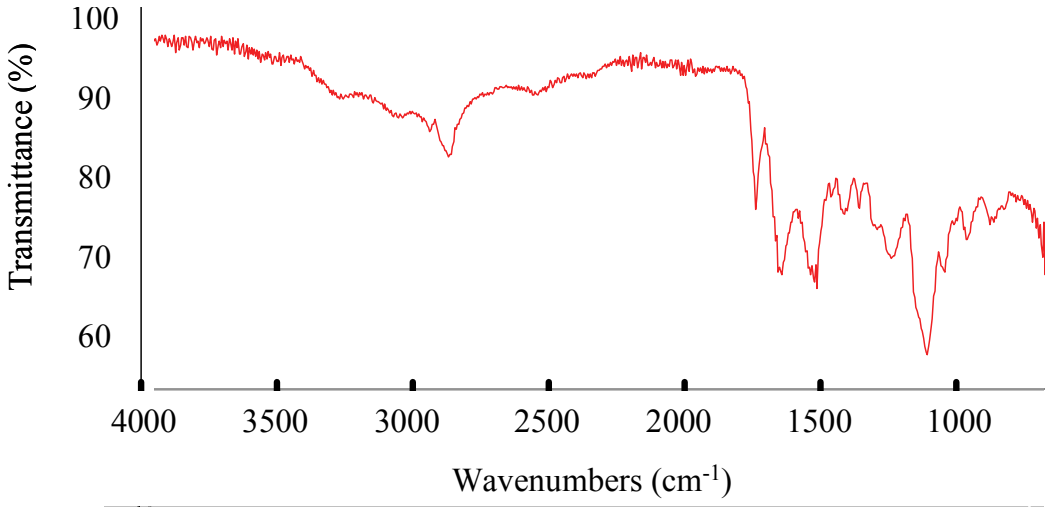

Figure 11.7. FT-IR spectrum of GS-SPEGS-SG, where disappearance of thiol S-H is noticable.

Oxidative stress imparts an imbalance of healthy ROS levels in cells causing damage to membrane lipids and proteins. H_2O_2 is often employed to induce oxidative stress on otherwise healthy cells to monitor oxidative stress in an *in vitro* model.[56] In the present investigation, SH-SY5Y cells were exposed to oxidative stress conditions with various concentrations of H_2O_2 (25 – 800 μM) for 24 h at 37 °C and subsequently were assessed for cell viability (Figure 11.8). As expected, cell viability decreased with increased H_2O_2 concentration in a dose-dependent

manner. The results of the H_2O_2 induced toxicity were consistent with results that Yu et al. described for SH-SY5Y cells.[57]

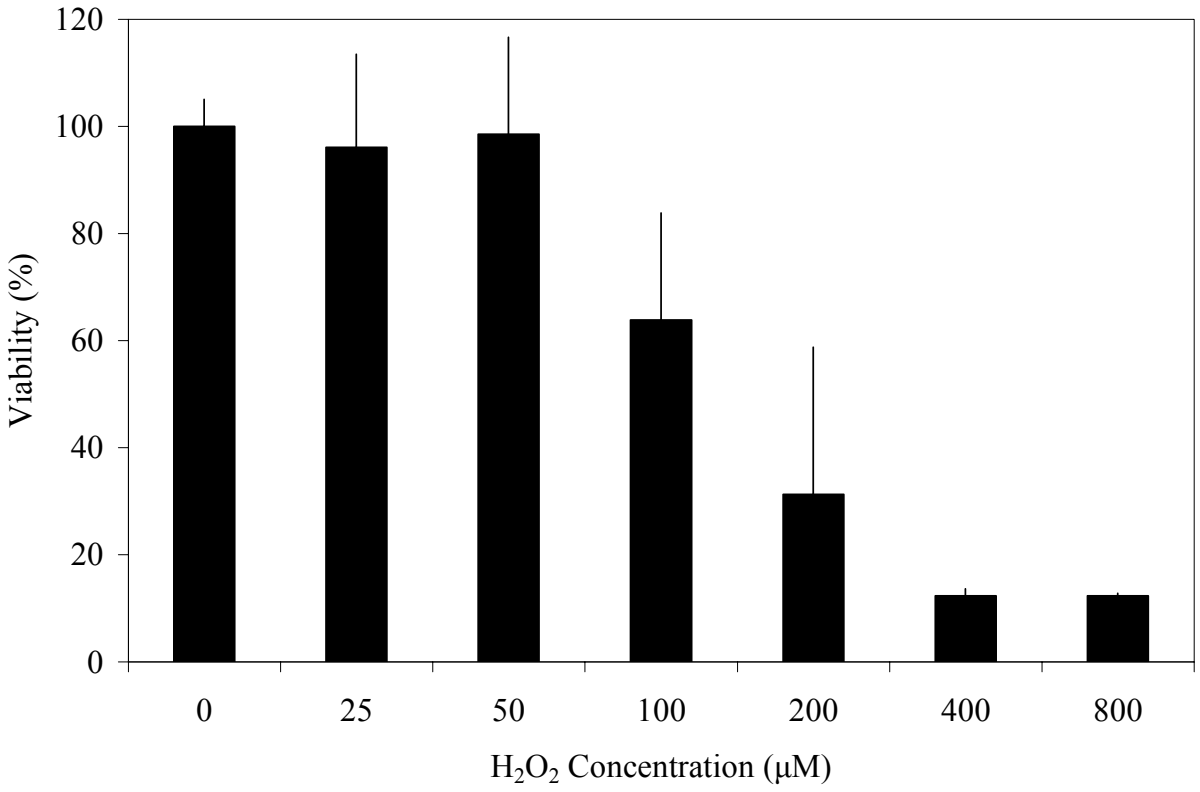

Figure 11.8. SH-SY5Y cell viability in the presence of various concentrations of H_2O_2. Viability determined with conventional MTT assay methodologies.

SH-SY5Y cells were incubated for 24 h in the presence of various concentrations of either Michael addition glutathione oligomers or disulfide-linked glutathione oligomers. After the 24 h incubation time, 100 μM H_2O_2 was added to induce oxidative stress. The MTT assay results are shown in Figure 11.9 and Figure 11.10 for the Michael addition glutathione oligomers and disulfide-linked glutathione oligomers, respectively. As expected, the Michael addition glutathione oligomers performed poorly, and did not protect the cells from oxidative damage, despite extremely high levels (500 and 1000 μM). As a positive control, SH-SY5Y cells were also treated with 100 μM GSH. As shown in both figures, GSH protected the cells from

oxidative stress, and nearly 100 % viability results were observed. A negative control, 100 μM H_2O_2, was also utilized in the experiments, and nearly 70 % of the cells were viable. As shown in Figure 11.9, the Michael addition oligomers were nearly as toxic as 100 μM H_2O_2.

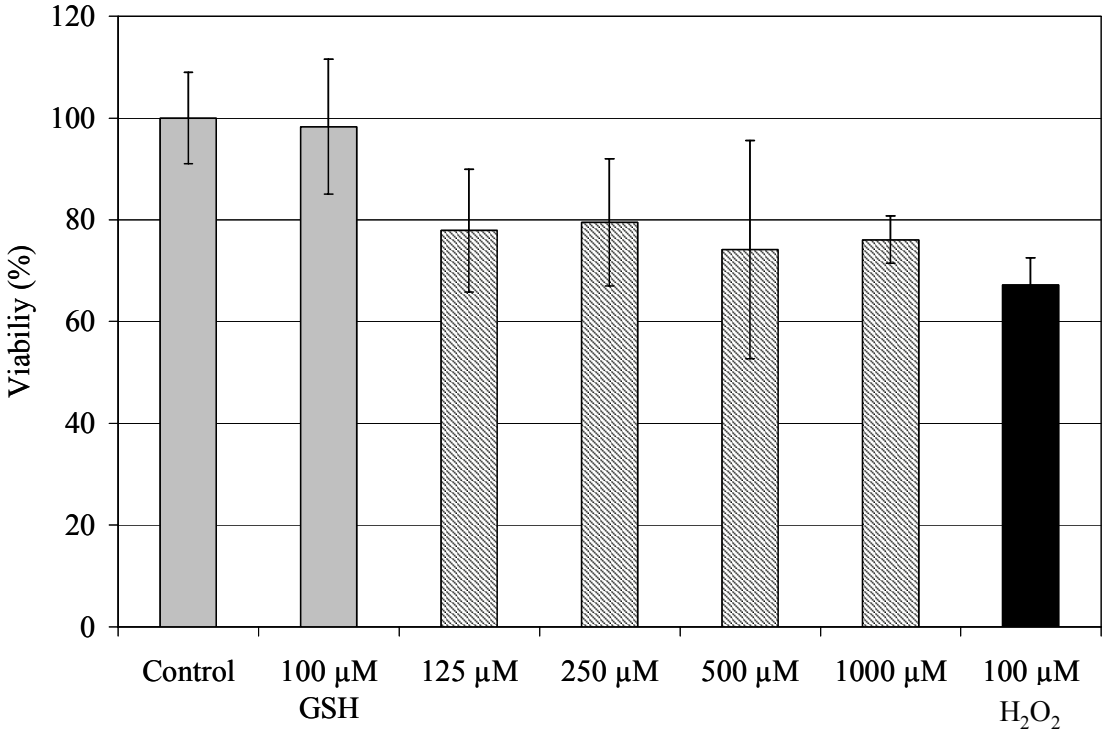

Figure 11.9. MTT assay results for GS-PEG 575-GS in the presence of 100 μm H_2O_2.

Conversely, GS-SPEGS-SG oligomers protected the cells from oxidative damage that resulted from exposure to 100 μM H_2O_2. The results of the MTT assay are shown in Figure 11.10. In this instance, the disulfide-linked glutathione oligomers were protective and helped to maintain cell viability. At 125 μM, approximately 80 % of the SH-SY5Y cells were viable. However, it was noted that a single 250 μM dose was sufficient to maintain 100 % cell viability. At higher GS-SPEGS-SG doses, cell viability was ≥ 100 %. Although a higher dose of GS-SPEGS-SG was required to protect the cells, relative to the positive control GSH, there are positives and negatives associated with both treatment strategies. First, perhaps the PEG

oligomer helped to protect the GSH until it was effectively delivered to the cell. Second, realizing now that the disulfide-linked glutathione oligomers were beneficial to the cells under oxidative stress, new delivery systems with active targeting vectors attached to PEG oligomers may enhance the therapeutic effects of the antioxidant delivery system.

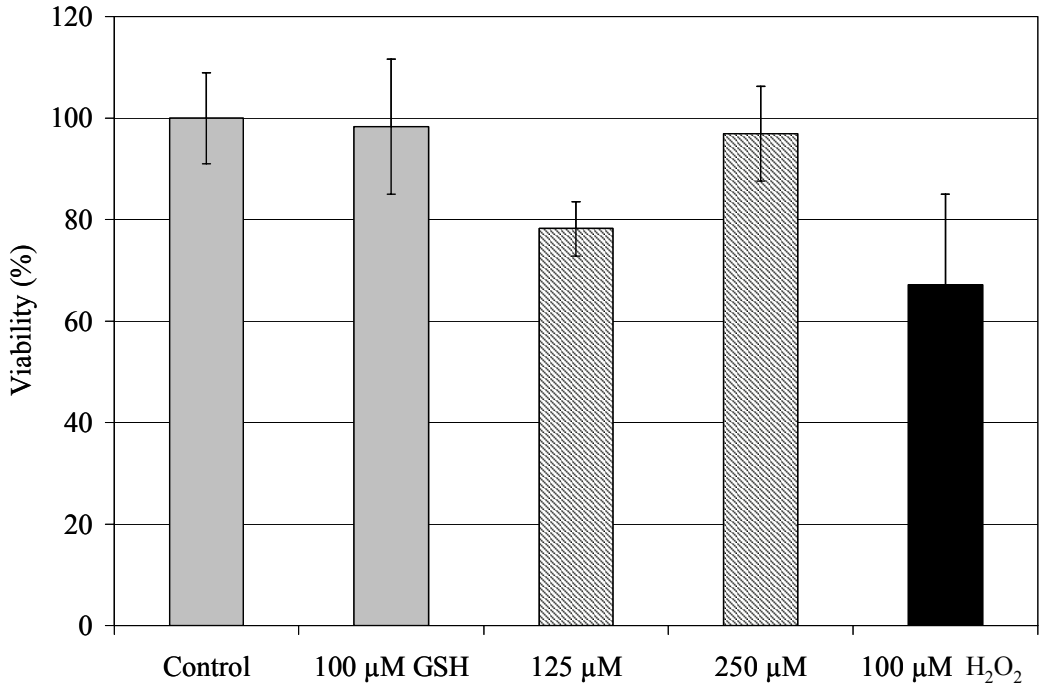

Figure 11.10. MTT assay results for GS-SPEGS-GS in the presence of 100 μM H_2O_2.

11.5 Conclusions

Novel Michael addition oligomers based on PEG and GSH were synthesized. DLS and TEM results indicated the formation of uniform nanoparticles, with sizes of 283 ± 4 nm via DLS measurements and ~100 nm via TEM. In addition, thiol-terminated PEG was synthesized and reacted with GSH to form novel disulfide-linked oligomers. SH-SY5Y cells were utilized in cell culture experiments, and oxidative stress was induced on the cells with H_2O_2. The Michael addition glutathione oligomers were not effective against protecting the cells from oxidative

stress, since the C-S bond was not labile. However, GS-SPEGS-SG oligomers were nearly 100 % effective at protecting the cells at 250 μM. With appropriate targeting reactive groups, perhaps targeted antioxidant delivery systems similar to those described herein could be employed for treating diseases typically associated with increased levels of ROS.

11.6 Acknowledgements

The authors acknowledge the financial support of the Macromolecular Interfaces with Life Sciences (MILES) Integrative Graduate Education and Research Traineeship (IGERT) of the National Science Foundation under agreement number DGE-0333378. This material is based upon work supported in part by the U.S. Army Research Office under grant number W911NF-07-1-0452 Ionic Liquids in Electro-Active Devices (ILEAD) MURI. The authors thank Kristi DeCourcy for assistance with confocal microscopy and Kristel Fuhrman for assistance with cell culture techniques.

11.7 References

(1) Cottone, R. J. J.; Rowland, S. M.; Davis, H. R.; Kutryk, M. J. B. Progenitor endothelial cell capturing with a drug eluting implantable medical device. US 20050271701, 2005.
(2) Coviello, T.; Alhaique, F.; Parisi, C.; Matricardi, P.; Bocchinfuso, G.; Grassi, M. *J. Controlled Release* **2006,** 102, 643-656.
(3) Espuelas, M. S.; Legrand, P.; Loiseau, P. M.; Bories, C.; Barratt, G.; Irache, J. M. *J. Drug Targeting* **2002,** 10, (8), 593-599.
(4) Gref, R.; Minamitake, Y.; Peracchia, M. T.; Trubetskoy, V.; Torchilin, V.; Langer, R. *Science* **1994,** 263, (5153), 1600-1603.
(5) Li, H.; Tran, V. V.; Hu, Y.; Saltzman, W. M.; Barnstable, C. J.; Tombran-Tink, J. *Exp. Eye Res.* **2006,** 83, (4), 824-833.
(6) Line, B. R.; Mitra, A.; Nan, A.; Ghandehari, H. *J. Nucl. Med.* **2005,** 46, (1552-1560).
(7) Olivier, L. Pharmaceutical compositions comprising polyethylene glycol having a molecular weight of less than 600 daltons. WO 2005120453, 2005.
(8) Ye, S.; Wang, C.; Liu, X.; Tong, Z.; Ren, B.; Zeng, F. *J. Controlled Release* **2006,** 112, (1), 79-87.
(9) Funhoff, A. M.; van Nostrum, C. F.; Lok, M. C.; Kruijtzer, J. A. W.; Crommelin, D. J. A.; Hennink, W. E. *J. Controlled Release* **2005,** 101, 233-246.
(10) Reches, M.; Gazit, E. *Science* **2003,** 300, 625-627.

(11) Hartgerink, J. D.; Granja, J. R.; Milligan, R. A.; Ghadiri, M. R. *J. Am. Chem. Soc.* **1996,** 118, (1), 43-50.
(12) Kisiday, J.; Jin, M.; Kurz, B.; Hung, H.; Semino, C.; Zhang, S.; Grodzinsky, A. J. *Proc. Natl. Acad. Sci. USA* **2002,** 99, (15), 9996.
(13) Claussen, R. C.; Rabatic, B. M.; Stupp, S. I. *J. Am. Chem. Soc.* **2003,** 125, (42), 12680-12681.
(14) Kiick, K. L. *Soft Matter* **2008,** 4, (1), 29-37.
(15) Nie, T.; Baldwin, A.; Yamaguchi, N.; Kiick, K. L. *J. Controlled Release* **2007,** 122, (3), 287-296.
(16) Zhang, L.; Furst, E. M.; Kiick, K. L. *J. Controlled Release* **2006,** 114, (2), 130-142.
(17) Yamaguchi, N.; Chae, B. S.; Zhang, L.; Kiick, K. L.; Furst, E. M. *Biomacromolecules* **2005,** 6, (4), 1931-1940.
(18) Yamaguchi, N.; Kiick, K. L. *Biomacromolecules* **2005,** 6, (4), 1921-1930.
(19) Yamaguchi, N.; Zhang, L.; Chae, B. S.; Palla, C. S.; Furst, E. M.; Kiick, K. L. *J. Am. Chem. Soc.* **2007,** 129, (11), 3040-+.
(20) Rizzi, S. C.; Ehrbar, M.; Halstenberg, S.; Raeber, G. P.; Schmoekel, H. G.; Hagenmuller, H.; Muller, R.; Weber, F. E.; Hubbell, J. A. *Biomacromolecules* **2006,** 7, (11), 3019-3029.
(21) Rizzi, S. C.; Hubbell, J. A. *Biomacromolecules* **2005,** 6, (3), 1226-1238.
(22) Gerschman, R.; Gilbert, D. L.; Nye, S. W.; Dwyer, P.; Fenn, W. O. *Science* **1954,** 119, (3097), 623-626.
(23) Gilbert, D. L. *Persp. Biol. Med.* **1960,** 4, 58-71.
(24) Gilbert, D. L., Fifty years of radical ideas. In *Reactive oxygen species from radiation to molecular biology: A festschrift in honor of Daniel L. Gilbert*, Chiueh, C. C., Ed. The New York Academy of Sciences: New York, 2000; Vol. 899, pp 1-14.
(25) Ames, B. N.; Shigenaga, M. K., Oxidants are a major contributor to cancer and aging. In *DNA and free radicals*, Halliwell, B.; Aruoma, O. I., Eds. Ellis Horwood Limited: New York, 1993; pp 1-15.
(26) Geurrieri, F.; Pellecchia, G.; Papa, S., Reactive oxygen species and alteration of F0F1-ATP synthase in aging and liver regeneration. In *Free radicals, oxidative stress, and antioxidants pathological and physiological significance*, Ozben, T., Ed. Plenum Press: New York, 1998; Vol. 296, pp 109-119.
(27) Gonzalez-Lima, F.; Valla, J.; Cada, A., Brain cytochrome oxidase activity and how it relates to the pathophysiology of memory and Alzheimer's disease. In *Free radicals, oxidative stress, and antioxidants pathological and physiological significance*, Ozben, T., Ed. Plenum Press: New York, 1998; Vol. 296, pp 205-227.
(28) Stadtman, E. R., The role of free radical mediation of protein oxidation in aging and disease. In *Free radicals, oxidative stress, and antioxidants pathological and physiological significance*, Ozben, T., Ed. Plenum Press: New York, 1998; Vol. 296, pp 131-143.
(29) Shiva, S.; Oh, J. Y.; Landar, A. L.; Ulasova, E.; Venkatraman, A.; Bailey, S. M.; Darley-Usmar, V. M. *Free Radical Biol. Med.* **2005,** 38, (3), 297-306.
(30) Beyer, R. E. *Free Rad. Biol. Med.* **1990,** 8, (6), 545-565.
(31) Abuja, P. M. A., R. *Clin. Chim. Acta* **2001,** 306, (1-2), 1-17.
(32) Halliwell, B.; Gutteridge, J. M. C., *Free Radicals in Biology and Medicine*. 3rd ed.; Oxford Science Publications: Oxford, 1999.
(33) Al-Malaika, S. *Int. Mat. Rev.* **2003,** 48, (3), 165-185.

(34) Gutteridge, J. M. C., Iron in free radical reactions and antioxidant protection. In *Free radicals, oxidative stress, and antioxidants pathological and physiological significance*, Ozben, T., Ed. Plenum Press: New York, 1998; Vol. 296, pp 1-14.
(35) O'Connor, J. E.; Kimler, B. F.; Morgan, M. C.; Tempas, K. J. *Cytometry A* **1988,** 9, (6), 529 - 532.
(36) Masella, R.; Benedetto, R. D.; Varı, R.; Filesi, C.; Giovannini, C. *J. Nutr. Biochem.* **2005,** 16, 577-586.
(37) Briviba, K.; Sies, H., Nonenzymatic antioxidant defense systems. In *Natural antioxidants in human health and disease*, Frei, B., Ed. Academic Press: San Diego, 1994; pp 107-122.
(38) Mather, B. D.; Viswanathan, K. V.; Miller, K. M.; Long, T. E. *Prog. Polym. Sci.* **2006,** 31, (5), 487-531.
(39) Robb, S. A.; Lee, B. H.; McLemore, R.; Vernon, B. L. *Biomacromolecules* **2007,** 8, (7), 2294-2300.
(40) Hiemstra, C.; van der Aa, L. J.; Zhong, Z.; Dijkstra, P. J.; Feijen, J. *Biomacromolecules* **2007,** 8, (5), 1548-1556.
(41) Hiemstra, C.; Van der Aa, L. J.; Zhong, Z.; Dijkstra, P. J.; Feijen, J. *Macromolecules* **2007,** 40, (4), 1165-1173.
(42) van de Wetering, P.; Metters, A. T.; Schoenmakers, R. G.; Hubbell, J. A. *J. Controlled Release* **2005,** 102, (3), 619-627.
(43) Heggli, M.; Tirelli, N.; Zisch, A.; Hubbell, J. A. *Bioconjugate Chem.* **2003,** 14, (5), 967-973.
(44) Metters, A.; Hubbell, J. *Biomacromolecules* **2005,** 6, (1), 290-301.
(45) Mather, B. D.; Williams, S. R.; Long, T. E. *Macromol. Chem. Phys.* **2007,** 208, (18), 1949-1955.
(46) Williams, S. R.; Mather, B. D.; Miller, K. M.; Long, T. E. *J. Polym. Sci. A-Polym. Chem.* **2007,** 45, (17), 4118-4128.
(47) Williams, S. R.; Miller, K. M.; Long, T. E. *Prog. React. Kin. Mech.* **2007,** 32, 165-194.
(48) Du, Y. J.; Brash, J. L. *J. Appl. Polym. Sci.* **2003,** 90, 594-607.
(49) Zhang, L., Yu, H., Sun, Y., Lin, X., Chen, B., Tan, C., Coa, G., Wang, Z. *European Journal of Pharmocology* **2007,** 564, 18-25.
(50) Alcantar, N. A.; Aydil, E. S.; Israelachvili, J. N. *J. Biomed. Mater. Res.* **2000,** 51, (3), 343-351.
(51) Collier, J. H.; Messersmith, P. B. *Adv. Mater.* **2004,** 16, (11), 907-910.
(52) Marsden, H. R.; Korobko, A. V.; Leeuwen, E. N. M. v.; Pouget, E. M.; Veen, S. J.; Sommerdijk, N. A. J. M.; Kros, A. *J. Am. Chem. Soc.* **2008,** 130, 9386-9393.
(53) Pourcelle, V.; Devouge, S.; Garinot, M.; Preat, V.; Marchand-Brynaert, J. *Biomacromolecules* **2007,** 8, (12), 3977-3983.
(54) Odian, G., *Priciples of Polymerization*. 4th ed.; Wiley-Interscience: Hoboken, 2004.
(55) Stevens, M. P., *Polymer Chemistry*. 3rd ed.; Oxford University Press: Oxford, 1999.
(56) Satoh, T.; Sakai, N.; Enokido, Y.; Uchiyama, Y.; Hatanaka, H. *J. Biochem.* **1996,** 120, 540-546.
(57) Zhang, L.; Yu, H.; Sun, Y.; Lin, X.; Chen, B.; Tan, C.; Cao, G.; Wang, Z. *Eur. J. Pharm.* **2007,** 564, 18-25.

Chapter 12 : Oxidative Degradation of Biological Macromolecules

12.1 Abstract

Sugar and protein based macromolecules offer potential applications in many areas including medical devices, drug delivery, and packaging. Thus, it is important to consider the degradation process that occurs while the macromolecule is exposed to oxygen. The primary focus of this literature review is the mechanism of oxidative degradation of biological macromolecules, specifically focusing on sugars and proteins. Free radical interactions with biologically derived materials and methods for minimizing the deleterious effects of free radical interactions are discussed. Furthermore, protein and sugar oxidation are investigated in detail. Finally, several methods for measuring oxidative stress are illustrated.

12.2 Scientific rational and perspective

When designing a structure, it is imperative to consider the degradation process that will occur during the lifetime of the material. Researchers have extensively studied the oxidation of synthetic polymers for decades. However, only in recent years have researchers incorporated naturally occurring molecules into synthetic macromolecular backbones and studied the oxidative degradation. There are many reasons for the inclusion of biologically derived materials, but the most obvious reason is the limited supply of petroleum-based chemicals that the world will have to face in future generations.[1,2] The use of biologically based materials generally also provides other advantage—lower toxicity.

Biologically based materials such as sugars and amino acids are easily modified into monomers that are used in polymerizations.[3-9] While incorporating sugars, amino acids, and

short peptides, it is important to consider how the materials compare in mechanical properties and performance to similar petroleum based products.

Sugar and protein based polymers have potential applications in many areas including medical devices,[3] drug delivery,[3] and packaging.[10] Thus, it is important to consider the degradation process that occurs while the material is exposed to oxygen. The basic mechanism of radical formation and the implication it has on biological macromolecules is described in further sections. The primary focus of this literature review is the mechanisms of oxidative degradation of biological macromolecules, specifically sugars and proteins.

12.3 Free radical interactions

12.3.1 Oxygen balance in biological systems

One of the greatest dilemmas of biological systems is their dependence on oxygen and their concurrent degradation due to oxidation. While oxygen is required for life in eukaryotic and prokaryotic cells, it promotes oxidative degradation of biological molecules via assisting in the formation of radical species.[11-13] It is hypothesized that oxygen was first produced during photosynthesis of blue-green algae.[14] In recent times, oxygen is thought of as a major contributor to the cause of many diseases and ailments including Alzheimer's disease, aging, ischemic injuries, and cancer.[15-18] Many researchers have collaborated to analyze this delicate balance of oxygen in a system. In the following section, the result of an imbalance in oxygen in biological and chemical systems is described.

12.3.1.1 Reactive oxygen species and their interactions with biological macromolecules

Oxidants, such as reactive oxygen species (ROS) and reactive nitrogen species (RNS), are typically radicals or molecules that convert other molecules into reactive species. For

example, peroxides are considered ROS because under the appropriate conditions, peroxides can undergo homolytic bond cleavage to yield two radical species. Typical ROS and RNS are shown in Table 12.1. ROS and RNS are formed in many ways, and X-rays, γ-rays, and ultraviolet rays are examples of radiation that can generate ROS. Furthermore, visible light can promote radical formation when the primary chromophore is transparent to the irradiation if a sensitizer is present. Alternatively, at high temperatures, not only is thermal degradation a likely pathway, a greater abundance of reactive species can form that will cause degradation of the biological or chemical compound. Xenobiotic agents, such as pollution from ozone, cigarette smoke, NO_2, and N_2O_2 also contribute to the production of ROS.

It is imperative to consider the consequence of forming ROS in biological systems, since macromolecules, such as proteins and DNA, are constantly bombarded with radicals produced via single-electron reactions in the body. The major contributor to production of ROS in the body is the mitochondria.[19] ROS are products of the electron transport chain, specifically during the redox reaction consisting of the reduction of oxygen to superoxide anion and the oxidation of ubisemiquinone radical in protein – lipid complexes I, II, and III in the inner membrane of the mitochondria. NADPH oxidases in neutrophils and macrophages also generate superoxide anion.[20,21] Other natural processes that produce ROS include lipid peroxidation, inflammatory responses, and oxidation of various electron carriers.[22] The formation of radicals causes consecutive one-electron oxidation reactions to occur, damaging the system, *in vivo* or *ex vivo*.

Alkoxyl radical	RO•
Hydroperoxide	ROOH
Hydroperoxyl radical	HOO•
Hypochlorite	$^{-}$OCl
Hydrogen peroxide	H_2O_2
Hydroxyl radical	HO•
Nitric oxide radical	NO•
Peroxyl radical	ROO•
Peroxynitrite	$ONOO^{-}$
Singlet Oxygen	$^{1}\Delta O_2$

Table 12.1. Reactive oxygen and nitrogen species.[23]

12.3.2 Radical reactions involving reactive oxygen species

The autoxidation process of polymers was first established in the 1940's following the British Rubber Producers Association's analysis of olefins.[24-26] Since then, researchers have extensively studied the basic mechanism of autoxidation, consisting of three major steps: initiation, propagation, and termination, as shown in Scheme 12.1.[27]

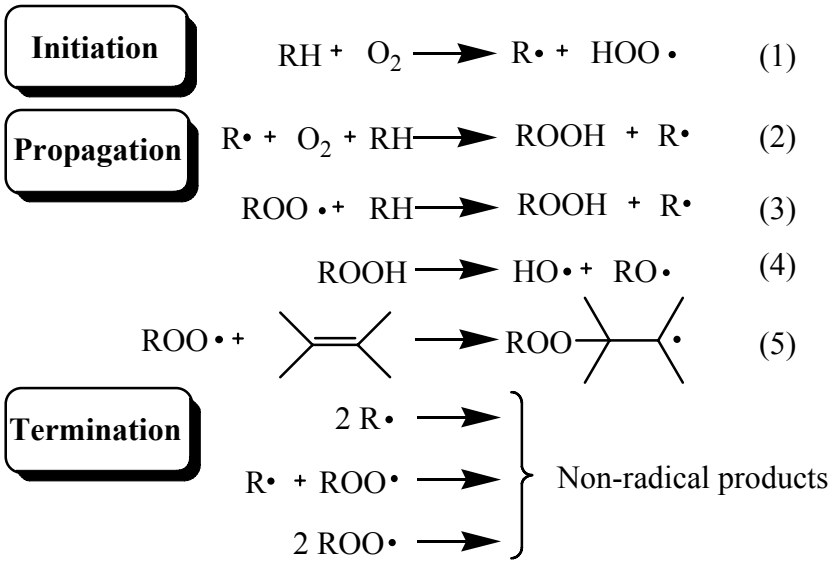

Scheme 12.1. The autoxidation reaction scheme.[27]

Due to the high bond dissociation energies of C – H (413 kJ/mol),[28] initiation is slow at room temperature, if it proceeds as shown in equation (1) of Scheme 12.1.[27] As oxidation proceeds, alkyl peroxides can decompose into alkyl peroxyl, hydroxyl, and alkoxyl radicals, which are favored over the radical species formed in the general initiation step mentioned above. A variety of factors influences the rate of alkyl peroxide decomposition, including the choice of solvent and whether acids or metals are present.[27] Propagation occurs via reactions (2), (3), (4), and (5) of Scheme 12.1. Reaction (2), a coupling reaction, proceeds with little to no activation energy; the rate constants are typically greater than 10^9 $M^{-1}s^{-1}$. The hydrogen abstraction reaction (3) occurs with activated C – H bonds, and is the rate-determining step in autoxidation. The low bond dissociation energy of HO-OR (~210 kJ/mol) allows reaction (4) to proceed in the formation of two radical species. Unsubstituted alkenes can react with peroxyl radicals (5). In many cases, poly(peroxide)s can form. Any of the last three reactions listed in Scheme 12.1 can cause termination.[27]

Radicals easily undergo disproportionation or dimerization reactions to form more stable oxidized and reduced products. Selectivity is a critical factor that one must take into account when considering the thermodynamics of a radical reaction. From enthalpies of formation and steric hindrance, dimerization is exceptionally favorable. However, according to Koppenol et al.,[29] disproportionation has an slightly higher enthalpic advantage to dimerization, in most cases, of several kJ/mol.

Radicals are both oxidizing and reducing, and must have some preference to react at sites that are stabilized through neighboring substituents. Such stabilizing substituents include heteroatoms and aromatic rings that can stabilize the unpaired electron through delocalization.[30] However, few radicals have the reactivity of the hydroxyl radical. Many research groups have shown that the hydroxyl radical is oxidizing and electrophilic.[29-31] The hydroxyl radical is formed in a variety of ways.[32] Since they are highly reactive electrophiles, hydroxyl radicals readily add to unsaturated bonds, abstract a proton from carbon atoms,[33] and oxidize hydroxyl functionalities.[34] Yet, due to the strength O – H bonds, it is much easier for a radical to react with C – H. In 1899, Fenton[35] showed that the hydroxyl radical is formed in a reaction of hydrogen peroxide with iron in the presence of hydrogen ions. This reaction is shown below with iron complexed to adenosine triphosphate (ATP).[30]

$$Fe^{2+}ATP + H_2O_2 + H^+ \longrightarrow Fe^{3+}ATP + HO\cdot + H_2O$$

In this process, a transition metal activates hydrogen peroxide, a ROS, to oxidize a substrate, as hydrogen peroxide has a high oxidation potential (E_0 = 1.76 V) in the half reaction:[33]

$$H_2O_2 + 2H^+ + 2e^- \longrightarrow 2\,H_2O$$

When hydrogen peroxide reacts with a transition metal such as Fe^{3+} or Fe^{4+}, it forms the Fenton reagents[35] via the Haber-Weiss[36] mechanism. Hydrogen peroxide, with a pK_a of 11.6, will rapidly form perhydroxyl anions (HOO^-) at an elevated pH when hydroxyl ions are present.[33]

While the above discussion details the formation of radical species, there are two additional aspects to consider in biological systems. First, the initial radical reaction takes a substantial amount of energy input to proceed. Usually, the first reaction with a macromolecule will not induce much damage to a biological or chemical system. The ensuing reactions that occur as a result of autoxidation are the origin for complete oxidative degradation. Secondly, since iron is present in biological systems, the hydroxyl radical can easily form. This has potential to result in severe biological consequences if there is an oxygen imbalance because hydroxyl radicals can react readily in a non-selective process.

12.3.3 Defense and repair mechanisms for biological and synthetic macromolecules

Oxidative stress is an imbalance of oxidants and antioxidants. To slow the process of oxidative degradation, antioxidants are synthesized naturally in a biological system or are incorporated during chemical synthesis. Antioxidants are synthetic or natural compounds that inhibit or slow the rate of oxidative damage resulting from ROS in a system. There are two key classes of antioxidants. Chain-breaking antioxidants, or primary antioxidants, eliminate radical species. Preventative antioxidants, or secondary antioxidants, obstruct radical formation. Primary antioxidants include sterically hindered phenols, sterically hindered aromatic amines, hydroxylamine, quinines, and lactones. Phosphite esters, thioesters, metal dithiolates, metal chelating molecules, 2-hydroxybenzophenone derivatives, and 2-hydroxybenzotriazole derivatives comprise the class of secondary antioxidants.[37] Antioxidants synthesized naturally

are superoxide dismutase, catalases, peroxidases, glutathione and other thiol containing compounds, urate, and ubiquinol.[31]

12.4 Protein oxidative degradation via reactive oxygen species

Research indicates that modification of proteins with reactive oxygen species plays a role in pathological disorders and aging.[38-44] The following section will discuss the intricate steps involved in amino acid degradation and hence modification of proteins. Following the next section is Table 12.2, which defines several rate constants for reactions of amino acids with various radical species, including HO•, HOO•, O_2•-, and H• at various pH.[30,37]

12.4.1 Oxidative degradation of amino acids

Researchers have previously determined that the exact sites of attack of ROS and the resulting products differ among aliphatic, aromatic and heterocyclic, and sulfur-containing amino acids. To understand the way in which amino acids degrade could help determine the degradation process of a protein. The following sections will summarize what researchers have discovered to this point. It is important to note the lack of research on oxidative degradation of more complex macromolecules, such as a synthetic polymer that incorporates a sugar or amino acid unit in the backbone. It is desirable to know the exact degradation process of these intricate structures, especially if the macromolecule is subjected to a living organism, in the form of a drug delivery vehicle or medical device.

12.4.1.1 Aliphatic amino acids

Amino acids with aliphatic substituents include glycine, alanine, valine, leucine, and isoleucine. In the absence of oxygen, these amino acids will form dimers upon radical hydrogen atom abstraction. With oxygen present, ROS can abstract a methylene proton and form a carbon

centered radical. Oxygen can then react with the radical to form peroxyl radicals. Hydroperoxides, hydroxides, or carbonyl compounds can then formed from peroxyl radicals.[30]

Serine, threonine, aspartic acid, asparagine, glutamic acid, glutamine, arginine, and lysine are aliphatic amino acids that contain a heteroatom—either oxygen or nitrogen in the substituent. The ROS appears to have increased selectivity when a heteroatom is part of the aliphatic substituent.[30]

Serine and threonine have side chains containing hydroxyl substituents that, upon ROS attack, are deprotonated alpha to the hydroxyl functionality. This occurs because the resulting radical is stabilized via the hydroxyl group (Scheme 12.2).

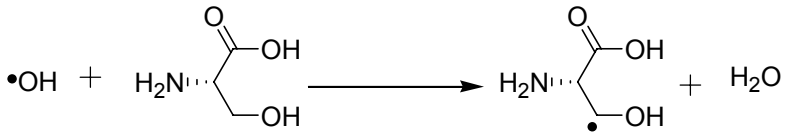

Scheme 12.2. Hydrogen atom abstraction of serine.

Lysine, having an amine functionality on the side chain, forms a carbon centered radical as a consequence of hydrogen atom abstraction on the fourth or fifth carbon in the side chain, as shown in Scheme 12.3. Interestingly, arginine's oxidative degradation results in a biomarker for protein damage as a result of radical attack. When the ROS abstracts a proton from the fourth carbon, 5-hydroxy-2-aminovaleric acid (HAVA) forms.[30]

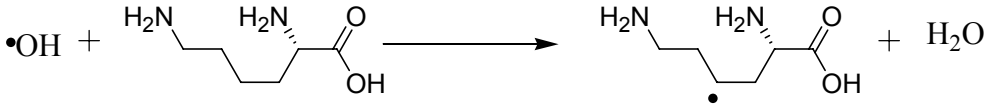

Scheme 12.3. Hydrogen atom abstraction of lysine.

12.4.1.2 Aromatic and heterocyclic amino acids

Typically, if an aromatic functionality is present, an addition reaction occurs on aromatic units of amino acids during oxidation rather than hydrogen atom abstraction. Histidine,

phenylalanine, tryptophan, tyrosine, and proline each contain either a heterocyclic or an aromatic substituent. Phenylalanine reacts with hydroxyl radicals to form tyrosine. Tyrosine forms 3,4-dihydrophenylalanine (DOPA) and rarely 2,4,5-trihydroxyphenylalanine (TOPA) as a result of hydroxyl radical addition to the phenyl ring. Although researchers have studied the formation of DOPA extensively, researchers have not studied the formation of TOPA.[30] The formation of DOPA from tyrosine is shown in Scheme 12.4. In addition, it is also possible to form tyrosine – tyrosine cross-links.

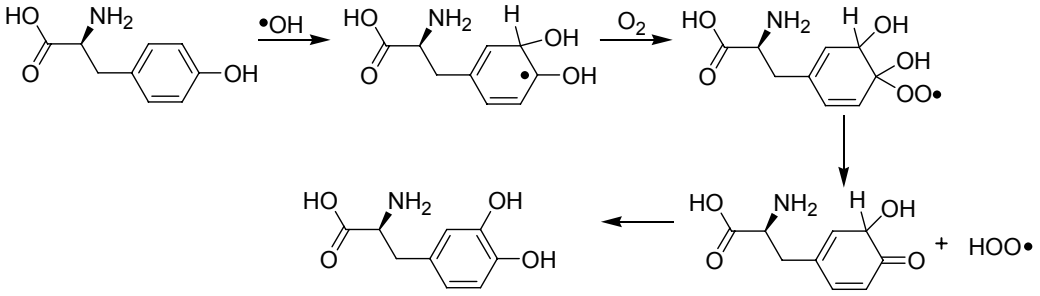

Scheme 12.4. Formation of 3, 4-dihydrophenylalanine (DOPA).[30]

Phenylalanine simply forms 2-, 3-, or 4-hydroxyphenylalanine upon attack via hydroxyl radical. If concentrations of ROS are great enough, dihydroxyphenylalanine species can form. Histidine residues will oxidize at rates that are dependent on the placement of the amino acid in the structure of the protein. Interestingly, under hydrolytic conditions, oxidized histidine can form aspartic acid.[45]

12.4.1.3 Amino acids containing sulfur atoms

Sulfur atoms impart special reactivity when concerning amino acid oxidation. Cysteine and methionine both contain sulfur in the pendant group of the amino acid. In the presence of oxygen, disulfide linkages form. Protein – protein intramolecular and intermolecular cross-links can form in this manner. In addition, cysteine and methionine can add hydroxyl, peroxyl, and acid functionalities upon oxidation. It is interesting that the cross-links are reversible. The

regeneration of both amino acids occurs in two ways: NADPH dependent hydrogenases and glutathione, which contains a thiol substituent.[30,46]

Substrate	Attacking Radical	Rate Constant ($dm^3\ mol^{-1}\ s^{-1}$)	pH
Glycine	HO·	1.7×10^7	5.8 - 6
	HOO·	< 49	1.5
	$O_2\cdot^-$	< 0.42	8.8
	H·	7.7×10^4	7
Alanine	HO·	7.7×10^7	5.5 - 6
Valine	HO·	7.6×10^8	6.6 - 6.9
	HOO·	< 10	1.5
	$O_2\cdot^-$	< 0.18	10.1
	H·	1.2×10^7	7
Leucine	HO·	1.7×10^9	5.5 - 6
Serine	HO·	3.2×10^8	5.5 - 6
Threonine	HO·	5.1×10^8	6.6
Cysteine	HO·	3.4×10^{10}	5.8 - 7
	H·	1.8×10^9	6
	HOO·	$< 6 \times 10^2$	1.4
	$O_2\cdot^-$	< 15	10.9
Cystine	HO·	2.1×10^9	6.5
Methionine	HO·	8.3×10^9	5.5 - 7
Aspartic Acid	HO·	7.5×10^7	6.8 - 7
Glutamic Acid	HO·	2.3×10^8	6.5
Lysine	HO·	3.5×10^7	6.6
Arginine	HO·	3.5×10^9	6.5 - 7.5
Asparagine	HO·	4.9×10^7	6.6
Phenylalanine	HO·	6.5×10^9	5.5 - 8
Tyrosine	HO·	1.3×10^{10}	4 - 7
Histidine	HO·	1.3×10^{10}	4 - 7
	HOO·	< 95	1.8
	$O_2\cdot^-$	< 1	10
Tryptophan	HO·	1.3×10^{19}	6.1 - 8.5
	H·	2×10^9	6
	$O_2\cdot^-$	< 24	10.6

Table 12.2. Rate constants of reactions of amino acids with radicals. [30,37]

12.4.2 Reactive oxygen species promoting peptide bond cleavage

The reactive hydroxyl radical can easily abstract an α-hydrogen from carbon on an amino acid within a peptide chain, thus producing a carbon centered radical. In the presence of oxygen, a peroxyl radical may form, which is capable of producing a peroxide. An autoxidative process can occur, in which both an alkoxyl radical and hydroxyl radical are formed, which can thus promote peptide bond cleavage, which leads to protein fragmentation.

12.4.3 Formation of carbonyl functionalities in amino acids

As described earlier, proteins can form reactive carbonyl groups when oxidized with ROS. Cleavage of a protein can occur and a carbonyl may form via the α-amidation pathway and diamide pathway, as Garrison et al. described in detail.[22,47] It is also possible to form carbonyls when glutamyl groups are oxidized, as shown in Scheme 12.5.[46,22]

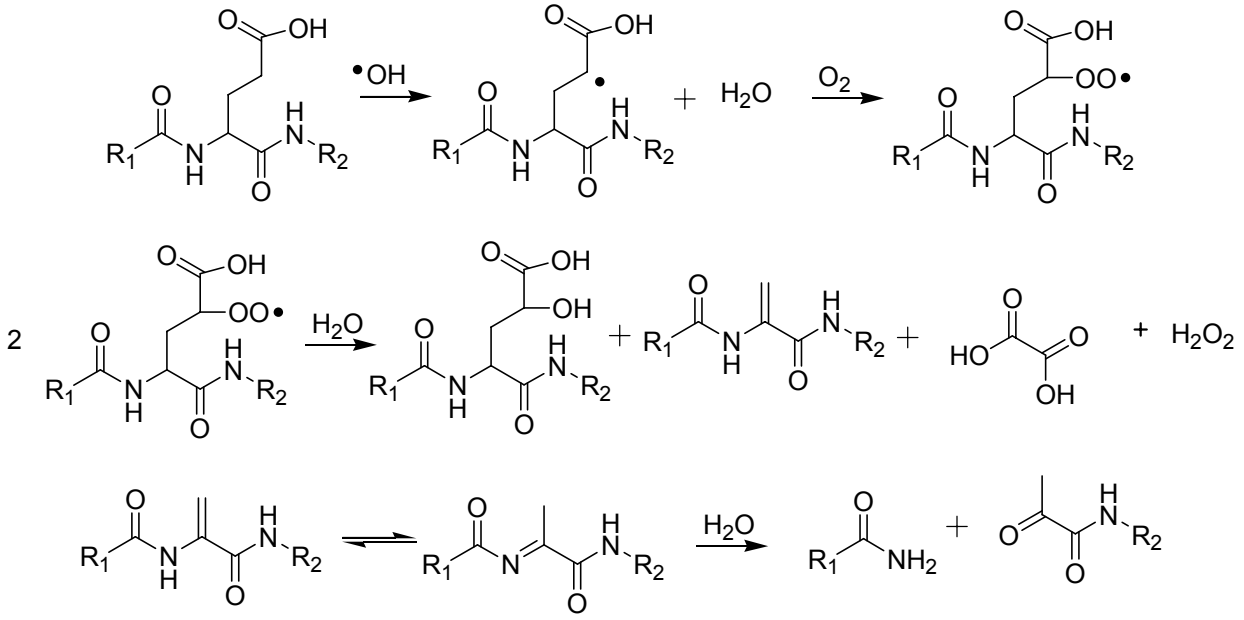

Scheme 12.5. Formation of carbonyl compounds upon oxidation of glutamyl residues. [47]

Lysine, arginine, proline, and threonine form various carbonyl containing species when subjected to metal catalyzed oxidation.[46] Lysine can also react with reducing sugars and their

oxidation products in glycation or glycoxidation reactions to form carbonyl groups, as shown in Scheme 12.6.[48]

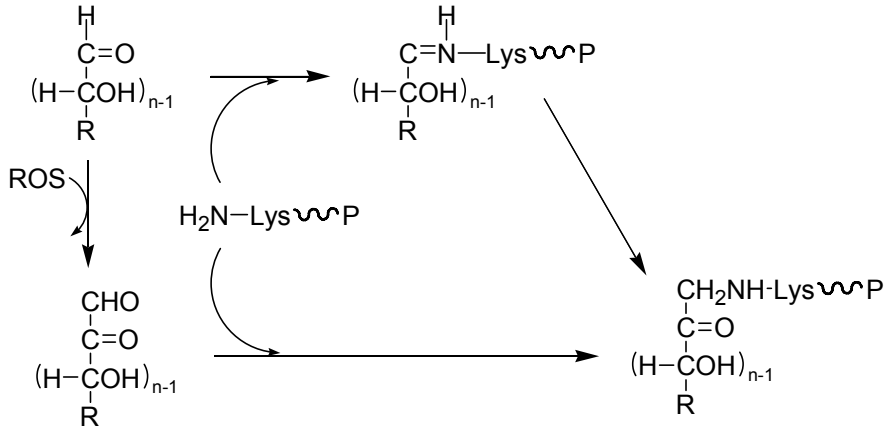

Scheme 12.6. Lysine oxidation though glycation – glycoxidation reaction. P represents the protein backbone.[48]

In addition, lysine, cysteine, or histidine amino acids can undergo carbon Michael addition reactions with α, β-peroxidation products of unsaturated fatty acids, such as 4-hydroxy-2-nonenal (HNE).[49,50] Products from this type of reaction for these amino acids is shown in Figure 12.1 below.

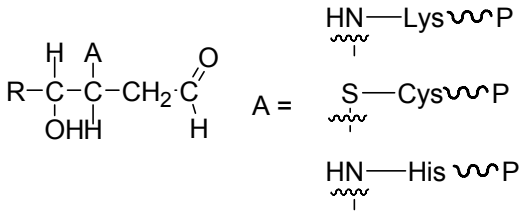

Figure 12.1. Oxidation products with carbonyl functionalities of proteins containing lysine, cysteine, and histidine.[48]

One can study oxidative damage to cells through the increase of carbonyl content of tissues. Oxidative damage due to ischemia reperfusion, hyperoxia, cigarette smoke, and various other factors that induce oxidative stress cause an increase in carbonyl content in proteins.[51] Researchers have developed many assays to measure carbonyl content.[52]

Carbonyl content is considered a marker for aging. As the age increases, the amount of carbonyls in the protein increases. In fact, the carbonyl content of muscles in older rats was nearly 50 % greater than that in younger rats.[53] Similar observations were previously made in many tissues, including human erythrocytes,[54] human lens proteins,[55] human brains,[56] and rat hepatocytes.[57]

12.4.4 Protein cross-linking as a result of oxidative degradation

It is generally accepted that, with oxygen present, there are six general mechanisms through which protein – protein cross-linking can occur. The first cross-linking reaction involves two protein chains with carbon-centered radicals present which come together to form a carbon – carbon bond (Scheme 12.7.1).[47,48] Tyrosyl radicals on two protein chains can react to form a cross-linked network (Scheme 12.7.2).[47] Malondialdehyde, a lipid peroxidation product, can react with two lysine residues on separate proteins (Scheme 12.7.3).[48] Fourthly, a HNE – Michael type derivative of one protein can react with the lysine of another protein to form a cross-link (Scheme 12.7.4).[48-50] A protein with a pendant lysine or arginine can react with a protein with a carbonyl of a glycation derivative to form a protein cross-link (Scheme 12.7.5).[48,58-60] Finally, two proteins with pendant cysteine residues can react when oxidized to form a cross-linked protein network (Scheme 12.7.6).[47,48]

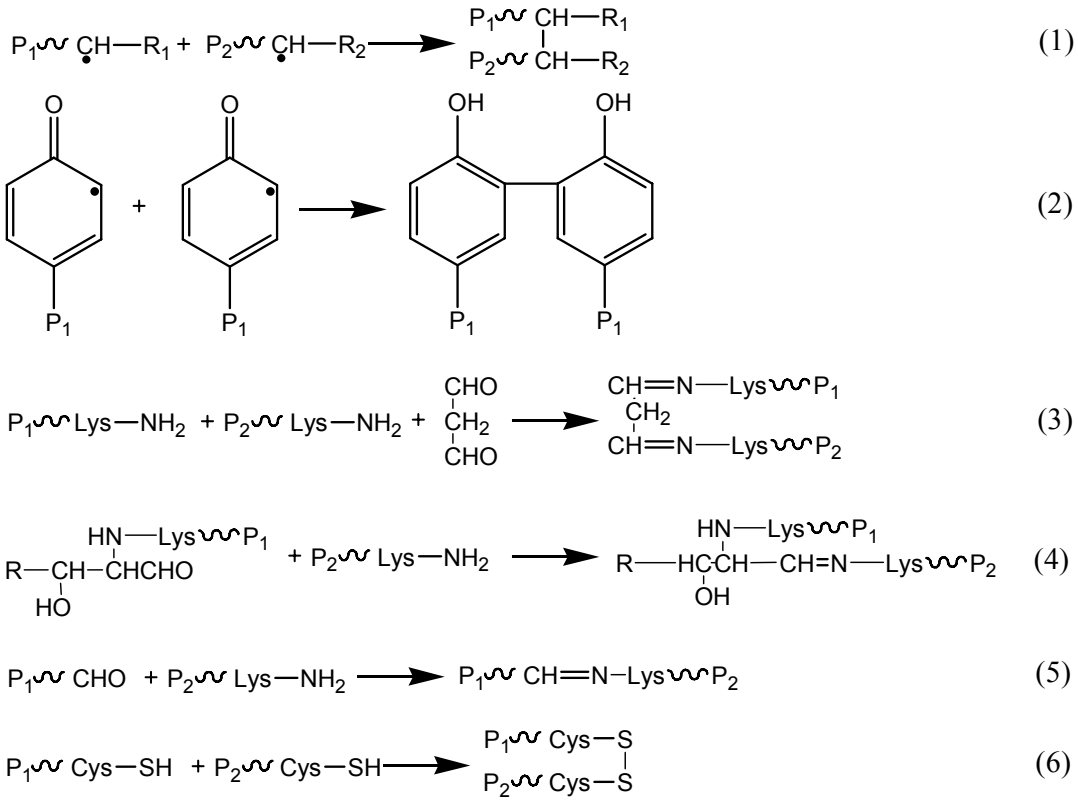

Scheme 12.7. Protein – protein cross-linking reactions.[48]

Accumulated cross-linked proteins in the body can cause damage. Under ordinary conditions, the 20 S proteosome degrades the proteins when the body no longer requires them for normal functions. However, upon accumulation of cross-linked proteins, the 20 S proteosome can no longer function properly. Not only does the proteosome not degrade cross-linked proteins, but also it does not degrade normal proteins. This accumulation has potential to greatly contribute to aging and disease.

12.5 Carbohydrate oxidative degradation via reactive oxygen species

Reactive oxygen species have a detrimental effect on polysaccharide containing macromolecules. Radicals and ROS can cleave the sugar phosphate backbone of DNA. The sugar in DNA is 2-deoxyribose (Figure 12.2). ROS can attack all carbon atoms on the phosphate sugar backbone of DNA.

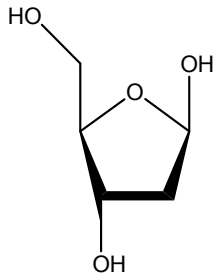

Figure 12.2. 2-deoxyribose, the monosaccharide in DNA.

In plants, oxidation of the polysaccharides of the plant cell walls, such as xyloglucan, glucuronoarabinoxylans, and (β-1,3), (β-1,4)-glucans, can greatly alter the intrinsic viscosity, solubility, and gel forming properties.[61] These properties are altered due to the depolymerization of the polysaccharides.

12.5.1 Oxidative degradation of reducing sugars and related compounds

The degradation of reducing sugars is dependent on the temperature and concentration of radicals or ROS. An increase in temperature or an increase in the concentration will promote degradation. However, if radical-scavenging antioxidants are present, the rate of degradation will decrease. To analyze the reactions and deduce the structures of the radical species, one may utilize electron paramagnetic resonance (EPR) spectroscopy. Gilbert and co-workers[62] investigated polysaccharide oxidative degradation through the hydroxyl radical via EPR. Using a series of dextrans of increasing molecular weights (10000 g/mol – 500000 g/mol), they concluded that at pH = 4, the hydroxyl radical would react at all positions except C-1. At lower pH, acid catalyzed rearrangements dominated. At higher pH, base catalyzed products were obtained. Through these studies, Gilbert and co-workers[62] determined that degradation of dextran is pH dependent.

Most carbohydrates are readily oxidized at basic pH.[33,34,63] Typically carbohydrates do not react with hydrogen peroxide in acidic media, primarily due to the absence of hydroperoxide

anion, according to Isbell and Frush.[63] In the presence of a ROS and water, aldoses are oxidized to the lower aldonic acid and formic acid, as shown in Scheme 12.8.[33,34,63,64]

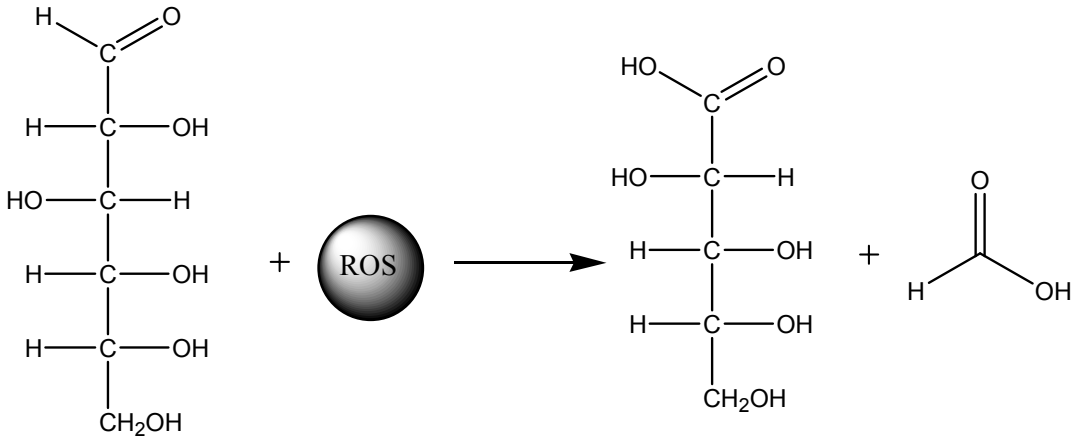

Scheme 12.8. Oxidation of an aldose yielding its lower aldonic acid and formic acid.

Steric hindrance plays an important role in the oxidation of saccharide functionalities on polymers. Thus, primary alcohols are oxidized more readily than secondary alcohols. Axial hydroxyl functionalities are attacked in five-membered ring systems if secondary alcohols are the only source of hydroxyl available for oxidation. If cyclic structures are attached to the saccharide functionality, attack is likely to occur at the carbon attached to an *endo* alcohol functionality.[64]

In a preliminary investigation, Isbell and Frush[34] found that alditols and aldonic acids are oxidized rapidly in alkaline hydrogen peroxide at 40 °C, but slowly at 0 °C. Additionally, Isabell and co-workers[63] investigated the oxidation of disaccharides with alkaline hydrogen peroxide. They studied cellobiose, lactose, and maltose, and concluded that the aldonic acid was formed, and then the lower aldonic acid, 2-*O*-D-glucopyranosyl-D-erythronic acid and formic acid were formed. Whistler and co-workers[65] found that when cornstarch amylopectin, a polysaccharide, is treated with alkaline hydrogen peroxide and hydrolyzed, no polysaccharide remains and mostly glucose is formed. Many other polysaccharides react analogously.

12.5.1.1 The pro-oxidant and antioxidant abilities of saccharides

Saccharides will react readily with reactive oxygen species. For example, Neta and co-workers[66] determined that carbohydrates react with hydroxyl radicals at rates ranging from 10^8 to 10^{10} $M^{-1}s^{-1}$. However, more recently, some authors suggested that saccharides have antioxidant capabilities. Although they are sometimes vague in their explanations, it appears the saccharide has antioxidant ability only when molecules that are more susceptible to oxidation are not present in solution.

Mooradian and co-workers[67] described the autoxidative and antioxidative abilities of simple carbohydrates. They utilized a fluorescence assay of porphyridium cruentum β-phycoerythrin protein, which is sensitive to changes in chemical structure. The concentration of hydroxyl and peroxyl radicals is proportional to the change in fluorescence over time. The authors used this relationship to deduce the extent of oxidative damage to the porphyridium cruentum β-phycoerythrin protein in the presence of reducing sugars. The authors determined that the autoxidative potential of reducing sugars is minimal, and that the antioxidative capabilities are somewhat lower than those of most known antioxidants when a known peroxyl radical generator was present. As shown in Table 12.3,[67] deoxyribose had the greatest antioxidant potential, and its ability was comparable to the antioxidant ascorbate.

Sugar	Percent of Oxidation Inhibition
Glucose (5 mM)	44.9 ± 2.4
Glucose (25 mM)	61.5 ± 0.7
Fructose (5 mM)	30.2 ± 1.9
Maltose (5 mM)	49.1 ±1.2
Lactose (5 mM)	53.5 ± 1.6
Deoxyribose (5 mM)	68.8 ± 1.7
Ribose (5 mM)	64.7 ± 1.8
Ascorbate (5 mM)	69.5 ± 1.0

Table 12.3. Antioxidant capabilities of some saccharides.[67]

In another study, Lo Scalzo et al.[68] evaluated the radical scavenging abilities of several carbohydrates under Fenton oxidizing conditions. Using thiobarbituric acid (TBA), gas chromatography to measure formic acid evolution, high performance liquid chromatography (HPLC) of sugars before and after Fenton treatments, and EPR spectroscopy, changes in carbohydrate composition at various conditions were evaluated. According to the article, carbohydrates, especially disaccharides such as maltose and sucrose, are good at scavenging hydroxyl radicals in Fenton-type conditions. Consequently, one may wish to incorporate a carbohydrate in a system as a sacrificial component to react with hydroxyl radicals.

12.5.2 Nitroxide-mediated oxidation of polysaccharides

Rheumatoid arthritis occurs when hyaluronan, a glycosaminoglycan, degrades around joints in the body. To slow the depolymerization process, antioxidants, such as superoxide dismutase and catalase, are used. More recently, persistent nitroxides such as 2,2,6,6-tetramethylpiperidinoxyl (TEMPO), shown in Figure 12.3, were considered effective antioxidants. The exact mechanism of this process is not fully understood. It is typically believed that persistent nitroxides cycle through three states, the hydroxylamine (TEMPOH), the radical ($TEMPO^{\cdot}$), and the nitrosonium cation ($TEMPO^{+}$).

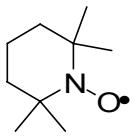

Figure 12.3. Structure of TEMPO, a persistent nitroxide.

Somewhere in the oxidative process, the nitroxide develops its antioxidant capability. The radical state is likely the responsible antioxidant species. But, many researchers have debated over the effectiveness of nitroxides as antioxidants, as they also catalyze the oxidation of alcohol functionalities.[69-71] Samuni and co-workers[70] determined the rate of oxidation of

hyaluronic acid with the TEMPO cation. The rate constant, k = (1.1 ± 0.1) x 10^{-1} $M^{-1}s^{-1}$, is considerably lower than the rate at which persistent nitroxides trap active hydroxyl radicals. The nitroxides trap hydroxyl radicals and prevent them from oxidizing the polysaccharide. Thus, according to Sumuni and co-workers,[70] persistent nitroxides protect polysaccharides from highly reactive radicals, such as hydroxyl radical, even though it is well known that nitroxides selectively catalyze the oxidation of alcohol functionalities, including those on mono-, di-, and polysaccharides.[72] Typically, persistent nitroxides are used in combination with other reagents such as hypochlorite, copper salt/bipyridine complexes, and enzymes to selectively oxidize of alcohol functionalities. The high selectivity almost certainly contributes to their slow reaction rate. More recently, Belgsir and co-workers[71] have developed a mechanism for the nitroxide-mediated electrochemical oxidation of alcohols, as shown in Scheme 12.9.

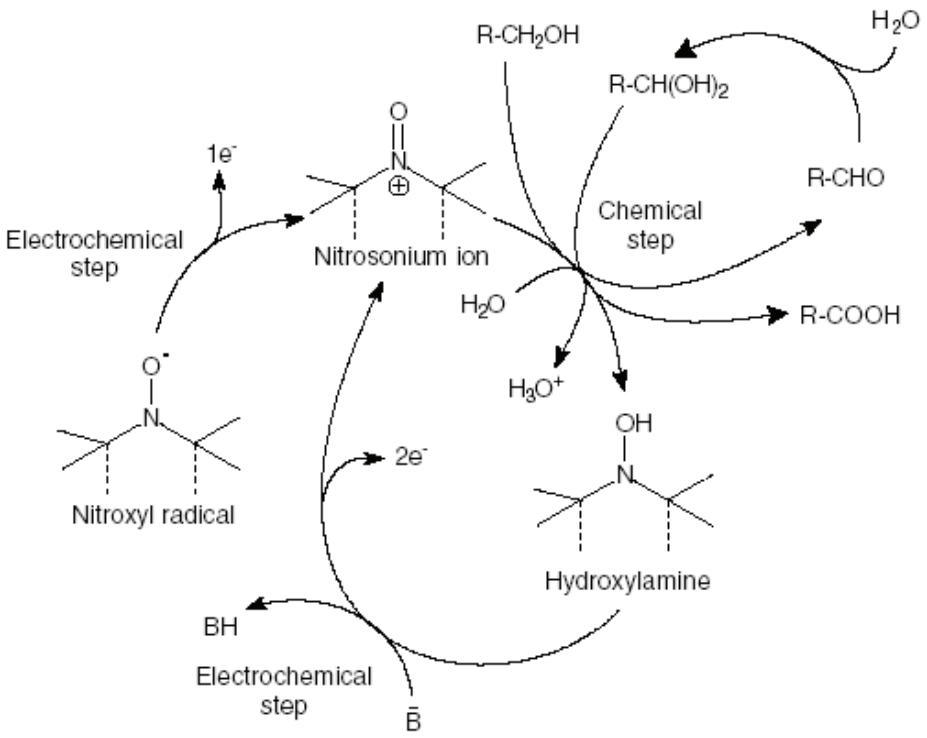

Scheme 12.9. Nitroxide mediated oxidation of alcohols.[71]

12.5.3 Oxidative stability of polymers with saccharide pendant groups

Polymers containing saccharide residues remain an area of scientific importance. These novel materials, termed glycopolymers, may contain saccharide units in different architectures, including terminal or pendant saccharide functionalities;[73,74] examples of such structures are given in Figure 12.4.

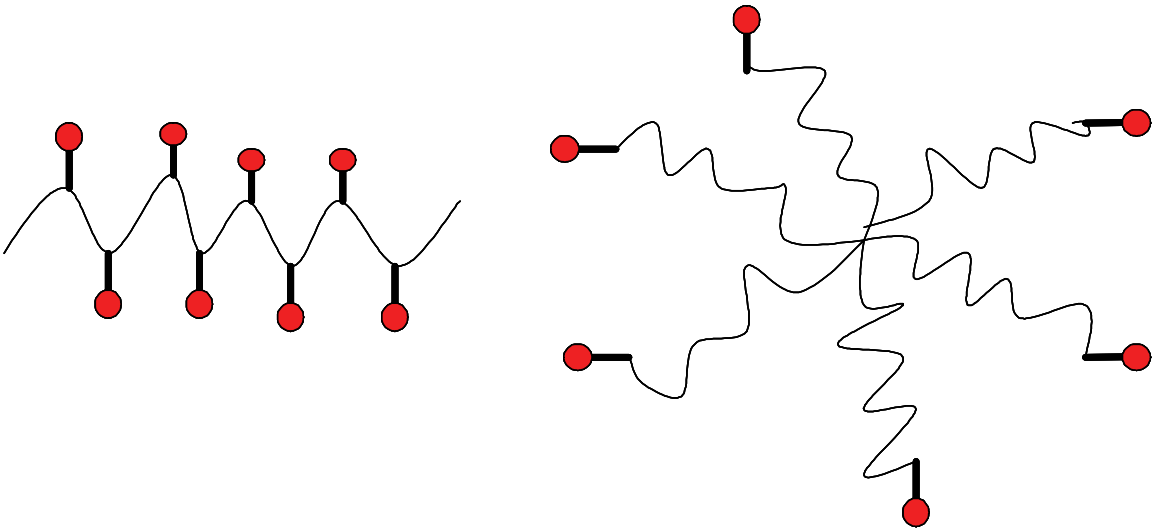

Figure 12.4. Examples of glycopolymers, both linear and dendritic, where sugar portions are shown in red.

Polymeric materials have limited lifetimes; the greatest factor determining the lifetime of a polymer is oxidative degradation.[76] Many chemists have synthesized saccharide – containing polymers, creating novel compounds that may possess better properties than natural analogues. The pendant or terminal saccharide unit imparts biomimetic ability to the polymer system. Biomimetics involves a synthetic molecule bearing functional groups that mimic natural analogues.[77] To meet critical physical and mechanical properties that are defined through the end use of the material, the backbone of the polymer is specifically tailored. Biocompatibility and biodegradability is improved through the incorporation of polymer blends, copolymers, and dendrimers containing saccharide residues. This marked increase in biocompatibility is due to an

increase in association constants. Typically, a single saccharide unit can weakly bind a receptor and produce an association constant of less than 10^{-6} M^{-1}.[73] This type of association is monovalent. However, with multivalent dendrimers and other molecules with increased number of saccharide residues, the association constants are greater. Lee and co-workers[78] termed this phenomenon "cluster effect."

The hydroxyl groups of glycopolymers are oxidized more readily than typical alcohol functionalities. This is because the hydroxyl groups of saccharides are more acidic than those of typical alcohols. Oxygen in neutral or basic conditions will readily oxidize saccharide pendants on glycopolymers. However, many other organic compounds can oxidize glycopolymers, including halogen-based compounds, peroxy acids, phenylhydrazine, hydrogen peroxide, metal oxides, and nitrogen-based compounds, including nitric acid, nitrogen dioxide, and nitroxyl radicals.[79] Thus, glycopolymers oxidatively degrade in a manner similar to true saccharides.

12.6 Effective means for measuring oxidative stress in biological macromolecular systems

It is imperative to understand the mechanisms through which materials oxidatively degrade when subjected to oxidative stress. The rate of oxidation determines the lifetime of a material. In order to study oxidative degradation of materials, researchers have developed many detection methods. The detection method that is most suitable largely depends on the application. The following section will outline briefly current techniques employed to determine oxidative stability in biological macromolecular systems.

12.6.1 Techniques for measuring oxidative stress or oxidative degradation

Most methods for measuring oxidative stress are spectroscopic methods. Unfortunately, few techniques detect only radicals. Thus, measuring oxidative stress via radical formations is a growing field.

12.6.1.1 Electron paramagnetic resonance spectroscopy

Perhaps the most reliable means for determining oxidative stability of materials is electron paramagnetic resonance (EPR) spectroscopy, also known as electron spin resonance spectroscopy (ESR).[80] This analytical technique detects paramagnetic species. The paramagnetic species is placed in a magnetic field and irradiated with microwave radiation. Absorption of the radiation allows certain spin states to transition. The change in energy from the transition is given in the equation below.

$$\Delta E = g\beta H = h\nu$$

where ΔE is the energy absorbed, g is the g-factor (2.00232 for a free electron), β is the Bohr magneton, H is the applied field strength, h is Planck's constant, and ν is the frequency of electromagnetic radiation.[81]

One can determine absorptions of specific compounds. EPR spectroscopy can detect nanomolar radical concentrations. However, in biological systems, the radical concentration is typically much lower, and radicals have short lifetimes. One option for detecting radicals at these low concentrations is spin trapping. This technique involves a short – lived radical of interest reacting with a non-radical molecule, such as a nitrone, to yield a nitroxyl radical, a more stable radical with a longer lifetime. Reasonable spin traps include N-*tert*-butyl-α-phenylnitrone (PBN), 5,5-dimethyl-1-pyrroline-N-oxide (DMPO), and α-(4-pyridyl-1-oxide)-N-*tert*-butylnitrone (4-POBN).[80] Spin trapping with EPR spectroscopy does have some disadvantages.

First, spin traps are often toxic, so their use is somewhat limited. Second, adducts formed through radicals reacting with the spin trap are not as informative as the original radicals themselves. Another option for detecting short – lived radicals at low concentrations is to use rapid freezing, but this technique will result in broadened peaks.[30]

12.6.1.2 Chemiluminescence and differential scanning calorimetry

Chemiluminescence is a rapid way to determine oxidative stability of polymers.[76] This technique relies on light emission. In the process, reactants in the ground state are converted to an excited transition state and then to an excited product. The product then releases a photon of light as it returns to the ground state.[82,83] Two types of chemiluminescence experiments are possible. The first type is performed at a constant temperature in an oxygen atmosphere to measure the oxidation induction time (OIT) and the oxidation rate. The second type is performed at variable temperature in an inert gas to measure the OIT. The latter technique is useful for determining storage lifetimes of materials. Specifically, one could use this technique to monitor the lifetimes of biologically based macromolecules. Differential scanning calorimetry (DSC) is another technique utilized to determine oxidative stability through the heat flow of a material. The experiment is performed isothermally and OIT is taken as the onset of an exotherm. A third possibility for determining the oxidative stability of polymers is utilizing a combination of DSC and chemiluminescence, allowing one to examine both heat flow and light emission. Billingham and co-workers[84] have developed this technique using a DSC with a chemiluminescence detector attached. The data obtained correlates well over a broad range of temperatures that is unattainable with chemiluminescence alone, and chemiluminescence can detect lower levels of peroxides than DSC. It is possible to combine the two techniques because

there is a linear relationship between heat flow and the square root of the intensity of the light emitted.[84]

12.6.1.3 Oxygen uptake

Another technique for evaluating the oxidative stability of polymers is oxygen uptake. The amount of oxygen consumed over a period of time is measured in a closed vessel at a constant temperature. The change in pressure of the system is correlated to the oxygen uptake value, which varies based on several kinetic parameters including induction period, process rate, and activation energy. It is possible to obtain kinetic data on the oxidation of macromolecules and determine if antioxidants are efficient at oxygen scavenging.[85] This technique has some advantages over other techniques because the instrument is relatively inexpensive and requires small sample sizes—approximately 20 milligrams.

12.6.1.4 Infrared spectroscopy

Infrared spectroscopy is an additional technique used to determine the presence of oxidized compounds. Many instruments have the capability to measure absorbance *in situ*. During the oxidation process, the chemical composition of species changes, often leading to modifications of the infrared spectrum. Specifically, the disappearance and appearance of functional groups indicates that oxidative degradation is occurring. The most monitored area on a spectrum is the carbonyl region, as aldehydes are common functionalities formed during oxidation reactions. The formation of alcohol functionalities are often observed as well. Figure 12.5 shows the appearance of a carbonyl functionality and hydroxyl functionality during the oxidation of poly(propylene) films.

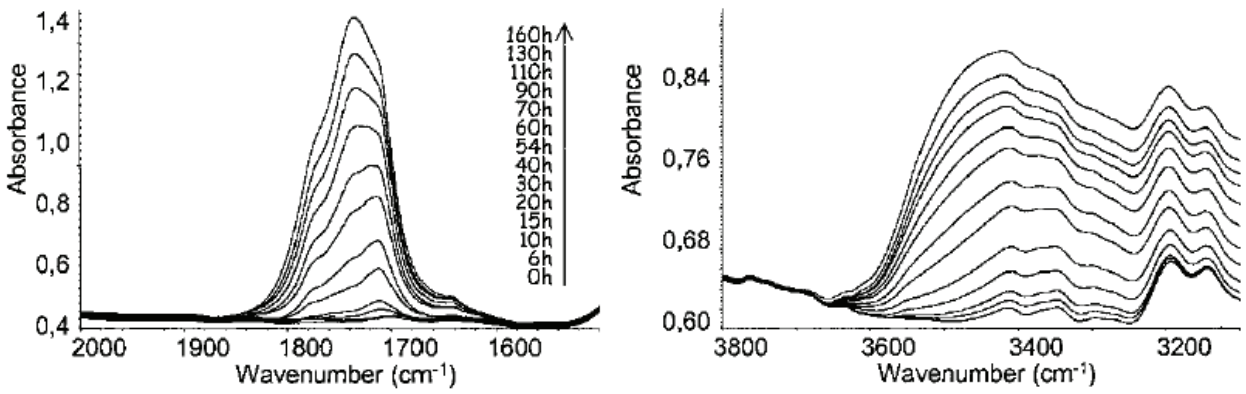

Figure 12.5. Infrared spectra of carbonyl and hydroxyl functionalities of oxidized poly(propylene) films over time.[86]

The absorbance at the carbonyl region and hydroxyl region increase as a function of time, indicating that oxidation is occurring. One can determine valuable kinetic data, such as the rate of oxidation, via constructing a plot of absorbance versus elapsed time. A kinetic plot from the poly(propylene) film data is given in Figure 12.6. The initial time during which the absorbance does not increase quickly over time, is called the induction period. After the induction period, the rate of oxidation is constant.[86]

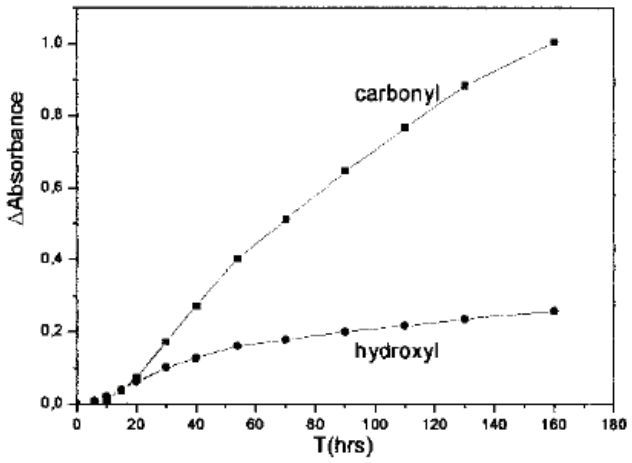

Figure 12.6. A kinetic plot to determine the rate of oxidation in carbonyl and hydroxyl functionalities of oxidized poly(propylene) films.[86]

12.7 Conclusions

In conclusion, measuring oxidation of biologically based macromolecules is an emerging area of interest. Current research efforts incorporate the role of oxidation of macromolecules in three distinct areas. These focused areas include (1) polymer synthesis in order to understand the effect of chemical structure on oxidation and free radical processes, (2) polymer characterization in order to investigate the effect of oxidation on mechanical properties of polymers and biopolymers, and (3) characterization to determine oxidation rates and processes of polymers.

12.8 References

(1) Deming, D. In *Oil: Are We Running Out?*, Second Wallace E. Pratt Memorial Conference, San Diego, CA, January 12-15, 2000, 2000; San Diego, CA, 2000.
(2) Deffeyes, K. S., *Hubbert's Peak: The Impending World Oil Shortage*. Princeton University Press: Princeton, New Jersey, 2001.
(3) Wang, Q.; Dordick, J. S.; Linhardt, R. J. *Chemistry of Materials* **2002,** 14, 3232-3244.
(4) Narain, R.; Armes, S. P. *Chemical Communications* **2002**, (23), 2776-2777.
(5) Chen, Y.; Wulff, G. *Macromolecular Chemistry and Physics* **2002,** 202, (17), 3426-3431.
(6) Chen, Y.; Wulff, G. *Macromolecular Chemistry and Physics* **2001,** 2002, (17), 3273-3278.
(7) Narain, R.; Dhanjay, J.; Wulff, G. *European Polymer Journal* **2002,** 38, (2), 273-280.
(8) Paramonov, S.; Gauba, V.; Hartgerink, J. D. *Macromolecules* **2005,** 38, (18), 7555-7561.
(9) Smeenk, J. M.; Loewik, D. W. P. M.; van Hest, J. C. M. *Current Organic Chemistry* **2005,** 9, (12), 1115-1125.
(10) Bloembergen, S.; McIennan, I. J.; Narayan, R. *Journal of the Adhesive and Sealant Council* **1997**, 367-395.
(11) Gerschman, R.; Gilbert, D. L.; Nye, S. W.; Dwyer, P.; Fenn, W. O. *Science* **1954,** 119, (3097), 623-626.
(12) Gilbert, D. L. *Perspectives in Biology and Medicine* **1960,** 4, 58-71.
(13) Gilbert, D. L., Fifty Years of Radical Ideas. In *Reactive Oxygen Species From Radiation to Molecular Biology: A Festschrift in Honor of Daniel L. Gilbert*, Chiueh, C. C., Ed. The New York Academy of Sciences: New York, 2000; Vol. 899, pp 1-14.
(14) Halliwell, B.; Gutteridge, J. M., *Free Radicals in Biology and Medicine*. 3rd ed.; Oxford University Press: Avon, England, 1999.
(15) Ames, B. N.; Shigenaga, M. K., Oxidants are a Major Contributor to Cancer and Aging. In *DNA and Free Radicals*, Halliwell, B.; Aruoma, O. I., Eds. Ellis Horwood Limited: New York, 1993; pp 1-15.
(16) Geurrieri, F.; Pellecchia, G.; Papa, S., Reactive Oxygen Species and Alteration of F0F1-ATP Synthase in Aging and Liver Regeneration. In *Free Radicals, Oxidative Stress, and*

Antioxidants Pathological and Physiological Significance, Ozben, T., Ed. Plenum Press: New York, 1998; Vol. 296, pp 109-119.
(17) Gonzalez-Lima, F.; Valla, J.; Cada, A., Brain Cytochrome Oxidase Activity and How It Relates to the Pathophysiology of Memory and Alzheimer's Disease. In *Free Radicals, Oxidative Stress, and Antioxidants Pathological and Physiological Significance*, Ozben, T., Ed. Plenum Press New York, 1998; Vol. 296, pp 205-227.
(18) Stadtman, E. R., The Role of Free Radical Mediation of Protein Oxidation in Aging and Disease. In *Free Radicals, Oxidative Stress, and Antioxidants Pathological and Physiological Significance* Ozben, T., Ed. Plenum Press: New York, 1998; Vol. 296, pp 131-143.
(19) Shiva, S.; Oh, J. Y.; Landar, A. L.; Ulasova, E.; Venkatraman, A.; Bailey, S. M.; Darley-Usmar, V. M. *Free Radical Biology and Medicine* **2005,** 38, 297-306.
(20) Beyer, R. E. *Free Radical Biology and Medicine* **1990,** 8, (6), 545-565.
(21) Turrens, J. F.; Alexandre, A.; Lehninger, A. L. *Archives of Biochemistry and Biophysics* **1985,** 237, (2), 408-414.
(22) Stadtman, E. R.; Levine, R. L., Protein Oxidation. In *Reactive Oxygen Species From Radiation to Molecular Biology: A Festschrift in Honor of Daniel L. Gilbert*, Chiueh, C. C., Ed. The New York Academy of Sciences: New York, 2000; Vol. 899, pp 191-208.
(23) Abuja, P. M. A., R. *Clinica Chimica Acta* **2001,** 306, (1-2), 1-17.
(24) Bateman, L. *Quarterly Reviews* **1954,** 8, 147-167.
(25) Bolland, J. L. *Quarterly Reviews* **1949,** 3, 1-21.
(26) Bolland, J. L.; Have, P. T. *Transactions of the Faraday Society* **1947,** 43, 201-210.
(27) Al-Malaika, S., Autoxidation. In *Atmospheric Oxidation and Antioxidants*, Scott, G., Ed. Elsevier: Amsterdam, 1993; Vol. I, pp 45-82.
(28) Silberberg, M. S., *Chemistry: The Molecular Nature of Matter and Change*. 2nd ed.; McGraw-Hill: Boston, 2000.
(29) Koppenol, W. H., The Chemical Reactivity of Radicals. In *Free Radical Toxicology*, Wallace, K. B., Ed. Taylor and Francis: Washington, D. C., 1997; pp 3-14.
(30) Davies, M. J.; Dean, R. T., *Radical-Mediated Protein Oxidation From Chemistry to Medicine*. Oxford University Press: Oxford, 1997.
(31) Gutteridge, J. M. C., Iron in Free Radical Reactions and Antioxidant Protection. In *Free Radicals, Oxidative Stress, and Antioxidants Pathological and Physiological Significance*, Ozben, T., Ed. Plenum Press: New York, 1998; Vol. 296, pp 1-14.
(32) Stadtman, E. R., Free Radical Mediated Oxidation of Proteins. In *Free Radicals, Oxidative Stress, and Antioxidants Pathological and Physiological Significance*, Ozben, T., Ed. Plenum Press: New York, 1998; Vol. 296, pp 51-64.
(33) Arts, S. J. H. F.; Mombarg, E. J. M.; Van Bekkum, H.; Sheldon, R. A. *Synthesis* **1997**, 597-613.
(34) Isbell, H. S.; Frush, H. L. *Carbohydrate Research* **1977,** 59, C25-C31.
(35) Fenton, H. J. H.; Jackson, H. *Journal of the Chemical Society* **1899,** 75, 1-11.
(36) Haber, F.; Weiss, J. J. *Proceedings of the Royal Society of London, Series A* **1934,** 147, 332-351.
(37) Al-Malaika, S. *International Materials Review* **2003,** 48, (3), 165-185.
(38) Hensley, K.; Floyd, R. A. *Archives of Biochemistry and Biophysics* **2002,** 397, (2), 377-383.

(39) Linton, S.; Davies, M. J.; Dean, R. T. *Experimental Gerontology* **2001,** 36, (9), 1503-1518.
(40) Oliver, C. N.; Fulks, R.; Levine, R. L.; Fucci, L.; Rivett, A. J.; Roseman, J. E.; Stadtman, E. R., Oxidative Inactivation of Key Metobolic Enzymes During Aging. In *Molecular Basis of Aging*, Roy, A. K.; Chatterjee, B., Eds. Academic Press: New York, 1984; pp 235-262.
(41) Stadtman, E. R. *Science* **1992,** 257, 1220-1224.
(42) Stadtman, E. R., The Status of Oxidatively Modified Proteins as a Marker of Aging. In *Molecular Aspects of Aging*, Esser, K.; Martin, G. M., Eds. John Wiley & Sons: New York, 1995; pp 130-143.
(43) Stadtman, E. R., Reactive Oxygen-Mediated Protein Oxidation in Aging and Disease. In *Annals of the New York Academy of Sciences*, 2000; Vol. 928, pp 22-38.
(44) Stadtman, E. R.; Berlett, B. S. *Drug Metabolism Reviews* **1998,** 30, (2), 225-243.
(45) Bertlett, B. S.; Levine, R. L.; Stadtman, E. R. *Journal of Biological Chemistry* **1996,** 271, (8), 4177-4182.
(46) Stadtman, E. R.; Berlett, B. S., Free-Radical-Mediated Modification of Proteins. In *Free Radical Toxicology*, Wallace, K. B., Ed. Taylor & Francis: Washington, D. C., 1997; pp 71-87.
(47) Garrison, W. M. *Chemical Reviews* **1987,** 87, 381-398.
(48) Stadtman, E. R.; Levine, R. L. *Amino Acids* **2003,** 25, 207-218.
(49) Friget, B.; Stadtman, E. R.; Szweda, L. *Journal of Biological Chemistry* **1994,** 269, 21639-21643.
(50) Uchida, K.; Stadtman, E. R. *Journal of Biological Chemistry* **1993,** 268, 6388-6393.
(51) Bertlett, B. S.; Stadtman, E. R. *Journal of Biological Chemistry* **1997,** 272, 20313-20316.
(52) Levine, R. L.; Williams, J. A.; Stadtman, E. R.; Schacter, E. *Methods in Enzymology* **1994,** 233, 346-357.
(53) Reznick, A. Z.; Packer, L. *Methods in Enzymology* **1994,** 233, 357-363.
(54) Oliver, C. N.; Ahn, B.-W.; Moerman, E. J.; Goldstein, S.; Stadtman, E. R. *Journal of Biological Chemistry* **1987,** 262, 5488-5491.
(55) Garland, D.; Russel, P.; Zigler, J. S., The Oxidative Modification of Lens Protein. In *Oxygen Radicals in Biology and Medicine*, Simic, M. G.; Taylor, K. S.; Ward, J. F.; von Sontag, V., Eds. Plenum: New York, 1988; pp 347-353.
(56) Smith, C. D.; Carney, J. M.; Stark-Reed, P. E.; Oliver, C. N.; Stadtman, E. R.; Floyd, R. A. *Proceedings of the National Academy of Sciences USA* **1991,** 88, 10540-10543.
(57) Stark-Reed, P. E.; Oliver, C. N. *Arch biochem Biophys* **1989,** 275, 559-567.
(58) Gradhee, S.; Monnier, V. M. *Journal of Biological Chemistry* **1991,** 266, (11649-11653).
(59) Verzijl, N.; De Groot, J.; Oldehinkel, E.; Bank, R. A.; Thorpe, S. R.; Baynes, J. W.; Bayliss, M. T.; Bijlsma, W., J.; Lafeber, F. P. J. G.; Tekoppele, J. M. *Biochem J* **2000,** 350, 381-387.
(60) Wells-Knecht, K. J.; Zyzak, D. V.; Litchfield, J. E.; Thorpe, S. R.; Baynes, J. W. *Biochemistry* **1995,** 34, (3702-3709).
(61) Schweikert, C.; Liszkay, A.; Schopfer, P. *Phytochemistry* **2002,** 61, 31-35.
(62) Glibert, B. C.; King, D. M.; Thomas, B. *Carbohydrate Research* **1984,** 125, 217-235.
(63) Isbell, H. S.; Frush, H. L. *Carbohydrate Research* **1987,** 161, 181-193.

(64) Green, J. W., In *The Carbohydrates: Chemistry and Biochemistry*, 2nd ed.; Pigman, W.; Horton, D.; Wander, J. D., Eds. Academic Press: New York, 1980; Vol. IB, pp 1101-1156.
(65) Whistler, R. L.; Schweiger, R. *Journal of the American Chemical Society* **1959,** 81, (12), 3126-3139.
(66) Anbar, M.; Neta, P. *International Journal of Applied Radiation and Isotopes* **1967,** 18, 493-523.
(67) Wehmeier, K. R.; Mooradian, A. D. *Free Radical Biology and Medicine* **1994,** 17, (1), 83-86.
(68) Morelli, R.; Russo-Volpe, S.; Bruno, N.; Lo Scalzo, R. *Journal of Agricultural and Food Chemistry* **2003,** 51, 7418-7425.
(69) Jiang, B.; Drouet, E.; Milas, M.; Rinaudo, M. *Carbohydrate Research* **2000,** 327, 455-461.
(70) Lurie, Z.; Offer, T.; Russo, A.; Samuni, A.; Nitzan, D. *Free Radical Biology and Medicine* **2003,** 35, (2), 169-178.
(71) Liaigre, D.; Breton, T.; Belgsir, E. M. *Electrochemistry Communications* **2005,** 7, 312-316.
(72) Bragd, P. L.; van Bekkum, H.; Besemer, A. C. *Topics in Catalysis* **2004,** 27, (1-4), 49-66.
(73) Ladmiral, V.; Melia, E.; Haddleton, D. M. *European Polymer Journal* **2004,** 40, 431-449.
(74) Okada, M. *Progress in Polymer Science* **2001,** 26, 67-104.
(75) Rele, S. M.; Cui, W.; Wang, L.; Hou, S.; Barr-Zarse, G.; Tatton, D.; Gnanou, Y.; Esko, J. D.; Chaikof, E. L. *Journal of the American Chemical Society* **2005,** 127, 10132-10133.
(76) Boxhammer, J. *Macromolecular Symposium* **2002,** 178, 11-24.
(77) Kao, W. J., In *Polymeric Biomaterials*, 2nd ed.; Dumitriu, S., Ed. Marcel Dekker, Inc.: New York, 2002; pp 63-77.
(78) Lee, Y. C.; T., L. R.; Rice, K.; Ichikawa, Y.; Wong, T.-C. *Pure and Applied Chemistry* **1991,** 63, 499.
(79) Varela, O. *Advances in Carbohydrate Chemistry and Biochemistry* **2003,** 58, 307-369.
(80) Rimbach, G.; Hohler, D.; Fischer, A.; Roy, S.; Virgili, F.; Pallauf, J.; Packer, L. *Archives of Animal Nutrition* **1999,** 52, (203-222).
(81) Villamena, F. A.; Zweier, J. L. *Antioxidants and Redox Signaling* **2004,** 6, (3), 619-629.
(82) Zlatkevich, L. *Journal of Polymer Science: Part B: Polymer Physics* **1990,** 28, 425-429.
(83) Adam, W.; Kazakov, D. V.; Kazakov, V. P. *Chemical Reviews* **2005,** 105, (9), 3371-3387.
(84) Fearon, P. K. B., S. W.; Billingham, N. C. *Journal of Thermal Analysis and Calorimetry* **2004,** 76, (1), 75-83.
(85) Zaharescu, T. *Materials Research Innovations* **2001,** 5, 35-39.
(86) Rivaton, A.; Gardette, J.-L.; Mailhot, B.; Morlat-Therlas, S. *Macromolecular Symposia* **2005,** 225, 129-146.

Chapter 13 : Introduction of Saccharide Functionality into Polymers: Synthesis and Applications

13.1 Abstract

Glycopolymers may contain saccharide units in different architectures, including terminal saccharide or pendant saccharide functionalities, and show great potential as novel compounds that offer properties useful for biomimetics and biomedical applications such as glycopolymer-protein interactions, treatments of infectious viruses, drug delivery, separation science, and package materials. Glycopolymer synthesis is accomplished through a variety of polymerization techniques such as conventional free radical polymerization, ionic polymerization, controlled free radical polymerization, ring opening metathesis polymerization, and ring opening polymerization. Of these methods, conventional free radical polymerization and controlled free radical polymerization are described herein. In addition, polymer oxidative degradation is introduced and compared to glycopolymer oxidative degradation.

13.2 Research objectives and scientific importance

In recent years, research in the chemistry-biology interface has received renewed interest, particularly the polymer-biology interface. Possible reasons for this include the increasing cost and depletion of non-renewable petroleum supplies. Rather than utilizing petroleum based materials for research, chemists are now studying the use of renewable feedstocks, such as saccharides, in their research.[1] As the depletion rate of petrochemicals has increased, the demand to replace current petroleum based materials for natural renewable feedstocks has also increased. Many polymeric materials synthesized from renewable resources do not consume

valuable petroleum based chemicals, produce fewer greenhouse gases, and are synthesized with less toxic materials.

Another interest in utilizing renewable feedstocks has resulted from the growing field of biomimetics. According to definition, biomimetics involves a synthetic molecule bearing functional groups that mimics a natural analog.[2] In order to interact with other biological systems, it is required that the polymers are biocompatible and possess acceptable chemical and physicomechanical properties. To this end, polysaccharides are ideal for biomaterials, possessing both the desired biocompatibility and biodegradability.

Thus, research concerning polymers containing saccharide residues remains an area of scientific importance. These novel materials, termed glycopolymers, may contain saccharide units in different architectures, including terminal saccharide or pendant saccharide functionalities.[3,4] According to some definitions, glycopolymers also pertain to natural polysaccharide polymers; however, this literature review focuses on synthetic glycopolymers and their potential applications. Many chemists have synthesized these saccharide polymers, creating novel compounds that potentially possess improved properties compared to natural analogs. The pendant or terminal saccharide unit imparts biomimetic ability to the polymer system. The backbone of the polymer is specifically tailored to meet critical physical and mechanical properties that are defined through the end use of the material. Biocompatibility and biodegradability has improved via the incorporation of polymer blends, copolymers, and dendrimers containing saccharide residues. This marked increase in biocompatibility was due to an increase in association constants. Typically, a single saccharide unit can enter a receptor and produce an association constant of less than 10^{-6} M^{-1}.[3] This type of association is monovalent. However, with multivalent dendrimers and other molecules that can increase the number of

saccharide residues, the association constants are greater. Lee et al. termed this phenomenon the "cluster effect."[5]

Initially, renewable materials were studied for packaging applications. However, the most widely studied area for natural materials today is biomedical applications. For glycopolymers, research areas of interest include drug delivery, gene delivery, tissue engineering, enzyme inhibition, and disease treatment applications. Through biomimetics, the polymers can interact with cellular material. The saccharide units of the glycopolymer can bind to specific lectins, which typically bind to naturally occurring polysaccharides.[6] The exact mechanism for this process is not fully understood at this point,[3] although it is believed to occur through an aggregation process.[7] Investigations on the binding of glycopolymers to lectin are accomplished through enzyme-linked lectin assays (ELLA).[3] This assay identifies saccharide functionalities on cellular surfaces via an enzyme-linked immunosorbent assay (ELISA).[8]

Given that these biomaterials are utilized in the presence of living organisms, it is imperative to consider the degradation process. Oxidative stress of glycopolymers, including mechanistic routes of degradation, and means to prevent or slow the process is described in further sections.

13.3 Advantages of utilizing bio-derived materials

In recent years, the number of potential uses for glycopolymers has increased. The decreasing supply of petroleum based starting materials and an increasing supply of agricultural, renewable feedstocks attributed to the interest. Many scientists are thus actively investigating the use of renewable feedstocks in place of petrochemicals in the synthesis of polymers. Further, many polymers are utilized only for a limited use lifetime. Furthermore, petroleum-based plastics tend to take an extended amount of time to degrade, long after the materials are needed.

If bio-derived materials are used in products that require shorter lifetimes, such as food packaging and in medicine, the polymer will degrade in a shorter amount of time.[9]

13.3.1 Potential applications of glycopolymers

Most importantly, glycopolymers are finding many applications in biomedical areas. This is due to the ability to mimic molecules that bind to cellular materials. These interactions could potentially apply to gene delivery, drug delivery, and tissue scaffolds.

An increasingly popular area of research is the investigation of glycopolymer-protein interactions.[10-15] Most protein-glycopolymer interactions need short, five to six oligosaccharide chains either to inhibit interactions[15] or elicit a response from a protein.[16] Thus, a single saccharide unit is not sufficient to inhibit an interaction of a protein to a harmful agent. For this reason, multivalent glycopolymers are studied as synthetic inhibitors. Since inhibition and actuation are based on the number of interactions between the glycopolymer and protein, branched and comb structures provide the greatest multivalent structure possible. As stated previously, this is due to the cluster effect.[5] Aoi et al.[11] synthesized dendrimers for receptor binding, transport, and adhesion. Glycopolymers not only mimic a cellular surface, but they also are utilized as medicinal agents. Simanek and co-workers[10] studied mimics to inhibit cell-cell interactions. Specifically, their efforts involve inhibiting lymphocytes from binding to cell surface receptors. Many health issues, such as rheumatoid arthritis, are caused as a result of this type of cell-cell interaction. Molecular weight and the architecture of the polymer are thus quite important for this specific application. If the molecular weight is too low or the structure does not contain enough saccharide functionalities, glycopolymer interactions with the protein are minimal.[15]

Usui and co-workers[17] studied treatments of infectious viruses with glycopolymers. The research group prepared glycopolymers containing sialyl oligosaccharide functionalities that successfully inhibited influenza A and B viruses. Measurements on the inhibition of MDCK cells were evaluated. It was shown that the viruses preferentially bound to the polymer, which inhibited the virus from attaching to the cell. Furthermore, an increase in molecular weight and sialic acid functionalities increased the amount of inhibition.

Drug delivery is another potential application for glycopolymers. Drugs delivered in hydrogels, three dimensional polymer networks made insoluble via crosslinking, are capable of absorbing liquids such as water and solvent. The hydrophilic nature of the polymer allows for maximum interactions with polar molecules. Peppas et al. developed a method for synthesizing pH sensitive hydrogels for oral protein delivery and reported that in an acidic environment, such as the stomach, the hydrogels were collapsed, thus protecting the proteins.[18] In basic or neutral areas of the body, the drug was released from the hydrogel. This area of research is increasingly popular, and many more studies are anticipated. In addition, hydrogels were utilized in biomedical applications as water absorbers and in contact lenses.[19] Poly(siloxane)s, typical materials found in contact lenses, are hydrophobic in nature, but it was found that poly(siloxane)s with saccharide functionalities provide more biocompatibility and wettability.[20] Dordick and co-workers[21] synthesized novel acrylate hydrogels crosslinked with *N,N'*-methylenebis(acry1amide). In addition, amphiphilic block copolymers are also useful drug carriers. Cunliffe[16] attributed this capacity to the ability of the copolymers to bind to lectins and self-assemble. Other pH sensitive polymers, such as poly(2-lactobionamidoethyl methacrylate)-*b*-poly(2-(diethylamino)ethyl methacrylate, also have potential as drug delivery systems.

Chiral saccharide polymers are often utilized in separation science as chromatographic support.[22-27] In addition, DeSimone and co-workers[28] have synthesized amphiphilic glycopolymers that are CO_2 soluble. This discovery may show a way to dissolve materials otherwise insoluble materials into CO_2, allowing for novel, solvent-free, separation techniques.

In addition to biomedical applications, glycopolymers have shown capability in packaging as a replacement for urethane plastics. As stated previously, natural saccharides have many advantages over petroleum-based products. Glycopolymers have good physical properties and are potentially more affordable than petrochemical-based polymers. Therefore, in place of the non-renewable polymers, glycopolymers utilized in the production of packaging materials, adhesives, elastomers, and coatings are potentially a superior alternative. Another point to consider is the lower toxicity of glycopolymers. Urethanes are produced with isocyanates that can react with water to produce suspected carcinogenic compounds.[29] Glycopolymers are thus much safer in food packaging than isocyanate components. The well-known carbon Michael chemistry utilized to cure saccharide-based monomers with natural materials, such as glycerol, isosorbide, and modified agricultural crop oils, have potential to produce safe, biodegradable packaging products.

13.4 Incorporation of saccharide functionalities into vinyl polymers

Many synthetic polymers are currently utilized at the interface of biology and chemistry. For example, poly(ethylene oxide), or PEO, is widely known as a biocompatible material.[16] There are several reasons why chemists have focused on the incorporation of saccharide functionalities into polymers. First, if the polymer is utilized in drug delivery, it must bind specific targets via interactions at various functional groups in the polymer. In order to accomplish this, the polymers must have well-defined architecture. Second, saccharides are

renewable resources, thus petroleum-based materials are not consumed. Third, saccharide-containing polymers possess biodegradable characteristics. As stated previously, "glycopolymer" is typically the term given to the class of polymers that contain saccharide units, either in the backbone of the polymer or as a functional pendant group. This section will focus on the various synthetic techniques chemists utilize to make well-defined glycopolymers.

13.4.1 Protection and deprotection chemistry

It is necessary to protect specific hydroxyl groups of saccharide functionalities in monomers before polymerization occurs. Typically, isopropylidene and benzylidene groups are utilized for this purpose. The isopropylidene group is attached to 1,2-*cis* hydroxyl groups to make a five-membered ketal ring with acetone, using a sulfuric acid or zinc chloride catalyst.[30,31] The benzylidene group is formed on 1,3-*cis* hydroxyl groups upon reaction with benzaldehyde to yield a six-membered acetal ring.[31] Acyl esters are frequently utilized in protecting hydroxyl groups. Synthesized via reacting pyridine with an anhydride or acid chloride, they are stable under acidic conditions, but are reactive towards bases.[32] Figure 13.1 demonstrates several examples of these protected saccharides.

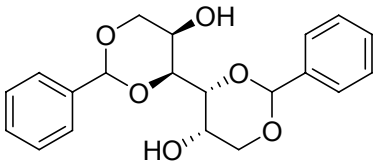

1,3;4,6-di-O-benzylidene galactitol

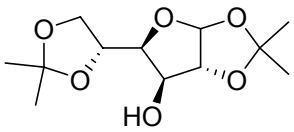

1,2;5,6-di-O-isopropylidene-D-glucofuranoside

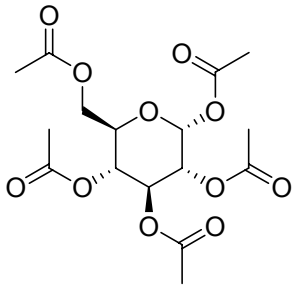

α-D-glucose pentaacetate

Figure 13.1. Examples of protected saccharides.[31]

Acid-catalyzed hydrolysis is utilized to deprotect hydroxyl groups after polymerization has occurred. Careful control of the pH is necessary in order to avoid depolymerization, esterification, or formation of insoluble polymers.[30] Coles et al.[33] have shown that isopropylidene groups are selectively removed at a faster rate from certain diols than from others. This is considered advantageous if certain chemical reactions are desired only at particular diols. Water solubility is achieved via complete deprotection to make the polymers hydrophilic. The most widely utilized reagents for deprotection of isopropylidene and benzylidene are 90 % trifluoroacetic acid in water,[34] 80 % formic acid in water,[35] and I_2 in methanol.[31]

Several groups have shown that protective groups are not required for certain polymerizations, including some atom transfer radical polymerization (ATRP), ring opening metathesis polymerization (ROMP), and cyanoxyl mediated reactions. Examples of such chemistry are described in later sections. However, protective chemistry is widely utilized in the synthesis of well-defined glycopolymers.

13.4.2 Synthesis

Due to the numerous equally reactive hydroxyl groups in glycopolymers, syntheses are somewhat challenging. Many efforts to protect the proper hydroxyl groups so that polymerization yields stereoregular polymers are necessary. There are several chemical compositions of glycopolymers. Linear, dendritic, graft, and cross-linked polymers are synthesized in a variety of ways. The following sections will discuss these concepts further.

13.4.2.1 Conventional free radical polymerization

Free radical polymerizations are widely utilized in polymer synthesis. In fact, over 80 % of commercial polymers are made using this process.[36] Advantages of this technique are numerous. Reaction conditions and monomer functionality are varied largely, the required solvent and monomer purity is not difficult to achieve, and initiators are inexpensive. However, the main disadvantages include broad polydispersities and difficulty in controlling molecular weight.

The first glycopolymer was synthesized in 1978. Horejsi et al.[37] synthesized poly(acrylamide) and (poly)allylic glycosides with ammonium persulfate as the initiator and tetramethylethylenediamine (TMEDA) as the catalyst. Since then, many researchers have reported syntheses of poly(vinyl saccharide)s and other glycopolymers via conventional free radical polymerization. Wulff described the saccharide pendant attachment through various functional groups, including ethers, esters, amides, ureas, or carbon-carbon bonds.[30,38] Utilizing water as the solvent in glycopolymer synthesis is advantageous over petroleum based solvents. Zhou et al.[26] synthesized high molecular weight urea-linked polystyrene with pendant lactose in water. Today, conventional free radical polymerization is not typically employed as a means to synthesize glycopolymers, due to the lack of control using this technique. Control of all aspects

of the polymerization is critical, as the final use of the polymer dictates that the materials lack any defects that would lessen the efficacy of the biomaterial. More advanced techniques, such as "living" polymerizations, are utilized to control the architectural structure and molecular weight of the polymer.

13.4.2.2 Ionic polymerization

Few glycopolymers synthesized using both cationic and anionic polymerizations are reported. Both "living" anionic and cationic polymerizations have several advantages, including low polydispersities (typically less than 1.20), controlled molecular weight, controlled stereochemistry, and minimal chain transfer. However, there are several disadvantages of "living" ionic polymerizations. First, polar hydroxyl groups affect the solvating ability of the solvent[39] and could promote chain transfer or termination.[40] Second, ionic polymerizations generally require lower temperatures than typical free radical polymerizations;[39] consequently, industrial scale-up is limited. Finally, monomer variety is restricted. Cationic polymerizations favor monomers containing electron-donating groups, while anionic polymerizations favor electron-withdrawing substituents.[39]

Nevertheless, it is possible to synthesize glycopolymers using ionic polymerization. Higishimura et al.[41] and Miyamoto et al.[6] synthesized derivatized styrenes and ethers using cationic polymerization via the optimization of initiators composed of weak Lewis acids and hydrogen iodide. Yamada et al.[42] successfully polymerized 1-*O*-(vinyloxy)ethyl-3,4,6-tri-*O*-acetyl-2-deoxy-2-phthalimide-β-D-glucopyranoside with an initiating system consisting of TFA/$EtAlCl_2$ through cationic polymerization, as well as block copolymers consisting of the vinyl ether of 3,4,6-tri-*O*-acetyl-2-deoxy-2-phthalimido-β-D-glucose and isobutyl vinylether.[6] In addition, the same researchers discovered that using zinc iodide and hydrogen chloride as the

initiating system for the copolymerization of 3-*O*-(vinyloxy)ethyl-1,2:5,6-di-*O*-isopropylidene-D-glucofuranose and isobutyl vinylether produced amphiphilic block copolymers.[43]

D'Agosto et al. applied a kinetic study to their work to determine if the polymerization of 1,2:3,4-di-*O*-isopropylidene-6-*O*-(2-vinyloxyethyl)-D-galactopyranose, with an initiating system of acetaldehyde diethylacetal/trimethylsilyl iodide/$ZnCl_2$, can tolerate polar functional groups.[40,44] The research group constructed a linear conversion versus time plot from size exclusion chromatography and ^{1}H NMR kinetic studies, and the results confirmed a lack of chain transfer and termination.[40]

Due to the many limitations stated previously, researchers have only recently begun exploring "living" anionic polymerization of glycopolymers. In 1998, Hirao et al. synthesized six monosaccharide-derivatized styrenes using anionic polymerization.[45] The monomers were first protected with acetal groups, polymerized with *sec*-butyl lithium as the initiator at –78 °C, terminated with methanol, and then deprotected under acidic conditions. The research group noted the typical orange-red color of the anion in solution.

DeSimone et al.[28] first employed glycosides to make glycopolymers via anionic polymerization in 2001. The research group successfully polymerized poly(3-*O*-methacryloyl-1,2:5,6-di-*O*-isopropylidene-D-glucofuranose) and block copolymers of poly(3-*O*-methacryloyl-1,2:5,6-di-*O*-isopropylidene-D-glucofuranose) and poly(1,1-dihydroperfluorooctyl methacrylate).

13.4.2.3 Controlled free radical polymerization

Controlled free radical polymerizations are also classified as "living" polymerizations. According to definition, "living" polymerizations are devoid of termination and chain transfer steps found in typical free radical polymerization. In addition, the rate is first order with respect

to monomer concentration.[39] For successful controlled polymerizations, the initiation step must proceed at a rate greater than or equal to that of propagation. This type of polymerization was developed to overcome the various disadvantages of conventional free radical polymerization discussed previously. Improved control of molecular weight, lower polydispersity, and enhanced understanding of structure-property relationships are gained in controlled free radical polymerization. There are several types of techniques that were developed in recent years including nitroxide- and copper-mediated controlled polymerizations. In addition, ATRP has recently become an increasingly popular way to synthesize polymers containing saccharide pendant groups with defined architecture, while controlling the molecular weight and polydispersity.

Fukuda et al. were the first to perform controlled free radical polymerizations through ATRP[46] and nitroxide mediated polymerization (NMP)[47] methods of styryl and methacryloyl glycopolymers. 3-*O*-methacryloyl-1,2:5,6-di-*O*-isopropylidene-D-glucofuranose was polymerized as a homopolymer and as a copolymer with styrene using ATRP with an alkyl halide and copper complex. Meng et al.[48] synthesized poly(6-*O*-methacryloyl-1,2;3,4-di-*O*-isopropylidene-D-galactopyranose) using ATRP and reported that in polar solvents, ATRP was optimized through varying initiators, catalysts, ligands, and temperatures. Narain et al.[49,50] recently reported the first ATRP synthesis of unprotected hydroxyl groups on glycopolymers. The research group reported that various functional groups were unaffected in ATRP synthesis, including hydroxyl groups; thus, ATRP provides a simple, direct route for the synthesis of glycopolymers under mild conditions. Mueller and co-workers[51,52] have recently applied ATRP in the synthesis of 2-(2-bromopropionyloxy)ethyl acrylate, 3-*O*-acryloyl-1,2:5,6-di-*O*-isopropylidene-α-D-glucofuranoside and 2-(2-bromoisbutyryloxy)ethyl methacrylate, as well as

3-*O*-methacryloyl-1,2:5,6-di-*O*-isopropylidene-α-D-glucofuranoside highly branched glycopolymers, for biomedical applications.

Nitroxide-mediated controlled free radical polymerization and copper-mediated living radical polymerization (CMLRP) also are considered controlled polymerizations. Nitroxide-mediated polymerizations are favored over CMLRP as there is no transition metal to remove. In addition, the reactions are performed without solvent. The molecular weight is controlled and polydispersities are lowered with nitroxide-mediated free radical polymerization.[34] These characteristics are desirable for high performance materials that are potentially suitable as biomaterials. Typical nitroxides capable of mediating polymerization include 2,2,6,6-tetramethylpiperidinoxyl (TEMPO), di-*tert*-butyl nitroxide, *tert*-butyl-2-methyl-1-phenylpropyl nitroxide, and *tert*-butyl-1-diethylphosphono-2,2-dimethyl nitroxide.[39] Structures of these nitroxides are shown in Figure 13.2.

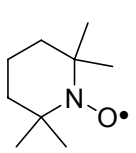

2,2,6,6-tetramethyl-1-piperidinoxyl

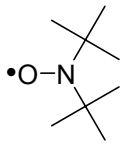

di t-butyl nitroxide

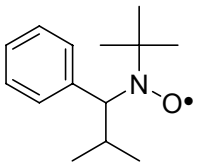

t-butyl 2-methyl-1-phenylpropyl nitroxide

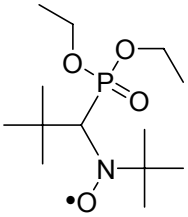

t-butyl 1-diethylphosphono-2,2-dimethylpropyl nitroxide

Figure 13.2. Typical nitroxides utilized in controlled free radical polymerization.[39]

It is possible to synthesize block copolymers using nitroxide-mediated polymerization. The nitroxide-capped radicals can further react with another monomer and initiate polymerization. Wulff et al.[34,53] synthesized polystyrene with reactive saccharide functionalities

using TEMPO as the initiator to yield monodisperse products. The styrene-saccharide unit formed at a carbon-carbon bond, thus creating a stable molecule. In addition, copolymers of various feed compositions were successfully synthesized. Kinetic studies were performed to demonstrate the controlled fashion of the polymerization.

Fukuda et al.[54] synthesized novel *N*-*p*-vinylbenzyl-2,3,5,6-tetra-*O*-acetyl-4-*O*-(2,3,4,6-tetra-*O*-acetyl-*b*-D-galactopyranosyl)-D-gluconamide under controlled polymerization conditions. This glycopolymer is an artificial glycolipid that has potential in drug delivery systems. Hawker and co-workers[55] have also synthesized biocompatible mimics for cellular membrane material with novel lipo-glycopolymers that also have potential in drug delivery. The initiator (Figure 13.3) utilized in the process of these amphiphilic polymers must have a non-polar tail group, just as a natural cellular lipid does.

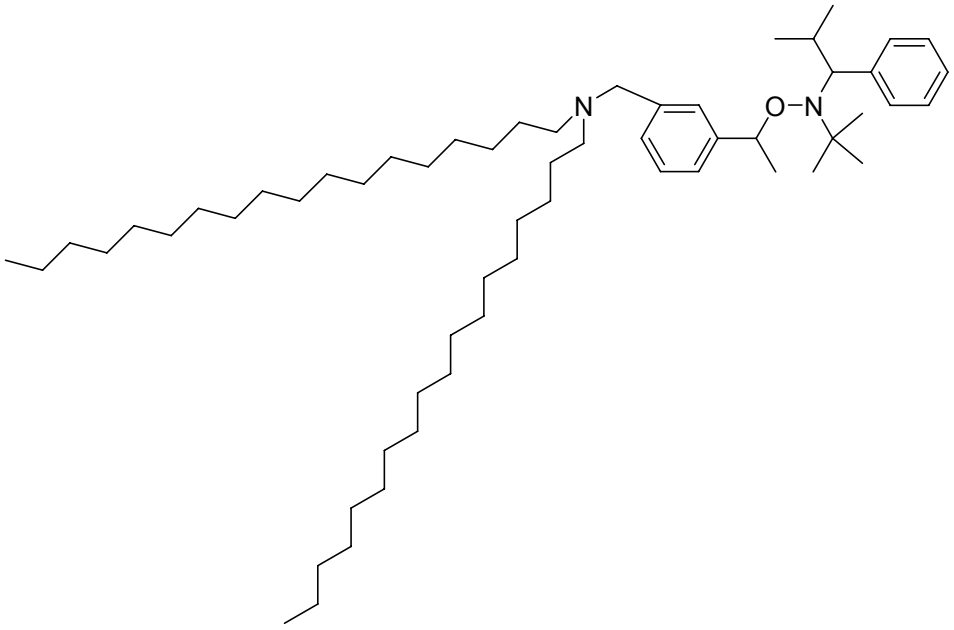

Figure 13.3. Novel nitroxide initiator developed for lipo-glycopolymerization.[55]

Chaikof and co-workers[56-60] developed cyanoxyl-mediated (·OC≡N) polymerizations for glycopolymers. In this technique, it is unnecessary to protect the monomers before synthesis, which makes the polymerization process facile. An extensive collection of functional groups,

such as -OH, -NH_2, -COOH, and –SO_3^- can tolerate the polymerization conditions without protective groups.[59,60] Chaikof et al. synthesized sulfonated and non-sulfonated acrylamide,[56,58,59] acrylate[57], and alkene[57] based glycopolymers bearing lactose pendants. These polymers exhibit remarkable binding activity and serve as ligands.[58]

13.4.2.4 Ring opening metathesis polymerization

Ring opening metathesis polymerization (ROMP) is quite valuable for polymer chemists. The primary advantage is that monomer protection at hydroxyl or other polar ends is not required, due to the catalysts utilized. This makes the synthesis of the polymers much simpler, as protection and deprotection chemistry can become complicated. Second, low polydispersities and controlled molecular weight are attainable. Third, it is possible to synthesize block copolymers.

Typical ring opening metathesis polymerizations proceed with molybdenum alkylidene initiators. Schrock and co-workers[61] employed Mo(CHCMe_2Ph)(N-2,6-*i*-$Pr_2C_6H_3$)(O-*t*-Bu)$_2$ as the initiator in the polymerization of four isopropylidene protected norbornene monomers. Low molecular weight distributions (less than 1.25), were obtained successfully for water-soluble homopolymers and block copolymers.

However, these initiators are not appropriate for every type of monomer. Grubbs et al. discovered that ruthenium carbene initiators[62] (Figure 13.4) work exceptionally well for ROMP. However, removal of the ruthenium metal is required if the polymer is used in biomedical applications. Few types of monomers are currently employed in ROMP due to catalyst and monomer incompatibility.[3]

Figure 13.4. Novel ruthenium initiators developed for ROMP.[62]

Grubbs et al.[62] compared reaction rates in various solvents, and revealed that the polymerization proceeds at a faster rate in methylene chloride than in benzene. The reactions are typically performed at room temperature. Nevertheless, if the initiator is less reactive, namely, the triphenylphosphine initiator shown on the left in Figure 4, temperatures up to 50 °C are required for polymerization to proceed.

13.4.2.5 Ring opening polymerization

Ring opening polymerizations occur cationically with anhydro saccharides. Aoi et al. first reported the cationic ring opening polymerizations in 1994.[63] Saccharide-substituted *α*-amino acid N-carboxyanhydrides (NCAs) were prepared using triethylamine or acetonitrile as the initiator. Acetonitrile yielded the polymer with the highest molecular weight (1.9×10^4 g/mol). Later, in 1997, Aoi and co-workers[64] prepared novel block copolymers, poly(2-methyl-2-oxazoline)-*b*-poly(L-phenylalanine), poly(2-methyl-2-oxazoline)-*b*-poly(*γ*-benzyl-L-glutamate), poly(2-methyl-2-oxazoline)-*b*-poly-[*O*-(tetra-*O*-acetyl-β-D-glucopyranosyl)-L-serine], and poly(2-phenyl-2-oxazoline)-*b*-poly[*O*-(tetra-*O*-acetyl-β-D-glucopyranosyl)-L-serine] using cationic ring opening polymerization.

Hatanaka and co-workers[65] synthesized comb-shaped polymers from 1,6-anhydro-3-*O*-benzyl-2-deoxy-4-*O*-(2',3',4',6'-tetra-*O*-benzyl-*α*-D-glucopyranosyl)-*β*-D-arabino-hexopyranose with mostly *α*-1,6 linkages in the backbone and some cyclic oligosaccharides. The authors reported that the comb characteristics of the polymer contributed to the enhanced biological activity, as there were more carbohydrate sites in the polymer. Similarly, Patten et al.[66]

synthesized 1,6-anhydro-3,4-di-*O*-benzyl-2-deoxy-*β*-D-glucose polymers from cationic ring opening polymerization. The group concluded that the process was primarily controlled, with minimal hydrochloric acid initiation and backbiting. Their conclusions were drawn from extensive mass spectroscopy analysis of the polymer and its endgroups.

Ring opening polymerizations were used in conjunction with ATRP to synthesize glycopolymers. Combined, these processes have created more complex glycopolymer architectures, such as star and comb-type polymer structures. Dong et al.[67] synthesized glycopolymer-polypeptide triblock copolymers of poly(L-alanine)-*b*-poly(2-acryloyloxyethyllactoside)-*b*-poly(L-alanine) that show potential in biomedical applications due to their natural ability to self-assemble. This was accomplished through polymerizing the glycopolymer 2-*O*-acryloyloxyethoxyl-(2,3,4,6-tetra-*O*-acetyl-*β*-D-galactopyranosyl)-(1-4)-2,3,6-tri-*O*-acetyl-*β*-D-glucopyranoside using ATRP and functionalizing the endgroups to diamines. This macroinitiator was then utilized with L-alanine-*N*-carboxyanhydrides in ring opening polymerization to ultimately yield the triblock copolymer. Chen and co-workers[35] were the first to synthesize polyester/poly(vinyl saccharide) star block copolymers. The novel molecules were prepared using ring opening polymerization of *ε*-caprolactone, then ATRP was utilized for the methacrylate with a galactose pendant saccharide.

13.5 Oxidative stress of polymers

Oxidative stress is an imbalance in oxidants. To alleviate this problem, antioxidants or other defense mechanisms are used. Oxidants, such as reactive oxygen species (ROS), are typically free radicals or molecules that cause free radicals to form. Typical ROS are given in Table 13.1. The free radicals then cause consecutive one-electron oxidation reactions to occur, damaging the system, a biomolecule *in vivo* or *ex vivo*.[68]

Alkoxyl radical	RO•
Hydroperoxide	ROOH
Hydroperoxyl radical	HOO•
Hypochlorite	$^{-}$Ocl
Hydrogen peroxide	H_2O_2
Hydroxyl radical	HO•
Nitric oxide radical	NO•
Peroxyl radical	ROO•
Peroxynitrite	$ONOO^{-}$
Singlet Oxygen	$^{1}\Delta O_2$

Table 13.1. Reactive oxygen species.[68]

As stated previously, glycopolymers are almost exclusively utilized as biomaterials for medical applications. With this is mind, it is imperative to consider the result of inserting the polymers into the human body environment. In physiological systems, molecules are constantly bombarded with radicals produced via single-electron reactions. The major contributor to production of ROS in the body is the mitochondria.[69] In addition, ROS are a product of the electron transport chain.

To slow the process of oxidative degradation, antioxidants are used. Antioxidants are synthetic or natural materials that inhibit or slow the rate of oxidative damage, produced via radical species, to a system. The two key classes of antioxidants are chain-breaking antioxidants, or primary antioxidants—those that eliminate polymer radicals, and preventative anti-oxidants, or secondary antioxidants—those that obstruct radical formation. Primary radicals include hindered phenols, hindered aromatic amines, hydroxyamines, quinines, and lactones. Phosphite

esters, thioesters, metal dithiolates, metal chelating molecules, 2-hydroxybenzophenone derivatives, and 2-hydroxybenzotriazole derivatives formulate the class of secondary antioxidants.[70]

Medical devices are typically sterilized using either chemical or heating processes. The use of ionizing radiation is a fast, simple way to sterilize materials. However, Woo and co-workers discovered that this sterilization technique caused enhanced rates in the oxidative degradation of biomaterials, as the materials analyzed were protected with phenol-based antioxidants. [71] The effect was measured via differential scanning calorimetry (DSC) using ASTM standardized methods to analyze oxidative induction time (OIT) isothermally. The results indicated that radical reactions were created upon ionization from high-energy electrons, and the antioxidant was sacrificed as a proton source to end the radical reaction process.

13.5.1 Techniques to measure oxidative stability

Researchers have developed many detection methods to investigate oxidative degradation of macromolecules. Chemiluminescence, a technique relies on light emission that occurs during oxidation reactions, is a rapid way to determine oxidative stability of polymers.[72] Two types of chemiluminescence experiments are possible. The first is performed at a constant temperature in an oxygen atmosphere to measure the oxidation induction time (OIT). The second is performed at variable temperature in an inert gas to measure the OIT. DSC is another technique utilized to determine oxidative stability. The instrument is run isothermally and OIT is taken as the onset of an exotherm. A third method for determining the oxidative stability of polymers is utilizing a combination of DSC and chemiluminescence. Fearon and co-workers[73] have developed this technique via a DSC with a chemiluminescence detector attached. The data obtained correlates

well over a broad range of temperatures that is unattainable with chemiluminescence alone, and chemiluminescence can detect peroxides at lower levels than can DSC alone.

Perhaps the most reliable means for determining oxidative stability of materials is using electron paramagnetic resonance spectroscopy (EPR), also known as electron spin resonance spectroscopy (ESR).[74] This analytical technique detects free radical formation. However, many radical formations have short lifetimes, therefore, spin trapping is utilized. Spin trapping involves a reaction of a radical species with a more stable free radical, such as a nitroxide, yielding a more stable radical species with a longer lifetime. Reasonable spin traps include N-*tert*-butyl-α-phenylnitrone (PBN), 5,5-dimethyl-1-pyrroline-*N*-oxide (DMPO), and α-(4-pyridyl-1-oxide)-*N*-*tert*-butylnitrone (4-POBN).[74] EPR is usually performed *in vitro*, due to hesitation of utilizing the toxic spin traps in the body.

A fifth technique for evaluating the oxidative stability of polymers is oxygen uptake. The amount of oxygen consumed over a period of time is measured, and this value varies based on several kinetic parameters including induction period, process rate, and activation energy.[75] Other techniques, such as infrared spectroscopy, are performed *in situ*. The disappearance and appearance of functional groups is indicative that oxidative degradation is occurring.

13.5.2 Oxidative stability of polymers with saccharide pendant groups

Polymeric materials have characteristic lifetimes; the greatest factor contributing to this lifetime is oxidative degradation.[72] Over time, materials tend to degrade via scission reactions due to oxygen in the atmosphere. Polymer degradation is similar to low molecular weight organic molecule degradation. First, heat, light, stress, transition metals, and various other sources catalyze reactions that form alkyl radicals. The reaction of the alkyl radicals with oxygen produces peroxy radicals (ROO·). Auto-oxidation then takes place, producing a variety

of smaller molecules and radicals, as shown in Figure 13.5.[70] Ultimately, termination takes place, when two radicals combine, yielding less reactive materials.

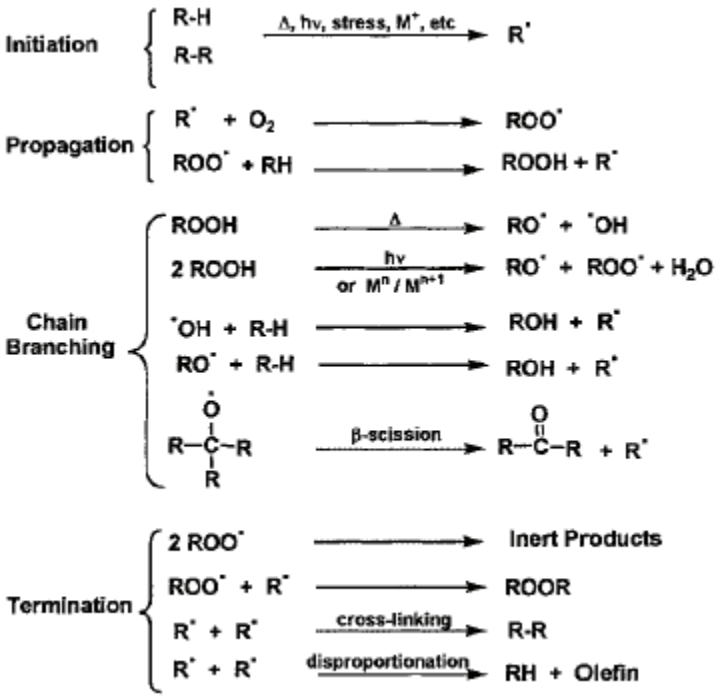

Figure 13.5. The auto-oxidation process in the degradation of polymers.[70]

The hydroxyl groups of glycopolymers are oxidized more readily than typical alcohol functionalities. This is because the hydroxyl group of saccharides is more acidic than are typical alcohols. Oxygen in neutral or basic conditions will readily oxidize saccharide pendants on glycopolymers. However, glycopolymers can become oxidized with many other organic compounds, including halogen-based compounds, peroxy acids, phenylhydrazine, hydrogen peroxide, metal oxides, and nitrogen-based compounds, including nitric acid, nitrogen dioxide, and nitroxyl radicals.[76]

When reducing saccharides are oxidized, aldonic acids are formed.[77] Sterics play an important role in the oxidation of saccharide functionalities on polymers. Thus, primary alcohols are oxidized more readily than are secondary alcohols. Axial carbons with hydroxyl

functionalities are attacked in five-membered ring systems if secondary alcohols are the only source of hydroxyl available for oxidation. If cyclic structures are attached to the saccharide functionality, attack is likely to occur at the carbon attached to an *endo* alcohol functionality.[78]

13.6 Conclusions

This literature review described the synthesis of glycopolymers containing terminal saccharide or pendant saccharide functionalities. The macromolecules offer properties useful for biomimetics, glycopolymer-protein interactions, treatments of infectious viruses, drug delivery, separation science, and packaging materials. Conventional free radical polymerization and controlled free radical polymerization techniques were described as successful methods for synthesizing glycopolymers. In addition, methods for detecting oxidative degradation were described, and polymer oxidative degradation was introduced and compared to glycopolymer oxidative degradation.

13.7 References

(1) Singh, S. K.; Gross, R. A., Overview: Introduction to Polysaccharides, Agroproteins, and Poly(amino acids). In *Biopolymers from Polysaccharides and Agroproteins*, Gross, R. A.; Scholz, C., Eds. American Chemical Society: Washington DC, 2001.
(2) Kao, W. J., Biomimetics. In *Polymeric Biomaterials*, 2nd ed.; Dumitriu, S., Ed. Marcel Dekker, Inc.: New York, 2002; pp 63-77.
(3) Ladmiral, V.; Melia, E.; Haddleton, D. M. *European Polymer Journal* **2004,** 40, 431-449.
(4) Okada, M. *Progress in Polymer Science* **2001,** 26, 67-104.
(5) Lee, Y. C.; Lee, R. T.; Rice, K.; Ichikawa, Y.; Wong, T.-C. *Pure and Applied Chemistry* **1991,** 63, 499.
(6) Yamada, K.; Minoda, M.; Miyamoto, T. *Macromolecules* **1999,** 32, 3553-3558.
(7) Lundquist, J. J.; Toone, E. J. *Chemical Reviews* **2002,** 102, 555-578.
(8) McCoy, J. P.; Varani, J.; Goldstein, I. J. *Experimental Cell Research* **1984,** 151, (1), 96-103.
(9) Warwel, S.; Bruse, F.; Demes, C.; Kunz, M.; Klaas, M. R. *Chemosphere* **2001,** 43, 39-48.
(10) Simanek, E. E.; McGarvey, G. J.; Jablonowski, J. A.; Wong, C. H. *Chemical Reviews* **1998,** 98, 833-862.
(11) Aoi, K.; Itoh, K.; Okada, M. *Macromolecules* **1995,** 28, 5391-5393.

(12) Strong, L. E.; Kiessling, L. L. *Journal of the American Chemical Society* **1999,** 121, 6193.
(13) Cairo, C. W.; Gestwicki, J. E.; Kanai, M.; Kiessling, L. L. *Journal of the American Chemical Society* **2002,** 124, 1615.
(14) Gestwicki, J. E.; Cairo, C. W.; Strong, L. E.; Oetjen, K. A.; Kiessling, L. L. *Journal of the American Chemical Society* **2002,** 124, 14992.
(15) Roy, R. *Current Opinion in Structural Biology* **1996,** 6, 692-702.
(16) Cunliffe, D.; Pennadam, S.; Alexander, C. *European Polymer Journal* **2004,** 40, 5-25.
(17) Totani, K.; Kubota, T.; Kuroda, T.; Murata, T.; Hidari, K. I. P. J.; Suzuki, T.; Suzuki, Y.; Kobayashi, K.; Ashida, H.; Yamamoto, K.; Usui, T. *Glycobiology* **2003,** 13, (5), 315-326.
(18) Peppas, N. A.; Kim, B. *Journal of Biomaterials Science Polymer Edition* **2002,** 13, (11), 1271-1281.
(19) Caneiro, M. J.; Fernandes, A.; Figneiredo, C. M.; Fortes, A. G.; Freitas, A. M. *Carbohydrate Polymers* **2001,** 45, 135-138.
(20) Volker, B.; Stadler, R. *Polymer* **1998,** 39, 1617.
(21) Chen, X. C.; Dordick, J. S.; Rethwisch, D. G. *Macromolecules* **1995,** 28, 6014-6019.
(22) Liu, X. C.; Dordick, J. S. *Journal of Polymer Science: Part A: Polymer Chemistry* **1999,** 37, (11), 1665-1671.
(23) Kobayashi, K.; Sumitomo, H. *Macromolecules* **1980,** 13, (2), 234-239.
(24) Roy, R.; Tropper, F. D. *Journal of Chemical Society, Chemical Communications* **1988**, (15), 1058-1060.
(25) Kobayashi, K.; Sumitomo, H.; Ina, Y. *Polymer Journal* **1985,** 17, (4), 567-575.
(26) Zhou, W.; Kurth, M. J.; Hsieh, Y. L.; Krotcha, J. M. *Macromolecules* **1999,** 32, 5507-5513.
(27) Wulff, G.; Schmidt, J.; Venhoff. *Macromolecular Chemistry and Physics* **1996,** 197, 259-274.
(28) Ye, W.; Wells, S.; Desimone, J. M. *Journal of Polymer Science: Part A: Polymer Chemistry* **2001,** 39, 3841-3849.
(29) Bourma, K.; Wijma, E. *Migration of Primary Aromatic Amines from Multilayer Films for Food Packaging*; ND1FC004/01; 2001.
(30) Narain, R.; Jhurry, D.; Wulff, G. *European Polymer Journal* **2002,** 38, (2), 273-280.
(31) Robyt, J. F., *Essentials of Carbohydrate Chemistry*. Springer: New York, 1998.
(32) Dekker, C. A.; Goodman, L., Chemical Reaction of the Sugar Portion of Nucleosides. In *The Carbohydrates: Chemistry and Biochemistry*, 2nd ed.; Pigman, W.; Horton, D.; Herp, A., Eds. Academic Press: New York, 1970; Vol. IIA, pp 26-27.
(33) Coles, H. W.; Goodhue, L. D.; Hixon, R. M. *Journal of the American Chemical Society* **1929,** 51, 523-525.
(34) Chen, Y.; Wulff, G. *Macromolecular Chemistry and Physics* **2001,** 202, (17), 3426-3431.
(35) Chen, Y. M.; Wulff, G. *Macromolecular Rapid Communications* **2002,** 23, 59-63.
(36) *Chemical and Engineering News* **1991**.
(37) Horejsi, V.; Smolek, P.; Kocourek, J. *Biochimica et Biophysica Acta* **1978,** 538, (2), 293-298.
(38) Varma, A. J.; Kennedy, J. F.; Galgali, P. *Carbohydrate Polymers* **2004,** 56, 429-445.
(39) Odian, G., *Principles of Polymerization*. 4th ed.; John Wiley & Sons, Inc.: Hoboken, New Jersey, 2004.

(40) D'Agosto, F.; Charreyre, M.-T.; Delolme, F.; Dessalces, G.; Cramail, H.; Deffieux, A.; Pichot, C. *Macromolecules* **2002,** 35, 7911-7918.
(41) Higashimura, T.; Sawamoto, M., In *Comprehensive Polymer Science*, Eastmond, G. C.; Ledwith, A.; Russo, S.; Sigwalt, P., Eds. Pergamon Press: Oxford, 1989; Vol. 3, pp 673-696.
(42) Yamada, K.; Minoda, M.; Miyamoto, T. *Journal of Polymer Science: Part A: Polymer Chemistry* **1997,** 35, 751-757.
(43) Yamada, K.; Yamaoka, K.; Minoda, M.; Miyamoto, T. *Journal of Polymer Science: Part A: Polymer Chemistry* **1997,** 35, 255-261.
(44) D'Agosto, F.; Charreyre, M.-T.; Pichot, C.; Mandrand, B. *Macromolecular Chemistry and Physics* **2002,** 203, 146-154.
(45) Loykulnant, A.; Hayashi, M.; Hirao, A. *Macromolecules* **1998,** 31, 9121-9126.
(46) Ohno, K.; Tsujii, Y.; Fukada, T. *Journal of Polymer Science: Part A: Polymer Chemistry* **1998,** 36, (14), 2473-2481.
(47) Ohno, K.; Tsujii, Y.; Miyamoto, T.; Fukada, T.; Goto, M.; Kobayashi, K.; Akaike, T. *Macromolecules* **1998,** 31, (4), 1064-1069.
(48) Meng, J. Q.; Du, F. S.; Liu, Y. S.; Li, Z. C. *Journal of Polymer Science: Part A: Polymer Chemistry* **2005,** 43, 752-762.
(49) Narain, R.; Armes, S. P. *Chemical Communications* **2002,** 23, 2276-2777.
(50) Narain, R.; Armes, S. P. *Macromolecules* **2003,** 36, (13), 4675-4678.
(51) Muthukrishnan, S.; Jutz, G.; Andre, X.; Mori, H.; Mueller, A. H. E. *Macromolecules* **2005,** 38, 9-18.
(52) Muthukrishnan, S.; Mori, H.; Mueller, A. H. E. *Macromolecules* **2005,** in press.
(53) Chen, Y.; Wulff, G. *Macromolecular Chemistry and Physics* **2001,** 202, (17), 3273-3278.
(54) Ohno, K.; Fukada, T.; Kitano, H. *Macromolecular Chemistry and Physics* **1998,** 199, 2193-2197.
(55) Gotz, H.; Harth, E.; Schiller, S. M.; Frank, C. W.; Knoll, W.; Hawker, C. J. *Journal of Polymer Science: Part A: Polymer Chemistry* **2002,** 40, 3379-3391.
(56) Grande, D.; Baskaran, S.; Baskaran, C.; Gnanou, Y.; Chaikof, E. L. *Macromolecules* **2000,** 33, 1123-1125.
(57) Grande, D.; Baskaran, S.; Chaikof, E. L. *Macromolecules* **2001,** 34, 1640-1646.
(58) Sun, X. L.; Faucher, K. M.; Houston, M.; Grande, D.; Chaikof, E. L. *Journal of the American Chemical Society* **2002,** 124, 7258-7259.
(59) Sun, X. L.; Grande, D.; Baskaran, S.; Hanson, S. R.; Chaikof, E. L. *Biomacromolecules* **2002,** 3, 1065-1070.
(60) Hou, S.; Sun, X. L.; Dong, C. M.; Chaikof, E. L. *Bioconjugate Chemistry* **2004,** 15, 954-959.
(61) Schrock, R. R.; Nomura, K. *Macromolecules* **1996,** 29, 540-545.
(62) Grubbs, R. H.; Fraser, C. *Macromolecules* **1995,** 28, (21), 7248-7255.
(63) Aoi, K.; Tsutsumiuchi, K.; Okada, M. *Macromolecules* **1994,** 27, 875-877.
(64) Tsutsumiuchi, K.; Aoi, K.; Okada, M. *Macromolecules* **1997,** 30, 4013-4017.
(65) Kasuya, M. C.; Hatanaka, K. *Macromolecules* **1999,** 32, 2131-2136.
(66) Liang, Y.-Z.; Franz, A. H.; Newbury, C.; Lebrilla, C. B.; Patten, T. E. *Macromolecules* **2002,** 35, 3402-3412.
(67) Dong, C. M.; Sun, X. L.; Faucher, K. M.; Apkarian, R. P.; Chaikof, E. L. *Biomacromolecules* **2004,** 5, 224-231.

(68) Abuja, P. M.; Albertini, R. *Clinica Chimica Acta* **2001,** 306, 1-17.
(69) Shiva, S.; Oh, J. Y.; Landar, A. L.; Ulasova, E.; Venkatraman, A.; Bailey, S. M.; Darley-Usmar, V. M. *Free Radical Biology and Medicine* **2005,** 38, 297-306.
(70) Al-Malaika. *International Materials Review* **2003,** 48, (3), 165-185.
(71) Woo, L.; Ling, M. T. K.; Ding, S. Y.; Westphal, S. P. *Thermochimica Acta* **1998,** 324, 179-185.
(72) Boxhammer, J. *Macromolecular Symposium* **2002,** 178, 11-24.
(73) Fearon, P. K.; Bigger, S. W.; Billingham, N. C. *Journal of Thermal Analysis and Calorimetry* **2004,** 76, 75-83.
(74) Rimbach, G.; Hohler, D.; Fischer, A.; Roy, S.; Virgili, F.; Pallauf, J.; Packer, L. *Archives of Animal Nutrition* **1999,** 52, 203-222.
(75) Zaharescu, T. *Materials Research and Innovations* **2001,** 5, 35-39.
(76) Varela, O. *Advances in Carbohydrate Chemistry and Biochemistry* **2003,** 58, 307-369.
(77) Arts, S. J. H. F.; Mombarg, E. J. M.; Van Bekkum, H.; Sheldon, R. A. *Synthesis* **1997**, 597-613.
(78) Green, J. W., Oxidative Reactions and Degradations. In *The Carbohydrates: Chemistry and Biochemistry*, 2nd ed.; Pigman, W.; Horton, D.; Wander, J. D., Eds. Academic Press: New York, 1980; Vol. IB, pp 1101-1156.

Chapter 14 : Overall Conclusions

The synthesis and characterization of novel Michael addition networks, ionene families, and ion-containing polyurethanes was described, with the underlying theme of investigating the structure-property relationships of segmented macromolecules.

With regard to ionenes, the Menschutkin reaction was used to prepare a series of water-soluble 12,12-ammonium ionenes from 1,12-dibromododecane and 1,12-bis(N,N-dimethylamino)dodecane. Absolute molecular weights were determined for the first time via MALLS with aqueous SEC, and structure-property relationships were established using tensile testing and DMA behavior as molecular weight varied. Specifically, DMA revealed glass transition temperatures that increased as molecular weight increased and ionic aggregate disassociation temperatures of 85 – 88 °C. Tensile analysis, reported for the first time, revealed the ionenes possessed excellent mechanical properties. X-ray scattering indicated the formation of ion-rich domains, with an average separation that correlated with the methylene spacer length between the ammonium cations. In addition, 12,12-ammonium ionenes were able to undergo triggered depolymerization in the presence of base. Since ionenes are ideal candidates for model polyelectrolytes in biomedical applications, a thorough analysis was conducted on SY5Y and COS-7 cell lines to determine the cytotoxicity of ionenes at various concentrations that are typical for gene transfection and antimicrobial action. Concentrations of ionenes ranged from 1-800 μg/mL, and significant cell viability was observed at concentrations less than 25 μg/mL, regardless of cell line utilized. There also was not a direct correlation between ionene weight-average molecular weight and cell viability.

For the first time, the ionenes were functionalized with either cinnamate or styrene groups and were then chain-extended or cross-linked via UV irradiation to impart improved

mechanical performance. 12,12-Ammonium ionenes containing cinnamate end groups were chain extended via UV irradiation and possessed enhanced mechanical properties (43.1 ± 0.4 MPa tensile stress and 640 ± 140 % elongation), which was a notable improvement compared to the non-UV irradiated analog. Thin films of ionene copolymers that possessed cinnamate functionality along the polymer backbone and at the chain ends and styrene-functionalized 12,12-ammonium ionenes were successfully cross-linked in the presence of UV light, and UV spectra were recorded over time to monitor the cross-linking reactions. These results demonstrated that cross-linked ionenes show promise as mechanically durable polyelectrolytes that have potential as membrane materials. This novel technique is a viable option to synthesize high molecular weight polymers using step-growth polymerization techniques in conjunction with UV irradiation.

The first synthesis of imidazolium-cation containing ionene copolymers was achieved through the use of PTMO dibromide oligomers, 1,12-dibromododecane, and 1,1'-(1,4-butanediyl)bis(imidazole). Hard segment contents ranged from 6-100 wt%, and structure-property relationships were established as a function of hard segment content. Thermal properties were measured via TGA and DSC, and the imidazolium ionene copolymers were thermally stable to temperatures greater than 257 °C, and crystallinity was observed via DSC for the copolymers containing PTMO soft segments. Film formation characteristics varied as a function of hard segment content, and free-standing films were obtained when hard segment content increased. Dynamic mechanical behavior of the 20 and 38 wt % hard segment copolymers demonstrated microphase separation. Tensile analysis indicated that the imidazolium copolymers that formed free-standing films were not elastomeric. X-ray scattering showed PTMO crystallinity for the imidazolium ionene containing 6 wt% hard segment. The

IAXS and SAXS curves demonstrated microphase separation for the same PTMO-imidazolium ionene. The X-ray scattering profile for the imidazolium ionene containing 100 wt% hard segment showed peaks at q~15.59 nm^{-1} and at q~2.70 nm^{-1}, which indicated the ionene was amorphous and possessed ionic aggregation, respectively.

Novel phosphonium-containing polyurethanes were synthesized and characterized using a variety of methods. For comparative purposes, polyurethanes containing 1,4-butanediol as the chain extender was also synthesized. DSC revealed that phosphonium polyurethanes were more crystalline, since they possessed both a T_c (-35 °C) and a T_m (14 °C). In addition, hydrogen bonding in the non-charged polyurethane restricted polymer mobility, and reduced PTMO crystallinity. FT-IR spectroscopy demonstrated that the hydrogen bonding interactions were significantly reduced due to the presence of phosphonium cations, with broad N-H regions (3300 cm^{-1}) and the absence of hydrogen bond carbonyls at ~1715-1730 cm^{-1}. The FT-IR spectroscopy data correlated well with tensile properties. The non-charged polyurethanes had excellent tensile strengths (23.97 ± 1.23 MPa) and elongation (1330 ± 63 %) values compared to the phosphonium polyurethane (19.24 ± 1.09 MPa, 1170 ± 180 %). WAXS demonstrated that the phosphonium and non-charged polyurethanes possessed low levels of crystallinity or were essentially amorphous at ambient temperature, while SAXS indicated that they exhibited hard segment microphase separation. STEM was employed to further investigate the ionic domains of the phosphonium polyurethanes, which revealed ion-rich domains within the hard segment. EDS during STEM imaging revealed the elemental composition of the ionic aggregates, which are enriched with bromine and phosphorus from the chain extender. This type of phosphonium diol chain extender opens a wide field of potential research in polyurethane ionomers.

Polyurethanes that contained bisimidazolium functionality in the hard segment were also synthesized. Again, the mechanical, morphological, and thermal properties of the ion-containing polyurethane were compared to a non-ion containing polyurethane, and revealed that the incorporation of the imidazolium hard segment caused the polyurethanes to demonstrate unique behavior. Specifically, the influence of incorporating imidazolium salt hard segments in polyurethanes was examined via TGA, DSC, DMA, FT-IR spectroscopy, X-ray scattering, STEM, and EDS. Thermal analysis indicated that the polyurethanes had similar thermal stabilities and the imidazolium salt-containing polyurethane possessed crystallinity, which was also observed for the phosphonium salt-containing polyurethanes described above. FT-IR spectroscopy indicated disruption of hydrogen bonding when ionic functionality was present. X-ray scattering, STEM, EDS, and DMA all indicated the presence of microphase separation.

In addition, a large portion of this dissertation focused on the Michael addition reaction. Initially, investigations on the kinetics of model Michael addition reactions were conducted with ethyl hexyl acrylate and ethyl acetoacetate to determine the effect of solvent, base, base concentration, and reactant molar ratio on the observed rate constant, which were determined via *in-situ* FTIR. A DOE analysis was conducted for reactions using DBU or K_2CO_3 as the base at various concentrations. Once conditions were established for small molecule Michael reactions, cross-linked films were prepared from PPG BisAcAc and PPGDA in the presence of either base. Again, *in-situ* FTIR spectroscopy was utilized to observe changes in the reaction over time, and observed rate constants were calculated. As expected, as the molecular weight of the PPG BisAcAc segment increased, the observed rate constant decreased. A dependence on PPG BisAcAc molecular weight on gel fraction analysis was observed, and revealed that increasing the molecular weight of PPG BisAcAc precursor resulted in lower gel fractions. However, the

base did not change the mechanical properties, according to the DMA results. Therefore, it appeared that base type was significant for the rate of the reaction, but not for the mechanical properties.

The influence of hydrogen bonding on mechanical and thermal behavior of Michael addition cross-linked networks was ascertained. PPG was successfully functionalized to incorporate acetoacetate endgroups via a transesterification reaction. EA-HMDI-EA, which contained urethane functionality, or NPGDA were then reacted with PPG AcAcs to prepare cross-linked films. The influence of PPG AcAc molecular weight on tensile and dynamic mechanical behavior was determined for both NPGDA and EA-HMDI-EA carbon-Michael networks. The stress at break and elongations at break for PPG BisAcAc (or TrisAcAc) – NPGDA networks ranged from 0.27 to 0.43 MPa and 52-117%, respectively. The urethane functionality significantly improved network mechanical performance. The stress at break and elongations at break for PPG BisAcAc – EA-HMDI-EA networks ranged from 0.10 to 0.54 MPa and 96-507%, respectively. A dependence on PPG AcAc molecular weight on gel fraction analysis was also observed, and revealed that increasing the molecular weight of PPG AcAc precursor resulted in lower gel fractions. These results were consistent with the PPG-based networks described in the previous paragraph. The networks could find potential applications in packaging and adhesives.

The Michael addition was also utilized to prepare poly(ethylene glycol) (PEG)-glutathione (GSH, an antioxidant) oligomers. DLS and TEM results indicated the formation of uniform nanoparticles, with particle sizes of 283 ± 4 nm via DLS and ~100 nm via TEM. However, the Michael addition products were not effective for antioxidant delivery since the thiol functional group was not free to react. Therefore, thiol-terminated PEG was synthesized

and reacted with GSH to form disulfide-linked oligomers, which were able to cleave to free thiol functional groups at the appropriate pH. SH-SY5Y cells were utilized in the cell culture experiments, and oxidative stress was induced on the cells with the use of H_2O_2. As expected, the Michael addition GSH-containing oligomers were not effective against protecting the cells from oxidative stress, since the C-S bond was not labile. However, disulfide-linked GSH-containing oligomers were 100 % effective at protecting the cells at a concentration of 250 μM.

Chapter 15: Suggested Future Work

15.1 Synthesis and structure-property relationships of novel ionenes

Several chapters of this thesis were devoted to ionene synthesis and structure-property relationships. Although ionene syntheses are well documented in the literature, there still remain many unexplored polymer compositions. First, poly(ethylene glycol) (PEG)-containing ionenes are not well documented throughout the literature, although PEG-containing polymers are known for their biocompatibility and use in conductive polymer applications. PEG-based ionenes with varying distance between charge sites should be synthesized. Different molecular weights of PEG will influence the mechanical and morphological performance of the ionenes, which will thus influence the final application properties, whether for gene transfection or electroactive devices.

Size exclusion chromatography (SEC) of ion-containing polymers is often complicated due to aggregation effects and interactions of the polymer with the column and mobile phase. However, our research group has shown successful separation and exact molecular weight determination of many ion-containing polymers, including the 12,12-ammonium ionenes described in this thesis. In the future, molecular weight characterization should be performed on all ion-containing polymers, including ionenes. Molecular weight is a critical polymer parameter that influences many thermal, mechanical, and morphological properties. Thus, it is self-evident that molecular weight analysis is required for accurate structure-property relationship investigations.

Most ionenes synthesized in our research group possess bromide counterions. However, a thorough investigation of the role of counteranion on ionene thermomechanical, morphological,

and solution behavior should be accomplished. Counteranion selection influences many properties due to changes in the ability to aggregate.

All of the ionenes described in this thesis are linear. The area of branched and cross-linked ionenes remains widely unexplored, as shown in chapter 2. Future efforts should focus on the synthesis and characterization of branched and cross-linked ionenes. The cross-linked ionenes would be ideal candidates for electroactive device membranes.

Chapter 2 also described the work of Galin et al.,[1-3] where zwitterionomers were compared to ionenes. Our research group focuses on the synthesis of zwitterionomers and ionenes. Therefore, novel ionene structures should be compared to similar zwitterionomers. The influence of a free counteranion versus one that is bound to the polymer chain has a distinct influence on the polymer properties.

Research in our lab has also focused on random ionene block copolymers. However, block copolymers, where the hard segment is preformed, will have different morphological and thermomechanical behavior. Therefore, future research efforts should focus on the synthesis of ionene copolymers with block structures. In addition, the effect of varying the soft segment composition and molecular weight should be investigated.

In chapter 3, a series 12,12-ammonium ionenes of various molecular weights were synthesized and their thermomechanical and morphological properties were investigated. An investigation of the solution properties in the presence of and in the absence of salt should be studied via DLS and solution rheology. Many researchers have reported the influence of charge density on the rheological properties of ammonium ionenes, but no one has reported the effect of molecular weight. As shown in Figure 15.1, an initial study of the solution rheology of a 12,12-ammonium ionene demonstrated that several transitions were observed concentration increased.

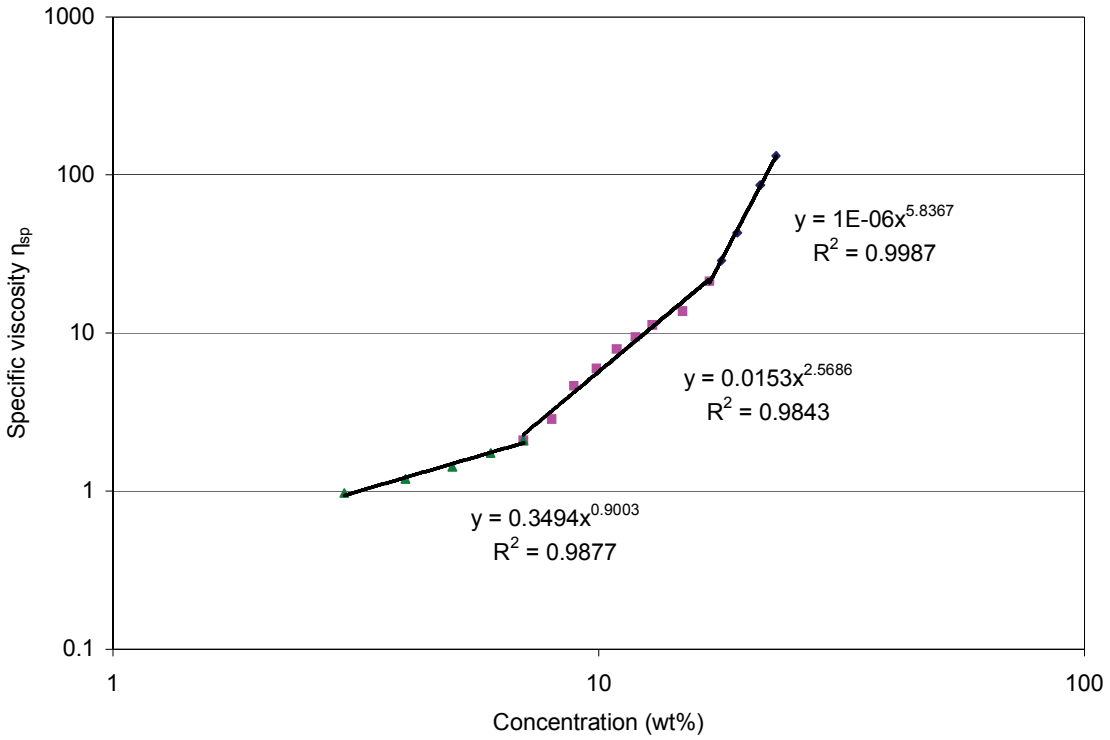

Figure 15.1. Solution rheology of 15700 g/mol 12,12-ammonium ionene. Conditions: AR-G2, 25 °C, concentric cylinder geometry.

All ionene films were cast under the same conditions as reported in chapter 3. However, in the future, the effect of casting conditions on the morphology should be examined. In addition, ionic aggregation should be studied with X-ray scattering as a function of hard segment content, temperature, and elongation.

No one has reported the use of ionenes as polymer brushes attached to surfaces. Surfaces modified with ionenes would be stimuli-responsive, since ionenes are sensitive to many factors such as moisture, ionic strength, and temperature (Figure 15.2). A systematic study on the synthesis of surfaces modified with ionenes should be conducted. In addition, when the modified surface is no longer required, the ionene brush could be degraded in a similar manner to the 12,12-ammonium ionenes described in chapter three.

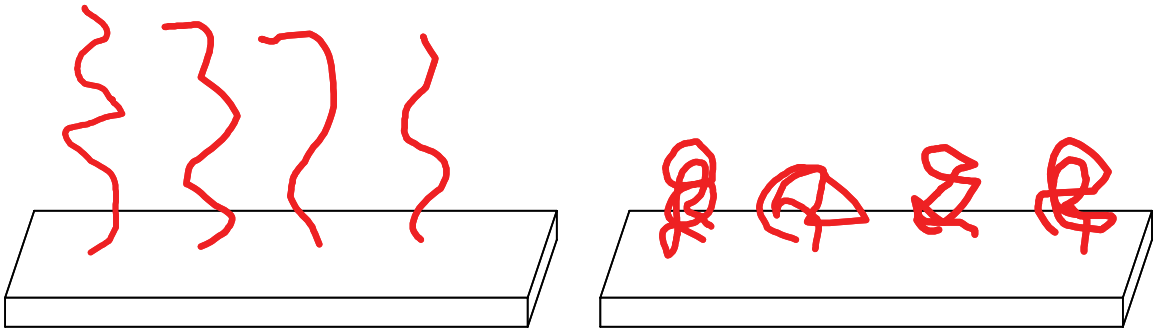

Figure 15.2. Schematic of ionene brushes as environmental factors are varied.

Ionenes are used in a variety of applications, including antimicrobial coatings. In the future, the antimicrobial properties of novel ionene polymers should be evaluated. Relatively hydrophobic ionenes could be electrospun into fibers for antimicrobial mats.

Chapter 3 demonstrated that 12,12-ammonium ionenes possessed shape memory and self-healing properties. Future studies should focus on these properties as a function of molecular weight and hard segment/soft segment composition.

The synthesis of cinnamate-functionalized 12,12-ammonium ionenes was reported in chapter 5. Andreopoulos et al. demonstrated that nitrocinnamates are more photoreactive than conventional cinnamates.[4] Therefore, their use will result in more efficient chain extension and cross-linking of the ammonium ionenes. Also, it is known that cinnamate dimerization in reversible; therefore, cleaving the chain extended and cross-linked networks should be investigated with the use of UV light at wavelengths less than 250 nm.

Chapter six described the first report of imidazolium ionene copolymers containing PTMO soft segments. Only two other reports of imidazolium ionenes exist in the literature, therefore this research area is quite new. A series of imidazolium ionenes of various molecular weights should be synthesized in a similar manner to the 12,12-ammonium ionenes described in chapter 3. The thermomechanical and morphological properties should vary as function of molecular weight. In addition, the behavior as a function of counteranion should be investigated,

since the structure and size of the counteranion influences properties. In addition, the solution properties should be studied using DLS and solution rheology as a function of salt concentration. Imidazolium cation containing polymers are often used in electroactive device fabrication. Conductivity measurements should be investigated as the soft segment composition and counteranion varies. It is proposed that imidazolium ionenes containing PEG soft segments will have the greatest conductivity values. This thesis reported the self-healing and shape memory properties of ammonium ionenes. The imidazolium ionenes should be evaluated in a similar manner. The bisimidazole monomer used in the synthesis possessed four methylene units between the imidazole functional groups. The spacer length between imidazole functional groups will affect many properties, including the morphology. Thermal, mechanical, and morphological properties will also change as the hard segment concentration changes. Therefore, a series of imidazolium ionene copolymers containing various amounts of PEG and PPG soft segments should be synthesized and characterized. In addition, all of the imidazolium ionene copolymers synthesized by our research group have a random structure. Synthesis of imidazolium ionene block copolymers should be performed, and the resulting polymers should be compared to the random copolymers already reported. Finally, no one has reported the synthesis of phosphonium cation-containing ionenes. Initial studies in our research group established that phosphonium ionene synthesis was successful, as shown in Scheme 15.1. Therefore, structure-property relationships should be evaluated for phosphonium ionenes.

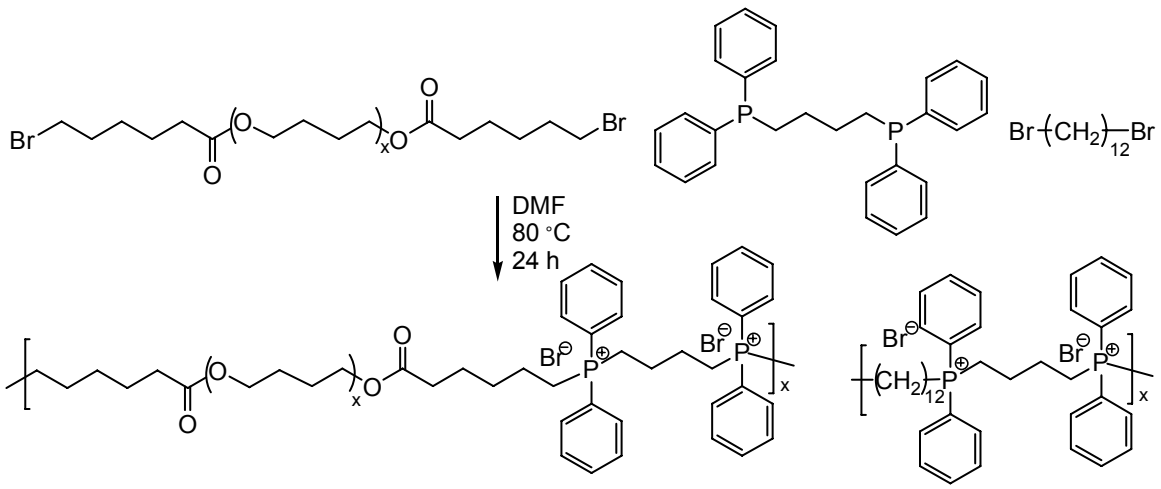

Scheme 15.1. Synthesis of phosphonium cation-containing ionenes with PTMO soft segments.

15.2 Synthesis and applications of ion-containing polyurethanes and polyureas

In chapters seven and eight, imidazolium and phosphonium polyurethane syntheses were described, respectively. X-ray scattering as a function of temperature would provide more information about the ionic domains. In these chapters, only one composition of ionic content was studied. In the future, the ion content should be systematically varied to elucidate the effect of ion content on mechanical performance and morphological properties. In addition, only 2000 g/mol poly(tetramethylene oxide) (PTMO) soft segments were utilized. A fundamental investigation of varying soft segment molecular weight will provide interesting results, especially for polymer crystallization properties. Other oligomeric soft segments, such as poly(propylene glycol) (PPG), PEG, and poly(caprolactone) (PCL) will offer interesting film forming properties or be water dispersible. The effect of counteranion will also have an influence on the thermal, mechanical, and morphological properties. Another study should focus on the effect of varying the alkyl spacer length between the charge sites of the chain extender. The novel synthesis of ion-containing polyurethane-ureas and polyureas would elucidate the effect that dominates properties—ionic interactions or hydrogen bonding. Branched polymers

behave differently than linear polymers. Therefore, a fundamental investigation on the effect of branching on the properties of ion-containing polyurethanes should be conducted.

There is increasing interest in using ionic liquids as polymerization solvents. Synthesis of ion-containing polyurethanes in ionic liquids could provide a preparation method that is more environmentally friendly. Furthermore, if some of the ionic liquid remains and swells the polyurethane, interesting conductive properties could result. Electrospinning ion-containing polyurethanes and polyureas into fibers perhaps will create novel membrane materials for membrane and antimicrobial applications. Finally, toxicity analysis should be conducted on the novel ion-containing polyurethanes to determine if they are suitable for biomedical applications.

15.3 Synthesis of Michael addition networks containing ammonium, imidazolium, and phosphonium salt monomers

Michael addition to formed cross-linked networks was described in several chapters of this thesis. As shown in chapters seven and eight, ion-containing diols were prepared for polyurethane synthesis. Ion-containing diols with longer alkyl segments are ideal candidates for monomer precursors for Michael chemistry. The short alkyl length spacers used for polyurethane synthesis would undergo an elimination reaction during the acetoacetate functionalization. Preliminary results demonstrated that acetoacetate functionalized phosphonium diols dissolved in chloroform cross-linked with diacrylates in the presence of 1,8-diazbicyclo[5.4.0]undec-7-ene (DBU). A thorough investigation of the effect of diacrylate structure on cross-linked film mechanical properties should be conducted. In addition, urethane diacrylates, such as those described in chapter eleven, could be used in cross-linking reactions to investigate the interaction of hydrogen bonding and ionic interactions.

15.4 Glutathione nanoparticles for antioxidant delivery

As shown in chapter 11, the formation of glutathione nanoparticles was analyzed in water. However, the behavior of the nanoparticles should be investigated as a function of the cellular environment using DLS.

15.5 References

(1) Grassl, B.; Galin, J. C. *Macromolecules* **1995,** 28, (21), 7035-7045.
(2) Grassl, B.; Mathis, A.; Rawiso, M.; Galin, J. C. *Macromolecules* **1997,** 30, 2075-2084.
(3) Grassl, B.; Meurer, B.; Scheer, M.; Galin, J. C. *Macromolecules* **1997,** 30, 236-245.
(4) Zheng, Y.; Andreopoulos, F. M.; Micic, M.; Huo, Q.; Pham, S. M.; Leblanc, R. M. *Adv. Funct. Mater.* **2001,** 11, (1), 37-40.